The Effect of Riverine Particulate Material on Primary Productivity and the Global Organic Carbon Cycle

Christian Grimm

Université Fédérale
Toulouse Midi-Pyrénées

THÈSE

En vue de l'obtention du

DOCTORAT DE L'UNIVERSITÉ DE TOULOUSE

Délivré par :

Université Toulouse 3 Paul Sabatier (UT3 Paul Sabatier)

Présentée et soutenue par :
GRIMM, Christian

le jeudi 12 octobre 2017

Titre :

Charge particulaire fluviale - Effet sur productivité primaire et implications sur le cycle global du carbone organique

---

École doctorale et discipline ou spécialité :
ED SDU2E : Sciences de la Terre et des Planètes Solides

Unité de recherche :
Géosciences Environnement Toulouse (UMR 5563)

Directeur/trice(s) de Thèse :

OELKERS, Eric H.

Jury :
GISLASON, Sigurður R. (rapporteur)
GUYOT, François (rapporteur)
JEANDEL, Catherine (examinatrice)
SCHOTT, Jacques (invité)
POKROVSKY, Oleg S. (invité)
OELKERS, Eric H. (directeur de Thèse)

PhD Thesis

The Effect of Riverine Particulate Material on Primary Productivity and the Global Organic Carbon Cycle

by

Christian Grimm

Extended Abstract

The supply of riverine particulate material to natural waters plays a vital role in the global cycle of the elements and is considered to significantly influence the organic carbon cycle in two ways. First, riverine particulates comprise a vast source of nutrients which can increase primary production in the oceans. For example, the global riverine particulate flux of limiting nutrients such as Si, P and Fe exceeds its corresponding dissolved flux by factors of 50, 100 and 350. Second, the supply of riverine particulates to the oceans is a major control of organic matter burial, an essential process in the long term CO_2 drawdown via the organic pathway.

To explore the link between particulate matter supply and primary production in natural waters, a series of microcosm growth experiments was performed with two common primary producing microbes, the freshwater cyanobacteria *Synechococcus sp.* and the marine diatom *Thalassiosira weissflogii*. Growth experiments were performed in the presence and absence of different riverine particulates at different initial nutrient levels. Results unambiguously demonstrate that riverine particulates significantly increase bacterial biomass growth as a function of particulate concentration. Notably, in experiments conducted with the freshwater cyanobacteria *Synechococcus sp.*, the presence of particulates 1) triggered bacterial growth in otherwise unfavorable conditions, 2) increased total biomass concentration, and 3) induced steady bacterial growth even after consumption of the initial nutrients. The positive effect of riverine particulates on the growth of the marine diatom *Thalassiosira weissflogii* was most obvious in nutrient free experiments where cultures grew linearly with time in the presence of sediments, whereas these cultures died in particulate free controls.

Furthermore, SEM investigations showed direct physical contact between microbes or microbially excreted organic substances and the particulates. In accord with reports in the literature, we suggest that microbes may acquire vital nutrients directly from the rock, which would again enhance the potential of riverine particulates as source of limiting nutrients. The direct physical contact also suggests an increase in the burial efficiency of organic carbon through either 1) increasing organic carbon content absorbed on mineral surfaces, 2) increasing agglomeration and marine snow formation of organic and inorganic particles or 3) increasing organic matter settling velocities through mineral ballasting. The direct physical attachment of microbes on mineral surfaces was also observed in natural samples obtained from a field study at the Icelandic South coast. The positive effect of particulates on microbial growth and its

effect on organic carbon burial are complimentary. Agglomeration is a function of suspended particle concentration, organic or inorganic. An elevated biomass concentration induced by the presence of riverine particulates results in a high total suspended matter concentration, thus increasing the particle agglomeration rate.

Taken together, this study provides experimental evidence for the importance of riverine particulates in the organic carbon cycle through its positive impact on primary production. Furthermore, it compiles evidence that particulates may facilitate organic matter burial through direct attachment of microbes on sediment surfaces or the formation of fast settling mineral/microbe agglomerations.

Complimentary studies were performed to assess the quality of carbon isotope compositions to preserve estimates of organic carbon burial rates over geological time. Variations in the degree of primary production and organic matter burial during Earths' history are recorded in the carbon isotopic signature of marine carbonates. The use of carbon isotopic signatures in carbonates to reconstruct past environmental conditions, however, requires that these signatures are preserved over vast timescales. Experimental results demonstrate, that the carbon isotopic composition of calcite continuously evolves towards mineral-fluid isotopic equilibrium. This observation suggests that calcite C-isotopic compositions might change noticeably if the calcite were continuously in isotopic disequilibria with its co-existing fluid.

Résumé étendu

L´apport de matière particulaire aux eaux naturelles joue un rôle essentiel dans le cycle global des éléments et notamment influence le cycle du carbone organique de deux façons: premièrement, les particules fluviales comprennent une source très importante d'éléments nutritifs qui peuvent augmenter la production primaire dans les océans. Par exemple, le flux global de particules de nutriments limitants tels que Si, P et Fe dépasse son flux dissous par des facteurs de 50, 100 et 350 au sein des rivières. Deuxièmement, l'apport des particules des continents aux océans est un contrôle majeur de la séquestration du carbone organique, un processus essentiel dans la réduction du CO_2 à long terme par le cycle de carbone organique.

Pour explorer le lien entre l'approvisionnement de matières particulaires et la production primaire dans les eaux naturelles, une série d'expériences de croissance dans des microcosmes a été réalisée impliquant deux producteurs primaires abondants: la cyanobactérie d'eau douce *Synechococcus sp*., et la diatomée marine *Thalassiosira weissflogii*. Des expériences de croissance ont été réalisées en présence et en l'absence de différentes particules de rivières et à différents niveaux nutritifs initiaux. Les résultats démontrent sans ambiguïté que les particules fluviales augmentent nettement la croissance de la biomasse en fonction de la concentration du matériel particulaire. Notamment, dans les expériences menées avec la cyanobactérie d'eau douce *Synechococcus sp.*, la présence de particules a 1) déclenché une croissance bactérienne dans des conditions pourtant défavorables, 2) augmenté la concentration totale de biomasse et 3) déclenché une croissance bactérienne constante même après la consommation des nutriments initiaux. L'effet positif des particules de rivières sur la croissance de la diatomée marine *Thalassiosira weissflogii* a été le plus évident pour les expériences n'impliquant pas de nutriments, où les concentrations des diatomées ont augmenté linéairement en présence de sédiments alors que ces cultures sont mortes dans des expériences menées sans la présence de particules.

De plus, des études MEB ont montré un contact physique direct entre les microbes ou les substances organiques excrétées par les microbes et les particules de rivières. Conformément aux travaux issus de la littérature, nous suggérons que les microbes peuvent acquérir des nutriments essentiels directement à partir des minéraux, ce qui augmenterait encore le potentiel des particules fluviales en tant que source de nutriments limitants. Le contact physique direct suggère également une augmentation de l'efficacité de piégeage du carbone organique par 1) l'augmentation du contenu de carbone organique absorbé sur les surfaces minérales, 2)

l'augmentation de l'agglomération des particules organiques et inorganiques et donc la formation de neige marine ou 3) l'augmentation des vitesses de chute de la matière organique par «mineral ballasting». La fixation physique directe des microbes sur les surfaces minérales a également été observée dans les échantillons naturels obtenus au cours d'une étude de terrain sur la côte sud islandaise. L'effet positif des particules sur la croissance microbienne et son effet sur la séquestration du carbone organique sont complémentaires. L'agglomération est une fonction de la concentration des particules en suspension, de nature organique ou inorganique. Une concentration élevée de biomasse induite par la présence de particules de rivières en suspension résulte en une concentration élevée de matière en suspension totale, ce qui augmente le taux d'agglomération des particules et la formation de neige marine.

Dans l'ensemble, cette étude fournit des preuves expérimentales de l'importance des particules de rivières dans le cycle du carbone organique grâce à son impact positif sur la production primaire. En outre, ces travaux rassemblent les preuves que les particules peuvent faciliter l'inhumation de matières organiques grâce à la fixation directe de microbes sur les surfaces de sédiments ou à la formation des agglomérats minéraux-microbes qui chutent rapidement dans la colonne d´eau.

Des études complémentaires ont été effectuées pour évaluer la qualité des compositions isotopiques du carbone, afin de préserver les estimations des taux de séquestration du carbone organique à travers une période géologique donnée. Les variations du degré de production primaire et du piégeage de la matière organique dans les sols au cours des temps géologiques sont conservées dans la signature isotopique du carbone des carbonates marins. L'utilisation de signatures isotopiques du carbone des carbonates pour reconstruire les conditions environnementales passées exige cependant que ces signatures soient conservées pour des vastes échelles de temps. Les résultats expérimentaux démontrent que la composition isotopique du carbone de la calcite évolue continuellement vers l'équilibre isotopique entre les fluides et les minéraux. Cette observation suggère que les compositions isotopiques de carbone dans la calcite pourraient changer notablement si la calcite était constamment dans un déséquilibre isotopique avec son fluide coexistant.

.

Preface

This PhD thesis presents the results of the research work carried out by the author from November 2013 to June 2017 at the Géosciences Environnement Toulouse / Centre National de la Recherche Scientifique (CNRS UMR 5563 GET) Laboratory in Toulouse, France. This study was funded by the Marie Curie EU-FP7 CO2-REACT Research and Training Network. The work is comprised of six chapters:

Chapter 1 is an extended introduction addressing the aim and motivation of this study as well as a compilation of previous research related to the subject. Chapter 2 describes the methodology applied during the experimental work in detail, extending the description in the corresponding main chapters where additional explanation is appropriate. Chapter 6 represents the general conclusions of the research as well as suggestions for future research.

Chapters 3, 4 and 5 describe the main research work of this thesis, which is comprised of three scientific research manuscripts. These chapters have been either submitted (Chapter 5), or prepared for submission to peer-reviewed journals (Chapters 3 and 4).

Chapter 3 describes the content of the completed manuscript: “Riverine particulate material as hot spots of cyanobacterial growth: results of laboratory experiments with *Synechococcus sp*.“. This chapter has been prepared for submission to an international peer-reviewed journal and is authored by C. Grimm, R. E. Martinez, O. S. Pokrovsky, L. G. Benning and E. H. Oelkers with the following contributions: The experimental and analytical work was performed by myself, and if appropriate, together with a corresponding technician. The manuscript was written by myself, and the co-authors, notably Eric Oelkers, provided comments and suggestions on the experimental work and the obtained data and furthermore critically reviewed the manuscript.

Chapter 4 describes the content of the completed manuscript: “Effect of riverine particulate material on the growth of marine diatoms: results of laboratory experiments with *Thalassiosira weissflogii*“, which has been prepared for submission to a peer-reviewed journal authored as follows: C. Grimm, A. Feurtet-Nazel, O. S. Pokrovsky and E. H. Oelkers with the following contributions: The experimental work and cell counting were performed by myself. The culturing of the diatom strain prior to the experimental work was conducted by Bruno Etcheverria at the EPOC, Station Marine d´Arcachon. The manuscript was written by myself,

and the co-authors, notably Eric Oelkers, provided comments and suggestions on the experimental work and the obtained data and critically reviewed the manuscript.

Chapter 5 is comprised of the manuscript "The temporal evolution of carbon isotopes in calcite in the presence of cyanobacteria", which has been submitted to *Geochimica et Cosmochimica Acta* on the 2nd of May 2017, authored as C. Grimm, V. Mavromatis, A. Leis, O. S. Pokrovsky and E. H. Oelkers and is currently under review (Manuscript Number GCA-D-17-00321). The experimental work and wet-chemical analysis were conducted by myself, whereas the carbon isotope analyses, including sample preparation, was performed by the co-author Albrecht Leis at the R-AquaConSol GmbH in Graz, Austria. The manuscript was written by myself, and the co-authors, notably Eric Oelkers, provided comments and suggestions on the experimental work and the obtained data and critically reviewed the manuscript.

The Annex is comprised of data tables which show the electronic supplement material of the corresponding chapters. Furthermore, Annex 3 presents the published article "Martinez R. E., Weber S. and Grimm C. (2016) Effects of freshwater Synechococcus sp. cyanobacteria pH buffering on $CaCO_3$ precipitation: Implications for CO_2 sequestration. *Applied Geochemistry* 75, 76–89.", of which I am the third author. My contributions were minor assistance with experimental work during a stay at the University of Freiburg in spring 2014, the completion of SEM analyses including sample processing, the preparation of the corresponding methods paragraph, as well as a review of the manuscript.

Acknowledgements

This thesis would not have been possible without the help of many people. First of all, I want to thank my advisor Eric Oelkers for the great support during the last years and for generously sharing his time, his expertise and his enthusiasm. In particular, his reviewing work during the formulation of the thesis, manuscripts, presentations, or conference abstracts is highly appreciated. Also his readiness and helpfulness to adjust work and private life are sincerely appreciated.

Next, I would like to thank the examiners and jury members for spending their time in evaluating this thesis.

I would furthermore like to thank all student and PI members, as well as industry partners of the European Marie Curie Initial training network CO2-React for their constructive criticism and advice in scientific or other career-related topics during our meetings. Above all, I would like to thank all of them for providing such a pleasant working atmosphere. I highly appreciated the good training sessions, nice field trips, enthusiastic sport sessions and convivial evenings throughout our network events.

I thank the current and former graduate students of the GET, Cristina Castillo, Anna Harrison, Andrea Perez, Franziska Stamm, Ulf-Niklas Berninger, Aridane Gonzalez, Thomas Rinder and Martin Voigt for the good times spent together during conferences, week-end trips, Petanque matches, lunch and coffee breaks, drinking Fridays and all other activities. A special thanks to Aridane Gonzalez for his readiness to help with my bio-related challenges. Moreover, I acknowledge Vasileios Mavromatis, Oleg Pokrovsky and Jacques Schott for their precious advice, insightful ideas and their support during experimental and analytical work and writing but also for their tips considering Pyrenees-outdoor activities. At this place I would like to dedicate a few extra lines to Martin Voigt. First, I would like to thank him for the many insightful scientific discussions, his help with solving complex calculations or with administrative work. Apart from this, I very much enjoyed our regular leisure activities such as ping-pong sessions, lunch à dehors, baignade en Arriège, snorkeling or the hours spent in front of the relief of the Pyrenees and the subsequent hiking trips. May there be many more mountains to climb and summit coffees to drink in the future!

I am much obliged to the technicians Carole Causserand, Thierry Aigouy, Alain Castillo, Aurélie Lanzanova, Frédéric Candaudap and Michel Thibaut for their assistance with

wet-chemical analyses, SEM- and BET- analyses, ICP-MS measurements, and XRD analyses, respectively. I would also like to thank Vincent Fournier, Carine Baritaud, Gaelle Combier, Marlène Larroque and Elisabeth Soulié for their administrative work. In terms of lab support, my work has greatly benefited from the assistance of Liudmila Shirokova, who readily answered all my question considering culturing, sterilization, etc. and taught my some basic biogeochemical techniques.

I would also like to thank the many other PhD students at the GET or the adjoining laboratories of the OMP for making the time in Toulouse so pleasant. Notably, I appreciated the early morning "cafe martinal convivial", basketball sessions, lunch football or lunch Pala matches and the elaborately organized ACDC meetings. A special thanks to Sylvain Pinet, first of all for revising the French translations in this thesis, and moreover for convincing me to join him in his rugby club.

At the University of Freiburg, where I spent the first weeks of my PhD, I was kindly received by the head of the Mineralogy/Geochemistry department Kurt Bucher (at this time) and the staff of the department, notably Sigrid Hirth Walter and Sebastian Weber to whom I send my acknowledgements. A special thanks to Raul Martinez for teaching me the basics in sterile work, cell-culturing, biogeochemical experimental work and for all his valuable scientific input.

Furthermore, I acknowledge Stefanie Lutz, Maren Kahl, Martin Fuller and Richard Walshaw from the School of Earth and Environment, University of Leeds for their help during SEM investigations and Daniela van den Heuvel for the warm welcome in Leeds. I am much obliged to Liane Benning from the University of Leeds, and the GFZ Potsdam, for kindly receiving me for the SEM work in Leeds and for insightful discussions, her support and encouragement.

I thank the bamby group at the Earth Science Institute of the University of Iceland, Deirdre Clark, Eydís Eiríksdóttir, Iwona Galeczka, Becca Neely, Sandra Snaebjörnsdóttir and Siggi Gíslason for sharing their time and expertise. Notably, Siggi and Eydis supported me lot during my work in Iceland and Eydis provided some of the tediously sampled riverine particulate material used during this study. A special thanks to Deirdre and Becca who joined me on an unforgettable sampling cruise where we had to suffer a lot, so that it became a strong bonding day for us and a peculiar lifetime experience. Moreover, I thank Jón Ólafsson from the

University of Iceland and Kristín Valsdóttir from the Icelandic Marine Research Institute for their advice and help with chlorophyll measurements.

Bruno Etcheverria from the EPOC, Station Marine d´Arcachon is thanked for tediously culturing the diatom strain and for his advice concerning diatom culturing and maintaining. Furthermore, I thank Agnès Feurtet-Mazel for her cooperativeness and her scientific input, as well as Oleg Pokrovsky for establishing the contact to Arcachon.

I would also like to thank Karen Johannesson from the Department of Earth and Environmental Sciences of Tulane University in New Orleans for providing Mississippi sediments.

Moreover, I would like to thank Pierre-Paul Riquet for having had the great ideas and geo-engineering skills to realize to completion of the Canal du Midi back in the 17th century. The canal served for three years as commute (by bike) from the city center of Toulouse down to the OMP, without a single annoying traffic light.

Finally, I would like to thank my family and friends at home and abroad, who supported me during the creation of this thesis either by providing on open ear whenever needed or by any sort of diverting activities dragging my bag into the real world.
Most importantly, I want to express my deepest gratitude to my wife Elisabeth Grimm, who readily followed me to France so that I could follow my professional interests. Her invaluable assistance and support throughout this time, notably during the final phase of the thesis, was very admirable. Merci!

Contents

1 Introduction

1.1 General Introduction / Motivation

Global warming is amongst the most polarizing subjects over the past decades. Sixteen of the 17 warmest years since modern recordkeeping began in 1880 occurred since the year 2001 and the year 2016 was the third consecutive year with a new record global average surface temperature (Potter et al., 2017). A large body of evidence demonstrates that global warming stems from an increase in atmospheric CO_2 concentration. As such, historic CO_2 concentrations are closely correlated to surface temperatures (Oelkers and Cole, 2008; Petit et al., 1999). Ice records reveal that atmospheric CO_2 concentrations fluctuated between glacial and interglacial cycles but have not exceeded 300 ppm during the last 400`000 years of Earths' history. Since the beginning of the industrial revolution and due to the exhaustive use of fossil fuels as energy source, the atmospheric CO_2 concentration has been steadily increasing from 280 ppm to more than 400 ppm today and the globally-averaged surface temperature has already risen about 1.1 °C since the late 19^{th} century (Potter et al., 2017). With the aim, or hope to "prevent dangerous anthropogenic interferences with the climate system (The United Nations Framework Convention on Climate Change (1992), Article2, p.9)", the worlds governments defined the target of ceiling global mean temperature increase below 2 °C relative to pre-industrial levels. The first and fundamental step to reach this target is to reduce anthropogenic CO_2 emissions through approaches such as the intensified use of renewable energy sources, energy saving strategies, an environmentally sustainable development of the transport sector or carbon capture and storage technologies.

Climate scientists however, increasingly agree that negative carbon emissions are required in order to reach the 2 °C target (Edmonds et al., 2013; Krey et al., 2014; Rogelj et al., 2013; Smith et al., 2015; van Vuuren et al., 2013). Whereas traditional mitigation technologies aim at reducing CO_2 emissions from point sources such as power plants, new technologies need to be established focusing on the removal of CO_2 directly from the atmosphere. For a compilation of possible negative emission technologies (NET) see for example Smith et al. (2015) and references therein.

The fundamental approach, however, is to study and understand how the planet Earth naturally controls atmospheric CO_2 concentrations and to evaluate how humans eventually affect these processes. The natural control of atmospheric CO_2 concentrations over geological timescales can be summarized by two elementary chemical reactions (Berner et al., 1983; Berner, 2003, 2006; Garrels et al., 1976):

$$(Mg, Ca)SiO_3 + CO_2 \leftrightarrow (Mg, Ca)CO_3 + SiO_2 \quad (1\text{-}1)$$

$$CO_2 + H_2O \leftrightarrow CH_2O + O_2 \quad (1\text{-}2)$$

Reaction (1-1) is key to the "inorganic carbon cycle" which is comprised of the weathering of continental Mg,Ca-silicates by CO_2 and the subsequent precipitation and deposition of Mg,Ca-carbonates in the oceans (Reaction (1-1) from left to right) and the release of CO_2 by the thermal decomposition of carbonates via volcanism, metamorphism or diagenesis (Reaction (1-1) from right to left).

Reaction (1-2) is the basis for the "organic carbon cycle" which notably affects atmospheric CO_2 and O_2 concentrations. The organic carbon cycle is comprised of the formation of organic matter from inorganic carbon via photosynthesis (Reaction (1-2) from left to right) and the release of CO_2 through respiration and decomposition (Reaction (1-2) from right to left on a timescale of days to months) or the release of CO_2 via oxidative weathering and thermal decomposition of organic matter after it had been buried and stored at depth (Reaction (1-2) from right to left on geological timescales). These two fundamental processes are illustrated in Figure 1-1, which additionally shows the major anthropogenic impact on these natural cycles: the burning of fossil fuels and the production of cement, both emitting CO_2 to the atmosphere which had been stored in depth for millions of years.

The particular interest of this work lies on Reaction (1-2), or more specifically on the link between Reactions (1-1) and (1-2) and on its climate sensitivity. The organic pathway is composed of two fundamental steps: First, the production of biomass via photosynthesis and second, the burial of organic matter to prevent its immediate decomposition. Both steps are crucially linked to the inorganic pathway since 1) weathering of continental rocks is the primordial source of nutrients driving primary production and 2) the supply of particulate material from continents to the oceans is the primary control of organic matter burial and preservation. These two processes are highlighted in blue in Figure 1-1.

The riverine transport of elements plays a key role in both carbon cycles since it provides the oceans with divalent cations, ready to form carbonates, and with nutrients supporting primary production. These processes are illustrated schematically in Figure 1-2. Notably, rivers transport elements derived from continental weathering to the oceans in dissolved and in particulate form and recent estimates demonstrate that the suspended material flux dominates the dissolved flux for essentially all elements (Jeandel and Oelkers, 2015; Oelkers et al., 2011; 2012). The supply of dissolved and particulate matter to the oceans is controlled by weathering rates and continental runoff (Eiriksdottir et al., 2015; Gislason et al., 2006; 2009; Ludwig et al., 1998; Ludwig and Probst, 1998) and increases with increasing temperature and rainfall. A recent field study conducted by Gislason et al. (2006) in NE Iceland demonstrates that the flux of riverine particulate material to the ocean is far more climate sensitive than the corresponding dissolved flux. This implies that riverine particulates derived from continental weathering potentially represent an important parameter in drawing down CO_2 and moderating climate by 1) providing limiting nutrients, thereby increasing primary production and 2) increasing organic carbon burial rates. The scope of this work is to validate the capability of riverine particulates to increase primary production and discuss their role in the organic carbon cycle.

Climate reconstructions take advantage of the pronounced carbon isotopic fractionation during photosynthesis. Organic matter is on average 2.5 ‰ more depleted in the heavier carbon isotope (^{13}C) compared to inorganic carbon dissolved in the ocean or fixed in carbonates (Broecker, 1970; Craig, 1953). As a result, the carbon isotopic history of the Earth, as recorded in marine carbonates, can be used to reveal differences in organic matter production and burial rates and thus to trace the link between biological activity and the evolution of the atmospheric CO_2 and O_2 concentrations. The use of carbon isotopic signatures to reconstruct past environmental conditions, however, requires that these signatures are preserved over vast timescales. This is the motivation of the fifth chapter of this work which aims to assess the rate of carbon isotope signature alteration in calcite caused by microbial-induced modifications of the carbon isotope composition of a co-existing fluid phase.

1.1b Introduction générale / Motivation

Le réchauffement climatique est certainement un des sujets les plus polarisants au cours des dernières décennies. Seize des dix-sept années les plus chaudes depuis la tenue de dossiers modernes en 1880 ont été enregistrées depuis 2001. De plus, l'année 2016 a été la troisième année consécutive avec un nouveau maximum de température mondiale globale de surface (Potter et al., 2017). Un grand nombre de preuves démontrent que le réchauffement climatique provient d'une augmentation de la concentration atmosphérique de CO_2. Notamment, les concentrations historiques de CO_2 sont étroitement liées aux températures de surface (Petit et al., 1999; Oelkers et Cole, 2008). Les données sur les carottes glacières révèlent que les concentrations atmosphériques de CO_2 ont fluctué entre les cycles glaciaires et non-glaciaires mais n'ont pas dépassé 300 ppm au cours des 400’000 dernières années de l'histoire de la Terre. Depuis le début de la révolution industrielle et du fait de l'utilisation exhaustive des combustibles fossiles comme source d'énergie, la concentration de CO_2 dans l´atmosphère a augmenté constamment de 280 ppm à plus de 400 ppm aujourd'hui et la température de surface moyenne a déjà augmenté environ 1.1 °C depuis la fin du 19ème siècle (Potter et al., 2017). Dans le but ou l'espoir de «prevent dangerous anthropogenic interferences with the climate system (The United Nations Framework Convention on Climate Change (1992), Article2, p.9)», les gouvernements mondiaux ont défini l'objectif de restreindre l'augmentation de la température moyenne globale au-dessous 2 °C par rapport aux niveaux préindustriels. La première étape fondamentale pour atteindre cet objectif est de réduire les émissions de CO_2 anthropiques à travers certaines approches telles que l'utilisation accrue des sources d'énergies renouvelables, des stratégies d'économie d'énergie, un développement écologique du secteur des transports ou des technologies de capture et de stockage du carbone.

Toutefois, les scientifiques du climat conviennent de plus en plus que des émissions de carbone négatives sont nécessaires pour atteindre l'objectif de 2 °C (Edmonds et al., 2013; Rogelj et al., 2013; van Vuuren et al., 2013; Krey et al., 2014; Smith et al., 2015). Alors que les technologies d'atténuation traditionnelles visent principalement à réduire les émissions de CO_2 provenant de sources ponctuelles telles que les centrales électriques, de nouvelles technologies focalisées sur l'élimination directe du CO_2 atmosphérique doivent être développées. Les travaux de Smith et al. (2015) et les références qui s’y trouvent sont un exemple de compilation des technologies possibles d'émission négative (NET).

L’approche fondamentale, cependant, consiste à étudier et comprendre comment la planète Terre régule naturellement les concentrations atmosphériques de CO_2 et viser à évaluer

comment les activités anthropiques influencent éventuellement ces processus. Le contrôle naturel des concentrations atmosphériques de CO_2 par rapport aux temps géologiques peut être résumé par deux réactions chimiques élémentaires (Garrels et al., 1976; Berner et al., 1983; Berner, 2003; 2006):

$$(Mg, Ca)SiO_3 + CO_2 \leftrightarrow (Mg, Ca)CO_3 + SiO_2 \quad (1\text{-}3)$$

$$CO_2 + H_2O \leftrightarrow CH_2O + O_2 \quad (1\text{-}4)$$

La réaction (1-1) est la clé du «cycle du carbone inorganique» qui comprend l'altération des silicates de Mg et Ca continentaux par le CO_2 et les précipitations et dépositions subséquentes de carbonates de Mg et Ca dans les océans (Réaction (1-1) de gauche à droite) et la libération de CO_2 par décomposition thermique des carbonates par volcanisme, métamorphisme ou diagénèse (Réaction (1-1) de droite à gauche).

La réaction (1-2) est à la base du «cycle du carbone organique» qui affecte notamment les concentrations atmosphériques de CO_2 et O_2. Le cycle du carbone organique comprend la formation de matière organique à partir du carbone inorganique via la photosynthèse (Réaction (1-2) de gauche à droite) et la libération de CO_2 par respiration et décomposition (Réaction (1-2) de droite à gauche sur une échelle de quelques jours à quelques mois) ou la libération de CO_2 par altération oxydatives et la décomposition thermique de la matière organique après avoir été enterré et stocké en profondeur (Réaction (1-2) de droite à gauche à l'échelle des temps géologiques). Ces deux processus fondamentaux sont illustrés dans la figure 1-1, qui montre en outre l'impact anthropique majeur sur ces cycles naturels: l'ignition des combustibles fossiles et la production de ciment, tous deux émettant dans l'atmosphère du CO_2 qui a été stocké en profondeur pendant des millions d'années.

L'intérêt particulier de ce travail repose sur la réaction (1-2), ou plus exactement sur le lien entre les réactions (1-1) et (1-2) ainsi que sur leur sensibilité au climat. Le cycle du carbone organique à long terme se compose de deux étapes fondamentales: premièrement, la production de biomasse par la photosynthèse et deuxièmement, l'enfouissement de la matière organique pour éviter sa décomposition immédiate. Ces deux étapes sont étroitement liées au cycle du carbone inorganique car 1) l'altération des roches continentales est la source primordiale des nutriments qui alimentent la production primaire et 2) l'apport des matières particulaires des continents vers les océans correspond au facteur principal de contrôle du piégeage et de la conservation des matières organiques. Ces deux processus sont mis en évidence en bleu sur la figure 1-1.

Le transport fluvial d'éléments joue un rôle clé dans les deux cycles du carbone, car il fournit aux océans des cations divalents, prêts à former des carbonates et des nutriments soutenant la production primaire. Ces procédés sont illustrés schématiquement dans la figure 1-2. Notamment, les rivières transportent des éléments dérivés de l´altération continentale vers les océans sous forme dissoute et sous forme particulaire. Des estimations récentes démontrent que le flux de matière en suspension domine le flux dissous essentiellement pour tous les éléments (Oelkers et al., 2011; 2012; Jeandel et Oelkers, 2015). L'apport de matières dissoutes et particulaires aux océans est contrôlé par les taux d'altération et le ruissellement continental (Ludwig et al., 1998; Ludwig et Probst, 1998; Gislason et al., 2006; 2009; Eiriksdottir et al., 2015) et augmente avec l'augmentation de la température et des précipitations. Une étude de terrain récente menée par Gislason et al. (2006) dans le nord-est de l'Islande démontre que le flux de matière particulaire fluviale vers l'océan est beaucoup plus sensible au climat que le flux dissous correspondant. Cela implique que les particules fluviales dérivées de l´altération continentale représentent potentiellement un paramètre important dans la réduction du CO_2 atmosphérique et la modération du climat par 1) un apport en nutriments limitants, augmentant ainsi la production primaire et 2) une augmentation des taux de séquestration du carbone organique. Les objectifs principaux de ces travaux sont de valider la capacité des particules fluviales à augmenter la production primaire et d´évaluer le rôle des particules fluviales dans le cycle du carbone organique.

Les reconstructions climatiques tirent partie du fractionnement isotopique prononcé du carbone pendant la photosynthèse. La matière organique est en moyenne 2.5 % moins chargée en isotope de carbone lourd (^{13}C) par rapport au carbone inorganique dissous dans l'océan ou fixé dans les carbonates (Craig, 1953; Broecker, 1970). En conséquence, l'histoire isotopique du carbone de la Terre, conservée dans les carbonates marins, peut être utilisée pour révéler les différences des taux de productivité primaire et de piégeage de matière organique et ainsi permet de tracer le lien entre l'activité biologique et l'évolution des concentrations atmosphériques de CO_2 et O_2. L'utilisation de signatures isotopiques de carbone pour reconstruire les conditions environnementales passées, cependant, exige que ces signatures soient conservées sur des vastes échelles de temps. C'est la motivation du dernier chapitre de ces travaux qui vise à évaluer le taux d'altération de la signature isotopique du carbone dans la calcite causée par des modifications de la composition isotopique du carbone de la phase fluide coexistante incitée par l´activité microbienne.

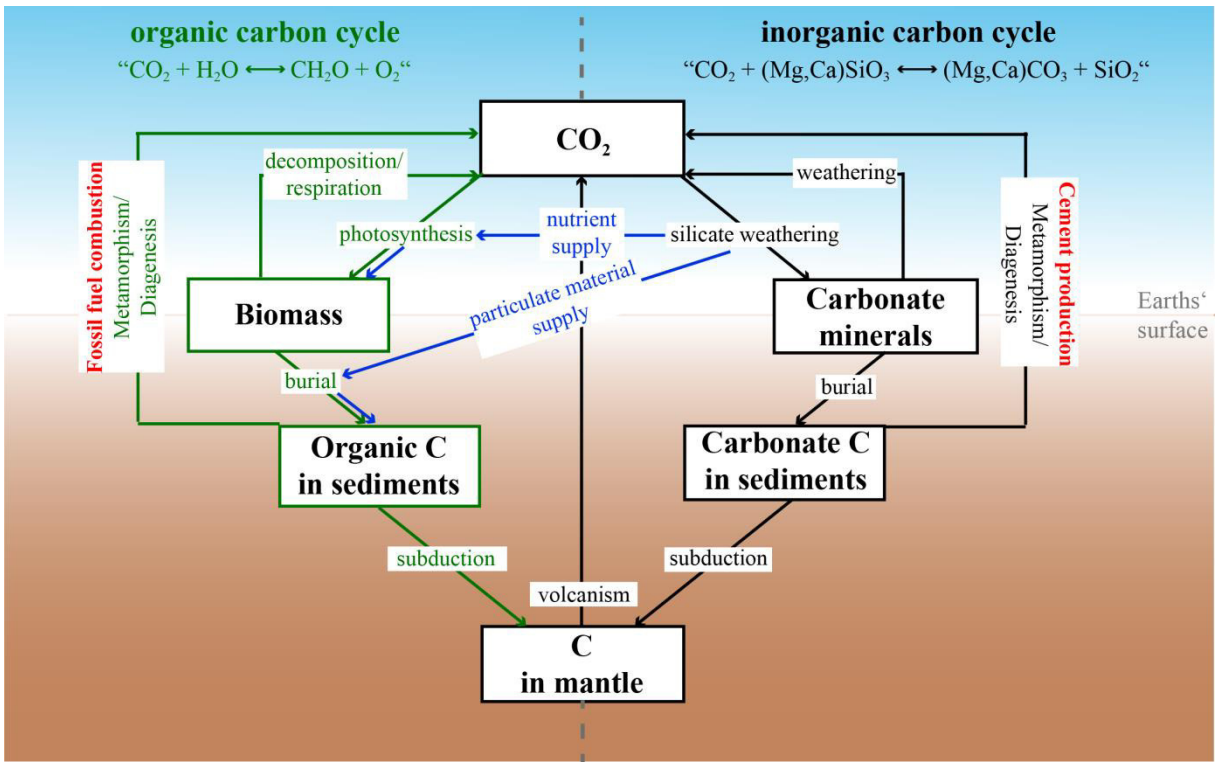

Figure 1-1. A model of the long-term carbon cycle modified from Berner (2003). The cycle can be subdivided into two subcycles: The organic carbon cycle, which includes organic matter formation and burial (left side of the figure) and the inorganic carbon cycle (right side of the figure), involving silicate weathering and deposition of carbonates. The major anthropogenic interventions on these cycles are highlighted in red. The supply of particulate material and nutrients derived from continental weathering represents a distinct link between the two cycles.

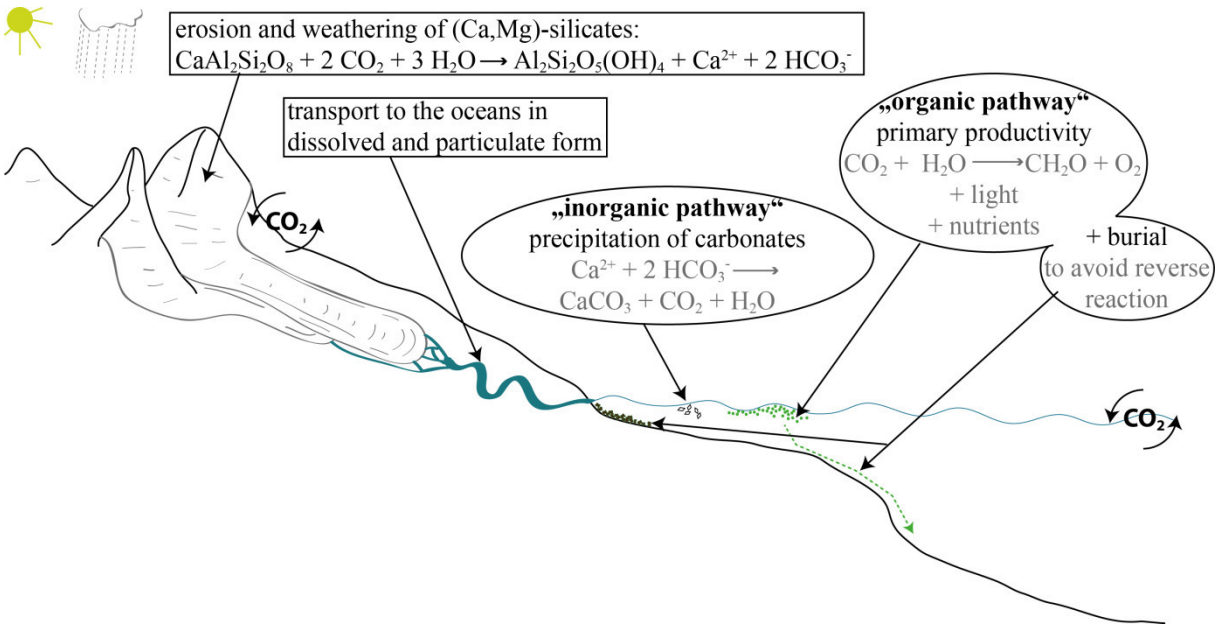

Figure 1-2. Schematic sketch showing the key role of riverine element fluxes as transport mechanism of dissolved and particulate material driving the inorganic and the organic C-cycle in the oceans.

1.2 The global carbon cycles

There are two major natural carbon cycles on Earth, which determine the atmospheric CO_2 concentration: The inorganic and the organic carbon cycle (Garrels et al., 1976). The inorganic carbon cycle is dictated by tectonics and weathering and its impacts are observed on geological timescales of multimillion years (Berner, 1990; Falkowski, 2014). CO_2 in the inorganic cycle is released to the atmosphere mainly through volcanism and seafloor spreading and is primarily removed from the atmosphere through weathering of silicates and the subsequent formation of carbonates in the oceans (Falkowski, 2014). The organic cycle comprises the formation of biomass from inorganic carbon sources, mainly through oxygenic photosynthesis. This C-cycle affects atmospheric CO_2 concentration on timescales of days to millennia (Falkowski, 2014). The majority of the organic matter produced in this C-cycle is oxidized back to inorganic carbon by respiration or heterotrophic degradation, but a small fraction escapes oxidation through fast burial in the ocean and enters the long term carbon cycle (Falkowski, 2014). In the following section, these carbon cycles are addressed in more detail with a focus on the biologically mediated carbon cycle.

1.2.1 The inorganic carbon cycle

The inorganic carbon cycle is driven by the transformation of silicate rocks to carbonates by weathering and sedimentation and their retransformation back to silicates through metamorphism or magmatism (Berner et al., 1983; Berner, 1992). Magmatism and metamorphism are the major sources of CO_2 to the atmosphere and chemical weathering of silicates is the major sink. The inorganic carbon cycle is closely related to plate tectonics: Seafloor spreading rates control 1) the CO_2 input to the atmosphere through degassing at spreading centers and heating plus decarbonation at convergent plate boundaries and 2) the CO_2 removal through continental weathering due to changes in continental surface area (Berner et al., 1983).

Weathering of (Mg,Ca)-silicates is a sink of atmospheric carbon because it consumes CO_2 and releases divalent cations during mineral dissolution which are transported through rivers to the oceans and combine with bicarbonate to form carbonates (Berner et al., 1983; Berner, 2004; Berner and Kothavala, 2001; Gislason et al., 2006; Walker et al., 1981; Wallmann, 2001). Reactions (1-5), (1-6) and (1-7) show representative weathering reactions of anorthite, wollastonite and forsterite (Mg-olivine):

$$\underbrace{CaAl_2Si_2O_8}_{Anorthite} + 3H_2O + 2CO_2 \rightarrow \underbrace{Al_2Si_2O_5(OH)_4}_{Kaolinite} + Ca^{2+} + 2HCO_3^- \quad (1\text{-}5)$$

$$\underbrace{CaSiO_3}_{Wollastonite} + 3H_2O + 2CO_2 \rightarrow H_4SiO_4 + Ca^{2+} + 2HCO_3^- \quad (1\text{-}6)$$

$$\underbrace{Mg_2SiO_4}_{Forsterite} + 4H_2O + 4CO_2 \rightarrow H_4SiO_4 + 2Mg^{2+} + 4HCO_3^- \quad (1\text{-}7)$$

During anorthite weathering, atmospheric CO_2 is consumed and dissolved Ca and bicarbonate are released into solution, whereas aluminum and silica are incorporated into the hydrated phyllosilicate Kaolinite ($Al_2Si_2O_5(OH)_4$). Similarly, during wollastonite and forsterite weathering, CO_2 is consumed, whereas Ca^{2+} or Mg^{2+} and HCO_3^- are released into solution. The divalent cations released during (Mg,Ca)-silicate weathering are then transported by rivers form the continents to the oceans where they react with bicarbonate to form carbonate minerals via reactions such as:

$$Ca^{2+} + 2HCO_3^- \rightarrow \underbrace{CaCO_3}_{Calcite} + H_2O + CO_2 \quad (1\text{-}8)$$

The overall reactions can thus be summarized to:

$$\underbrace{CaAl_2Si_2O_8}_{Anorthite} + 2H_2O + CO_2 \rightarrow \underbrace{Al_2Si_2O_5(OH)_4}_{Kaolinite} + \underbrace{CaCO_3}_{Calcite} \quad (1\text{-}9)$$

$$\underbrace{CaSiO_3}_{Wollastonite} + 2H_2O + CO_2 \rightarrow H_4SiO_4 + \underbrace{CaCO_3}_{Calcite} \quad (1\text{-}10)$$

$$\underbrace{Mg_2SiO_4}_{Forsterite} + 2H_2O + 2CO_2 \rightarrow H_4SiO_4 + 2\,\underbrace{MgCO_3}_{Magnesite} \quad (1\text{-}11)$$

Reactions (1-9), (1-10) and (1-11) illustrate, that the weathering of (Mg,Ca)-silicates is a net sink of atmospheric CO_2. Notably, for each mole olivine, two moles of CO_2 are consumed during weathering, which is why mafic and ultramafic rocks are of special interest for mineral carbonation technologies. Note, that in the current ocean Mg-carbonates do not precipitate but Mg^{2+} exchanges at the oceanic ridges for Ca^{2+}, which ultimately precipitates as carbonate minerals (Coogan and Dosso, 2012; Higgins and Schrag, 2015; Seyfried and Bischoff, 1981). As the newly precipitated carbonates get progressively buried in the oceans forming huge limestone reservoirs, the once atmospheric carbon is immobilized over geological timescales. Thus, the long term CO_2 fixation from the atmosphere is proportional to the release rate of divalent cations (notably Ca) from silicate rocks and hence, the chemical weathering rate of

silicates (Berner et al., 1983; Gislason et al., 2006; Walker et al., 1981). This is a slow process operating on time scales of millions of years (Falkowski, 2014; Kasting, 1993).

The rate of chemical weathering is a function of temperature and precipitation (Amiotte Suchet and Probst, 1993; Dessert et al., 2003; Eiriksdottir et al., 2013; Eiriksdottir, 2016; Gislason et al., 2009; White and Blum, 1995) and increases with increasing surface temperatures and precipitation rates (Berner et al., 1983). This link between air temperature, precipitation and CO_2 drawdown via chemical weathering creates a negative feedback, referred to as the internal thermostat of the Earth (Berner et al., 1983; Eiriksdottir, 2016; Gislason et al., 2006; Walker et al., 1981). At elevated atmospheric CO_2 concentration, the greenhouse effect causes air temperatures and precipitation rates to increase, which itself facilitates CO_2 drawdown through enhanced chemical weathering. As such, chemical weathering rates are proposed to change by 2-10 % for each degree air temperature change (Berner and Kothavala, 2001; Wallmann, 2001). In a long-term river-monitoring study in NE-Iceland, Gislason et al. (2009) found that for each degree of temperature increase, the chemical weathering flux increased by 4-14 % and the mechanical weathering flux by 8-30 %. Similarly, Gislason et al. (2006) reported daily dissolved and particulate Ca fluxes in a glacial river in NE-Iceland and noted that particulate fluxes vary by as much as 4.5 orders of magnitude during the year, whereas dissolved fluxes fluctuate no more than 1.5 orders of magnitude, both maximizing during spring and early summer, when temperature and rainfall are high. These studies demonstrate that the riverine particulate flux is far more sensitive to climate change compared to the dissolved flux. Based on these observations, Gislason et al. (2006) proposed that mechanical weathering and the partial dissolution of riverine particulates in the oceans provides a more powerful negative feedback on climate change via the inorganic pathway than chemical weathering on the continents (Jeandel and Oelkers, 2015).

Moreover, the transport of riverine particulates from the continents to the oceans is considered to play a crucial role in the CO_2 drawdown via the organic pathway since it comprises a huge source of nutrients and controls the burial efficiency of organic carbon (Jeandel and Oelkers, 2015). This will be discussed in more detail in the following section 1.2.2.

1.2.2 The organic carbon cycle

Terrestrial and oceanic biological processes markedly affect the global carbon cycle through the production of organic matter from an inorganic carbon source. The synthesis of organic matter from CO_2 is summarized by the term primary production, which forms the basis for all life on Earth (Falkowski, 2014). The reduction of inorganic carbon to organic matter is

an endothermic reaction and requires energy. Chemoautotrophic organisms use chemical energy whereas the far dominant group of photoautotrophic organisms uses sunlight as energy source. Collectively, chemoautotrophs and photoautotrophs are called primary producers. The major primary producers in marine ecosystems are autotrophic microorganisms floating in the sunlit surface layer of the oceans, collectively termed phytoplankton. Phytoplankton can be subdivided into several categories such as diatoms, coccolithophores, dinoflaggelates and cyanobacteria. Diatoms account for ~40 % of the total current marine primary production and for ~75 % of the primary production in upwelling systems and coastal regions (De La Rocha and Passow, 2004; Nelson et al., 1995), whereas the open ocean is currently dominated by prokaryotic picoplankton (Chisholm et al., 1988; De La Rocha and Passow, 2014; Liu et al., 1999; Steinberg et al., 2001). Notably, the two cyanobacteria Synechococcus and Prochlorococcus dominate biomass in nutrient poor low latitude oceans (Goericke and Welschmeyer, 1993; Li, 1995; Partensky et al., 1999; Rocap et al., 2002; Rohwer and Thurber, 2009; Veldhuis et al., 1997).

Virtually all organic matter is synthesized from CO_2 by oxygenic photosynthesis (Field et al., 1998). During this process, CO_2 is reduced with the use of H_2O as reductant. The splitting of water requires a high energy input, provided by the photosynthetic pigment chlorophyll-a, which efficiently harvests light energy (Falkowski, 2014). Thus, the oxygenic photosynthesis can be described in its simplest form according to:

$$CO_2 + H_2O + Light + Nutrients \xrightarrow{Chl-a} CH_2O + O_2 \qquad (1\text{-}12)$$

The total amount of biomass built by primary producers is referred to as gross primary production (GPP). A fraction of these carbon products, however, is consumed by the autotrophs for cell maintenance and cell respiration (Sigman and Hain, 2012). The resulting difference between GPP and respiration describes the net primary production (NPP), which defines the carbon available for further plant growth or consumption by heterotrophs. Due to CO_2 consumption during photosynthesis according to Reaction (1-12), NPP is a key determinant of carbon sinks and sources (Field et al., 1998). NPP is commonly presented in units of mass of carbon per area per time (g C m^{-2} yr^{-1}). Based on satellite data and ^{14}C incubation measurements, the average oceanic primary production has been estimated to be 140 g C m^{-2} yr^{-1}, with open ocean levels of ~130 g C m^{-2} yr^{-1}, coastal levels of 250 g C m^{-2} yr^{-1} and levels of 420 g C m^{-2} yr^{-1} in upwelling zones (De La Rocha and Passow, 2014; Falkowski, 2014; Field et al., 1998; Martin et al., 1987). These estimates yield a total of 45-50 Gt C fixed in the surface ocean by

phytoplankton per year, which represents roughly half of the annual primary production of 104.9 Gt C occurring on Earth (Falkowski, 2014; Field et al., 1998). Note, that the oceanic primary production is driven by a phytoplankton biomass of <1 Gt C (less than 1 % of the total photosynthetic biomass on Earth), which implies that phytoplankton biomass turns over every 2-6 days, emphasizing the fast production of organic carbon in the oceans (De La Rocha and Passow, 2014; Falkowski, 2014).

As oceanic primary production is a fundamental part of the carbon cycle, the modelling of global scale NPP has become an important discipline in Earth Sciences. Estimations of global oceanic net primary production are obtained from satellite-derived sea-surface chlorophyll concentrations. As such, the Sea-viewing Field of View Sensor (SeaWiFS) measures the variation of light absorption and creates ocean color maps in order to track the concentration of the green chlorophyll pigment. The more recently launched satellite Moderate Resolution Imaging Spectrophotometer (MODIS) creates fluorescence data and additionally allows for the determination of the physiological state of phytoplankton. Figure 1-3 shows the composite distribution of chlorophyll-a concentration in the ocean during June and December 2016 (SNPP VIIRS, OCI Algorithm) obtained from NASA OceanColorWEB (http://oceancolor.gsfc.nasa.gov/cgi/l3).

As illustrated in Figure 1-3, global oceanic chlorophyll concentrations, as indicator for the variation in primary production, vary seasonally and geographically. Seasonal variations are principally driven by variations of light availability and water mixing or shoaling effects (Siegel et al., 2002; Sigman and Hain, 2012). Seasonality is greatest at high latitudes where light availability varies extremely throughout the year. This results in higher chlorophyll concentrations during summer, as shown in the upper panel of Figure 1-3 for the northern hemisphere and the lower panel for the southern hemisphere. Furthermore, the overall pattern exhibits elevated chlorophyll concentrations at high latitudes, at the equator and along the coasts. This pattern is most of all driven by upwelling or mixing of nutrient-rich waters into the sunlit surface layer of the ocean (Boyd et al., 2014; Kessler, 2006; Pennington et al., 2006; Sigman and Hain, 2012). One such mechanism is coastal upwelling, which brings nutrient rich deep waters to the surface where it fuels primary production. Coastal upwelling is initiated through the rising sea floor which pushes cold, nutrient-rich water to the surface combined with along-shore winds that initiate Ekman transport of water masses (Kosro et al., 1991; Picado et al., 2013; Strub et al., 1987). The elevated chlorophyll concentration close to the equator results from equatorial upwelling, where nutrient-rich deep waters are transported to the surface through transverse currents (Kessler, 2006; Wyrtki, 1981).

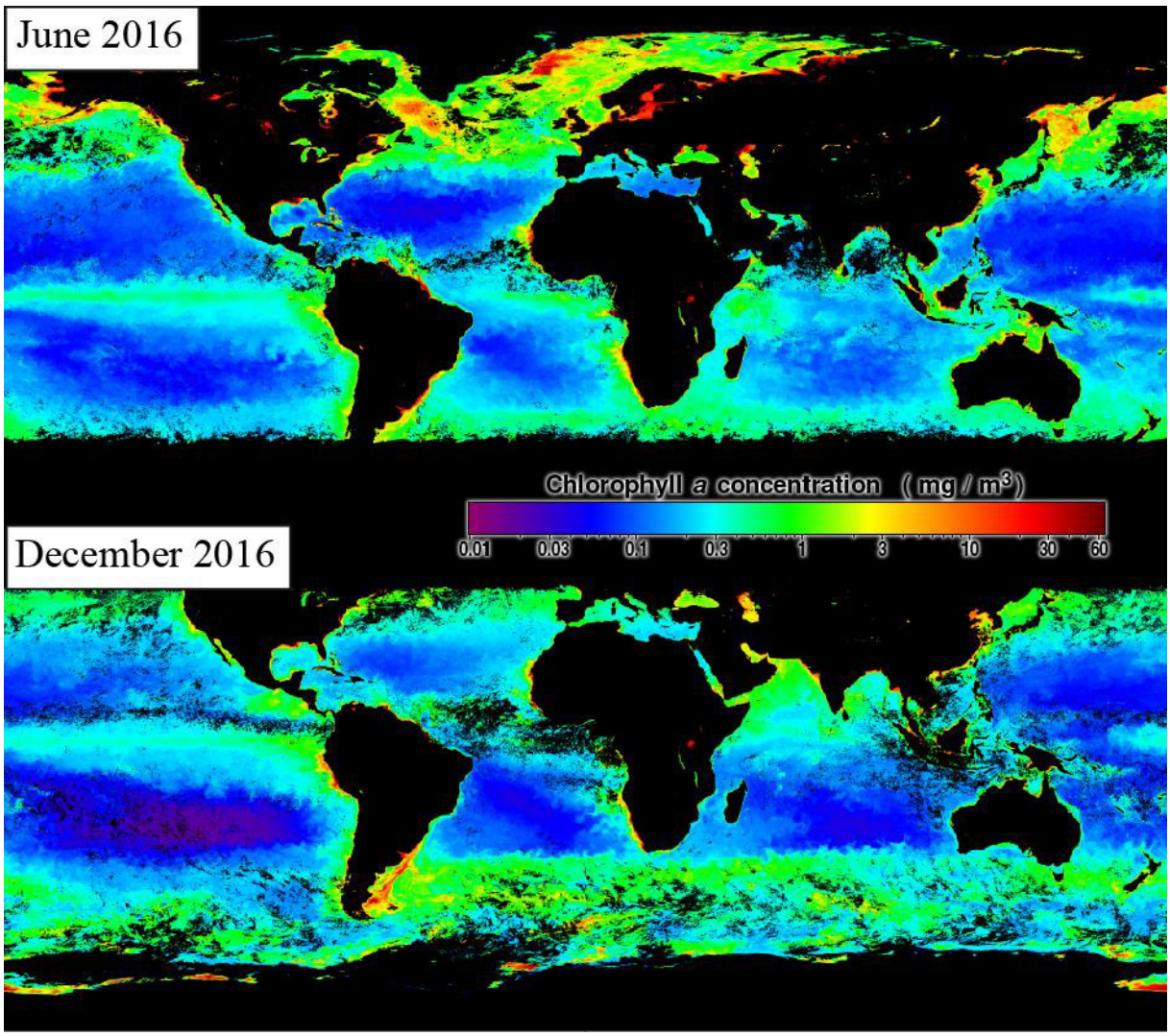

Figure 1-3. Global composite satellite-derived chlorophyll concentrations during the northern hemisphere summer (upper panel) and the southern hemisphere summer (lower panel). The data is available through NASA´s OceanColor website (http://oceancolor.gsfc.nasa.gov/cgi/l3).

The coastal ocean (water depth <200 m) is of particular importance as it covers only ~7 % of the of the surface of the global ocean but accounts for 14-30 % of the oceanic primary production (Gattuso et al., 1998). This high productivity is due to the high nutrient runoff from land and efficient nutrient recycling from bottom sediments in well-mixed shelf waters.

Large areas of the open ocean, exhibit only minor primary production even though they are rich in most major nutrients. These areas are referred to as high nitrate, low chlorophyll (HNLC) areas. Reduced productivity in these regions is due to the absence of one or more limiting nutrient, commonly iron (Boyd et al., 1998; 2004; de Baar et al., 2005; Hamme et al., 2010; Harrison et al., 2004).

The use of satellite derived chlorophyll concentration alone to deduce primary production, however, has certain restraints. Chlorophyll concentration alone correlates to gross

rather than to net primary production. For example, in high turbidity maxima of estuaries, chlorophyll concentrations are commonly high, whereas net primary production is practically zero due to light limitation (Azhikodan and Yokoyama, 2016; Cloern, 1987; Cloern et al., 2014; Domingues et al., 2011; Irigoien and Castel, 1997). Furthermore, satellite ocean color measurements do not reach the base of the euphotic zone but rather extend only to the upper tens of meters (Sigman and Hain, 2012). Nutrient depleted regions, commonly exhibit a deep chlorophyll maximum at several tens of meters depth, where the interplay between light availability and nutrient supply from depth are optimal (Sigman and Hain, 2012). To overcome these restrictions, recent models of net primary production include algorithms as the Vertically Generalized Production Model (VGPM) (Behrenfeld and Falkowski, 1997), which are based on chlorophyll concentrations but also take sea surface temperature, photosynthetically available radiation (PAR) and mixed layer depths into account (Behrenfeld and Falkowski, 1997; Falkowski et al., 1998).

1.2.2.1 What limits primary production?

As shown in Reaction (1-12), photosynthesis requires nutrients and light as energy source. Either of those may locally limit oceanic primary production. In a water body, the gradients of nutrients and light are commonly reversed. Primary production near the sunlit surface depletes surface waters in nutrients. The organically bound nutrients are transported down the water column where they eventually get oxidized to their inorganic forms (Falkowski, 2014). Thus, the pools of inorganic nutrients at depth are much higher compared to surface waters but the absence of light inhibits primary production in deep waters. Note, that the term "limiting" might refer to the total phytoplankton biomass (yield) or the rate of biomass formation (Falkowski et al., 1992; 1998). For example, light and temperature may limit the rate of primary production but as long as nutrients are consumed by the production of biomass, the vertical flux of nutrients is sustained (Falkowski et al., 1998). The limitation of the yield of photosynthesis, controlled by the least available nutrient relative to the requirement, is more relevant to biogeochemical cycles, whereas the rate is more critical to species distribution in ecosystems (Falkowski, 2014).

1.2.2.1.1 Light

Sunlight is the ultimate energy source of photosynthesizing life. Light is absorbed and scattered in the ocean so that little penetrates deeper than 150 m (Sigman and Hain, 2012). The depth in the water column at which the photosynthetic available radiation (PAR) is reduced to 1 % of its surface intensity is defined as the euphotic zone depth. The average euphotic zone

depth of the world ocean is ~54 m (Falkowski, 2014) but it reaches >150 m in low productive subpolar latitudes (Sigman and Hain, 2012) and is restricted to <1 m in estuarine systems with high particulate loads (Azhikodan and Yokoyama, 2016). Besides incident solar radiation, the euphotic zone depth is a function of suspended matter concentration which determines light attenuation. Light attenuation in turbid estuaries is commonly dominated by suspended sediments (Cloern, 1987; May et al., 2003; Wofsy, 1983), whereas phytoplankton concentration itself restricts the euphotic zone depth in the open ocean (Lee et al., 2007). Sunlight furthermore heats the surface water creating a buoyant layer floating on the denser deep ocean (Sigman and Hain, 2012). This buoyant, well mixed surface layer (referred to as "mixed layer") is crucial for phytoplankton growth since deep mixing would otherwise carry phytoplankton out of the sunlit zone. The interplay between mixed layer depth, euphotic zone depth and nutrient availability is principally determining primary production.

1.2.2.1.2 Nutrients

Phytoplankton requires a suite of nutrients to build organic cells and maintain its metabolism. A lack of nutrients can limit primary production as originally defined by "Liebig´s law of the Minimum" which describes the limitation for biomass synthesis by the substance that is least available relative to its requirements (Falkowski et al., 1992). The nutrients required in the highest quantities (primary macronutrients) are C, N and P which define the mean elemental ratio of marine organic matter as 106C/16N/1P, known as the Redfield ratio (Redfield, 1958). Further macronutrients are K and Si, whereas Si is only a nutrient for specific plankton like diatoms, which use Si for their hard parts (Sigman and Hain, 2012). Calcium, Mg and S are commonly found in large quantities and are therefore termed as secondary macronutrients, which are usually not limiting primary production (Eiriksdottir, 2016). The group of micronutrients comprises bio-essential trace metals like Fe, Mn, Zn, Ni, Cu, Se, Mo, V and B, which are constituents of structural materials, enzymes or pigments or are present within cells for osmoregulation or charge balance (De La Rocha and Passow, 2014).

It is generally assumed that the availability of either P or N limits global oceanic primary production (Broecker, 1982; Falkowski, 1997; Redfield, 1958). The oceanic phosphorous budget is largely controlled by geological processes and has no significant new biological or atmospheric source (Falkowski et al., 1998; Sigman and Hain, 2012). Nitrogen, on the other hand, is abundant in the atmosphere and its oceanic budget is largely biologically controlled since atmospheric N_2 can be reduced to bioavailable ammonia by diazotrophs (N_2-fixing phytoplankton) such as the cyanobacteria *Trichodesmium* (Capone et al., 2005; Capone and

Carpenter, 1982; Kranz et al., 2010; Mulholland et al., 2006). Since the rate of supply of P is much lower than that of N, the former has a significantly longer residence time (1-5×10^4 years for P and ~1×10^3 years for N; Filippelli and Delaney (1996) and Brandes and Devol (2002)). This longer residence time of P compared to N implies that the source of P limits its availability for consumers (Falkowski et al., 1998). Thus, it has been argued that rather P than N limits primary production over geological times (Broecker, 1982; Mills et al., 2004; Redfield, 1958; Trommer et al., 2013). However, oceanographers have demonstrated through nutrient enrichment experiments and nutrient distribution patterns, that phytoplankton productivity is often limited by the availability of inorganic nitrogen (Barber and Chavez, 1991; Dugdale, 1967; Eppley et al., 1979; Falkowski et al., 1998). Furthermore, a number of studies proposed that reduced denitrification during ice ages increased the oceanic N reservoir which led to higher primary productivity and the reduction of atmospheric CO_2 during ice ages (Altabet et al., 1995; Christensen, 1994; Ganeshram et al., 1995). De La Rocha and Passow (2014) summarized that nitrogen input to the surface ocean limits primary production over short timescales, whereas the phosphorous input limits global ocean primary production over timescales exceeding the residence time of phosphorus (>1-5×10^4 years).

Note also, that in large areas of the open ocean, the major nutrients N and P are never entirely consumed and other micronutrients are critical to limiting primary production through their role during metabolism. Numerous studies have demonstrated that Fe is the missing nutrient in these HNLC regions (Boyd et al., 1998; 2004; de Baar et al., 2005; De La Rocha and Passow, 2014; Hamme et al., 2010; Harrison et al., 2004). Iron deficiency is estimated to limit oceanic primary production and carbon export in as much as 40 % of the world´s oceans (Elrod et al., 2004; Martin, 1990; Moore et al., 2001). Furthermore, low levels of silicic acid in surface waters have been shown to limit the growth of diatoms, one of the most abundant type of phytoplankton (De La Rocha and Passow, 2014; Egge and Aksnes, 1992; Nelson and Dortch, 1996; Rzezinski and Nelson, 1996). As such, the supply of silicate has been linked to changes in ocean primary production from glacial to interglacial periods (Archer et al., 2000; Jeandel and Oelkers, 2015; Opfergelt et al., 2013).

Thus, the supply of the nutrients P, N, Si and Fe to the euphotic zone is considered to set the upper limit of primary production in most parts of the ocean. Which nutrient or nutrients effectively limit production may vary regionally and seasonally and furthermore differs for different types of phytoplankton. The next subsection will briefly describe the major nutrient fluxes to the surface ocean.

1.2.2.2 Nutrient fluxes to the euphotic zone

There are two major sources of nutrients to the euphotic zone: The local recycling of nutrients through microbial degradation and the influx of new nutrients from the deep ocean, the atmosphere or from terrestrial runoff (Falkowski, 2014). Whereas in the open ocean, upwelling of nutrient rich deep ocean water and atmospheric input may dominate nutrient fluxes and thus primary production, the coastal zone nutrient supply in dominated by continental inputs. Even though the Coastal zone (<200 m water depth) covers only approximately 7 % of the total surface area of the ocean, it accounts for 15-30 % of oceanic primary production (Frankignoulle and Borges, 2001; Gattuso et al., 1998). It plays a considerable role in global biogeochemical cycles because it receives vast terrestrial inputs of organic matter and nutrients which are exchanged in large amounts with the open ocean (Gattuso et al., 1998). The importance of coastal zones in the global carbon cycle stems not only from its high rates of primary production but notably from its predominant role in organic matter burial. This will be discussed in more detail in subsection 1.2.2.3 on page 20.

1.2.2.2.1 Terrestrial derived nutrient fluxes

The continental flux of new nutrients to the oceans is controlled by river runoff (Eiriksdottir et al., 2015; Eiriksdottir, 2016), Aeolian dust (Jickells et al., 2005) and volcanic ash (Jones and Gislason, 2008; Lindenthal et al., 2013; Olgun et al., 2011). Jickells et al. (2005) estimated the Aeolian dust flux to the oceans to be 0.4-2 Gt year^{-1} and a large number of studies has focused on quantifying its potential to fertilize the oceans and its effect on global primary production and elemental cycles (Jickells et al., 2005; Maher et al., 2010; Mahowald et al., 2005). The global dissolved riverine flux is approximately 1 Gt year^{-1} (Gaillardet et al., 1999; 2003; Viers et al., 2009) and the riverine supply of dissolved elements to the ocean has been the focus of numerous scientific studies (Dessert et al., 2003; Gaillardet et al., 1999). The global flux of riverine particulate material to the ocean is estimated to be 16.6 – 30 Gt year^{-1}, of which 15-20 Gt are transported as suspended load and 1.6-10 Gt as bedload (Jeandel and Oelkers, 2015; Meybeck et al., 2003; Syvitski et al., 2003; Walling, 2006). Thus, the global particulate flux exceeds the dissolved flux by a factor of 16.6-30 and the aeolian dust flux by a factor of 8-75. This implies that the overwhelming majority of continental weathering products arrive the oceans in the form of river-transported particulate material, as illustrated in Figure 1-4. The elemental ratio of the riverine particulate flux over dissolved flux is a function of the solubility of the elements. As such, the dissolved flux exceeds the corresponding particulate flux only for the most soluble elements like Na, whereas the particulate flux of insoluble elements including rare earth elements, Al or Fe comprises >99 % of the total riverine flux (Oelkers et al., 2011;

2012). This implies that the dissolution of only 5 % of riverine particulates arriving the oceans would be enough to dominate the chemical evolution of seawater and the feedback between continental weathering and climate (Gislason et al., 2006; Oelkers et al., 2012). A growing interest in suspended sediment fluxes has also arisen from their role in contaminant transport, reservoir sedimentation, soil erosion and loss, harbor and channel silting or water quality trends (Horowitz, 2008). Water quality regulations in many countries are solely based on dissolved constituents, as they are presumed to be bioavailable (Horowitz, 2008), whereas the bioavailability of the elements in the sediment-associated counterparts has yet to be assessed.

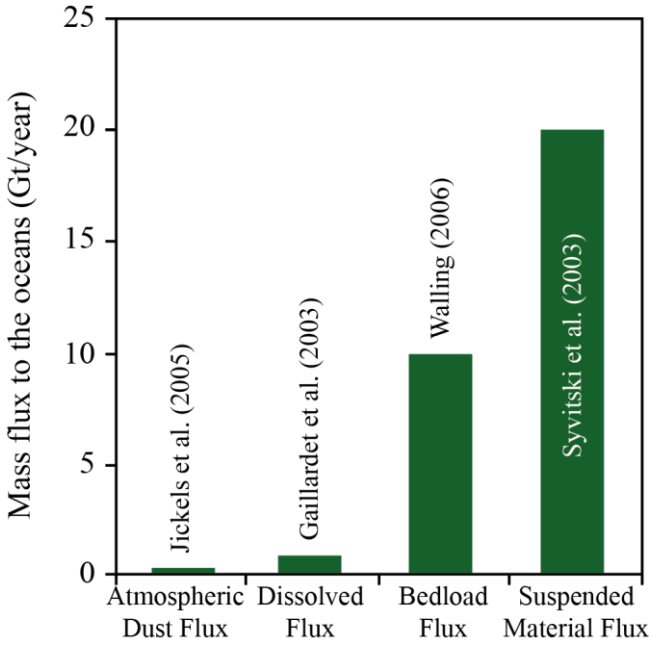

Figure 1-4. Estimates of the total mass of material transported annually from the continents to the oceans by selected processes (modified after Oelkers et al. (2012)).

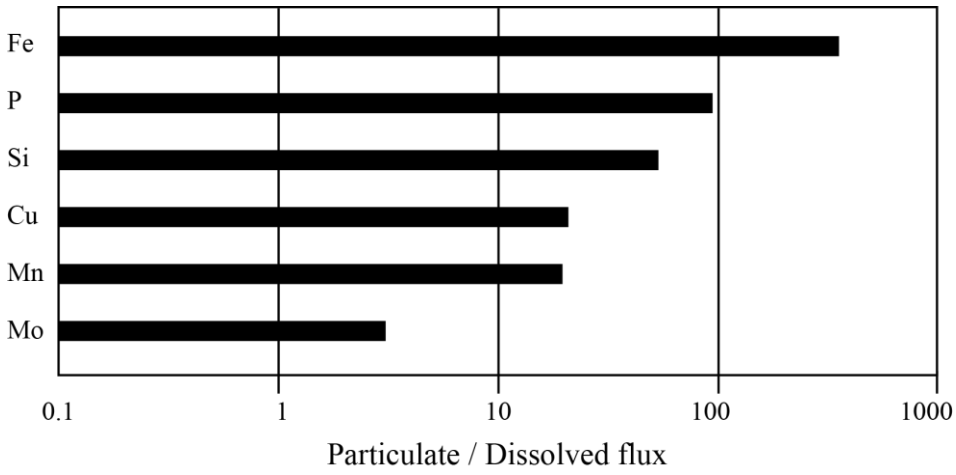

Figure 1-5. The ratio of global riverine particulate flux to the corresponding dissolved flux for selected nutrients. Figure modified after Oelkers et al. (2011).

Figure 1-5 shows the ratio of the riverine particulate flux over the dissolved flux for a selection of vital nutrients. As such, for nutrients potentially limiting primary production like Si, P and Fe, the particulate flux exceeds the corresponding dissolved flux by factors of 50, 100 and 350. This implies that vast amounts of essential nutrients are stored and transported in riverine particulates, which could considerably effect oceanic productivity and global elemental cycles (Jeandel and Oelkers, 2015).

Riverine particulates reaching the oceans have been largely ignored by the scientific community as potential source of nutrients for primary production (Jeandel et al., 2011; Jeandel and Oelkers, 2015). This is presumably due to the saturation or supersaturation of seawater with respect to most of the mineral phases entering the oceans in particulate form (Jeandel and Oelkers, 2015; Oelkers et al., 2011). As such, these minerals are thought to have a minor significance on the ocean budgets of most of the elements due to negligible dissolution or the rapid precipitation of secondary phases (Jeandel and Oelkers, 2015; Oelkers et al., 2011). Jeandel and Oelkers (2015) however summarized the fate of riverine particulate material upon its arrival to the ocean and elucidate that particulates may well significantly influence the oceanic budgets of certain elements like Sr, Nd, rare earth elements, Si, Mg and Fe. As such, suspended sediments likely act as nutrient buffer, slowly releasing nutrients via mineral dissolution, constantly replenishing the dissolved nutrient pool, once consumed by primary production.

Silica, for example, is considered as one of the limiting nutrients in coastal oceans, where diatoms are the dominant phytoplankton species. During phytoplankton blooms, diatoms consume all dissolved Si to form their silica hard shells (Egge and Aksnes, 1992; Eiriksdottir, 2016; Nelson and Dortch, 1996; Rzezinski and Nelson, 1996). Jeandel and Oelkers (2015) characterize two examples, the Mediterranean Sea and the Kerguelen Plateau, where Si mass balance calculations require a previously undefined external silica source to balance the Si budget and they conclude that riverine particulate dissolution upon arrival to the ocean margins may be the missing external Si source. This hypothesis is supported by Kress et al. (2014) who concluded that internal weathering of alumosilicates is the key to balancing Eastern Mediterranean Si budget and by experimental studies from Jones et al. (2012) and Pearce et al. (2013) who quantified Si release rates of riverine particulate material in seawater.

The supply of iron to the ocean from terrestrial particulate material has received notable attention due to its influence on primary production and the dissolution of Fe in continental shelf sediments has been attributed as major source of Fe to the oceans. John et al. (2012)

suggested that the reductive dissolution (suboxic dissolution triggered by the decomposition of organic matter in sediments) of particulate material from the continental margins accounts for 4-12 % of the global oceanic dissolved Fe budget. Moreover, Elrod et al. (2004) reported that the Fe input from shelf sediments is at least as significant as the global input from aerosols, which is considered to be the major external Fe source to the oceans. Elrod et al. (2004) furthermore reported, that the influence of near-shore Fe-input is observed at least 600 km offshore. Similarly, Radic et al. (2011), Slemons et al. (2012) and Homoky et al. (2012) proposed the non-reductive dissolution of continental margin sediments as a major input of dissolved Fe to the oceans and stated that this Fe may be transported hundreds of kilometers to Fe-depleted surface ocean settings. Notably, Homoky et al. (2012) reported that suspended particles are not only a significant buffer of dissolved Fe in shelf sediments but also an important Fe-transport mechanism and they concluded that suspended particulate material regulates the dissolved Fe concentration in the ocean.

Thus, the potential role of terrestrial particulates on delivering essential nutrients nourishing oceanic primary production has been demonstrated in several studies. These studies commonly discuss the delivery of nutrients through particulate dissolution. Note, however, that primary producers may access vital nutrients "directly" from the sediment so that the intermediate step of particle dissolution is eventually not resolvable. Phytoplankton is known to have developed powerful strategies to gain access to vital nutrients, some of these will be discussed in more detail in subsection 1.3 on page 23.

1.2.2.3 Organic carbon burial

The photosynthetically driven synthesis of biomass from dissolved inorganic carbon lowers the partial pressure of CO_2 in the upper ocean which promotes the absorption of atmospheric carbon, thus reducing atmospheric CO_2 levels (De La Rocha and Passow, 2014; Falkowski et al., 2000). To effectively remove CO_2 from the atmosphere, this organic carbon needs to be buried into the anoxic zone before decomposition, since decomposition will reverse Reaction (1-12) and ultimately release CO_2 back into the atmosphere (Falkowski, 1997). The transport of organic matter from the surface to the oceans interior is referred to as the biological carbon pump which dominates the distribution of carbon, nutrients and oxygen in the ocean (De La Rocha and Passow, 2014; Ridgwell, 2011). The biological pump consists of the production of organic matter and biominerals in the surface ocean, the settling of these particles and the decomposition or sedimentation in the deep ocean. While most of the biomass formed will be recycled in the upper few hundred meters of the oceans, some portion will be transported to the

deep layers where it may escape mineralization and remain in the sedimentary reservoir (De La Rocha and Passow, 2014). The international Panel of Climate change (IPCC 2007) has declared that the long-term carbon sequestration requires the removal of carbon from the atmosphere for >100 years. In the open ocean this criterion is met when organic carbon settled below 1000 m in the water column (Passow and Carlson, 2012; Primeau, 2005).

Of the 45-50 Gt C fixed into biomass through oceanic primary production each year (Falkowski et al., 1998; Field et al., 1998; Longhurst et al., 1995), roughly 11-16 Gt C are transported to the deep ocean (De La Rocha and Passow, 2014; Falkowski et al., 2000). Falkowski et al. (2000) reported that this vertical carbon flux keeps the atmospheric CO_2 level 150-200 ppm lower than it would be in the absence of oceanic phytoplankton. Of the 11-16 Gt C transported to the deep ocean, only about 0.16 Gt C are actually preserved in ocean sediments (De La Rocha and Passow, 2014; Hedges and Keil, 1995). This organic carbon burial and preservation in the ocean exhibits a pronounced special variation. Hedges and Keil (1995) reported that > 90 % of the total organic carbon preserved in the oceans is buried on continental shelves and slopes. Factors controlling burial in the open ocean and the coastal zone are discussed in more detail in the following subsections.

1.2.2.3.1 Burial in the open ocean

The burial efficiency of organic matter in the open ocean is closely related to the formation of aggregates and their capability of rapid sedimentation (Alldredge et al., 1995; Jackson and Lochmann, 1992). These larger particles are collectively known as “marine snow”. Marine snow is either formed biologically as fecal pellets or physically through coagulation of smaller particles (De La Rocha and Passow, 2014; McCave, 1984), whereby the physical aggregation accounts for the bulk of marine snow formation (De La Rocha and Passow, 2014; Hill, 1992; Smetacek, 1985; Turner, 2002). Particle coagulation requires the collision of particles and the subsequent attachment. The particle collision, mainly through shear, scales with the square of the particle concentration (Hill, 1992; Jackson, 1990; Smetacek, 1985) and high particle concentration combined with abundant non-phytoplankton background particles are necessary to match observed aggregation and sedimentation rates in the ocean (Alldredge et al., 1995; Hill, 1992). The stickiness of particles is controlled by their physical and chemical surface properties (Alldredge and Jackson, 1995; De La Rocha and Passow, 2014; Jackson and Burd, 1998). Analyses of sediment traps indicate that diatoms frequently dominate large sedimentation events due to their capability to form large, fast-sinking aggregates (Alldredge et al., 1995; Goldman, 1993; Passow and Carlson, 2012; Seebah et al., 2014).

Furthermore, mineral particles have been found to promote particle coagulation: First, their presence increases the absolute particle concentration, thus increasing collision frequency. Second, mineral fragments may increase adhesion due to electrostatic forces or hydrogen bonds (Avnimelech et al., 1982; Beaulieu et al., 2005; Ding and Henrichs, 2002; Passow et al., 2014; Verspagen et al., 2006). As such, clay particles have been successfully used to remove harmful algae blooms from the water column through the formation and settling of clay/algal flocs (Avnimelech et al., 1982; Beaulieu et al., 2005; Verspagen et al., 2006). The scavenging of high density mineral fragments into marine snow might furthermore increase their settling velocity, thus increasing the burial efficiency (De La Rocha and Passow, 2007; Ploug et al., 2008a; 2008b). This process, known as the "ballast effect", was described to match the observed correlation between particulate organic carbon and mineral fluxes in the deep ocean (Armstrong et al., 2001; Francois et al., 2002; Klaas and Archer, 2002; Le Moigne et al., 2014). As such, Le Moigne et al. (2014) reported, that 60 % of the particulate organic carbon flux in the high-latitude North Atlantic is associated with ballast minerals. Fragments of minerals were moreover described to drive organic carbon fluxes by physically protecting the organic carbon from degradation (Gehlen et al., 2006; Le Moigne et al., 2014; Yool et al., 2013).

Note also, that exopolymeric substances, notably transparent exopolymeric particles (TEPs), have recently received great attention due to their role in the transport of carbon to the deep ocean (Alldredge et al., 1993; De La Rocha and Passow, 2014; Passow et al., 2001; Passow, 2002). As such, Logan et al. (1995) reported that the formation of fast sinking aggregates is controlled by TEP abundance which greatly increases the probability of particle sticking. Moreover, TEPs contain C and N in proportions exceeding the Redfield ratio, thus, providing a powerful mechanism of pumping organic carbon to the deep ocean (De La Rocha and Passow, 2014; Engel et al., 2002; Engel and Passow, 2001; Mari et al., 2001).

1.2.2.3.2 Organic carbon burial in the coastal zone

As mentioned above, the overwhelming majority of organic carbon burial in the ocean occurs in coastal regions and several studies elucidate the role of particulate material in the process of organic carbon accumulation and preservation (France-Lanord and Derry, 1997; Galy et al., 2007; Ingall and van Cappellen, 1990; Jeandel and Oelkers, 2015). As such, high riverine sediment supply to the coast increases the sediment accumulation rate, thus reducing sediment exposure time to oxygen and consequently organic matter decomposition (Jeandel and Oelkers, 2015). Furthermore, organic matter has been shown to be bound to mineral surfaces (Lalonde et al., 2012) and several studies reported a direct proportionality between

organic matter concentration and sediment specific surface area (Mayer, 1994). As a result, the long term preservation of organic carbon is suggested to be controlled by the sorption of organic matter onto mineral surfaces and thus, by the delivery of particulate surface area to the ocean (Berner, 1989; Hedges and Keil, 1995; Jeandel and Oelkers, 2015; Keil and Hedges, 1993; Kennedy et al., 2002; Mayer, 1994; Salmon et al., 2000).

This link between continental particle supply and organic carbon burial in the oceans is perhaps strongest during the end of glacial cycles where glacial processes produce vast amounts of fine-grained particles (Alley et al., 1997; Galeczka et al., 2014; Stefánsdóttir and Gíslason, 2005). As such, Jeandel and Oelkers (2015) proposed that this intense particulate supply and the contaminant high rate of organic carbon burial may significantly draw down atmospheric CO_2 and thus moderate global warming at the end of glacial times. An intensification of CO_2 drawdown via the organic carbon cycle towards the end of glaciations is furthermore facilitated through the input of huge amounts of nutrients, notably by icebergs, which may carry nutrients to remote regions of the ocean (Broecker, 1994; Hawkings et al., 2017; Hemming, 2004; Raiswell et al., 2016). Increased organic carbon burial during glaciations was also reported from Cartapanis et al. (2016) and Lyle (1988) and has been attributed to increased primary productivity by Sarnthein et al. (1988) and Pedersen (1983).

In summary, there exists extensive evidence that the supply of riverine particulates to the ocean facilitates organic matter burial and preservation, either through its effect on particle agglomeration and settling velocity, or, more evidently, through the delivery of mineral surface area to the coastal ocean, which is readily adsorbed by organic matter. The observed correlation between organic carbon and mineral surface combined with the vast source of essential nutrients present in suspended minerals furthermore suggests a deliberate mineral-microbe interaction, with microbes acquiring vital nutrients directly from the mineral.

1.3 Mineral microbe interactions

Any physical attachment of organic matter on particulate material could increase burial efficiency of organic carbon. The direct attachment of microbes or any organic substance onto mineral surfaces might be of physio-chemical origin caused by electrostatic forces or by the stickiness of organic ligands or exopolymeric substances. Microbes, however, have been shown to have developed sophisticated strategies to gain access to vital nutrients from inorganic sources and direct or indirect interactions between minerals and microbes are omnipresent in natural systems (Dong, 2010; Mapelli et al., 2012; Rogers and Bennett, 2004; Sudek et al., 2017; Uroz et al., 2009). The potential of primary producers to access nutrients directly from

particulate material significantly strengthens the importance of riverine particulates in the global carbon cycle since these particulates represent a vast source of potentially limiting nutrients.

The capability of microbes to acquire nutrients directly from a mineral source has been demonstrated in several experimental and field studies. For example, Bailey et al. (2009), revealed in an experimental study that microbes can obtain required nutrients and energy directly from basaltic glass in nutrient-deplete environments. They reported enhanced microbial growth on basaltic glasses compared to a reference borosilicate glass and concluded that nutrients present within the basaltic silicate matrix drive metabolic activity. Similar experimental and field studies were conducted by Stevens and McKinley (1995), Rogers et al. (1998), Rogers and Bennett (2004), Perez et al. (2016) and Sudek et al. (2017) who all reported enhanced microbial growth in the presence of nutrient bearing mineral substrates compared to nutrient free substrates. Notably, Sudek et al. (2017) reported that the physical contact between microbes and the substrate is critical in this process. Furthermore, Rogers and Bennett (2004) concluded that microorganisms extract inorganic P directly from rocks while destroying the silicate surface, thereby facilitating mineral dissolution. This is in agreement with work by Edwards et al. (2004) who observed a vivid microbial activity in seafloor basalts and a 6-8 fold increase in basalt dissolution rates in the presence of microbes compared to abiotic systems.

The potential role of microbial activity during mineral dissolution has been demonstrated in numerous experimental studies (Bennett et al., 2001; Drever and Stillings, 1997; Olsson-Francis et al., 2012; Perez et al., 2016; Rogers and Bennett, 2004; Stockmann et al., 2012; Uroz et al., 2009; Wu et al., 2007; 2008). Microorganisms may accelerate mineral dissolution either through 1) altering pH or 2) through the excretion of organic ligands which complex metals in solution, form Si-destabilizing surface complexes or change mineral saturation states in the vicinity of the surface (Edwards et al., 2004; Rogers and Bennett, 2004). Notably, Rogers and Bennett (2004) reported that microorganisms significantly alter Si-solubility by perturbing mineral-water equilibria in their microenvironment particularly when directly attached to mineral surfaces. Figure 1-6 A shows a schematic sketch illustrating the potential positive feedback between bacterial growth in mineral proximity and mineral dissolution.

It is still a matter of discussion whether this interaction is the deliberate strategy of microorganisms to obtain vital nutrients directly from the mineral source, or simply the coincidental side effect of microbial metabolism (Bennett et al., 2001). However, several

evident mechanisms indicate that primary producers developed these strategies to their advantage. For example, bacteria and blue-green algae excrete siderophores, complexing agents with a high affinity and specificity for ferric iron. These siderophores can solubilize hydrous Fe-oxide, which is afterwards recognized by receptor sites on the cell surface and transported across the cell membrane (Anderson and Morel, 1982). Similarly, chelators have been shown to stimulate phytoplankton growth in nature and in cultures, through depression of toxic metal activities or through solubilizing hydrous Fe-oxide (Anderson and Morel, 1982). Furthermore, iron oxides have been observed to be adsorbed onto diatom frustules and are thought to be made bioavailable through "biochemical reactions" at the cell surface (Anderson and Morel, 1982). One such mechanism to acquire this iron source might simply be the alteration of pH in the cell microenvironment during metabolism. Depending on the carbon uptake mechanism of the primary producer, the pH in the cell microenvironment may increase or decrease, which then influences the solubility of inorganic nutrient-bearing sources in the cell vicinity (Milligan et al., 2009; Wolf-Gladrow and Riebesell, 1997). As such, Milligan et al. (2009) and Shaked et al. (2005) proposed that acidification in the cell environment increases the availability of iron through enhanced dissolution of Fe-oxides.

In addition to the effect of microorganisms on mineral dissolution, their effect on mineral precipitation has been shown in several experimental and natural studies (Dittrich et al., 2003; Dittrich and Sibler, 2010; Hodell et al., 1998; Lee et al., 2006; Stabel, 1986; Thompson et al., 1997; Zhu and Dittrich, 2016). Notably, cyanobacteria have been shown to catalyze calcium carbonate precipitation through the creation of a highly alkaline environment around the cell. The link between photosynthesis and alkalinity stems from molecular CO_2 reduction. Molecular CO_2 is reduced to organic compounds by Ribulose-1,5 biphosphat carboxylase/Oxygenase (RuBisCO) and is the ultimate carbon species used for carbon fixation (Cooper et al., 1969; Wolf-Gladrow and Riebesell, 1997). For aquatic cyanobacteria and algae, however, molecular CO_2 might be poorly available. To overcome potential CO_2 limitations, a wide range of microorganisms have developed a mechanism to use HCO_3^- via the carbon concentration mechanism (Kamennaya et al., 2012; Wolf-Gladrow and Riebesell, 1997). During this carbon concentration mechanism, HCO_3^- is transported into the cell where it is converted to OH^- and CO_2 by the enzyme carbonic anhydrase (Dupraz et al., 2009; Jansson and Northen, 2010; Kamennaya et al., 2012). CO_2 is then fixed during cell construction, whereas OH^- is released from the cell surface creating a highly alkaline microenvironment. This process is illustrated schematically in Figure 1-6 B. The alkalinization, combined with an accumulation of Ca^{2+} at the cell surface attracted by negatively charged functional groups or EPS (Bundeleva

et al., 2014; Dupraz et al., 2009; Kamennaya et al., 2012; Zhu and Dittrich, 2016) may locally provoke calcium carbonate supersaturation and ultimately carbonate precipitation. Notably, cyanobacteria have been shown to trigger "whiting events", the sudden precipitation of calcium carbonates in aqueous environments (Swart et al., 2014; Thompson et al., 1997). As such, cyanobacteria have received increased attention due to their potential use in CO_2 sequestration technologies (Jansson and Northen, 2010; Kamennaya et al., 2012; Kumar et al., 2011; Martinez et al., 2016; Zhu and Dittrich, 2016).

This summary of mineral microbe interactions demonstrates that the interplay between organic and the inorganic processes is fundamental to quantify the carbon cycles. As such, the inorganic and organic carbon cycles, as illustrated in Figure 1-1 and represented by Equations (1-1) and (1-2), are closely related to each other. Biota is ubiquitous and closely involved in apparently inorganic mineral dissolution or precipitation process and reversely, inorganic minerals are fundamental for the biotic world since they build the basis of the food-chain as supplier of nutrients for primary production.

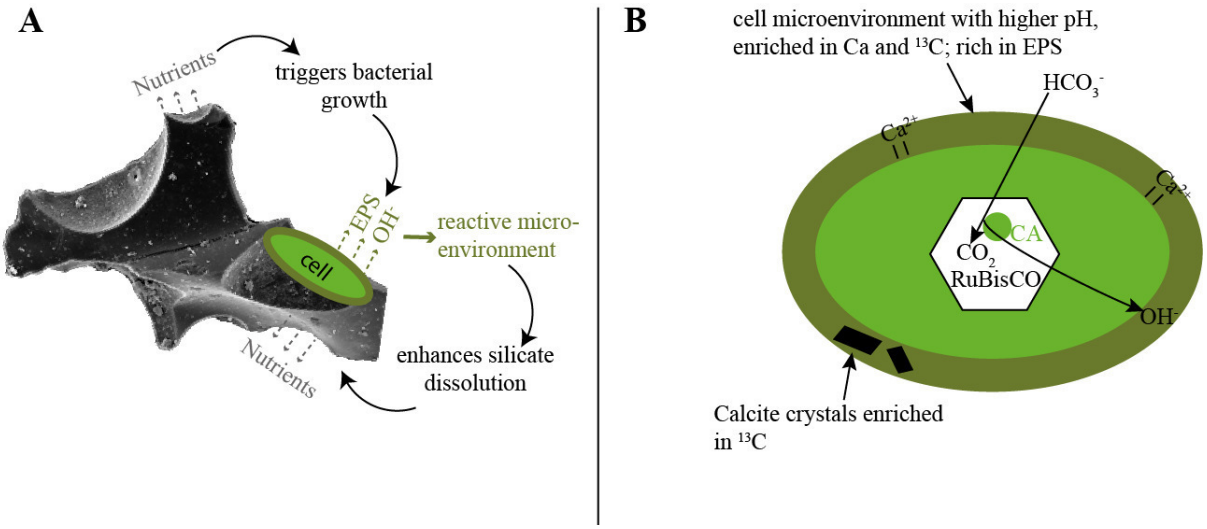

Figure 1-6. Schematic sketch of possible mineral microbe interactions. **A:** Bacterial growth in close proximity to mineral surfaces might facilitate mineral dissolution (see text) which itself might increase to availability of nutrients, thus facilitating bacterial growth and creating a positive feedback. **B:** Simplified model of the CO_2-concentration mechanism (CCM) and resulting calcite precipitation in the cell microenvironment. CA refers to the enzyme carboxyl anhydrase. Modified from Kamennaya et al. (2012) and Thompson et al. (1997).

1.4 The use of carbon isotopes as environmental proxy

The global impact of photosynthesis and organic carbon burial on the atmospheric CO_2 concentration and its connection to the rise of atmospheric oxygen has been discussed in detail in the scientific literature (Broecker, 1970; Schrag et al., 2013). The reconstruction of the global carbon cycle over geological timescales was enabled by the observation of carbon isotopic

fractionation during photosynthesis, first described by Urey (1948). The carbon isotopic composition of a substance is commonly presented in the delta notation given by:

$$\delta^{13}\mathrm{C} = 1000 \cdot \left(\frac{^{13/12}\mathrm{C}_{sample}}{^{13/12}\mathrm{C}_{V-PDB}} - 1 \right) [‰], \quad (1\text{-}13)$$

where $^{13/12}\mathrm{C}_{sample}$ and $^{13/12}\mathrm{C}_{V-PDB}$ refer to the isotopic ratios of the sample of interest and the V-PDB international standard and $\delta^{13}\mathrm{C}$ designates the normalized ratio of the sample of interest presented in per mil.

During the formation of organic material through photosynthesis, the light carbon isotope $^{12}\mathrm{C}$ is preferentially incorporated into biomass, thereby enriching the co-exiting aqueous phase in heavier $^{13}\mathrm{C}$ (Craig, 1953; O'Leary, 1988). The extent to which organic matter is depleted in $^{13}\mathrm{C}$ is controlled by the plant photosynthesis (C3, C4 or CAM, for further details see e.g. O'Leary (1988)). Most photosynthetic terrestrial plants have a $\delta^{13}\mathrm{C}$ value between -25 and -30 ‰. In marine vascular plants, $\delta^{13}\mathrm{C}$ varies between -8 and -12 ‰ (Deines, 1980; Swart, 2015), whereas marine algae exhibit a more negative $\delta^{13}\mathrm{C}$ value between -20 and -24 ‰ (Degens et al., 1968; Swart, 2015). The carbon isotopic signature of all organic matter averages at roughly -25 ‰ (Schrag et al., 2013). Dissolved inorganic carbon in seawater and in calcium carbonate have similar carbon isotopic signatures of ~0 ‰ (Schrag et al., 2013). Thus, organic carbon contains on average 2.5 % less $^{13}\mathrm{C}$ relative to carbonate carbon (Broecker, 1970; Craig, 1953). A prominent example for the difference in carbon isotopic signatures between inorganic and organic sources is the recent decrease in $\delta^{13}\mathrm{C}$ in the atmosphere, resulting from the injection of isotopically light carbon from fossil fuel combustion (Keeling et al., 2010).

Changes in the isotopic composition in marine carbonates have been interpreted as changes in the fractional burial of carbonate carbon relative to organic carbon (Schrag et al., 2013). During times of enhanced organic matter burial and preservation, $\delta^{13}\mathrm{C}$ of dissolved inorganic carbon and precipitating carbonates was elevated because heavily depleted organic carbon was removed from the system. Conversely, during times of reduced organic matter burial or enhanced oxidation, $\delta^{13}\mathrm{C}$ values of dissolved inorganic carbon and carbonates decreased because few $^{12}\mathrm{C}$ was stored in biomass (Swart, 2008, 2015). This is manifested in the Earths' marine carbonate records, notably as carbon excursions, during which carbon isotopic signatures differ several ‰ compared to background levels. For example, during Early Carboniferous, a time when abundant coal deposits were formed, the $\delta^{13}\mathrm{C}$ values increased by 3-4 ‰ (Saltzman et al., 2004; Swart, 2015; Tipple et al., 2010; Veizer et al., 1999).

Variations in carbon isotopic signatures in marine carbonates have thus been used to reconstruct environmental conditions present over geological time, to provide insight into past carbon cycling or to trace the link between primary productivity and the rise of atmospheric oxygen (Assayag et al., 2008; Bartley and Kah, 2004; Botz et al., 1996; Broecker, 1970; Hayes et al., 1999; Schrag et al., 2013; Whiticar, 1999).

The use of carbon isotopic signatures to reconstruct past environmental conditions, however, requires that these signatures are preserved over vast timescales. A part of this thesis aims to assess the rates of carbon isotope signature alteration in calcite due to bacterial-induced changes in the carbon isotope composition of a co-existing fluid phase. Towards this goal, we conducted calcite precipitation experiments in the presence of cyanobacteria and monitored the temporal $\delta^{13}C$ isotope evolution of the fluid and solid phases. These observations were used to evaluate the rate and degree to which stable carbon isotope compositions are altered in calcite.

2 Materials and methods

Microcosm growth experiments in this thesis were designed to determine 1) the effect of riverine particulate material on the growht of cyanobacteria and diatoms (Chapters 3 and 4) or 2) the effect of the presence of cyanobacteria on the carbon isotope signatures of calcite (Chapter 5). In this chapter, we describe the material and methods used during these studies as well as the corresponding experimental design of these experiments.

2.1 Primary producers

2.1.1 Cyanobacteria – *Synechococcus*

Cyanobacteria are prokaryotic microorganisms in the domain of bacteria. The term prokaryotic implies that cyanobacteria lack a nucleus and organelles, the characteristics of eukaryotes. However, cyanobacteria contain the green pigment chlorophyll-a and are thus the only prokaryotes capable of oxygenic photosynthesis (Falkowski and Knoll, 2007; Hamilton et al., 2016). Cyanobacteria are the oldest known organisms with a fossil evidence recorded in stromatolites tracing back to ~3.5 Ga (Schopf, 2012) They are suggested to have provided the first large-scale source of biogenic oxygen, thus controlling the evolution of the early Earths' atmosphere (Hamilton et al., 2016; Schopf, 2012). Cyanobacteria are considered as most successful group of microorganisms and are quantitatively amongst the most important organisms on Earth (Dvořák et al., 2014; Whitton and Potts, 2012). Flombaum et al. (2013) suggested that marine cyanobacteria are responsible for 25 % of the ocean net primary production. Cyanobacteria colonize almost every terrestrial and aquatic habitat and are even found in most extreme conditions. As such, certain cyanobacteria are capable of living in the extreme environments of Antarctica or in thermal springs, or may even survive for long periods in complete darkness (Zanchett and Oliveira-Filho, 2013). Cyanobacteria occur as single cells, as filaments or in colonies. Cells vary in size from <1 µm (picoplankton) to greater than 20 µm (Wehr et al., 2015). Furthermore, cyanobacteria form blooms in freshwater and marine environments, which can be toxic and hazardous for humans or other animals and aquatic organisms (Paul, 2008). Many cyanobacteria are diazotroph and can convert inorganic nitrogen to bioavailable ammonia (Capone et al., 2005). Due to their great abundance, cyanobacteria

play an important role in global biogeochemical cycles of several elements, such as C, O, N, and P.

Synechococcus is an abundant group of cyanobacteria and a significant global primary producer. They colonize marine and freshwater habitats and are ubiquitous in nearly all environments (Dvořák et al., 2014). Flombaum et al. (2013) estimated a global net primary production of 8 Gt year^{-1} (16.7 % of ocean net primary production) for *Synechococcus*. *Synechococci* are found as single rod-shaped cells or as clusters and pairs. They are gram-negative with highly structured cell walls. *Synechococcus* is well known for its capacity to precipitate calcium carbonate (Bundeleva et al., 2014; Dittrich et al., 2003; Dittrich and Sibler, 2006; 2010; Kamennaya et al., 2012; Martinez et al., 2016; Obst et al., 2006; 2009b; 2009a; Thompson et al., 1997) and to play and important role in metal sorption processes (Dittrich and Sibler, 2006; Saito et al., 2005).

2.1.2 Diatoms – *Thalassiosira weissflogii*

Diatoms are unicellular eukaryotes with a usual size ranging between 2 and 200 µm, which commonly form colonies or filaments (Kooistra et al., 2007). The unique feature of diatoms is their silica hard shell, called frustule, which exists in great diversity of architectures (Round et al., 1990). Diatoms are among the most common components of phytoplankton on Earth and are widespread in the oceans and in freshwater environments (Kooistra et al., 2007). They are especially abundant in nutrient rich waters of the ocean and are considered to account for as much as 40-45 % of the oceanic primary production and 20 % of the global photosynthetic carbon fixation (Mann 1999), fixing roughly 20 Gt of C per year (Field et al., 1998; Kooistra et al., 2007; Mann, 1999). Notably, this is more than all the worlds tropical rainforests (Field et al., 1998; Mann, 1999). Moreover, diatoms often dominate the microphytobenthos, populations of microalgae living in the surface layers of sediments in coastal waters with sufficient light for photosynthesis (Thornton et al., 2002; Thornton, 2012). Diatoms frequently form blooms, which terminate by aggregate formation, contributing significantly to the flux of organic carbon from the surface water to the deep ocean (Thornton et al., 2002; Thornton, 2012). Diatoms have been shown to be highly adaptable to environmental conditions. For example, they are adapted to grow in deeply mixed turbulent waters with reduced light availability and are capable of storing nutrients for the use during nutrient deficiency (Kooistra et al., 2007; Mitchell and Holm-Hansen, 1991). Diatoms are known to occur in such large concentrations that they form sediments composed almost entirely of diatoms frustules, known as diatomites. Due to their

remarkable abundance, diatoms play an important part in the global biogeochemical cycling of several elements, particularly carbon and silicon.

Thalassiosira weissflogii (TW) is a centric (exhibit a radial symmetry) diatom, forming cylinders of 4 -32 µm diameter (Johansen and Theriot, 1987) which occur singly or in groups. TW is widespread and can be found in marine, brackish and freshwater environments, especially at salinities above 5 ‰ (Vrieling et al., 1999). This non-toxic diatom is known to grow in relatively high pH waters (8-9.4; Sala (1997)) and it exhibits increasing growth rates with increasing temperature (Lomas and Glibert, 1999). TW growth might be limited by the availability of nickel, zinc, iron, nitrogen or silica (De La Rocha and Passow, 2004; Fryxell and Hasle, 1977; Lee et al., 1995; Morel et al., 1994). Due to their large size, *Thalassiosira weissflogii* are used to feed shrimp and shellfish in aquaculture.

2.2 Microbial growth

Figure 2-1 shows a typical bacterial growth curve of a batch culture. Initially, the culture enters the lag phase during which growth is temporarily absent and bacteria adjust to the ambient growth conditions. The lag phase is followed by the acceleration phase and the exponential growth phase, which is characterized by cell doubling. During this exponential growth, the growth rate is constant, resulting in a straight line on a logarithmic plot. The slope of this line describes the growth rate constant. As the growth rate declines, the culture enters the deceleration phase until it reaches the stationary phase, where the cell concentration remains constant. The stationary growth phase is commonly reached when an essential nutrient is exhausted or when the accumulation of growth inhibiting products prevents further growth (Hall et al., 2014). Note, that during the stationary phase, cell division usually still occurs but the growth rate equals the death rate of the culture so that no net growth occurs. The final phase is the dead phase during which bacteria die.

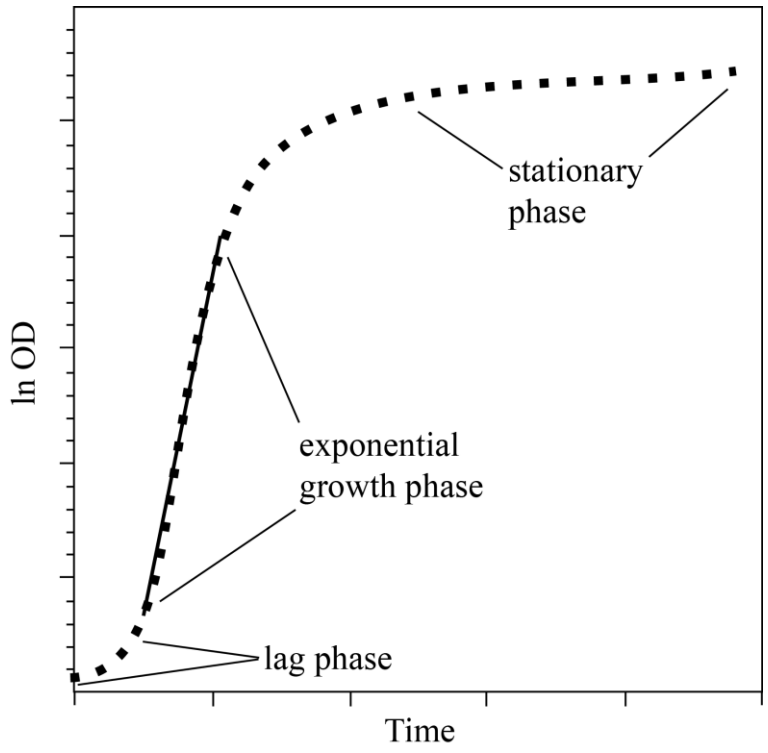

Figure 2-1. Typical bacterial growth illustrated as ln of optical density (OD) versus time. After an initial lag period, bacterial growth accelerates and reaches an exponential growth phase during which the growth rate is constant. After the exponential phase, growth rates decelerate until the culture enters the stationary phase during which little or no growth occurs.

2.2.1 Control of biomass production in turbid samples

During this thesis, cell growth was controlled differently depending on the microorganism used. Note, that the presence of suspended particulates significantly influenced bacterial biomass determination so that common methods had to be adjusted to quantify biomass in our experiments.

In case of the diatom *Thalassiosira weissflogii*, growth was monitored by optical cell counting using a Nageotte counting chamber. A Nageotte counting chamber is a glass chamber with a marked grid, as illustrated in Figure 2-2. It consists of 40 fields, which each measure 10 x 0.25 x 0.5 mm. Thus, the volume of each field is 1.25 µl and that of the total chamber is 50 µl. The samples were diluted prior to counting to reach a range of 10-100 diatoms per field. To reach accurate cell concentrations, 10 fields were counted for each sample. The average counts per field were then converted to cells/ml by multiplication by the factor 800 (1000/1.25 µl) and the corresponding sample dilution.

The presence of suspended particulates did not hamper diatom cell counts significantly since mineral fragments and diatoms could be discriminated readily during counting. However, at elevated suspended sediment concentrations, the diatom concentration was likely

underestimated since diatoms were covered within the high sediment load. Figure 2-3 shows a representative microscope photograph illustrating diatoms and mineral fragments in the counting chamber. This method is tedious and time consuming but yields a precise measure of the cell concentration.

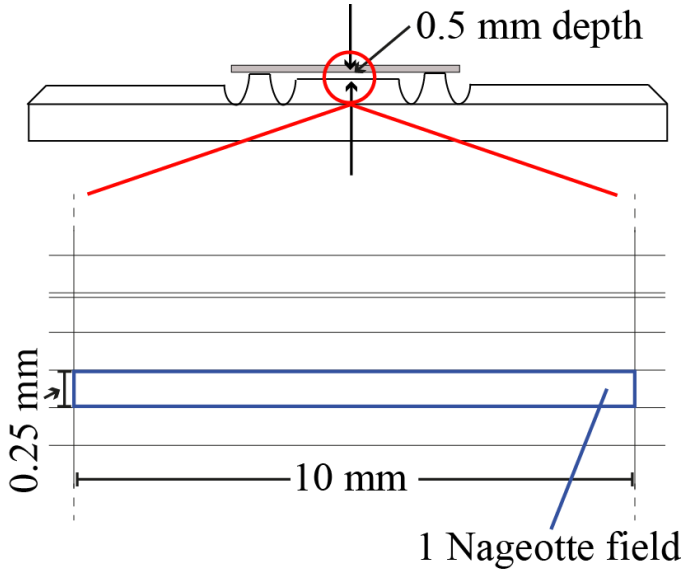

Figure 2-2. The principle of cell counting using a Nageotte counting chamber. An aliquot of the sample (~100 µl) is placed in the chamber and covered by a cover glass. The sample volume in the counting area is thus defined as 50 µl. The marked grid is composed of 40 identical fields of 10 x 0.25 x 0.5 mm, defining a volume of 1.25 µl. Cells are counted in at least 10 fields to get a statistically relevant cell count.

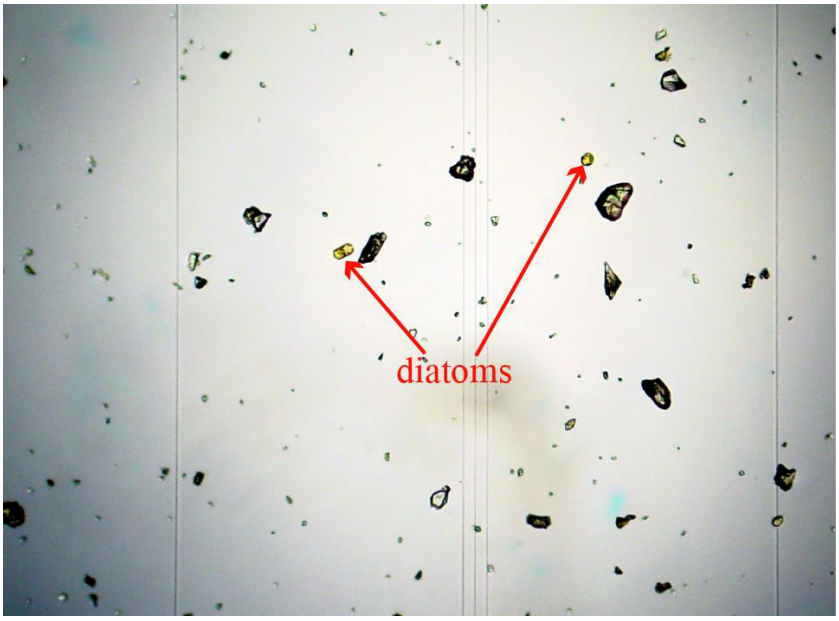

Figure 2-3. Microphotograph of a sample containing 1500 mg/l Mississippi sediment and diatoms illustrating the different appearance of mineral fragments and diatoms in the counting chamber. The vertical lines represent the marked grid of the Nageotte counting chamber. The distance between the lines is 0.25 mm, as illustrated in Figure 2-2.

UV-Vis spectrophotometry is the most commonly-used method for estimation of cell concentrations in liquid culture. A spectrophotometer quantifies the optical density (OD) of a liquid substance by comparing a known incoming light source with the intensity of that light after passing through the sample. Light is absorbed or scattered in the sample, reducing the incoming intensity according to Lambert-Beer's law. In pigmented samples like a cyanobacteria solution, the distinction between light scattering and absorbance is fundamental to choose an appropriate wavelength. As such, OD can be measured at "robust" or at "sensitive" wavelengths. A robust wavelength is away from pigment absorption peaks so that scattering is the predominant light attenuation mechanism. Thus, measurements at robust wavelengths measure the turbidity of a sample. The measurement at 750 nm has become a common convention for the determination of cyanobacteria biomass (Bundeleva et al., 2014; Ernst et al., 2005; Mavromatis et al., 2015; Myers et al., 2013). In contrast, the light attenuation at a sensitive wavelength (at the peak absorption of a pigment) is controlled by scattering and absorption and OD is subject to change with culture conditions, which may influence the relative pigment concentration in a given biomass. Despite this uncertainty, the use of sensitive wavelengths such as the peak absorption of chlorophyll-a at 680 nm is preferred for the estimation of phytoplankton levels if concentrations are low or if the water is turbid due to other substances (Myers et al., 2013). Furthermore, the OD at a pigment-dependent absorption wavelength can be corrected for its scattering component by measuring ratios or differences between sensitive and robust wavelengths.

In this study, we conducted growth experiments in reactors containing different concentrations of suspended matter. This suspended matter contributed significantly to sample turbidity, thus excluding the use of a robust wavelength as growth control (see Figure 2-4 and Figure 2-5 B). Figure 2-4 illustrates the contribution of the suspended sediments on sample turbidity. Reactor 4 on the right contains the highest biomass concentration whereas the turbidity (and thus OD reading) is much higher in Reactor 2, since sediments in this reactor are more fine grained and remain in suspension. Reactor 1 does not contain suspended sediments but a small concentration of biomass. Hence, we controlled cyanobacteria growth at the peak absorption of chlorophyll-a (here determined at 682 nm) and corrected this measure for the scattering of the particles by subtracting the OD measured at the robust wavelength at 750 nm (see Figure 2-5 A and B). This procedure also gave a measure of the physiological state of the culture since the chlorophyll peak shifted towards a lower wavelength when bacteria started to die, whereas dead bacteria still contributed to turbidity at 750 nm (see Figure 2-5 C). To further correct the data, we repeated the same protocol with an abiotic control and subtracted this

contribution from the biotic suspension sample. The OD measurements at 682-750 nm were then correlated to biomass dry weight as illustrated in Figure 2-6. Dry weight was determined at five different optical density readings by centrifugation of a 50 ml sample and weighing the biomass pellet after freeze drying for >24h. This resulted in precise estimates of the cyanobacteria biomass concentration, independent of different suspended sediment loads.

Note, however, that bacteria attached on sediment particles are not accounted for with this method, since sediment-bacteria agglomerations settled in the cuvette used for OD readings and were thus not in the light penetration path of the spectrophotometer. Bacteria attached on minerals may have contributed significantly to total biomass and as such, bacteria concentrations in the presence of sediments may be somewhat underestimated.

Figure 2-4. Photograph of three reactors illustrating the different optical appearance at different biomass concentrations. Reactor 1 contains a low biomass concentration but no suspended sediments. Reactors 2 and 4 contain about the same biomass concentration (slightly higher in Reactor 4) but reactor 2 appears much more turbid, which is due to a high load of fine-grained suspended sediments.

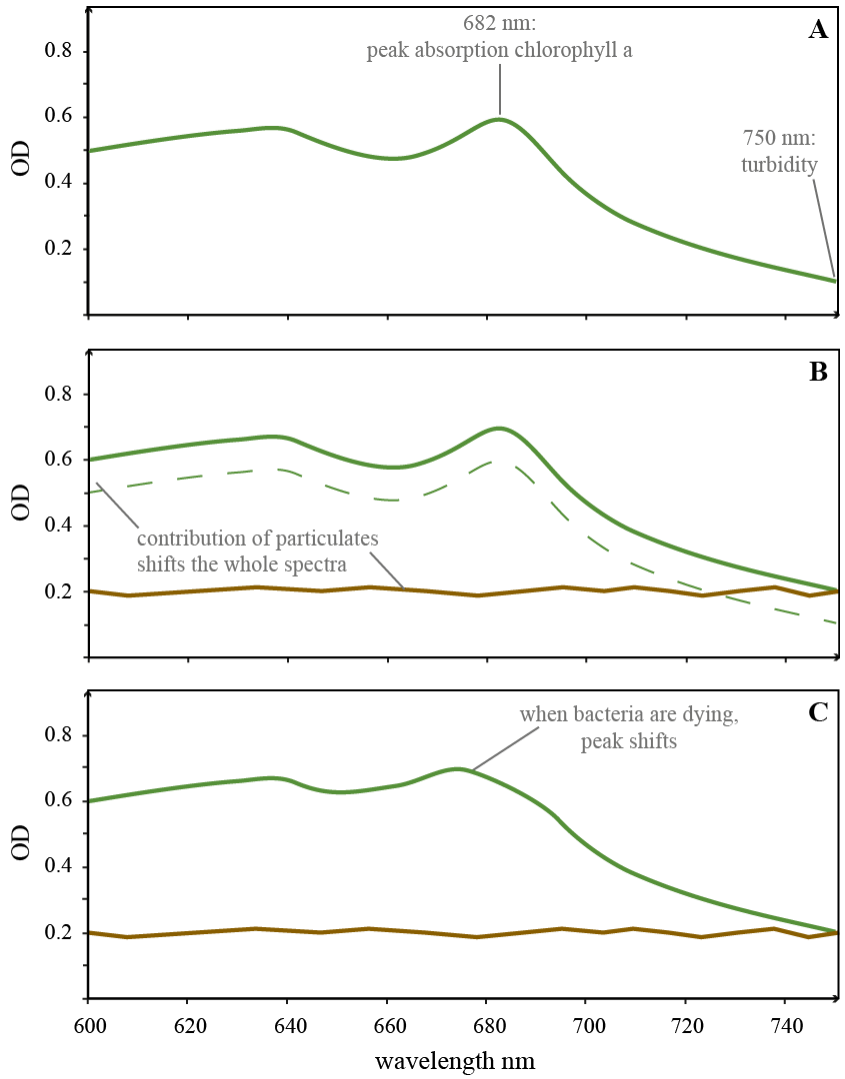

Figure 2-5. Spectrophotometric scans of cyanobacteria from 600 to 750 nm showing the difference between a sensitive (~680 nm) and a robust (commonly 750 nm) wavelength (**A**). The presence of sediments shifts the Synechococcus curve to higher total values without changing Δ682-750 (**B**). For dying cyanobacteria Δ682-750 decreases due to a shift of the peak absorption to lower wavelengths (**C**).

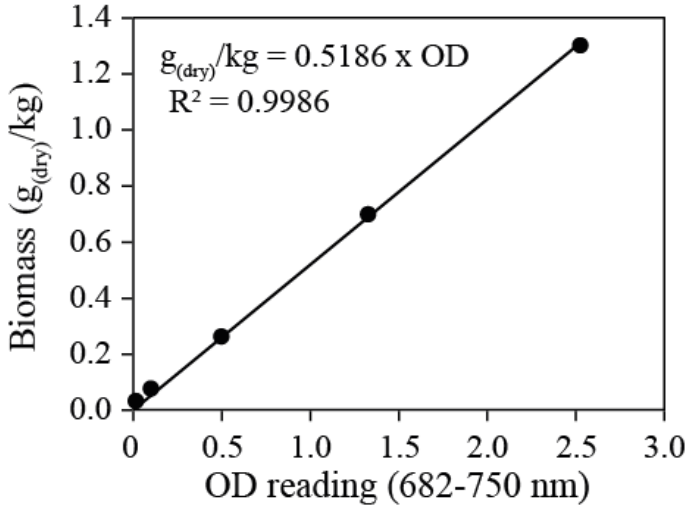

Figure 2-6. Optical density (OD) versus biomass ($g_{(dry)}$/kg) calibration curve for determination of biomass concentrations in a liquid cell culture.

2.3 Experimental approach

Growth experiments with cyanobacteria and diatoms, as presented in Chapters 3 and 4, were performed in sterile Polycarbonate flasks. These flasks were placed at room temperature on an orbital shaker (250 1/min) under an intermittent light source, illuminating the cultures for 12h at 3000 LUX cool white fluorescence light during daytime. Flasks were closed using BIO-SILICO© N stoppers that allowed sterile equilibration with the atmosphere. All reactive fluids, as well as the experimental equipment were either filter-sterilized or autoclaved at 121 °C for 20 minutes prior to the experiment. The riverine particulates added to the reactors were sterilized either overnight in the oven at 121 °C with or without previous ethanol rinsing, or by H_2O_2 treatment, or burned in the oven at 450 °C for 2.5 hours. Aliquots of homogenous samples were taken from each experiment in a sterile laminar hood box periodically, 6h after the onset of illumination. Figure 2-7 shows a sketch of the experimental design.

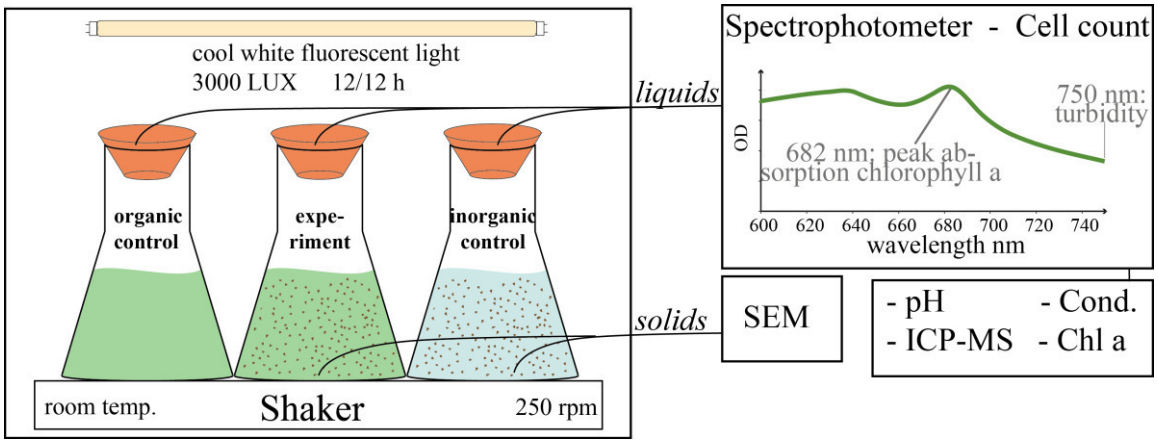

Figure 2-7. Experimental design used to study the growth of cyanobacteria and diatoms in the presence of riverine particulate material (Chapters 3 and 4).

Calcite precipitation experiments in the presence of cyanobacteria, presented in Chapter 5, were performed in sterile Schott glass bottles. Other than the growth experiments presented above, bottles were continuously illuminated at 3000 LUX cool whit fluorescence light, bubbled with sterile humidified air to assure equilibration with the atmosphere and stirred with stirring bars. All reactive fluids, as well as the experimental equipment were either filter-sterilized or autoclaved at 121 °C for 20 minutes prior to the experiment. Aliquots of homogenous samples were taken from each experiment in a sterile laminar hood box. Figure 2-8 shows a photograph of the experimental design.

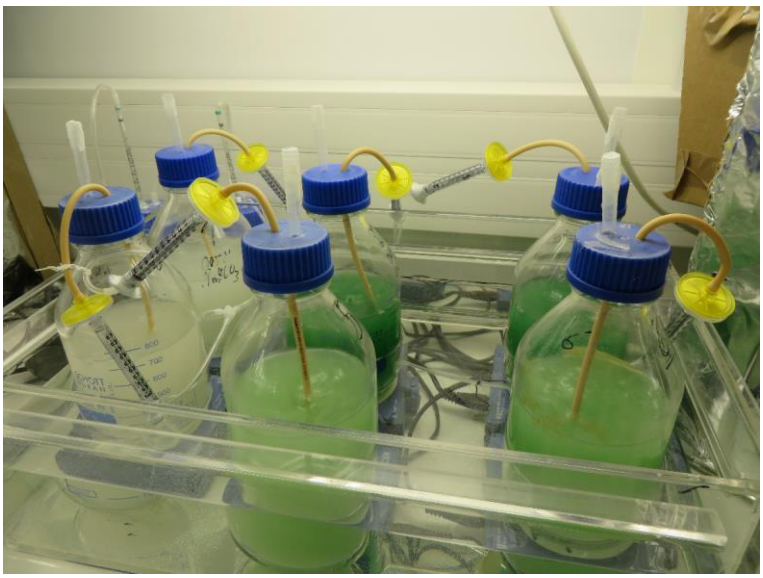

Figure 2-8. Experimental design used for calcite precipitation experiments in the presence of cyanobacteria (Chapter 5).

2.4 Natural samples

During spring 2014 (May 7th 2014), we conducted a samplng trip off the Southcoast of the Reykjanes Peninsular in SW-Iceland to sample suspended particles to evaluate mineral microbe interactions. Samples were collected from the Ölfusá river in Selfoss (sampling from the bridge of highway 1, 63°56'20''N, 21°00'17''W), downstream the Ölfusá river at its estuary mouth (sampling from the bridge of highway 34, 63°52'44''W, 21°12'36''N) and from a boat ~40 km west of the estuary, where riverine sediments are transported by a westward current along the shore (63°46'45''N, 22°04'56''W). Samples were taken into sterile bottles and treated in the lab by Glutaraldehyde fixation (see Chapter 3) for SEM analyses. Selected SEM images are presented in Chapter 3.

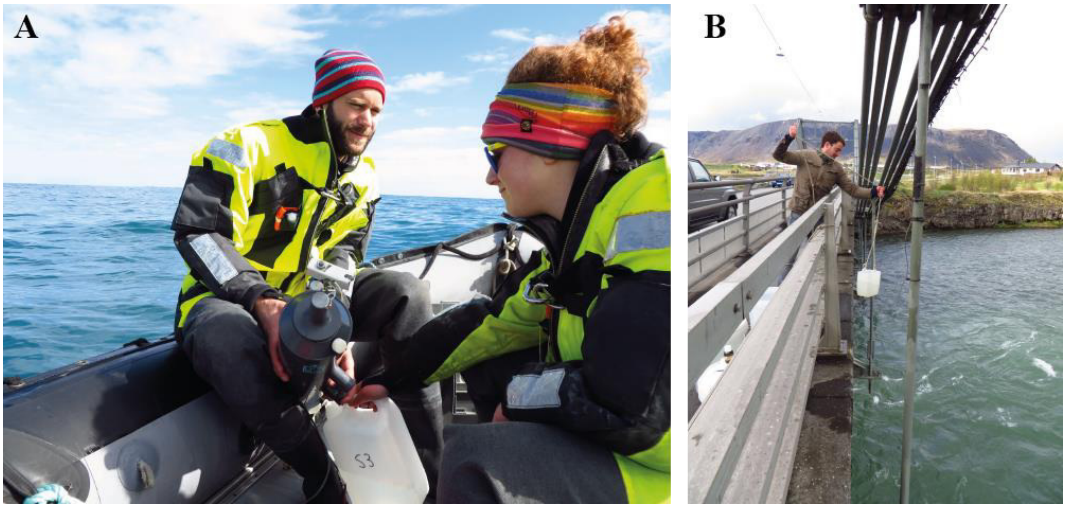

Figure 2-9. Sampling at the Icelandic southcoast south of Krisuvik **(A)** and at the Ölfusá river in Selfoss **(B)**.

3 Effect of riverine particulates on the growth of the freshwater cyanobacteria *Synechococcus sp*.

Résumé

L'apport des matières particulaires continentales dans des eaux naturelles joue un rôle essentiel dans les cycles globaux des éléments. Notamment, la masse de la plupart des éléments transportés par les rivières vers les océans en forme des particules dépasse de loin le flux en forme dissous correspondant. Par exemple, le flux global des nutriments essentiels Si, P et Fe sous forme particulaire dépasse le flux dissous correspondant par des facteurs de 50, 100 et 350, respectivement. Les microbes peuvent alors avoir accès à ces nutriments soit indirectement par dissolution des particules, soit directement par attaque microbienne. Donc, il semble raisonnable de s´attendre à un lien étroit entre l'approvisionnement en matière particulaire et la productivité primaire dans les eaux naturelles. Pour explorer ce lien, des séries d'expériences de croissance dans des microcosmes ont été réalisées avec une cyanobactérie typique d'eau douce, *Synechococcus sp*., cultivée dans une dilution du milieu de culture BG-11, en présence et en l'absence de particules basaltiques et continentales. Les résultats démontrent que les particules de rivières augmentent notamment la biomasse bactérienne 1) en provoquant une croissance bactérienne dans des conditions défavorables, 2) en augmentant la concentration totale de biomasse en fonction de la concentration des particules et 3) en provoquant une croissance bactérienne constante en phase post-exponentielle en fonction de la concentration en particules. En outre, les résultats suggèrent une réaction positive entre la présence de particules et celle des bactéries croissantes, car la dissolution des sédiments augmente la croissance bactérienne, ce qui favorise davantage la dissolution des sédiments en modifiant le pH de la phase liquide. Des analyses MEB ont montré un contact physique direct entre les particules et les cyanobactéries par des fibres organiques, ce qui suggère que les bactéries se fixent directement sur les surfaces minérales pour obtenir des nutriments nécessaires. En outre, des agglomérats de bactéries ont fréquemment été observés associés à des particules de sédiments, indiquant ainsi une accumulation plus fréquente des bactéries en présence de matières particulaires, ce qui pourrait faciliter l'efficacité de séquestration du carbone organique.

Riverine particulate material as hot spots of cyanobacterial growth: results of laboratory experiments with *Synechococcus sp.*

Christian Grimm[1*], Raul E. Martinez[2], Oleg S. Pokrovsky[1,3], Liane G. Benning[4,5] and Eric H. Oelkers[1,6]

[1] GET, CNRS/URM 5563, Université Paul-Sabatier, 14 avenue Edouard-Belin, 31400 Toulouse, France
[2] Geo- und Umweltnaturwissenschaften, Albert-Ludwigs Universität, 79104 Freiburg, Germany
[3] N. Laverov Federal Center of Integrated Arctic Research, Russian Academy of Science, Arkhangelsk, Russia
[4] School of Earth and Environment, University of Leeds, LS2 9JT, UK
[5] GFZ German Research Centre for Geosciences, 14473 Potsdam, Germany
[6] Earth Sciences, University College London, Gower Street London WC1E 6BT, UK

[*]Corresponding author: grimm@get.obs.mip.fr

This manuscript is completed for submission

Keywords: CO_2, cyanobacteria, organic carbon cycle, primary production, riverine particulate material, nutrients, mineral-microbe interaction, carbon burial

Abstract

The supply of riverine particulate material to natural waters plays a vital role on global cycles of certain elements. Notably, the mass of most elements transported by rivers to the oceans as particulates far exceeds the corresponding dissolved flux. For example, the global riverine particulate flux of the essential nutrients Si, P and Fe exceeds the corresponding dissolved flux by factors of 50, 100 and 350. Microbes might gain access to these nutrients either indirectly through dissolution of the particulates or directly through microbial attack. As such, it seems reasonable to expect a close link between the particulate material supply and primary productivity in natural waters. To explore this link, a series of microcosm growth experiments were performed with a typical freshwater cyanobacteria *Synechococcus sp.* grown in dilute BG-11 culture media in the presence and absence of basaltic and continental riverine particulate material. Results demonstrate that riverine particulates significantly increase bacterial biomass by 1) triggering bacterial growth in otherwise unfavourable conditions, 2) increasing total biomass concentration as a function of particulate concentration and 3) inducing steady bacterial growth during the post-exponential phase as a function of particulate concentration. Results also indicate a positive feedback between the presence of particulates and growing bacteria, where dissolving particulates enhance bacterial growth, which further promotes particulate dissolution by altering fluid pH. SEM analysis showed direct physical contact between particulates and cyanobacteria, suggesting that bacteria attach directly on mineral surfaces to gain required nutrients. Furthermore, frequent bacteria clusters were observed associated with particulates, indicating an increasing accumulation of bacteria in the presence of particulate material, which may facilitate a higher burial efficiency of organic carbon.

3.1 Introduction

Atmospheric CO_2 concentrations have been steadily increasing since the beginning of the industrial revolution and there is exhaustive research linking it to global climate change. Carbon dioxide is removed from the atmosphere by two major mechanisms: The ‘inorganic pathway’, which couples the dissolution of divalent metal bearing silicate minerals to the formation of carbonate minerals and the ‘organic pathway’, which removes CO_2 from the atmosphere by photosynthesis and the subsequent burial of organic matter (Berner, 1982; Berner et al., 1983; Berner and Kothavala, 2001; Falkowski et al., 1998; Gislason et al., 2009; Walker et al., 1981; Wallmann, 2001). Burial of organic matter is required for the long-term

drawdown of CO_2 via the 'organic pathway' because it prevents organic matter decomposition and thus the return of CO_2 to the atmosphere (Berner, 1982; Falkowski et al., 1998; Jeandel and Oelkers, 2015). Besides CO_2 and light, photosynthesizing microorganisms require nutrients that serve as electron donors and acceptors for their metabolic activity. A lack of nutrients, such as P, N, Si, or Fe can be the limiting factor for primary production (Broecker, 1982; Falkowski et al., 1998; Jickells et al., 2005; Mills et al., 2004), whereas in turbid environments, light can limit bacterial growth (Anderson et al., 2002). The two major sources of nutrients in natural waters are the recycling of organic compounds due to microbial degradation and the influx of new nutrients through rivers, aeolian dust or volcanic ash (Eiriksdottir et al., 2015; Eiriksdottir, 2016; Falkowski, 2014; Jickells et al., 2005; Jones and Gislason, 2008; Olsson et al., 2013).

Rivers carry elements derived from continental weathering in dissolved and particulate form. Whereas the dissolved riverine transport has received much greater interest in the past, more recent estimates of riverine particulate fluxes concluded that the suspended material flux dominates the dissolved flux for essentially all elements except for the most soluble like Na (Gislason et al., 2006; Jeandel and Oelkers, 2015; Jones et al., 2012; Oelkers et al., 2011; 2012). The estimated global dissolved riverine flux is approximately 1 Gt $year^{-1}$ (Gaillardet et al., 1999; 2003; Meybeck et al., 2003; Viers et al., 2009), whereas the suspended particulate land-to-ocean flux is estimated to be 15-20 Gt $year^{-1}$, thus at least an order of magnitude greater (Meybeck et al., 2003; Oelkers et al., 2011; Syvitski et al., 2003; Walling, 2006). Including the estimated bedload component of 1.6 to 10 Gt $year^{-1}$, the total particulate flux exceeds the dissolved flux by a factor of 17 to 30 (Jeandel and Oelkers, 2015; Walling, 2006). The aeolian dust flux to the oceans is estimated to be 0.4-2 Gt $year^{-1}$, thus 8 to 75 times less than the estimated particulate flux (Jeandel and Oelkers, 2015; Jickells et al., 2005). The predominance of particulate over dissolved transport is depicted in Figure 3-1 for a selection of vital and often limiting nutrients. For example, the riverine particulate flux of Si, P and Fe exceeds the corresponding dissolved flux by factors of 50, 100 and 350, respectively (Jeandel and Oelkers, 2015; Oelkers et al., 2011). Moreover, much of what is commonly measured as dissolved flux may in fact be present as colloids and nanoparticles (Gaillardet et al., 2003). Given the huge flux of riverine particulate material, only a tiny fraction of it needs to dissolve to substantially influence bio-geochemical cycles.

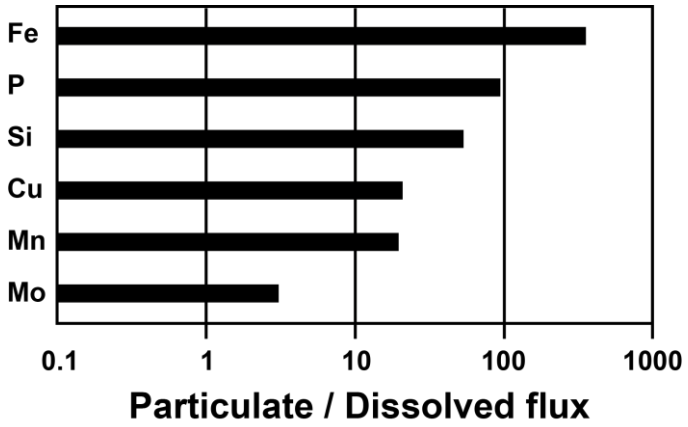

Figure 3-1. The ratio of global riverine particulate flux to the corresponding dissolved flux for selected nutrients. Particulate fluxes of vital nutrients like Si, P and Fe exceed the corresponding dissolved fluxes by factors of 50, 100 and 350. Figure modified after Oelkers et al. (2011).

Jeandel and Oelkers (2015) summarized the role of riverine particulate material in the burial and preservation of organic carbon. First, an increasing supply of particulate material accelerates the sediment accumulation rate, thus reducing organic material exposure time to oxygen and the organic matter decomposition. Secondly, the supply of mineral surfaces is viewed as major control of organic matter burial due to strong organic material sorption onto mineral grains (Burdige, 2007; Kennedy et al., 2002; Lalonde et al., 2012; Mayer, 1994). Note also, that the delivery of riverine particulate material to the oceans is particularly climate sensitive (Gislason et al., 2009; Jeandel and Oelkers, 2015). An increasing CO_2 concentration in the atmosphere leads to higher air temperatures, changing precipitations patterns and increasing runoff, which leads to elevated chemical and physical weathering rates (Alley et al., 1997; Gedney et al., 2006; Gislason et al., 2006; 2009; Labat et al., 2004). The increasing weathering rates in turn drive the CO_2 drawdown via both the 'inorganic' and 'organic pathway' through the delivery of divalent cations as well as limiting nutrients. This link between increasing CO_2 concentration leading to increased weathering rates and the subsequent precipitation of carbonate minerals has been referred to as the internal thermostat of the Earth (Berner et al., 1983; Walker et al., 1981). Note, that Gislason et al. (2006) and (2009) observed in a field study in NE Iceland that the riverine suspended particulate load is far more sensitive to climate change compared to the dissolved load. Taken together, these observations suggest a strong feedback between the riverine particulate material flux and the CO_2 consumption via the 'organic pathway'.

The significance of terrestrial sediments in primary production has received some attention, notably due to its potential source of bio-available Fe. The reductive and non-

reductive dissolution of Fe in continental shelf sediments has been attributed as major source of dissolved Fe to the oceans (Elrod et al., 2004; Jeandel and Oelkers, 2015; Jones et al., 2011; Radic et al., 2011). However, the direct effect of riverine particulates on phytoplankton growth has not been investigated in detail. Direct and indirect interactions between minerals and microbes, however, are common or even omnipresent in natural systems. For example, Bailey et al. (2009) demonstrated in an experimental study the capability of microbes to obtain required nutrients directly from basaltic glass. Similarly, Rogers et al. (1998) and Rogers and Bennett (2004) showed in a field and experimental study that P-bearing silicates were heavily colonized and weathered by subsurface microorganisms, whereas P-free silicates were not. They concluded that microorganisms extract inorganic P from the minerals while destroying the silicate matrix. More recently, Sudek et al. (2017) observed elevated growth of the heterotrophic bacterium *Pseudomonas stutzeri VS-10* in the presence of basaltic glass and concluded that the physical contact between the bacterium and the glass is critical in this process. Perez et al. (2016) described elevated growth of the heterotrophic bacterium *Pseudomonas aeruginosa* in the presence of Fe-bearing basaltic glass compared to Fe-free basalts and control experiments without basalt.

Moreover, microorganisms have been shown to influence mineral dissolution and precipitation. For example in lacustrine settings, the growth of cyanobacteria has been demonstrated to catalyze calcium carbonate formation through the creation of an alkaline growth environment around the cell (Dittrich et al., 2003; Hodell et al., 1998; Lee et al., 2006; Stabel, 1986; Thompson et al., 1997). In addition, microorganisms can accelerate the dissolution of a variety of silicates through their effect on pH, or through microbially produced organic ligands that complex metals in solutions or form Si-framework destabilizing surface complexes (Bennett et al., 2001; Drever and Stillings, 1997; Olsson-Francis et al., 2012; Perez et al., 2016; Rogers and Bennett, 2004; Stockmann et al., 2012; Uroz et al., 2009; Wu et al., 2007; 2008). Notably, when directly attached to mineral surfaces, microorganisms significantly alter Si-solubility by perturbing mineral-water equilibria in their highly reactive microenvironment (Rogers and Bennett, 2004). However, it is a matter of discussion whether this interaction is the coincidental effect of the microbial metabolism, or a deliberate strategy of the microorganisms to get access to vital nutrients directly from the rocks (Bennett et al., 2001).

The interactions of microbes and minerals described above, together with the vast source of nutrients present in riverine particulates, suggest an influence of riverine particulate material

on primary productivity. This study aims to explore the effect of riverine particulate material on the growth of freshwater cyanobacteria. Towards this goal, we conducted microcosm growth experiments with the freshwater cyanobacteria *Synechococcus sp.*, a widespread cyanobacterium in marine and freshwater environments, in the presence of two types of riverine particulate material. The purpose of this paper is to present the results of this experimental study and to use these results to assess the potential role of riverine particulates on microbial growth in natural system.

3.2 Materials

3.2.1 Riverine Particulate Material

Two different types of riverine particulate material (RPM) with distinct chemical and mineralogical compositions were used in this study. The bulk chemical compositions as well as BET surface areas of these particulates are listed in Table 3-1. In one experimental series, zircon particles were added to the reactors to mimic the presence of inert mineral surfaces. The riverine particulates used in this study were:

1) **MS**, bedload material from the Mississippi river collected in July 2010 in western New Orleans, USA. This sample is described in detail in Jones et al. (2012) where the chemical composition and the BET surface area were reported. The Mississippi RPM consists of almost 80 % SiO_2 and is mainly composed of quartz and feldspars with minor concentrations of sheet silicates. It was chosen as a representative of continental riverine material. The BET surface area of this material is 3.05 m^2g^{-1}. The XRD spectrum of this sample, provided in Figure A 3-1, shows a smooth pattern with well localized peaks which can almost perfectly be fit assuming the sample contained only quartz and feldspar.

2) **ICE**, suspended basaltic particulates from Jökulsá á Fjöllum, a glacial river in Eastern Iceland. The major chemical components of this Iceland RPM are 51.5 % SiO_2, 13.6 % Al_2O_3, 12.2 % FeO and 10.4 % CaO. It is mainly composed of basaltic glass and basalt fragments. The XRD spectrum, illustrated in Figure A 3-1, shows a pattern typical for glassy material. The observed peaks can be best fit with a combination of plagioclase and pyroxenes. This sample is representative of the high relief, volcanic and tectonic active islands that contribute over 45 % of river suspended material to the oceans (Eiriksdottir et al., 2008; Milliman and Syvitski, 1992). Details on sampling and filtration methods can be found in Eiriksdottir et al. (2008) where the chemical composition was taken from (sample ID 01A033 therein).

Table 3-1. Whole rock analyses and specific surface areas of riverine particulate material used in this study. Mississippi (MS) data is from Jones et al. (2012), Iceland (ICE) data from Eiriksdottir et al. (2008). Note that total Fe is presented as FeO or Fe_2O_3, respectively, for the ICE and MS samples.

Name	**ICE**	**MS**
Type	suspended	Bedload
BET (m^2g^{-1})	8.92	3.05
SiO_2 (%)	51.54	79.25
Na_2O (%)	2.67	1.56
MgO (%)	5.86	0.51
Al_2O_3 (%)	13.62	6.38
P_2O_5 (%)	0.28	0.10
K_2O (%)	0.47	1.71
CaO (%)	10.44	1.34
TiO_2 (%)	2.52	0.43
MnO (%)	0.22	0.03
FeO (ICE) (%) Fe_2O_3 (MS) (%)	12.24	1.39

3.2.2 Cyanobacteria

The unicellular freshwater cyanobacteria *Synechococcus sp. PCC 7942* used in this study were cultured in sterile conditions in BG-11 Freshwater Solution Medium (Sigma-Aldrich C3061) at room temperature, 24h illumination at 3000 LUX cool white fluorescence light and bubbling of humidified air to achieve constant mixing. *Synechococcus* were chosen for this study because of their great abundance in freshwater and marine environments (Obst et al., 2009b; 2009a). The cyanobacteria *Synechococcus sp*. and *Prochlorococcus sp*. are responsible for >25 % of global photosynthesis (Rohwer and Thurber, 2009). Further details about this cyanobacteria are provided in Dittrich and Sibler (2006), Obst et al. (2009b), Obst et al. (2009a) and Bundeleva et al. (2014). The initial cyanobacteria cultures showed minor heterotrophic cortege (<5 % of the biomass).

3.3 Methods

3.3.1 Growth Experiments

Inoculation experiments were performed in sterile 250 and 500 ml Polycarbonate flasks with 12 h/12 h illumination/dark cycles (3000 LUX cool white fluorescence light during daytime), circular shaking at 250 1/min, and room temperature. Reactors were closed with BIO-SILICO© N stoppers that allowed sterile equilibration with the atmosphere. The reactive fluids were composed of 1:1000 or 1:375 dilutions of the 50x concentrated BG-11 Freshwater Solution culture medium to obtain a 5 % and 13.3 % dilution of the original BG-11 culture

medium. The resulting chemical compositions are listed in Table 3-2. The majority of the experiments were performed in 5 % BG-11 media, whereas a few were conducted at higher nutrient conditions. The riverine particulate material was cleaned and sterilized following different protocols. They were either sterilized overnight in the oven at 121 °C with or without previous Ethanol rinsing, or sterilized by H_2O_2 treatment, or burned in the oven at 450 °C for 2.5 hours. Note, that these treatments potentially alter the particle surfaces distinctly, potentially creating more fresh inorganic sites while reducing the number of reactive organic sites. Particulates were added in concentrations of 75 mg/kg and 1500 mg/kg, resulting in a low and a high natural riverine particulate concentrations according to Meybeck et al. (2003). Additionally, a series of Mississippi RPM experiments was performed with intermediate concentrations of 500 and 1000 mg/kg. In one experimental series (Series S*Vb*), 1500 mg/kg MS and ICE RPM were equilibrated for one month in diluted BG-11 media (1:1000 dilution) and subsequently filtered to remove the particulates prior to inoculation. Biotic controls without RPM and abiotic controls with particulates but without bacteria were run as part of each experimental series. All reactive fluids, as well as the experimental equipment were either filter-sterilized or autoclaved at 121 °C for 20 minutes prior to the experiment.

Aliquots of the bacteria stocks were harvested from the stationary growth stage (4-6 weeks after initial culturing) and rinsed three times in the experimental electrolyte fluid by centrifugation/resuspension cycles prior to inoculation. Cyanobacteria were inoculated into the reactors at the low, mid or high initial biomass concentrations of 0.007, 0.018, and 0.041 $g_{(dry)}$/kg, respectively. Table A 3-1 summarizes the initial conditions of all experiments.

Table 3-2. Composition of BG-11 Freshwater culture solution and the 1:1000 and 1:375 dilutions used for the growth experiments. FAC means Ferric Ammonium Citrate. BG-11 concentration from Rippka et al. (1979).

mMol/kg	**BG-11 100%**	**5% (1:1000)**	**13.33% (1:375)**
$NaNO_3$	17.60	0.88	2.347
K_2HPO_4	0.23	1.15×10^{-2}	3.07×10^{-2}
$MgSO_4*7H_2O$	0.30	1.50×10^{-2}	4.00×10^{-2}
$CaCl_2*2H_2O$	0.24	1.20×10^{-2}	3.20×10^{-2}
Citric Acid$*H_2O$	0.031	1.55×10^{-3}	4.13×10^{-2}
FAC	0.021	1.05×10^{-3}	2.80×10^{-2}
$Na_2EDTA*2H_2O$	0.0027	1.35×10^{-4}	3.60×10^{-4}
Na_2CO_3	0.19	9.50×10^{-3}	2.53×10^{-2}
H_3BO_3	0.046	2.30×10^{-3}	6.13×10^{-3}
$MnCl_2*4H_2O$	0.009	4.50×10^{-4}	1.20×10^{-3}
$ZnSO_4*7H_2O$	0.00077	3.85×10^{-5}	1.03×10^{-4}
$Na_2MoO_4*2H_2O$	0.0016	8.00×10^{-5}	2.13×10^{-4}
$CuSO_4*5H_2O$	0.0003	1.50×10^{-5}	4.00×10^{-5}
$Co(NO_3)_2*6H_2O$	0.00017	8.50×10^{-6}	2.27×10^{-5}

3.3.2 Sampling

Aliquots of homogenous samples were taken from each experiment in a sterile laminar hood box periodically, 6h after the onset of illumination. Solids were thoroughly resuspended prior to sampling to preserve constant RPM and bacteria concentrations during the experiment. The sample volume was 3 ml for 250 ml reactors where only biomass and pH were measured, and 15 ml for 500 ml reactors where the aqueous fluids were further analyzed for elemental composition, dissolved inorganic carbon (DIC) and non-purgeable organic carbon (NPOC). In selected reactors, solids were sampled during and after the experiment and prepared for SEM analyses. Optical density and pH were measured immediately after sampling in suspension samples, whilst fluid supernatants were filtered using a MilliPore 0.45 µm cellulose acetate filter for further analyses.

3.3.3 Analytical methods

3.3.3.1 Biomass concentration

Biomass concentration was monitored from the suspension sample optical density measured at the peak absorption of chlorophyll a (682 nm) after subtracting the contribution of turbidity determined at 750 nm. The Varian Cary50Scan Spectrophotometer used for this analysis allowed simultaneous measurements of these two wavelengths. Optical density (OD) was then converted to dry biomass using a linear calibration curve over the concentration range of the experiments (see Figure 2-6). This approach accounts for the contribution of riverine

particulates or cell debris on the OD measurements. As depicted in Figure 3-2 A, the effect of different particulate concentrations on optical density was accurately accounted for by the difference of two wavelengths. Note the 682 nm peak shifts towards a lower wavelength when cyanobacteria die, which gives an indication of their physical state. Abiotic controls of each particulate concentration were measured following the same protocol to correct for the OD (682-750 nm) of the particulates and to control for possible contamination. Measurements of the abiotic controls were subtracted from the biotic experiments. The optical density of each sample was measured in triplicate and total uncertainty was estimated to be below 10 %.

To validate the OD measurement of biomass, bacterial growth was also monitored by chlorophyll a measurements via pigment extraction in one set of experiments. Chlorophyll analyses were performed by first diluting a 0.3 ml suspension sample in a glass vial with 2.7 ml acetone to produce a 90 % acetone solution. After storage for two days at -20 °C with occasional shaking, the samples were centrifuged for 10 min at 4500 rpm and absorbance was measured with a spectrophotometer at 750 nm, 663 nm, 645 nm and 633 nm. Chlorophyll a concentration was then calculated using the SCOR-Unesco Report (1966) equation: chlorophyll a = 11.96 x (663nm-750nm) - 2.16 x (645-750nm) + 0.1 x (630-750nm). Figure 3-2 B shows the correlation of the two different methods for biomass measurement in three experiments. The good correlation (R^2 = 0.93) validates our biomass concentrations determinations using optical density measurements.

3.3.3.2 DIC/NPOC

Dissolved inorganic (DIC) and non-purgeable organic carbon (NPOC) were measured using a Shimadzu TOC-VCSN Carbon Analyzer with a ASI-V sample unit at the CNRS laboratory Géosciences Environnement Toulouse. The quantification limits were 0.57 ppm and 0.47 ppm for DIC and NPOC and the uncertainty below 3 %.

3.3.3.3 ICP-MS

In two experimental series, aqueous major and trace element concentrations were determined by High Resolution Inductively Coupled Plasma Mass Spectrometry (HR-ICP-MS) using a Thermo-Finnigan Element-XR at the Géosciences Environnement Toulouse. Multi-element standard solutions were used for calibration. The analytical uncertainty of these measurements was below 2 %.

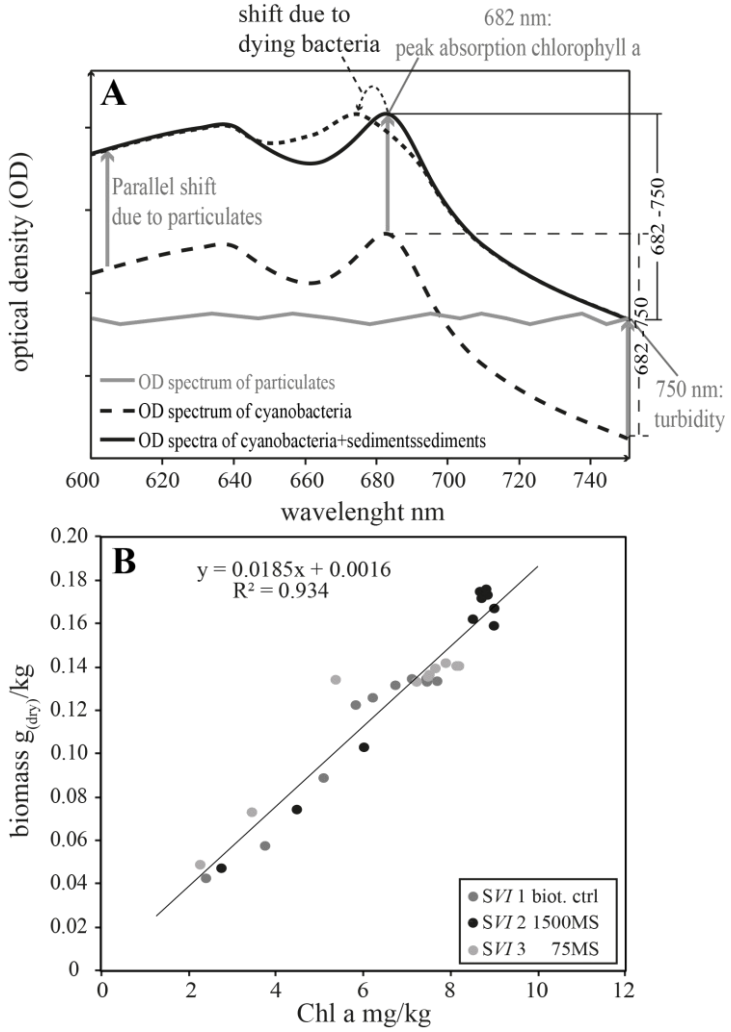

Figure 3-2. A: Spectrophotometric scan of cyanobacteria with (solid black line) and without (dashed black line) sediments (grey line) from 600 to 750 nm. The presence of sediments shifts the Synechococcus curve to higher total values without changing Δ682-750. For dying cyanobacteria Δ682-750 decreases due to a shift of the peak absorption to lower wavelengths **B:** Correlation of measured biomass and chlorophyll-a concentration in experiments where both were measured.

3.3.3.4 Scanning electron microscopy (SEM)

Solid samples (particulate-bacteria mixtures) were analyzed using a FEI Quanta 650 FEG-ESEM Scanning Electron Microscope (SEM) at the School of Earth and Environment at the University of Leeds. To avoid destruction of the bacteria in high vacuum, samples were previously fixed by Glutaraldehyde treatment as follows: The recovered particulate/bacteria mixtures were stored for one night in sterile 2.5 % Glutaraldehyde solution (25 % stock solution diluted 1:10 in 50 mM Na_3PO_4) to preserve the bacteria. Subsequently, the samples were ethanol exchanged by suspending them in gradually increasing ethanol concentrations through to pure ethanol. Finally, samples were critical point dried, mounted on sample stubs and gold coated prior to analysis.

3.3.4 Growth rate calculation

Bacterial growth rates were calculated using the *GrowthRates* software (Version 2.1, December 11, 2015) developed by Barry G. Hall and others at the Bellingham Research Institute (Hall et al., 2014). Figure 3-3 illustrates a typical temporal bacterial growth curve, which is composed of an initial lag period followed by an acceleration phase and an exponential growth phase, during which the growth rate is constant. After the exponential growth, rates decelerate until the culture enters the stationary phase during which little or no growth occurs. The specific growth rate constant μ is calculated only on the basis of the exponential growth phase according to:

$$\mu = \frac{(lnN_{t_2} - lnN_{t_1})}{(t_2 - t_1)} \tag{3-1}$$

where N represents the biomass concentration at time t. The dimension of μ is reciprocal time. The results obtained from the *GrowthRates* program were verified for each experiment and if appropriate recalculated manually. The uncertainty is given by the error of the linear regression of the biomass concentrations considered to calculate the rate. If only two points were used for the calculation, an uncertainty of 20 % was estimated. The bacterial growth behavior in the stationary phase was quantified by linear regression and is presented as growth rate in stationary phase μ_{stat} in this study.

For the logistic fit of the biomass concentration we applied the equation from Ernst et al. (2005):

$$y = \frac{a}{1 + e^{-k(t-c)}} + a_0 \tag{3-2}$$

where a represents the upper asymptote of the sigmoidal growth curve, a_0 reflects the initial offset in biomass concentration, k stands for a rate parameter describing the rate at which growth initially accelerates and c designates a time constant describing the time elapsed between the beginning of the experiment and the turning point (point of maximal increase in biomass concentration).

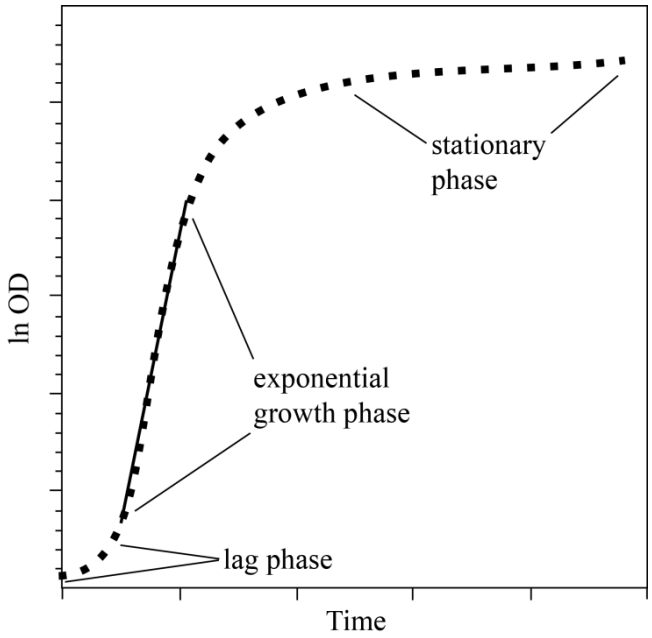

Figure 3-3. Typical bacterial growth in ln of biomass concentration versus time. After an initial lag period, bacterial growth accelerates and reaches an exponential growth phase during which the growth rate is constant. After the exponential growth, rates decelerate until the culture enters the stationary phase during which little or no growth occurs.

3.4 Results

Table A 3-2 summarizes the observed maximum biomass concentration, the calculated growth rate constant μ, and the growth in the stationary phase μ_{stat} for all experiments. A detailed list of all measurements can be found in the thesis Annex 1 on page 182ff. The bacterial cultures showed typical logistic bacterial growth, however, distinct differences were observed depending on the presence or absence of Iceland and Mississippi riverine particulate material (RPM).

3.4.1 Temporal evolution of biomass concentration in the presence and absence of 1500 mg/kg Mississippi and Iceland RPM

Figure 3-4 shows the temporal evolution of biomass concentration of representative growth experiments in the presence and absence of 1500 mg/kg Mississippi (Figure 3-4 A) and 1500 mg/kg Iceland (Figure 3-4 B) riverine particulate material. These experiments were performed at an initial pH of 5.9, a low initial nutrient concentration (BG-11 1:1000) and a medium (medium defined in the methods as 0.018 $g_{(dry)}$/kg) initial biomass concentration. The different colors in the figure correspond to different protocols of sterilization of the riverine particulate material. No bacterial growth was observed in biotic control experiments without additional RPM. However, in the presence of 1500 mg/kg MS and ICE RPM, bacteria cultures showed typical logistic growth to average maximal biomass concentrations of 0.151±0.008

$g_{(dry)}$/kg and 0.151±0.012 $g_{(dry)}$/kg, respectively. The calculated growth rate constant μ during the exponential growth phase was 0.41±0.08 and 0.37±0.08 day^{-1} for 1500 mg/kg MS and ICE RPM, respectively. In the presence of MS RPM, the exponential growth was followed by a steady increase in biomass concentration during the stationary phase at an average rate μ_{stat}= (8.4±2.2)×10^{-04} $g_{(dry)}$/kg/day. The numbers presented give the average and standard deviations of the four replicates shown in the figures. In the presence of 1500 mg/kg ICE RPM, bacteria concentration stayed constant or slightly decreased during the stationary phase. Two reactors doped with ICE RPM were stopped immediately after the exponential growth phase. The results presented in Figure 3-4 also illustrate the experimental reproducibility. The absence of bacterial growth in the biotic controls without additional RPM was consistent throughout all experimental series performed at these conditions. In the presence of 1500 mg/kg Mississippi RPM, the observed growth behavior was very consistent in all experimental series with maximal biomass concentrations varying by only ±5 %. The calculated growth rate constant μ and the post-exponential growth behavior μ_{stat} were reproducible to ±19and ±26 %. In the presence of 1500 mg/kg Iceland RPM, the maximum biomass concentration varied by ±8 % and the growth rate constant by 22 %. For both types of riverine particulate material, only the reactor where RPM were treated with H_2O_2 showed a slight offset towards lower biomass concentrations.

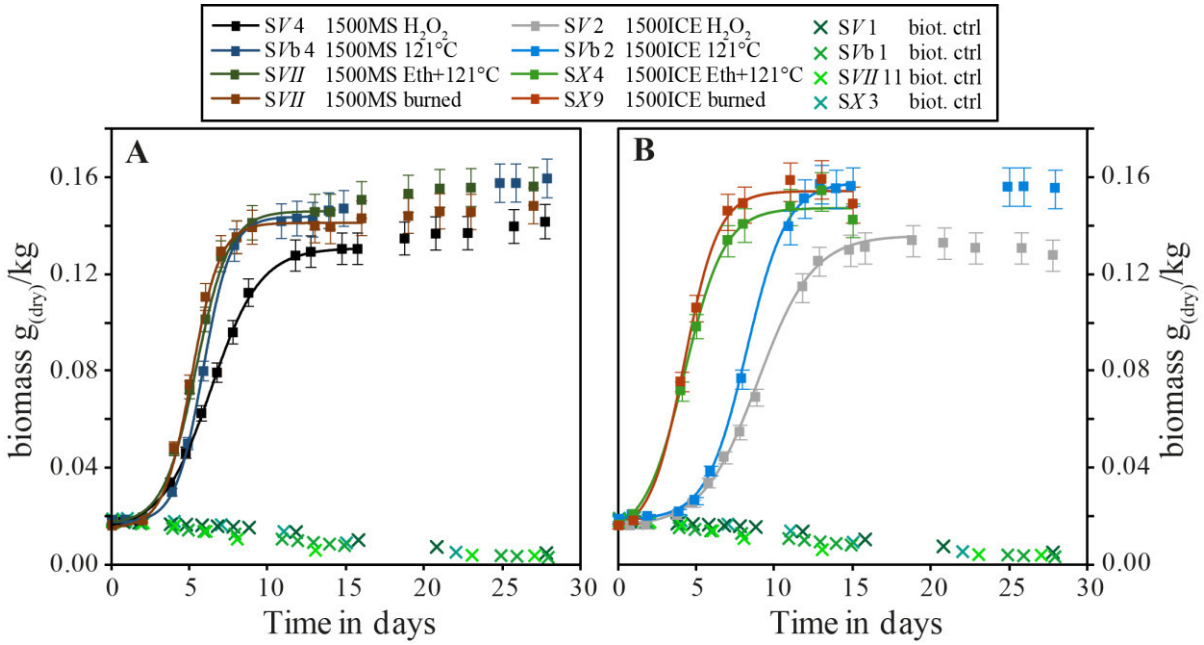

Figure 3-4. Temporal evolution of biomass concentration in selected reactors of experimental series S*V*, S*Vb*, S*VII* and S*X*. The crosses show biotic control experiments performed without riverine particulate material. Figure **A** shows experiments performed in the presence of 1500 mg/kg Mississippi RPM and Figure **B** experiments performed in the presence of 1500 mg/kg Iceland RPM. The different colors indicate different protocols followed for the sterilization of the riverine particulates. The lines indicate the fits of the logistic growth function.

3.4.2 The effect of initial biomass concentration on bacterial growth

Figure 3-5 shows the temporal evolution of biomass concentration of representative growth experiments at different initial biomass concentrations in the presence and absence of 1500 mg/kg MS and ICE riverine particulate material, respectively. The experiments were performed at initial pH of 5.9, low initial nutrient concentration (BG-11 1:1000) and 3 different initial biomass concentrations (l = low (0.007 $g_{(dry)}$/kg), m = medium (0.018 $g_{(dry)}$/kg), h = high (0.041 $g_{(dry)}$/kg)), represented by different colors. No bacterial growth was observed in biotic control experiments without additional RPM, independent of the initial biomass concentration. In the presence of MS and ICE RPM, the bacteria showed typical logistic growth in all reactors. No significant effect of the different initial biomass concentrations on the bacterial growth was observed as the growth curves were shifted parallel to one another as a function of the initial biomass concentration. However, computed growth rate constants μ increased with decreasing initial biomass concentration (find rates in Table A 3-2 in the appendix of this chapter). The post-exponential increase in biomass concentration observed in MS experiments occurred at an average rate of μ_{stat}= (11.3±2.6)×10^{-04} $g_{(dry)}$/kg/day exhibiting a good experimental reproducibility even at different initial biomass concentrations.

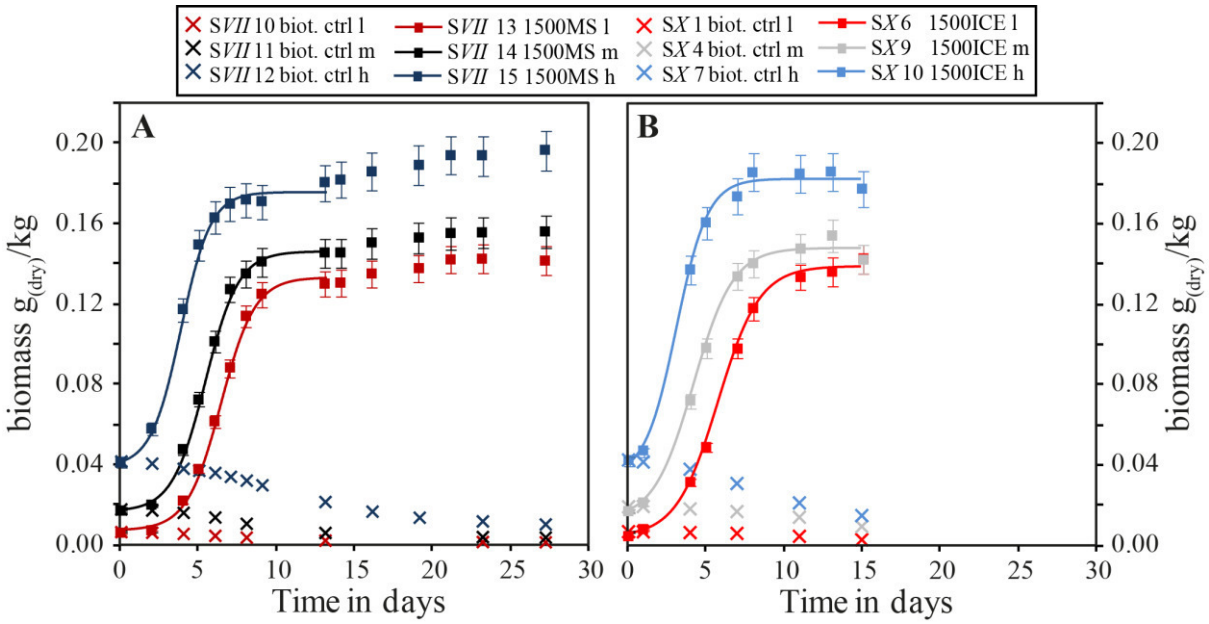

Figure 3-5. Temporal evolution of biomass concentration in selected reactors of experimental series S*VII* and S*X*. The crosses show biotic control experiments performed without riverine particulate material. Figure **A** shows experiments performed in the presence of 1500 mg/kg Mississippi RPM and Figure **B** experiments performed in the presence of 1500 mg/kg Iceland RPM which were stopped after the exponential growth phase for technical reasons. The different colors indicate different initial biomass concentrations. The lines indicate the fits of the logistic growth function.

3.4.3 Comparison of the effect of Mississippi and Iceland RPM on bacterial growth

Figure 3-6 shows the temporal evolution of biomass concentration for representative growth experiments emphasizing the distinct effects on bacterial growth of MS and ICE RPM. These experiments were performed in the presence and absence of Mississippi and Iceland RPM at an initial pH of 5.9, a low initial nutrient concentration (BG-11 1:1000) and a medium initial biomass concentration. No bacterial growth was observed in the biotic control experiments without additional RPM. Likewise, no bacterial growth was observed in the presence of 75 mg/kg MS and ICE RPM, respectively. Notably, the initial biomass concentrations decreased even faster in the presence of 75 mg/kg ICE RPM compared to 75 mg/kg MS RPM and the biotic control. In the presence of 1500 mg/kg MS and ICE RPM, bacteria showed typical logistic growth but small differences between MS and ICE experiments were evident. The maximum bacterial growth was observed 2-3 days earlier in the presence of MS RPM compared to ICE RPM (Figure 3-6 A and B). As a result, the post exponential increase in biomass concentration was notably more pronounced in MS experiments (μ_{stat}= (8.4±0.5)×10^{-04} and (10.6±0.5)×10^{-04} $g_{(dry)}$/kg/day) compared to ICE experiments, where bacteria concentrations remained constant or decreased with time (μ_{stat}= (-1.7±1.6)×10^{-04} and (-3.7±4.3)×10^{-05} $g_{(dry)}$/kg/day). The measured maximum biomass concentrations were similar for MS (0.142 and 0.159 $g_{(dry)}$/kg) and ICE (0.134 and 0.157 $g_{(dry)}$/kg) RPM. The calculated growth rate constant μ was slightly greater in MS compared to ICE experiments. Figure 3-6 B also exhibits two experiments performed in diluted BG-11 solutions (1:1000) that were previously equilibrated for one month with 1500 mg/kg MS and ICE RPM and subsequently filtered (0.22 μm filter) to remove to particulates. Again, the exponential growth phase begun notably earlier in the electrolyte equilibrated with MS compared to ICE RPM. Furthermore, the measured maximum biomass concentration was 19 % higher in the electrolyte that was equilibrated with MS RPM. In both experiments, no post-exponential growth occurred. Note however, that the total biomass concentrations were much greater in experiments performed in presence of particulates compared to the experiments in which the reactive fluids were previously equilibrated with the RPM and subsequently filtered to remove the particulates.

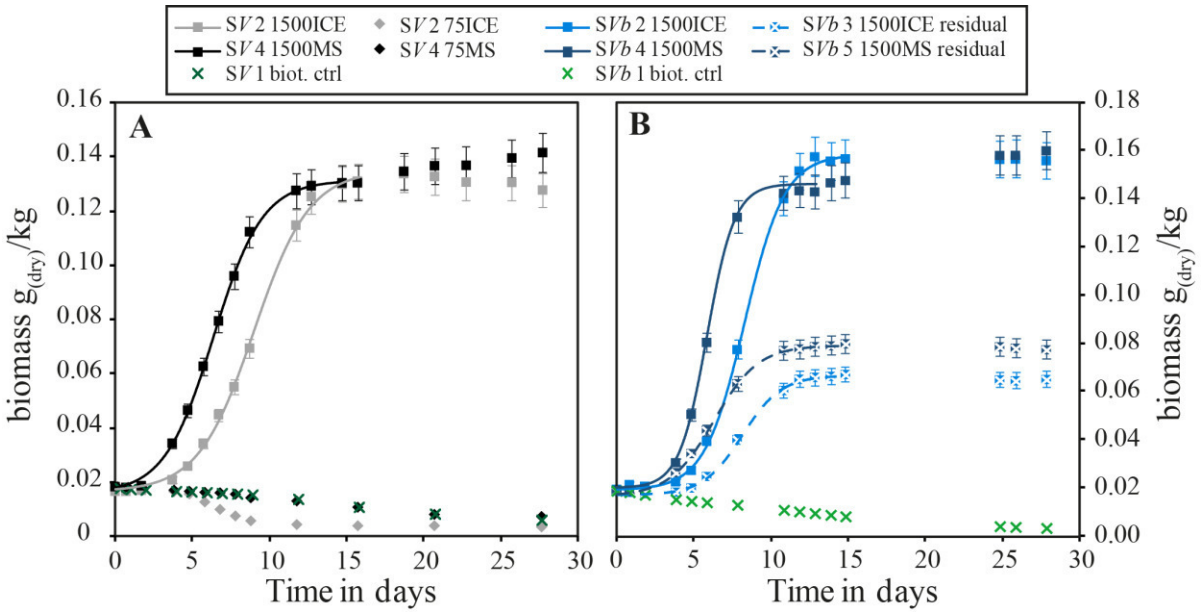

Figure 3-6. Temporal evolution of biomass concentration in selected reactors of experimental series S*V* (**A**) and S*Vb* (**B**). The x-symbols show biotic control experiments performed without riverine particulate material. Squares indicate experiments performed in the presence of 1500 mg/kg Mississippi and Iceland RPM, diamonds represent concentrations of 75 mg/kg of the indicated RPM. The crossed squares in Figure **B** depict experiments performed in solutions equilibrated with MS or ICE particulates and subsequently filtered to remove the particles before starting the experiments. The curves indicate the fits of the logistic growth function.

3.4.4 Effect of different initial conditions on bacterial growth

Figure 3-7 shows the evolution of biomass, conductivity and pH of seven experiments run at the different initial conditions summarized in Table 3-3. All biotic experiments were performed in triplicate with three different initial biomass concentrations of which the highest is shown in these figures. Bacterial growth was observed only in the reactor doped with 1500 mg/kg MS RPM and in the two reactors run at higher initial pH through the addition of NaOH and $NaHCO_3$. No growth was observed in the biotic controls without RPM, at higher initial conductivity and in the presence of 1500 mg/kg zircon particles. Note, that maximum biomass concentrations were on average 57±15 % higher in experiments doped with 1500 mg/kg Mississippi RPM compared to the control performed at an elevated initial pH through the addition of NaOH and 23±9 % higher than the control performed at higher initial pH through the addition of $NaHCO_3$. Furthermore, the biomass concentration in the presence of 1500 mg/kg Mississippi RPM increased steadily after the exponential growth phase, whereas concentrations decreased in the reactors without RPM. Details of the evolution of pH and conductivity will be discussed in section 3.4.6 together with the evolution of the aqueous fluid composition. Figure 3-8 shows the temporal evolution of biomass concentration of experiments performed with pH buffered by the addition of 0.1 mol/kg $NaHCO_3$:Na_2CO_3 in a 90:10 ratio to the diluted BG-11 nutrient solution. In all reactors instantaneous bacterial growth was observed, however, the

addition of 500 mg/kg MS RPM resulted in 12 and 20 % higher maximum biomass concentrations compared to the control reactors without RPM.

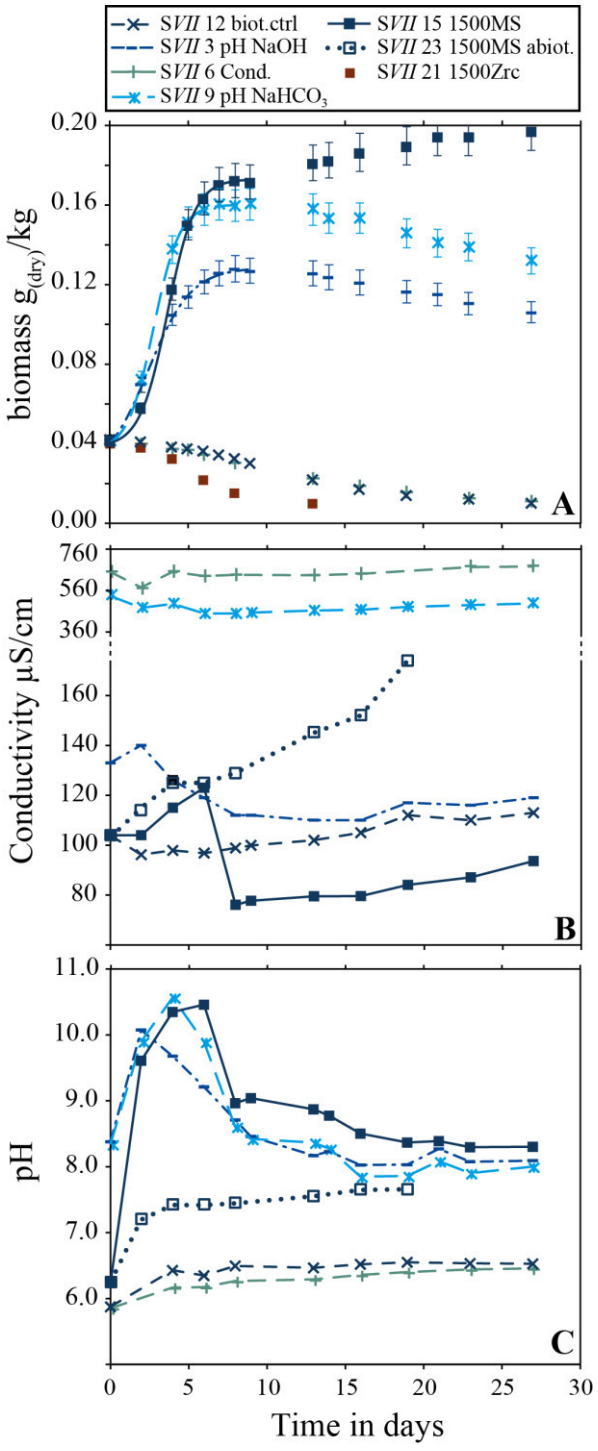

Figure 3-7. Temporal evolution of biomass concentration (**A**), Conductivity (**B**) and pH (**C**) in selected experiments of experimental series S*VII*. The lines in Figure **A** indicate the fits of the logistic growth function, lines in Figures **B** and **C** are connecting lines between data points to better illustrate the temporal evolution.

Table 3-3. Summary of experimental conditions for seven experiments performed at different initial conditions to evaluate the potential effect of pH, conductivity, Mississippi (MS) riverine particulate material (RPM) and zircon (Zrc) particles on the growth of cyanobacteria. Corresponding growth plots are shown in Figure 3-7.

Reactor ID	BG-11 dilution	Initial pH	RPM [mg/kg]	Biomass initial [$g_{(dry)}$/kg]	Conductivity [µS/cm]
S*VII* 12 biot. Ctrl	1:1000	5.9	--	0.043	104
S*VII* 3 pH NaOH	1:1000	8.4	--	0.043	133
S*VII* 6 Cond.	1:1000	5.9	--	0.043	650
S*VII* 9 pH NaHCO3	1:1000	8.3	--	0.043	535
S*VII* 15 1500MS	1:1000	6.2	1500 MS	0.043	104
S*VII* 23 1500MS abiot.	1:1000	6.3	1500 MS	no	103
S*VII* 21 1500Zrc	1:1000	n.d.	1500 Zrc	0.041	n.d.

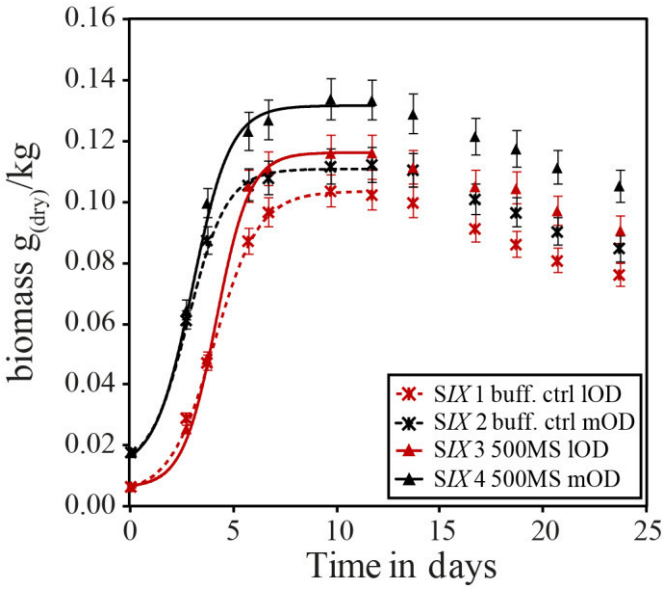

Figure 3-8. Temporal evolution of biomass concentration of experimental series S*IX*, performed in carbonate buffer solution ($pH_{initial}$ = 9.4). Crosses indicate biotic control experiments without additional RPM, triangles indicate experiments performed with 500 mg/kg MS RPM. Red colors indicate experiments performed at low initial biomass concentration, black colors indicate experiments performed at medium initial biomass concentration. The lines indicate the fits of the logistic growth function.

3.4.5 Effect of different riverine particulate material concentrations on bacterial growth

Figure 3-9 illustrates the effect of different RPM concentrations on bacterial growth. These experiments were performed at a low initial nutrient concentration (BG-11 1:1000) and high initial biomass concentration in the absence and presence of various concentrations of MS RPM. Note that corresponding experiments were not performed using the Icelandic RPM. At an initial pH of 5.9 (Figure 3-9 A), no bacterial growth was observed in the biotic control in the absence of RPM. The addition of 500, 1000 and 1500 mg/kg MS RPM triggered instantaneous bacterial growth whereby the maximum biomass concentration increased with increasing RPM concentration. The addition of 75 mg/kg MS particulates provoked growth only after a lag phase

of about twenty days. Furthermore, the post-exponential increase in biomass concentration was more pronounced at higher RPM concentrations. At a slightly higher initial pH of 6.8 (Figure 3-9 B), bacteria in all reactors including the biotic control grew instantaneously. The effect of higher initial pH on the growth of the biotic control was also observed in the other experiments described above. However, with increasing RPM concentration, exponential growth was observed earlier and the maximum biomass concentrations were higher. The measured maximum biomass concentrations presented in Figure 3-9 B increased by 5, 16, 19 and 32 % with the addition of 75, 500, 1000 and 1500 mg/kg MS RPM compared to the biotic control. Again, the post-exponential increase in biomass concentration was more pronounced at higher RPM concentrations. Figure 3-10 illustrates the effect of different RPM concentrations on bacterial growth in experiments performed at 2.67 times higher initial nutrient concentrations (BG-11 1:375). The biotic control experiment without RPM showed bacterial growth only after a lag phase of about two weeks, whereas experiments run in the presence of Mississippi RPM showed either instantaneous bacterial growth or a significantly shorter lag phase. Furthermore, the presence of riverine particulates noticeably increased the total biomass concentration as a function of RPM concentration. The measured maximum biomass concentrations presented in Figure 3-10 increased by 6, 14, 15 and 21 % with the addition of 75, 500, 1000 and 1500 mg/kg MS RPM compared to the biotic control. There was no post-exponential bacteria growth observed in this experimental series.

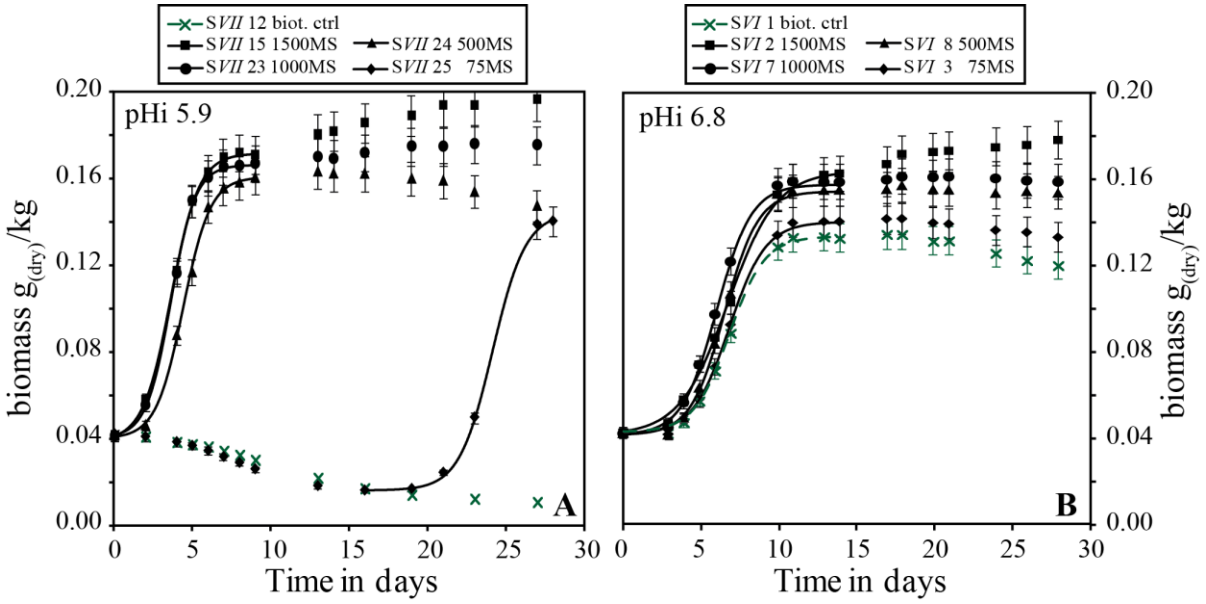

Figure 3-9. Temporal evolution of biomass concentration in selected experiments of experimental series S*VII* (**A**), performed at an initial pH of 5.9 and experimental series S*VI* (**B**), performed at an initial pH of 6.8. Crosses indicate biotic controls, diamonds, triangles, circles and squares represent 75, 500, 1000 and 1500 mg/kg Mississippi RPM, respectively. The lines indicate the fits of the logistic growth function.

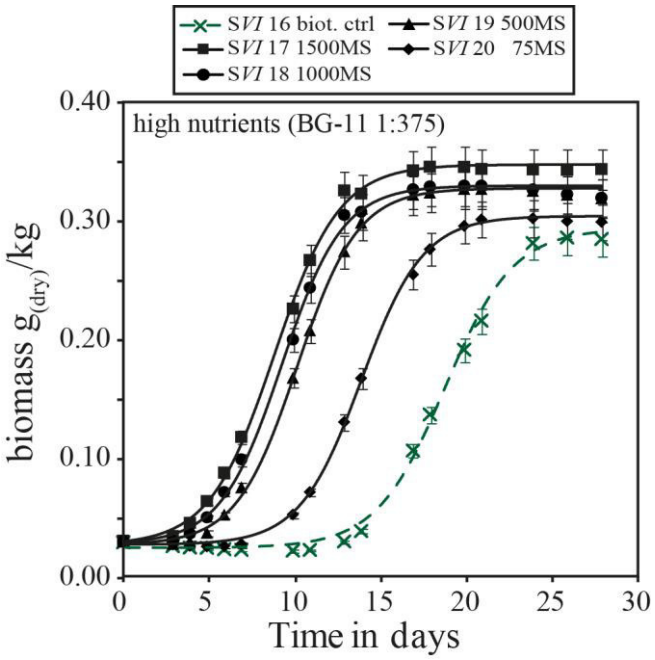

Figure 3-10. The evolution of biomass concentration in selected experiments of experimental series S*VI*, performed at elevated initial nutrient concentrations. Crosses indicate biotic controls, diamonds, triangles, circles and squares represent 75, 500, 1000 and 1500 mg/kg Mississippi RPM, respectively. The lines indicate the fits of the logistic growth function.

3.4.6 The temporal evolution of the reactive fluid compositions

3.4.6.1 The temporal evolution of pH and dissolved inorganic carbon (DIC)

Figure 3-11 shows the temporal evolution of biomass, pH and DIC concentration of the reactive fluids collected during experimental series S*V*. In the biotic control experiment, no growth was observed and pH increased slightly from initially 5.9 to a final pH of 6.6. In the abiotic control experiments, pH increased from 5.9 to 7.6 and 7.0 for reactors doped with 1500 mg/kg MS and ICE RPM, respectively. In the biotic experiments doped with 1500 mg/kg MS and ICE RPM, the bacterial growth resulted in a pH increase from initially 5.9 to 10.6 and 10.1, respectively. The elevated pH persisted during the exponential growth phase and was followed by a pH drop to final values of 8.2 and 7.6, respectively. This pH evolution is closely linked to the DIC concentration. In the biotic control, DIC concentrations were constant at 0.7 - 0.9 ppm throughout the experiment. In the abiotic control doped with 1500 mg/kg MS RPM, DIC increased from 0.8 to 4.9 ppm during the experiment, while DIC in the abiotic control doped with 1500 mg/kg ICE RPM only slightly increased from 0.8 to 1.4 ppm. The greater increase observed in the presence of MS compared to ICE RPM is consistent with the higher pH in MS experiments and the increasing solubility of $CO_{2(g)}$ at higher pH. In both biotic experiments in the presence of RPM, DIC increased significantly as a consequence of the high pH resulting from the photosynthetic activity of the growing bacteria. During the exponential growth phase,

DIC increased from 1.0 to 8.5 ppm and from 0.8 to 6.6 ppm in the presence of 1500 mg/kg MS and ICE RPM, respectively. After the exponential growth, DIC increased slightly from 8.5 to 9.6 ppm in the MS experiment and dropped from 6.6 to 5.3 ppm in the ICE experiment.

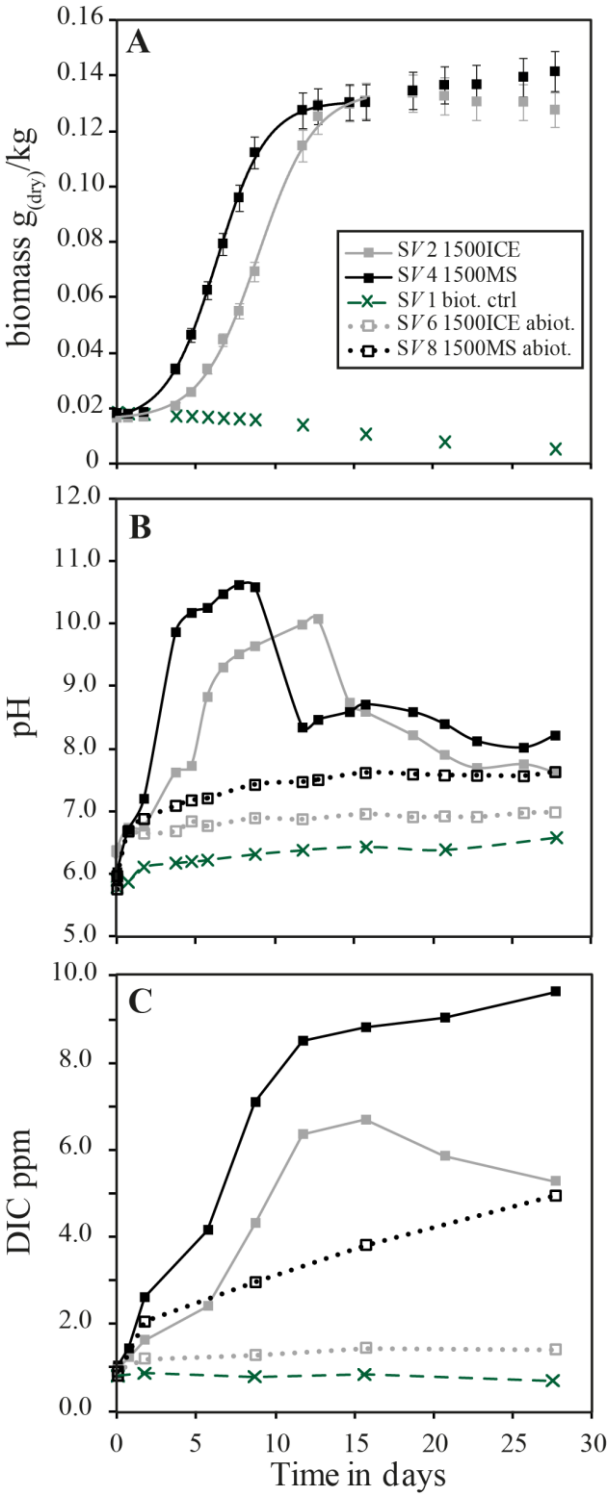

Figure 3-11. Temporal evolution of biomass concentration (**A**), pH (**B**) and dissolved inorganic carbon (**C**) in selected experiments of experimental series S*V*. Crosses represent biotic controls, squares indicated experiments performed in the presence of 1500 mg/kg MS and ICE RPM. Open squares indicate abiotic controls. The lines in Figure **A** indicate the fits of the logistic growth function, lines in Figures **B** and **C** are connecting lines between data points to better illustrate the temporal evolution.

3.4.6.2 The evolution of major and trace elements

Figure 3-12 shows the temporal evolution of selected elements in reactive fluid samples collected from experimental series S*V*. The green dashed line represents the biotic control experiment without RPM, the open squares depict the abiotic control experiments with 1500 mg/kg MS and ICE RPM but without bacteria and the filled squares depict the experiments with RPM and bacteria. Note that no growth was observed in the biotic control without RPM (see Figure 3-11 A). Figure 3-12 A depicts the temporal evolution of Si concentration; Si concentration increases due to the dissolution of silicate minerals. The Si concentration in the biotic control remained constant at 218±36 ppb. Silicon concentrations in the abiotic and biotic reactors doped with Mississippi RPM showed an initial increase from 225 ppb and 116 ppb to 367±34 ppb and 382±25 ppb, where they remained constant through the rest of the experiments. Silicon concentrations in the abiotic and biotic reactors doped with Iceland RPM increased during the first five days at a similar rate from 206 ppb and 144 ppb to 994±12 ppb and 1064±18 ppb. During the following 22 days, the Si concentration in the biotic ICE experiment increased to a much greater extent reaching a final concentration of 4360±8 ppb compared to 2221±8 ppb in the abiotic control. A similar temporal evolution was observed for dissolved aluminum concentrations.

Figure 3-12 B shows the temporal evolution of Ca concentration. Calcium concentration in the biotic control increased during the experiment from 294±2 ppb to 432±3 ppb. The Ca concentration in the abiotic controls increased from initially 803±5 ppb and 970±3 ppb to 4567±16 ppb and 1776±8 ppb in the presence of dissolving Mississippi and Iceland RPM, respectively. In the biotic experiments doped with MS and ICE RPM, Ca concentrations increased during the first four days from 694±9 ppb and 956±5 ppb to 1221±2 ppb and 1221±1 ppb, then decreased to 113±1 ppb and 234±7 ppb, respectively. Similar trends were observed for the concentrations of Mn and Mg.

Figure 3-12 C and D show the temporal evolution of dissolved Fe and P concentrations, representing possible limiting nutrients. Initial Fe concentrations were at 35±6 ppb in all reactors. In the biotic control, Fe concentration decreased during the first days to 6 ppb and subsequently increased to a final concentration of 16 ppb. In the abiotic MS control, Fe concentration decreased to 9 ppb, whereas Fe concentration remained constant at 37±8 ppb in the control doped with ICE RPM. Similarly, the biotic experiments doped with MS and ICE RPM showed distinct temporal evolutions of Fe concentrations. In the biotic MS experiment, Fe decreased to about 4 ppb, whereas Fe concentrations in the biotic ICE experiment increased

continuously to 257±4 ppb. Phosphate concentrations were initially at about 260 ppb in all reactors. In the biotic control, P concentration initially dropped below detection limit and subsequently increased again towards the initial concentration. P concentration remained constant in the abiotic MS control at 251±15 ppb, whereas it decreased steadily in the abiotic ICE control from initially 262±2 ppb to 105 ppb. In the biotic MS and ICE experiments, P concentrations initially dropped to less than 10 ppb. In the biotic MS experiment, the concentration remained near zero throughout the experiment. In the biotic ICE experiment, the initial drop in P concentrations was followed by a steady increase to a final concentration of 24 ppb.

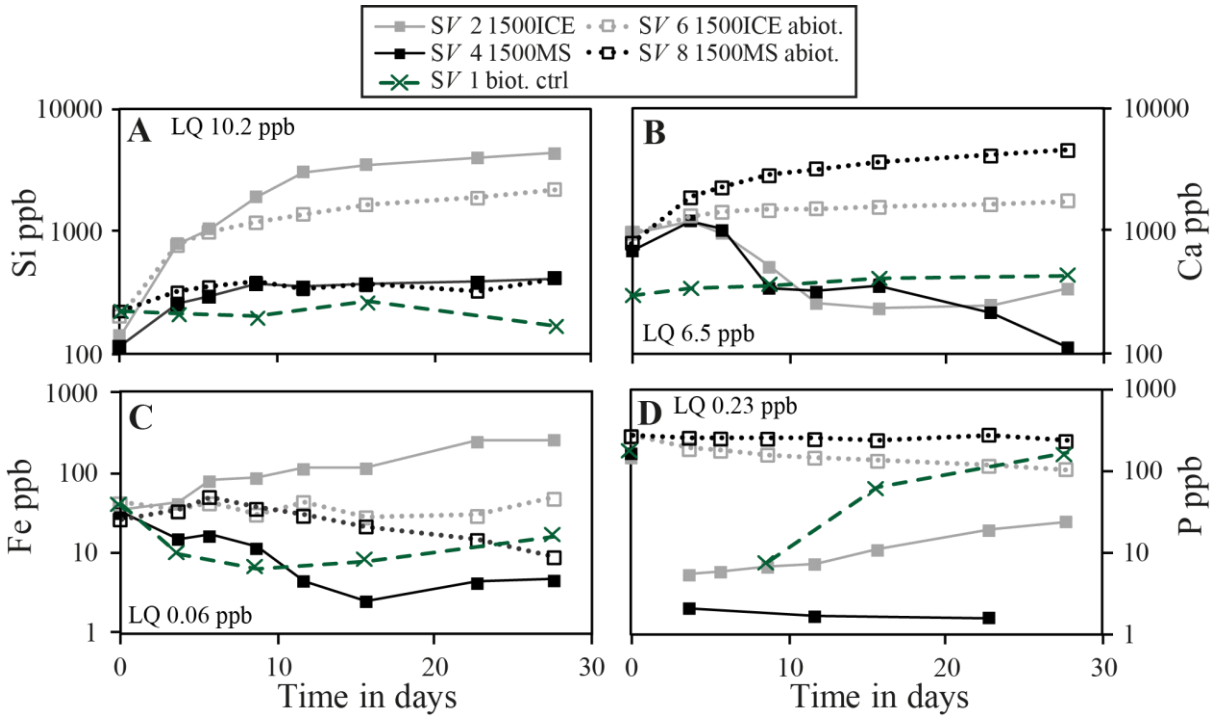

Figure 3-12. Temporal silicon (**A**), calcium (**B**), iron (**C**) and phosphorus (**D**) concentration of selected experiments of experimental series S*V*. Crosses represent biotic controls, squares indicated experiments performed in the presence of 1500 mg/kg MS and ICE RPM. Open squares indicate abiotic controls. The lines are connecting lines between data points to better illustrate the temporal evolution.

3.4.7 SEM investigation of riverine particulate material

In experimental series S*III*, a few mg of the ICE and MS riverine particulate material were sampled during the exponential growth phase of the bacteria and were investigated by SEM. Figures 3-13 A-D show representative SEM images of Mississippi particulate material. No morphological differences were evident between the initial particulates and the particulates sampled during bacterial growth but occasionally, bacteria were found attached to feldspar grains (Figure 3-13 B). Clusters of agglomerated bacteria were frequent, as evident in Figure 3-13 A and depicted in detail in Figure 3-13 C. These agglomerations were associated with mineral fragments (Figure 3-13 D), predominantly clays. Figures 3-13 E-F show representative images of Iceland particulate material. Again, no major morphological changes compared to the initial material were evident. However, the basaltic glass particles were frequently covered by cyanobacteria, as indicated in Figure 3-13 E and illustrated in Figure 3-13 F. The bacteria appeared mostly in vesicles of basaltic glass particles. In closer detail, the cyanobacteria were found to be attached to the mineral surface through organic fibers (Figure 3-13 G and Figure 3-13 H). Note, that the bacteria attached on mineral surfaces are not accounted for in the spectrophotometric determination of biomass concentration due to settling of particles in the cuvette. Consequently, the total biomass concentration in experiments doped with RPM is likely higher than the values reported.

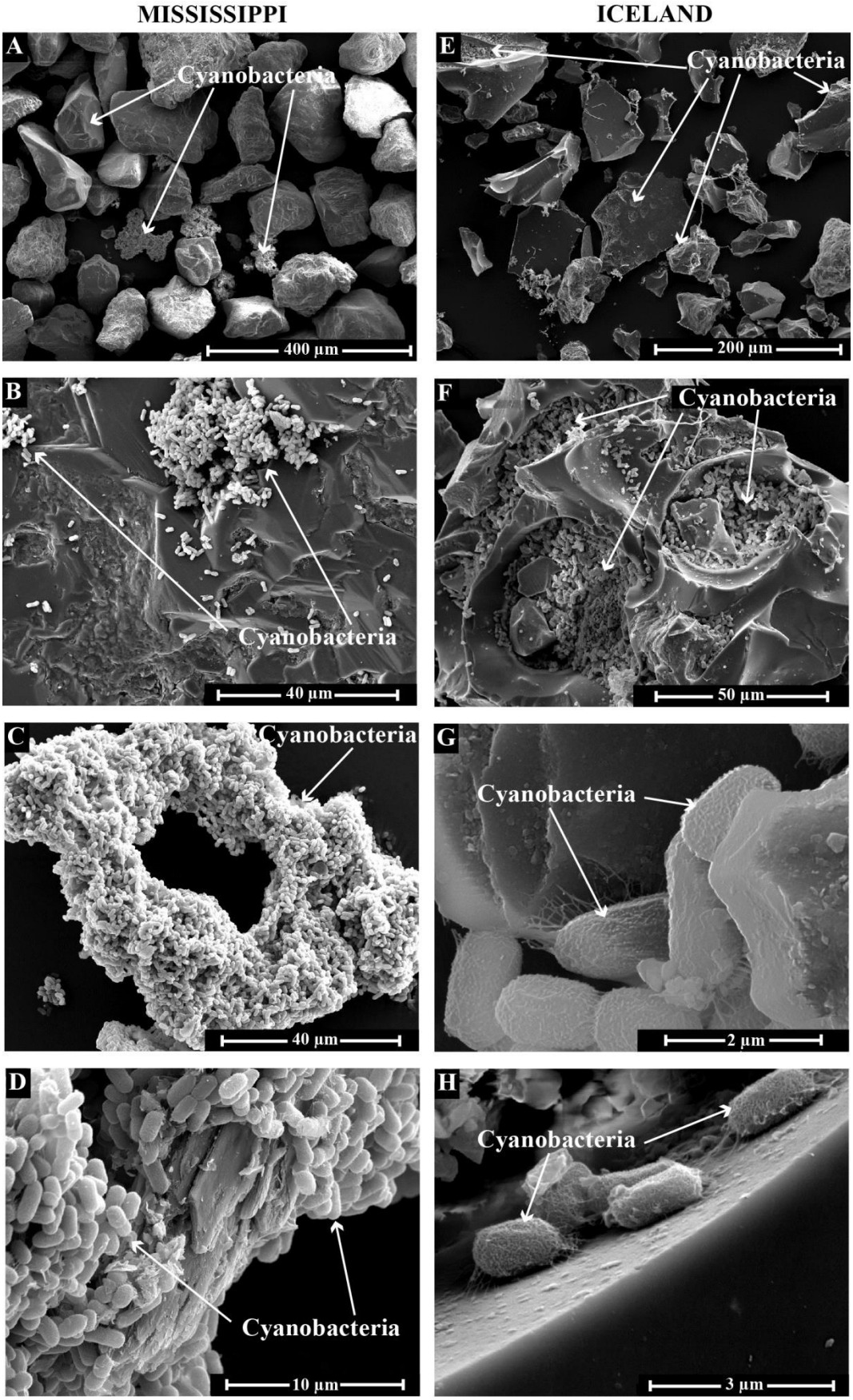

Figure 3-13. SEM microphotographs of Mississippi (**A**-**D**) and Iceland (**E**-**H**) riverine particulate material sampled during the exponential growth phase of experimental series S*III*.

3.5 Discussion

3.5.1 The effects of riverine particulate material on the growth of Synechococcus sp. freshwater cyanobacteria

The results presented above illustrate the distinct effects of riverine particulate material on the growth of *Synechococcus sp.* freshwater cyanobacteria. Firstly, at low initial nutrient concentrations and an initial pH of 5.9, the presence of Mississippi and Iceland RPM triggered bacterial growth whereas bacteria cultures in biotic controls without riverine particulates did not grow. This growth triggering effect is best illustrated in Figures 3-4, 3-5, 3-6, 3-7 A, 3-9 A and 3-11 A. In growth experiments performed at higher initial pH, bacterial growth was observed in the biotic control experiments, as illustrated in Figures 3-7 A, 3-8, and 3-9 B. Similarly bacterial growth was observed in biotic control experiments in an experiment run at high initial nutrient concentration (see Figure 3-10). Bacterial growth, however, occurred earlier in the presence of riverine particulate material. This is best illustrated in Figure 3-10, where the maximum bacterial growth was observed after 8.7, 9.1, 10.0 and 13.8 days in growth experiments performed in the presence of 1500, 1000, 500 and 75 mg/kg MS RPM and only after 18.7 in the biotic control without RPM. Furthermore, the maximum biomass concentrations increased as a function of RPM concentration. This effect is summarized for all experiments containing Mississippi RPM in Figure 3-14, which shows the highest biomass concentration measured in each experiment plotted against the MS RPM concentration added to the reactors. The illustrated biotic controls at zero RPM were all conducted at $pH_{inital} \geq 6.8$ because no growth was observed at lower pH. The biomass concentration in these biotic controls is limited by the initial nutrient concentration and varies as a function of BG-11 dilution (black symbols show experiments performed at higher nutrient concentration). Additional bacterial growth at a given BG-11 concentration only occurs from the additional nutrients delivered from dissolving the riverine particulates. To a first approximation, the maximum biomass concentration increased linearly with increasing MS RPM concentration as shown in Figure 3-14 by the linear regression of the data. The maximum biomass concentration increased by $(2.5\pm0.5)\times10^{-5}$ and $(4.8\pm0.9)\times10^{-5}$ $g_{(dry)}$/kg with each mg/kg MS RPM added to the reactor. This yields an increase of about 15, 35 and 32 % for the addition of 500, 1000 and 1500 mg/kg MS riverine particulate material compared to biotic controls without RPM. The presence of riverine particulates also influenced the evolution of the biomass concentration in the stationary phase. The presence of MS RPM resulted in a continuous increase of the biomass concentration after the exponential growth phase, whereas biomass concentration stayed constant or

decreased when no particulates were added to the reactors. This observation is most evident in Figure 3-7 A, where bacteria concentration continuously increased in the stationary phase in the presence of 1500 mg/kg MS RPM but notably decreased in biotic controls without particulates.Figure 3-9 illustrates the same effect as a function of particulate concentration. Figure 3-15 summarizes the post-exponential growth behavior obtained by linear regression of the biomass concentration measured after the exponential growth phase as a function of the riverine particulate concentration (only for MS) for all experiments. In the biotic controls, biomass concentrations decreased at an average rate of μ_{stat}= (-12.0±6.2)×10^{-4} $g_{(dry)}$/kg/day. With increasing MS RPM concentration this rate became positive reaching an average of μ_{stat}= (+9.3±3.6)×10^{-4} $g_{(dry)}$/kg/day in the presence of 1500 mg/kg MS particulates. The effect of both types of RPM on the growth rate constant μ was small and no clear trend was evident.

In summary, riverine particulate material has three major effects on the growth of freshwater cyanobacteria *Synechococcus sp*. First, RPM triggers bacterial growth if the pH of the aqueous fluid is below 6. Second, the presence of RPM increases the total biomass concentration with increasing particulate concentration and third, the presence of particulate material causes a post-exponential long-term growth of the cyanobacteria, likewise as a function of RPM concentration.

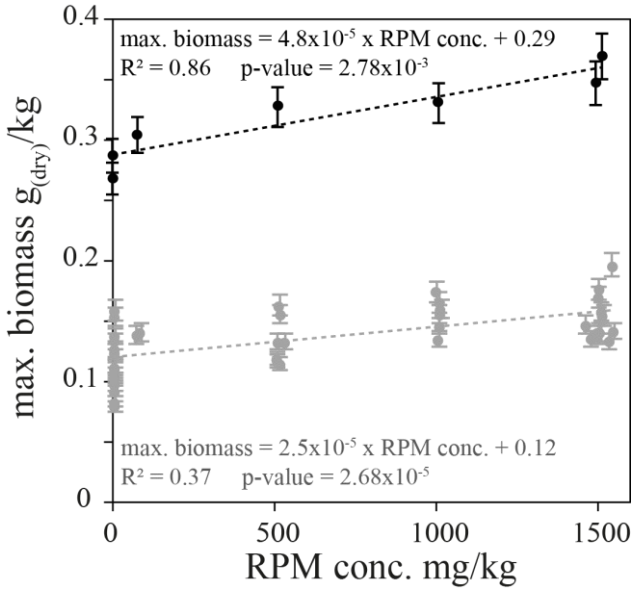

Figure 3-14. Highest biomass concentration measured in each reactor where growth was observed plotted against the Mississippi RPM concentration added to the reactors. Biotic controls at zero RPM were all conducted at elevated initial pH≥6.8. The black symbols indicate experiments performed at elevated nutrient concentration (BG11 1:375 dilution), the grey symbols indicate experiments performed at lower nutrient concentrations (BG11 1:1000 dilution). The dotted lines represent linear regressions of the data.

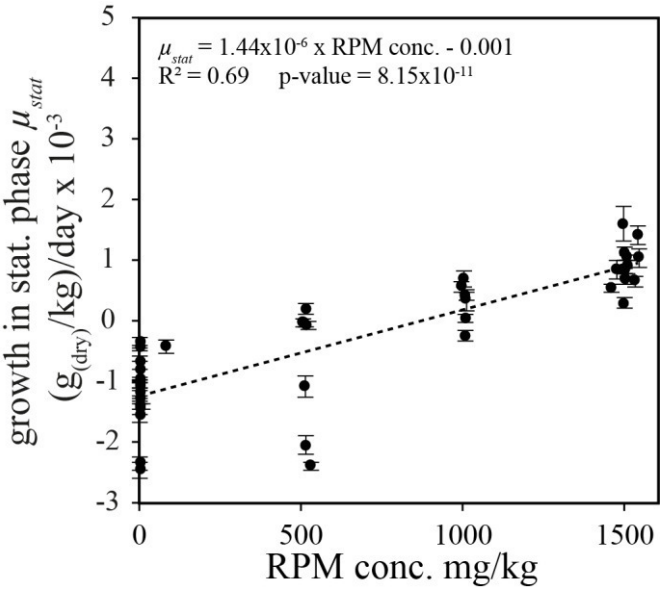

Figure 3-15. Growth behavior in the stationary phase as a function of Mississippi RPM concentration. Biotic controls at zero RPM were all conducted at elevated initial pH≥6.8. The growth in stationary phase μ_{stat} was obtained by linear regression of the biomass concentrations after the exponential growth phase. The dotted line depicts the linear regression of the plotted data.

3.5.2 How does riverine particulate material increase bacterial growth?

To evaluate what triggered bacterial growth in the presence of RPM, five possible influencing factors were tested: 1) the addition of organic compounds stemming from the particulates, 2) the physical presence of the particulate surfaces, 3) the slight increase in ionic strength resulting from dissolving particulates, 4) a pH increase resulting from particulate dissolution, and 5) an increased nutrient concentration due to particulate dissolution. To address these factors, growth experiments were performed with distinct initial conditions including: 1) RPM burning at 450 °C to exclude external potential organic compounds, 2) addition of zircon particles to mimic the presence of inert mineral surfaces, 3) higher initial ionic strength by the addition of NaCl, 4) higher initial pH by addition of NaOH or carbonate buffers and 5) higher initial nutrient concentrations.

Results of these experiments are shown in Figures 3-4, 3-7, 3-8 and 3-10. Figure 3-4 shows the evolution of biomass of four replicate experiments performed in different experimental series whereby the replicates differ only in the protocol applied for the sterilization of the riverine particulate material. To eliminate a potential organic contamination introduced by the RPM, the particulates were sterilized by either H_2O_2 treatment, by dry sterilization at 121 °C for 12 h with or without previous ethanol treatment, or by heating for 2.5 h at 450 °C. Similar bacterial growth was observed in all reactors suggesting that organic contamination was not a major factor influencing growth rates and that different treatments did

not result in major surface change effects. Only the reactor where RPM were treated with H_2O_2 showed a slight offset towards lower biomass concentrations.

Figure 3-7 shows the evolution of biomass, conductivity and pH of seven reactors run at different initial conditions, summarized in Table 3-3. In the biotic control experiments performed at higher initial pH, bacteria showed logistic growth, however, to 23-57 % lower final biomass concentrations compared to reactors run with 1500 mg/kg Mississippi RPM. This observation suggests that the initial growth triggering effect of the RPM stems at least in part from the increase in pH caused by the dissolution of the particulates. This is in agreement with growth experiments performed by Bundeleva et al. (2014) who observed growth only at pH ≥7.3 for the same species. Neither the presence of zircon nor increasing ionic strength changed bacterial growth rates. However, the biotic control where pH was increased through the addition of $NaHCO_3$ showed higher biomass concentrations compared to the control where initial pH was increased by NaOH. This suggests that C-availability is also critical for the bacterial growth. Thus, a series of experiments was performed in carbonate buffer solutions (0.1 mol/kg DIC) to keep pH constant and provide sufficient C for bacterial growth. These results, presented in Figure 3-8, show that even at these conditions, the presence of 500 mg/kg Mississippi RPM increased the maximum biomass concentrations by 12 and 20 % compared to the control reactors without RPM. Similarly, at high nutrient concentrations, biotic controls showed lagged growth but the presence of RPM resulted in 6-21 % greater biomass concentrations (see Figure 3-10).

In summary, results indicate that one factor leading to increased biomass in the presence of RPM is the increase of pH due to mineral dissolution. However, even at favorable initial conditions (higher initial pH, carbonate buffered fluid or higher initial nutrient concentration), the presence of RPM resulted in 1) higher maximum biomass concentrations and 2) a continuous post-exponential increase in biomass concentration at high RPM concentrations. The post-exponential growth was only evident for MS particulates, which were studied in more detail. It therefore seems likely that such additional growth stems from nutrient release from the RPM. To illuminate this hypothesis, the chemical evolution of the aqueous fluid was investigated in selected experiments and results are presented in Figure 3-11 and Figure 3-12. Note, that the interpretation of the aqueous fluid composition in these experiments is challenging since multiple biogeochemical processes occur simultaneously. Besides dissolution of the riverine particulate material and consumption of nutrients by growing cyanobacteria, processes as secondary phase precipitation or ad- and desorption of elements on mineral or

bacteria surfaces may influence the temporal evolution of each element. Furthermore, changes in pH and dissolved organic matter concentration change the solubility of each element during the experiments. Figure 3-12 A shows the evolution of Si concentration, which changes due to silicate mineral dissolution. Two important observations are evident in this figure. First, the silicates in Iceland RPM dissolve faster than those in Mississippi particulates. Note that Mississippi RPM is primarily composed of quartz and feldspar whereas Iceland RPM is composed of basalt and basaltic glass which dissolve faster at these conditions (Gislason and Oelkers, 2003). Second, the silicate minerals in the biotic reactors dissolve faster compared to those in the abiotic reactors due to the pH increase induced by growing cyanobacteria and the decreased stability of alumosilicate minerals at higher pH. Figure 3-12 B shows the temporal evolution of Ca concentration. Again, two important observations are evident in this figure. First, Mississippi RPM releases far more Ca (as well as Mn and Mg) to the aqueous fluid compared to Iceland RPM, likely due to trace amounts of carbonate minerals in these RPM. Second, in the biotic experiments doped with MS and ICE RPM, Ca concentrations dropped after a few days. This drop in Ca (also observed for Mg and Mn) coincides with the drop in conductivity (see Figure 3-7 B) and may stem from the precipitation of carbonate minerals triggered by increasing pH due to the metabolic activity of the growing cyanobacteria. Figure 3-12 C and Figure 3-12 D show the temporal evolution of Fe and P concentrations. The ICE particulates delivered much more Fe compared to the MS RPM, which did however not result in a more pronounced bacterial growth as can be seen in Figure 3-11 A. Phosphate concentrations in all biotic experiments indicate complete consumption of this element by the biomass, even in the biotic control where no growth was observed. The concentrations close to zero throughout the biotic experiment doped with 1500 mg/kg MS RPM, which exhibited post-exponential bacterial growth, indicate that growth was P limited. However, MS RPM did not release significant amounts of P to the fluid phase in the absence of bacteria as indicated by the corresponding abiotic control. It is remarkable that MS RPM showed a greater increase in biomass compared to the ICE RPM, even though Iceland particulates contain much more Fe and P and the silicate minerals in these particulates dissolve more rapidly. One possibility is that the attachment of bacteria to the surface of the minerals in this RPM limits particle dissolution of mafic minerals such as observed by Oelkers et al. (2015). Moreover, we suggest that certain accessory phases, such as carbonates or clay minerals, which readily exchange their interlayer cations, or the presence of highly reactive nanoparticles adhering to larger grains (Poulton and Raiswell, 2005) might be most efficient in increasing bacterial growth. Furthermore, the stronger effect of Mississippi particulates might stem from a higher

concentration of adsorbed nutrients on MS particle surfaces, impacted by anthropogenic and agricultural activity.

The SEM investigations of the riverine particulate material showed that cyanobacteria were frequently found attached through organic fibers on particle surfaces, especially on clays in Mississippi RPM and on basaltic glass fragments in Iceland RPM (see Figure 3-13). This direct attachment of microbes on the particle surfaces suggests that the cyanobacteria are able to directly acquire the limiting nutrient from the minerals through an increase in production of exopolymeric substances (EPS) and transparent exopolymeric particles (TEP). The ability of microbes to acquire limiting nutrients directly from the mineral phase has been shown by numerous past studies including Bailey et al. (2009), Rogers et al. (1998), Rogers and Bennett (2004), Bonneville et al. (2011), Smits et al. (2012) and Sudek et al. (2017).

Furthermore, the direct attachment of bacteria on the mineral surface together with the highly alkaline pH produced by the bacteria can increase the dissolution rate of the silicate minerals in the particulates. This has been shown in numerous studies (Bennett et al., 2001; Drever and Stillings, 1997; Olsson-Francis et al., 2012; Rogers and Bennett, 2004; Uroz et al., 2009; Wu et al., 2007; 2008). In this study, bacteria likewise indirectly enhanced mineral dissolution by altering pH and potentially also through the production of organic ligands. This creates a positive interplay between bacteria and minerals where mineral dissolution enhances bacterial growth though nutrient release and the enhanced bacterial activity accelerates mineral dissolution through altering the aqueous solution concentration. This feedback may also be facilitated and enhanced by the direct attachment of the bacteria to the mineral surfaces. As shown in Figure 3-16, the direct attachment of bacteria on mineral surfaces was also observed in natural samples. These samples were collected in early May 2014 at the South coast of Iceland, at the river mouth of Ölfusá river and were prepared as described for the experimental samples. Microbes were frequently found attached on basaltic particulate material.

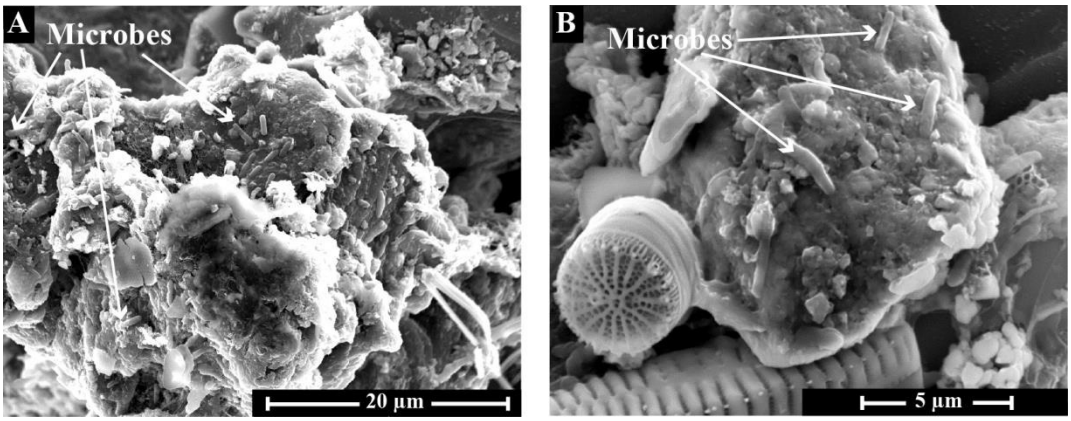

Figure 3-16. SEM images showing microbes attached on mineral surfaces in natural systems. Samples were taken in an estuary at the South coast of Iceland in spring 2014.

3.5.3 Potential role of riverine particulate material in natural environments

The potential role of river transported particulate material on global element cycles has received attention as particulates dominate the transport of limiting nutrients to the oceans compared to dissolved riverine transport (Jeandel and Oelkers, 2015). Nutrients transported in particulate form likely act as slow release fertilizer for primary productivity. The results obtained in this study validate the role of particulate material on primary productivity in freshwater environments and suggest that such particles influence the natural biotic carbon cycle.

Riverine particulate material likely enhance bacterial growth in natural nutrient limited systems. Moreover, in certain environments, particulates might trigger calcite precipitation. A number of studies described calcite precipitation induced by algae or cyanobacteria blooms in natural lakes (Hodell et al., 1998; Stabel, 1986; Thompson et al., 1997). Notably, Thompson et al. (1997) emphasized *Synechococcus sp.* cyanobacteria as especially suitable for calcite precipitation and observed calcite precipitates in the alkaline microenvironment around the cells. Thompson et al. (1997) furthermore mentioned that *Synechococcus sp.* also exhibit a benthic growth habit, colonizing various surfaces. As shown in this study, dissolving particulates deliver limiting nutrients available for bacterial growth and may act as substrates on which bacteria can grow. The physical contact between the cells and the particle surface can accelerate their dissolution, thus liberating, depending on the mineralogy of the particulates, divalent cations ready to form carbonates. Thus, we hypothesize a potential role of particulate material in triggering algae blooms and simultaneously occurring whiting events.

Phytoplankton blooms commonly occur during spring and early summer, when temperature rises and light availability is maximize. During spring, however, fluxes of riverine

particulate material also maximize. Gislason et al. (2006) reported a variation in Ca particulate fluxes of 4.5 orders of magnitude over the course of a year in a glacial river in NE Iceland with maximum particulate fluxes during spring and late summer. Thus, times of increased primary production coincide with times of highest particulate nutrient fluxes. The effect of riverine particulate material on phytoplankton growth in natural systems, however, requires a case-by-case study depending on various environmental factors such as nutrient availability and nutrient ratios, light conditions and the distribution of phytoplankton species. For example, Baisre and Arboleya (2006) described a drastic reduction in nutrient concentrations resulting from decreasing sediment concentration in a Cuban estuary following upstream dam constructions. This had a profound negative influence on the estuary ecosystem and hence, on local fisheries. In contrast, Jiang et al. (2014) and Chen et al. (2017) observed increasing chlorophyll a concentrations with decreasing suspended sediment input in Chinese estuaries, as a consequence of dam constructions. This might occur in highly eutrophic systems, where light availability limits primary productivity.

The global impact of river damming on biogeochemical cycles has long been recognized and numerous studies described the degree and the consequences of retention of particulates and nutrients in dammed river systems (Baisre and Arboleya, 2006; Bergkamp et al., 2000; Eiriksdottir et al., 2017; Friedl and Wüest, 2002; Humborg et al., 2000; Maavara et al., 2015; Syvitski et al., 2005; Teodoru and Wehrli, 2005; Vörösmarty et al., 2003; Walling, 2006). Syvitski et al. (2005) estimated a reduction of the global riverine flux of particulates to the oceans by 1.4 Gt $year^{-1}$ due to retention within reservoirs. The main negative impacts of these trapped particulates mentioned are the reduced storage capacity and thus, the reduced operational time of the reservoirs, as well as coastal retreat due to reduced particulate supply to coastal regions (Bergkamp et al., 2000; Syvitski et al., 2005). Studies exploring the effect of river damming on nutrient dynamics usually consider the dissolved and organic nutrient fluxes and assume that the inorganic particulate flux is not bioavailable. Maavara et al. (2015) for example estimated a global annual P retention for the year 2000 of 42 Gmol from which 18 Gmol was ‘reactive phosphorous’ and 24 Gmol considered as ‘unreactive particulate P’, mainly composed of crystalline phosphate-bearing minerals. The results obtained in this study, however, suggest that inorganic particulates may as well be bioavailable and may directly serve as slow release fertilizer for phytoplankton. Besides the drastic reduction of particulate material, dam construction causes notable alterations of nutrient ratios (Friedl and Wüest, 2002; Humborg et al., 2000; Maavara et al., 2015). Whereas the retention of P and N in artificial

reservoirs counteracts anthropogenic eutrophication, the retention of Si is believed to cause harmful algae blooms in downstream environments due to changing phytoplankton species distribution (Chen et al., 2017; Humborg et al., 2000). The role of riverine suspended material in buffering nutrient ratios and thus, its effect on algae blooms has yet to be investigated.

Note that the role of riverine particulate material on primary productivity is likely of global importance in marine systems. Jeandel and Oelkers (2015) summarized the effects of riverine particulate material on ocean elemental budgets and on the global carbon cycle. They conclude that riverine particulates may affect the atmospheric carbon cycle through 1) the release of limiting nutrients enhancing primary productivity and 2) the delivery of particulate surface area which increases organic carbon burial and thus preservation, a fundamental step for the long-term removal of carbon (see references in Jeandel and Oelkers , 2015). The direct attachment of bacteria on mineral surfaces presented in this study support this possibility. Moreover, the frequent occurrence of cyanobacteria aggregates associated with particulates observed in this study (see Figure 3-13), suggests a positive effect of the particulates on the aggregation of cyanobacteria. Similarly, Deng et al. (2015), observed an increasing number, though decreasing size in marine *Synechococcus* aggregates with increasing clay mineral concentrations, thus supporting the 'ballast hypothesis' which proposes that mineral particles accelerate organic carbon transport through the water column (Armstrong et al., 2001; Deng et al., 2015), thus increasing burial efficiency.

3.6 Conclusions

The results presented in this study demonstrate the positive effect of riverine suspended material on the growth of freshwater cyanobacteria *Synechococcus sp.* Riverine particulates exhibited three distinct effects on bacterial growth, which are 1) triggering bacterial growth in otherwise unfavourable growth conditions (e.g. by increasing pH), 2) increasing total biomass concentration as a function of particulate concentration, and 3) inducing steady bacterial growth in post-exponential growth phase as a function of particulate concentration. Results furthermore suggest a positive feedback between particulates and growing bacteria, where dissolving particulates enhance bacterial growth which in turn enhances silicate mineral dissolution by altering fluid pH. SEM investigations showed direct physical contact between particulates and cyanobacteria through organic fibres, suggesting that bacteria attach on mineral surfaces to gain required nutrients. Furthermore, frequent bacteria clusters were observed associated with

particulates, suggesting an increasing accumulation of bacteria in the presence of particulate material.

These results indicate a notable influence of riverine particulate material on phytoplankton growth in freshwater environments. However, its effect requires a case-by-case study depending on various environmental factors such as nutrient availability and nutrient ratios, light intensity or phytoplankton species distribution. Given the predominance of potentially limiting nutrients transported in riverine particulates compared to its dissolved flux, it seems obvious that particulates enhance bacterial growth whenever growth is limited by nutrient availability. The global role of riverine particulates, however, is revealed in marine environments and its effect on marine primary productivity has to be subject of further investigations. Riverine particulates are expected to deliver limiting nutrients to coastal regions, thus increasing primary productivity. Furthermore, the direct attachment of bacteria on mineral surfaces underscores the importance of riverine particulates on the burial efficiency of organic carbon. These effects combined suggest a significant impact of particulate material on the global carbon cycle.

Acknowledgements

This research was supported by the Marie Curie EU-FP7 CO2-REACT Research and Training Network. The authors would like to thank Liudmila Shirokova, Carole Causserand, Aurélie Lanzanova, Frédéric Candaudap and Michel Thibaut from the Géosciences Environnement Toulouse for their help with experimental work, wet chemical analyses, and XRD- measurements, respectively. Stefanie Lutz, Maren Kahl, Martin Fuller and Richard Walshaw from the School of Earth and Environment, University of Leeds are acknowledged for their help with SEM investigations. Eydis Eiriksdottir, Deirdre Clark, Rebecca Neely and Sigurdur Gislason from the Earth Science Institute of the University of Iceland are acknowledged for the provision of suspended particulate material and for support during field work. Sigrid Hirth-Walther, Sebastian Weber and Kurt Bucher from the institute of Geo- und Umweltnaturwissenschaften, Albert-Ludwigs Universität, are likewise acknowledged for their cooperation and help during this study.

3.7 References

See References on page 157ff.

Appendix Chapter 3

Table A 3-1. Summary of experimental conditions. RPM means Riverine Particulate Material. ICE means Iceland and MS Mississippi particulates.

	ID	Electrolyte BG-11 dilution	type of RPM	RPM [mg/kg]	sterilization of sediments	biomass initial [$g_{(dry)}$/kg]	pH initial	pH max	duration [days]	parameter controlled
S.2	*SII* 1	1:375	organic ctrl			0.022	nd	nd	28	OD
	SII 2	1:375	ICE	1505	no sterilization	0.021	nd	nd	28	OD
	SII 3	1:375	MS	1506	no sterilization	0.022	nd	nd	28	OD
Series 3	*SIII* 1	1:1000	organic ctrl			0.032	nd	nd	36	OD
	SIII 2	1:1000	ICE	501	no sterilization	0.033	nd	nd	36	OD
	SIII 3	1:1000	ICE	1503	no sterilization	0.033	nd	nd	36	OD
	SIII 4	1:1000	MS	498	no sterilization	0.033	nd	nd	36	OD
	SIII 5	1:1000	MS	1498	no sterilization	0.034	nd	nd	36	OD
Series 4	*SIV* 1	1:1000	ICE	1501	12h at 121°C	1	6.0	9.8	22	OD, pH
	SIV 2	1:1000	ICE	76	12h at 121°C	1	6.0	6.3	22	OD, pH
	SIV 3	1:1000	MS	1495	12h at 121°C	1	6.0	10.7	22	OD, pH
	SIV 4	1:1000	MS	75	12h at 121°C	1	6.0	6.5	22	OD, pH
	SIV 5	1:1000	ICE	1499	12h at 121°C	inorg. Ctrl	6.0	7.1	22	OD, pH
	SIV 6	1:1000	ICE	75	12h at 121°C	inorg. Ctrl	6.0	6.2	22	OD, pH
	SIV 7	1:1000	MS	1500	12h at 121°C	inorg. Ctrl	6.0	7.8	22	OD, pH
	SIV 8	1:1000	MS	76	12h at 121°C	inorg. Ctrl	6.0	6.6	22	OD, pH
	SIV 9	1:1000	organic ctrl			1	6.0	6.3	22	OD, pH
Series 5	*SV* 1	1:1000	organic ctrl			m	6.0	6.6	28	OD, pH, NPOC, DIC, ICP-MS
	SV 2	1:1000	ICE	1489	10 % H_2O_2	m	6.0	10.1	28	OD, pH, NPOC, DIC, ICP-MS
	SV 3	1:1000	ICE	76	10 % H_2O_2	m	6.0	6.5	28	OD, pH, NPOC, DIC, ICP-MS
	SV 4	1:1000	MS	1501	10 % H_2O_2	m	6.0	10.6	28	OD, pH, NPOC, DIC, ICP-MS
	SV 5	1:1000	MS	76	10 % H_2O_2	m	6.0	6.9	28	OD, pH, NPOC, DIC, ICP-MS
	SV 6	1:1000	ICE	1495	10 % H_2O_2	inorg. Ctrl	6.0	6.9	28	OD, pH, NPOC, DIC, ICP-MS
	SV 7	1:1000	ICE	77	10 % H_2O_2	inorg. Ctrl	6.0	6.4	28	OD, pH, NPOC, DIC, ICP-MS
	SV 8	1:1000	MS	1502	10 % H_2O_2	inorg. Ctrl	6.0	7.6	28	OD, pH, NPOC, DIC, ICP-MS
	SV 9	1:1000	MS	75	10 % H_2O_2	inorg. Ctrl	6.0	6.7	28	OD, pH, NPOC, DIC, ICP-MS
	SV 10	1:1000	blank				6.0	6.2	28	OD, pH, NPOC, DIC, ICP-MS
Series 5b	*SVb* 1	1:1000	organic ctrl			m	nd		28	OD
	SVb 2	1:1000	ICE	1517	12h at 121°C	m	nd	nd	28	OD
	SVb 3	resid. SV 6				m	6.8	nd	28	OD
	SVb 4	1:1000	MS	1506	12h at 121°C	m	nd	nd	28	OD
	SVb 5	resid. SV 8				m	7.6	nd	28	OD
	SVb 6	1:1000	ICE	1500	12h at 121°C	inorg. Ctrl	nd	nd	28	OD

Table A 3-1. Continuation.

ID	Electrolyte BG-11 dilution	type of RPM	RPM [mg/kg]	sterilization of sediments	biomass initial [$g_{(dry)}$/kg]	pH initial	pH max	duration [days]	parameter controlled
SVb 7	1:1000	MS	1524	12h at 121°C	inorg. Ctrl	nd	nd	28	OD
SVI 1	1:1000 + NaOH	organic ctrl			h	6.8	10.6	28	OD, pH
SVI 2	1:1000 + NaOH	MS	1499	Eth + 12h 121°C	h	6.8	10.8	28	OD, pH
SVI 3	1:1000 + NaOH	MS	78	Eth + 12h 121°C	h	6.8	10.6	28	OD, pH
SVI 4	1:1000 + NaOH	MS	1501	Eth + 12h 121°C	inorg. Ctrl	6.8	7.8	28	OD, pH
SVI 5	1:1000 + NaOH	MS	76	Eth + 12h 121°C	inorg. Ctrl	6.8	7.1	28	OD, pH
SVI 6	1:1000 + NaOH	blank			inorg. Ctrl	6.8	6.9	28	OD, pH
SVI 7	1:1000 + NaOH	MS	1007	Eth + 12h 121°C	h	6.8	nd	28	OD
SVI 8	1:1000 + NaOH	MS	514	Eth + 12h 121°C	h	6.8	nd	28	OD
SVI 9	1:1000 + NaOH	MS	1005	Eth + 12h 121°C	m	6.8	nd	28	OD
SVI 10	1:1000 + NaOH	MS	506	Eth + 12h 121°C	m	6.8	nd	28	OD
SVI 11	1:1000 + NaOH	MS	1493	Eth + 12h 121°C	l	6.8	nd	28	OD
SVI 12	1:1000 + NaOH	MS	1006	Eth + 12h 121°C	l	6.8	nd	28	OD
SVI 13	1:1000 + NaOH	MS	502	Eth + 12h 121°C	l	6.8	nd	28	OD
SVI 14	1:1000 + NaOH	MS	1010	Eth + 12h 121°C	inorg. Ctrl	6.8	nd	28	OD
SVI 15	1:1000 + NaOH	MS	497	Eth + 12h 121°C	inorg. Ctrl	6.8	nd	28	OD
SVI 16	1:375	organic ctrl			0.030	nd	nd	28	OD
SVI 17	1:375	MS	1487	Eth + 12h 121°C	0.032	nd	nd	28	OD
SVI 18	1:375	MS	1000	Eth + 12h 121°C	0.030	nd	nd	28	OD
SVI 19	1:375	MS	508	Eth + 12h 121°C	0.030	nd	nd	28	OD
SVI 20	1:375	MS	74	Eth + 12h 121°C	0.030	nd	nd	28	OD
SVII 1	1:1000 + NaOH				l	7.4	9.4	27	OD, pH, Cond
SVII 2	1:1000 + NaOH				m	7.6	9.7	27	OD, pH, Cond
SVII 3	1:1000 + NaOH				h	7.6	10.1	27	OD, pH, Cond
SVII 4	1:1000 + 0.3g/kg NaCl				l	6.0	6.3	27	OD, pH, Cond
SVII 5	1:1000 + 0.3g/kg NaCl				m	6.0	6.3	27	OD, pH, Cond
SVII 6	1:1000 + 0.3g/kg NaCl				h	6.0	6.5	27	OD, pH, Cond
SVII 7	1:1000 + HCO_3/Ca				l	7.6	9.9	27	OD, pH, Cond
SVII 8	1:1000 + HCO_3/Ca				m	7.6	10.4	27	OD, pH, Cond
SVII 9	1:1000 + HCO3/Ca				h	7.8	10.6	27	OD, pH, Cond
SVII 10	1:1000	organic ctrl			l	6.1	6.6	27	OD, pH, Cond
SVII 11	1:1000	organic ctrl			m	6.1	6.5	27	OD, pH, Cond
SVII 12	1:1000	organic ctrl			h	6.0	6.6	27	OD, pH, Cond, Chl a
SVII 13	1:1000	MS	1543	Eth + 12h 121°C	l	6.0	10.3	27	OD, pH, Cond
SVII 14	1:1000	MS	1509	Eth + 12h 121°C	m	5.9	10.3	27	OD, pH, Cond

Series 6

Series 7

Table A 3-1. Continuation.

	ID	Electrolyte BG-11 dilution	type of RPM	RPM [mg/kg]	sterilization of sediments	biomass initial [$g_{(dry)}$/kg]	pH initial	pH max	duration [days]	parameter controlled
Series 8	*SVII* 15	1:1000	MS	1541	Eth + 12h 121°C	h	5.9	10.5	27	OD, pH, Cond, Chl a
	SVII 16	1:1000	MS	1001	Eth + 12h 121°C	l	nd	nd	27	OD
	SVII 17	1:1000	MS	1474	burned	l	nd	nd	27	OD
	SVII 18	1:1000	MS	1458	burned	m	nd	nd	27	OD
	SVII 19	1:1000	MS	1497	burned	h	nd	nd	27	OD
	SVII 20	1:1000	Zircone	1452	Eth + 12h 121°C	l	nd	nd	13	OD
	SVII 21	1:1000	Zircone	1497	Eth + 12h 121°C	h	nd	nd	13	OD
	SVII 22	1:1000	MS	1477	Eth + 12h 121°C	inorg. Ctrl	5.9	7.7	19	OD, pH
	SVII 23	1:1000	MS	994	Eth + 12h 121°C	h	nd	nd	27	OD, pH, Cond
	SVII 24	1:1000	MS	508	Eth + 12h 121°C	h	nd	nd	27	OD, Chl a
	SVII 25	1:1000	MS	70	Eth + 12h 121°C	h	nd	nd	28	OD
	SVIII 1	1:1000 + NaOH				l	7.1	9.5	27	OD, pH
	SVIII 2	1:1000 + NaOH				m	7.1	9.5	27	OD, pH
	SVIII 3	1:1000 + NaOH				h	7.1	10.5	27	OD, pH
	SVIII 4	1:1000	MS	1007	Eth + 12h 121°C	h	6.1	10.1	27	OD, pH
	SVIII 5	1:1000				h	6.1	6.2	12	OD, pH
	SVIII 6	1:1000				h	6.1	6.2	12	OD, pH
Series 9	*SIX* 1	1:1000 + carb buff.				l	9.4	9.6	24	OD, pH
	SIX 2	1:1000 + carb buff.				m	9.4	9.7	24	OD, pH
	SIX 3	1:1000 + carb buff.	MS	512	Eth + 12h 121°C	l	9.4	9.8	24	OD, pH
	SIX 4	1:1000 + carb buff.	MS	526	Eth + 12h 121°C	m	9.4	9.6	24	OD, pH
Series 10	*SX* 1	1:1000	organic ctrl			l	5.8	6.2	15	OD, pH, Cond
	SX 2	1:1000	ICE	1497	Eth + 12h 121°C	l	6.6	10.0	15	OD, pH, Cond
	SX 3	1:1000	organic ctrl			m	5.8	6.4	15	OD, pH, Cond
	SX 4	1:1000	ICE	1482	Eth + 12h 121°C	m	6.4	10.0	15	OD, pH, Cond
	SX 5	1:1000	organic ctrl			h	5.8	6.5	15	OD, pH, Cond, Chl a
	SX 6	1:1000	ICE	81	Eth + 12h 121°C	h	nd	nd	15	OD
	SX 7	1:1000	ICE	1504	Eth + 12h 121°C	h	6.9	10.4	15	OD, pH, Cond Chl a
	SX 8	1:1000	ICE	1478	Eth + 12h 121°C	inorg. Ctrl	6.6	7.0	15	OD, pH, Cond
	SX 9	1:1000	ICE	1468	burned	m	nd	nd	15	OD
	SX 10	1:1000 + NaOH				h	7.1	9.9	25	OD, pH
	SX 11	1:1000 + NaOH				m	7.2	9.7	25	OD, pH
	SX 12	1:1000	MS	1464	Eth + 12h 121°C	inorg. Ctrl	6.2	7.6	25	OD, pH, Cond
	SX 13	1:1000	MS	1531	Eth + 12h 121°C	l	nd	nd	25	OD
	SX 14	1:1000	MS	505	Eth + 12h 121°C	l	nd	nd	25	OD

Table A 3-2. Initial conditions, maximal biomass concentration and computed growth rate constants in exponential (μ) and in stationary phase (μ_{stat}) for all reactors.

	ID	RPM [mg/kg]	type of RPM	biomass initial [$g_{(dry)}$/kg]	pH initial	pH max	max biomass [$g_{(dry)}$/kg]	Growth rate constant μ [$days^{-1}$]	± [$days^{-1}$]	Slope in stat. phase μ_{stat} [$g_{(dry)}$/kg/day]	± [$g_{(dry)}$/kg/day]
S.2	*SII* 1	organic ctrl		0.022	nd	nd	0.267	0.431	0.010	-9.75×10^{-4}	7.62×10^{-4}
	SII 2	1505	ICE	0.021	nd	nd	0.343	0.476	0.095	3.35×10^{-3}	7.33×10^{-4}
	SII 3	1506	MS	0.022	nd	nd	0.368	0.435	0.096	4.30×10^{-3}	2.93×10^{-4}
Series 3	*SIII* 1	organic ctrl		0.032	nd	nd	0.115	0.466	0.093	1.80×10^{-4}	5.70×10^{-5}
	SIII 2	501	ICE	0.033	nd	nd	0.141	0.395	0.008	2.17×10^{-4}	7.32×10^{-5}
	SIII 3	1503	ICE	0.033	nd	nd	0.157	0.431	0.062	-2.92×10^{-4}	1.24×10^{-4}
	SIII 4	498	MS	0.033	nd	nd	0.153	0.388	0.127	8.18×10^{-4}	6.19×10^{-5}
	SIII 5	1498	MS	0.034	nd	nd	0.219	0.382	0.010	2.68×10^{-3}	1.01×10^{-4}
Series 4	*SIV* 1	1501	ICE	1	6.0	9.8	0.133	0.390	0.007	6.92×10^{-4}	6.54×10^{-5}
	SIV 2	76	ICE	1	6.0	6.3			no growth		
	SIV 3	1495	MS	1	6.0	10.7	0.140	0.465	0.038	1.59×10^{-3}	2.91×10^{-4}
	SIV 4	75	MS	1	6.0	6.5			no growth		
	SIV 9	organic ctrl		1	6.0	6.3			no growth		
Series 5	*SV* 1	organic ctrl		m	6.0	6.6			no growth		
	SV 2	1489	ICE	m	6.0	10.1	0.134	0.274	0.005	-1.69×10^{-4}	1.62×10^{-4}
	SV 3	76	ICE	m	6.0	6.5			no growth		
	SV 4	1501	MS	m	6.0	10.6	0.142	0.301	0.001	8.42×10^{-4}	5.03×10^{-5}
	SV 5	76	MS	m	6.0	6.9			no growth		
Series 5b	*SVb* 1	organic ctrl		m	nd				no growth		
	SVb 2	1517	ICE	m	nd	nd	0.157	0.348	0.011	-3.74×10^{-5}	4.26×10^{-5}
	SVb 3	Residual *SV* 6		m	6.8	nd	0.067	0.234	0.012	-1.54×10^{-4}	4.05×10^{-5}
	SVb 4	1506	MS	m	nd	nd	0.159	0.483	0.018	1.06×10^{-3}	5.17×10^{-5}
	SVb 5	Residual *SV* 8		m	7.6	nd	0.080	0.255	0.007	-1.24×10^{-4}	4.04×10^{-5}
Series 6	*SVI* 1	organic ctrl		h	6.8	10.6	0.135	0.209	0.005	-7.99×10^{-4}	1.64×10^{-4}
	SVI 2	1499	MS	h	6.8	10.8	0.178	0.228	0.019	1.12×10^{-3}	1.06×10^{-4}
	SVI 3	78	MS	h	6.8	10.6	0.142	0.215	0.013	-4.11×10^{-4}	1.03×10^{-4}
	SVI 7	1007	MS	h	6.8	nd	0.161	0.253	0.005	4.28×10^{-5}	6.35×10^{-5}
	SVI 8	514	MS	h	6.8	nd	0.157	0.240	0.010	-6.84×10^{-5}	5.88×10^{-5}
	SVI 9	1005	MS	m	6.8	nd	0.147	0.346	0.009	4.23×10^{-4}	7.70×10^{-5}
	SVI 10	506	MS	m	6.8	nd	0.134	0.355	0.021	-2.54×10^{-5}	5.35×10^{-5}
	SVI 11	1493	MS	l	6.8	nd	0.142	0.473	0.003	8.48×10^{-4}	7.09×10^{-5}
	SVI 12	1006	MS	l	6.8	nd	0.167	0.399	0.011	-2.48×10^{-4}	8.50×10^{-5}

Table A 3-2. Continuation.

	ID	RPM [mg/kg]	type of RPM	biomass initial [$g_{(dry)}$/kg]	pH initial	pH max	max biomass [$g_{(dry)}$/kg]	Growth rate constant μ [$days^{-1}$]	±	[$days^{-1}$]	Slope in stat. phase μ_{stat} [$g_{(dry)}$/kg/day]	± [$g_{(dry)}$/kg/day]
Series 7	*SVI* 13	502	MS	1	6.8	nd	0.120	0.403		0.012	-1.88×10^{-3}	7.32×10^{-5}
	SVI 16	organic ctrl		0.030	nd	nd	0.286	0.310		0.012		
	SVI 17	1487	MS	0.032	nd	nd	0.346	0.309		0.005		1.24×10^{-4}
	SVI 18	1000	MS	0.030	nd	nd	0.33	0.301		0.017		2.04×10^{-4}
	SVI 19	508	MS	0.030	nd	nd	0.327	0.283		0.009		1.63×10^{-4}
	SVI 20	74	MS	0.030	nd	nd	0.303	0.291		0.009		2.15×10^{-4}
	SVII 1	ctrl high pH		1	7.4	9.4	0.081	0.410		0.043	-1.27×10^{-3}	4.78×10^{-5}
	SVII 2	ctrl high pH		m	7.6	9.7	0.099	0.347		0.020	-1.06×10^{-3}	7.09×10^{-5}
	SVII 3	ctrl high pH		h	7.6	10.1	0.128	0.230		0.026	-1.39×10^{-3}	5.25×10^{-5}
	SVII 4	ctrl high cond.		1	6.0	6.3				no growth		
	SVII 5	ctrl high cond.		m	6.0	6.3				no growth		
	SVII 6	ctrl high cond.		h	6.0	6.5				no growth		
	SVII 7	ctrl high cond.&pH		1	7.6	9.9	0.107	0.591		0.107	-6.68×10^{-4}	1.18×10^{-4}
	SVII 8	ctrl high cond.&pH		m	7.6	10.4	0.125	0.411		0.020	-9.53×10^{-4}	2.35×10^{-5}
	SVII 9	ctrl high cond.&pH		h	7.8	10.6	0.160	0.300		0.021	-1.55×10^{-3}	1.21×10^{-4}
	SVII 10	organic ctrl		1	6.1	6.6				no growth		
	SVII 11	organic ctrl		m	6.1	6.5				no growth		
	SVII 12	organic ctrl		h	6.0	6.6				no growth		
	SVII 13	1543	MS	1	6.0	10.3	0.143	0.505		0.022	1.05×10^{-3}	1.48×10^{-4}
	SVII 14	1509	MS	m	5.9	10.3	0.156	0.409		0.020	9.14×10^{-4}	1.19×10^{-4}
	SVII 15	1541	MS	h	5.9	10.5	0.197	0.322		0.045	1.42×10^{-3}	1.47×10^{-4}
	SVII 16	1001	MS	1	nd	nd	0.136	0.531		0.012	6.98×10^{-4}	1.39×10^{-4}
	SVII 17	1474	MS	1	nd	nd	0.137	0.526		0.027	8.51×10^{-4}	1.61×10^{-4}
	SVII 18	1458	MS	m	nd	nd	0.148	0.446		0.019	5.46×10^{-4}	6.21×10^{-5}
	SVII 19	1497	MS	h	nd	nd	0.171	0.390		0.078	2.85×10^{-4}	8.37×10^{-5}
	SVII 20	1452	Zircone	1	nd	nd				no growth		
	SVII 21	1497	Zircone	h	nd	nd				no growth		
	SVII 23	994	MS	h	nd	nd	0.176	0.338		0.047	5.76×10^{-4}	6.94×10^{-5}
	SVII 24	508	MS	h	nd	nd	0.164	0.292		0.019	-1.07×10^{-3}	1.66×10^{-4}
	SVII 25	70	MS	h	nd	nd	0.140	0.271		0.022		
Series 8	*SVIII* 1	ctrl high pH		1	7.1	9.5	0.084	0.512		0.102	-3.42×10^{-4}	8.91×10^{-5}
	SVIII 2	ctrl high pH		m	7.1	9.5	0.093	0.326		0.065	-4.28×10^{-4}	5.18×10^{-5}
	SVIII 3	ctrl high pH		h	7.1	10.5	0.155	0.198		0.040	-1.00×10^{-3}	1.01×10^{-4}
	SVIII 4	1007	MS	h	6.1	10.1	0.157	0.411		0.082	3.66×10^{-4}	1.69×10^{-4}

Table A 3-2. Continuation.

	ID	RPM [mg/kg]	type of RPM	biomass initial [$g_{(dry)}$/kg]	pH initial	pH max	max biomass [$g_{(dry)}$/kg]	Growth rate constant μ [$days^{-1}$]	± [$days^{-1}$]	Slope in stat. phase μ_{stat} [$g_{(dry)}$/kg/day]	± [$g_{(dry)}$/kg/day]
Series 9	*SVIII* 5	organic ctrl		h	6.1	6.2			no growth		
	SVIII 6	organic ctrl		h	6.1	6.2			no growth		
	SIX 1	ctrl carb buff.		l	9.4	9.6	0.104	0.532	0.023	-2.33×10^{-3}	1.20×10^{-4}
	SIX 2	ctrl carb buff.		m	9.4	9.7	0.112	0.434	0.036	-2.44×10^{-3}	1.36×10^{-4}
	SIX 3	512	MS	l	9.4	9.8	0.116	0.527	0.049	-2.05×10^{-3}	1.49×10^{-4}
	SIX 4	526	MS	m	9.4	9.6	0.134	0.467	0.015	-2.37×10^{-3}	5.51×10^{-5}
Series 10	*SX* 1	organic ctrl		l	5.8	6.2			no growth		
	SX 2	1497	ICE	l	6.6	10.0	0.143	0.470	0.018		
	SX 3	organic ctrl		m	5.8	6.4			no growth		
	SX 4	1482	ICE	m	6.4	10.0	0.154	0.405	0.081		
	SX 5	organic ctrl		h	5.8	6.5			no growth		
	SX 6	81	ICE	h	nd	nd			no growth		
	SX 7	1504	ICE	h	6.9	10.4	0.186	0.361	0.072		
	SX 9	1468	ICE	m	nd	nd	0.159	0.465	0.093		
	SX 10	ctrl high pH		h	7.1	9.9	0.139	0.304	0.061	-1.43×10^{-3}	8.32×10^{-5}
	SX 11	ctrl high pH		m	7.2	9.7	0.113	0.472	0.094	-1.17×10^{-3}	8.25×10^{-5}
	SX 13	1531	MS	l	nd	nd	0.135	0.566	0.042	6.69×10^{-4}	8.77×10^{-5}
	SX 14	505	MS	l	nd	nd	0.118	0.462	0.045	1.95×10^{-4}	8.70×10^{-5}

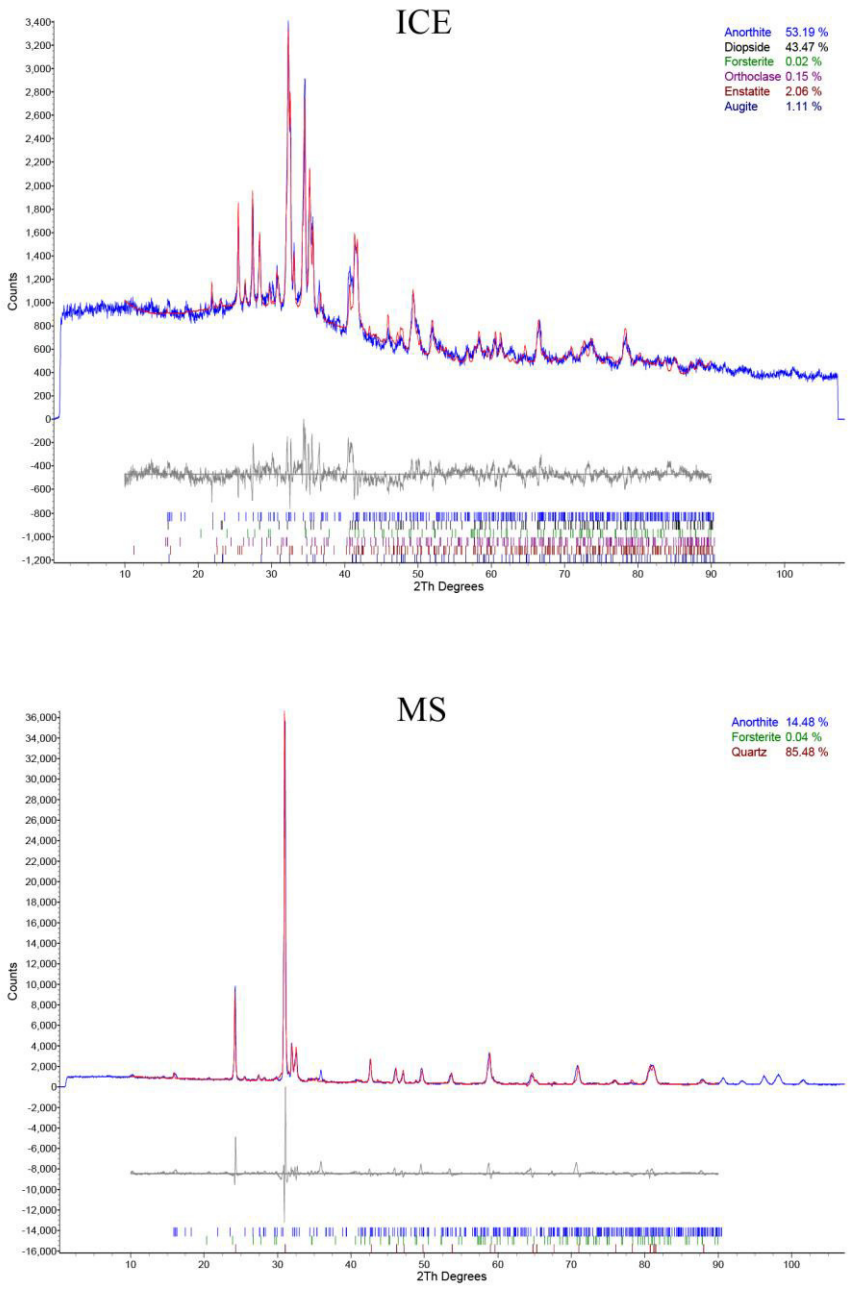

Figure A 3-1. XRD spectra of Iceland (ICE) and Mississippi (MS) riverine particulate material used in this study.

4 Effect of riverine particulate material on the growth of the marine diatom *Thalassiosira weissflogii*

Résumé

L'apport en matière particulaire des continents vers les océans joue un rôle essentiel sur les cycles globaux des éléments, car le flux de particules dépasse par plusieurs ordres de grandeur le flux dissous correspondant pour pratiquement tous les éléments du tableau périodique. Les particules fluviales sont le moyen de transport principal de nombreux éléments nutritifs essentiels comme le silicium, le fer ou le phosphore. Arrivant aux marges de l'océan, les particules favorisent la production primaire en agissant comme engrais naturel et en libérant des nutriments tamponnés. En outre, l´apport en surface de particules dans l'océan régule principalement le piégeage du carbone organique. Ces considérations suggèrent un lien substantiel entre l'apport de matière particulaire fluviale et le cycle du carbone organique. Pour explorer ce lien, nous avons mené des expériences de croissance du microcosme, en étudiant la croissance de la diatomée marine *Thalassiosira weissflogii* en présence et en l'absence de différents types et concentrations de matières particulaires de rivières afin de caractériser leur effet sur la productivité des diatomées. Les résultats démontrent un fort effet positif du matériel particulaire fluvial sur la croissance des diatomées avec une augmentation des concentrations totales de diatomées et des taux de mortalité post-exponentiels ralentis en fonction de la concentration en sédiments. De plus, les études de microscopie optique et électronique suggèrent que les particules fluviales peuvent faciliter la séquestration du carbone organique grâce à leur rôle dans l'agrégation et la sédimentation du phytoplancton, ainsi que par l'apport de surfaces disponibles à être occupées par des composés organiques. Il a été montré que la charge en matière particulaire fluviale est particulièrement sensible au climat avec des flux de particules croissants avec une augmentation des températures et du ruissellement global. Cette sensibilité climatique prononcée implique que les particules fluviales peuvent contribuer considérablement à réguler les concentrations atmosphériques de CO_2 par leur rôle dans le cycle du carbone organique.

Effect of riverine particulate material on the growth of marine diatoms: results of laboratory experiments with *Thalassiosira weissflogii*

Christian Grimm[1*], Agnès Feurtet-Mazel[2], Oleg S. Pokrovsky[1,3] and Eric H. Oelkers[1,4]

[1] GET, CNRS/URM 5563, Université Paul-Sabatier, 14 avenue Edouard-Belin, 31400 Toulouse, France
[2] University of Bordeaux, CNRS, UMR EPOC 5805, Aquatic Ecotoxicology, Arcachon, France
[3] N. Laverov Federal Center of Integrated Arctic Research, Russian Academy of Science, Arkhangelsk, Russia
[4] Earth Sciences, University College London, Gower Street London WC1E 6BT, UK

[*]Corresponding author: grimm@get.obs.mip.fr

This manuscript is in preparation for submission

Keywords: CO_2, organic carbon cycle, diatoms, primary production, riverine particulate material, nutrients, mineral-microbe interactions, carbon burial

Abstract

The supply of riverine particulate material from the continents to the oceans plays a vital role in the global cycles of the elements. Notably, the riverine particulate flux exceeds the corresponding dissolved flux for practically all elements of the periodic table by orders of magnitude. As such, riverine particulates dominate the transport of vital nutrients like Si, Fe or P to the ocean margins, where they may increase primary production by acting as slow release fertilizer. Furthermore, the supply of particulate surface area to the ocean is considered to control organic carbon burial. Taken together, these observations suggest a close link between the supply of riverine particulate material and the organic carbon cycle. To explore this link, we conducted microcosm experiments, to measure the growth of the marine diatom *Thalassiosira weissflogii* in the presence and absence of different types and concentrations of riverine particulate material. Results demonstrate a strong positive effect of riverine particulate material on diatom growth with increased total diatom concentrations and slowed post-exponential death rates with increasing particulate concentration. Moreover, SEM and optical microscope investigations suggest that riverine particulates may facilitate organic carbon burial through their role in the aggregation and sedimentation of phytoplankton. The supply of riverine particulate material has been shown to be markedly climate sensitive with their fluxes increasing dramatically with increasing global temperature and runoff. This pronounced climate sensitivity implies that riverine particulates may contribute substantially in regulating atmospheric CO_2 concentrations through their role in the organic carbon cycle.

4.1 Introduction

The atmospheric concentration of carbon dioxide has been steadily increasing since the beginning of the industrial revolution and exhaustive evidence demonstrates its link to global climate change (IPCC, 2007; Oelkers and Cole, 2008; Petit et al., 1999). Over geological time, atmospheric CO_2 concentrations have been profoundly influenced 1) by oceanic primary productivity and the subsequent burial of organic matter (Falkowski et al., 1998; 2000), referred to as the 'biological pump' or the 'organic pathway' and 2) by weathering of Ca-Mg-silicates and the subsequent precipitation of carbonates, referred to as the 'inorganic pathway' (Berner, 1982; Berner et al., 1983; Berner and Kothavala, 2001; Falkowski et al., 1998; Gislason et al., 2009; Walker et al., 1981; Wallmann, 2001). Several studies have demonstrated a feedback between climate change and the inorganic pathway. This feedback stems from global air temperatures increasing in response to increasing atmospheric CO_2 concentrations, leading to

changing precipitation patterns, increasing continental runoff and elevated chemical and physical weathering rates (Gislason et al., 2009). Increasing weathering rates drive CO_2 drawdown via through the delivery of divalent cations and the subsequent precipitation of carbonates in the oceans (Gedney et al., 2006; Gislason et al., 2006; 2009; Labat et al., 2004). This has been referred to as the internal thermostat of the Earth (Berner et al., 1983; Walker et al., 1981).

The effect of a changing climate on the global biological pump has been subject of numerous studies including the consequence of changing temperature and CO_2 partial pressure (pCO_2) on marine primary production (Clark and Flynn, 2000; Engel et al., 2013; Feng et al., 2009; Hein and Sand-Jensen, 1997; Passow and Carlson, 2012; Riebesell et al., 2000; 2007; Rost et al., 2008; Tortell et al., 2002). Currently, the marine science community cannot confidently predict whether the biological pump will weaken or strengthen in a high CO_2 world (Feng et al., 2009; Passow and Carlson, 2012; Passow and Laws, 2015; Seebah et al., 2014). The common hypothesis is that increasing temperature and ocean acidification will result in increased carbon fluxes creating a negative feedback on the biological carbon pump (Arrigo, 2007; Riebesell et al., 2007).

The response of phytoplankton to environmental stress associated with climate change comprises not only elevated pCO_2, temperature and concomitant ocean acidification but also changing nutrient availabilities. The two major sources of nutrients to the ocean are the recycling of organic compounds and the influx of new nutrients through rivers, aeolian dust or volcanic ash (Eiriksdottir et al., 2015; 2017; Frogner et al., 2001; Jickells et al., 2005; Jones and Gislason, 2008; Olsson et al., 2013). Of these influxes, the riverine particulate input is the most important. Estimates suggest global land-to-ocean fluxes of 15-20 Gt $year^{-1}$ for suspended riverine particulate material, 1.6-10 Gt $year^{-1}$ for riverine bedload material, ~1 Gt $year^{-1}$ for riverine dissolved load and 0.4-2 Gt $year^{-1}$ for aeolian dust (Gaillardet et al., 1999; 2003; Jeandel and Oelkers, 2015; Meybeck et al., 2003; Oelkers et al., 2011; 2012; Syvitski et al., 2003; Viers et al., 2009; Walling, 2006). Thus, the riverine particulate flux exceeds the dissolved flux by a factor of 17-30 and the aeolian dust flux by a factor of 8-75. Notably, due to their low solubility, the particulate flux of limiting nutrients like Si, P and Fe exceeds the corresponding dissolved flux by factors of 50, 100 and 350 (Jeandel and Oelkers, 2015; Oelkers et al., 2011). Such observations suggest a major impact of riverine particulates on primary production. Jeandel and Oelkers (2015) summarized the fate of riverine particulate material reaching the coastal ocean

and highlight its role in the global cycle of the elements and its feedback on climate change through serving as slow release fertilizer for marine primary production.

Ocean water is largely depleted in dissolved silica and thus its availability limits primary production in various marine settings (De La Rocha and Passow, 2004). Diatoms account for 75 % of the primary productivity in high nutrient and coastal regions and 40 % of the total annual marine primary production (Arrigo, 2007; De La Rocha and Passow, 2004; Field et al., 1998). About half the total global primary productivity occurs in the oceans, thus, diatoms contribute about 20 % of the annual total primary production that occurs on Earth (De La Rocha and Passow, 2004). Furthermore, diatoms are efficient in transporting organic carbon from the surface water to the deep ocean by forming large aggregates with high settling velocities (Passow and Carlson, 2012; Smetacek, 1985; 1998).

To effectively remove CO_2 from the atmosphere via the organic pathway, organic carbon produced during photosynthesis needs to be transported down the water column to escape decomposition (Berner et al., 1983; Falkowski et al., 1998; Jeandel and Oelkers, 2015). Thus, besides the net primary productivity, the export of atmospheric CO_2 via the organic pathway depends on the burial efficiency of organic matter, which is closely related to the formation of aggregates and their sedimentation capability (Alldredge et al., 1995; Alldredge and Jackson, 1995; Jackson and Lochmann, 1992). A significant proportion of surface-derived organic matter sinks to the ocean floor as 'marine snow' (aggregates >500 µm), formed during phytoplankton blooms (Alldredge et al., 1995; Alldredge and Jackson, 1995). Marine snow can be formed biologically as fecal pellets through grazing and excretion or through physical aggregation (McCave, 1984), whereby physical aggregation explains the bulk of post-bloom particle aggregation (Hill, 1992; Smetacek, 1985). The coagulation of small particles to larger aggregates scales with the square of particle concentration (Hill, 1992; Jackson, 1990; Smetacek, 1985). Hill (1992) concluded in his coagulation model, that high particle concentrations and abundant non-phytoplankton particles are necessary to match the observed aggregation and sedimentation rates in the ocean (Alldredge et al., 1995). Mineral particles have been found to promote particle coagulation through electrostatic forces or hydrogen bonds (Avnimelech et al., 1982; Beaulieu et al., 2005; Ding and Henrichs, 2002; Passow et al., 2014; Verspagen et al., 2006). Furthermore, the incorporation of mineral particles with a high specific density into marine snow usually leads to higher sinking velocities (Ploug et al., 2008a; 2008b), although the reverse effect might occur, due to the fragmentation of aggregates in the presence of mineral particles (De La Rocha and Passow, 2007; Passow and De La Rocha, 2006). Notably,

large sedimentation events are frequently dominated by diatoms due to their capability to form marine snow sized aggregates (Alldredge et al., 1995; Passow and Carlson, 2012; Seebah et al., 2014).

The supply of mineral particles to the ocean is predicted to change significantly with climate change (Gislason et al., 2006; 2009; Passow et al., 2014) but the specific details and consequences of this change are still unclear. Gislason et al. (2006) observed that the riverine particulate flux is far more climate sensitive compared to the corresponding dissolved flux. The potential influence of a changing particulate flux to the oceans on the biological pump are expected to have global consequences because riverine particulates 1) deliver limiting nutrients, thus increasing marine primary production and 2) increase organic carbon burial rates due to the strong organic material sorption onto mineral surfaces (Lalonde et al., 2012; Mayer, 1994). However, experimental calibration of the effect of river suspended material on growth of coastal primary producers and related carbon sequestration remains limited.

This study aims to explore the effect of riverine particulate material on the growth of marine diatoms. Towards this goal, we conducted growth experiments with the marine diatom *Thalassiosira weissflogii* in the presence of different types and concentrations of riverine particulate material. We hypothesize that the presence of particulate matter may 1) accelerate the cell growth by providing nutrients and 2) scavenge cell exametabolites via adsorption on the particulate surfaces. The purpose of this paper is to verify these hypotheses and to discuss the potential role of riverine particulate material on the organic carbon cycle.

4.2 Materials and Methods

In this study, we performed microcosm experiments, investigating the growth of the marine diatom *Thalassiosira weissflogii* in the presence and absence of different types and concentrations of riverine particulate material to characterize the effect of riverine particulates on diatom productivity.

4.2.1 Riverine Particulate Material

Two types of riverine particulate material with distinct mineralogical and chemical compositions were used in this study. Bulk chemical compositions as well as BET surface areas of these particulates are listed in Table 4-1.

1) Mississippi (**MS**) bedload material collected in autumn 2015 in New Orleans near to the Department of Earth and Environmental Science of Tulane University. Due to the low water

level in autumn 2015, the mud sample was collected from the usually flooded river bed. The sample consists of roughly 80 % SiO_2 and is mainly composed of quartz, and feldspars with minor quantities of sheet silicates. It was chosen as a representative of continental riverine material.

2) Iceland (**ICE**) suspended particulates collected from Jökulsá á Dal at Brú, a glacial river in Eastern Iceland. The ICE riverine particulate material mainly consists of basaltic glass and crystalline basalt fragments. This sample is representative of the high relief, volcanic and tectonic active islands that contribute over 45 % of river suspended material to the oceans (Eiriksdottir et al., 2008; Milliman and Syvitski, 1992). Details on sampling and filtration methods can be found in Eiriksdottir et al. (2008), where the chemical composition is provided (sample ID 01A034 therein).

Table 4-1. Whole rock analyses and specific surface areas of the Mississippi (MS) and Iceland (ICE) riverine particulate material used in this study. ICE data is from Eiriksdottir et al. (2008). Note that total Fe is presented as FeO or Fe_2O_3, respectively, for the ICE and MS samples.

Name	**ICE**	**MS**
Type	suspended	bedload
BET (m^2/g)	36.83	16.27
SiO_2 (%)	51.87	77.65
Na_2O (%)	2.22	1.20
MgO (%)	6.00	0.91
Al_2O_3 (%)	13.87	9.55
P_2O_5 (%)	0.24	0.14
K_2O (%)	0.40	1.70
CaO (%)	10.15	1.67
TiO_2 (%)	2.42	0.58
MnO (%)	0.21	0.09
FeO (ICE) (%)	12.49	
Fe_2O_3 (MS) (%)		2.60
LOI		3.78

4.2.2 Diatoms

The marine planktonic diatom *Thalassiosira weissflogii* (TW) used in this study was cultured under sterile conditions in Guillard´s f/2 enriched Instant Ocean© artificial seawater in a thermo-regulated growth chamber at the EPOC laboratory, University of Bordeaux in Arcachon. The chemical composition of the Instant Ocean© sea salt and the modified Guillard´s f/2 culture medium (Guillard, 1975) used in the culture are provided in Table 4-2 and Table 4-3, respectively. *Thalassiosira weissflogii* is a common unicellular, bloom-forming diatom found in marine, estuarine and freshwater environments. It forms 4-32 µm diameter cylindrical silica valves (Johansen and Theriot, 1987) which occur as single cells or in groups. Figure 4-1 A shows a SEM image of a single TW cell and Figure 4-1 B shows an optical microscope image

of several TW cells in a Nageotte counting chamber. Amongst them, some occur as single cells and others are arranged in pairs or chains. Due to its large mean size (~10 µm) TW is commonly used to feed shrimps and oysters. Further details about this diatom are provided in De La Rocha and Passow (2004), De La Rocha et al. (2010), Johansen and Theriot (1987), Roberts et al. (1997) and Sorhannus et al. (2010).

Table 4-2. Elemental composition of Instant Ocean (IO) and natural seawater (SW). Data obtained from Atkinson et al. (1999).

	IO	**SW**
Major cations (mmol/kg)		
Na^+	462	470
K^+	9.4	10.2
Mg^{2+}	52	53
Ca^{2+}	9.4	10.3
Sr^{2+}	0.19	0.09
Major anions (mmol/kg)		
Cl^-	550	550
SO_4^{2-}	23	28
Trace elements (µmol/kg)		
Li	54	20
Si	16	5
Mo	1.8	0.1
Ba	0.85	0.04
V	2.95	0.04
Ni	1.7	0.004
Cr	7.5	0.003
Al	240	0.002
Cu	1.8	0.001
Zn	0.5	0.001
Mn	1.2	0.0004
Fe	0.24	0.0001
Cd	0.24	0.0001
Pb	2.1	0.00006
Co	1.3	0.00005
Ag	2.3	0.00001
Ti	0.67	0.00001

Table 4-3. Nutrient concentrations of modified pure and 5 % Guillard´s f/2 culture medium (Guillard, 1975). Note that no additional silica was added to the reactors except for the Si present in the Instant Ocean© as described in Table 4-2.

	pure f/2	**5 % f/2**
	(mmol/kg)	
$NaNO_3$	8.82×10^{-01}	4.41×10^{-02}
NaH_2PO_4	3.62×10^{-02}	1.81×10^{-03}
$FeCl_3$	1.17×10^{-02}	5.83×10^{-04}
$CuSO_4$	3.92×10^{-02}	1.96×10^{-03}
Na_2MoO_4	2.60×10^{-02}	1.30×10^{-03}
$CoSO_4$	3.56×10^{-02}	1.78×10^{-03}
$MnCl_2$	9.10×10^{-02}	4.55×10^{-03}
thiamine HCl (V B_1)	2.96×10^{-04}	1.48×10^{-05}
biotine (V H)	2.05×10^{-06}	1.03×10^{-07}
cyanocobalamin (V B_{12})	3.69×10^{-07}	1.85×10^{-08}

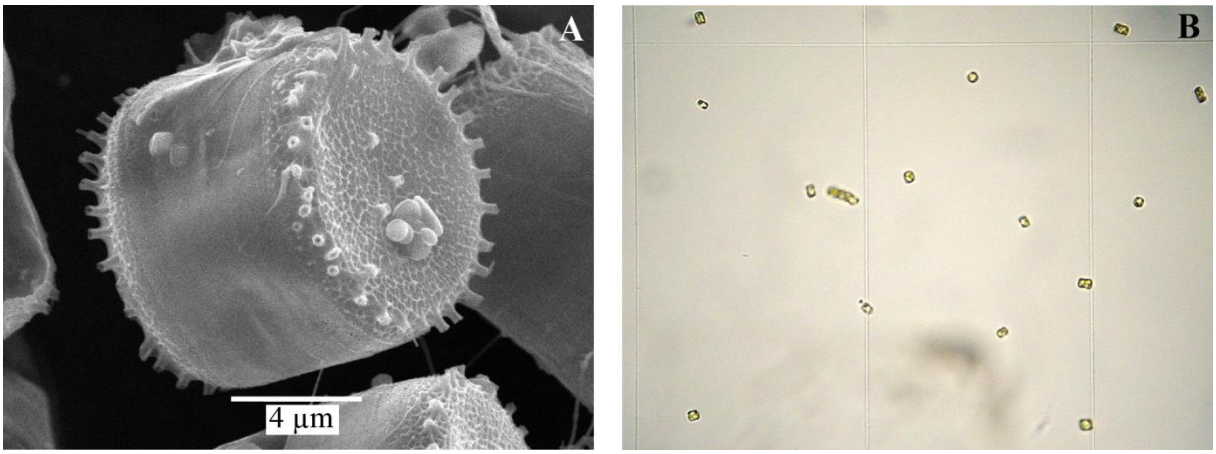

Figure 4-1. SEM photopgraph of a single Thalassiosira weissflogii (TW) cell (**A**) and light microspoce photopgraph of several TW cells in the Nageotte counting chamber (**B**). The distance between the vertical lines in (**B**) is 250 µm.

4.2.3 Growth experiments

Inoculation experiments were performed in sterile 250 or 500 ml Polycarbonate flasks with 12 h/12 h illumination/dark cycles (3000 LUX cool white fluorescence light during daytime), circular shaking at 250 1/min, and room temperature. The polycarbonate flasks were closed with BIO-SILICO© N stoppers that allowed the sterile equilibration of the microcosms with the atmosphere. The reactive fluids were composed of either pure Instant Ocean© (IO) artificial sea salt solution or Instant Ocean© artificial seawater enriched with 5 % modified Guillard´s f/2 culture medium. One experimental series was performed in seawater enriched with 100 % Guillard´s f/2 culture medium. Note that no additional silica was added to the reactors except for the Si present in the Instant Ocean© sea salt solution. The chemical composition of Instant Ocean© and natural seawater are provided in Table 4-2, and the nutrient concentrations of pure and 5 % modified Guillard´s f/2 culture medium are given in Table 4-3. Salinities and pH were initially between 32-34‰ and 8.1-8.4 in each reactor. The riverine particulate material was cleaned with ethanol and flushed 3 times with deionized water and subsequently sterilized for >12h in the oven at 121°C. Particulates were added in concentrations of 75, 100, 250, 500 and 750 mg/kg. Biotic controls without particulates and abiotic controls with particulates, but without bacteria were run as part of each experimental series. All reactive fluids, as well as the experimental equipment were either filter-sterilized or autoclaved at 121 °C for 20 minutes prior to the experiment.

Aliquots of the diatoms were harvested from the stock solutions and rinsed three times in the experimental electrolyte solution by centrifugation/resuspension cycles prior to

inoculation. Diatoms were inoculated at a concentration of ~10^4 cells/ml. All experiments were run in triplicate.

4.2.4 Sampling and analytical methods

Three ml aliquots of homogenous samples were periodically taken from each experiment in a sterile laminar hood box 6h after the onset of illumination; all solids were thoroughly resuspended prior to sampling. Cell density and pH measurements were performed immediately after sampling in collected suspension samples. Solids were sampled after selected experiments and prepared for SEM analysis.

Cell densities were determined using a Nageotte counting chamber (grid of 40 fields of 1.25 µl each, 0.5 mm depth). Suspension samples were diluted prior to counting to attain a range of 10-100 cells per Nageotte field. To obtain accurate cell concentrations, 10 fields were counted for each sample. The pH was measured using a VWR semi-micro electrode with an uncertainty of ± 0.05. To fit of the temporal evolution of the diatom concentration we applied (Ernst et al., 2005):

$$y = \frac{a}{1 + e^{-k(t-c)}} + a_0 \qquad (4\text{-}1)$$

where a represents the upper asymptote of the sigmoidal growth curve, a_0 reflects the initial diatom concentration, k is a rate parameter describing the initial growth and c designates a time constant describing the time elapsed between the beginning of the experiment and the turning point (point of maximal increase in diatom concentration).

Sampled solids were characterized by scanning electron microscopy using a Jeol JSM 6360LV at the Laboratoire Géoscience Environnement Toulouse.

4.3 Results

A total of 5 experimental series were conducted, three in nutrient enriched artificial seawater solution (series TW1, TW2, and TW4) and two in artificial seawater without added dissolved nutrients (series TW3 and TW5). Table A 4-1 in the appendix of this chapter summarizes the experimental conditions as well as the observed temporal evolution of diatom concentrations and pH during all experimental series. A detailed list of experiments and results is provided in the thesis Annex 2 on page 201ff.

The diatom cultures showed typical logistic growth in fluids comprised of Instant Ocean© (IO) artificial seawater enriched with Guillard´s f/2 (series TW1, TW2 and TW4),

whereas diatom cultures did not exhibit an exponential growth stage during experiments carried out in Instant Ocean© without additional nutrients (series TW3 and TW5) but exhibited linear growth in the presence of riverine particulates. In all experimental series, distinct differences were observed depending on the presence or absence of riverine particulate material.

4.3.1 Temporal evolution of diatom concentrations in experiments carried out in in nutrient enriched Instant Ocean© - Experiments TW1, TW2, and TW4

Figure 4-2 shows the temporal evolution of the diatom concentration and pH in experimental series TW1 performed in Guillard´s f/2 enriched (100 % f/2 nutrient concentrations) Instant Ocean©, in the presence and absence of 500 mg/kg MS and ICE riverine particulates. All diatom cultures exhibited exponential growth until the end of the experiment. Experiments were stopped before the cultures reached the stationary growth stage. Notably, initial diatom growth occurred earlier in the presence of riverine particulates compared to the biotic control and the final diatom concentration was 1.21±0.05 times greater in the presence of 500 mg/kg ICE particulates compared to the biotic control. The experiment performed in the presence of 500 mg/kg MS particulates showed a similar final diatom concentration as the biotic control. The pH in the biotic experiments (Figure 4-2 B) increased from initially ~8.2 to 9.2-9.4. This >1 pH unit increase results from diatom photosynthetic activity. As carbon accumulates in the cells, HCO_3^- is converted by the enzyme carbonic anhydrase to CO_2, producing one mole of OH^- per mole of carbon (Roberts et al., 1997). The pH in the abiotic control experiments increased during the first 2 days slightly from ~8.2 to ~8.4 and remained constant until the end of these experiments.

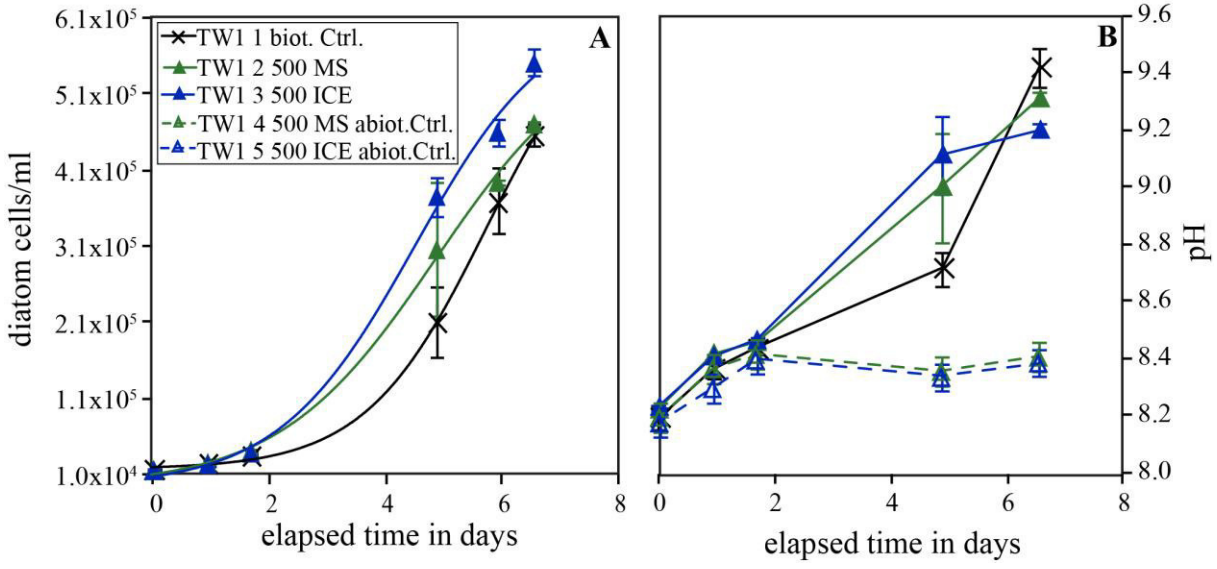

Figure 4-2. Temporal evolution of diatom concentration (**A**) and pH (**B**) during experimental series TW1 carried out in Instant Ocean© enriched with pure Guillard´s f/2 culture medium. The error bars represent the standard deviation of the triplicates.

Figure 4-3 shows the temporal evolution of diatom concentration and pH in experimental series TW2 performed in Instant Ocean© artificial seawater solution enriched with 5 % Guillard´s f/2 culture medium, in the presence and absence of 75 and 500 mg/kg MS and ICE riverine particulates. All biotic experiments showed typical logistic growth, however, distinct differences were observed depending on the presence or absence of riverine particulate material. Note, that for the biotic control and the experiments performed in the presence of 500 mg/kg MS and ICE particulates, two of the triplicates were conducted in 250 ml flasks and one in a 500 ml flask. Since the diatoms in the larger reactors showed notably more pronounced growth, they are illustrated separately (Figure 4-3 A and C for small reactors, Figure 4-3 B and D for big reactors). Diatoms grew exponentially from the onset of the experiments for ~10 days when they reached the stationary phase. In the 500 ml reactors (Figure 4-3 B), diatom concentrations remained constant after the exponential growth until the end of the experiment. In the 250 ml reactors, diatom concentrations remained constant after exponential growth only in the presence of 500 mg/kg MS particulates and decreased in all other experiments. The maximum diatom concentrations determined for each series in the small reactors increased by factors of 1.07±0.18 and 1.06 ± 0.09 with the addition of 75 mg/kg MS and ICE particulates but by factors of 1.92 ± 0.08 and 1.32 ± 0.08 with the addition of 500 mg/kg MS and ICE particulates relative to the biotic control. In the 500 ml reactors, the presence of 500 mg/kg MS and ICE particulates resulted in an 1.42 ± 0.07 and 1.18 ± 0.07 times higher maximum diatom concentration relative to the biotic control without particulates. The pH in the biotic experiments increased slightly during the first 3-5 days from 8.35 to 8.5-8.6 and subsequently decreased to 8.2-8.3. Notably, pH in the biotic reactors doped with 500 mg/kg ICE particulates attained the final pH of 8.2-8.3 after only 5 days following a rapid decrease from 8.5 to 8.2. The pH in the abiotic controls increased during the first 3 days from 8.35 to 8.4-8.5 whereas it remained constant for reactors doped with MS particulates. In contrast, the pH dropped from 8.5 to 8.2 towards the end of the experiment in abiotic controls doped with ICE particulates.

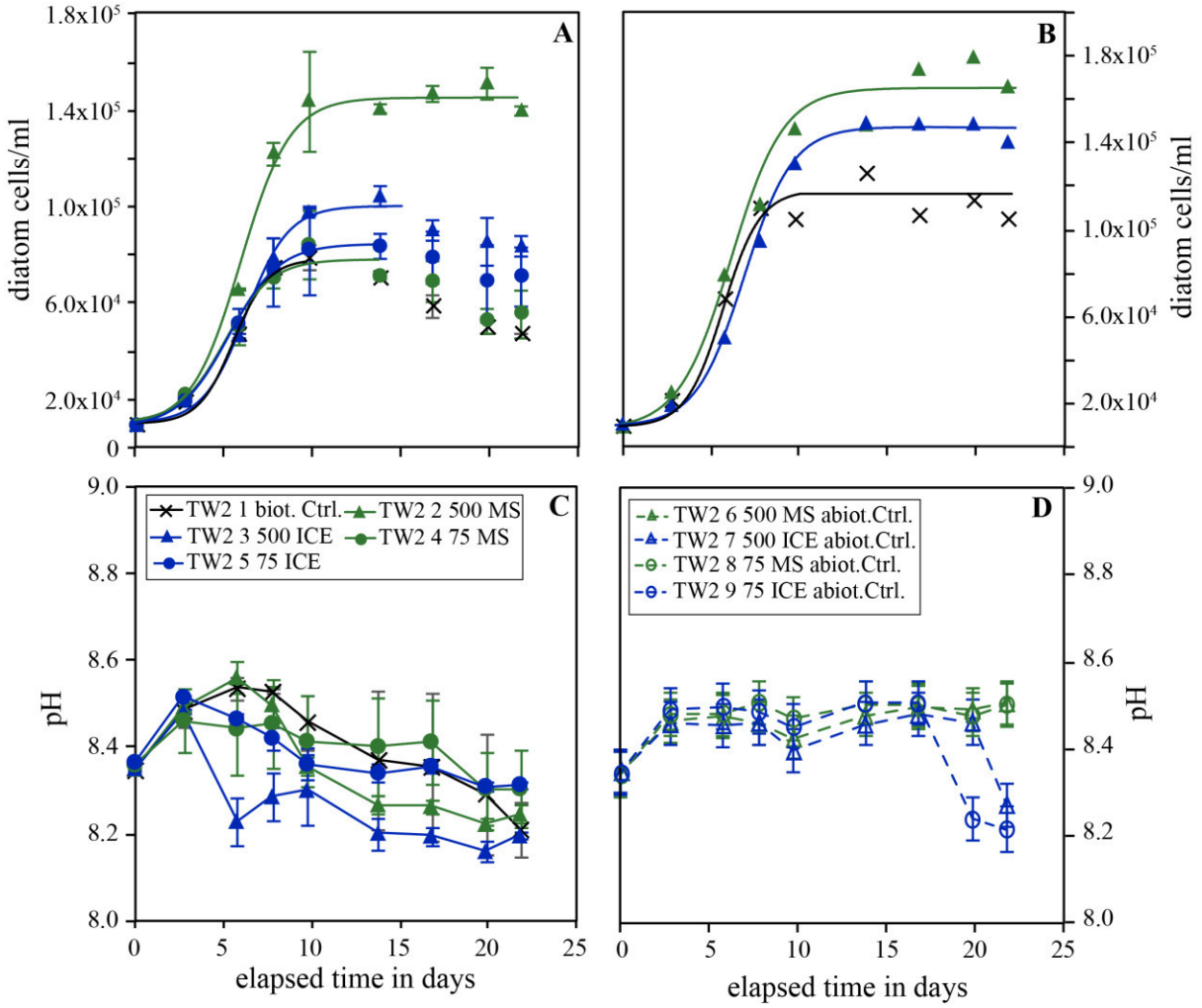

Figure 4-3. Temporal evolution of diatom concentration (**A**, **B**) and pH (**C**, **D**) in experimental series TW2 carried out in Instant Ocean© enriched with 5 % Guillard´s f/2 culture medium. Figure **A** shows the evolution of diatom concentration of experiments performed in 250 ml reactors, whereas Figure **B** shows the evolution in experiments performed in 500 ml reactors. Figure **C** shows the pH evolution of the biotic experiments and Figure **D** the pH evolution of the abiotic experiments. The error bars in **A** represent the standard deviation of the duplicates, in **C** and **D** of the triplicates. The uncertainty in diatom concentrations in Figure **C** is estimated to be below 10 %.

Figure 4-4 shows the temporal evolution of TW concentration and pH during experimental series TW4 performed in Instant Ocean© enriched with 5 % Guillard´s f/2 culture medium, in the presence and absence of 250 and 750 mg/kg MS and ICE riverine particulates. All TW cultures showed exponential growth from the onset of the experiment until day 12-15 when the cultures attained the stationary phase and cell concentrations started to decrease in all reactors. This post-exponential decay was most pronounced in the biotic control experiment without particulates. In the presence of 750 mg/kg ICE particulates, growth occurred, but lagged by 3-4 days. The measured maximum diatom concentration increased by factors of 1.10 ± 0.07 and 1.27 ± 0.08 in the presence of 250 and 750 mg/kg MS particulates and slightly by factors of 1.08 ± 0.09 and 1.04 ± 0.13 in the presence of 250 and 750 mg/kg ICE particulates relative to the biotic control. The pH in the biotic experiments doped with MS particulates increased

initially from 8.45 to 8.6, then decreased to 8.3 and remained constant during the last 8 days of experiment. In the biotic control and the reactors doped with ICE particulates, pH decreased during the first 3 days from 8.45 to 8.3-8.4 and 8.2-8.3, then it remained constant. The pH in the abiotic controls doped with MS particulates increased slightly from 8.45 to 8.55 during the course of the experiment. In abiotic controls doped with ICE particulates, pH remained constant at ~8.45 for the first 10 days but then decreased to 8.2 towards the end of the experiment.

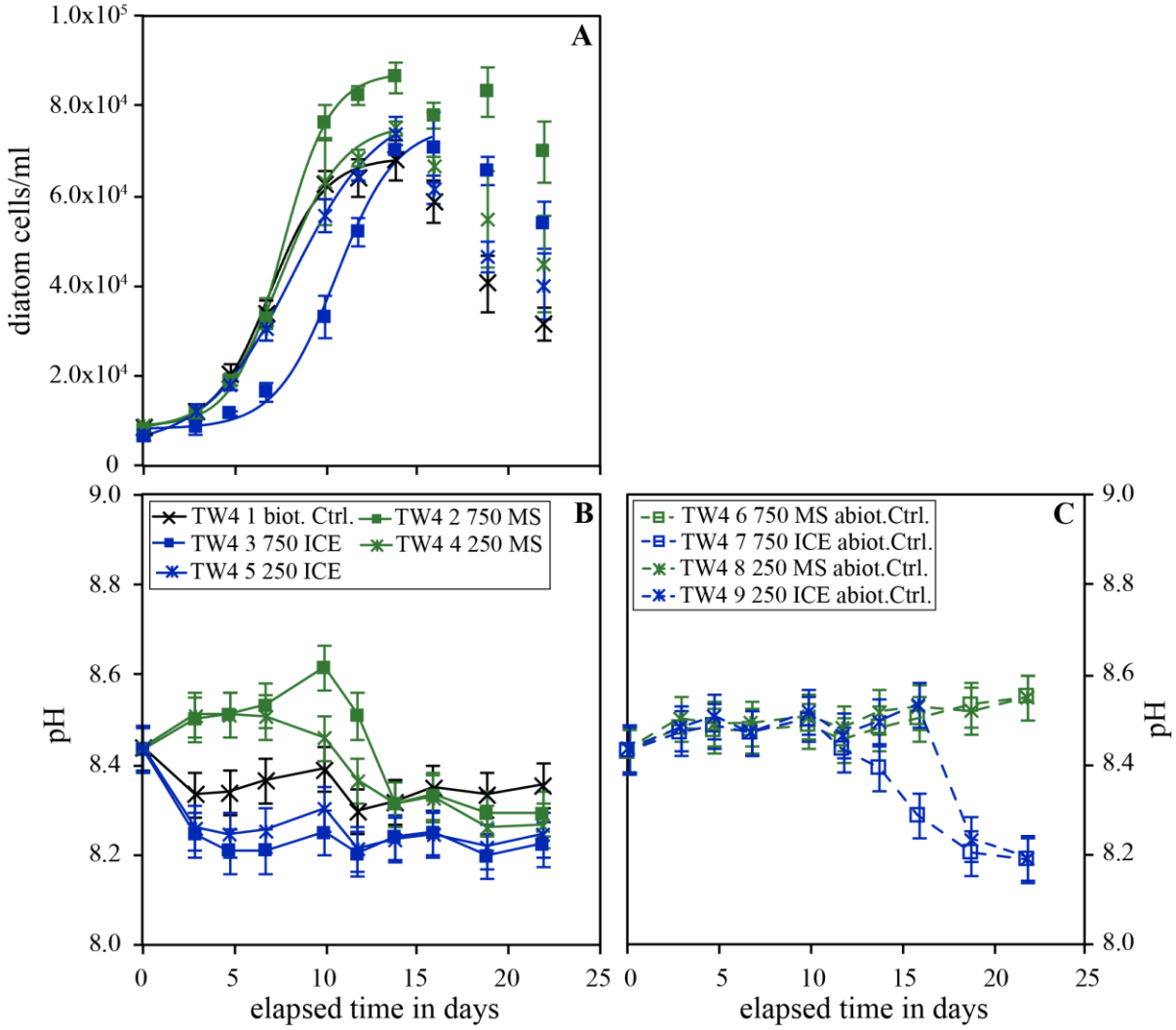

Figure 4-4. Temporal evolution of diatom concentration (**A**), pH (**B**) and pH in the abiotic control (**C**) of experimental series TW4 carried out in Instant Ocean© enriched with 5 % Guillard´s f/2 culture medium. The error bars represent the standard deviation of the triplicates.

4.3.2 Temporal evolution of diatom concentrations in Instant Ocean© without added dissolved nutrients - Experiments TW3 and TW5

In experiments conducted in Instant Ocean© without additional nutrients, diatom cultures did not exhibit an exponential growth stage. However, a pronounced positive effect of riverine particulates on diatom growth was observed in these experiments.

Figure 4-5 shows the temporal evolution of diatom concentration and pH in experimental series TW3 performed in Instant Ocean© in the presence and absence of 100 and 500 mg/kg MS and ICE riverine particulates. The initial diatom concentration was identical in all reactors since the solutions were all derived from the same dilution of the original culture. Thus, the observed lower concentration at the onset of the experiments doped with particulates is likely an artifact resulting from the increased turbidity and a concomitant underestimation of diatom concentration due to a more difficult traceability of the diatoms in the counting chamber.

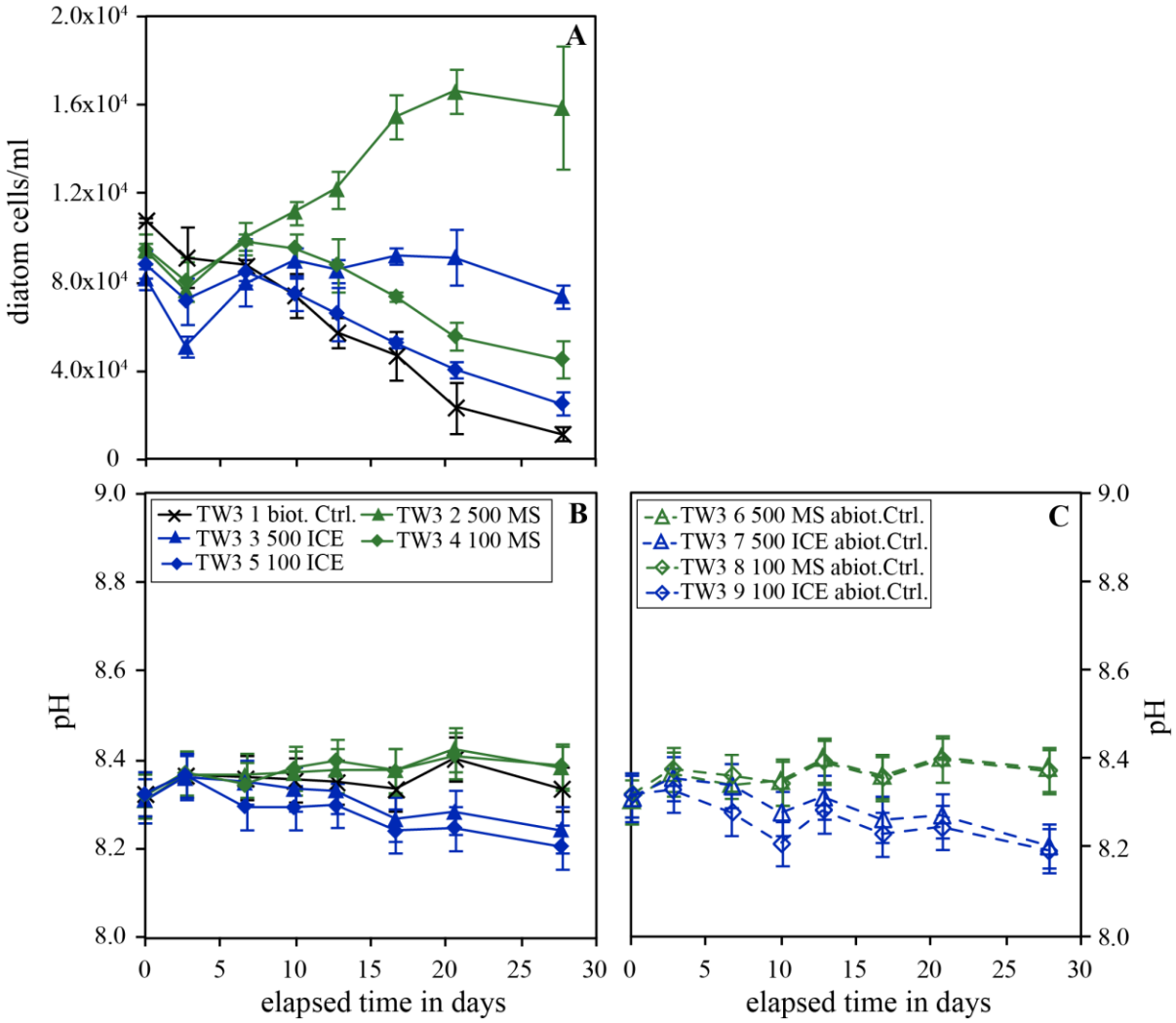

Figure 4-5. Temporal evolution of diatom concentration (**A**), pH (**B**) and pH in the abiotic control (**C**) of experimental series TW3 carried out in Instant Ocean© without additional nutrients. The error bars represent the standard deviation of the triplicates.

This is particularly evident for the more fine-grained ICE particulates. Diatom concentrations in the biotic control continuously decreased during the experiments. In the presence of 500 mg/kg MS particulates, diatom concentrations increased linearly from day 3 to 20 of the experiment resulting in a 13.55 ± 0.31 times greater final diatom concentration compared to the biotic control. In the presence of 500 mg/kg ICE particulates, this linear growth was less pronounced but diatoms likewise grew during day 3 to 20 resulting in a 6.30 ± 0.26 times greater final diatom concentration compared to the biotic control. Continuous growth was not observed in reactors doped with 100 mg/kg MS or ICE particulates but diatom concentrations notably decreased less rapidly compared to the biotic control, resulting in 3.86 ± 0.31 and 2.16 ± 0.32 times greater final diatom concentrations, respectively. The pH evolution was similar as in previously described experiments with a constant or slightly increasing pH in reactors doped with MS particulates and a decrease in pH by ~0.2 pH units in reactors doped with ICE particulates.

Figure 4-6 shows the temporal evolution of diatom concentration and pH in experimental series TW5 performed in Instant Ocean© in the presence and absence of 250 and 750 mg/kg MS and ICE riverine particulates. Similar as shown in Figure 4-5, diatom concentrations in the biotic control experiments continuously decreased during the experiments. In the presence of 750 mg/kg MS particulates, however, diatom concentration increased linearly throughout the experiment. In experiments doped with 250 mg/kg MS or ICE, and 750 mg/kg ICE particulates, diatom concentrations increased during days 1-9 and 1-15 of the experiment, respectively. This resulted in final diatom concentrations 7.87 ± 0.16 and 4.25 ± 0.17 times greater than the biotic control in the presence of 750 mg/kg MS and ICE particulates, respectively. With the addition of 250 mg/kg MS and ICE particulates, the final diatom concentrations increased by factors of 2.87 ± 0.17 and 1.20 ± 0.20 relative to the biotic control. The pH remained constant at 8.3-8.4 after an initial increase from 8.1 in all biotic and abiotic reactors.

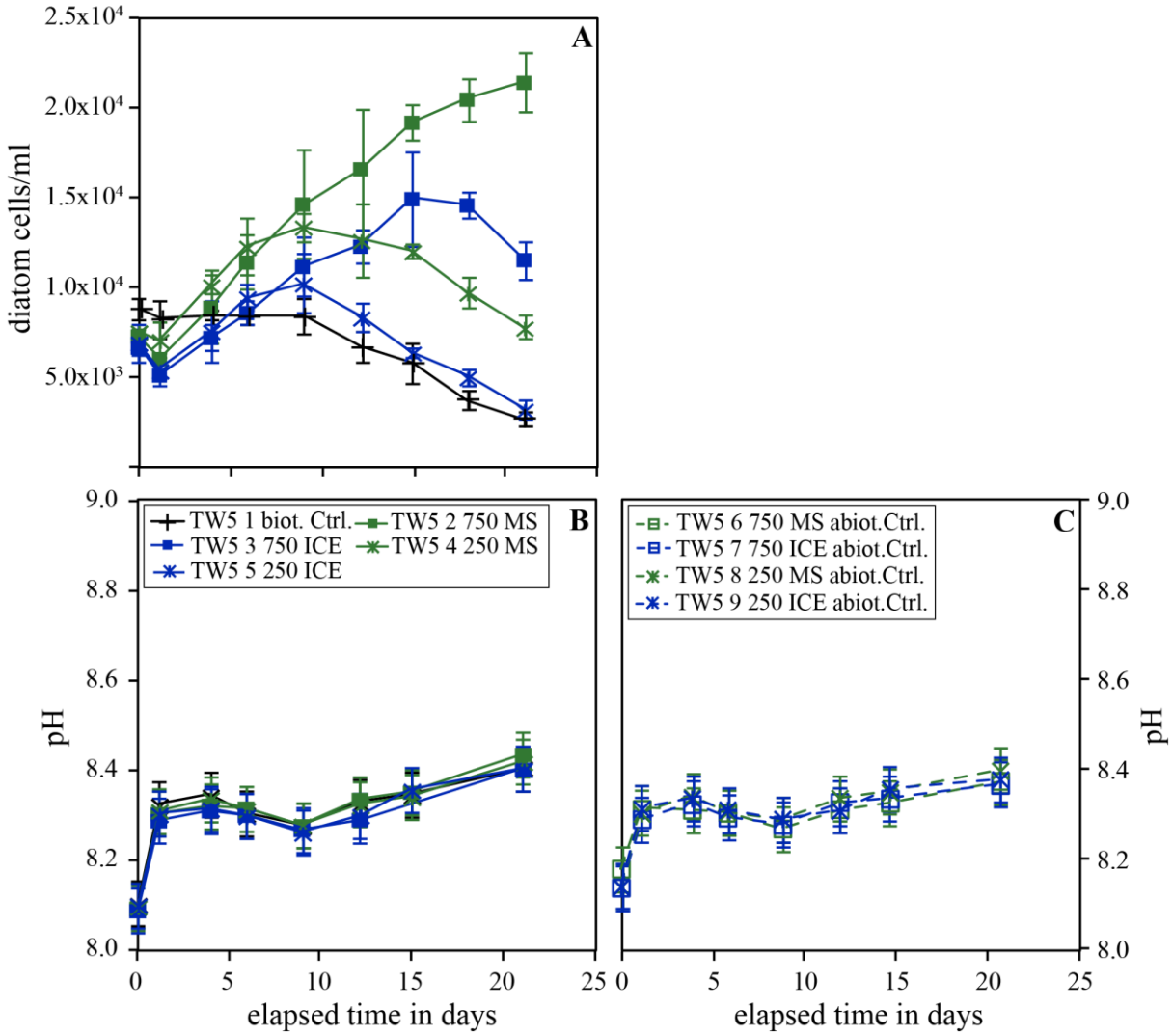

Figure 4-6. Temporal evolution of diatom concentration (**A**), pH (**B**) and the pH in the abiotic control (**C**) of experimental series TW5 carried out in Instant Ocean© without additional nutrients. The error bars represent the standard deviation of the triplicates.

4.3.3 SEM and optical microscopy

During cell counting using the optical microscope, diatoms were frequently found agglomerated in groups of about 10-50 cells mingled with sediment particles. This was evident for all experiments performed in the presence of MS and ICE particulates. This observation was confirmed by SEM investigations (see Figure 4-7) showing agglomerates of diatoms and sediment particles which appear to be held within organic substances (Figure 4-7 C).

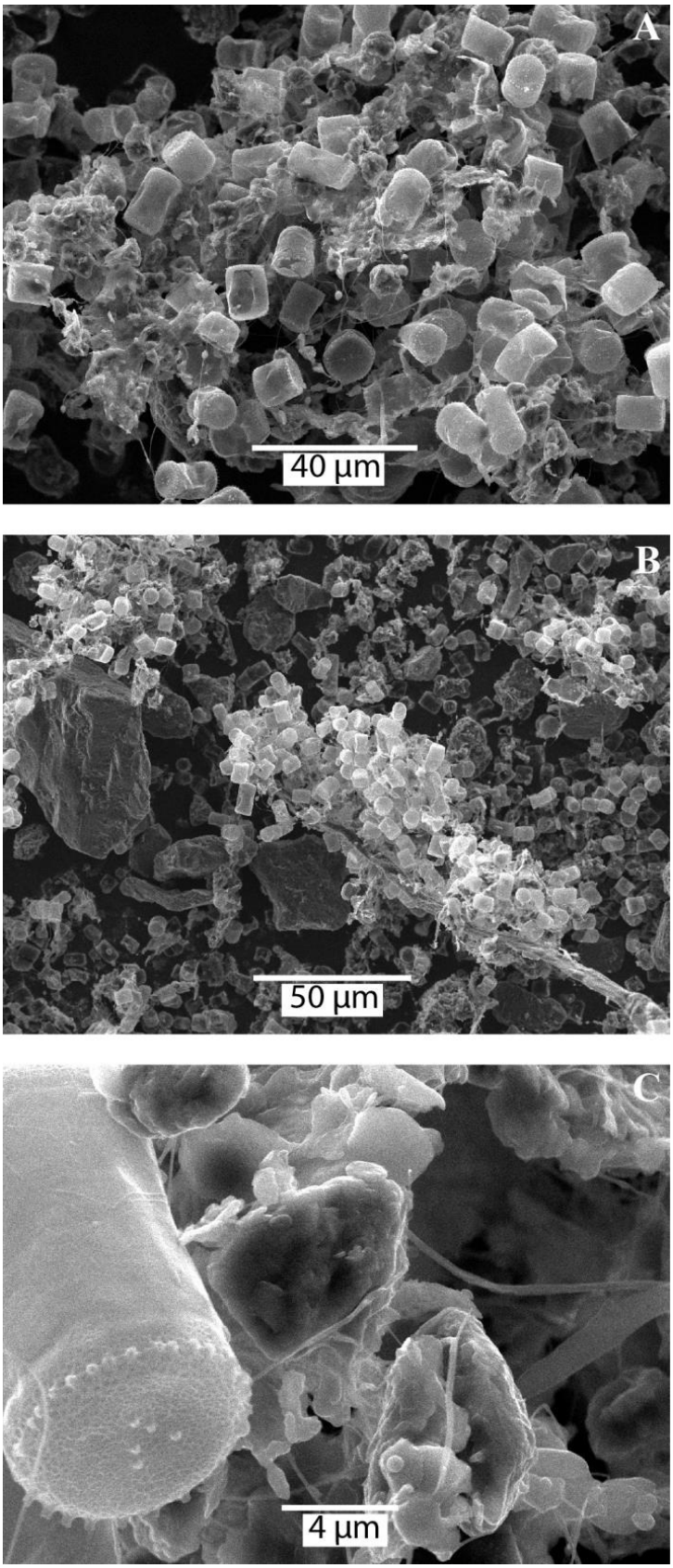

Figure 4-7. SEM photographs of experiment TW2 2-R1 performed in Instant Ocean© enriched with 5 % Guillard´s f/2 culture medium, in the presence of 500 mg/kg MS particulates. Diatoms were frequently found agglomerated with sediments, glued by organic substances.

4.4 Discussion

4.4.1 Summary of the effect of MS and ICE riverine particulate material on diatom growth

The microcosm growth experiments performed in this study can be subdivided into two categories with different initial conditions: a) series TW1, TW2 and TW4 were performed in nutrient enriched artificial seawater and b) series TW3 and TW5 were performed in artificial seawater without additional nutrients. In both initial conditions, the presence of riverine particulate material increased diatom growth or maintained its viability.

The effect of riverine particulate material on the growth of diatom in nutrient enriched artificial seawater is summarized in Figure 4-8, which shows the maximum (TW_{max}) and final (TW_{final}) diatom concentrations as a function of MS (Figure 4-8 A) and ICE (Figure 4-8 B) particulate concentrations. Throughout all experiments, the maximum and final diatom concentrations increased with increasing sediment concentration. However, this effect was more pronounced in the presence of MS compared to ICE particulates. Furthermore, the post-exponential decrease from the maximum diatom concentrations (TW_{max}) to the final concentration (TW_{final}) was distinctly less pronounced in experiments performed in the presence of riverine particulates compared to the biotic control. This is evidenced by the steeper slope of the regression lines of the TW_{final} compared to the TW_{max} concentrations and the resulting convergence of the two linear fit lines shown in Figure 4-8 A and B.

The effect of riverine particulate material on the diatom growth in artificial seawater without nutrient enrichment is summarized in Figure 4-9, which shows the temporal evolution of diatom concentrations in the presence of MS particulates (Figure 4-9 A), in the presence of ICE particulates (Figure 4-9 B) and the biotic controls in the absence of added particulates (Figure 4-9 C) during the same time interval. In all biotic controls, diatom concentrations continuously decreased during the experiments, whereas linear growth was observed in experiments doped with ≥100 mg/kg MS and ICE particulates. In the presence of 100 mg/kg MS and ICE particulates, diatom concentrations stayed close to constant or decreased slightly but less rapidly than in the biotic controls, resulting in higher final diatom concentrations. The linear growth observed during the experiments containing ≥100 mg/kg particulates is highlighted in Figure 4-10 which shows the slope of the best linear fits given in Figure 4-9, as a function of MS and ICE particulate concentrations added to the reactors. To a first approximation, these data are linear functions of particulate concentration, and consistent with rates of 1.42 ± 0.31 (R^2 = 0.87) and 1.13 ± 0.18 (R^2 = 0.92) diatom cells/ml/day per mg/kg MS

and ICE particulate material, respectively. With a diatom (TW) cell organic carbon content of about 30-180 pg C/cell (De La Rocha et al., 2010; De La Rocha and Passow, 2004; Waite et al., 1997), this corresponds to organic carbon formation rates ranging from 43 ± 9 to 255 ± 57 and 34 ± 6 to 203 ± 33 pg C/ml/day per each mg/kg MS and ICE particulate material, respectively. This estimate only takes cellular organic carbon into account and thus excluded extracellular C_{org}, which may significantly contribute to the total organic carbon content. Similar to the experiments performed in nutrient enriched Instant Ocean©, MS particulates showed a greater effect on diatom growth than ICE particulates.

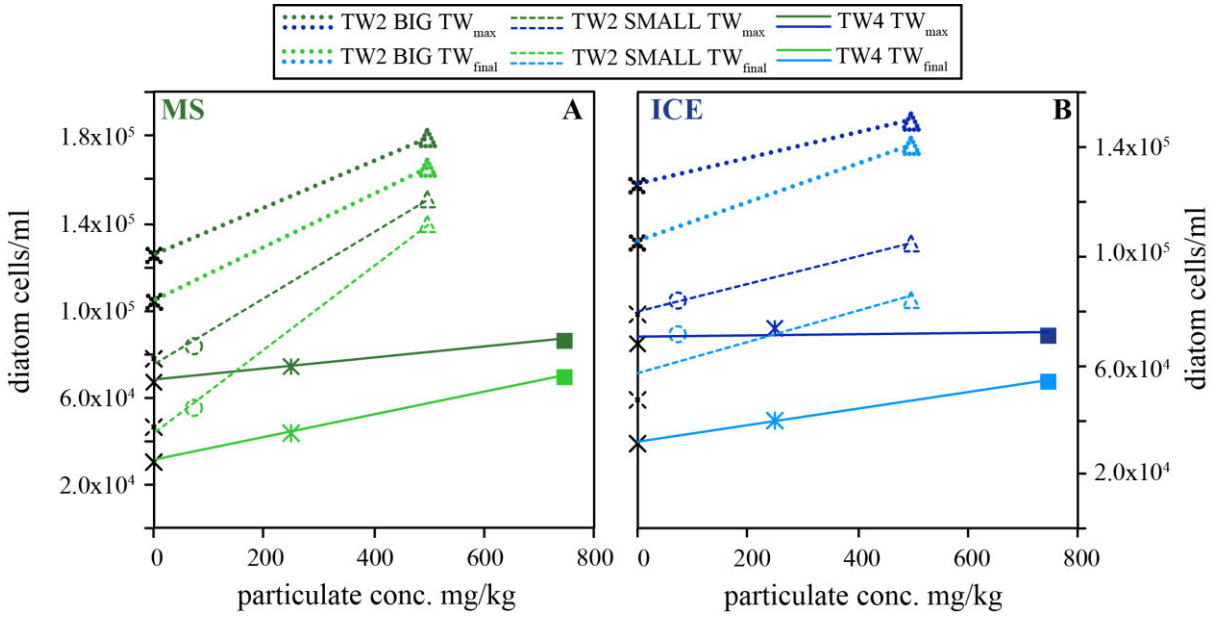

Figure 4-8. . Measured maximum (TW_{max}) and final (TW_{final}) diatom concentrations as a function of MS (**A**) and ICE (**B**) riverine particulate concentration for experimental series TW2 and TW4 performed in Instant Ocean© enriched with 5% Guillard´s f/2 culture medium. BIG and SMALL refers to the 500 ml and 250 ml reactors used in series TW2. Biotic controls without particulates are indicated as black crosses on the y-axes. Increasing particulate concentration raised diatom concentrations compared to the biotic control without particulates.

During this study, growth experiments were performed using only one single species of phytoplankton, the diatom *Thalassiosira weissflogii*. The two types of riverine particulate material used in the study cover a wide range of chemical compositions (silicic to basaltic). The basaltic sediment from Iceland might be expected to have a greater effect on diatom growth due to the more rapid release of silica, the main constituent of the diatom frustules (Brady and Walther, 1990; Gislason and Oelkers, 2003). However, Mississippi particulates showed a more pronounced effect on diatom growth compared to Iceland particulates in all experimental series. Thus, the observed positive effect of particulate material on phytoplankton growth may be due to the presence of minor phases, such as clays, or the presence of highly reactive nanoparticles adhering to larger grains (Poulton and Raiswell, 2005). Furthermore, we suggest that the

stronger effect of MS particulates compared to ICE particulates might stem from a higher concentration of adsorbed macro- and micronutrients on the surfaces of the Mississippi River sediments, impacted by anthropogenic and agricultural activity. Abiotic experiments of nutrient desorption from riverine particulate material would be necessary to quantify this difference.

The observation that silica release rates from sediments may not be the most important factor limiting diatom growth rates suggests that the release of nutrients from riverine particulates may be critical to the primary productivity in natural waters. As such, it seems likely that the presence of particles will positively affect the growth of other primary producers, which do not depend on silica, such as cyanobacteria, the oldest known organisms on Earth. Thus, riverine particulates might be expected to affect global primary production and consequently global biogeochemical cycles of several elements, today and in the past.

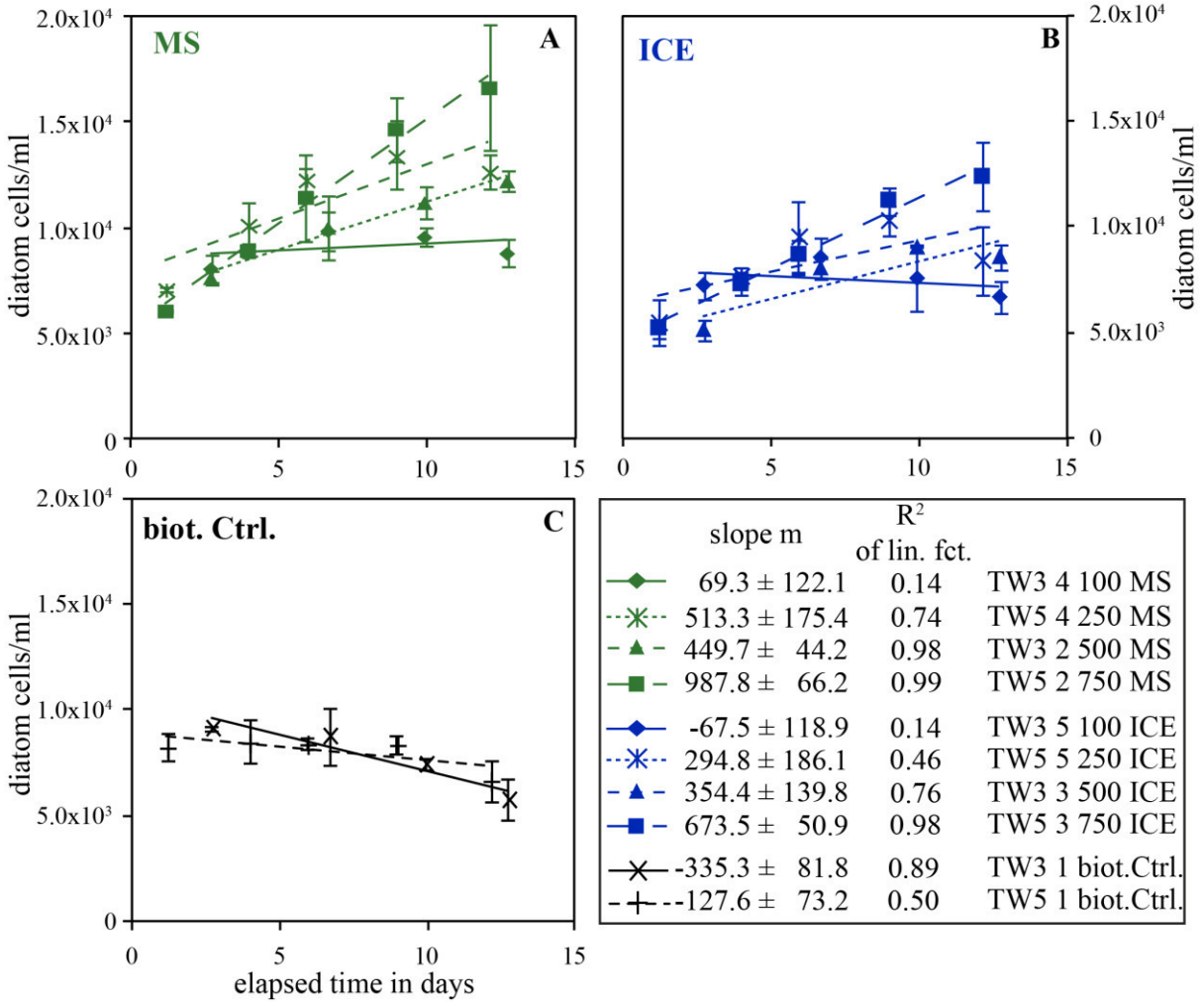

Figure 4-9. Temporal evolution of diatom concentration during the first 13 days of experimental series TW3 and TW5, performed in Instant Ocean© without additional nutrient enrichment. **A** and **B** show results from experiments performed in the presence of MS and ICE particulates and **C** shows results of the biotic controls without particulates. Lines show linear best fits of the data, the slopes of these fits are provided in the lower right box. The presence of particulates caused a linear diatom growth, whereas diatom numbers decreased with time in the biotic controls without particulates.

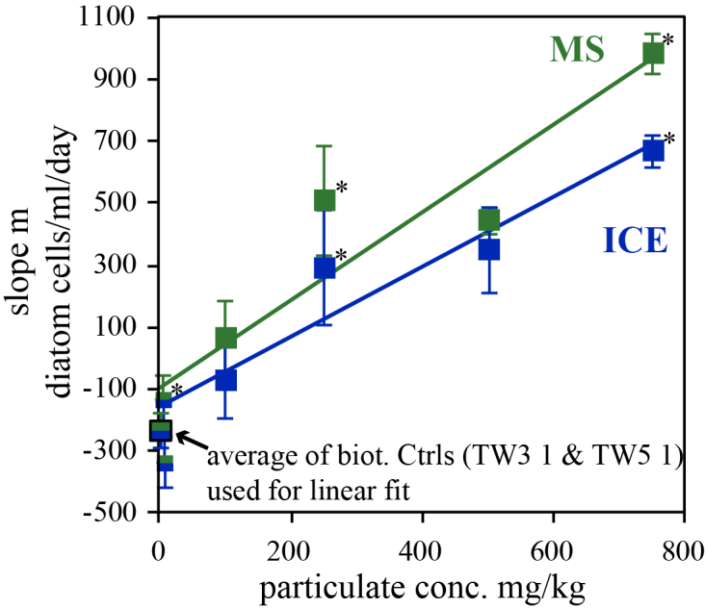

Figure 4-10. Slope of the linear best fits given in Fig. 8 plotted against the particulate concentration added to the reactors. Data points with a star (*) represent results of experimental series TW3, those without a star are from series TW5. Solid lines represent linear best fits of the data, whereby the average of the two biotic controls at 0 mg/kg particulates was used. Error bars reflect the uncertainty of the slope (see box in Figure 4-9).

4.4.2 Potential role of riverine particulate material in natural systems

Jeandel and Oelkers (2015) concluded that riverine particulate material has a large influence on ocean chemistry and the global cycle of the elements. Therein, Jeandel and Oelkers highlighted the potential role of riverine particulate material as slow release fertilizer supporting oceanic primary productivity and organic carbon burial. The results obtained in this study demonstrate that riverine particulates enhance diatom growth in seawater and thus validate the influence of terrigenous sediments on marine primary productivity.

Diatom blooms commonly occur during spring and early summer when light availability maximizes, seawater temperatures rise and oceanic water stratification is favorable. In the Arctic and subarctic, this coincides with the peak of the suspended matter delivery by the rivers to the ocean during freshet (Gordeev et al., 1996; Pokrovsky et al., 2012). Moreover, Gislason et al. (2006) observed that the maximum particulate fluxes in rivers in NE Iceland occur during the spring when ice melting maximizes. Thus, in times of highest oceanic primary productivity, riverine particulate fluxes from the continents to the oceans also maximize suggesting an important role of these particulates in delivering limiting nutrients such as silica. Moreover, at this time during the year, the less dense particulate and thus nutrient-rich river water floats on top of the denser seawater, creating a surface layer favorable for primary production. The potential effect of riverine particulates on primary production, however, depends on the environment. Whenever nutrients limit phytoplankton growth, riverine particulates could be

expected to increase growth due to the delivery of limiting nutrients. Evidence for this can be found following the damming of rivers. Dam construction reduces sediment arrival to estuarine ecosystems. This can have a major impact on primary productivity. For example, Baisre and Arboleya (2006) described a reduction in nutrient concentrations resulting from decreasing suspended sediment input in a Cuban estuary, which had a profound negative influence on the local ecosystem and on the regional fish industry. However, suspended particulates can also reduce light transmittance in the water column, which might decrease primary production if growth is light limited. For example, Jiang et al. (2014) and Chen et al. (2017) observed increasing chlorophyll a concentrations with decreasing suspended sediment input in Chinese estuaries, as a consequence of dam constructions. Note, however, these studies also report a concurrent increased occurrence of harmful algae blooms in these estuaries.

The large input of anthropogenic dissolved phosphate and nitrogen from agricultural use to coastal waters is known the increase eutrophication, potentially causing harmful algae blooms. Riverine particulates, however, release nutrients through mineral dissolution. The consumption of nutrients from seawater lowers the degree of saturation of nutrient-bearing minerals, thereby enhancing their release by accelerating mineral dissolution. Thus, particulates act as slow release fertilizer providing nutrients for phytoplankton growth in a buffered manner. Furthermore, particulates oppose harmful algal blooms through their ability to form sediment/algal flocs which sediment rapidly in the water column (Beaulieu et al., 2005). As shown in Figure 4-7, the diatoms in this study agglomerated into larger groups when particulates were present in the reactors. This observation suggests a potential effect of riverine particulates on organic carbon burial since larger agglomerates have greater settling velocities than single diatom cells. This supports the ‘ballast hypothesis’ from e.g. Armstrong et al. (2001), which proposes that mineral fragments increase organic carbon burial due to the formation of fast-settling mineral-phytoplankton aggregates.

Phytoplankton is known to have developed powerful strategies to gain access to vital nutrients. For example, bacteria and blue-green algae release siderophores with a high affinity for iron, which are recognized by receptor sites on the cell surface and transported across the cell membrane (Anderson and Morel, 1982). Similarly, chelators are known to depress toxic metal activity or to increase ferric oxide solubility making Fe bio-available (Anderson and Morel, 1982; Milligan et al., 2009). Furthermore, depending on the mechanism of carbon uptake, phytoplankton may alter the surrounding pH (Milligan et al., 2009; Wolf-Gladrow and Riebesell, 1997), which can increase nutrient availability through enhanced mineral dissolution

in the cell microenvironment (Milligan et al., 2009; Shaked et al., 2005). Direct and indirect interactions of microbes and inorganic substances are omnipresent in natural systems and several studies have demonstrated the ability of microbes to acquire nutrients directly from minerals (Bailey et al., 2009; Rogers et al., 1998; Rogers and Bennett, 2004; Sudek et al., 2017). Riverine particles can release elements to the oceans by desorption, exchange or dissolution; several examples are summarized in Jeandel and Oelkers (2015). Furthermore, we hypothesize that phytoplankton might access limiting nutrients directly from the sediments within the microniches at the particle surfaces. The direct physical contact between phytoplankton or their extracted organic compounds might further reinforce the role of particulates as nutrient supplier and transport agent for organic carbon to the deep ocean. This, however, needs further experimental and in-situ studies exploring the effect of riverine particulates on the growth of different types of phytoplankton and their mechanisms of nutrient uptake as well as the role of particulates in agglomeration and sedimentation of organic carbon.

The link between climate and riverine particulate transport is likely strongest during the end of glacial cycles, when glacial activity produces vast quantities of fine-grained material, transported to the oceans by glacial meltwater (Alley et al., 1997; Eiriksdottir et al., 2015; Jeandel and Oelkers, 2015). Furthermore, the transport of particulate material to the oceans during this time is likely facilitated through the influx of icebergs, which may transport nutrients to remote regions of the open ocean. The increased supply of particulate material to the ocean likely increases primary productivity and organic carbon burial, thus contributing to drawing down atmospheric CO_2 levels and moderating global warming. As the CO_2 drawdown via the organic carbon cycle is concomitant with a rise in oxygen, produced during oxygenic photosynthesis, the enhanced organic carbon cycle towards the end of major glaciations may have played a major role in the atmospheric oxygenation events. The two major oxygenation events of the Earths' atmosphere occurred about 2.4-1.8 Ga ago (Great Oxidation Event (GOE, e.g. Holland, 2002; Shields-Zhou and Och, 2011)) and during the Neoproterozoic, and both coincide with major "Snowball Earth" events, which occurred 2.4-2.1 Ga ago (Huronian glaciation, e.g. Tang and Chen, 2013) and during the Cryogenian period (Sturtian and Marionoan glaciations, ~0.7 Ga and ~0.65 Ga ago e.g. Arnaud et al., 2011; Rooney et al., 2015). These major oxygenation and glaciation events furthermore coincide with carbon isotope excursions recorded in marine carbonates, which are interpreted as variations in organic matter burial (Holland, 2006; Shields-Zhou and Och, 2011). Such observations suggest that the stabilization of the Earths' temperature through photosynthetic CO_2 drawdown and the oxygenation of the Earths' atmosphere through photosynthetic O_2 production may have been

caused, at least in part, by particulate driven enhanced primary production and organic carbon burial.

4.5 Conclusions

The results obtained in this study demonstrate a positive effect of riverine particulate material on the growth of the marine diatom *Thalassiosira weissflogii*. In Guillard´s f/2 culture medium enriched Instant Ocean©, the presence of riverine particulates increased the total diatom concentration and slowed post-exponential net diatom death rates. In Instant Ocean© without additional nutrients, riverine particulates led to a linear increase in diatom concentrations as a function of particulate concentration, whereas diatom cultures died in controls without particulates. These results indicate a strong positive influence of riverine particulates on phytoplankton growth in coastal environments. Moreover, the presence of particulates is suggested to facilitate organic carbon burial through the delivery of surface area available for adsorption of organic compounds and through their role in the aggregation and sedimentation of phytoplankton. These combined effects suggest a major role of riverine particulates in the global carbon cycle, which becomes especially important in view of serious anthropogenic perturbations of global particle fluxes.

Acknowledgements

This research was supported by the Marie Curie EU-FP7 CO2-REACT Research and Training Network. The authors would like to thank Liudmila Shirokova, Thierry Aigouy and Alain Castillo from the Géosciences Environnement Toulouse for their help with the experimental work, SEM- and BET- measurements, respectively. OSP acknowledges partial support from RFBR grant No 17-05-00348_a and RSF grant No 15-17-10009. The authors furthermore acknowledge Bruno Etcheverria from the EPOC laboratory, University of Bordeaux, Station Marine d´Arcachon for providing the diatom culture and for his advice concerning diatom culturing and maintaining. Eydis Eiriksdottir from the Department of Earth Sciences at the University of Iceland and Karen Johannesson from the Department of Earth and Environmental Sciences of Tulane University, New Orleans, are acknowledged for the provision of Iceland and Mississippi riverine particulate material, respectively.

4.6 References

See References on page 157ff.

Appendix Chapter 4

Table A 4-1. Summary of experimental conditions as well as the measured maximal (TW_{max}) and final (TW_{final}) TW concentrations.

Experiment ID	electrolyte	particulates [mg/kg] - type	duration [days]	pH initial	pH range	$TW_{initial}$ $\times 10^4$ [cells/kg]	TW_{max} $\times 10^4$ [cells/kg]	TW_{final} $\times 10^4$ [cells/kg]	% increase rel. to biotic ctrl	observation
TW1 1	IO + 100 % f/2	biotic ctrl	6.6	8.20	8.2-9.4	1.87	45.72	45.72		exp. Growth
TW1 2	IO + 100 % f/2	500 MS	6.6	8.22	8.2-9.3	1.77	47.20	47.20	3.2	exp. Growth
TW1 3	IO + 100 % f/2	500 ICE	6.6	8.23	8.2-9.3	1.67	55.20	55.20	20.7	exp. Growth
TW1 4	IO + 100 % f/2	500 MS	6.6	8.20	8.2-8.4		abiotic ctrl			
TW1 5	IO + 100 % f/2	500 ICE	6.6	8.18	8.2-8.4		abiotic ctrl			
TW2 1	IO + 5 % f/2	biotic ctrl	21.8	8.34	8.1-8.6	0.99	7.90	10.51		exp. Growth
TW2 1b	IO + 5 % f/2	biot. ctrl BIG	21.8	8.35	8.2-8.5	0.96	12.62	4.77		exp. Growth
TW2 2	IO + 5 % f/2	500 MS	21.8	8.35	8.2-8.5	0.99	15.16	16.60	91.8	exp. Growth
TW2 2b	IO + 5 % f/2	500 MS BIG	21.8	8.35	8.2-8.6	0.92	17.96	14.02	42.3	exp. Growth
TW2 3	IO + 5 % f/2	500 ICE	21.8	8.35	8.2-8.5	0.94	10.46	14.04	32.4	exp. Growth
TW2 3b	IO + 5 % f/2	500 ICE BIG	21.8	8.35	8.1-8.5	1.05	14.93	8.39	18.3	exp. Growth
TW2 4	IO + 5 % f/2	75 MS	21.8	8.36	8.3-8.5	0.94	8.43	5.60	6.6	exp. Growth
TW2 5	IO + 5 % f/2	75 ICE	21.8	8.37	8.3-8.5	0.94	8.37	7.14	5.9	exp. Growth
TW2 6	IO + 5 % f/2	500 MS	21.8	8.35	8.4-8.5		abiotic ctrl			
TW2 7	IO + 5 % f/2	500 ICE	21.8	8.35	8.3-8.5		abiotic ctrl			
TW2 8	IO + 5 % f/2	75 MS	21.8	8.34	8.3-8.5		abiotic ctrl			
TW2 9	IO + 5 % f/2	75 ICE	21.8	8.35	8.2-8.5		abiotic ctrl			
TW3 1	IO	biotic ctrl	27.7	8.32	8.3-8.4	1.08	1.08	0.12		no growth
TW3 2	IO	500 MS	27.7	8.31	8.3-8.4	0.95	1.66	1.59	1254.5*	linear growth
TW3 3	IO	500 ICE	27.7	8.31	8.2-8.4	0.82	0.92	0.74	529.5*	linear growth
TW3 4	IO	100 MS	27.7	8.32	8.3-8.4	0.95	0.99	0.45	286.4*	no growth
TW3 5	IO	100 ICE	27.7	8.32	8.2-8.4	0.88	0.88	0.25	115.9*	no growth
TW3 6	IO	500 MS	27.7	8.30	8.3-8.4		abiotic ctrl			
TW3 7	IO	500 ICE	27.7	8.32	8.2-8.4		abiotic ctrl			
TW3 8	IO	100 MS	27.7	8.31	8.3-8.4		abiotic ctrl			
TW3 9	IO	100 ICE	27.7	8.32	8.2-8.3		abiotic ctrl			
TW4 1	IO + 5 % f/2	biotic ctrl	21.8	8.44	8.3-8.4	0.86	6.83	3.17		exp. Growth
TW4 2	IO + 5 % f/2	750 MS	21.8	8.43	8.3-8.6	0.81	8.67	7.01	27.0	exp. Growth

Table A 4-1. Continuation.

Experiment ID	electrolyte	particulates [mg/kg] - type	duration [days]	pH initial	pH range	$TW_{initial}$ $\times 10^4$ [cells/kg]	TW_{max} $\times 10^4$ [cells/kg]	TW_{final} $\times 10^4$ [cells/kg]	% increase rel. to biotic ctrl	observation
TW4 3	IO + 5 % f/2	750 ICE	21.8	8.44	8.2-8.4	0.65	7.08	5.40	3.8	exp. Growth
TW4 4	IO + 5 % f/2	250 MS	21.8	8.44	8.3-8.5	0.91	7.54	4.49	10.5	exp. Growth
TW4 5	IO + 5 % f/2	250 ICE	21.8	8.44	8.2-8.4	0.70	7.39	4.01	8.3	exp. Growth
TW4 6	IO + 5 % f/2	750 MS	21.8	8.43	8.4-8.6		abiotic ctrl			
TW4 7	IO + 5 % f/2	750 ICE	21.8	8.43	8.2-8.5		abiotic ctrl			
TW4 8	IO + 5 % f/2	250 MS	21.8	8.44	8.4-8.6		abiotic ctrl			
TW4 9	IO + 5 % f/2	250 ICE	21.8	8.44	8.2-8.5		abiotic ctrl			
TW5 1	IO	biotic ctrl	21.0	8.10	8.1-8.4	0.89	0.89	0.27		no growth
TW5 2	IO	750 MS	21.0	8.09	8.1-8.4	0.73	2.14	2.14	687.3*	linear growth
TW5 3	IO	750 ICE	21.0	8.09	8.1-8.4	0.67	1.50	1.16	325.5*	linear growth
TW5 4	IO	250 MS	21.0	8.10	8.1-8.4	0.76	1.34	0.78	187.3*	initially lin. growth
TW5 5	IO	250 ICE	21.0	8.10	8.1-8.4	0.70	1.03	0.33	19.6*	initially lin. growth
TW5 6	IO	750 MS	21.0	8.18	8.1-8.4		abiotic ctrl			
TW5 7	IO	750 ICE	21.0	8.14	8.1-8.4		abiotic ctrl			
TW5 8	IO	250 MS	21.0	8.14	8.1-8.4		abiotic ctrl			
TW5 9	IO	250 ICE	21.0	8.14	8.1-8.4		abiotic ctrl			

*In experimental series TW3 and TW5, where no exponential growth occurred, the % increase relative to the biotic control is based on the final TW concentration and not on the maximal concentration as for experimental series TW1, TW2 and TW4 where exponential growth occurred.

5 The temporal evolution of carbon isotopes in calcite in the presence of cyanobacteria

Résumé

La calcite a été précipitée en présence et en l'absence des cyanobactéries *Synechococcus sp.* dans des réacteurs discontinus. L'évolution temporelle de l'isotope du carbone de la calcite ($\delta^{13}C_{Calcite}$) et du carbone inorganique dissous ($\delta^{13}C_{DIC}$) a été surveillée pour évaluer le taux et le degré d´altération des compositions d'isotopes du carbone dans la calcite. La présence de cyanobactéries a favorisé la formation de carbonate de calcium et a modifié considérablement la composition isotopique du carbone inorganique de la phase liquide en raison de l'incorporation préférentielle de ^{12}C dans la biomasse. La composition isotopique du carbone de la calcite a évolué en continu vers l'équilibre isotopique entre les fluides et les minéraux après la complète précipitation de la calcite. Les taux normalisés à la surface géométrique des minéraux atteignaient 1.75×10^{-14} à 1.71×10^{-13} mol $^{13}C/m^2/s$. Ces taux mesurés suggèrent que les compositions de $\delta^{13}C_{DIC}$ des fluides dans les roches riches en carbonate seraient généralement tamponnées par la signature $\delta^{13}C_{Calcite}$ de la calcite coexistante. D'autres calculs du bilan de masse suggèrent que la composition isotopique du carbone de la calcite ($\delta^{13}C_{Calcite}$) pourrait changer notablement si la calcite était continuellement en déséquilibre isotopique avec son fluide coexistant, par exemple par la présence d'un puits local de ^{12}C comme des microorganismes photosynthétiques ou d'une source de ^{12}C telle que celle engendrée par la décomposition de matières organiques.

The temporal evolution of carbon isotopes in calcite in the presence of cyanobacteria

Christian Grimm[1*], Vasileios Mavromatis[1,2], Albrecht Leis[3], Oleg S. Pokrovsky[1], Eric H. Oelkers[1,4]

[1] Géosciences Environnement Toulouse, CNRS-UPS-OMP, 14 av. Édouard Belin, 31400 Toulouse, France.

[2] Institute of Applied Geosciences, Graz University of Technology, Rechbauerstraße 12, 8010 Graz, Austria.

[3] R-AquaConSol GmbH, Steyrergasse 21, 8010 Graz, Austria.

[4] Department of Earth Sciences, UCL, Gower Street, WC1E 6BT London, United Kingdom.

* Corresponding author e-mail: grimm@get.obs-mip.fr

This manuscript has been submitted to *Geochimica et Cosmochimica Acta*

Keywords: Carbon isotopes, calcite, cyanobacteria, isotope re-equilibration

Abstract

Calcite was precipitated in the presence and absence of *Synechococcus sp.* cyanobacteria in batch reactors. The temporal carbon isotope evolution of calcite ($\delta^{13}C_{Calcite}$) and dissolved inorganic carbon ($\delta^{13}C_{DIC}$) was monitored to evaluate the rate and degree to which stable carbon isotope compositions in calcite are modified after the precipitation is complete. The presence of cyanobacteria promoted calcium carbonate formation and changed significantly the carbon isotope composition of dissolved inorganic carbon due to the preferential incorporation of ^{12}C into the biomass, generating an isotopic disequilibrium between the precipitated calcite and the ambient aqueous fluid phase. The carbon isotope composition of the calcite evolved continuously towards mineral-fluid isotopic equilibrium after calcite precipitation was complete at geometric surface area normalized rates ranging from 1.75×10^{-14} to 1.71×10^{-13} mol $^{13}C/m^2/s$. These measured rates suggest that the $\delta^{13}C_{DIC}$ compositions of fluids in carbonate-rich rocks would commonly be buffered by the $\delta^{13}C_{Calcite}$ of the co-existing calcite. Further mass balance calculations suggest that the carbon isotope composition of calcite ($\delta^{13}C_{Calcite}$) might change noticeably if the calcite were continuously in isotopic disequilibria with its co-existing fluid, for example through the presence of a local ^{12}C sink such as photosynthetic microorganisms or ^{12}C source such as decomposition of organic material.

5.1 Introduction

The precipitation of carbonate minerals is a fundamental process in the Earth´s carbon cycle. Notably, the stable isotope compositions of carbonate minerals reflect the conditions prevailing during mineral precipitation (e.g. Broecker, 1970; Epstein et al., 1953; Kump and Arthur, 1999; McCrea, 1950; McDermott, 2004; Schidlowski and Junge, 1981; Urey et al., 1951). As such, these compositions have become a widespread tool to reconstruct the environmental conditions present over geologic time. For example, the carbon isotope signature $\delta^{13}C$ has been used to provide insight into past carbon cycling (Assayag et al., 2008; Bartley and Kah, 2004; Hayes et al., 1999) and to trace the link between biological activity and the rise of atmospheric oxygen (e.g. Botz et al., 1996; Broecker, 1970; Schrag et al., 2013; Whiticar, 1999). The presence of positive or negative 'carbon excursions' in the marine carbonate record are amongst the most notable observations in the sedimentary record. For instance a negative carbon excursion occurred at the Paleocene-Eocene thermal maximum (PETM) with stable carbon isotopes being 2-3 ‰ more negative than background levels (e.g. Koch et al., 1992;

Dickens et al., 1995). These events were interpreted to record significant changes in primary productivity and organic carbon burial (Brasier et al., 1994; Kump, 1991; Kump and Arthur, 1999). Organic carbon exhibits distinct carbon isotopic signatures due to the preferential uptake of ^{12}C during photosynthesis (Johnston and Fischer, 2012; O'Leary, 1988). Thus, at times of high primary productivity and organic carbon burial, carbon isotopes in the atmosphere, in dissolved inorganic carbon, and in precipitated carbonate minerals are enriched in the heavier ^{13}C isotope. The use of the $\delta^{13}C$ signatures of carbonate minerals in the geological record to interpret past environmental conditions, however, requires that these signatures are preserved over vast timescales. The carbonate minerals calcite and aragonite are of particular interest in this regard due to their abundance in modern and ancient natural systems.

The degree to which carbon and other isotopic signatures of carbonates can be preserved over geological timescales has been recently questioned by the scientific community. As such, Mavromatis et al. (2015) observed the rapid re-equilibration of carbon isotope signatures of precipitated hydrous Mg-carbonates in contact with an aqueous fluid. Moreover, Mavromatis et al. (2012) and Shirokova et al. (2013) observed a similar re-equilibration of Mg isotopes in hydromagnesite and dypingite, and Mavromatis et al. (2016) reported a rapid equilibration of Ba isotopes in witherite in contact with an aqueous fluid even after fluid-mineral chemical equilibrium was attained. Similarly, Mavromatis et al. (2017) observed a pronounced Mg-isotope shift during the transformation of amorphous calcium carbonate to $(Ca,Mg)CO_3$, followed by a progressive change of Mg-isotopes in the Mg-calcite towards isotopic equilibrium with respect to the aqueous fluid. The chemical exchange between carbonates and the ambient fluid phase during diagenesis and a resulting isotopic modification of the solid have been described in detail the literature (Banner and Hanson, 1990; Brand and Veizer, 1980, 1981; Gorski and Fantle, 2017). This early diagenetic mineral stabilization depends on 1) the stability and reactivity of the mineral phase, 2) the difference in composition of the formation fluid and newly infiltrating aqueous fluids, 3) the water/rock ratio representing the openness of the system and 4) the isotopic fractionation factor. The mechanism is described as a dissolution-precipitation process occurring near the mineral-fluid interface where each step includes a new mineral-fluid equilibration. Thereby, the degree of isotopic exchange depends on the isotopic disequilibrium between the mineral and the fluid phase and is thus subject to the maintenance of the disequilibrium, controlled by the openness of the system (Brand and Veizer, 1980, 1981). For example, Patterson and Walter (1994a) and Patterson and Walter (1994b) concluded that the $\delta^{13}C$ in shelf limestones is partly controlled by chemically evolved pore waters rather than

by the open ocean seawater from which it originally precipitated. Similarly, Oehlert and Swart (2014) observed the simultaneous post-depositional alteration of organic and carbonate $\delta^{13}C$ values in carbonates from the Great Bahama Banks due to freshwater alteration and marine diagenesis and Allan and Matthews (1982) describe variations of $\delta^{13}C$ signatures in carbonates associated with early meteoric diagenesis. This isotopic modification during diagenesis may be amplified by the authigenic precipitation of new mineral phases in the pore-fluid as described by Schrag et al. (2013) who proposed that authigenic carbonate precipitation in sediment pore fluids during early diagenesis leads to local variations in carbon isotope signatures which may help to explain major carbon isotope variations in the geological record. Moreover, field (Eichinger, 1983)and laboratory (Mozeto et al., 1984; Wendt, 1971) evidence affirms that carbon isotope exchange between different carbon bearing phases is an important process in groundwater and needs to be taken into account to accurately determine the ^{14}C ages of groundwaters (Gonfiantini and Zuppi, 2003; Han et al., 2014; Han and Plummer, 2013). These examples describe potential isotopic modifications occurring during mineral stabilization at the fluid-solid interface and raise the question how well these minerals are preserved over long timescales and how well they record the penecontemporaneous depositional environment.

Bacterial activity has been shown to markedly influence the carbon isotope compositions of fluid-carbonate systems. The presence of cyanobacteria effects the carbon isotope signatures of dissolved inorganic carbon and of the precipitating carbonates through their metabolic activity, which preferentially uptake ^{12}C during photosynthesis (e.g. Ferris et al., 1997; Andres et al., 2006; Jimenez-Lopez et al., 2006; Power et al., 2011; Brady et al., 2013; Mavromatis et al., 2015). Furthermore, a range of studies have shown that cyanobacteria can promote carbonate mineral precipitation by increasing pH during photosynthesis (Dittrich et al., 2003; Kranz et al., 2010; Mavromatis et al., 2012; 2015; Obst et al., 2009b; Shirokova et al., 2011; 2013; Thompson et al., 1997). As such, bacterial activity is a major control of the carbon isotope composition of DIC in natural waters, which in turn influences the isotopic composition of carbonates precipitated at or near to isotopic equilibrium with these fluids (Craig, 1953; Nelson and Smith, 1996; Swart, 2015).

This study aims to assess the rates of carbon isotope signature modification in calcite due to bacterial-induced changes in the carbon isotope composition of a co-existing fluid phase. Towards this goal, we conducted a series of batch calcite precipitation experiments in the presence of cyanobacteria and monitored the temporal $\delta^{13}C$ isotope evolution of the fluid and solid phases. These observations were used to evaluate the rate and degree to which stable

carbon isotope compositions are modified in calcite. The purpose of this paper is to report the results of this experimental study and to use these results to assess the degree to which calcite carbon isotope signatures might change with time in natural systems.

5.2 Theoretical considerations

Carbon isotope compositions in this paper are presented in the delta notation given by:

$$\delta^{13}\mathrm{C}\ (‰) = 10^3 \cdot \left(\frac{^{13/12}\mathrm{C}_{sample}}{^{13/12}\mathrm{C}_{V-PDB}} - 1 \right), \qquad (5\text{-}1)$$

where $^{13/12}\mathrm{C}$ refers to the indicated isotope ratio of C, $\delta^{13}\mathrm{C}$ provides the normalized value of this ratio and the subscripts *sample* and *V-PDB* represent the sample of interest and the *V-PDB* international standard, respectively. Note, that all calcite $\delta^{13}\mathrm{C}$ values ($\delta^{13}\mathrm{C}_{Calcite}$) reported in this study refer to the average bulk isotopic composition of the solid.

In this study, calcite was precipitated from aqueous carbonate solutions in the presence of cyanobacteria and in contact with the atmosphere (details about the experimental conditions are described in the methods section). In such systems there are four major processes that affect the carbon isotope composition of dissolved inorganic carbon as summarized in Figure 5-1. The $\delta^{13}\mathrm{C}_{DIC}$ in these experiments is initially controlled by the carbon isotope composition of the sodium carbonate and bicarbonate used to produce the aqueous fluids. This value is subsequently influenced by 1) carbon exchange with the atmospheric CO_2 that was continuously bubbled in the reactors, 2) photosynthetic uptake of DIC by growing cyanobacteria, 3) respiration and cell death together with the subsequent heterotrophic degradation of organic compounds to dissolved carbon species, and 4) DIC removal from the fluid by calcite precipitation. These processes are described in detail in the following section.

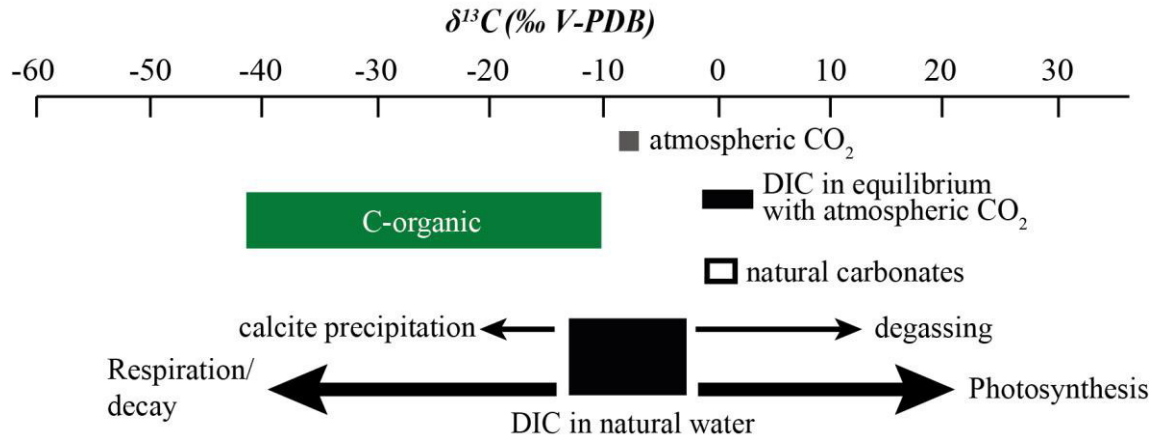

Figure 5-1. Carbon isotope signatures of various components of the carbon cycle. The grey symbol indicates gaseous carbon, the filled black symbols represent carbon in DIC and the black open symbols indicate carbon in carbonate minerals. Arrows indicate processes effecting $\delta^{13}C$ (modified from Schulte et al. (2011)).

5.2.1 Carbon exchange with the atmosphere

5.2.1.1 Equilibrium fractionation between atmospheric CO_2 and DIC

An estimate of $\delta^{13}C_{DIC}$ in equilibrium with the atmosphere can be made by taking account of the distinct equilibrium fractionation factors of each major carbon species present in the aqueous fluids using (Myrttinen et al., 2012):

$$\delta^{13}C_{DIC} = \sum_i \left(x_i \cdot \left(\delta^{13}C_{CO_2} + 10^3 \ln \alpha^{13}C_{i-CO_{2(g)}} \right) \right) \qquad (5\text{-}2)$$

where x_i designates the molar fraction of each aqueous carbon species computed using PHREEQC (see below) and $\delta^{13}C_{CO_2}$ designates the carbon isotope composition of atmospheric CO_2 which was taken from Mavromatis et al. (2015), who conducted experiments in the same laboratory $\left(\delta^{13}C_{CO_2} = -8.5 \pm 1‰\right)$. The term $10^3 ln\alpha^{13}C_{i-CO_{2(g)}}$ refers to the equilibrium fractionation factor between the indicated aqueous carbon species and $CO_{2(g)}$. Note that as the equilibrium fractionation factor for each aqueous carbon species is distinct, the $\delta^{13}C_{DIC}$ in equilibrium with the atmosphere is equally a function of fluid pH. This variation of fractionation factors with pH has led to discrepancies in $CO_3^{2-} - CO_{2(g)}$ equilibrium isotope fractionation factors reported in the literature (see Myrtinnen et al., 2012). The fractionation factors $10^3 ln\alpha^{13}C_{HCO_3^- - CO_{2(g)}} = 7.9$ and $10^3 ln\alpha^{13}C_{CO_3^{2-} - CO_{2(g)}} = 2.7$ adopted in this study for 25°C were taken from Mook et al. (1974) and Halas et al. (1997), respectively. These fractionation factors indicate that $\delta^{13}C_{DIC}$ compositions in equilibrium with atmospheric CO_2 become more depleted in ^{13}C with increasing pH at pH>7.

5.2.1.2 Carbon degassing

The effect of carbon degassing to the atmosphere can be quantified using a modified Rayleigh equation (Wynn et al., 2005):

$$\delta^{13}C_f = \left(10^3 \cdot \left(F^{\left(\alpha^{13}C_{DIC-CO_{2(g)}}-1\right)} - 1\right)\right) + \delta^{13}C_i \cdot F^{\left(\alpha^{13}C_{DIC-CO_{2(g)}}-1\right)}. \quad (5\text{-}3)$$

Equation (5-3) allows calculation of the carbon isotope composition of the fluid, $\delta^{13}C_f$, after the fraction $(1-F)$ of carbon has been removed from the DIC pool by degassing. The initial carbon isotope signature of the fluid is given by $\delta^{13}C_i$. The term $\alpha^{13}C_{DIC-CO_{2(g)}}$ designates the $DIC - CO_{2(g)}$ equilibrium isotope fractionation factor, which will vary during degassing due to fluid pH changes. This can be calculated taking account of the carbon species present in the aqueous fluid using (Zhang et al., 1995):

$$10^3 ln\alpha^{13}C_{DIC-CO_{2(g)}} = \sum_i (x_i \cdot 10^3 \ln \alpha^{13}C_{i-CO_{2(g)}}), \quad (5\text{-}4)$$

where $10^3 ln\alpha^{13}C_{i-CO_{2(g)}}$ refers to the fractionation factor and x_i to the mole fraction of the subscripted aqueous carbon species present in the aqueous solution.

5.2.2 Effect of cyanobacteria on $\delta^{13}C_{DIC}$

Biomass produced during photosynthesis preferentially consumes ^{12}C thus increasing $\delta^{13}C_{DIC}$ as demonstrated in Figure 5-1 (e.g. O´Leary, 1988; Johnston and Fischer, 2012). This has been observed in numerous natural and experimental studies (e.g. Ferris et al., 1997; Andres et al., 2006; Jimenez-Lopez et al., 2006; Power et al., 2011; Brady et al., 2013; Mavromatis et al., 2015). Cyanobacteria may release ^{12}C to the fluid phase during cell lysis and death and if respiration predominates over photosynthesis as is common in many natural environments (Schulte et al., 2011), thereby lowering $\delta^{13}C_{DIC}$ of the ambient fluid phase.

5.2.3 Calcium carbonate precipitation

The offset of carbon isotope compositions between calcite and DIC can be expressed by a fractionation factor $\left(\Delta^{13}C_{Calcite-DIC}\right)$ given by:

$$\Delta^{13}C_{Calcite-DIC} = \delta^{13}C_{Calcite} - \delta^{13}C_{DIC} \quad (5\text{-}5)$$

At isotopic equilibrium, 25°C, and in aqueous solutions where dissolved carbon is dominated by the HCO_3^- species, $\Delta^{13}C_{Calcite-DIC}$ has been reported to range between $+0.83$ ‰ and $+1.96$ ‰ (Deines et al., 1974; Jimenez-Lopez et al., 2006; Polag et al., 2010; Romanek et al., 1992), consistent with the preferential incorporation of ^{13}C into calcite compared to its co-existing aqueous fluid. Isotopic equilibrium, however, may not be attained in a rapidly precipitating system; McCrea (1950) suggested that rapidly precipitated carbonate will have a $\delta^{13}C$ value identical to its DIC reservoir.

5.3 Methods

5.3.1 Microcosm precipitation experiments

The experimental protocol adopted in this study is similar to that used by Mavromatis et al., 2012; 2015). Calcite precipitation was performed in sterile 1000 ml borosilicate glass reactors containing Sigma-Aldrich C3061 BG-11 growth medium. The initial fluid compositions of each experiment are provided in Table 5-1 and were chosen to promote sufficient calcium carbonate precipitation to produce adequate calcite and dissolved carbonate concentrations for chemical/isotopic analyses, but avoiding unfavorable growth conditions for the cyanobacteria. The high supersaturation ($1.8 \leq SI_{Calcite} \leq 3.0$) of these initial fluids with respect to calcite ensured its rapid homogeneous precipitation. All initial reactive fluids were either autoclaved for 15 minutes at 121°C using a Systec™ DB23 autoclave or sterilized by filtration (MilliPore 0.22 µm cellulose acetate filter) prior to each experiment. Known quantities of previously grown *Synechococcus sp.* were added to the sterile aqueous carbonate solution of all biotic reactors. Aliquots of concentrated aqueous $CaCl_2$ (50 mmol/kg) solution were then added to all reactors to obtain the desired Ca concentration of 8.5 mmol/kg. Reactors were constantly bubbled with sterile humidified air (filtered through sterile MilliPore 0.22 µm cellulose acetate filter), stirred with magnetic stirring bars and kept under continuous 3000 LUX illumination throughout each experiment. Temperature was kept constant at 24°C with maximum deviations of ± 1°C. Duplicates and abiotic controls were performed at each experimental condition.

The unicellular freshwater cyanobacteria *Synechococcus sp. PCC 7942* used in the experiments were previously cultured under sterile conditions in BG-11 Freshwater Solution Medium at room temperature and continuous illumination with a 3000 LUX cool white fluorescence light while bubbling humidified air to achieve constant mixing. Further details about this cyanobacteria are provided by Obst et al. (2009b; 2009a) and Bundeleva et al. (2014). The initial cyanobacterial cultures showed minor heterotrophic cortege (<5 % of the biomass).

Table 5-1. Experimental conditions of all experiments.

Initial Conditions:

ID	Duration (days)	$NaHCO_3$ (mmol/kg)	Na_2CO_3 (mmol/kg)	$CaCl_2$ (mmol/kg)	SI calcite	BG-11 (g/kg)	biomass ($g_{(dry)}$/kg)
SolA-1i	35	10		8.6	1.8	20	
SolA-2	35	10		8.6	1.8	20	0.016
SolA-3	35	10		8.6	1.8	20	0.015
SolB-1i	19	50		8.5	2.6	20	
SolB-2	33	50		8.5	2.6	20	0.017
SolB-3	33	50		8.5	2.6	20	0.017
SolC-1i	26	25	25	8.5	3.0	20	
SolC-2	33	25	25	8.5	3.0	20	0.017
SolC-3	33	25	25	8.5	3.0	20	0.017

Conditions during experiment:

ID	Biomass range ($g_{(dry)}$/kg)	pH range	Ca conc. range (mmol/kg)	DIC range (mmol/kg)	Alkalinity range (mmol/kg)
SolA-1i	abiotic	8.31 - 8.68	8.63 - 4.89	9.05 - 3.11	
SolA-2	0.016 - 1.852	8.32 - 10.76	8.60 - 0.10	9.10 - 0.28	
SolA-3	0.015 - 1.755	8.26 - 10.94	8.53 - 0.05	9.05 - 0.23	
SolB-1i	abiotic	8.31 - 9.60	8.50 - 0.02	46.9 - 27.4	51.5 - 32.1
SolB-2	0.017 - 1.070	8.20 - 11.65	8.50 - 0.02	46.9 - 20.2	51.5 - 32.4
SolB-3	0.017 - 0.357	8.25 - 11.85	8.50 - 0.02	46.9 - 19.5	51.5 - 33.3
SolC-1i	abiotic	9.76 - 10.14	8.50 - 0.01	48.8 - 44.3	71.6 - 56.1
SolC-2	0.017 - 1.339	9.92 - 11.12	8.50 - 0.02	47.7 - 28.9	71.6 - 57.1
SolC-3	0.017 - 1.342	9.89 - 10.73	8.50 - 0.03	47.7 - 39.7	71.6 - 56.7

5.3.2 Sampling and Analytical methods

Fifty ml aliquots of homogenous suspensions were sampled periodically from the reactors in a sterile laminar hood box. The optical density (OD) and pH were measured in these suspension samples, whereas the fluid supernatants were centrifuged for 10 min at 5000 rpm and filtered using a MilliPore 0.45 µm cellulose acetate filter prior to alkalinity, dissolved inorganic carbon (DIC), Ca concentration and $\delta^{13}C_{DIC}$ measurements. Biomass concentration was monitored from the measured suspension sample optical density at the peak absorption of chlorophyll-a (682 nm) after subtracting the contribution of turbidity determined at 750 nm. The Varian Cary50Scan Spectrophotometer used for this analysis allowed simultaneous measurements of these two wavelengths. This approach thereby reduced the contribution of mineral precipitates or cell debris on the OD measurements. Optical density was converted to dry biomass using a linear calibration curve (see Figure 2-6). The uncertainty of the resulting biomass concentration was estimated to be ±10 %. The pH was measured using a VWR semi-

micro electrode with an uncertainty of ±0.05. Alkalinity was measured following a standard HCl titration procedure using a Schott TitroLine alpha plus titrator with an uncertainty of ±2 %. The concentration of dissolved inorganic carbon (DIC) was measured using a Shimadzu TOC-VCSN carbon Analyzer with an ASI-V sample unit with a quantification limit of 0.57 ppm and an uncertainty of 3 %. Calcium concentrations were measured by flame atomic absorption spectroscopy using a Perkin Elmer AAnalysit 400 with an uncertainty of ±2 %. Fluids for the determination of $\delta^{13}C_{DIC}$ values were placed into sterile 24 ml amber serum flasks closed with Wheaton Bromobutyl stoppers and aluminum caps to seal them from the atmosphere and stored at 4°C prior to their analyses. Solid samples for carbon isotope analyses were obtained via centrifugation, stored at -80°C and freeze-dried 1-2 weeks after sampling. No H_2O_2 treatment of these solids was performed as centrifugation successfully separated mineral precipitates from the biomass due to the higher density of the mineral compared to the organic phase. Sampled solids were characterized by scanning electron microscopy using a Jeol JSM 6360LV and by X-ray diffraction using a G3000 INEL with a CuKα source.

The $\delta^{13}C$ values of DIC and carbonate minerals were measured at the stable isotope laboratory of the Joanneum Research Institute in Graz, Austria. Details of the analytical procedure can be found in Spötl (2005) and Alemayehu et al. (2011) for the liquids and in Révész and Landwehr (2002), Spötl and Vennemann (2003), Paul and Skrzypek (2007) and Dietzel et al. (2009) for the solids. In brief, the liquid samples were injected into gas tight vials, which were previously flushed with helium gas and preloaded with six droplets of phosphoric acid. For the solids, 200-400 µg of calcite were placed into sealed Exetainer vials, flushed with helium gas to remove residual air and digested in excess pure phosphoric acid for 2 h at 90°C. Acidification converted the total sample carbonate into aqueous and gaseous CO_2, which was then analyzed using a fully automated peripheral continuous-flow gas preparation device (Gasbench II) connected to a Finnigan DELTAplus XP mass spectrometer. NSB-19 and two in-house lab standards were measured for calibration. The method of Santrock et al. (1985) was applied for ^{17}O correction, whereby the data were processed by the build in SSH-correction algorithm of the software package ISODAT 3.0 (Thermo Scientific). The analytical reproducibility of $\delta^{13}C$ was ±0.1 ‰ (1σ).

The geochemical code PHREEQC (Parkhurst and Appelo, 1999) was used to calculate, chemical speciation and CO_2 pressure of the fluid phase (pCO_2). The standard state adopted in these calculations for solid phases and H_2O is the pure phase, while a hypothetical 1 mol/kg aqueous solution referenced to infinite dilution is chosen for unit activity of aqueous species,

both at the temperature and pressure of interest. The Lawrence Livermore National Laboratory aqueous model (Wolery and Daveler, 1992), which uses the extended Debye-Hückel equation (Helgeson, 1969) was used to calculate activity coefficients of aqueous species. As a result of the low aqueous fluid calcium concentrations compared to the total biomass concentration (up to 1.85 $g_{(dry)}$/kg), and l) the unknown concentration of metabolic products, 2) lack of thermodynamic properties for aqueous complexes that may have formed among the dissolved Ca and these products it was not possible to accurately calculate the saturation state of calcite during the experiments.

5.4 Results

Three distinct experimental series were performed in this study. Each series consisted of one abiotic and two biotic experiments performed over 19 to 35 days. All experiments were initiated with 8.6 mmol/kg Ca present in the aqueous fluid and each biotic experiment was initiated with 16±1 mg/kg of biomass in the reactors. Experimental series SolA was performed in aqueous fluids initially containing 10 mmol/kg $NaHCO_3$, experimental series SolB was performed in aqueous fluids initially containing 50 mmol/kg $NaHCO_3$, and experimental series SolC was performed in aqueous fluids initially containing a 50 mmol/kg $NaHCO_3/Na_2CO_3$ buffer (see Table 5-1). The chemical composition of sampled fluids and the carbon isotope composition of dissolved inorganic carbon and calcite in all experiments are listed in Table A 5-1 in the appendix of this chapter on page 145ff, together with the volume of aqueous fluid and the mass of calcite present in each reactor after each sampling. These results are summarized below.

5.4.1 Chemical evolution of the reactive fluid

The temporal evolution of biomass, pH, Ca concentrations, and alkalinity are shown in Figure 5-2 A-D, Figure 5-3 A-D and Figure 5-3 E-H for experimental series SolA, SolB, and SolC, respectively. Due to its much lower initial alkalinity, SolA exhibited a distinct fluid compositional evolution compared to SolB and SolC.

During the abiotic experiment SolA-1i (Figure 5-2), Ca and DIC concentrations decreased due to carbonate precipitation at the onset of the experiment, after which concentrations remained constant at around 5 mmol/kg for Ca and 3.1 mmol/kg for DIC. The pH remained constant at 8.6±0.1 after an initial increase from 8.3. During the biotic experiments SolA-2 and SolA-3, Ca concentration decreased at the onset of the experiment by the same

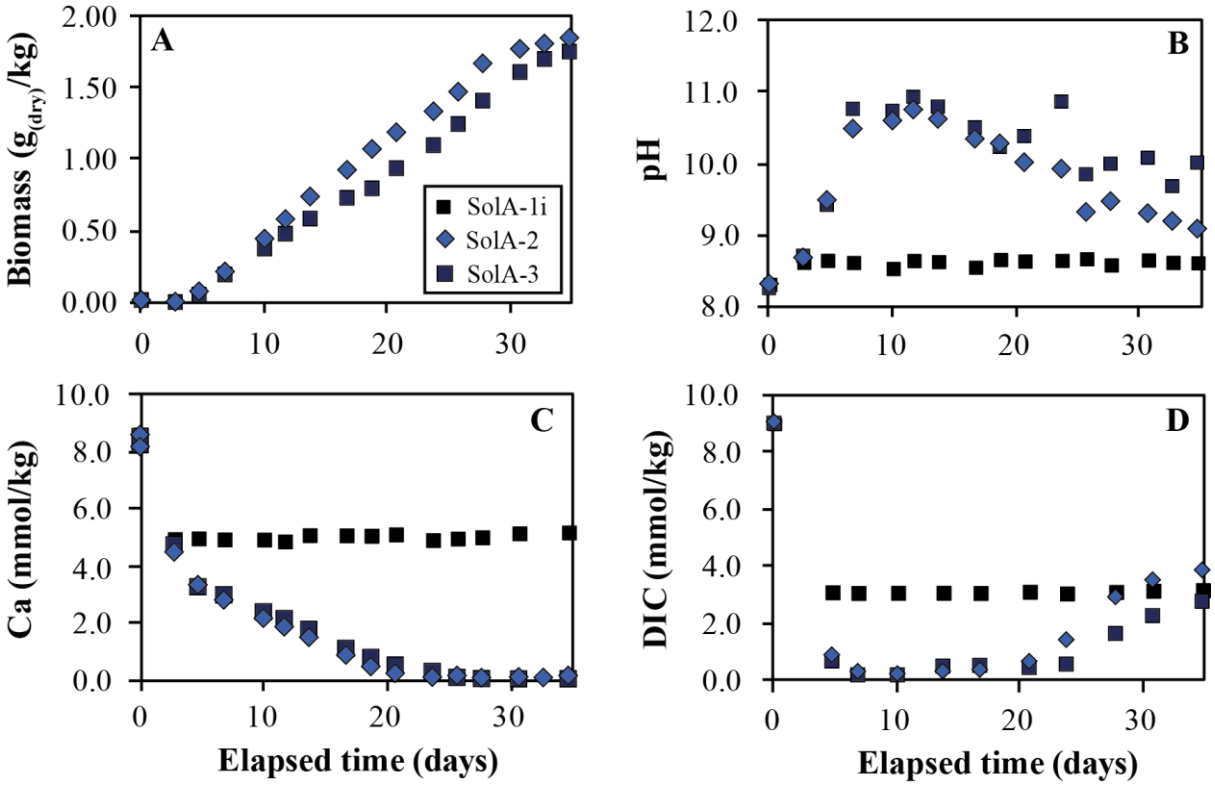

Figure 5-2. The temporal evolution of biomass concentration (**A**), pH (**B**), Ca concentration (**C**) and DIC (**D**) during experimental series SolA. The uncertainty of biomass concentration is ±5% whereas the analytical uncertainties of pH, Ca concentration and DIC are smaller than the symbol sizes. The symbols are identified in Figure 5-2 **A**.

amount as in the abiotic control, whereas the DIC concentration immediately dropped to near zero. The biomass concentration continually increased from 0.02 $g_{(dry)}$/kg to 1.76-1.85 $g_{(dry)}$/kg and the pH in the reactive fluids increased from initially 8.3 to ~10.9 due to the metabolic activity of growing cyanobacteria. This elevated pH resulted in further Ca-carbonate precipitation. From day 4 until day 21, the fluid Ca concentration continuously decreased while DIC remained near zero until the Ca in the fluid phase approached zero and DIC concentrations increased to final concentrations of 2.8-3.9 mmol/kg.

As depicted in Figure 5-3, experimental series SolB and SolC showed distinct chemical evolutions due to their higher initial aqueous carbonate concentrations, resulting in higher calcite saturation states (see SI values in Table 5-1). Consequently, the reactive fluid Ca concentrations decreased from 8.5 mmol/kg to less than 0.1 mmol/kg during the first hours of all SolB and SolC experiments. After an initial rapid change from pH 8.6, the pH in the abiotic reactor SolB-1i remained constant at pH 9.6; similarly, after an initial rapid change from pH 10.1, the pH in the abiotic reactor SolC-1i remained constant at 9.8. In the biotic experiments SolB-2 and SolB-3, the biomass concentration increased from 0.02 $g_{(dry)}$/kg to 1.07 $g_{(dry)}$/kg and 0.58 $g_{(dry)}$/kg, respectively. During experiment SolB-3, the biomass concentration decreased

during the last 10 days of experiment to 0.36 $g_{(dry)}$/kg. the biomass concentration continuously increased from 0.02 $g_{(dry)}$/kg to 1.34 $g_{(dry)}$/kg and the pH increased decrease in pH to final values of 10.5 and 10.3. Alkalinity during experimental series SolB dropped from an initial value of

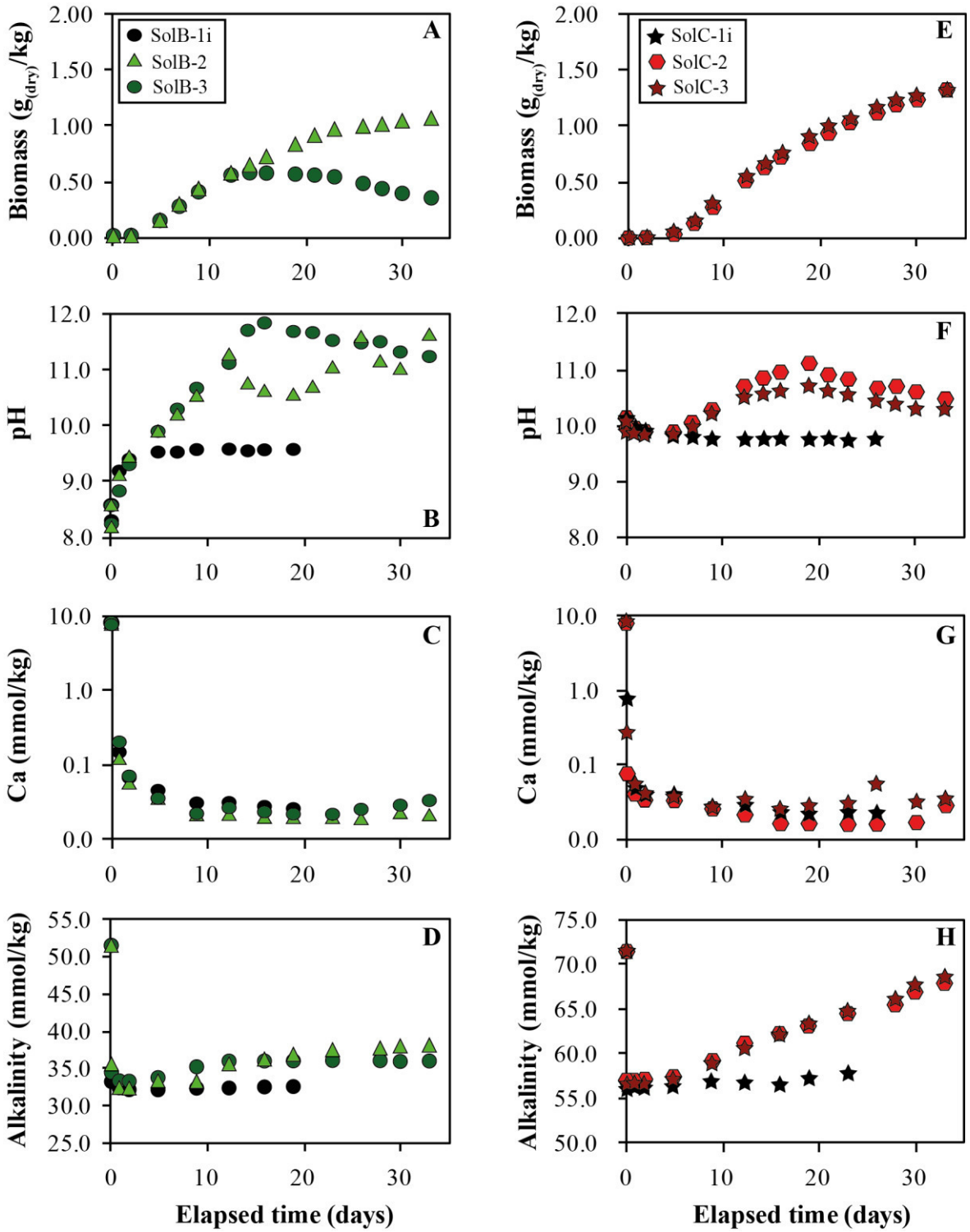

Figure 5-3. The temporal evolution of biomass concentration (**A**, **E**), pH (**B**, **F**), Ca concentration (**C**, **G**) and alkalinity (**D**, **H**) during experimental series SolB and SolC. Note, that Ca concentrations are shown on logarithmic scale. The uncertainty of biomass concentration is ±5% whereas analytical uncertainties on pH, Ca concentrations and alkalinities are smaller than the symbol sizes. The symbols are identified in Figures 5-3 **A** and **E**.

51.5 mmol/kg to 33 mmol/kg and increased again slightly in the biotic reactors to 38 mmol/kg and 36 mmol/kg. During experimental series SolC, alkalinity dropped from 71.6 mmol/kg to 57 mmol/kg and subsequently increased in the biotic reactors to 68 mmol/kg. Note that the reactive fluids containing 50 mmol/kg HCO_3^- (experimental series SolB) and 25 mmol/kg HCO_3^- + 25 mmol/kg CO_3^{2-} (experimental series SolC) were not initially in equilibrium with the atmosphere. Computed pCO_2 values of the initial SolB fluids ranged from $10^{-2.0}$ to $10^{-2.2}$ and were thus significantly higher than atmospheric pCO_2. As such, immediately after the onset of these experiments some DIC was lost to the atmosphere through CO_2 outgassing, such that pCO_2 dropped to $10^{-3.6}$ during the abiotic experiment. In contrast, the computed fluid phase pCO_2 in the SolC series fluids was initially at $10^{-4.3}$ and thus lower than atmospheric pCO_2. Consequently, atmospheric CO_2 diffused into the reactive fluid until atmospheric level of pCO_2 was attained (see Figure 5-4).

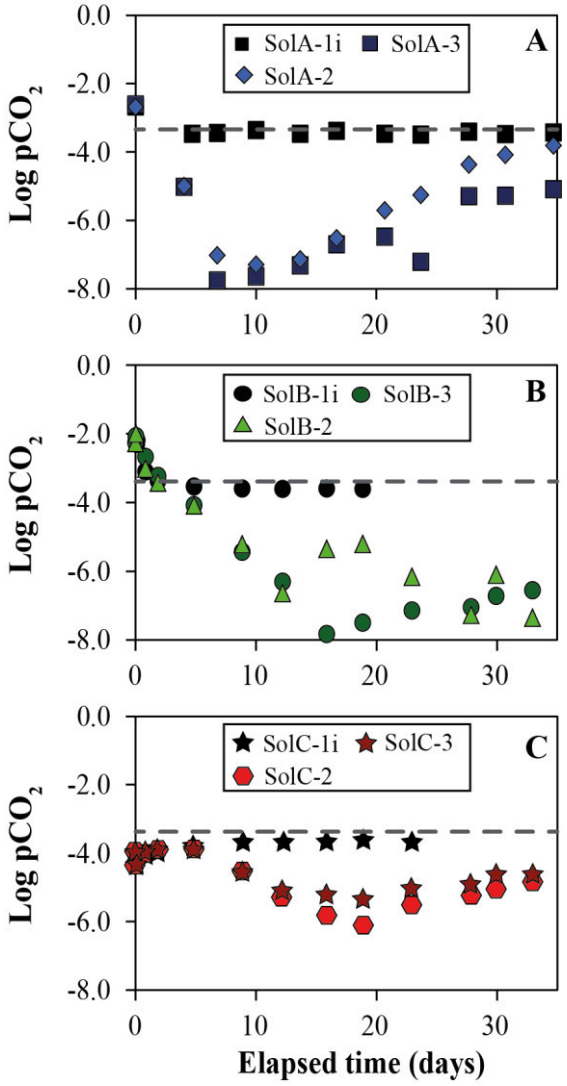

Figure 5-4. The temporal evolution of pCO_2 during experimental series SolA (**A**), SolB (**B**) and SolC (**C**). pCO_2 was calculated from measured aqueous fluid composition using PHREEQC. The symbols are identified in the figures. Dashed lines indicated atmospheric saturation.

5.4.2 Mineralogy of the sampled solids

Calcium carbonate formation was observed in all experiments and evidenced by the decrease in fluid phase Ca and DIC concentrations. All analyzed solids consisted of pure calcite within XRD detection limits (i.e. ±1 wt.%) (see Figure A 5-1). Representative SEM images of the solids after 4.8 days are shown in Figure 5-5 A-D, whereas Figure 5-5 E-H show solids collected at the end of these experiments. Figure 5-5 A, E and Figure 5-5 C, G show solids collected from abiotic experiments SolB-1i and SolC-1i, respectively. Figure 5-5 B, F and Figure 5-5 D, H show the solids collected from the biotic experiments SolB-3 and SolC-2. The calcite precipitated in hypidiomorphic morphologies with existing crystal surfaces indicating a rhombohedral shape. The grain size ranged from 2 to 5 µm. These features indicate a spontaneous rapid precipitation as evidence by the milky fluid at the onset of the experiments. Since bacteria were added to the already milky fluid after a large portion of calcite precipitation was complete, there is no evidence for biotic effects on crystal nucleation and morphology. No morphological differences are evident between the solids sampled from abiotic compared to the biotic experiments, nor are there morphological differences in these solids between the onset and the end of the experiments. However, calcite precipitated during experimental series SolB (Figure 5-5 A, B, E, F) are notably smaller (~2 µm diameter) compared to those precipitated during in the more supersaturated series SolC (Figure 5-5 C, D, G, H), where calcite crystal were on average about 5 µm in diameter.

5.4.3 Carbon isotope evolution of dissolved inorganic carbon and calcite during experimental series SolA

As the $\delta^{13}C$ values measured in the DIC and calcite during experimental series SolA showed a distinct behavior compared to those in series SolB and SolC, they are described separately in this section. The temporal evolution of $\delta^{13}C_{DIC}$ and $\delta^{13}C_{Calcite}$ values of SolA-1i, SolA-2 and SolA-3 are shown in Figure 5-6 A and B, respectively. The carbon isotope composition of the DIC in the abiotic experiment SolA-1i initially increased from -6.08 ‰ to -3.33±0.93 ‰. respectively. The $\delta^{13}C_{DIC}$ values in the abiotic experiment SolA-1i initially increased from -6.08 ‰ to -3.33±0.93 ‰. It subsequently remained stable for 20 days then decreased to -9.53±0.45 ‰ near the end of the experiment. The carbon isotope composition of the calcite during this experiment was constant at -3.25±0.15 ‰. In contrast, the carbon isotope composition of the DIC and calcite in the biotic experiments SolA-2 and SolA-3 evolved with time. After an initial increase in $\delta^{13}C_{DIC}$ from values of -4.64 ‰ and -6.37 ‰ to +4.25 ‰ and +6.25 ‰, the fluid carbon isotope composition became substantially more negative attaining

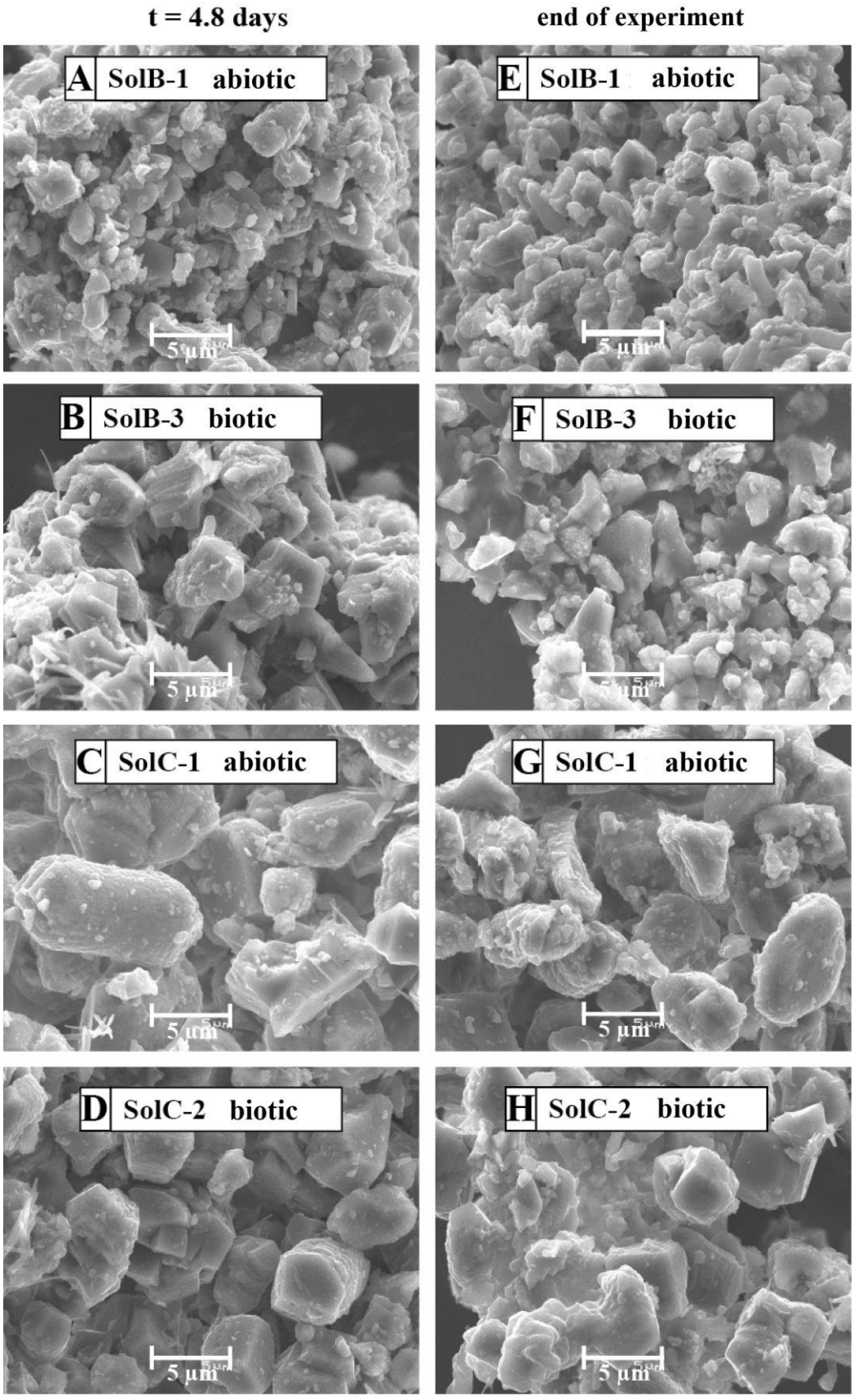

Figure 5-5. Representative SEM images of the calcite precipitated in this study. The images on the left show calcite sampled after 4.8 days of experiments SolB-1i (**A**), SolB-3 (**B**), SolC-1i (**C**) and SolC-3 (**D**), whereas the images on the right show calcite sampled after the corresponding experiment.

values as low as -24.38 ‰ in SolA-3. This negative $\delta^{13}C_{DIC}$ signature persisted as long as the DIC concentrations in the fluid remained below 1 mmol/kg. Once calcite precipitation was essentially complete, DIC and $\delta^{13}C_{DIC}$ increased again. Gaps evident in the datasets are due to DIC concentrations being too low to measure carbon isotope compositions. Carbon isotopes in the calcite also decreased with time while it precipitated (see Figure 5-6 B). Starting at values of around 0 ‰, the $\delta^{13}C_{Calcite}$ values became progressively more negative reaching values of -6 ‰. It can be seen, however, that $\delta^{13}C_{Calcite}$ values slightly increased during the final 15 days of the biotic experiments after calcite precipitation was complete. The final increase in $\delta^{13}C_{Calcite}$ was coherent with the increase in $\delta^{13}C_{DIC}$ and the total DIC concentration following the completion of calcite precipitation.

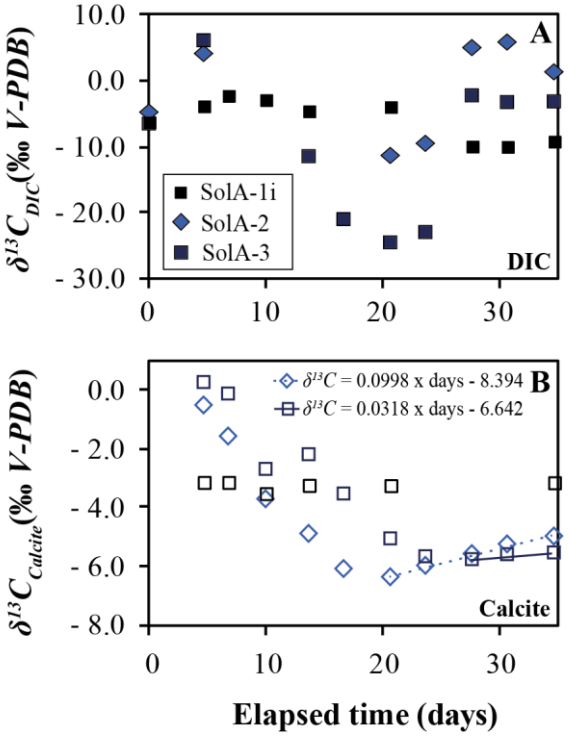

Figure 5-6. The temporal evolution of $\delta^{13}C_{DIC}$ (**A**) and $\delta^{13}C_{Calcite}$ (**B**) during experimental series SolA. The analytical uncertainties (1σ) of the carbon isotope measurement are 0.1‰ and are smaller than the symbol size. Lines in (**B**) are linear regressions of the $\delta^{13}C_{Calcite}$ evolution after completion of calcite precipitation. Equations shown in Figure 5-6 **B** correspond to the regression of the results of experiments SolA-2 (dashed line) and SolA-3 (solid line) – see text. The symbols are identified in Figure 5-6 **A**. The filled symbols designate the carbon isotope signatures of DIC, the open symbols represent the carbon isotope signatures of calcite samples.

5.4.4 Carbon isotope compositions of dissolved inorganic carbon and calcite during experimental series SolB and SolC

After an initial rapid change, the $\delta^{13}C_{DIC}$ value in the abiotic experiments SolB-1i and SolC-1i, remained stable at -2.62±0.18 ‰ and -4.60±0.36 ‰, respectively (Figure 5-7 C and F). Note that the carbon isotope ratios of the bicarbonate and carbonate powders used to produce

the aqueous fluids were -5.96 ‰ ($NaHCO_3$) and -2.69 ‰ (Na_2CO_3). The longer-term $\delta^{13}C_{DIC}$ value in SolB-1i was ~3.3 ‰ higher than that of the bicarbonate used to produce to initial reactive fluids. In contrast, the longer-term $\delta^{13}C_{DIC}$ value of experiment SolC-1i of -4.6 ‰ was close to that calculated from a 50/50 mixture of the $NaHCO_3$ and Na_2CO_3 reagents used to make this fluid.

Similar to the $\delta^{13}C_{DIC}$value, the calcite precipitated during these abiotic experiments exhibited only small variations in their $\delta^{13}C$ values after an initial rapid change. In SolB-1i and SolC-1i, the long-term $\delta^{13}C_{Calcite}$ values were -4.80±0.20 ‰ and -3.15±0.24 ‰, respectively (Figure 5-7 C and F). Note that the $\delta^{13}C_{Calcite}$ value was higher than the $\delta^{13}C_{DIC}$ value in experiment SolC-1i but lower than the $\delta^{13}C_{DIC}$ value in experiment SolB-1i. This results in $\Delta^{13}C_{Calcite-DIC}$ values of -2.15±0.38 ‰ in SolB-1i and 1.49±0.60 ‰ in experiments SolC-1i.

The isotopic composition of dissolved inorganic carbon showed distinctly different trends depending on the presence or absence of cyanobacteria (see Figure 5-7). In the biotic experiments SolB-2 and SolB-3, the $\delta^{13}C_{DIC}$ values increased over the first 12 days by more than 16 ‰ from initial values of -7‰ to +10 ‰ then decreased by 6-9 ‰ at the end of the experiment (see Figure 5-7 A). The biotic experiments SolC-2 and SolC-3 showed a similar behavior but the initial $\delta^{13}C_{DIC}$ increase was delayed by four days and $\delta^{13}C_{DIC}$ values increased only by around 10 ‰, from initial values of ~-5 ‰ to a maximum of ~+6.5 ‰ (Figure 5-7 D). Likewise, the decrease in $\delta^{13}C_{DIC}$ at the end of the experiments SolC-2 and SolC-3 was less distinct. The observed final $\delta^{13}C_{DIC}$ values were similar in all biotic experiments of SolB and SolC at values between +3.28 ‰ and +3.75 ‰.

In contrast to the abiotic control experiments, after an initial relatively rapid change, the $\delta^{13}C$ values in calcite became progressively more positive over time during the biotic experiments. In SolB-2 and SolB-3, $\delta^{13}C_{Calcite}$ values increased by about 0.5 ‰ and 1.3 ‰ after the initial change during the experiment (Figure 5-7 B). The increase was less pronounced in SolC-2 and SolC-3, where $\delta^{13}C_{Calcite}$ increased by 0.7 ‰ and 0.5 ‰ during the last 30 days of the experiment (see Figure 5-7 E). Note that the bulk of these carbon isotope compositional changes occurred after calcite precipitation was complete, as evidenced by stable Ca concentrations.

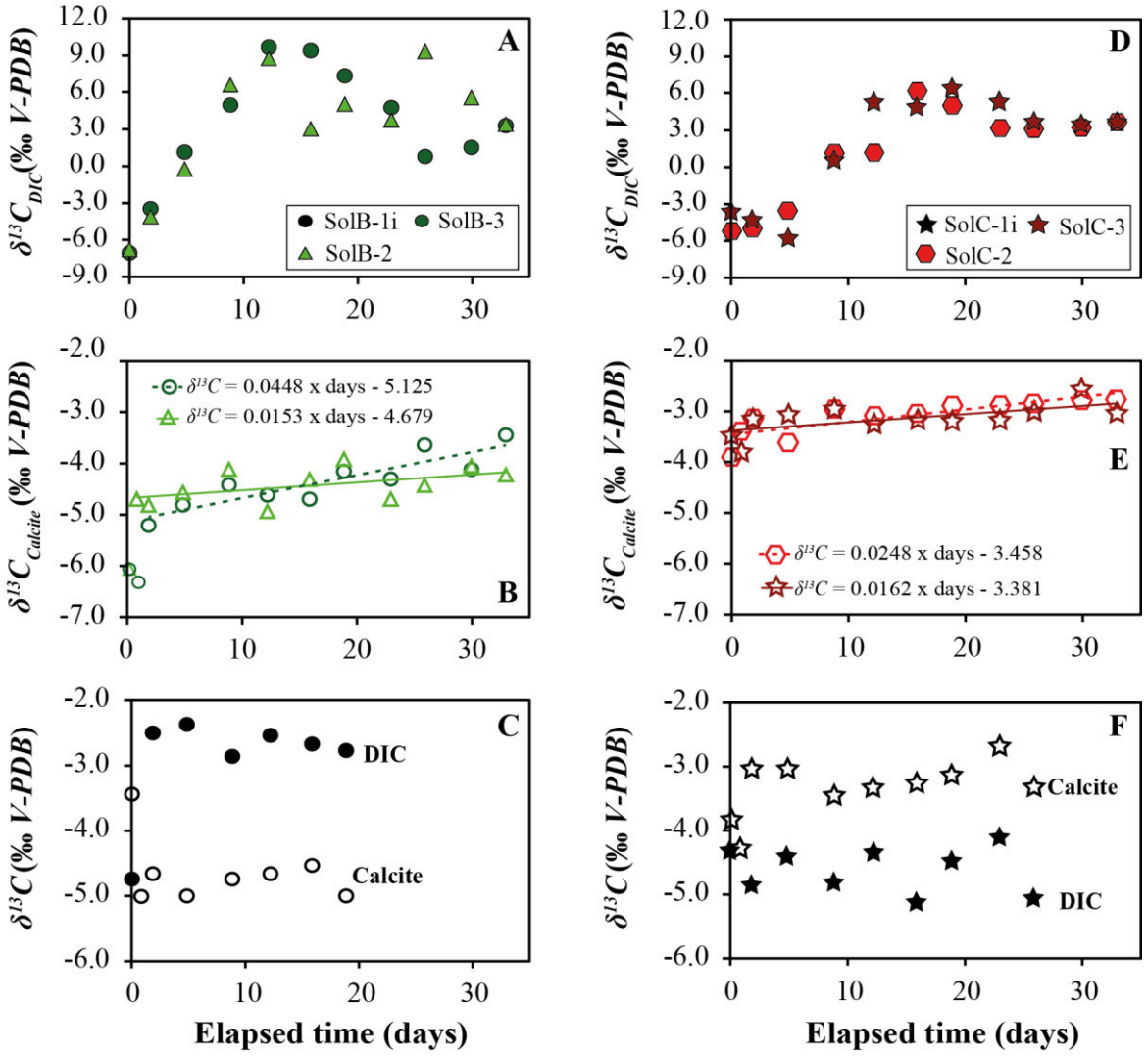

Figure 5-7. The temporal evolution of $\delta^{13}C_{DIC}$ (**A**, **D**) and $\delta^{13}C_{Calcite}$ (**B**, **E**) in the biotic reactors of experimental series SolB and SolC. The evolution of $\delta^{13}C_{DIC}$ and $\delta^{13}C_{Calcite}$ in the abiotic controls SolB-1i and SolC-1i are shown in plots **C** and **F**. The analytical uncertainties (1σ) of the measurement are 0.1‰ and are smaller than the symbol size. The lines in Figs. B and E are linear regressions of the temporal $\delta^{13}C_{Calcite}$ evolution after completion of calcite precipitation. Corresponding equations are provided in Figure **B** for reactors SolB-2 (solid line) and SolB-3 (dashed line) and in Figure **E** for reactors SolC-2 (dashed line) and SolC-3 (solid line) – see text. The symbols are identified in Figures 5-7 **A** and **D**. The filled symbols designate carbon isotope signatures in DIC, the open symbols represent the carbon isotope signatures of calcite samples.

5.5 Discussion

5.5.1 Carbon isotopic fractionation during the abiotic experiments

The $\delta^{13}C_{DIC}$ value in the absence of cyanobacteria is initially set by the bicarbonate and carbonate reagents used to produce the initial reactive fluids and subsequently changes due to calcite precipitation and CO_2 exchange with the atmosphere. Note that calcite precipitated rapidly during the experiments due to sizable initial supersaturations ($1.8 \leq SI_{Calcite} \leq 3.0$). McCrea (1950) and Turner (1982) reported that the enrichment of ^{13}C in carbonates decreases with increasing precipitation rate suggesting that rapidly precipitated carbonate minerals will

have an isotopic composition identical to its DIC reservoir. Table 5-2 summarizes the measured and calculated carbon isotope compositions of all abiotic experiments. The $\delta^{13}C_{DIC}$ values of the abiotic experiments SolA-1i and SolB-1i are close to constant at -3.33±0.93 ‰ and -2.62±0.18 ‰ after an initial increase of about 2.7 ‰ and 2.2 ‰ (see Figure 5-6 A and C). The calculated $\Delta^{13}C_{Calcite-DIC}$ values were close to constant from days 5-21 at +0.06±1.07 ‰ in experiment SolA-1i, and close to constant after 5 days at -2.15±0.38 ‰ in experiment SolB-1i, suggesting a small isotopic disequilibrium between the calcite and the aqueous fluid phase compared to previously published $Calcite - HCO_3^-$ equilibrium fractionation factors (e.g. ranging from +0.83 ‰ to +1.96 ‰; Deines et al., 1974; Jimenez-Lopez et al., 2006; Polag et al., 2010; Romanek et al., 1992). The observed initial increase of the $\delta^{13}C_{DIC}$ values in SolA-1i and SolB-1i and fluid-calcite isotopic disequilibrium is likely the result of preferential loss of ^{12}C during CO_2 during atmospheric equilibration. Mass balance calculations taking account of $DIC_{tot} = DIC_{initial} - (DIC_{lost\ by\ degassing} + DIC_{precipitated\ calcite})$ indicate that 42 % and 30 % of the carbon present in the reactors was degassed to the atmosphere during the first hours of experiments SolA-1i and SolB-1i, respectively. The degassing of these fluids is also consistent with the observed pCO_2 evolution shown in Figure 5-4. The effect of degassing on $\delta^{13}C_{DIC}$ has been calculated using Eqns. (5-3) and (5-4). Since degassing essentially occurred in a single step at the beginning of the experiments, the calculated $10^3 ln\alpha^{13}C_{DIC-CO_{2(g)}}$ used in for this calculation was that of the initial aqueous fluid. The results shown in indicate that the observed carbon isotope compositions of DIC are in close agreement with those calculated due to degassing. In contrast to experiments SolA-1i and SolB1i, negligible carbon loss was observed from the abiotic reactor SolC-1i according to mass balance calculations. The $\delta^{13}C_{DIC}$ value remained close to constant after 3 days in experiment SolC-1i at -4.60±0.36 ‰ (see Figure 5-7 F), which is similar to the carbon isotope composition of the $Na_2CO_3/NaHCO_3$ mixture used to prepare the reactive fluid. The calculated $\Delta^{13}C_{Calcite-DIC}$ over this time in SolC-1i is +1.49±0.60 ‰ and agrees with previously published $Calcite - HCO_3^-$ equilibrium fractionation factors. In contrast, the $\delta^{13}C_{DIC}$ compositions calculated to be in equilibrium with the atmosphere are significantly higher than those measured (see Table 5-2) suggesting that isotopic equilibration between the fluid and the atmosphere was slower than that between the fluid and the precipitating calcite.

Table 5-2. Measured and calculated carbon isotope fractionation in the abiotic experiments. The calculated initial values are determined from the isotope composition of the reagents used to produce the initial reactive fluids together with mass balance constraints. The calculated compositions in equilibrium with atmospheric CO_2 and after CO_2 degassing were determined according to Eqns. (5-2) and (5-3).

	$\delta^{13}C_{DIC}$ (‰)					$\delta^{13}C_{Calcite}$ (‰)	$\Delta^{13}C_{Calcite\text{-}DIC}$
ID	**initial (measured)**	**calculated initial (powder)**	**average steady-state (measured)**	**calc. in equilibrium with $CO_{2(atm)}$**	**calc. after C loss**	**average steady-state (measured)**	**$\delta^{13}C_{Calcite}$ - $\delta^{13}C_{DIC}$**
SolA-1i	-6.08 ± 0.1	-5.96 ± 0.1	-3.33 ± 0.93	-0.72 ± 1	-1.88	-3.25 ± 0.15	+0.06 ± 1.07
SolB-1i	-4.74 ± 0.1	-5.96 ± 0.1	-2.62 ± 0.18	-1.85 ± 1	-2.27	-4.80 ± 0.20	-2.15 ± 0.38
SolC-1i	-4.31 ± 0.1	-4.33 ± 0.1	-4.60 ± 0.36	-2.47 ± 1	no C loss	-3.15 ± 0.24	+1.49 ± 0.60

5.5.2 Carbon isotope fractionation in the presence of cyanobacteria

5.5.2.1 CO_2 limited calcite precipitation - Experiments SolA-2 and SolA-3

Mass balance calculations indicate that calcite precipitation during the biotic experiments SolA-2 and SolA-3 is limited by CO_2 dissolution from the atmosphere: the initial 9 mmol/kg DIC present in the reactor was consumed within the first few days of each experiment and the DIC concentrations stayed below 1 mmol/kg in the reactor fluid until calcite precipitation was complete and DIC again increased (see Figure 5-2). Calcite precipitated at a close to constant rate as evidenced by the linear decrease in Ca concentrations over time (see Figure 5-2 C). The combination of atmospheric CO_2 dissolution, biotic activity, and calcite precipitation resulted in the distinct carbon isotope signatures in the DIC and precipitated calcite as shown in Figure 5-6 A and B.

The initial measured $\delta^{13}C_{DIC}$ values of experiments SolA-2 and SolA-3 was similar to that of their corresponding abiotic control SolA-1i and similar to that of the bicarbonate powder used to make these aqueous solutions. Within the first five days, the $\delta^{13}C_{DIC}$ value increased from around -6 ‰ to +6.25 ‰. This increase can be attributed to the preferential uptake of ^{12}C by photosynthesis producing a fluid enriched in ^{13}C. This trend stopped when the carbon concentrations of the fluid dropped to near zero. New carbon entering the fluid via CO_2 dissolution from the atmosphere was rapidly consumed by the precipitating calcite and the measured $\delta^{13}C_{DIC}$ values ranged from -9.4 ‰ to -24.4 ‰ between day 5 and 24. A predominant consumption of DIC by biota would result in more positive $\delta^{13}C_{DIC}$ values. This suggests that the calcite precipitation is controlled by the kinetics of CO_2 dissolution rather than by the competing consumption of DIC by biota. Once calcite precipitation stopped and DIC concentrations increased, $\delta^{13}C_{DIC}$ values increased to +1.46 ‰ and -3.01 ‰ in SolA-2 and SolA-3, respectively. During the first few days of the experiments, the calcite precipitated with

a $\delta^{13}C_{Calcite}$ value of around 0 ‰. Subsequently, when calcite precipitation was limited by carbon influx from the atmosphere, the $\delta^{13}C_{Calcite}$ value decreased to less than -6 ‰. Similar highly depleted carbon isotope signatures were previously described in experimental studies by Wilson et al. (2010) and Clark et al. (1992), as well as in natural aragonite and calcite travertines and "scums" in the western United States and the Oman described by O'Neil and Barnes (1971), Clark et al. (1992) and Falk et al. (2016). These highly negative $\delta^{13}C$ signatures have been attributed to kinetic isotope effects during CO_2 uptake from the atmosphere into alkaline aqueous fluids. Finally, after the completion of calcite precipitation an upward temporal trend in $\delta^{13}C_{Calcite}$ values towards calcite-aqueous fluid isotopic equilibrium is apparentThe initial measured $\delta^{13}C_{DIC}$ values of experiments SolA-2 and SolA-3 was similar to that of their corresponding abiotic control SolA-1i and similar to that of the bicarbonate powder used to make these aqueous solutions. Within the first five days, the $\delta^{13}C_{DIC}$ value increased from around -6 ‰ to +6.25 ‰. This increase can be attributed to the preferential uptake of ^{12}C by photosynthesis producing a fluid enriched in ^{13}C. This trend stopped when the carbon concentrations of the fluid dropped to near zero. New carbon entering the fluid via CO_2 dissolution from the atmosphere was rapidly consumed by the precipitating calcite and the measured $\delta^{13}C_{DIC}$ values ranged from -9.4 ‰ to -24.4 ‰ between day 5 and 24. A predominant consumption of DIC by biota would result in more positive $\delta^{13}C_{DIC}$ values. This suggests that the calcite precipitation is controlled by the kinetics of CO_2 dissolution rather than by the competing consumption of DIC by biota. Once calcite precipitation stopped and DIC concentrations increased, $\delta^{13}C_{DIC}$ values increased to +1.46 ‰ and -3.01 ‰ in SolA-2 and SolA-3, respectively. During the first few days of the experiments, the calcite precipitated with a $\delta^{13}C_{Calcite}$ value of around 0 ‰. Subsequently, when calcite precipitation was limited by carbon influx from the atmosphere, the $\delta^{13}C_{Calcite}$ value decreased to less than -6 ‰. Similar highly depleted carbon isotope signatures were previously described in experimental studies by Wilson et al. (2010) and Clark et al. (1992), as well as in natural aragonite and calcite travertines and "scums" in the western United States and the Oman described by O'Neil and Barnes (1971), Clark et al. (1992) and Falk et al. (2016). These highly negative $\delta^{13}C$ signatures have been attributed to kinetic isotope effects during CO_2 uptake from the atmosphere into alkaline aqueous fluids. Finally, after the completion of calcite precipitation an upward temporal trend in $\delta^{13}C_{Calcite}$ values towards calcite-aqueous fluid isotopic equilibrium is apparent (see Figure 5-6 B).

5.5.2.2 Carbon isotope fractionation in the presence of cyanobacteria during experiments SolB-2, SolB-3, SolC-2 and SolC-3

The carbon isotopes of dissolved inorganic carbon in the presence of cyanobacteria show a characteristic trend defined by the metabolic activity of the growing biomass (see Figure 5-7 A and D). During photosynthesis, cyanobacteria preferentially consume the light ^{12}C isotope (Johnston and Fischer, 2012; O'Leary, 1988) thus significantly increasing $\delta^{13}C_{DIC}$ values over time (arrow 1 in Figure 5-8 B). In the biotic experiments SolB-2, SolB-3, SolC-2 and SolC-3 this occurred during the first 10-15 days of the experiments when the $\delta^{13}C_{DIC}$ values increased by 16-17 ‰ in SolB-2 and SolB-3 and by about 12 ‰ in SolC-2 and SolC-3. This strong increase in $\delta^{13}C_{DIC}$ was followed by a decrease to final values of +3.3±0.1 ‰ in SolB-2 and SolB-3 and +3.5±0.3 ‰ in SolC-2 and SolC-3, respectively. The decrease at the end of the experiments (arrow 2 in Figure 5-8 B) might be caused by either 1) cell lysis and death and subsequent degradation to abiotic carbon species, 2) predominance of respiration over photosynthesis, as common in natural environments (Schulte et al., 2011), 3) the rate of atmospheric CO_2 influx exceeding photosynthesis or 4) a combination of these processes.

The close link between photosynthetic activity and the $\delta^{13}C_{DIC}$ values is illustrated in Figure 5-8 A and B. . In the abiotic experiments, pCO_2 was close to equilibrium with respect to the atmosphere and $\delta^{13}C_{DIC}$ remained close to constant after an initial adjustment. In the biotic experiments, the production of biomass removed aqueous carbon and increased pH thereby reducing the pCO_2 in the fluid phase to ~10^{-8} atm. The preferential uptake of ^{12}C into biomass caused a strong inverse correlation between $\delta^{13}C_{DIC}$ and pCO_2 as shown in Figure 5-8 A. Figure 5-8 B illustrates the correlation between the $\delta^{13}C_{DIC}$ values and biomass. With increasing biomass concentration, $\delta^{13}C_{DIC}$ values increased due to photosynthesis until a biomass concentration of about 0.6 $g_{(dry)}$/kg was reached and subsequently $\delta^{13}C_{DIC}$ values decreased due to ^{12}C input as described above. These observations are in close agreement with those of Mavromatis et al. (2015), who precipitated hydrous Mg-carbonates in the presence of cyanobacteria in similar experiments and of Pentecost and Spiro (1990), who observed an increase in $\delta^{13}C_{DIC}$ of 2 ‰ caused by the photosynthetic activity of a *Rivularia sp.* colony. An increase in $\delta^{13}C_{DIC}$ during high productivity events can also be observed in natural systems as described by Parker et al. (2010) and Pokrovsky and Shirokova (2013).

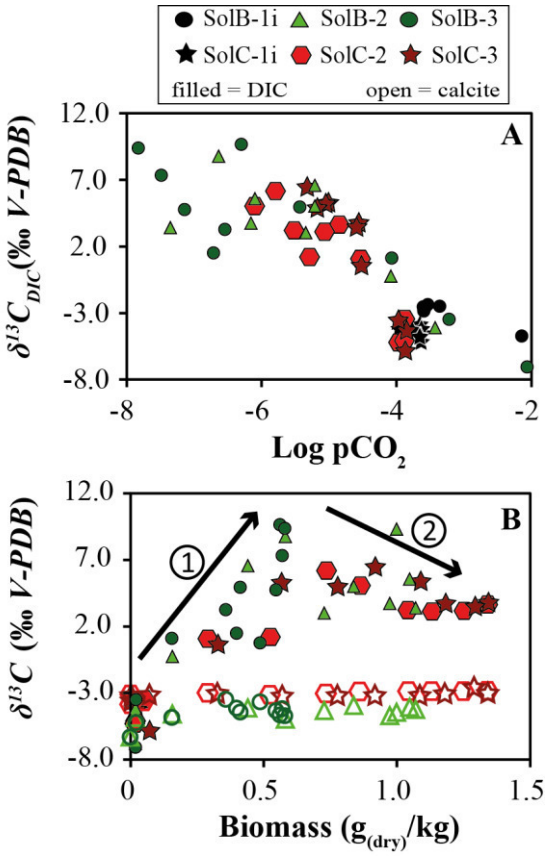

Figure 5-8. Plot of $\delta^{13}C_{DIC}$ as a function of pCO_2 in all experiments of series SolB and SolC (**A**) and of $\delta^{13}C_{DIC}$ (black symbols) and $\delta^{13}C_{Calcite}$ (grey symbols) as a function of biomass concentration in biotic experiments SolB-2, SolB-3, SolC-2 and SolC-3 (**B**). Arrow (1) highlights the $\delta^{13}C_{DIC}$ increase resulting from photosynthesis which preferentially consumes ^{12}C creating a liquid more enriched in ^{13}C. Arrow (2) highlights the decrease in $\delta^{13}C_{DIC}$ resulting from cell death and decomposition - see text. The symbols are identified above the figure.

5.5.2.3 Carbon isotope fractionation in calcite after its complete precipitation

In all biotic experiments the $\delta^{13}C_{Calcite}$ value evolved towards fluid-calcite equilibrium after calcite precipitation was completed (see Figure 5-6 B and Figure 5-7 B and E). In experiments SolA-2, $\delta^{13}C_{Calcite}$ increased from -6.39 ‰ to -5.00 ‰ after calcite precipitation was complete during the last 14 days of the experiment. In SolA-3, the $\delta^{13}C_{Calcite}$ value increased from -5.79 ‰ to -5.56 ‰ over the last 7 days of the experiment. The $\delta^{13}C_{Calcite}$ values measured during the biotic experiments evolved from -4.72 ‰ to -4.23 ‰ in SolB-2, from -5.21 ‰ to -3.45 ‰ in SolB-3, from -3.89 ‰ to -2.77 ‰ in SolC-2 and from -3.79 ‰ to -3.03 ‰ in SolC-3 after calcite precipitation had stopped. Nevertheless, the calculated $\Delta^{13}C_{Calcite-DIC}$ throughout these biotic experiments are highly negative due to the large changes in $\delta^{13}C_{DIC}$ compared to those of $\delta^{13}C_{Calcite}$, and thus remain out of isotopic equilibrium at the end of the experiments. This observation contrasts with those of Mavromatis et al. (2015), who precipitated the hydrous Mg-carbonates dypingite and nesquehonite in similar experiments and observed a co-variance of $\delta^{13}C_{DIC}$ and $\delta^{13}C_{Solid}$ in their biotic experiments.

The most striking observation in Mavromatis et al. (2015) is that $\Delta^{13}C_{(Hydrous\ Mg-carbonate)-DIC}$ remained close to constant and close to isotopic equilibrium, even after the majority of carbon had precipitated from the fluid phase and the aqueous fluid is in bulk chemical equilibrium. This observation requires the continuous equilibration of the carbon isotope composition of these solid and fluid phases. The contrasting behaviors of these hydrous Mg-carbonates compared to calcite is likely due to the faster mineral fluid reaction rates of these hydrous Mg-carbonates compared to calcite.

It seems likely that the observed enrichment in ^{13}C in calcite following its complete precipitation in this study is driven by the large isotopic disequilibrium resulting from the preferential uptake of ^{12}C by cyanobacteria. To a first approximation, the $\delta^{13}C$ values of the calcite increase at a constant rate in each experiment following their complete precipitation. Linear regression of these variations are shown in Figure 5-6 B and Figure 5-7 B and E; the slopes of these regression lines are provided in Table 5-3.

The rate of ^{13}C transferred to and from the solid can be quantified by taking account of the first derivative of Eqn. (5-1) with respect to time:

$$\frac{d\left(^{13/12}C_{Calcite}\right)}{dt} = \frac{^{13/12}C_{V-PDB}}{1000} \cdot \frac{d(\delta^{13}C_{Calcite})}{dt}, \qquad (5\text{-}6)$$

where $^{13/12}C_{V-PDB}$ again refers to the isotopic ratio of the *V-PDB* standard; $^{13/12}C_{V-PDB}$= 0.01118 (Hayes, 1983) $^{13/12}C_{Calcite}$ designates the atomic C isotope ratio of the calcite and $\delta^{13}C_{Calcite}$ refers to the measured calcite isotope signature in per mil. Because the total ^{13}C within calcite in the reactor ($^{13}C_{tot}$) is related to its carbon isotope ratio $^{13/12}C_{Calcite}$, according to:

$$^{13}C_{tot} = m_{Calcite} \cdot \frac{^{13/12}C_{Calcite}}{\left(^{13/12}C_{Calcite} + 1\right)}, \qquad (5\text{-}7)$$

where $m_{Calcite}$ refers to the total mass of calcite in the reactor, it follows that:

$$\frac{d\left(^{13}C_{tot}\right)}{dt} = m_{Calcite} \cdot \frac{^{13/12}C_{V-PDB}}{1000} \cdot \left(\frac{1}{\left(^{13/12}C_{Calcite} + 1\right)^2}\right) \cdot \frac{d(\delta^{13}C_{Calcite})}{dt} \qquad (5\text{-}8)$$

Note, that as $^{13/12}C_{Calcite}$ commonly varies by less than ±5 % in natural samples, it can be assumed to be a constant equal to $^{13/12}C_{V-PDB}$ such that $\left(\frac{1}{\left(^{13/12}C_{Calcite}+1\right)^2}\right) \approx 0.98$. Equation (5-8) was used together with the average $^{13/12}C_{Calcite}$ values provided in Table 5-3 and the $\frac{d(\delta^{13}C_{Calcite})}{dt}$ values generated from the linear regressions shown in Figure 5-6 B and Figure 5-7 B and E, and provided in Table 5-3 to compute corresponding values of $\frac{d(^{13}C_{tot})}{dt}$. This latter time derivative was normalized to the total surface area A_{tot} of calcite in the reactors to obtain the surface area normalized carbon isotope equilibration rate r according to:

$$r = \frac{d(^{13}C_{tot})}{dt} \cdot \frac{1}{A_{tot}} \tag{5-9}$$

This normalization describes the rate at which the mass of ^{13}C is transferred into and out of the calcite structure. Rates generated by this approach have the same dimensions as mineral dissolution and precipitation rates common in the literature, mass/(time·length^2) (Liu and Dreybrod, 1997; Oelkers et al., 1994). Due to the small mass of calcite precipitated during the experiments, it was not possible to measure their BET surface areas. As such, the surface area used to calculate rates in Eqn. (5-9) was the total geometric surface area A_{tot}, calculated assuming that particles are smooth spheres according to:

$$A_{tot} = \frac{6 \cdot m_{Calcite}}{\rho \cdot d}, \tag{5-10}$$

where $m_{Calcite}$ refers to the total mass of calcite present in the reactor, ρ designates the density of calcite (2.715×10^{06} g/m^3) and d designates the average grain diameter, estimated from SEM images. As the calcite grain size is constant within the reactor after its precipitation, the mass to surface ratio remains constant. These calculations yield carbon isotope equilibration rates r ranging from 1.75×10^{-14} to 1.71×10^{-13} mol^{13}C/m^2/s (see Table 5-3).

Table 5-3. Estimated carbon isotope equilibration rates normalized to geometric surface area (r). The $\frac{d(\delta^{13}C_{Calcite})}{dt}$ values in ‰/s were obtained by linear regression of the $\delta^{13}C_{Calcite}$ measurements as shown in Figures 5-6 and 5-7. Calcite grain diameters d were estimated from SEM images to appraise geometric surface area A_{tot}. $^{13/12}C_{Calcite\ (t_i)}$ and $^{13/12}C_{Calcite\ (t_e)}$ designate the calculated $^{13/12}C$ at the beginning (t_i) of the carbon isotope re-equilibration and the end (t_e) of the experiment.

ID	$\frac{d(\delta^{13}C_{Calcite})}{dt}$ (‰/s) x 10^{-7}	$^{13/12}C_{Calcite\ (t_i)}$	$^{13/12}C_{Calcite\ (t_e)}$	r (mol^{13}C/m^2/s) x 10^{-14}
SolA-2	11.6 ± 0.72	0.011109	0.011125	17.1 ± 4.26
SolA-3	3.68 ± 1.34	0.011116	0.011118	5.45 ± 17.8
SolB-2	1.77 ± 1.00	0.011128	0.011134	1.75 ± 1.31
SolB-3	5.19 ± 0.95	0.011124	0.011139	5.13 ± 1.31
SolC-2	2.87 ± 0.66	0.011142	0.011151	7.09 ± 2.07
SolC-3	1.88 ± 0.71	0.011142	0.011148	4.64 ± 2.23

ID	Time elapsed (t_i-t_e) (days)	Calcite diameter d (µm)	$m_{Calcite}$ in reactor (mmol)	A_{tot} in reactor (m²)
SolA-2	14	3	4.78 - 3.02	0.22 - 0.35
SolA-3	7	3	3.98 - 3.04	0.22 - 0.29
SolB-2	32	2	7.01 - 2.76	0.31 - 0.78
SolB-3	31	2	6.93 - 2.75	0.30 - 0.77
SolC-2	33	5	7.13 - 2.75	0.12 - 0.32
SolC-3	33	5	7.07 - 2.75	0.12 – 0.31

5.5.2.4 Estimation of the extent of calcite-fluid carbon exchange following the completion of calcite precipitation

An estimate of the average depth of carbon isotope exchange within the calcite can be made by assuming that 1) the originally precipitated calcite was isotopically homogenous, and 2) a fraction of this calcite was isotopically equilibrated with the fluid. In such cases, the fraction f of the carbon in the calcite that has been isotopically equilibrated can be calculated from:

$$\delta^{13}C_{Calcite\ final} = f \cdot \delta^{13}C_{Calcite\ EQ} + (1-f) \cdot \delta^{13}C_{Calcite\ i}\ , \qquad (5\text{-}11)$$

where $\delta^{13}C_{Calcite\ final}$ designates the final measured $\delta^{13}C_{Calcite}$ at the end of the experiment, $\delta^{13}C_{Calcite\ i}$ refers to the $\delta^{13}C_{Calcite}$ immediately after the completion of calcite precipitation and $\delta^{13}C_{Calcite\ EQ}$ stands for the $\delta^{13}C_{Calcite}$ in equilibrium with the fluid phase. In this study, $\delta^{13}C_{Calcite\ EQ}$ was estimated by adding the equilibrium fractionation factor $\Delta^{13}C_{Calcite-HCO_3^-}$ of 1.96 ‰ (Deines et al., 1974) to the average $\delta^{13}C_{DIC}$ measured in the reactors after the completion of calcite precipitation. This is an approximation since $\delta^{13}C_{DIC}$ constantly evolved during our experiments due to bacterial activity. Insight into the mechanism of post-calcite precipitation carbon exchange can be gained by consideration of dissolution-reprecipitation processes or the solid-state diffusion rates in calcite. The solid-state diffusion rate of carbon in

calcite at 25°C is negligibly slow (~7.1×10-7 µm/year using the diffusion coefficient: D = 1.6×10-32 m2/s by Anderson (1969) and the diffusion-depth relation: $x = 2\sqrt{Dt}$ by Bird et al. (1960)) and very little evidence supports this mechanism. The isotopic modification of a bulk solid phase is commonly explained by the mechanism of coarsening or Ostwald ripening, which describes a dissolution-reprecipitation process where coarser grains grow in expense of smaller grains, as first described by Lifshitz and Slyozov (1961). This mechanism, however, requires a changing crystal size distribution as described for example by Kile et al. (2000), which has not been observed during this study based on SEM investigations at the beginning and the end of the experiment. This suggests that a process other than Ostwald ripening might play a role in the observed variation of carbon isotope signatures observed in this study. One such mechanism has been proposed by Putnis (2009) who described pervasive fluid infiltration into the reacting crystal through a porous reaction front generated by interface-coupled dissolution-reprecipitation reactions. Note, that a detailed crystal size evolution necessary to unambiguously exclude Ostwald ripening was not conducted.

Table 5-4 shows the results of this calculation for all biotic experiments. These results suggest from 4.0 to 15.2 % of the carbon in the originally precipitated calcite needed to be isotopically equilibrated with the reactive aqueous fluid after calcite had precipitated to match the observed total ^{13}C evolution observed in the experiments. This amount of isotopic equilibration would require a minimum isotopic exchange depth, assuming spherical calcite grains of 2 to 5 µm diameter, of 136 to 801 Å. Note that these values are only approximations, as they are based on the assumption that the original precipitated calcite was isotopically homogeneous and that the carbon incorporated into the calcite after its complete precipitation was in isotopic equilibrium with the fluid phase.

Insight into the mechanism of post-calcite precipitation carbon exchange can be gained by consideration of dissolution-reprecipitation processes or the solid-state diffusion rates in calcite. The solid-state diffusion rate of carbon in calcite at 25°C is negligibly slow (~7.1×10^{-7} µm/year using the diffusion coefficient: D = 1.6×10^{-32} m^2/s by Anderson (1969) and the diffusion-depth relation: $x = 2\sqrt{Dt}$ by Bird et al. (1960)) and very little evidence supports this mechanism. The isotopic modification of a bulk solid phase is commonly explained by the mechanism of coarsening or Ostwald ripening, which describes a dissolution-reprecipitation process where coarser grains grow in expense of smaller grains, as first described by Lifshitz and Slyozov (1961). This mechanism, however, requires a changing crystal size distribution as described for example by Kile et al. (2000), which has not been observed during this study

based on SEM investigations at the beginning and the end of the experiment. This suggests that a process other than Ostwald ripening might play a role in the observed variation of carbon isotope signatures observed in this study. One such mechanism has been proposed by Putnis (2009) who described pervasive fluid infiltration into the reacting crystal through a porous reaction front generated by interface-coupled dissolution-reprecipitation reactions. Note, that a detailed crystal size evolution necessary to unambiguously exclude Ostwald ripening was not conducted.

Table 5-4. Parameters used and results for the calculations of percentage calcite exchanged and the corresponding depth of carbon exchange from the calcite-fluid interface expressed as distance in Å. The % calcite exchanged corresponds to the fraction f calculated by Eqn. (5-11).

ID	Calcite diameter d (µm)	$\delta^{13}C_{Calcite\ i}$ (‰ V-PDB)	$\delta^{13}C_{Calcite\ end}$ (‰ V-PDB)	$\delta^{13}C_{Calcite\ EQ}$ (‰ V-PDB)	Average $\delta^{13}C_{DIC}$ (‰ V-PDB)	Calcite exchanged f (%)	Depth of C exchange (Å)
SolA-2	3	-6.39	-5.00	2.76	0.80	15.2	801
SolA-3	3	-5.79	-5.56	-0.78	-2.74	4.6	233
SolB-2	2	-4.66	-4.19	6.98	5.02	4.0	136
SolB-3	2	-5.05	-3.66	5.89	3.93	12.7	443
SolC-2	5	-3.46	-2.65	5.29	3.33	9.3	797
SolC-3	5	-3.38	-2.86	6.15	4.19	5.5	463

5.5.3 Estimation of carbon isotope equilibration rates in calcite in natural systems

The results summarized above suggest that carbon isotope re-equilibration between carbonate minerals and its co-existing fluid may occur whenever a significant isotopic disequilibrium exists between these phases. This can be achieved for example on carbonate platforms where limestone, which originally precipitated in isotopic equilibrium with seawater, becomes in contact with pore waters which are isotopically evolved through evaporation, freshwater discharge or biotic activity (Patterson and Walter, 1994a, 1994b). Furthermore, authigenic carbonates that precipitated in sediment pore waters, commonly exhibit highly depleted δ^{13}C signatures because the DIC from which they formed was generated by the oxidation of organic matter and is thus highly negative ^{13}C values (Oehlert and Swart, 2014). Isotopic disequilibrium would result if these depleted carbonates became in contact with seawater or other isotopically different diagenetic fluids.

The median calcite carbon isotope equilibration rate $r = 5.29\times10^{-14}$ mol^{13}C/m^2/s generated above can be used together with Eqns. (5-8) and (5-9) to estimate the rates of carbon isotope equilibration in natural systems. For a spherical calcite grain with diameter d, A_{tot} can be calculated according to Eqn. (5-10) and the molar mass, $m_{Calcite}$, determined from the sphere volume and the density of calcite. Multiplying the obtained ^{13}C equilibration rate by A_{tot} yields

the temporal change in ^{13}C. This rate can be converted to $\frac{d(\delta^{13}C_{Calcite})}{dt}$ via Eqn. and the time required to change the carbon isotope signature of a calcite grain by 1 ‰ can be calculated, provided that it is out of isotopic equilibrium with the fluid phase. The results of this calculation as a function of grain diameter from 1 µm to 1 cm are provided in Figure 5-9. Thus, a 1 µm diameter calcite grain in contact with a fluid which is out of isotopic equilibrium with this grain is calculated to change its carbon isotope composition by 1 ‰ in 10.8 days whereas it takes about 10^5 days or 296 years to change a calcite grain of 1 cm diameter by 1 ‰. Note that this calculation requires a sufficient large reservoir of DIC, and/or substantial fluid flow to maintain fluid-calcite disequilibria, which may be rare in many subsurface systems. Note also, that the rates obtained in this study were normalized to geometric surface area. Total reactive surface area and overall ^{13}C exchange rates might be notably higher due to surface roughness or nanoporosity (e.g. Mavromatis et al. (2017) Ritter et al., (2017).

In contrast, the rates generated in this study suggest that the carbon isotope composition of the fluid phase in carbonate-rich rocks might be strongly affected if it were out of isotopic

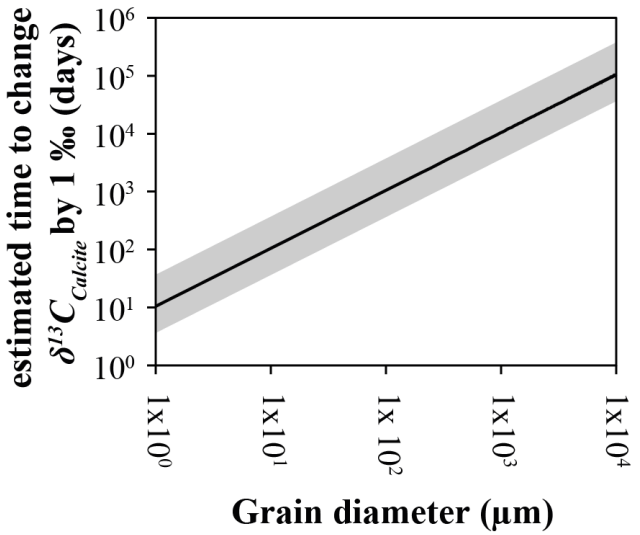

Figure 5-9. Estimated time required to change the $\delta^{13}C_{Calcite}$ of a spherical calcite grain by 1‰ as a function of grain size. Calculations are based on the median rate obtained in this study (see text). The grey area represents the uncertainty of the calculation, given by the variation of the obtained rates.

equilibrium with its co-existing solid phase. The carbon isotope evolution of DIC in the presence of calcite depends on the ratio of carbon in the solid to that in the liquid phase. In a system containing just calcite and an aqueous phase, such as a porous pure limestone, the ratio of carbon in calcite compared to DIC varies as a function of porosity and DIC concentration. Multiplying the average calcite carbon isotope equilibration rate by the surface area of a spherical pore yields the temporal change $\frac{d(^{13}C_{tot})}{dt}$. Using Eqn. (5-8), with $m_{Calcite}$ representing

the total mass of carbon in the pore fluid, the temporal carbon isotopic change $\frac{d(‰\delta^{13}C_{DIC})}{dt}$ of the pore fluid can be calculated. Such calculations were used to generate Figure 5-10, which shows the calculated time to change $\delta^{13}C_{DIC}$ of a pore fluid by 1 ‰ as a function of the pore diameter. For this calculation DIC concentrations of 0.1 mmol/kg, 2 mmol/kg (equals present day sea surface water concentration) and 5 mmol/kg were considered and the porosity was assumed to be composed of uniform individual spheres with diameters ranging from 1 to 25 mm. According to these calculations, it would take only 0.8 days to change the $\delta^{13}C_{DIC}$ by 1 ‰ in a pore fluid having a 2 mmol/kg DIC concentration if the pores had a 1 mm pore diameter and 19.9 days for 25 mm pores.

This result suggests that $\delta^{13}C_{DIC}$ in limestone would rapidly equilibrate with $\delta^{13}C_{Calcite}$ assuming that $\delta^{13}C_{DIC}$ is not perturbed by other processes such as $\delta^{13}C_{DIC}$ recharge, equilibration with a gas phase or microbial activity/decay. The rapid equilibration of $\delta^{13}C_{DIC}$ stems from mass balance constraints in these calcite dominated systems; the total carbon in DIC is small compared to the mass of carbon in the calcite. This is illustrated in Figure 5-10 B, which shows the ratio of carbon in calcite and carbon in the pore fluid having an exemplary DIC concentration of 2 mmol/kg. As such, in a hypothetical limestone with 50 % porosity, there is still about 10^4 time more C in calcite compared to the pore fluid. Similarly, Han and Plummer (2013) and Han et al. (2014) concluded that the carbon isotope composition of dissolved inorganic carbon in groundwater is ultimately controlled by carbonate minerals due to the considerably larger mass of solid carbonate compared to the mass of DIC. Note, however, our calculations were performed using a representative rate measured in the biotic experiments performed in the present study. The carbon isotopes of the calcite in the present study were as much as 14.3 per mil out of isotopic equilibrium with respect to their co-existing fluid phase. It seems likely that the rate of isotopic change in calcite will depend on the degree of calcite-aqueous fluid isotopic disequilibrium. For example, by analogy with the behavior of mineral dissolution and precipitation rates (Oelkers et al., 1994; Oelkers, 2001), carbon isotope equilibration rates likely decrease as fluid-mineral isotopic equilibrium is approached. Some evidence for this is seen in our abiotic experiments; the fluids in our abiotic experiments were closer to isotopic equilibrium with their precipitated calcite than our biotic experiments and the carbon isotope composition of the calcite in these abiotic experiments showed little variation after their complete precipitation during the experiments. As such, the results of calculations shown in Figure 5-9 and Figure 5-10 should be viewed as provisional estimates until a more

quantitative description of the rates of isotopic variation as a function of isotopic disequilibration become available.

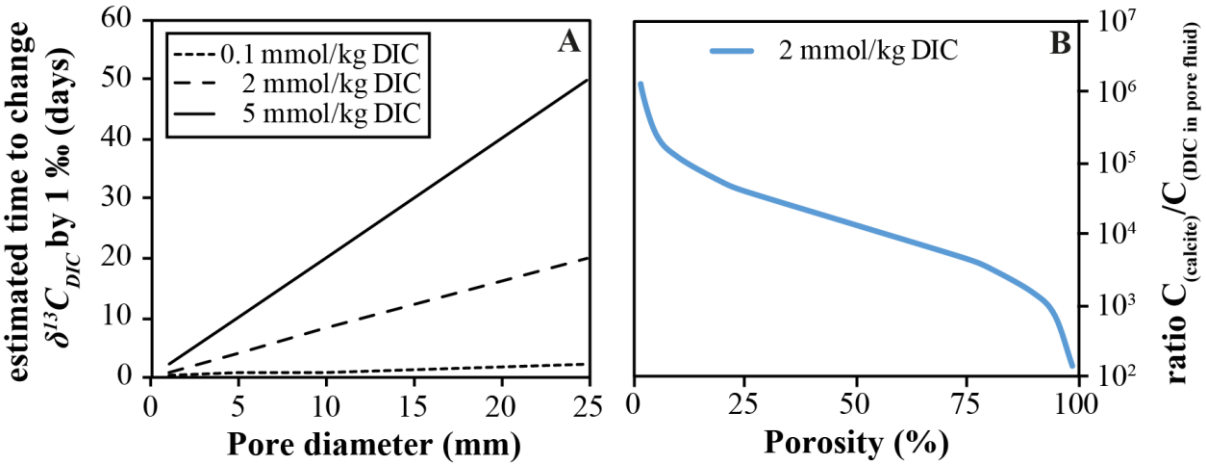

Figure 5-10. A: Estimated time required to change the $\delta^{13}C_{DIC}$ of porewater in a limestone by 1‰ as a function of the pore diameter which defines the reactive surface area as well as the total mass of aqueous carbon at a defined DIC concentration in the pore fluid. The three lines correspond to the pore water DIC concentrations defined in the plot. Calculations are based on the median rate obtained in this study (see text). The uncertainty, defined by the variation of the obtained rates, is approximately one order of magnitude. **B**: Ratio of carbon in calcite to dissolved carbon in pore fluid of a pure limestone showing that C is largely predominant in the solid phase even at high porosities.

5.6 Conclusions

The fractionation of carbon isotopes in calcite has been investigated in the presence of actively growing cyanobacteria. The major findings are:

1) When calcite precipitation is limited by CO_2 dissolution from the atmosphere into the fluid phase, the fluid and the precipitated solid show highly negative carbon isotope values despite the presence of cyanobacteria, which would tend to produce more positive DIC and calcite carbon isotope values due to the preferential uptake of ^{12}C into biomass. Consequently, the $\delta^{13}C$ values of DIC and calcite are significantly more negative than those that might be expected if the system were at equilibrium with the atmosphere. Similar observations were made in synthetically precipitated dypingite by Wilson et al. (2010) and in natural travertines (Clark et al., 1992; Falk et al., 2016; O'Neil and Barnes, 1971).

2) The $\delta^{13}C$ values of calcite were found to continuously evolve towards equilibrium after its complete precipitation at rates ranging from 1.75×10^{-14} to 1.71×10^{-13} mol $^{13}C/m^2/s$. This carbon isotope exchange rate is much lower than those of hydrous Mg-carbonates which appear to instantaneously reset their carbon isotope signature (Mavromatis et al., 2015).

3) The carbon isotope exchange rates determined in this study are sufficiently fast to modifiy significantly the carbon isotope signatures of calcite over geologic timespans. Nevertheless, mass balance calculations suggest that in closed systems and in the absence of an internal distinct carbon isotope source (e.g. organic carbon) calcite will preserve its carbon isotope signature by rapidly equilibrating the carbon isotope signature of its co-existing fluid phase with the reactive surface area.

Acknowledgements

This research was supported by the Marie Curie EU-FP7 CO2-REACT Research and Training Network. The authors would like to thank Liudmila S. Shirokova, Carole Causserand, Thierry Aigouy and Michel Thibaut for their help with experimental work, wet chemical analyses, SEM- and XRD- measurements, respectively. Elisabeth Grimm, Anna L. Harrison and Martin Voigt are acknowledged for their helpful ideas and contributions during the edition of this manuscript.

5.7 References

See References on page 157ff.

Appendix Chapter 5

Table A 5-1. Measured biomass concentration, pH, Ca concentration, dissolved inorganic carbon (DIC), alkalinity, C isotope composition of fluid and solid phase as well as the volume of aqueous fluid and the mass of calcite present in the reactor for all samples examined in this study. Note, that alkalinity was not measured in experiment SolA due to low carbon concentrations. *Moles of calcite were calculated from the decrease in Ca concentration and the volume of fluid in the reactor.

ID	Time elapsed (days)	Biomass conc. ($g_{(dry)}$/kg)	pH	Ca (mmol/kg)	DIC (mmol/kg)	Alkalinity (mmol /kg)	Fluid in reactor (g)	Calcite in reactor* (mmol)	$\delta^{13}C_{Calcite}$ (‰ V-PDB)	$\delta^{13}C_{DIC}$ (‰ V-PDB)
SolA-1i - 0	0.0			8.64			900			
SolA-1i - 1	0.0		8.31	8.25	9.05		894	0.34		-6.08
SolA-1i - 2	2.8		8.62	4.97			844	3.09		
SolA-1i - 3	4.7		8.64	5.00	3.16		838	3.05	-3.15	-3.66
SolA-1i - 4	6.8		8.61	4.96	3.13		788	2.90	-3.15	-2.08
SolA-1i - 5	10.0		8.54	4.96	3.14		738	2.71	-3.53	-2.71
SolA-1i - 6	11.7		8.65	4.89			688	2.58		
SolA-1i - 7	13.7		8.64	5.11	3.14		682	2.40	-3.25	-4.42
SolA-1i - 8	16.7		8.56	5.10	3.13		632	2.23		
SolA-1i - 9	18.7		8.67	5.09			582	2.06		
SolA-1i - 10	20.7		8.64	5.14	3.17		573	2.00	-3.26	-3.77
SolA-1i - 11	23.7		8.65	4.94	3.11		523	1.93		
SolA-1i - 12	25.7		8.68	4.99			473	1.72		
SolA-1i - 13	27.7		8.59	5.04	3.16		467	1.68		-9.76
SolA-1i - 14	30.7		8.66	5.18	3.21		417	1.44		-9.81
SolA-1i - 15	32.7		8.63				367			
SolA-1i - 16	34.7		8.62	5.20	3.23		359	1.23	-3.16	-9.01
SolA-2 - 0	0.0			8.60			900			
SolA-2 - 1	0.0	0.016	8.32	8.19	9.10		894	0.37	-13.61	-4.64
SolA-2 - 2	2.8	0.004	8.69	4.50			844	3.46		
SolA-2 - 3	4.7	0.076	9.49	3.35	0.94		838	4.40	-0.53	4.25
SolA-2 - 4	6.8	0.215	10.49	2.82	0.36		788	4.55	-1.59	
SolA-2 - 5	10.0	0.445	10.60	2.18	0.28		738	4.73	-3.73	
SolA-2 - 6	11.7	0.582	10.76	1.88			688	4.62		
SolA-2 - 7	13.7	0.740	10.62	1.51	0.37		682	4.83	-4.91	
SolA-2 - 8	16.7	0.927	10.35	0.89	0.42		632	4.87	-6.11	
SolA-2 - 9	18.7	1.073	10.28	0.49			582	4.72		
SolA-2 - 10	20.7	1.190	10.02	0.25	0.71		573	4.78	-6.39	-11.21
SolA-2 - 11	23.7	1.337	9.93	0.12	1.47		523	4.43	-6	-9.37
SolA-2 - 12	25.7	1.474	9.32	0.17			473	3.99		
SolA-2 - 13	27.7	1.672	9.47	0.10	2.97		467	3.97	-5.6	5.14
SolA-2 - 14	30.7	1.774	9.30	0.12	3.57		417	3.53	-5.27	5.98
SolA-2 - 15	32.7	1.811	9.20	0.10			367			
SolA-2 - 16	34.7	1.852	9.09	0.17	3.91		359	3.02	-5	1.46
SolA-3 - 0	0.0			8.54			900			
SolA-3 - 1	0.0	0.015	8.25	8.26	9.04		894	0.25	-9.1	-6.37
SolA-3 - 2	2.8	0.001	8.71	4.74			844	3.20		
SolA-3 - 3	4.7	0.053	9.42	3.28	0.72		838	4.40	0.25	6.25
SolA-3 - 4	6.8	0.194	10.77	3.00	0.23		788	4.36	-0.14	
SolA-3 - 5	10.0	0.376	10.74	2.40	0.24		738	4.53	-2.71	
SolA-3 - 6	11.7	0.480	10.94	2.16			688	4.38		
SolA-3 - 7	13.7	0.585	10.80	1.78	0.54		682	4.60	-2.21	-11.32
SolA-3 - 8	16.7	0.732	10.51	1.11	0.57		632	4.69	-3.55	-20.85
SolA-3 - 9	18.7	0.797	10.23	0.81			582	4.50		
SolA-3 - 10	20.7	0.939	10.38	0.53	0.50		573	4.58	-5.08	-24.38
SolA-3 - 11	23.7	1.100	10.87	0.31	0.62		523	4.30	-5.69	-22.82
SolA-3 - 12	25.7	1.248	9.85	0.11			473	3.98		
SolA-3 - 13	27.7	1.411	10.00	0.06	1.69		467	3.95	-5.79	-2.09
SolA-3 - 14	30.7	1.612	10.08	0.05	2.31		417	3.53	-5.62	-3.11
SolA-3 - 15	32.7	1.703	9.68				367			
SolA-3 - 16	34.7	1.755	10.01	0.06	2.82		359	3.04	-5.56	-3.01
SolB-1i - 1	0.0		8.59	8.50	47.60	51.53	897	0.00		
SolB-1i - 2	0.0	0.003	8.31	8.23	29.50	33.23	847	0.23	-3.44	-4.74
SolB-1i - 3	0.8		9.20	0.15		32.39	837	6.99	-5.01	
SolB-1i - 4	1.9	0.005	9.41	0.07	28.42	32.14	787	6.63	-4.66	-2.5
SolB-1i - 5	4.8	0.011	9.54	0.05	27.49	32.12	737	6.23	-5	-2.37
SolB-1i - 6	6.8	0.005	9.53				734			

Table A 5-1. Continuation.

ID	Time elapsed (days)	Biomass conc. ($g_{(dry)}$/kg)	pH	Ca (mmol/kg)	DIC (mmol/kg)	Alkalinity (mmol /kg)	Fluid in reactor (g)	Calcite in reactor* (mmol)	$\delta^{13}C_{Calcite}$ (‰ V-PDB)	$\delta^{13}C_{DIC}$ (‰ V-PDB)
SolB-1i - 7	8.8	0.002	9.58	0.03	28.56	32.34	684	5.79	-4.74	-2.86
SolB-1i - 8	12.2	0.008	9.59	0.03	28.64	32.37	634	5.37	-4.66	-2.54
SolB-1i - 9	14.1	0.002	9.56				631			
SolB-1i - 10	15.9	0.013	9.58	0.03	27.31	32.51	581	4.92	-4.53	-2.67
SolB-1i - 11	18.9	0.015	9.58	0.03	27.89	32.56	531	4.50	-5	-2.77
SolB-2 - 1	0.0	0.017	8.59	8.50	47.60	51.53	897	0.00		
SolB-2 - 2	0.0	0.018	8.20	7.98	32.37	35.60	847	0.44	-6.3	-6.78
SolB-2 - 3	0.8		9.13	0.13		32.44	837	7.01	-4.7	
SolB-2 - 4	1.9	0.018	9.46	0.06	28.96	32.37	787	6.64	-4.82	-4.11
SolB-2 - 5	4.8	0.157	9.91	0.04	26.19	33.34	737	6.24	-4.57	-0.25
SolB-2 - 6	6.8	0.302	10.22				734			
SolB-2 - 7	8.8	0.440	10.55	0.02	22.36	33.26	684	5.80	-4.12	6.58
SolB-2 - 8	12.2	0.580	11.29	0.02	21.92	35.61	634	5.37	-4.94	8.76
SolB-2 - 9	14.1	0.652	10.77				631			
SolB-2 - 10	15.9	0.727	10.64	0.02	23.99	36.25	581	4.93	-4.32	3.01
SolB-2 - 11	18.9	0.837	10.57	0.02	24.38	36.89	531	4.50	-3.92	5.02
SolB-2 - 12	20.9	0.918	10.71				528			
SolB-2 - 13	22.9	0.973	11.06	0.02	22.46	37.51	478	4.05	-4.7	3.74
SolB-2 - 14	25.9	0.999	11.60	0.02	20.55		428	3.63	-4.43	9.32
SolB-2 - 15	27.9	1.017	11.17			37.73	425			
SolB-2 - 16	29.9	1.047	11.03	0.02	24.32	38.01	375	3.18	-4.05	5.57
SolB-2 - 17	32.9	1.070	11.65	0.02	21.56	38.13	325	2.76	-4.23	3.39
SolB-3 - 1	0.0	0.017	8.58	8.50	47.60	51.53	897	0.00		
SolB-3 - 2	0.0	0.018	8.25	7.88	31.74	34.46	847	0.53	-6.3	-7.06
SolB-3 - 3	0.8		8.84	0.21		33.34	837	6.94	-6.56	
SolB-3 - 4	1.9	0.020	9.31	0.07	29.71	33.28	787	6.63	-5.21	-3.48
SolB-3 - 5	4.8	0.154	9.91	0.04	29.83	33.77	737	6.24	-4.81	1.13
SolB-3 - 6	6.8	0.281	10.30				734			
SolB-3 - 7	8.8	0.411	10.68	0.02	20.49	35.22	684	5.80	-4.42	4.95
SolB-3 - 8	12.2	0.561	11.12	0.03	19.80	35.99	634	5.37	-4.62	9.65
SolB-3 - 9	14.1	0.582	11.72				631			
SolB-3 - 10	15.9	0.579	11.85	0.02	27.72	36.00	581	4.92	-4.7	9.39
SolB-3 - 11	18.9	0.569	11.70	0.02	21.95	36.02	531	4.50	-4.16	7.34
SolB-3 - 12	20.9	0.561	11.68				528			
SolB-3 - 13	22.9	0.545	11.54	0.02	21.11	36.07	478	4.05	-4.31	4.76
SolB-3 - 14	25.9	0.486	11.49	0.03	18.54		428	3.63	-3.64	0.78
SolB-3 - 15	27.9	0.439	11.51			36.05	425			
SolB-3 - 16	29.9	0.397	11.33	0.03	20.99	35.94	375	3.18	-4.12	1.51
SolB-3 - 17	32.9	0.357	11.25	0.03	23.64	36.00	325	2.75	-3.45	3.28
SolC-1i - 1	0.0		10.14	8.50	48.94	71.61	897	0.00		
SolC-1i - 2	0.0	0.004	9.94	0.82	41.71	56.19	847	6.50	-3.84	-4.31
SolC-1i - 3	0.8		9.98	0.05		56.16	837	7.07	-4.26	
SolC-1i - 4	1.9	0.004	9.92	0.04	44.45	56.07	787	6.66	-3.04	-4.82
SolC-1i - 5	4.8	0.006	9.83	0.04	45.43	56.31	737	6.23	-3.04	-4.39
SolC-1i - 6	6.8	0.003	9.79				734			
SolC-1i - 7	8.8	0.007	9.78	0.03	46.66	57.02	684	5.79	-3.44	-4.81
SolC-1i - 8	12.2	0.012	9.77	0.03	47.77	56.78	634	5.37	-3.32	-4.34
SolC-1i - 9	14.1	0.008	9.75				631			
SolC-1i - 10	15.9	0.014	9.76	0.02	45.97	56.59	581	4.92	-3.25	-5.12
SolC-1i - 11	18.9	0.015	9.75	0.02	49.89	57.12	531	4.50	-3.13	-4.46
SolC-1i - 12	20.9	0.004	9.77				528			
SolC-1i - 13	22.9	0.020	9.76	0.02	46.28	57.65	478	4.05	-2.67	-4.09
SolC-1i - 14	25.9	0.018	9.80	0.02	45.86		428	3.60	-3.30	-5.04
SolC-2 - 1	0.0	0.017	10.14	8.50	48.94	71.61	897	0.00		
SolC-2 - 2	0.0	0.015	9.95	0.08	43.06	57.12	847	7.13	-3.89	-5.23
SolC-2 - 3	0.8		9.98	0.04		57.18	837	7.08	-3.38	
SolC-2 - 4	1.9	0.017	9.92	0.04	49.13	57.29	787	6.66	-3.13	-5.07
SolC-2 - 5	4.8	0.048	9.91	0.04	44.40	57.52	737	6.24	-3.61	-3.48
SolC-2 - 6	6.8	0.138	10.07				734			
SolC-2 - 7	8.8	0.289	10.29	0.03	42.07	59.27	684	5.80	-2.94	1.08
SolC-2 - 8	12.2	0.525	10.71	0.02	37.15	61.29	634	5.37	-3.08	1.21
SolC-2 - 9	14.1	0.645	10.86				631			
SolC-2 - 10	15.9	0.734	10.97	0.02	38.36	62.35	581	4.93	-3.03	6.2

Table A 5-1. Continuation.

ID	Time elapsed (days)	Biomass conc. ($g_{(dry)}$/kg)	pH	Ca (mmol/kg)	DIC (mmol/kg)	Alkalinity (mmol /kg)	Fluid in reactor (g)	Calcite in reactor* (mmol)	$\delta^{13}C_{Calcite}$ (‰ V-PDB)	$\delta^{13}C_{DIC}$ (‰ V-PDB)
SolC-2 - 11	18.9	0.860	11.12	0.02	35.30	63.20	531	4.50	-2.86	5.05
SolC-2 - 12	20.9	0.952	10.92				528			
SolC-2 - 13	22.9	1.041	10.83	0.02	37.57	64.55	478	4.06	-2.86	3.2
SolC-2 - 14	25.9	1.130	10.68	0.02	38.70		428	3.63	-2.82	3.13
SolC-2 - 15	27.9	1.201	10.70			65.58	425			
SolC-2 - 16	29.9	1.251	10.60	0.02	44.22	67.02	375	3.18	-2.79	3.16
SolC-2 - 17	32.9	1.339	10.50	0.03	43.28	67.93	325	2.75	-2.77	3.64
SolC-3 - 1	0.0	0.017	10.13	8.50	48.94	71.61	897	0.00		
SolC-3 - 2	0.0	0.017	9.96	0.27	44.82	56.68	847	6.97	-3.47	-3.51
SolC-3 - 3	0.8		9.95	0.06		56.86	837	7.07	-3.79	
SolC-3 - 4	1.9	0.019	9.89	0.04	48.76	56.75	787	6.66	-3.14	-4.26
SolC-3 - 5	4.8	0.069	9.90	0.04	46.59	57.21	737	6.24	-3.06	-5.81
SolC-3 - 6	6.8	0.171	10.05				734			
SolC-3 - 7	8.8	0.326	10.28	0.03	42.24	59.09	684	5.79	-2.94	0.59
SolC-3 - 8	12.2	0.566	10.57	0.03	36.29	60.67	634	5.37	-3.23	5.27
SolC-3 - 9	14.1	0.683	10.62				631			
SolC-3 - 10	15.9	0.775	10.65	0.03	40.25	62.22	581	4.92	-3.17	4.92
SolC-3 - 11	18.9	0.918	10.73	0.03	41.07	63.45	531	4.50	-3.18	6.46
SolC-3 - 12	20.9	1.022	10.63				528			
SolC-3 - 13	22.9	1.087	10.57	0.03	44.56	64.95	478	4.05	-3.16	5.35
SolC-3 - 14	25.9	1.180	10.50	0.06	43.89		428	3.61	-2.99	3.68
SolC-3 - 15	27.9	1.242	10.44			66.28	425			
SolC-3 - 16	29.9	1.290	10.35	0.03	47.24	67.80	375	3.18	-2.57	3.51
SolC-3 - 17	32.9	1.342	10.34	0.04	47.06	68.57	325	2.75	-3.03	3.75

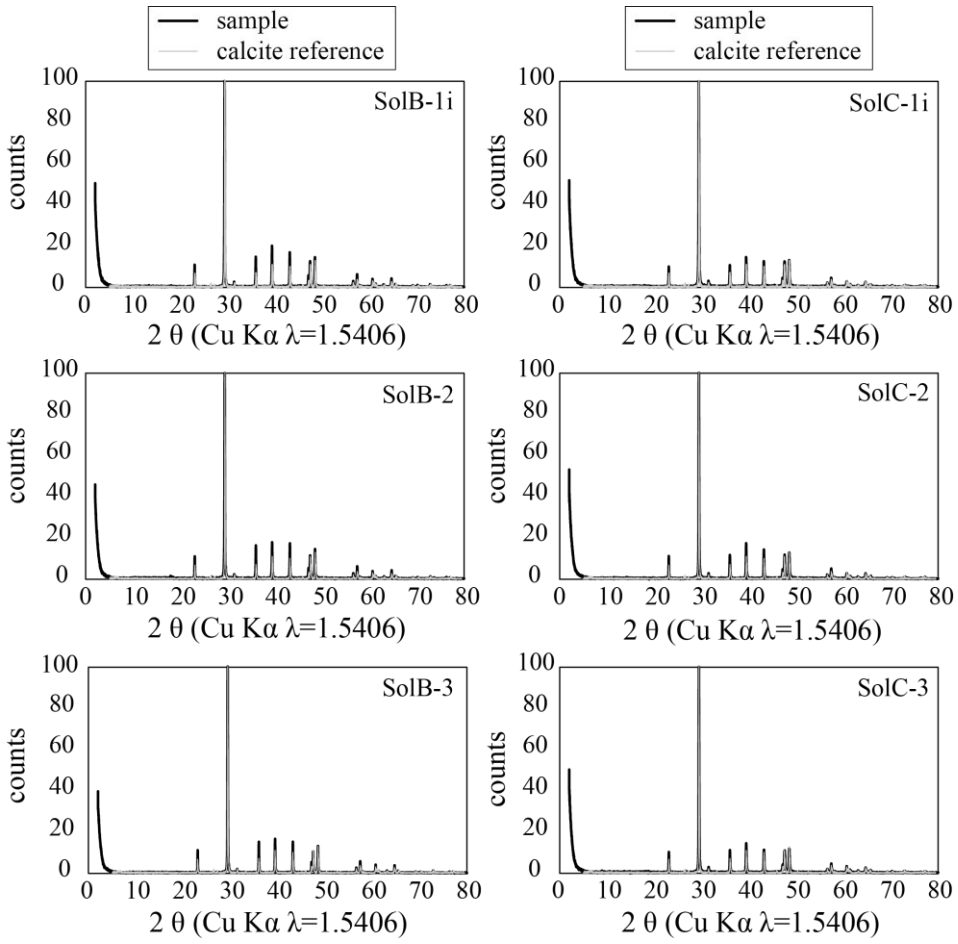

Figure A 5-1. XRD patterns of carbonates precipitated during experiments SolB and SolC. Black lines are the samples, grey lines show the calcite reference pattern.

6 Conclusions and outlook

This study was designed to evaluate the effect of riverine particulate material on the organic carbon cycle and to provide new insight into the negative feedback between global warming and the enhanced CO_2 drawdown via the organic pathway. To achieve this, we first investigated the effect of riverine particulates on primary production by conducting microcosm growth experiments with two common primary producing microorganisms, the cyanobacteria *Synechococcus sp*. and the diatom *Thalassiosira weissflogii*. Furthermore, we discussed the potential effect of riverine particulates on organic carbon burial, a fundamental step in drawing down atmospheric CO_2 over long timescales.

Results of the experimental study conducted with freshwater cyanobacteria displayed three distinct positive effects of riverine suspended material on bacterial growth: 1) particulates triggered bacterial growth in otherwise unfavorable growth conditions (e.g. by increasing pH), 2) particulates increased total biomass concentration as a function of particulate concentration, and 3) particulates induced steady bacterial growth in the post-exponential growth phase as a function of particulate concentration. In addition, the results of this study demonstrate a positive feedback between bacterial growth and sediment dissolution; dissolving sediments enhanced bacterial growth which itself enhanced alumosilicate particle dissolution by altering fluid pH. Scanning electron microscopy investigations revealed frequent bacteria clusters associated with sediment particles as well as abundant direct physical contact between particulates and cyanobacteria through organic fibers, suggesting that bacteria attach on mineral surfaces to gain required nutrients. Corresponding experiments conducted with marine diatoms also showed a strong positive effect of riverine particulate material on diatom growth. The presence of particulates increased total diatom concentrations and slowed post-exponential death rates. This effect is increased with increasing sediment concentration. An enhanced effect of suspended sediments on the burial efficiency of organic carbon was suggested by the occurrence of frequent diatom-sediment agglomerations. A direct physical attachment of microbes onto mineral surfaces was also observed in natural samples at the South coast of Iceland.

Taken together, this thesis provides experimental evidence for the close link between the arrival of riverine particulate material to the oceans and the organic carbon cycle through their positive impact on primary production and indicate that particulates facilitate organic

matter burial through direct attachment of microbes on sediment surfaces or the formation of fast settling mineral/microbe agglomerations. Suspended particulates act as nutrient buffer or slow release fertilizer, replenishing the dissolved nutrient pool, once consumed by primary production, or even serve directly as nutrient source. Note, however, that the effect of riverine particulates on phytoplankton growth in natural systems requires a case-by-case study depending on various environmental factors such as nutrient availability and nutrient ratios, light intensity, phytoplankton species distribution or the characteristics or the particulates. For example, a reduced sediment supply to estuaries following upstream dam constructions may decrease primary production due to a reduction in nutrient concentrations but may also increase photosynthetic activity as a consequence of elevated light availability. Note, that studies describing increased primary production in estuaries related to reduced sediment supply after dam construction frequently report a concomitant increase in the number or extent of harmful algae blooms.

The flux of riverine particulates from the continents to the oceans is subject to constant changes, either locally or globally, either naturally or man-made. The major direct anthropogenic intervention on the riverine particulate flux is the construction of dams, which cause an estimated 5-10 % reduction of the global riverine sediment flux to the oceans due to retention within reservoirs. Whereas the consequences of dam construction on the local environment have commonly been addressed, the potential global and long term effect of this human intervention has rather been relatively neglected. Riverine particulate fluxes have furthermore been reported to be particularly climate sensitive. An increasing atmospheric CO_2 concentration leads to higher air temperatures, changing precipitations patterns and increasing runoff, which leads to elevated chemical and physical weathering rates and thus, to higher suspended sediment fluxes. This is a naturally occurring process accelerated through the human input of CO_2 to the atmosphere from the burning of fossil fuels. This link between climate and riverine particulate transport is likely strongest during the end of glacial cycles, when glacial abrasion produces vast quantities of fine-grained material, easily transported to the oceans by glacial meltwater. The elevated supply of particulate material to the ocean may increase primary productivity and organic carbon burial, thus significantly contributing to drawing down atmospheric CO_2 and moderating global warming towards the end of glaciations. As the CO_2 drawdown via the organic carbon cycle is concomitant with a rise in oxygen, which is produced during oxygenic photosynthesis, the accelerated organic carbon cycle towards the end of a glaciation may furthermore be considered as mechanism responsible for the major atmospheric

oxygenation events, which coincide major "Snowball Earth" events in the Earths' historical record.

Major variations in the degree of primary production and organic carbon burial are observed in the carbon isotopic record of marine carbonates as "carbon excursions". Notably, the two major carbon excursions occurred during Earths' history also coincide with the major snowball Earth and global oxygenation events. These reconstructions of primary production, organic carbon burial rates and generally past climate conditions take advantage of the pronounced carbon isotopic fractionation during photosynthesis. Organic matter is on average 2.5 % more depleted in ^{13}C compared to inorganic carbon dissolved in the ocean or fixed in carbonates. As a result, changes in the isotopic composition of marine carbonates have been interpreted as changes in the fractional burial of carbonate carbon relative to organic carbon. The use of carbon isotopic signatures to reconstruct past environmental conditions, however, requires that these signatures are preserved over vast timescales.

This requirement was tested as a part of this thesis. We conducted calcite precipitation experiments in the presence of cyanobacteria and monitored the temporal evolution of the carbon isotopic signature of calcite and dissolved inorganic carbon to evaluate the rate and degree to which stable carbon isotopes in calcite might alter over time. Experimental results demonstrate, that the carbon isotopic composition of calcite continuously evolves towards mineral-fluid isotopic equilibrium. This observation suggests that calcite C-isotopic compositions might change noticeably if the calcite were continuously in isotopic disequilibria with its co-existing fluid.

Models of past atmospheric CO_2 concentrations, take account of primary production and organic carbon burial ("organic pathway"), as well as weathering, diagenesis, sedimentation, mantle degassing and metamorphism ("inorganic pathway"). We suggest that the supply of riverine particulate material to the oceans may provide a strong negative feedback for the regulation of the Earths' temperature through its role in the inorganic (supply of divalent cations) and especially the organic (supply of nutrients and facilitating organic carbon burial) carbon cycle and therefore needs to be included in climate models to accurately predict future global climate evolution.

To accurately quantify the effect of riverine particulate material on the global carbon cycle in order to define input data for precise climate modelling, further experimental and especially natural studies need to be conducted with different primary producing microbes or natural microbial communities. The use of natural communities would simultaneously

enlighten the effect of particulates on microbial species distribution and thus on the formation of harmful algae blooms.

We furthermore suggest that future efforts should aim to evaluate the potential role of suspended matter supply on the major global oxygenation events of the Earths' atmosphere, which remain still enigmatic. Further research should address the characterization and the quantification of the mass of particulate matter produced and transported to the oceans by glacial activity and the quantification of the associated particulate surface area available for reaction and organic carbon absorption. Moreover, precise quantification of release rates of nutrients from particulates should be determined and coupled with estimates of the total particulate supply. For a more accurate estimate of the role of suspended particulates in organic carbon burial, we furthermore encourage more research on the absorption of organic matter on mineral surfaces and the role of suspended matter in aggregate formation and organic matter settling.

Such efforts would further quantify the role of riverine particulate material in the global carbon cycle and test whether the stabilization of Earths' temperature through biological CO_2 drawdown and the oxygenation of the Earths' atmosphere via biological O_2 production may have been caused by particulate driven enhanced primary production and organic carbon burial.

6b Conclusions générales et perspectives

Cette étude a été conçue pour évaluer l'effet de la matière particulaire fluviale sur le cycle du carbone organique et pour donner un aperçu de la réaction négative entre l´effet de serre et une réduction améliorée de CO_2 par le cycle de carbone organique. Pour ce faire, nous avons d'abord étudié l'effet des particules de rivières sur la production primaire en effectuant des expériences de croissance du microcosme avec deux producteurs primaires communs, la cyanobactérie *Synechococcus sp.* et la diatomée *Thalassiosira weissflogii*. En outre, nous avons discuté l'effet potentiel des particules de rivières sur la séquestration du carbone organique, une étape fondamentale dans l'élimination du CO_2 atmosphérique sur de longues échelles de temps.

Les résultats de l'étude expérimentale réalisée avec des cyanobactéries d'eau douce ont montré trois effets positifs distincts de la matière en suspension sur la croissance bactérienne: 1) les particules ont déclenché une croissance bactérienne dans des conditions de croissance défavorables (par exemple en augmentant le pH), 2) les particules ont augmenté la concentration totale de biomasse en fonction de la concentration des particules, et 3) les particules ont induit une croissance bactérienne continue dans la phase de croissance post-exponentielle en fonction de la concentration particulaire. En outre, les résultats de cette étude démontrent une réaction positive entre la croissance bactérienne et la dissolution des sédiments: la dissolution des sédiments a amélioré la croissance bactérienne, et elle-même a amélioré la dissolution des particules d'alumosilicate en modifiant le pH du fluide. Les études de microscopie électronique à balayage ont révélé des agglomérats fréquents de bactéries associés à des particules sédimentaires ainsi qu'un contact physique direct abondant entre les particules et les cyanobactéries par des fibres organiques. Ceci suggère que les bactéries se fixent sur les surfaces minérales pour obtenir les nutriments requis. Les expériences correspondantes menées avec des diatomées marines ont également montré un fort effet positif du matériel particulaire de rivière sur la croissance des diatomées. La présence de particules a augmenté les concentrations totales de diatomées et ralenti les taux de mortalité post-exponentielle. Cet effet s'est accru avec l'augmentation de la concentration de sédiments. Un effet positif des sédiments en suspension sur l'efficacité de décantation du carbone organique a été suggéré par l'apparition d'agglomérats fréquents de diatomées et de sédiments. Une fixation physique directe des

microbes sur des surfaces minérales a également été observée dans des échantillons naturels sur la côte sud de l'Islande.

Ensemble, cette thèse fournit des preuves expérimentales du lien étroit qui existe entre l'arrivée de la matière particulaire fluviale vers les océans et le cycle du carbone organique grâce à leur impact positif sur la production primaire. De plus, les résultats indiquent que les particules facilitent le piégeage des matières organiques par fixation directe de microbes sur les surfaces sédimentaires ou la formation d'agglomérats minéraux/microbes décantant rapidement dans la colonne d´eau. Les particules en suspension agissent comme un tampon nutritif ou un engrais à libération lente, en reconstituant l´inventaire de nutriments dissous, une fois consommés par la production primaire, ou même en servant directement de source nutritive. Il est à noter cependant que l'effet des particules de rivières sur la croissance du phytoplancton dans les systèmes naturels nécessite une étude au cas par cas de l'impact de divers facteurs environnementaux tels que la disponibilité des nutriments et les rapports nutritionnels, l'intensité lumineuse, la répartition des espèces de phytoplancton ou surtout la caractéristique des particules arrivants. Par exemple, un approvisionnement réduit en sédiments dans les estuaires suivant des constructions de barrage en amont peut diminuer la production primaire en raison d'une réduction des concentrations de nutriments, mais peut également augmenter l'activité photosynthétique en raison de la disponibilité élevée de la lumière. Il est également à noter que les études décrivant l'augmentation de la production primaire dans les estuaires liée à l'approvisionnement réduit en sédiments après la construction des barrages reportent fréquemment aussi une augmentation concomitante du nombre ou de l'étendue des proliférations d'algues nuisibles.

Le flux de particules fluviales des continents vers les océans est soumis à des changements constants, localement ou globalement, soit d'origine naturelle, soit anthropique. L'impact anthropique majeur sur les flux de particules de rivières est issu de la construction de barrages, ce qui cause une réduction estimée de 5 à 10 % du flux global de sédiments fluviaux aux océans en raison de la rétention dans les réservoirs. Bien que les conséquences de la construction des barrages sur l'environnement local ont souvent été abordées, l'effet potentiel à l'échelle globale et à long terme de cette intervention humaine a plutôt été relativement négligé. En outre, il a été montré que les flux de particules fluviales sont particulièrement sensibles au climat. Une augmentation de la concentration atmosphérique de CO_2 conduit à des températures plus élevées, au changement des précipitations et à l'augmentation du ruissellement, ce qui entraîne des taux d'altération chimiques et physiques élevés et donc des flux de sédiments en

suspension plus élevés. Il s'agit d'un processus naturel qui s'est accéléré par l'apport humain de CO_2 dans l'atmosphère en conséquence de l´utilisation des combustibles fossiles. Ce lien entre le climat et le transport des particules de rivières est probablement le plus fort pendant des cycles glaciaires, lorsque l'abrasion glaciaire produit de grandes quantités de matières fines, facilement transportées vers les océans par l'eau de fonte glaciaire. L'apport élevé de matériaux particulaires à l'océan peut augmenter la productivité primaire et la séquestration du carbone organique, ce qui contribue largement à atténuer le CO_2 atmosphérique et à modérer le réchauffement climatique vers la fin des glaciations. Etant donné qu'une réduction du CO_2 atmosphérique par le cycle du carbone organique est concomitante avec une augmentation de l'oxygène, qui est produit pendant la photosynthèse, le cycle du carbone organique accéléré vers la fin d'une glaciation peut en outre être considéré comme un mécanisme responsable des événements majeurs d'oxygénation de l´atmosphère, qui coïncident avec les événements majeurs de «Snowball Earth» dans l´histoire de la Terre.

Des variations majeures du taux de production primaire et de séquestration du carbone organique pendant l´histoire de la Terre sont conservées dans les signatures isotopiques du carbone des carbonates marins comme «excursions de carbone». Notamment, les deux grandes excursions de carbone qui ont eu lieu lors de l'histoire de la Terre coïncident également avec les événements majeurs de «Snowball Earth» et de l'oxygénation atmosphérique. Ces reconstructions de la production primaire, les taux de piégeage du carbone organique et généralement les conditions climatiques passées profitent du fractionnement isotopique du carbone prononcé lors de la photosynthèse. La matière organique est en moyenne 2.5% plus appauvrie en ^{13}C par rapport au carbone inorganique dissous dans l'océan ou fixé dans les carbonates. En conséquence, les changements dans la composition isotopique des carbonates marins ont été interprétés comme des changements dans le piégeage du carbone de carbonate par rapport au carbone organique. L'utilisation de signatures isotopiques de carbone pour reconstruire les conditions environnementales passées, cependant, exige que ces signatures soient conservées sur de vastes échelles de temps.

Cette exigence a été testée dans le cadre de cette thèse. Dans ce chapitre, nous avons mené des expériences de précipitation de calcite en présence de cyanobactéries et nous avons surveillé l'évolution temporelle de la signature isotopique du carbone de la calcite et du carbone inorganique dissous pour évaluer le taux et le degré d'altération des isotopes de carbone dans la calcite au cours du temps. Les résultats expérimentaux démontrent que la composition isotopique du carbone de la calcite évolue continuellement vers l'équilibre isotopique entre les

fluides et les minéraux. Cette observation suggère que les compositions isotopiques du carbone de calcite pourraient changer notablement si la calcite était constamment dans des déséquilibres isotopiques avec son fluide coexistant.

Les modèles de concentrations de CO_2 atmosphériques passées tiennent compte de la production primaire et de la séquestration du carbone organique («cycle de carbone organique»), ainsi que des altérations continentales, de la diagénèse, de la sédimentation, du dégazage du manteau et du métamorphisme («cycle de carbone inorganique»). Nous suggérons que l'apport en matière particulaire fluviale aux océans peut induire une forte réaction négative pour la régulation de la température globale grâce à son rôle dans le cycle du carbone inorganique (apport en cations divalents) et en particulier dans le cycle du carbone organique (apport en nutriments et piégeage facilité du carbone organique) et doit donc être inclus dans les modèles climatiques pour prédire avec plus de précision l'évolution future du climat mondial.

Pour quantifier avec précision l'effet du matériel particulaire fluviale sur le cycle mondial du carbone afin de définir les données saisies pour une modélisation climatique précise, d'autres études expérimentales, et spécialement en conditions naturelles, doivent être menées avec différents producteurs primaires ou des communautés microbiennes naturelles. L'utilisation de communautés naturelles permettrait d'éclairer l'effet des particules sur la distribution des espèces microbiennes, et donc sur la formation de proliférations d'algues nuisibles.

Nous suggérons en outre que les efforts futurs devraient viser à évaluer le rôle potentiel de l'apport en matières en suspension sur les principaux événements d'oxygénation mondiale de l'atmosphère, qui restent encore énigmatiques. D'autres recherches devraient aborder la caractérisation et la quantification de la masse de particules produites et transportées vers les océans par l'activité glaciaire et la quantification de la surface particulaire disponible pour la réaction et l'absorption du carbone organique. De la même façon, une quantification précise des taux de libération des nutriments provenant des particules devrait être déterminée et associée à des estimations de l'apport total de particules. Pour une estimation plus précise du rôle des particules en suspension dans la séquestration du carbone organique, nous encourageons davantage la recherche sur l'absorption de la matière organique sur les surfaces minérales et le rôle des matières en suspension dans la formation d'agrégats et dans la décantation de matières organiques.

De tels efforts permettraient de quantifier plus précisément le rôle du matériel particulaire fluvial dans le cycle mondial du carbone et de tester si la stabilisation de la température de la Terre par la réduction biologique du CO_2 et l'oxygénation de l'atmosphère par la production biologique d'O_2 peut avoir été causée par une amélioration de la production primaire et de la séquestration de carbone organique liée à l´apport des particules fluviales en suspension.

7 References

Alemayehu, T., Leis, A., Eisenhauer, A., Dietzel, M., 2011. Multi-proxy approach ($^{2}H/H$, $^{18}O/^{16}O$, $^{13}C/^{12}C$ and $^{87}Sr/^{86}Sr$) for the evolution of carbonate-rich groundwater in basalt dominated aquifer of Axum area, northern Ethiopia. Chemie der Erde - Geochemistry 71 (2), 177–187.

Allan, J.R., Matthews, R.K., 1982. Isotope signatures associated with early meteoric diagenesis. Sedimentology 29 (6), 797–817.

Alldredge, A.L., Gotschalk, C., Passow, U., Riebesell, U., 1995. Mass aggregation of diatom blooms: Insights from a mesocosm study. Deep Sea Research Part II: Topical Studies in Oceanography 42 (1), 9–27.

Alldredge, A.L., Jackson, G.A., 1995. Preface: Aggregation in marine system. Deep Sea Research Part II: Topical Studies in Oceanography 42 (1), 1–7.

Alldredge, A.L., Passow, U., Logan, B.E., 1993. The abundance and significance of a class of large, transparent organic particles in the ocean. Deep Sea Research Part I: Oceanographic Research Papers 40 (6), 1131–1140.

Alley, R.B., Cuffey, K.M., Evenson, E.B., Strasser, J.C., Lawson, D.E., Larson, G.J., 1997. How glaciers entrain and transport basal sediment: Physical constraints. Quaternary Science Reviews 16 (9), 1017–1038.

Altabet, M.A., Francois, R., Murray, D.W., Prell, W.L., 1995. Climate-related variations in denitrification in the Arabian Sea from sediment $^{15}N/^{14}N$ ratios. Nature 373, 506-509.

Amiotte Suchet, P., Probst, J.L., 1993. Modelling of atmospheric CO_2 consumption by chemical weathering of rocks: Application to the Garonne, Congo and Amazon basins. Chemical Geology 107 (3), 205–210.

Anderson, D.M., Glibert, P.M., Burkholder, J.M., 2002. Harmful algal blooms and eutrophication: Nutrient sources, composition, and consequences. Estuaries 25 (4), 704–726.

Anderson, M.A., Morel, F.M., 1982. The influence of aqueous iron chemistry on the uptake of iron by the coastal diatom Thalassiosira weissflogii. Limnology and Oceanography 27 (5), 789–813.

Anderson, T.F., 1969. Self-diffusion of carbon and oxygen in calcite by isotope exchange with carbon dioxide. Journal of Geophysical Research 74 (15), 3918–3932.

Andres, M.S., Sumner, D.Y., Reid, R.P., Swart, P.K., 2006. Isotopic fingerprints of microbial respiration in aragonite from Bahamian stromatolites. Geology 34 (11), 973–976.

Archer, D., Winguth, A., Lea, D., Mahowald, N., 2000. What caused the glacial/interglacial atmospheric pCO_2 cycles? Reviews of Geophysics 38 (2), 159–189.

Armstrong, R.A., Lee, C., Hedges, J.I., Honjo, S., Wakeham, S.G., 2001. A new, mechanistic model for organic carbon fluxes in the ocean based on the quantitative association of POC with ballast minerals. Deep Sea Research Part II: Topical Studies in Oceanography 49 (1), 219–236.

Arnaud, E., Halverson, G.P., Shields-Zhou, G., 2011. Chapter 1: The geological record of Neoproterozoic ice ages. Geological Society, London, Memoirs 36 (1), 1–16.

Arrigo, K.R., 2007. Carbon cycle: Marine manipulations. Nature 450 (7196), 491–492.

Assayag, N., Jézéquel, D., Ader, M., Viollier, E., Michard, G., Prévot, F., Agrinier, P., 2008. Hydrological budget, carbon sources and biogeochemical processes in Lac Pavin (France): Constraints from $\delta^{18}O$ of water and $\delta^{13}C$ of dissolved inorganic carbon. Applied Geochemistry 23 (10), 2800–2816.

Atkinson, M.J., Barnett, H., Aceves, H., Langdon, C., Carpenter, S.J., McConnaughey, T., Hochberg, E., Smith, M., Marino, B.D.V., 1999. The Biosphere 2 coral reef biome. Ecological Engineering 13 (1), 147–172.

Avnimelech, Y., Troeger, B.W., Reed, L.W., 1982. Mutual Flocculation of Algae and Clay: Evidence and Implications. Science 216 (4541), 63.

Azhikodan, G., Yokoyama, K., 2016. Spatio-temporal variability of phytoplankton (Chlorophyll-a) in relation to salinity, suspended sediment concentration, and light intensity in a macrotidal estuary. Continental Shelf Research 126, 15–26.

Bailey, B., Templeton, A., Staudigel, H., Tebo, B.M., 2009. Utilization of Substrate Components during Basaltic Glass Colonization by Pseudomonas and Shewanella Isolates. Geomicrobiology Journal 26 (8), 648–656.

Baisre, J.A., Arboleya, Z., 2006. Going against the flow: Effects of river damming in Cuban fisheries. Fisheries Research 81 (2), 283–292.

Banner, J.L., Hanson, G.N., 1990. Calculation of simultaneous isotopic and trace element variations during water-rock interaction with applications to carbonate diagenesis. Geochimica et Cosmochimica Acta 54 (11), 3123–3137.

Barber, R.T., Chavez, F.P., 1991. Regulation of primary productivity rate in the equatorial Pacific. Limnology and Oceanography 36 (8), 1803–1815.

Bartley, J.K., Kah, L.C., 2004. Marine carbon reservoir, C_{org}-C_{carb} coupling, and the evolution of the Proterozoic carbon cycle. Geology 32 (2), 129–132.

Beaulieu, S.E., Sengco, M.R., Anderson, D.M., 2005. Using clay to control harmful algal blooms: Deposition and resuspension of clay/algal flocs. Harmful Algae 4 (1), 123–138.

Behrenfeld, M.J., Falkowski, P.G., 1997. Photosynthetic rates derived from satellite-based chlorophyll concentration. Limnology and Oceanography 42 (1), 1–20.

Bennett, P.C., Rogers, J.R., Choi, W.J., Hiebert, F.K., 2001. Silicates, Silicate Weathering, and Microbial Ecology. Geomicrobiology Journal 18 (1), 3–19.

Bergkamp, G., McCartney, M., Dugan, P., McNeely, J., Acreman, M., 2000. Dams, ecosystem functions and environmental restoration. WCD Thematic Review Environmental Issues II.1, prepared as an input to the World Commission on Dams, Capetown, www.dams.org.

Berner, R.A., 1982. Burial of organic carbon and pyrite sulfur in the modern ocean: Its geochemical and environmental significance. American Journal of Science 282, 451–473.

Berner, R.A., 1989. Biogeochemical cycles of carbon and sulfur and their effect on atmospheric oxygen over phanerozoic time. Global and Planetary Change 1 (1), 97–122.

Berner, R.A., 1990. Atmospheric Carbon Dioxide Levels Over Phanerozoic Time. Science 249 (4975), 1382–1386.

Berner, R.A., 1992. Weathering, plants, and the long-term carbon cycle. Geochimica et Cosmochimica Acta 56 (8), 3225–3231.

Berner, R.A., 2003. The long-term carbon cycle, fossil fuels and atmospheric composition. Nature 426, 323-326.

Berner, R.A., 2004. The Phanerozoic Carbon Cycle: CO_2 and O_2. Oxford University Press.

Berner, R.A., 2006. GEOCARBSULF: A combined model for Phanerozoic atmospheric O_2 and CO_2. Geochimica et Cosmochimica Acta 70 (23), 5653–5664.

Berner, R.A., Kothavala, Z., 2001. Geocarb III: A Revised Model of Atmospheric CO_2 over Phanerozoic Time. American Journal of Science 301 (2), 182–204.

Berner, R.A., Lasaga, A.C., Garrels, R.M., 1983. The carbonate-silicate geochemical cycle and its effect on atmospheric carbon dioxide over the past 100 million years. American Journal of Science 283 (7), 641–683.

Bird, R.B., Stewart, W.E., Lightfoot, E.N., 1960. Transport Phenomena. John Wiley & Sons, New York.

Bonneville, S., Morgan, D.J., Schmalenberger, A., Bray, A., Brown, A., Banwart, S.A., Benning, L.G., 2011. Tree-mycorrhiza symbiosis accelerate mineral weathering: Evidences from nanometer-scale elemental fluxes at the hypha–mineral interface. Geochimica et Cosmochimica Acta 75 (22), 6988–7005.

Botz, R., Pokojski, H.-D., Schmitt, M., Thomm, M., 1996. Carbon isotope fractionation during bacterial methanogenesis by CO_2 reduction. Organic Geochemistry 25 (3), 255–262.

Boyd, P.W., Law, C.S., Wong, C.S., Nojiri, Y., Tsuda, A., Levasseur, M., Takeda, S., Rivkin, R., Harrison, P.J., Strzepek, R., Gower, J., McKay, R.M., Abraham, E., Arychuk, M., Barwell-Clarke, J., Crawford, W., Crawford, D., Hale, M., Harada, K., Johnson, K., Kiyosawa, H., Kudo, I., Marchetti, A., Miller, W., Needoba, J., Nishioka, J., Ogawa, H., Page, J., Robert, M., Saito, H., Sastri, A., Sherry, N., Soutar, T., Sutherland, N., Taira, Y., Whitney, F., Wong, S.-K.E., Yoshimura, T., 2004. The decline and fate of an iron-induced subarctic phytoplankton bloom. Nature 428, 549–553.

Boyd, P.W., Sundby, S., Pörtner, H.-O., 2014. Cross-chapter box on net primary production in the ocean, in: , Climate Change: Impacts, Adaptation, and Vulnerability. Part A: Global and Sectoral Aspects. Contribution of Working Group II to the Fifth Assessment Report of the Intergovernmental Panel of Climate Change. Cambridge University Press, pp. 133–136.

Boyd, P.W., Wong, C.S., Merrill, J., Whitney, F., Snow, J., Harrison, P.J., Gower, J., 1998. Atmospheric iron supply and enhanced vertical carbon flux in the NE subarctic Pacific: Is there a connection? Global Biogeochemical Cycles 12 (3), 429–441.

Brady, A.L., Druschel, G., Leoni, L., Lim, D.S., Slater, G.F., 2013. Isotopic biosignatures in carbonate-rich, cyanobacteria-dominated microbial mats of the Cariboo Plateau, B.C. Geobiology 11 (5), 437–456.

Brady, P.V., Walther, J.V., 1990. Kinetics of quartz dissolution at low temperatures. Chemical Geology 82, 253–264.

Brand, U., Veizer, J., 1980. Chemical diagenesis of a multicomponent carbonate system-1: Trace elements. Journal of Sedimentary Research 50 (4).

Brand, U., Veizer, J., 1981. Chemical diagenesis of a multicomponent carbonate system-2: Stable isotopes. Journal of Sedimentary Research 51 (3).

Brandes, J.A., Devol, A.H., 2002. A global marine-fixed nitrogen isotopic budget: Implications for Holocene nitrogen cycling. Global Biogeochemical Cycles 16 (4), 1120.

Brasier, M.D., Corfield, R.M., Derry, L.A., Rozanov, A.Y., Zhuravlev, A.Y., 1994. Multiple $\delta^{13}C$ excursions spanning the Cambrian explosion to the Botomian crisis in Siberia. Geology 22 (5), 455–458.

Broecker, W.S., 1970. A boundary condition on the evolution of atmospheric oxygen. Journal of Geophysical Research 75 (18), 3553–3557.

Broecker, W.S., 1982. Glacial to interglacial changes in ocean chemistry. Progress in Oceanography 11 (2), 151–197.

Broecker, W.S., 1994. Massive iceberg discharges as triggers for global climate change. Nature 372, 421–424.

Bundeleva, I.A., Ménez, B., Augé, T., Bodénan, F., Recham, N., Guyot, F., 2014. Effect of cyanobacteria Synechococcus PCC 7942 on carbonation kinetics of olivine at 20°C. Minerals Engineering 59, 2–11.

Burdige, D.J., 2007. Preservation of Organic Matter in Marine Sediments: Controls, Mechanisms, and an Imbalance in Sediment Organic Carbon Budgets? Chemical Reviews 107 (2), 467–485.

Capone, D.G., Burns, J.A., Montoya, J.P., Subramaniam, A., Mahaffey, C., Gunderson, T., Michaels, A.F., Carpenter, E.J., 2005. Nitrogen fixation by Trichodesmium spp.: An important source of new nitrogen to the tropical and subtropical North Atlantic Ocean. Global Biogeochemical Cycles 19 (2), GB2024.

Capone, D.G., Carpenter, E.J., 1982. Nitrogen Fixation in the Marine Environment. Science 217 (4565), 1140–1142.

Cartapanis, O., Bianchi, D., Jaccard, S.L., Galbraith, E.D., 2016. Global pulses of organic carbon burial in deep-sea sediments during glacial maxima. Nature Communications 7, 10796.

Chen, C., Mao, Z., Tang, F., Han, G., Jiang, Y., 2017. Declining riverine sediment input impact on spring phytoplankton bloom off the Yangtze River Estuary from 17-year satellite observation. Continental Shelf Research 135, 86–91.

Chisholm, S.W., Olson, R.J., Zettler, E.R., Goericke, R., Waterbury, J.B., Welschmeyer, N.A., 1988. A novel free-living prochlorophyte abundant in the oceanic euphotic zone. Nature 334, 340-343.

Christensen, J.P., 1994. Carbon export from continental shelves, denitrification and atmospheric carbon dioxide. Continental Shelf Research 14 (5), 547–576.

Clark, D.R., Flynn, K.J., 2000. The relationship between the dissolved inorganic carbon concentration and growth rate in marine phytoplankton. Proceedings of the Royal Society of London. Series B: Biological Sciences 267 (1447), 953–959.

Clark, I.D., Fontes, J.-C., Fritz, P., 1992. Stable isotope disequilibria in travertine from high pH waters: Laboratory investigations and field observations from Oman. Geochimica et Cosmochimica Acta 56 (5), 2041–2050.

Cloern, J.E., 1987. Turbidity as a control on phytoplankton biomass and productivity in estuaries. Continental Shelf Research 7 (11), 1367–1381.

Cloern, J.E., Foster, S.Q., Kleckner, A.E., 2014. Phytoplankton primary production in the world's estuarine-coastal ecosystems. Biogeosciences 11, 2477–2501.

Coogan, L.A., Dosso, S., 2012. An internally consistent, probabilistic, determination of ridge-axis hydrothermal fluxes from basalt-hosted systems. Earth and Planetary Science Letters 323, 92–101.

Cooper, T.G., Filmer, D., Wishnick, M., Lane, M.D., 1969. The Active Species of "CO_2" Utilized by Ribulose Diphosphate Carboxylase. Journal of Biological Chemistry 244 (4), 1081–1083.

Craig, H., 1953. The geochemistry of the stable carbon isotopes. Geochimica et Cosmochimica Acta 3 (2), 53–92.

de Baar, H.J., Boyd, P.W., Coale, K.H., Landry, M.R., Tsuda, A., Assmy, P., Bakker, D.C., Bozec, Y., Barber, R.T., Brzezinski, M.A., Buesseler, K.O., Boyé, M., Croot, P.L., Gervais, F., Gorbunov, M.Y., Harrison, P.J., Hiscock, W.T., Laan, P., Lancelot, C., Law, C.S., Levasseur, M., Marchetti, A., Millero, F.J., Nishioka, J., Nojiri, Y., van Oijen, T., Riebesell, U., Rijkenberg, M.J., Saito, H., Takeda, S., Timmermans, K.R., Veldhuis, M.J., Waite, A.M., Wong, C.-S., 2005. Synthesis of iron fertilization experiments: From the Iron Age in the Age of Enlightenment. Journal of Geophysical Research 110 (C9), C09S16.

De La Rocha, C.L., Passow, U., 2004. Recovery of Thalassiosira weissflogii from nitrogen and silicon starvation. Limnology and Oceanography 49 (1), 245–255.

De La Rocha, C.L., Passow, U., 2007. Factors influencing the sinking of POC and the efficiency of the biological carbon pump. Deep Sea Research Part II: Topical Studies in Oceanography 54 (5), 639–658.

De La Rocha, C.L., Passow, U., 2014. 8.4 - The Biological Pump. In: Holland, H.D., Turekian K.K. (Eds.), Treatise on Geochemistry (Second Edition). Elsevier, Oxford, 93–122.

De La Rocha, C.L., Terbrüggen, A., Völker, C., Hohn, S., 2010. Response to and recovery from nitrogen and silicon starvation in Thalassiosira weissflogii: growth rates, nutrient uptake and C, Si and N content per cell. Marine Ecology Progress Series 412, 57–68.

Degens, E.T., Guillard, R.R.L., Sackett, W.M., Hellebust, J.A., 1968. Metabolic fractionation of carbon isotopes in marine plankton—I. Temperature and respiration experiments. Deep Sea Research and Oceanographic Abstracts 15 (1), 1–9.

Deines, P., 1980. The isotopic composition of reduced organic carbon. Handbook of Environmental Isotope Geochemistry 1, 329–406.

Deines, P., Langmuir, D., Harmon, R.S., 1974. Stable carbon isotope ratios and the existence of a gas phase in the evolution of carbonate ground waters. Geochimica et Cosmochimica Acta 38 (7), 1147–1164.

Deng, W., Monks, L., Neuer, S., 2015. Effects of clay minerals on the aggregation and subsequent settling of marine Synechococcus. Limnology and Oceanography 60 (3), 805–816.

Dessert, C., Dupré, B., Gaillardet, J., François, L.M., Allègre, C.J., 2003. Basalt weathering laws and the impact of basalt weathering on the global carbon cycle. Chemical Geology 202 (3), 257–273.

Dickens, G.R., O'Neil, J.R., Rea, D.K., Owen, R.M., 1995. Dissociation of oceanic methane hydrate as a cause of the carbon isotope excursion at the end of the Paleocene. Paleoceanography 10 (6), 965–971.

Dietzel, M., Tang, J., Leis, A., Köhler, S.J., 2009. Oxygen isotopic fractionation during inorganic calcite precipitation — Effects of temperature, precipitation rate and pH. Chemical Geology 268 (1), 107–115.

Ding, X., Henrichs, S.M., 2002. Adsorption and desorption of proteins and polyamino acids by clay minerals and marine sediments. Marine Chemistry 77 (4), 225–237.

Dittrich, M., Müller, B., Mavrocordatos, D., Wehrli, B., 2003. Induced Calcite Precipitation by Cyanobacterium Synechococcus. Acta hydrochimica et hydrobiologica 31 (2), 162–169.

Dittrich, M., Sibler, S., 2006. Influence of H^+ and Calcium Ions on Surface Functional Groups of Synechococcus PCC 7942 Cells. Langmuir 22 (12), 5435–5442.

Dittrich, M., Sibler, S., 2010. Calcium carbonate precipitation by cyanobacterial polysaccharides. Geological Society, London, Special Publications 336 (1), 51–63.

Domingues, R.B., Anselmo, T.P., Barbosa, A.B., Sommer, U., Galvão, H.M., 2011. Light as a driver of phytoplankton growth and production in the freshwater tidal zone of a turbid estuary. Estuarine, Coastal and Shelf Science 91 (4), 526–535.

Dong, H., 2010. Mineral-microbe interactions: A review. Frontiers of Earth Science in China 4 (2), 127–147.

Drever, J.I., Stillings, L.L., 1997. The role of organic acids in mineral weathering. Colloids and Surfaces A: Physicochemical and Engineering Aspects 120 (1), 167–181.

Dugdale, R.C., 1967. Nutrient limitation in the sea: Dynamics, identification and significance. Limnology and Oceanography 12 (4), 685–695.

Dupraz, C., Reid, R.P., Braissant, O., Decho, A.W., Norman, R.S., Visscher, P.T., 2009. Processes of carbonate precipitation in modern microbial mats. Earth-Science Reviews 96 (3), 141–162.

Dvořák, P., Casamatta, D.A., Poulíčková, A., Hašler, P., Ondřej, V., Sanges, R., 2014. Synechococcus: 3 billion years of global dominance. Molecular Ecology 23 (22), 5538–5551.

Edmonds, J., Luckow, P., Calvin, K., Wise, M., Dooley, J., Kyle, P., Kim, S.H., Patel, P., Clarke, L., 2013. Can radiative forcing be limited to 2.6 Wm^{-2} without negative emissions from bioenergy and CO_2 capture and storage? Climatic Change 118 (1), 29–43.

Edwards, K.J., Bach, W., McCollom, T.M., Rogers, D.R., 2004. Neutrophilic Iron-Oxidizing Bacteria in the Ocean: Their Habitats, Diversity, and Roles in Mineral Deposition, Rock Alteration, and Biomass Production in the Deep-Sea. Geomicrobiology Journal 21 (6), 393–404.

Egge, J.K., Aksnes, D.L., 1992. Silicate as regulating nutrient in phytoplankton competition. Marine Ecology Progress Series 83 (2), 281–289.

Eichinger, L., 1983. A Contribution to the Interpretation of ^{14}C Groundwater Ages Considering the Example of a Partially Confined Sandstone Aquifer. Radiocarbon 25 (2), 347–356.

Eiriksdottir, E.S., 2016. Weathering and riverine fluxes in pristine and controlled river catchments. PhD Dissertation, Faculty of Earth Sciences, University of Iceland.

Eiriksdottir, E.S., Gislason, S.R., Oelkers, E.H., 2013. Does temperature or runoff control the feedback between chemical denudation and climate? Insights from NE Iceland. Geochimica et Cosmochimica Acta 107, 65–81.

Eiriksdottir, E.S., Gislason, S.R., Oelkers, E.H., 2015. Direct evidence of the feedback between climate and nutrient, major, and trace element transport to the oceans. Geochimica et Cosmochimica Acta 166, 249–266.

Eiriksdottir, E.S., Louvat, P., Gislason, S.R., Óskarsson, N., Hardardóttir, J., 2008. Temporal variation of chemical and mechanical weathering in NE Iceland: Evaluation of a steady-state model of erosion. Earth and Planetary Science Letters 272 (1), 78–88.

Eiriksdottir, E.S., Oelkers, E.H., Hardardottir, J., Gislason, S.R., 2017. The impact of damming on riverine fluxes to the ocean: A case study from Eastern Iceland. Water Research 113, 124–138.

Elrod, V.A., Berelson, W.M., Coale, K.H., Johnson, K.S., 2004. The flux of iron from continental shelf sediments: A missing source for global budgets. Geophysical Research Letters 31 (12), L12307.

Engel, A., Borchard, C., Piontek, J., Schulz, K.G., Riebesell, U., Bellerby, R., 2013. CO_2 increases ^{14}C primary production in an Arctic plankton community. Biogeosciences 10 (3), 1291–1308.

Engel, A., Goldthwait, S., Passow, U., Alldredge, A., 2002. Temporal decoupling of carbon and nitrogen dynamics in a mesocosm diatom bloom. Limnology and Oceanography 47 (3), 753–761.

Engel, A., Passow, U., 2001. Carbon and nitrogen content of transparent exopolymer particles (TEP) in relation to their Alcian Blue adsorption. Marine Ecology Progress Series 219, 1–10.

Eppley, R.W., Render, E.H., Harrison, W.G., Cullen, J.J., 1979. Ammonium distribution in southern California coastal waters and its role in the growth of phytoplankton1. Limnology and Oceanography 24 (3), 495–509.

Epstein, S., Buchsbaum, R., Lowenstam, H.A., Urey, H.C., 1953. Revised Carbonate-Water Isotopic Temperature Scale. GSA Bulletin 64 (11), 1315–1326.

Ernst, A., Deicher, M., Herman, P.M., Wollenzien, U.I., 2005. Nitrate and Phosphate Affect Cultivability of Cyanobacteria from Environments with Low Nutrient Levels. Applied and Environmental Microbiology 71 (6), 3379–3383.

Falk, E.S., Guo, W., Paukert, A.N., Matter, J.M., Mervine, E.M., Kelemen, P.B., 2016. Controls on the stable isotope compositions of travertine from hyperalkaline springs in Oman: Insights from clumped isotope measurements. Geochimica et Cosmochimica Acta 192, 1–28.

Falkowski, P.G., 1997. Evolution of the nitrogen cycle and its influence on the biological sequestration of CO_2 in the ocean. Nature 387, 272–275.

Falkowski, P.G., 2014. 10.5 - Biogeochemistry of Primary Production, in: Holland, H.D., Turekian, K.K. (Eds.), Treatise on Geochemistry (Second Edition). Elsevier, Oxford, pp. 163–187.

Falkowski, P.G., Barber, R.T., Smetacek, V., 1998. Biogeochemical Controls and Feedbacks on Ocean Primary Production. Science 281 (5374), 200–206.

Falkowski, P.G., Greene, R.M., Geider, R.J., 1992. Physiological Limitations on Phytoplankton Productivity in the Ocean. Oceanography 5 (2), 84–91.

Falkowski, P.G., Knoll, A.H., 2007. CHAPTER 1 - An Introduction to Primary Producers in the Sea: Who They Are, What They Do, and When They Evolved, in: , Evolution of Primary Producers in the Sea. Academic Press, Burlington, pp. 1–6.

Falkowski, P.G., Scholes, R.J., Boyle, E., Canadell, J., Canfield, D., Elser, J., Gruber, N., Hibbard, K., Högberg, P., Linder, S., Mackenzie, F.T., Moore, B., Pedersen, T., Rosenthal,

Y., Seitzinger, S., Smetacek, V., Steffen, W., 2000. The Global Carbon Cycle: A Test of Our Knowledge of Earth as a System. Science 290 (5490), 291–296.

Feng, Y., Hare, C.E., Leblanc, K., Rose, J.M., Zhang, Y., DiTullio, G.R., Lee, P.A., Wilhelm, S.W., Rowe, J.M., Sun, J., Nemcek, N., Gueguen, C., Passow, U., Benner, I., Brown, C., Hutchins, D.A., 2009. Effects of increased pCO_2 and temperature on the North Atlantic spring bloom. I. The phytoplankton community and biogeochemical response. Marine Ecology Progress Series 388, 13–25.

Ferris, F.G., Thompson, J.B., Beveridge, T.J., 1997. Modern Freshwater Microbialites from Kelly Lake, British Columbia, Canada. PALAIOS 12 (3), 213–219.

Field, C.B., Behrenfeld, M.J., Randerson, J.T., Falkowski, P., 1998. Primary Production of the Biosphere: Integrating Terrestrial and Oceanic Components. Science 281 (5374), 237–240.

Filippelli, G.M., Delaney, M.L., 1996. Phosphorus geochemistry of equatorial Pacific sediments. Geochimica et Cosmochimica Acta 60 (9), 1479–1495.

Flombaum, P., Gallegos, J.L., Gordillo, R.A., Rincón, J., Zabala, L.L., Jiao, N., Karl, D.M., Li, W.K., Lomas, M.W., Veneziano, D., Vera, C.S., Vrugt, J.A., Martiny, A.C., 2013. Present and future global distributions of the marine Cyanobacteria *Prochlorococcus* and *Synechococcus*. Proceedings of the National Academy of Sciences 110 (24), 9824–9829.

France-Lanord, C., Derry, L.A., 1997. Organic carbon burial forcing of the carbon cycle from Himalayan erosion. Nature 390, 65-67.

Francois, R., Honjo, S., Krishfield, R., Manganini, S., 2002. Factors controlling the flux of organic carbon to the bathypelagic zone of the ocean. Global Biogeochemical Cycles 16 (4), 1087.

Frankignoulle, M., Borges, A.V., 2001. European continental shelf as a significant sink for atmospheric carbon dioxide. Global Biogeochemical Cycles 15 (3), 569–576.

Friedl, G., Wüest, A., 2002. Disrupting biogeochemical cycles - Consequences of damming. Aquatic Sciences 64 (1), 55–65.

Frogner, P., Gíslason, S.R., Óskarsson, N., 2001. Fertilizing potential of volcanic ash in ocean surface water. Geology 29 (6), 487–490.

Fryxell, G.A., Hasle, G.R., 1977. genus Thalassiosira: Some species with a modified ring of central strutted processes. Nova hedwigia. Beihefte 54, 67–98.

Gaillardet, J., Dupré, B., Allègre, C.J., 1999. Geochemistry of large river suspended sediments: Silicate weathering or recycling tracer? Geochimica et Cosmochimica Acta 63 (23), 4037–4051.

Gaillardet, J., Viers, J., Dupré, B., 2003. 5.09 - Trace Elements in River Waters, in: Holland, H.D., Turekian, K.K. (Eds.), Treatise on Geochemistry. Pergamon, Oxford, pp. 225–272.

Galeczka, I., Oelkers, E.H., Gislason, S.R., 2014. The chemistry and element fluxes of the July 2011 Múlakvísl and Kaldakvísl glacial floods, Iceland. Journal of Volcanology and Geothermal Research 273, 41–57.

Galy, V., France-Lanord, C., Beyssac, O., Faure, P., Kudrass, H., Palhol, F., 2007. Efficient organic carbon burial in the Bengal fan sustained by the Himalayan erosional system. Nature 450, 407-410.

Ganeshram, R.S., Pedersen, T.F., Calvert, S.E., Murray, J.W., 1995. Large changes in oceanic nutrient inventories from glacial to interglacial periods. Nature 376, 755-758.

Garrels, R.M., Lerman, A., Mackenzie, F.T., 1976. Controls of atmospheric O_2 and CO_2. American Scientist 64 (3), 306–315.

Gattuso, J.-P., Frankignoulle, M., Wollast, R., 1998. Carbon and carbonate metabolism in coastal aquatic ecosystems. Annual Review of Ecology and Systematics 29 (1), 405–434.

Gedney, N., Cox, P.M., Betts, R.A., Boucher, O., Huntingford, C., Stott, P.A., 2006. Detection of a direct carbon dioxide effect in continental river runoff records. Nature 439, 835–838.

Gehlen, M., Bopp, L., Emprin, N., Aumont, O., Heinze, C., Ragueneau, O., 2006. Reconciling surface ocean productivity, export fluxes and sediment composition in a global biogeochemical ocean model. Biogeosciences 3 (4), 521–537.

Gislason, S.R., Oelkers, E.H., 2003. Mechanism, rates, and consequences of basaltic glass dissolution: II. An experimental study of the dissolution rates of basaltic glass as a function of pH and temperature. Geochimica et Cosmochimica Acta 67 (20), 3817–3832.

Gislason, S.R., Oelkers, E.H., Eiriksdottir, E.S., Kardjilov, M.I., Gisladottir, G., Sigfusson, B., Snorrason, A., Elefsen, S., Hardardottir, J., Torssander, P., Oskarsson, N., 2009. Direct evidence of the feedback between climate and weathering. Earth and Planetary Science Letters 277 (1), 213–222.

Gislason, S.R., Oelkers, E.H., Snorrason, Á., 2006. Role of river-suspended material in the global carbon cycle. Geology 34 (1), 49–52.

Goericke, R., Welschmeyer, N.A., 1993. The marine prochlorophyte Prochlorococcus contributes significantly to phytoplankton biomass and primary production in the Sargasso Sea. Deep Sea Research Part I: Oceanographic Research Papers 40 (11), 2283–2294.

Goldman, J.C., 1993. Potential role of large oceanic diatoms in new primary production. Deep Sea Research Part I: Oceanographic Research Papers 40 (1), 159–168.

Gonfiantini, R., Zuppi, G.M., 2003. Carbon isotope exchange rate of DIC in karst groundwater. Chemical Geology 197 (1), 319–336.

Gordeev, V.V., Martin, J.M., Sidorov, I.S., Sidorova, M.V., 1996. A reassessment of the Eurasian river input of water, sediment, major elements, and nutrients to the Arctic Ocean. American Journal of Science 296 (6), 664–691.

Gorski, C.A., Fantle, M.S., 2017. Stable mineral recrystallization in low temperature aqueous systems: A critical review. Geochimica et Cosmochimica Acta 198, 439–465.

Guillard, R.R., 1975. Culture of Phytoplankton for Feeding Marine Invertebrates, in: Smith, W.L., Chanley, M.H. (Eds.), Culture of Marine Invertebrate Animals: Proceedings — 1st Conference on Culture of Marine Invertebrate Animals Greenport. Springer US, Boston, MA, pp. 29–60.

Halas, S., Szaran, J., Niezgoda, H., 1997. Experimental determination of carbon isotope equilibrium fractionation between dissolved carbonate and carbon dioxide. Geochimica et Cosmochimica Acta 61 (13), 2691–2695.

Hall, B.G., Acar, H., Nandipati, A., Barlow, M., 2014. Growth Rates Made Easy. Molecular Biology and Evolution 31 (1), 232–238.

Hamilton, T.L., Bryant, D.A., Macalady, J.L., 2016. The role of biology in planetary evolution: Cyanobacterial primary production in low-oxygen Proterozoic oceans. Environmental Microbiology 18 (2), 325–340.

Hamme, R.C., Webley, P.W., Crawford, W.R., Whitney, F.A., DeGrandpre, M.D., Emerson, S.R., Eriksen, C.C., Giesbrecht, K.E., Gower, J.F., Kavanaugh, M.T., Peña, M.A., Sabine,

C.L., Batten, S.D., Coogan, L.A., Grundle, D.S., Lockwood, D., 2010. Volcanic ash fuels anomalous plankton bloom in subarctic northeast Pacific. Geophysical Research Letters 37 (19), L19604.

Han, L.-F., Niel Plummer, L., Aggarwal, P., 2014. The curved ^{14}C vs. $\delta^{13}C$ relationship in dissolved inorganic carbon: A useful tool for groundwater age- and geochemical interpretations. Chemical Geology 387, 111–125.

Han, L.-F., Plummer, L.N., 2013. Revision of Fontes & Garnier's model for the initial ^{14}C content of dissolved inorganic carbon used in groundwater dating. Chemical Geology 351, 105–114.

Harrison, P.J., Whitney, F.A., Tsuda, A., Saito, H., Tadokoro, K., 2004. Nutrient and Plankton Dynamics in the NE and NW Gyres of the Subarctic Pacific Ocean. Journal of Oceanography 60 (1), 93–117.

Hawkings, J.R., Wadham, J.L., Benning, L.G., Hendry, K.R., Tranter, M., Tedstone, A., Nienow, P., Raiswell, R., 2017. Ice sheets as a missing source of silica to the polar oceans. Nature Communications 8, 14198.

Hayes, J.M., 1983. Practice and principles of isotopic measurements in organic geochemistry. Organic geochemistry of contemporaneous and ancient sediments 5, 1–25.

Hayes, J.M., Strauss, H., Kaufman, A.J., 1999. The abundance of ^{13}C in marine organic matter and isotopic fractionation in the global biogeochemical cycle of carbon during the past 800 Ma. Chemical Geology 161 (1), 103–125.

Hedges, J.I., Keil, R.G., 1995. Sedimentary organic matter preservation: An assessment and speculative synthesis. Marine Chemistry 49 (2), 81–115.

Hein, M., Sand-Jensen, K., 1997. CO_2 increases oceanic primary production. Nature 388 (6642), 526–527.

Helgeson, H.C., 1969. Thermodynamics of hydrothermal systems at elevated temperatures and pressures. American Journal of Science 267 (7), 729–804.

Hemming, S.R., 2004. Heinrich events: Massive late Pleistocene detritus layers of the North Atlantic and their global climate imprint. Reviews of Geophysics 42 (1), RG1005.

Higgins, J.A., Schrag, D.P., 2015. The Mg isotopic composition of Cenozoic seawater – evidence for a link between Mg-clays, seawater Mg/Ca, and climate. Earth and Planetary Science Letters 416, 73–81.

Hill, P.S., 1992. Reconciling aggregation theory with observed vertical fluxes following phytoplankton blooms. Journal of Geophysical Research: Oceans 97 (C2), 2295–2308.

Hodell, D.A., Schelske, C.L., Fahnenstiel, G.L., Robbins, L.L., 1998. Biologically induced calcite and its isotopic composition in Lake Ontario. Limnology and Oceanography 43 (2), 187–199.

Holland, H.D., 2002. Volcanic gases, black smokers, and the great oxidation event. Geochimica et Cosmochimica Acta 66 (21), 3811–3826.

Holland, H.D., 2006. The oxygenation of the atmosphere and oceans. Philosophical Transactions of the Royal Society B: Biological Sciences 361 (1470), 903–915.

Homoky, W.B., Severmann, S., McManus, J., Berelson, W.M., Riedel, T.E., Statham, P.J., Mills, R.A., 2012. Dissolved oxygen and suspended particles regulate the benthic flux of iron from continental margins. Marine Chemistry 134-135, 59–70.

Horowitz, A.J., 2008. Determining annual suspended sediment and sediment-associated trace element and nutrient fluxes. Science of The Total Environment 400 (1), 315–343.

Humborg, C., Conley, D.J., Rahm, L., Wulff, F., Cociasu, A., Ittekkot, V., 2000. Silicon Retention in River Basins: Far-reaching Effects on Biogeochemistry and Aquatic Food Webs in Coastal Marine Environments. AMBIO: A Journal of the Human Environment 29 (1), 45–50.

Ingall, E.D., van Cappellen, P., 1990. Relation between sedimentation rate and burial of organic phosphorus and organic carbon in marine sediments. Geochimica et Cosmochimica Acta 54 (2), 373–386.

IPCC, 2007. Climate Change 2007: The Physical Science Basis. *Contribution of Working Group I to the Fourth Assessment Report of the Intergovernmental Panel on Climate Change* (eds. S. Solomon, D. Qin, M. Manning, Z. Chen, M. Marquis, K.B. Averyt, M. Tignor and H.L. Miller), Cambridge University Press, Cambridge, United Kingdom and New York, NY, USA.

Irigoien, X., Castel, J., 1997. Light Limitation and Distribution of Chlorophyll Pigments in a Highly Turbid Estuary: The Gironde (SW France). Estuarine, Coastal and Shelf Science 44 (4), 507–517.

Jackson, G.A., 1990. A model of the formation of marine algal flocs by physical coagulation processes. Deep Sea Research Part A. Oceanographic Research Papers 37 (8), 1197–1211.

Jackson, G.A., Burd, A.B., 1998. Aggregation in the Marine Environment. Environmental Science & Technology 32 (19), 2805–2814.

Jackson, G.A., Lochmann, S.E., 1992. Effect of coagulation on nutrient and light limitation of an algal bloom. Limnology and Oceanography 37 (1), 77–89.

Jansson, C., Northen, T., 2010. Calcifying cyanobacteria - the potential of biomineralization for carbon capture and storage. Current Opinion in Biotechnology 21 (3), 365–371.

Jeandel, C., Oelkers, E.H., 2015. The influence of terrigenous particulate material dissolution on ocean chemistry and global element cycles. Chemical Geology 395, 50–66.

Jeandel, C., Peucker-Ehrenbrink, B., Jones, M.T., Pearce, C.R., Oelkers, E.H., Godderis, Y., Lacan, F., Aumont, O., Arsouze, T., 2011. Ocean margins: The missing term in oceanic element budgets? Eos, Transactions American Geophysical Union 92 (26), 217–218.

Jiang, Z., Liu, J., Chen, J., Chen, Q., Yan, X., Xuan, J., Zeng, J., 2014. Responses of summer phytoplankton community to drastic environmental changes in the Changjiang (Yangtze River) estuary during the past 50 years. Water Research 54, 1–11.

Jickells, T.D., An, Z.S., Andersen, K.K., Baker, A.R., Bergametti, G., Brooks, N., Cao, J.J., Boyd, P.W., Duce, R.A., Hunter, K.A., Kawahata, H., Kubilay, N., laRoche, J., Liss, P.S., Mahowald, N., Prospero, J.M., Ridgwell, A.J., Tegen, I., Torres, R., 2005. Global Iron Connections Between Desert Dust, Ocean Biogeochemistry, and Climate. Science 308 (5718), 67–71.

Jimenez-Lopez, C., Romanek, C.S., Caballero, E., 2006. Carbon isotope fractionation in synthetic magnesian calcite. Geochimica et Cosmochimica Acta 70 (5), 1163–1171.

Johansen, J.R., Theriot, E., 1987. The relationship between valve diameter and number of central flutoportulae in Thalassiosira weissflogii (Barcillariophyceae). Journal of Phycology 23 (4), 663–665.

John, S.G., Mendez, J., Moffett, J., Adkins, J., 2012. The flux of iron and iron isotopes from San Pedro Basin sediments. Geochimica et Cosmochimica Acta 93, 14–29.

Johnston, D.T., Fischer, W.W., 2012. Stable Isotope Geobiology, in: Knoll, A.H., Canfield, D.E., Konhauser, K.O. (Eds.), Fundamentals of Geobiology. John Wiley & Sons, Ltd, pp. 250–268.

Jones, M.E., Beckler, J.S., Taillefert, M., 2011. The flux of soluble organic-iron(III) complexes from sediments represents a source of stable iron(III) to estuarine waters and to the continental shelf. Limnology and Oceanography 56 (5), 1811–1823.

Jones, M.T., Gislason, S.R., 2008. Rapid releases of metal salts and nutrients following the deposition of volcanic ash into aqueous environments. Geochimica et Cosmochimica Acta 72 (15), 3661–3680.

Jones, M.T., Pearce, C.R., Jeandel, C., Gislason, S.R., Eiriksdottir, E.S., Mavromatis, V., Oelkers, E.H., 2012. Riverine particulate material dissolution as a significant flux of strontium to the oceans. Earth and Planetary Science Letters 355-356, 51–59.

Kamennaya, A.N., Ajo-Franklin, M.C., Northen, T., Jansson, C., 2012. Cyanobacteria as Biocatalysts for Carbonate Mineralization. Minerals 2 (4).

Kasting, J.F., 1993. Earth´s early atmosphere. Science 259 (5097), 920–926.

Keeling, C.D., Piper, S.C., Bollenbacher, A.F., Walker, S.J., 2010. Monthly Atmospheric $^{13}C/^{12}C$ Isotopic Ratios for 11 SIO Stations. Carbon Dioxide Information Analysis Center (CDIAC) Datasets.

Keil, R.G., Hedges, J.I., 1993. Sorption of organic matter to mineral surfaces and the preservation of organic matter in coastal marine sediments. Chemical Geology 107 (3), 385–388.

Kennedy, M.J., Pevear, D.R., Hill, R.J., 2002. Mineral Surface Control of Organic Carbon in Black Shale. Science 295 (5555), 657.

Kessler, W.S., 2006. The circulation of the eastern tropical Pacific: A review. Progress in Oceanography 69 (2), 181–217.

Kile, D.E., Eberl, D.D., Hoch, A.R., Reddy, M.M., 2000. An assessment of calcite crystal growth mechanisms based on crystal size distributions. Geochimica et Cosmochimica Acta 64 (17), 2937–2950.

Klaas, C., Archer, D.E., 2002. Association of sinking organic matter with various types of mineral ballast in the deep sea: Implications for the rain ratio. Global Biogeochemical Cycles 16 (4), 1116.

Koch, P.L., Zachos, J.C., Gingerich, P.D., 1992. Correlation between isotope records in marine and continental carbon reservoirs near the Palaeocene/Eocene boundary. Nature 358, 319–322.

Kooistra, W.H., Gersonde, R., Medlin, L.K., Mann, D.G., 2007. CHAPTER 11 - The Origin and Evolution of the Diatoms: Their Adaptation to a Planktonic Existence, in: Falkowski, P.G., Knoll, A.H. (Eds.), Evolution of Primary Producers in the Sea. Academic Press, Burlington, pp. 207–249.

Kosro, P.M., Huyer, A., Ramp, S.R., Smith, R.L., Chavez, F.P., Cowles, T.J., Abbott, M.R., Strub, P.T., Barber, R.T., Jessen, P., Small, L.F., 1991. The structure of the transition zone between coastal waters and the open ocean off northern California, winter and spring 1987. Journal of Geophysical Research 96 (C8), 14707–14730.

Kranz, S.A., Gladrow, D.W., Nehrke, G., Langer, G., Rosta, B., 2010. Calcium carbonate precipitation induced by the growth of the marine cyanobacteria Trichodesmium. Limnology and Oceanography 55 (6), 2563–2569.

Kress, N., Gertman, I., Herut, B., 2014. Temporal evolution of physical and chemical characteristics of the water column in the Easternmost Levantine basin (Eastern Mediterranean Sea) from 2002 to 2010. Journal of Marine Systems 135, 6–13.

Krey, V., Luderer, G., Clarke, L., Kriegler, E., 2014. Getting from here to there – energy technology transformation pathways in the EMF27 scenarios. Climatic Change 123 (3), 369–382.

Kumar, K., Dasgupta, C.N., Nayak, B., Lindblad, P., Das, D., 2011. Development of suitable photobioreactors for CO_2 sequestration addressing global warming using green algae and cyanobacteria. Bioresource Technology 102 (8), 4945–4953.

Kump, L.R., 1991. Interpreting carbon-isotope excursions: Strangelove oceans. Geology 19 (4), 299–302.

Kump, L.R., Arthur, M.A., 1999. Interpreting carbon-isotope excursions: Carbonates and organic matter. Chemical Geology 161 (1), 181–198.

Labat, D., Goddéris, Y., Probst, J.L., Guyot, J.L., 2004. Evidence for global runoff increase related to climate warming. Advances in Water Resources 27 (6), 631–642.

Lalonde, K., Mucci, A., Ouellet, A., Gélinas, Y., 2012. Preservation of organic matter in sediments promoted by iron. Nature 483 (7388), 198–200.

Le Moigne, F.A., Pabortsava, K., Marcinko, C.L., Martin, P., Sanders, R.J., 2014. Where is mineral ballast important for surface export of particulate organic carbon in the ocean? Geophysical Research Letters 41 (23), 8460–8468.

Lee, B.D., Apel, W.A., Walton, M.R., 2006. Calcium carbonate formation by Synechococcus sp. strain PCC 8806 and Synechococcus sp. strain PCC 8807. Bioresource Technology 97 (18), 2427–2434.

Lee, J.G., Roberts, S.B., Morel, F.M., 1995. Cadmium: A nutrient for the marine diatom Thalassiosira weissflogii. Limnology and Oceanography 40 (6), 1056–1063.

Lee, Z., Weidemann, A., Kindle, J., Arnone, R., Carder, K.L., Davis, C., 2007. Euphotic zone depth: Its derivation and implication to ocean-color remote sensing. Journal of Geophysical Research 112, C03009.

Li, W.K., 1995. Composition of ultraphytoplankton in the central North Atlantic. Marine Ecology Progress Series 122 (1), 1–8.

Lifshitz, I.M., Slyozov, V.V., 1961. The kinetics of precipitation from supersaturated solid solutions. Journal of Physics and Chemistry of Solids 19 (1), 35–50.

Lindenthal, A., Langmann, B., Pätsch, J., Lorkowski, I., Hort, M., 2013. The ocean response to volcanic iron fertilisation after the eruption of Kasatochi volcano: A regional-scale biogeochemical ocean model study. Biogeosciences 10 (6), 3715–3729.

Liu, H., Landry, M.R., Vaulot, D., Campbell, L., 1999. Prochlorococcus growth rates in the central equatorial Pacific: An application of the $f$max approach. Journal of Geophysical Research 104 (C2), 3391–3399.

Liu, Z., Dreybrod, W., 1997. Dissolution kinetics of calcium carbonate minerals in H_2O-CO_2 solutions in turbulent flow: The role of the diffusion boundary layer and the slow reaction $H_2O + CO_2 \rightarrow H^+ + HCO_3^-$. Geochimica et Cosmochimica Acta 61 (14), 2879–2889.

Logan, B.E., Passow, U., Alldredge, A.L., Grossartt, H.-P., Simont, M., 1995. Rapid formation and sedimentation of large aggregates is predictable from coagulation rates (half-lives) of

transparent exopolymer particles (TEP). Deep Sea Research Part II: Topical Studies in Oceanography 42 (1), 203–214.

Lomas, M.W., Glibert, P.M., 1999. Interactions between NH_4^+ and NO_3^- uptake and assimilation: Comparison of diatoms and dinoflagellates at several growth temperatures. Marine Biology 133 (3), 541–551.

Longhurst, A., Sathyendranath, S., Platt, T., Caverhill, C., 1995. An estimate of global primary production in the ocean from satellite radiometer data. Journal of Plankton Research 17 (6), 1245–1271.

Ludwig, W., Amiotte-Suchet, P., Munhoven, G., Probst, J.-L., 1998. Atmospheric CO_2 consumption by continental erosion: Present-day controls and implications for the last glacial maximum. Global and Planetary Change 16-17, 107–120.

Ludwig, W., Probst, J.-L., 1998. River sediment discharge to the oceans; present-day controls and global budgets. American Journal of Science 298 (4), 265–295.

Lyle, M., 1988. Climatically forced organic carbon burial in equatorial Atlantic and Pacific Oceans. Nature 335, 529-532.

Maavara, T., Parsons, C.T., Ridenour, C., Stojanovic, S., Dürr, H.H., Powley, H.R., van Cappellen, P., 2015. Global phosphorus retention by river damming. Proceedings of the National Academy of Sciences USA 112 (51), 15603–15608.

Maher, B.A., Prospero, J.M., Mackie, D., Gaiero, D., Hesse, P.P., Balkanski, Y., 2010. Global connections between aeolian dust, climate and ocean biogeochemistry at the present day and at the last glacial maximum. Earth-Science Reviews 99 (1), 61–97.

Mahowald, N.M., Baker, A.R., Bergametti, G., Brooks, N., Duce, R.A., Jickells, T.D., Kubilay, N., Prospero, J.M., Tegen, I., 2005. Atmospheric global dust cycle and iron inputs to the ocean. Global Biogeochemical Cycles 19 (4), GB4025.

Mann, D.G., 1999. The species concept in diatoms. Phycologia 38 (6), 437–495.

Mapelli, F., Marasco, R., Balloi, A., Rolli, E., Cappitelli, F., Daffonchio, D., Borin, S., 2012. Mineral–microbe interactions: Biotechnological potential of bioweathering. Journal of Biotechnology 157 (4), 473–481.

Mari, X., Beauvais, S., Lemée, R., Pedrotti, M.L., 2001. Non-Redfield C:N ratio of transparent exopolymeric particles in the northwestern Mediterranean Sea. Limnology and Oceanography 46 (7), 1831–1836.

Martin, J.H., 1990. Glacial-interglacial CO_2 change: The Iron Hypothesis. Paleoceanography and Paleoclimatology 5 (1), 1–13.

Martin, J.H., Knauer, G.A., Karl, D.M., Broenkow, W.W., 1987. VERTEX: Carbon cycling in the northeast Pacific. Deep Sea Research Part A. Oceanographic Research Papers 34 (2), 267–285.

Martinez, R.E., Weber, S., Grimm, C., 2016. Effects of freshwater Synechococcus sp. cyanobacteria pH buffering on $CaCO_3$ precipitation: Implications for CO_2 sequestration. Applied Geochemistry 75, 76–89.

Mavromatis, V., Bundeleva, I.A., Shirokova, L.S., Millo, C., Pokrovsky, O.S., Bénézeth, P., Ader, M., Oelkers, E.H., 2015. The continuous re-equilibration of carbon isotope compositions of hydrous Mg carbonates in the presence of cyanobacteria. Chemical Geology 404, 41–51.

Mavromatis, V., Pearce, C.R., Shirokova, L.S., Bundeleva, I.A., Pokrovsky, O.S., Benezeth, P., Oelkers, E.H., 2012. Magnesium isotope fractionation during hydrous magnesium carbonate precipitation with and without cyanobacteria. Geochimica et Cosmochimica Acta 76, 161–174.

Mavromatis, V., Purgstaller, B., Dietzel, M., Buhl, D., Immenhauser, A., Schott, J., 2017. Impact of amorphous precursor phases on magnesium isotope signatures of Mg-calcite. Earth and Planetary Science Letters 464, 227–236.

Mavromatis, V., van Zuilen, K., Purgstaller, B., Baldermann, A., Nägler, T.F., Dietzel, M., 2016. Barium isotope fractionation during witherite ($BaCO_3$) dissolution, precipitation and at equilibrium. Geochimica et Cosmochimica Acta 190, 72–84.

May, C.L., Koseff, J.R., Lucas, L.V., Cloern, J.E., Schoellhamer, D.H., 2003. Effects of spatial and temporal variability of turbidity on phytoplankton blooms. Marine Ecology Progress Series 254, 111–128.

Mayer, L.M., 1994. Surface area control of organic carbon accumulation in continental shelf sediments. Geochimica et Cosmochimica Acta 58 (4), 1271–1284.

McCave, I.N., 1984. Size spectra and aggregation of suspended particles in the deep ocean. Deep Sea Research Part A. Oceanographic Research Papers 31 (4), 329–352.

McCrea, J.M., 1950. On the Isotopic Chemistry of Carbonates and a Paleotemperature Scale. The Journal of Chemical Physics 18 (6), 849–857.

McDermott, F., 2004. Palaeo-climate reconstruction from stable isotope variations in speleothems: A review. Quaternary Science Reviews 23 (7), 901–918.

Meybeck, M., Laroche, L., Dürr, H.H., Syvitski, J.P.M., 2003. Global variability of daily total suspended solids and their fluxes in rivers. Global and Planetary Change 39 (1), 65–93.

Milligan, A.J., Mioni, C.E., Morel, F.M.M., 2009. Response of cell surface pH to pCO_2 and iron limitation in the marine diatom Thalassiosira weissflogii. Marine Chemistry 114 (1), 31–36.

Milliman, J.D., Syvitski, J.P., 1992. Geomorphic/Tectonic Control of Sediment Discharge to the Ocean: The Importance of Small Mountainous Rivers. The Journal of Geology 100 (5), 525–544.

Mills, M.M., Ridame, C., Davey, M., La Roche, J., Geider, R.J., 2004. Iron and phosphorus co-limit nitrogen fixation in the eastern tropical North Atlantic. Nature 429, 292–294.

Mitchell, B.G., Holm-Hansen, O., 1991. Observations of modeling of the Antartic phytoplankton crop in relation to mixing depth. Deep Sea Research Part A. Oceanographic Research Papers 38 (8), 981–1007.

Mook, W.G., Bommerson, J.C., Staverman, W.H., 1974. Carbon isotope fractionation between dissolved bicarbonate and gaseous carbon dioxide. Earth and Planetary Science Letters 22 (2), 169–176.

Moore, J.K., Doney, S.C., Glover, D.M., Fung, I.Y., 2001. Iron cycling and nutrient-limitation patterns in surface waters of the World Ocean. Deep Sea Research Part II: Topical Studies in Oceanography 49 (1), 463–507.

Morel, F.M., Reinfelder, J.R., Roberts, S.B., Chamberlain, C.P., Lee, J.G., Yee, D., 1994. Zinc and carbon co-limitation of marine phytoplankton. Nature 369, 740-742.

Mozeto, A.A., Fritz, P., Reardon, E.J., 1984. Experimental observations on carbon isotope exchange in carbonate-water systems. Geochimica et Cosmochimica Acta 48 (3), 495–504.

Mulholland, M.R., Bernhardt, P.W., Heil, C.A., Bronk, D.A., O'Neil, J.M., 2006. Nitrogen fixation and release of fixed nitrogen by Trichodesmium spp. in the Gulf of Mexico. Limnology and Oceanography 51 (4), 1762–1776.

Myers, J.A., Curtis, B.S., Curtis, W.R., 2013. Improving accuracy of cell and chromophore concentration measurements using optical density. BMC Biophysics 6 (1), 4.

Myrttinen, A., Becker, V., Barth, J.A.C., 2012. A review of methods used for equilibrium isotope fractionation investigations between dissolved inorganic carbon and CO_2. Earth-Science Reviews 115 (3), 192–199.

Nelson, C.S., Smith, A.M., 1996. Stable oxygen and carbon isotope compositional fields for skeletal and diagenetic components in New Zealand Cenozoic nontropical carbonate sediments and limestones: A synthesis and review. New Zealand Journal of Geology and Geophysics 39 (1), 93–107.

Nelson, D.M., Dortch, Q., 1996. Silicic acid depletion and silicon limitation in the plume of the Mississippi River: Evidence from kinetic studies in spring and summer. Marine Ecology Progress Series 136 (1/3), 163–178.

Nelson, D.M., Tréguer, P., Brzezinski, M.A., Leynaert, A., Quéguiner, B., 1995. Production and dissolution of biogenic silica in the ocean: Revised global estimates, comparison with regional data and relationship to biogenic sedimentation. Global Biogeochemical Cycles 9 (3), 359–372.

Obst, M., Dittrich, M., Kuehn, H., 2006. Calcium adsorption and changes of the surface microtopography of cyanobacteria studied by AFM, CFM, and TEM with respect to biogenic calcite nucleation. Geochemistry, Geophysics, Geosystems 7 (6), Q06011.

Obst, M., Dynes, J.J., Lawrence, J.R., Swerhone, G.D.W., Benzerara, K., Karunakaran, C., Kaznatcheev, K., Tyliszczak, T., Hitchcock, A.P., 2009a. Precipitation of amorphous $CaCO_3$ (aragonite-like) by cyanobacteria: A STXM study of the influence of EPS on the nucleation process. Geochimica et Cosmochimica Acta 73 (14), 4180–4198.

Obst, M., Wehrli, B., Dittrich, M., 2009b. $CaCO_3$ nucleation by cyanobacteria: Laboratory evidence for a passive, surface-induced mechanism. Geobiology 7 (3), 324–347.

Oehlert, A.M., Swart, P.K., 2014. Interpreting carbonate and organic carbon isotope covariance in the sedimentary record. Nature Communications 5, 4672.

Oelkers, E.H., 2001. General kinetic description of multioxide silicate mineral and glass dissolution. Geochimica et Cosmochimica Acta 65 (21), 3703–3719.

Oelkers, E.H., Benning, L.G., Lutz, S., Mavromatis, V., Pearce, C.R., Plümper, O., 2015. The efficient long-term inhibition of forsterite dissolution by common soil bacteria and fungi at Earth surface conditions. Geochimica et Cosmochimica Acta 168, 222–235.

Oelkers, E.H., Cole, D.R., 2008. Carbon Dioxide Sequestration A Solution to a Global Problem. Elements 4 (5), 305–310.

Oelkers, E.H., Gislason, S.R., Eiriksdottir, E.S., Jones, M., Pearce, C.R., Jeandel, C., 2011. The role of riverine particulate material on the global cycles of the elements. Applied Geochemistry 26, S365-S369.

Oelkers, E.H., Jones, M.T., Pearce, C.R., Jeandel, C., Eiriksdottir, E.S., Gislason, S.R., 2012. Riverine particulate material dissolution in seawater and its implications for the global cycles of the elements. Comptes Rendus Geoscience 344 (11), 646–651.

Oelkers, E.H., Schott, J., Devidal, J.-L., 1994. The effect of aluminum, pH, and chemical affinity on the rates of aluminosilicate dissolution reactions. Geochimica et Cosmochimica Acta 58 (9), 2011–2024.

O'Leary, M.H., 1988. Carbon Isotopes in Photosynthesis. BioScience 38 (5), 328–336.

Olgun, N., Duggen, S., Croot, P.L., Delmelle, P., Dietze, H., Schacht, U., Óskarsson, N., Siebe, C., Auer, A., Garbe-Schönberg, D., 2011. Surface ocean iron fertilization: The role of airborne volcanic ash from subduction zone and hot spot volcanoes and related iron fluxes into the Pacific Ocean. Global Biogeochemical Cycles 25 (4), GB4001.

Olsson, J., Stipp, S.L.S., Dalby, K.N., Gislason, S.R., 2013. Rapid release of metal salts and nutrients from the 2011 Grímsvötn, Iceland volcanic ash. Geochimica et Cosmochimica Acta 123, 134–149.

Olsson-Francis, K., Simpson, A.E., Wolff-Boenisch, D., Cockell, C.S., 2012. The effect of rock composition on cyanobacterial weathering of crystalline basalt and rhyolite. Geobiology 10 (5), 434–444.

O'Neil, J.R., Barnes, I., 1971. C^{13} and O^{18} compositions in some freshwater carbonates associated with ultramafic rocks and serpentinites: Western United States. Geochimica et Cosmochimica Acta 35 (7), 687–697.

Opfergelt, S., Burton, K.W., Pogge von Strandmann, P.A.E., Gislason, S.R., Halliday, A.N., 2013. Riverine silicon isotope variations in glaciated basaltic terrains: Implications for the Si delivery to the ocean over glacial–interglacial intervals. Earth and Planetary Science Letters 369-370, 211–219.

Parker, S.R., Gammons, C.H., Poulson, S.R., DeGrandpre, M.D., Weyer, C.L., Smith, M.G., Babcock, J.N., Oba, Y., 2010. Diel behavior of stable isotopes of dissolved oxygen and dissolved inorganic carbon in rivers over a range of trophic conditions, and in a mesocosm experiment. Chemical Geology 269 (1), 22–32.

Parkhurst, D.L., Appelo, C.A.J., 1999. User's guide to PHREEQC (Version 2): A computer program for speciation, batch-reaction, one-dimensional transport, and inverse geochemical calculations. Water-Resources Investigations Report 99-4259.

Partensky, F., Hess, W.R., Vaulot, D., 1999. Prochlorococcus, a marine photosynthetic prokaryote of global significance. Microbiology and molecular biology reviews 63 (1), 106–127.

Passow, U., 2002. Transparent exopolymer particles (TEP) in aquatic environments. Progress in Oceanography 55 (3), 287–333.

Passow, U., Carlson, C.A., 2012. The biological pump in a high CO_2 world. Marine Ecology Progress Series 470, 249–271.

Passow, U., De La Rocha, C., Fairfield, C., Schmidt, K., 2014. Aggregation as a function of and mineral particles. Limnology and Oceanography 59 (2), 532–547.

Passow, U., De La Rocha, C.L., 2006. Accumulation of mineral ballast on organic aggregates. Global Biogeochemical Cycles 20 (1), GB1013.

Passow, U., Laws, E.A., 2015. Ocean acidification as one of multiple stressors: Growth response of Thalassiosira weissflogii (diatom) under temperature and light stress. Marine Ecology Progress Series 541, 75–90.

Passow, U., Shipe, R.F., Murray, A., Pak, D.K., Brzezinski, M.A., Alldredge, A.L., 2001. The origin of transparent exopolymer particles (TEP) and their role in the sedimentation of particulate matter. Continental Shelf Research 21 (4), 327–346.

Patterson, W.P., Walter, L.M., 1994a. Depletion of ^{13}C in seawater ΣCO_2 on modern carbonate platforms: Significance for the carbon isotopic record of carbonates. Geology 22 (10), 885–888.

Patterson, W.P., Walter, L.M., 1994b. Syndepositional diagenesis of modern platform carbonates: Evidence from isotopic and minor element data. Geology 22 (2), 127–130.

Paul, D., Skrzypek, G., 2007. Assessment of carbonate-phosphoric acid analytical technique performed using GasBench II in continuous flow isotope ratio mass spectrometry. International Journal of Mass Spectrometry 262 (3), 180–186.

Paul, V.J., 2008. Global warming and cyanobacterial harmful algal blooms, in: Hudnell, H.K. (Ed.), Cyanobacterial Harmful Algal Blooms: State of the Science and Research Needs. Springer New York, New York, NY, pp. 239–257.

Pearce, C.R., Jones, M.T., Oelkers, E.H., Pradoux, C., Jeandel, C., 2013. The effect of particulate dissolution on the neodymium (Nd) isotope and Rare Earth Element (REE) composition of seawater. Earth and Planetary Science Letters 369-370, 138–147.

Pedersen, T.F., 1983. Increased productivity in the eastern equatorial Pacific during the last glacial maximum (19,000 to 14,000 yr B.P). Geology 11 (1), 16–19.

Pennington, J.T., Mahoney, K.L., Kuwahara, V.S., Kolber, D.D., Calienes, R., Chavez, F.P., 2006. Primary production in the eastern tropical Pacific: A review. Progress in Oceanography 69 (2), 285–317.

Pentecost, A., Spiro, B., 1990. Stable carbon and oxygen isotope composition of calcites associated with modern freshwater cyanobacteria and algae. Geomicrobiology Journal 8 (1), 17–26.

Perez, A., Rossano, S., Trcera, N., Huguenot, D., Fourdrin, C., Verney-Carron, A., van Hullebusch, E.D., Guyot, F., 2016. Bioalteration of synthetic Fe(III)-, Fe(II)-bearing basaltic glasses and Fe-free glass in the presence of the heterotrophic bacteria strain Pseudomonas aeruginosa: Impact of siderophores. Geochimica et Cosmochimica Acta 188, 147–162.

Petit, J.R., Jouzel, J., Raynaud, D., Barkov, N.I., Barnola, J.-M., Basile, I., Bender, M., Chappellaz, J., Davis, M., Delaygue, G., Delmotte, M., Kotlyakov, V.M., Legrand, M., Lipenkov, V.Y., Lorius, C., PÉpin, L., Ritz, C., Saltzman, E., Stievenard, M., 1999. Climate and atmospheric history of the past 420,000 years from the Vostok ice core, Antarctica. Nature 399 (6735), 429–436.

Picado, A., Alvarez, I., Vaz, N., Dias, J.M., 2013. Chlorophyll concentration along the northwestern coast of the Iberian Peninsula vs. atmosphere-ocean-land conditions. Journal of Coastal Research, 2047–2052.

Ploug, H., Iversen, M.H., Fischer, G., 2008a. Ballast, sinking velocity, and apparent diffusivity within marine snow and zooplankton fecal pellets: Implications for substrate turnover by attached bacteria. Limnology and Oceanography 53 (5), 1878–1886.

Ploug, H., Iversen, M.H., Koski, M., Buitenhuis, E.T., 2008b. Production, oxygen respiration rates, and sinking velocity of copepod fecal pellets: Direct measurements of ballasting by opal and calcite. Limnology and Oceanography 53 (2), 469–476.

Pokrovsky, O.S., Shirokova, L.S., 2013. Diurnal variations of dissolved and colloidal organic carbon and trace metals in a boreal lake during summer bloom. Water Research 47 (2), 922–932.

Pokrovsky, O.S., Viers, J., Dupré, B., Chabaux, F., Gaillardet, J., Audry, S., Prokushkin, A.S., Shirokova, L.S., Kirpotin, S.N., Lapitsky, S.A., Shevchenko, V.P., 2012. Biogeochemistry of carbon, major and trace elements in watersheds of northern Eurasia: The change of fluxes, sources and mechanisms under the climate warming prospectivedrained to the Arctic Ocean. Comptes Rendus Geoscience 344 (11), 663–677.

Polag, D., Scholz, D., Mühlinghaus, C., Spötl, C., Schröder-Ritzrau, A., Segl, M., Mangini, A., 2010. Stable isotope fractionation in speleothems: Laboratory experiments. Chemical Geology 279 (1), 31–39.

Potter, S., Cabbage, M., McCarthy, L., 2017. NASA, NOAA Data show 2016 warmest Year on Record Globally, press release, Jan. 19 (https://www.nasa.gov/press-release/nasa-noaadata-show-2016-warmest-year-on-record-globally).

Poulton, S.W., Raiswell, R., 2005. Chemical and physical characteristics of iron oxides in riverine and glacial meltwater sediments. Chemical Geology 218 (3), 203–221.

Power, I.M., Wilson, S.A., Dipple, G.M., Southam, G., 2011. Modern carbonate microbialites from an asbestos open pit pond, Yukon, Canada. Geobiology 9 (2), 180–195.

Primeau, F., 2005. Characterizing Transport between the Surface Mixed Layer and the Ocean Interior with a Forward and Adjoint Global Ocean Transport Model. Journal of Physical Oceanography 35 (4), 545–564.

Putnis, A., 2009. Mineral Replacement Reactions. Reviews in Mineralogy and Geochemistry 70 (1), 87–124.

Radic, A., Lacan, F., Murray, J.W., 2011. Iron isotopes in the seawater of the equatorial Pacific Ocean: New constraints for the oceanic iron cycle. Earth and Planetary Science Letters 306 (1), 1–10.

Raiswell, R., Hawkings, J.R., Benning, L.G., Baker, A.R., Death, R., Albani, S., Mahowald, N., Krom, M.D., Poulton, S.W., Wadham, J., Tranter, M., 2016. Potentially bioavailable iron delivery by iceberg-hosted sediments and atmospheric dust to the polar oceans. Biogeosciences 13 (13), 3887–3900.

Redfield, A.C., 1958. The biological control of chemical factor in the environment. American Scientist 46 (3), 230A-221.

Révész, K.M., Landwehr, J.M., 2002. $\delta^{13}C$ and $\delta^{18}O$ isotopic composition of $CaCO_3$ measured by continuous flow isotope ratio mass spectrometry: Statistical evaluation and verification by application to Devils Hole core DH-11 calcite. Rapid Communications in Mass Spectrometry 16 (22), 2102–2114.

Ridgwell, A., 2011. Evolution of the ocean´s "biological pump". Proceedings of the National Academy of Sciences 108 (40), 16485–16486.

Riebesell, U., Schulz, K.G., Bellerby, R.G., Botros, M., Fritsche, P., Meyerhöfer, M., Neill, C., Nondal, G., Oschlies, A., Wohlers, J., Zöllner, E., 2007. Enhanced biological carbon consumption in a high CO_2 ocean. Nature 450 (7169), 545–548.

Riebesell, U., Zondervan, I., Rost, B., Tortell, P.D., Zeebe, R.E., Morel, F.M., 2000. Reduced calcification of marine plankton in response to increased atmospheric CO_2. Nature 407 (6802), 364–367.

Rippka, R., Deruelles, J., Waterbury, J.B., Herdman, M., Stanier, R.Y., 1979. Generic Assignments, Strain Histories and Properties of Pure Cultures of Cyanobacteria. Microbiology 111 (1), 1–61.

Ritter, A.-C., Mavromatis, V., Dietzel, M., Kwiecien, O., Wiethoff, F., Griesshaber, E., Casella, L.A., Schmahl, W.W., Koelen, J., Neuser, R.D., Leis, A., Buhl, D., Niedermayr, A., Breitenbach, S.F., Bernasconi, S.M., Immenhauser, A., 2017. Exploring the impact of diagenesis on (isotope) geochemical and microstructural alteration features in biogenic aragonite. Sedimentology 64 (5), 1354–1380.

Roberts, S.B., Lane, T.W., Morel, F.M., 1997. Carbonic anhydrase in the marine diatom Thalassiosira weissflogii (Barcillariophyceae). Journal of Phycology 33 (5), 845–850.

Rocap, G., Distel, D.L., Waterbury, J.B., Chisholm, S.W., 2002. Resolution of Prochlorococcus and Synechococcus Ecotypes by Using 16S-23S Ribosomal DNA Internal Transcribed Spacer Sequences. Applied and Environmental Microbiology 68 (3), 1180–1191.

Rogelj, J., McCollum, D.L., Reisinger, A., Meinshausen, M., Riahi, K., 2013. Probabilistic cost estimates for climate change mitigation. Nature 493, 79-83.

Rogers, J.R., Bennett, P.C., 2004. Mineral stimulation of subsurface microorganisms: Release of limiting nutrients from silicates. Chemical Geology 203 (1), 91–108.

Rogers, J.R., Bennett, P.C., Choi, W.J., 1998. Feldspars as a source of nutrients for microorganisms. American Mineralogist 83 (11), 1532–1540.

Rohwer, F., Thurber, R.V., 2009. Viruses manipulate the marine environment. Nature 459 (7244), 207–212.

Romanek, C.S., Grossman, E.L., Morse, J.W., 1992. Carbon isotopic fractionation in synthetic aragonite and calcite: Effects of temperature and precipitation rate. Geochimica et Cosmochimica Acta 56 (1), 419–430.

Rooney, A.D., Strauss, J.V., Brandon, A.D., Macdonald, F.A., 2015. A Cryogenian chronology: Two long-lasting synchronous Neoproterozoic glaciations. Geology 43 (5), 459–462.

Rost, B., Zondervan, I., Wolf-Gladrow, D., 2008. Sensitivity of phytoplankton to future changes in ocean carbonate chemistry: Current knowledge, contradictions and research directions. Marine Ecology Progress Series 373, 227–238.

Round, F.E., Crawford, R.M., Mann, D.G., 1990. Diatoms: Biology and morphology of the genera. Cambridge University Press.

Rzezinski, M.A., Nelson, D.M., 1996. Chronic substrate limitation of silicic acid uptake rates in the western Sargasso Sea. Deep Sea Research Part II: Topical Studies in Oceanography 43 (2), 437–453.

Saito, M.A., Rocap, G., Moffett, J.W., 2005. Production of cobalt binding ligands in a Synechococcus feature at the Costa Rica upwelling dome. Limnology and Oceanography 50 (1), 279–290.

Sala, S.E., 1997. Diatom flora of Paso de las Piedras impounding, Buenos Aires Province IV: Order Centrales. Gayana 54, 1–14.

Salmon, V., Derenne, S., Lallier-Vergès, E., Largeau, C., Beaudoin, B., 2000. Protection of organic matter by mineral matrix in a Cenomanian black shale. Organic Geochemistry 31 (5), 463–474.

Saltzman, M.R., Groessens, E., Zhuravlev, A.V., 2004. Carbon cycle models based on extreme changes in $\delta^{13}C$: An example from the lower Mississippian. Palaeogeography, Palaeoclimatology, Palaeoecology 213 (3), 359–377.

Sands, P., 1992. The United Nations framework convention on climate change. Review of European Community & International Environmental Law 1 (3), 270–277.

Santrock, J., Studley, S.A., Hayes, J.M., 1985. Isotopic analyses based on the mass spectra of carbon dioxide. Analytical Chemistry 57 (7), 1444–1448.

Sarnthein, M., Winn, K., Duplessy, J.-C., Fontugne, M.R., 1988. Global variations of surface ocean productivity in low and mid latitudes: Influence on CO_2 reservoirs of the deep ocean and atmosphere during the last 21,000 years. Paleoceanography 3 (3), 361–399.

Schidlowski, M., Junge, C.E., 1981. Coupling among the terrestrial sulfur, carbon and oxygen cycles: Numerical modeling based on revised Phanerozoic carbon isotope record. Geochimica et Cosmochimica Acta 45 (4), 589–594.

Schopf, J.W., 2012. The Fossil Record of Cyanobacteria, in: Whitton, B.A. (Ed.), Ecology of Cyanobacteria II: Their Diversity in Space and Time. Springer Netherlands, Dordrecht, pp. 15–36.

Schrag, D.P., Higgins, J.A., Macdonald, F.A., Johnston, D.T., 2013. Authigenic Carbonate and the History of the Global Carbon Cycle. Science 339 (6119), 540–543.

Schulte, P., van Geldern, R., Freitag, H., Karim, A., Négrel, P., Petelet-Giraud, E., Probst, A., Probst, J.-L., Telmer, K., Veizer, J., Barth, J.A.C., 2011. Applications of stable water and carbon isotopes in watershed research: Weathering, carbon cycling, and water balances. Earth-Science Reviews 109 (1), 20–31.

SCOR UNESCO, 1966. Determination of photosynthetic pigments in seawater - Report of SCOR-UNESCO Working group 17 (Paris). Monographs on Oceanographic Methodology 1.

Seebah, S., Fairfield, C., Ullrich, M.S., Passow, U., 2014. Aggregation and Sedimentation of Thalassiosira weissflogii (diatom) in a Warmer and More Acidified Future Ocean. PLOS ONE 9 (11), e112379.

Seyfried, W.E., Bischoff, J.L., 1981. Experimental seawater-basalt interaction at 300°C, 500 bars, chemical exchange, secondary mineral formation and implications for the transport of heavy metals. Geochimica et Cosmochimica Acta 45 (2), 135–147.

Shaked, Y., Kustka, A.B., Morel, F.M., 2005. A general kinetic model for iron acquisition by eukaryotic phytoplankton. Limnology and Oceanography 50 (3), 872–882.

Shields-Zhou, G., Och, L., 2011. The case for a Neoproterozoic Oxygenation Event: Geochemical evidence and biological consequences. GSA Today 21 (3), 4–11.

Shirokova, L.S., Mavromatis, V., Bundeleva, I., Pokrovsky, O.S., Bénézeth, P., Pearce, C., Gérard, E., Balor, S., Oelkers, E.H., 2011. Can Mg isotopes be used to trace cyanobacteria-mediated magnesium carbonate precipitation in alkaline lakes? Biogeosciences Discussions 8 (4), 6473–6517.

Shirokova, L.S., Mavromatis, V., Bundeleva, I.A., Pokrovsky, O.S., Bénézeth, P., Gérard, E., Pearce, C.R., Oelkers, E.H., 2013. Using Mg Isotopes to Trace Cyanobacterially Mediated Magnesium Carbonate Precipitation in Alkaline Lakes. Aquatic Geochemistry 19 (1), 1–24.

Siegel, D.A., Doney, S.C., Yoder, J.A., 2002. The North Atlantic Spring Phytoplankton Bloom and Sverdrup´s Critical Depth Hypothesis. Science 296 (5568), 730–733.

Sigman, D.M., Hain, M.P., 2012. The Biological Productivity of the Ocean. Nature Education Knowledge 10 (3).

Slemons, L., Paul, B., Resing, J., Murray, J.W., 2012. Particulate iron, aluminum, and manganese in the Pacific equatorial undercurrent and low latitude western boundary current sources. Marine Chemistry 142-144, 54–67.

Smetacek, V., 1998. Biological oceanography: Diatoms and the silicate factor. Nature 391 (6664), 224–225.

Smetacek, V.S., 1985. Role of sinking in diatom life-history cycles: Ecological, evolutionary and geological significance. Marine Biology 84 (3), 239–251.

Smith, P., Davis, S.J., Creutzig, F., Fuss, S., Minx, J., Gabrielle, B., Kato, E., Jackson, R.B., Cowie, A., Kriegler, E., van Vuuren, D.P., Rogelj, J., Ciais, P., Milne, J., Canadell, J.G., McCollum, D., Peters, G., Andrew, R., Krey, V., Shrestha, G., Friedlingstein, P., Gasser, T., Grübler, A., Heidug, W.K., Jonas, M., Jones, C.D., Kraxner, F., Littleton, E., Lowe, J., Moreira, J.R., Nakicenovic, N., Obersteiner, M., Patwardhan, A., Rogner, M., Rubin, E., Sharifi, A., Torvanger, A., Yamagata, Y., Edmonds, J., Yongsung, C., 2015. Biophysical and economic limits to negative CO_2 emissions. Nature Climate Change 6, 42-50.

Smits, M.M., Bonneville, S., Benning, L.G., Banwart, S.A., Leake, J.R., 2012. Plant-driven weathering of apatite – the role of an ectomycorrhizal fungus. Geobiology 10 (5), 445–456.

Sorhannus, U., Ortiz, J.D., Wolf, M., Fox, M.G., 2010. Microevolution and Speciation in Thalassiosira weissflogii (Bacillariophyta). Protist 161 (2), 237–249.

Spötl, C., 2005. A robust and fast method of sampling and analysis of $\delta^{13}C$ of dissolved inorganic carbon in ground waters. Isotopes in Environmental and Health Studies 41 (3), 217–221.

Spötl, C., Vennemann, T.W., 2003. Continuous-flow isotope ratio mass spectrometric analysis of carbonate minerals. Rapid Communications in Mass Spectrometry 17 (9), 1004–1006.

Stabel, H.-H., 1986. Calcite precipitation in Lake Constance: Chemical equilibrium, sedimentation, and nucleation by algae1. Limnology and Oceanography 31 (5), 1081–1094.

Stefánsdóttir, M.B., Gíslason, S.R., 2005. The erosion and suspended matter/seawater interaction during and after the 1996 outburst flood from the Vatnajökull Glacier, Iceland. Earth and Planetary Science Letters 237 (3), 433–452.

Steinberg, D.K., Carlson, C.A., Bates, N.R., Johnson, R.J., Michaels, A.F., Knap, A.H., 2001. Overview of the US JGOFS Bermuda Atlantic Time-series Study (BATS): A decade-scale look at ocean biology and biogeochemistry. Deep Sea Research Part II: Topical Studies in Oceanography 48 (8), 1405–1447.

Stevens, T.O., McKinley, J.P., 1995. Lithoautotrophic Microbial Ecosystems in Deep Basalt Aquifers. Science 270 (5235), 450–455.

Stockmann, G.J., Shirokova, L.S., Pokrovsky, O.S., Bénézeth, P., Bovet, N., Gislason, S.R., Oelkers, E.H., 2012. Does the presence of heterotrophic bacterium Pseudomonas reactans affect basaltic glass dissolution rates? Chemical Geology 296-297, 1–18.

Strub, P.T., Allen, J.S., Huyer, A., Smith, R.L., 1987. Large-scale structure of the spring transition in the coastal ocean off western North America. Journal of Geophysical Research 92 (C2), 1527–1544.

Sudek, L.A., Wanger, G., Templeton, A.S., Staudigel, H., Tebo, B.M., 2017. Submarine Basaltic Glass Colonization by the Heterotrophic Fe(II)-Oxidizing and Siderophore-Producing Deep-Sea Bacterium Pseudomonas stutzeri VS-10: The Potential Role of Basalt in Enhancing Growth. Frontiers in Microbiology 8, 363.

Swart, P.K., 2008. Global synchronous changes in the carbon isotopic composition of carbonate sediments unrelated to changes in the global carbon cycle. Proceedings of the National Academy of Sciences 105 (37), 13741–13745.

Swart, P.K., 2015. The geochemistry of carbonate diagenesis: The past, present and future. Sedimentology 62 (5), 1233–1304.

Swart, P.K., Oehlert, A.M., Mackenzie, G.J., Eberli, G.P., Reijmer, J.J., 2014. The fertilization of the Bahamas by Saharan dust: A trigger for carbonate precipitation? Geology 42 (8), 671–674.

Syvitski, J.P., Peckham, S.D., Hilberman, R., Mulder, T., 2003. Predicting the terrestrial flux of sediment to the global ocean: A planetary perspective. Sedimentary Geology 162 (1), 5–24.

Syvitski, J.P., Vörösmarty, C.J., Kettner, A.J., Green, P., 2005. Impact of Humans on the Flux of Terrestrial Sediment to the Global Coastal Ocean. Science 308 (5720), 376–380.

Tang, H., Chen, Y., 2013. Global glaciations and atmospheric change at ca. 2.3 Ga. Geoscience Frontiers 4 (5), 583–596.

Teodoru, C., Wehrli, B., 2005. Retention of Sediments and Nutrients in the Iron Gate I Reservoir on the Danube River. Biogeochemistry 76 (3), 539–565.

Thompson, J.B., Schultze-Lam, S., Beveridge, T.J., Des Marais, D.J., 1997. Whiting events: Biogenic origin due to the photosynthetic activity of cyanobacterial picoplankton. Limnology and Oceanography 42 (1), 133–141.

Thornton, D.C., 2012. Primary production in the ocean. Advances in Photosynthesis–Fundamental Aspects, edited by: Najafpour, MM, InTech, Rijeka, Croatia, 63–588.

Thornton, D.C., Dong, L.F., Underwood, G.J., Nedwell, D.B., 2002. Factors affecting microphytobenthic biomass, species composition and production in the Colne Estuary (UK). Aquatic Microbial Ecology 27, 285–300.

Tipple, B.J., Meyers, S.R., Pagani, M., 2010. Carbon isotope ratio of Cenozoic CO_2: A comparative evaluation of available geochemical proxies. Paleoceanography 25 (3), PA3202.

Tortell, P.D., DiTullio, G.R., Sigman, D.M., Morel, F.M., 2002. CO_2 effects on taxonomic composition and nutrient utilization in an Equatorial Pacific phytoplankton assemblage. Marine Ecology Progress Series 236, 37–43.

Trommer, G., Leynaert, A., Klein, C., Naegelen, A., Beker, B., 2013. Phytoplankton phosphorus limitation in a North Atlantic coastal ecosystem not predicted by nutrient load. Journal of Plankton Research 35 (6), 1207–1219.

Turner, J.T., 2002. Zooplankton fecal pellets, marine snow and sinking phytoplankton blooms. Aquatic Microbial Ecology 27, 57–102.

Turner, J.V., 1982. Kinetic fractionation of carbon-13 during calcium carbonate precipitation. Geochimica et Cosmochimica Acta 46 (7), 1183–1191.

Urey, H.C., 1948. Oxygen Isotopes in Nature and in the Laboratory. Science 108 (2810), 489–496.

Urey, H.C., Lowenstam, H.A., Epstein, S., McKinney, C.R., 1951. Measurement of paleotemperatures and temperatures of the Upper Cretaceous of England, Denmark, and the southeastern United States. Geological Society of America Bulletin 62 (4), 399–416.

Uroz, S., Calvaruso, C., Turpault, M.-P., Frey-Klett, P., 2009. Mineral weathering by bacteria: Ecology, actors and mechanisms. Trends in Microbiology 17 (8), 378–387.

van Vuuren, D.P., Deetman, S., van Vliet, J., van den Berg, M., van Ruijven, B.J., Koelbl, B., 2013. The role of negative CO_2 emissions for reaching 2 °C—insights from integrated assessment modelling. Climatic Change 118 (1), 15–27.

Veizer, J., Ala, D., Azmy, K., Bruckschen, P., Buhl, D., Bruhn, F., Carden, G.A., Diener, A., Ebneth, S., Godderis, Y., Jasper, T., Korte, C., Pawellek, F., Podlaha, O.G., Strauss, H., 1999. $^{87}Sr/^{86}Sr$, $\delta^{13}C$ and $\delta^{18}O$ evolution of Phanerozoic seawater. Chemical Geology 161 (1), 59–88.

Veldhuis, M.J., Kraay, G.W., van Bleijswijk, J.D., Baars, M.A., 1997. Seasonal and spatial variability in phytoplankton biomass, productivity and growth in the northwestern Indian Ocean: The southwest and northeast monsoon, 1992–1993. Deep Sea Research Part I: Oceanographic Research Papers 44 (3), 425–449.

Verspagen, J.M., Visser, P.M., Huisman, J., 2006. Aggregation with clay causes sedimentation of the buoyant cyanobacteria Microcystis spp. Aquatic Microbial Ecology 44 (2), 165–174.

Viers, J., Dupré, B., Gaillardet, J., 2009. Chemical composition of suspended sediments in World Rivers: New insights from a new database. Science of The Total Environment 407 (2), 853–868.

Vörösmarty, C.J., Meybeck, M., Fekete, B., Sharma, K., Green, P., Syvitski, J.P., 2003. Anthropogenic sediment retention: Major global impact from registered river impoundments. Global and Planetary Change 39 (1), 169–190.

Vrieling, E.G., Poort, L., Beelen, T.P., Gieskes, W.W., 1999. Growth and silica content of the diatoms Thalassiosira weissflogii and Navicula salinarum at different salinities and enrichments with aluminium. European Journal of Phycology 34 (3), 307–316.

Waite, A., Fisher, A., Thompson, P.A., Harrison, P.J., 1997. Sinking rate versus cell volume relationships illuminate sinking rate control mechanisms in marine diatoms. Marine Ecology Progress Series 157, 97–108.

Walker, J.C., Hays, P.B., Kasting, J.F., 1981. A negative feedback mechanism for the long-term stabilization of Earth's surface temperature. Journal of Geophysical Research: Oceans 86 (C10), 9776–9782.

Walling, D.E., 2006. Human impact on land–ocean sediment transfer by the world's rivers. Geomorphology 79 (3), 192–216.

Wallmann, K., 2001. Controls on the cretaceous and cenozoic evolution of seawater composition, atmospheric CO_2 and climate. Geochimica et Cosmochimica Acta 65 (18), 3005–3025.

Wehr, J.D., Sheath, R.G., Kociolek, J.P., 2015. Freshwater algae of North America: Ecology and classification. Elsevier.

Wendt, I., 1971. Carbon and oxygen isotope exchange between HCO_3 in saline solution and solid $CaCO_3$. Earth and Planetary Science Letters 12 (4), 439–442.

White, A.F., Blum, A.E., 1995. Effects of climate on chemical weathering in watersheds. Geochimica et Cosmochimica Acta 59 (9), 1729–1747.

Whiticar, M.J., 1999. Carbon and hydrogen isotope systematics of bacterial formation and oxidation of methane. Chemical Geology 161 (1), 291–314.

Whitton, B.A., Potts, M., 2012. Introduction to the Cyanobacteria, in: Whitton, B.A. (Ed.), Ecology of Cyanobacteria II: Their Diversity in Space and Time. Springer Netherlands, Dordrecht, pp. 1–13.

Wilson, S.A., Barker, Shaun L. L., Dipple, G.M., Atudorei, V., 2010. Isotopic disequilibrium during uptake of atmospheric CO_2 into mine process waters: Implications for CO_2 sequestration. Environmental Science & Technology 44 (24), 9522–9529.

Wofsy, S.C., 1983. A simple model to predict extinction coefficients and phytoplankton biomass in eutrophic waters. Limnology and Oceanography 28 (6), 1144–1155.

Wolery, T.J., Daveler, S.A., 1992. EQ6, a computer program for reaction path modeling of aqueous geochemical systems: Theoretical manual, user's guide and related documentation (Version 7.0). Lawrence Livermore Laboratory, University of California Livermore, CA.

Wolf-Gladrow, D., Riebesell, U., 1997. Diffusion and reactions in the vicinity of plankton: A refined model for inorganic carbon transport. Marine Chemistry 59 (1), 17–34.

Wu, L., Jacobson, A.D., Chen, H.-C., Hausner, M., 2007. Characterization of elemental release during microbe–basalt interactions at T=28°C. Geochimica et Cosmochimica Acta 71 (9), 2224–2239.

Wu, L., Jacobson, A.D., Hausner, M., 2008. Characterization of elemental release during microbe–granite interactions at T=28°C. Geochimica et Cosmochimica Acta 72 (4), 1076–1095.

Wynn, J.G., Bird, M.I., Wong, V.N.L., 2005. Rayleigh distillation and the depth profile of $^{13}C/^{12}C$ ratios of soil organic carbon from soils of disparate texture in Iron Range National Park, Far North Queensland, Australia. Geochimica et Cosmochimica Acta 69 (8), 1961–1973.

Wyrtki, K., 1981. An Estimate of Equatorial Upwelling in the Pacific. Journal of Physical Oceanography 11 (9), 1205–1214.

Yool, A., Popova, E.E., Anderson, T.R., 2013. MEDUSA-2.0: An intermediate complexity biogeochemical model of the marine carbon cycle for climate change and ocean acidification studies. Geoscientific Model Development 6 (5), 1767–1811.

Zanchett, G., Oliveira-Filho, E.C., 2013. Cyanobacteria and cyanotoxins: From impacts on aquatic ecosystems and human health to anticarcinogenic effects. Toxins 5 (10), 1896–1917.

Zhang, J., Quay, P.D., Wilbur, D.O., 1995. Carbon isotope fractionation during gas-water exchange and dissolution of CO_2. Geochimica et Cosmochimica Acta 59 (1), 107–114.

Zhu, T., Dittrich, M., 2016. Carbonate Precipitation through Microbial Activities in Natural Environment, and Their Potential in Biotechnology: A Review. Frontiers in Bioengineering and Biotechnology 4, 4.

Annex

Annex 1: Electronic supplement of Chapter 3

Abbreviations used:

Particulate Material:

ICE	Iceland
MS	Mississippi
Zrc	Zircone

Experimental conditions:

hN	high initial nutrient concentration – BG11 dilution 1:375
hpH	high initial pH
hIS	high initial Ionic Strenght
hpH&hIS	high initial Ph and Ionic Strenght
buff.	buffered pH (carbonate-bicarbonate buffer)
lOD	low initial biomass concentration (OD = optical density); ~0.007 $g_{(dry)}$/kg
mOD	medium initial biomass concentration (OD = optical density); ~0.018 $g_{(dry)}$/kg
hOD	high initial biomass concentration (OD = optical density); ~0.041 $g_{(dry)}$/kg

Note:

All experiment without “hN” were performed at BG11 1:1000
All experiments without hpH were performed at an initial pH of 5.9-6.2

Others:

Biot. Ctrl.	biotic control – cyanobacteria but no particulate material
Abiot. Ctrl.	abiotic control – particulate material but no cyanobacteria
DIC	Dissolved inorganic carbon
NPOP	Non-purgeable organic carbon
b.d.l.	below detection limit
SD	Standard deviation

Note:

"Biomass" of the abiotic controls was determined following the same procedure as for the biotic experiments. The obtained values were subtracted from the corresponding biotic experiment. However, there was no biomass observed in the abiotic controls!

Annex 1 Table 1. Table 1 of the Electronic supplement of Chapter 3 – Results of experimental series S*II*.

		date/time	elapsed time [days]	biomass [g(dry)/kg]			date/time	elapsed time [days]	biomass [$g_{(dry)}$/kg]
***SII* 1 biot. Ctrl, hN**									
***SII* 1 biotic control, BG11 1:375**	*SII* 1_1	12.03.14 11:30	0.0	0.0215					
	SII 1_2	13.03.14 11:30	1.0	0.0216					
	SII 1_3	14.03.14 11:30	2.0	0.0218					
	SII 1_4	15.03.14 11:30	5.0	0.0231					
	SII 1_5	16.03.14 11:30	6.0	0.0259					
	SII 1_6	17.03.14 11:30	7.0	0.0345					
	SII 1_7	18.03.14 11:30	8.0	0.0540					
	SII 1_8	19.03.14 11:30	9.0	0.0834					
	SII 1_9	20.03.14 11:30	10.0	0.1247					
	SII 1_10	21.03.14 11:30	12.0	0.1755					
	SII 1_11	22.03.14 11:30	13.0	0.1936					
	SII 1_12	23.03.14 11:30	14.0	0.2169					
	SII 1_13	24.03.14 11:30	15.0	0.2399					
	SII 1_14	25.03.14 11:30	16.0	0.2539					
	SII 1_15	26.03.14 11:30	19.0	0.2483					
	SII 1_16	27.03.14 11:30	20.0	0.2669					
	SII 1_17	28.03.14 11:30	21.0	0.2582					
	SII 1_18	29.03.14 11:30	22.0	0.2609					
	SII 1_19	30.03.14 11:30	23.0	0.2443					
	SII 1_20	31.03.14 11:30	26.0	0.2377					
	SII 1_21	01.04.14 11:30	27.0	0.2478					
	SII 1_22	02.04.14 11:30	28.1	0.2519					
***SII* 2 1500ICE, hN**					***SII* 4 1500ICE, abiot. Ctrl., hN**				
***SII* 2, 1500 mg/l ICE, BG11 1:375**	*SII* 2_1	12.03.14 11:30	0.0	0.0211	***SII* 4, abiotic control, 1500 mg/l ICE, BG11 1:375**	*SII* 4_1	12.03.14 11:30	0.00	0.0062
	SII 2_2	13.03.14 12:10	1.0	0.0234		*SII* 4_2	13.03.14 12:10	1.03	0.0047
	SII 2_3	14.03.14 12:00	2.0	0.0253		*SII* 4_3	14.03.14 12:00	2.02	0.0073
	SII 2_4	17.03.14 12:00	5.0	0.0802		*SII* 4_4	17.03.14 12:00	5.02	0.0123
	SII 2_5	18.03.14 12:10	6.0	0.1296		*SII* 4_5	18.03.14 12:10	6.03	0.0099
	SII 2_6	19.03.14 12:15	7.0	0.1769		*SII* 4_6	19.03.14 12:15	7.03	0.0097
	SII 2_7	20.03.14 12:15	8.0	0.2196		*SII* 4_7	20.03.14 12:15	8.03	0.0111
	SII 2_8	21.03.14 12:00	9.0	0.2534		*SII* 4_8	21.03.14 12:00	9.02	0.0090
	SII 2_9	22.03.14 12:00	10.0	0.2720		*SII* 4_9	22.03.14 12:00	10.02	0.0101
	SII 2_10	24.03.14 12:10	12.0	0.2866		*SII* 4_10	24.03.14 12:10	12.03	0.0109
	SII 2_11	25.03.14 12:20	13.0	0.2825		*SII* 4_11	25.03.14 12:20	13.03	0.0094
	SII 2_12	26.03.14 12:20	14.0	0.2960		*SII* 4_12	26.03.14 12:20	14.03	0.0104
	SII 2_13	27.03.14 12:00	15.0	0.2991		*SII* 4_13	27.03.14 12:00	15.02	0.0095
	SII 2_14	28.03.14 12:15	16.0	0.2930		*SII* 4_14	28.03.14 12:15	16.03	0.0108
	SII 2_15	31.03.14 12:15	19.0	0.3332		*SII* 4_15	31.03.14 12:15	19.03	0.0127
	SII 2_16	01.04.14 11:45	20.0	0.3243		*SII* 4_16	01.04.14 11:45	20.01	0.0106
	SII 2_17	02.04.14 12:00	21.0	0.3405		*SII* 4_17	02.04.14 12:00	21.02	0.0114
	SII 2_18	03.04.14 12:00	22.0	0.3429		*SII* 4_18	03.04.14 12:00	22.02	0.0109
	SII 2_19	04.04.14 12:00	23.0	0.3399		*SII* 4_19	04.04.14 12:00	23.02	0.0106
	SII 2_20	07.04.14 12:10	26.0	0.3225		*SII* 4_20	07.04.14 12:10	26.03	0.0106
	SII 2_21	08.04.14 12:15	27.0	0.3365		*SII* 4_21	08.04.14 12:15	27.03	0.0105
	SII 2_22	09.04.14 13:20	28.1	0.3281		*SII* 4_22	09.04.14 13:20	28.08	0.0116
***SII* 3 1500MS, hN**					***SII* 5 1500MS, abiot. Ctrl., hN**				
***SII* 3, 1500 mg/l MS, BG11 1:375**	*SII* 3_1	12.03.14 11:30	0.0	0.0215	***SII* 5, abiotic control, 1500 mg/l MS, BG11 1:375**	*SII* 5_1	12.03.14 11:30	0.00	0.0009
	SII 3_2	13.03.14 12:10	1.0	0.0240		*SII* 5_2	13.03.14 12:10	1.03	0.0008
	SII 3_3	14.03.14 12:00	2.0	0.0299		*SII* 5_3	14.03.14 12:00	2.02	0.0004
	SII 3_4	17.03.14 12:00	5.0	0.1120		*SII* 5_4	17.03.14 12:00	5.02	0.0005
	SII 3_5	18.03.14 12:10	6.0	0.1694		*SII* 5_5	18.03.14 12:10	6.03	0.0006
	SII 3_6	19.03.14 12:15	7.0	0.2250		*SII* 5_6	19.03.14 12:15	7.03	0.0006
	SII 3_7	20.03.14 12:15	8.0	0.2615		*SII* 5_7	20.03.14 12:15	8.03	0.0007
	SII 3_8	21.03.14 12:00	9.0	0.2780		*SII* 5_8	21.03.14 12:00	9.02	0.0006
	SII 3_9	22.03.14 12:00	10.0	0.2834		*SII* 5_9	22.03.14 12:00	10.02	0.0010
	SII 3_10	24.03.14 12:10	12.0	0.2981		*SII* 5_10	24.03.14 12:10	12.03	0.0012
	SII 3_11	25.03.14 12:20	13.0	0.2999		*SII* 5_11	25.03.14 12:20	13.03	0.0013
	SII 3_12	26.03.14 12:20	14.0	0.3017		*SII* 5_12	26.03.14 12:20	14.03	0.0013
	SII 3_13	27.03.14 12:00	15.0	0.3086		*SII* 5_13	27.03.14 12:00	15.02	0.0012
	SII 3_14	28.03.14 12:15	16.0	0.3138		*SII* 5_14	28.03.14 12:15	16.03	0.0014
	SII 3_15	31.03.14 12:15	19.0	0.3228		*SII* 5_15	31.03.14 12:15	19.03	0.0007
	SII 3_16	01.04.14 11:45	20.0	0.3218		*SII* 5_16	01.04.14 11:45	20.01	0.0005
	SII 3_17	02.04.14 12:00	21.0	0.3247		*SII* 5_17	02.04.14 12:00	21.02	0.0004
	SII 3_18	03.04.14 12:00	22.0	0.3328		*SII* 5_18	03.04.14 12:00	22.02	0.0004
	SII 3_19	04.04.14 12:00	23.0	0.3468		*SII* 5_19	04.04.14 12:00	23.02	0.0003
	SII 3_20	07.04.14 12:10	26.0	0.3468		*SII* 5_20	07.04.14 12:10	26.03	0.0005
	SII 3_21	08.04.14 12:15	27.0	0.3667		*SII* 5_21	08.04.14 12:15	27.03	0.0005
	SII 3_22	09.04.14 13:20	28.1	0.3681		*SII* 5_22	09.04.14 13:20	28.08	0.0007

Annex 1 Table 2. Table 2 of the Electronic supplement of Chapter 3 – Results of experimental series S*III*.

		date/time	elapsed time [days]	biomass [g(dry)/kg]
***SIII* 1 biot. Ctrl**				
***SIII* 1, biotic control, 1:1000 BG11**	*SIII* 1_1	26.06.14 14:30	0.0	0.0320
	SIII 1_2	27.06.14 12:15	0.9	0.0311
	SIII 1_3	29.06.14 17:30	3.1	0.0306
	SIII 1_4	30.06.14 16:25	4.1	0.0303
	SIII 1_5	01.07.14 13:00	4.9	0.0317
	SIII 1_6	02.07.14 13:25	6.0	0.0340
	SIII 1_7	03.07.14 13:00	6.9	0.0373
	SIII 1_8	04.07.14 12:50	7.9	0.0471
	SIII 1_9	05.07.14 14:30	9.0	0.0775
	SIII 1_10	07.07.14 13:10	10.9	0.1093
	SIII 1_11	08.07.14 12:20	11.9	0.1105
	SIII 1_12	09.07.14 12:45	12.9	0.1108
	SIII 1_13	10.07.14 12:00	13.9	0.1062
	SIII 1_14	11.07.14 12:30	14.9	0.1114
	SIII 1_15	14.07.14 12:20	17.9	0.1097
	SIII 1_16	16.07.14 12:00	19.9	0.1115
	SIII 1_17	17.07.14 12:00	20.9	0.1066
	SIII 1_18	21.07.14 13:45	25.0	0.1092
	SIII 1_19	22.07.14 13:45	26.0	0.1096
	SIII 1_20	23.07.14 13:45	27.0	0.1093
	SIII 1_21	24.07.14 11:30	27.9	0.1124
	SIII 1_22	25.07.14 11:40	28.9	0.1121
	SIII 1_23	28.07.14 13:20	32.0	0.1119
	SIII 1_24	29.07.14 13:45	33.0	0.1135
	SIII 1_25	30.07.14 12:30	33.9	0.1142
	SIII 1_26	01.08.14 11:30	35.9	0.1149
***SIII* 2 500ICE**				
***SIII* 2, 500 mg/l ICE, 1:1000 BG11**	*SIII* 2_1	26.06.14 14:30	0.0	0.0331
	SIII 2_2	27.06.14 12:15	0.9	0.0313
	SIII 2_3	29.06.14 17:30	3.1	0.0312
	SIII 2_4	30.06.14 16:25	4.1	0.0318
	SIII 2_5	01.07.14 13:00	4.9	0.0404
	SIII 2_6	02.07.14 13:25	6.0	0.0599
	SIII 2_7	03.07.14 13:00	6.9	0.0890
	SIII 2_8	04.07.14 12:50	7.9	0.1161
	SIII 2_9	05.07.14 14:30	9.0	0.1269
	SIII 2_10	07.07.14 13:10	10.9	0.1357
	SIII 2_11	08.07.14 12:20	11.9	0.1359
	SIII 2_12	09.07.14 12:45	12.9	0.1352
	SIII 2_13	10.07.14 12:00	13.9	0.1330
	SIII 2_14	11.07.14 12:30	14.9	0.1345
	SIII 2_15	14.07.14 12:20	17.9	0.1297
	SIII 2_16	16.07.14 12:00	19.9	0.1326
	SIII 2_17	17.07.14 12:00	20.9	0.1325
	SIII 2_18	21.07.14 13:45	25.0	0.1327
	SIII 2_19	22.07.14 13:45	26.0	0.1339
	SIII 2_20	23.07.14 13:45	27.0	0.1384
	SIII 2_21	24.07.14 11:30	27.9	0.1368
	SIII 2_22	25.07.14 11:40	28.9	0.1348
	SIII 2_23	28.07.14 13:20	32.0	
	SIII 2_24	29.07.14 13:45	33.0	0.1392
	SIII 2_25	30.07.14 12:30	33.9	0.1394
	SIII 2_26	01.08.14 11:30	35.9	0.1411
***SIII* 3 1500ICE**				
***SIII* 3, 1500 mg/l ICE, 1:1000 BG11**	*SIII* 3_1	26.06.14 14:30	0.0	0.0329
	SIII 3_2	27.06.14 12:15	0.9	0.0298
	SIII 3_3	29.06.14 17:30	3.1	0.0397
	SIII 3_4	30.06.14 16:25	4.1	0.0499
	SIII 3_5	01.07.14 13:00	4.9	0.0769
	SIII 3_6	02.07.14 13:25	6.0	0.1124
	SIII 3_7	03.07.14 13:00	6.9	0.1353
	SIII 3_8	04.07.14 12:50	7.9	0.1368
	SIII 3_9	05.07.14 14:30	9.0	0.1400
	SIII 3_10	07.07.14 13:10	10.9	0.1571
	SIII 3_11	08.07.14 12:20	11.9	0.1554
	SIII 3_12	09.07.14 12:45	12.9	0.1515
	SIII 3_13	10.07.14 12:00	13.9	0.1499
	SIII 3_14	11.07.14 12:30	14.9	0.1536
	SIII 3_15	14.07.14 12:20	17.9	0.1448
	SIII 3_16	16.07.14 12:00	19.9	0.1446
	SIII 3_17	17.07.14 12:00	20.9	0.1464
	SIII 3_18	21.07.14 13:45	25.0	0.1472
	SIII 3_19	22.07.14 13:45	26.0	0.1468
	SIII 3_20	23.07.14 13:45	27.0	0.1473
	SIII 3_21	24.07.14 11:30	27.9	0.1425
	SIII 3_22	25.07.14 11:40	28.9	0.1435
	SIII 3_23	28.07.14 13:20	32.0	0.1412
***SIII* 6 500ICE, abiot. Ctrl.**				
***SIII* 6, abiotic control, 500 mg/l ICE 1:1000 BG11**	*SIII* 6_1	26.06.14 14:30	0.0	0.0008
	SIII 6_2	27.06.14 12:15	0.9	0.0009
	SIII 6_3	29.06.14 17:30	3.1	0.0014
	SIII 6_4	30.06.14 16:25	4.1	0.0015
	SIII 6_5	01.07.14 13:00	4.9	0.0016
	SIII 6_6	02.07.14 13:25	6.0	0.0014
	SIII 6_7	03.07.14 13:00	6.9	0.0013
	SIII 6_8	04.07.14 12:50	7.9	0.0014
	SIII 6_9	05.07.14 14:30	9.0	0.0015
	SIII 6_10	07.07.14 13:10	10.9	0.0016
	SIII 6_11	08.07.14 12:20	11.9	0.0021
	SIII 6_12	09.07.14 12:45	12.9	0.0021
	SIII 6_13	10.07.14 12:00	13.9	0.0016
	SIII 6_14	11.07.14 12:30	14.9	0.0014
	SIII 6_15	14.07.14 12:20	17.9	0.0017
	SIII 6_16	16.07.14 12:00	19.9	0.0020
	SIII 6_17	17.07.14 12:00	20.9	0.0025
	SIII 6_18	21.07.14 13:45	25.0	0.0024
	SIII 6_19	22.07.14 13:45	26.0	0.0025
	SIII 6_20	23.07.14 13:45	27.0	0.0022
	SIII 6_21	24.07.14 11:30	27.9	0.0021
	SIII 6_22	25.07.14 11:40	28.9	0.0024
	SIII 6_23	28.07.14 13:20	32.0	0.0016
	SIII 6_24	29.07.14 13:45	33.0	0.0019
	SIII 6_25	30.07.14 12:30	33.9	0.0019
	SIII 6_26	01.08.14 11:30	35.9	0.0021
***SIII* 7 1500ICE, abiot. Ctrl.**				
***SIII* 7,abiotic control, 1500 mg/l ICE, 1:1000 BG11**	*SIII* 7_1	26.06.14 14:30	0.0	0.0028
	SIII 7_2	27.06.14 12:15	0.9	0.0070
	SIII 7_3	29.06.14 17:30	3.1	0.0069
	SIII 7_4	30.06.14 16:25	4.1	0.0108
	SIII 7_5	01.07.14 13:00	4.9	0.0080
	SIII 7_6	02.07.14 13:25	6.0	0.0096
	SIII 7_7	03.07.14 13:00	6.9	0.0077
	SIII 7_8	04.07.14 12:50	7.9	0.0071
	SIII 7_9	05.07.14 14:30	9.0	0.0063
	SIII 7_10	07.07.14 13:10	10.9	0.0084
	SIII 7_11	08.07.14 12:20	11.9	0.0087
	SIII 7_12	09.07.14 12:45	12.9	0.0086
	SIII 7_13	10.07.14 12:00	13.9	0.0121
	SIII 7_14	11.07.14 12:30	14.9	0.0088
	SIII 7_15	14.07.14 12:20	17.9	0.0068
	SIII 7_16	16.07.14 12:00	19.9	0.0079
	SIII 7_17	17.07.14 12:00	20.9	0.0095
	SIII 7_18	21.07.14 13:45	25.0	0.0099
	SIII 7_19	22.07.14 13:45	26.0	0.0120
	SIII 7_20	23.07.14 13:45	27.0	0.0124
	SIII 7_21	24.07.14 11:30	27.9	0.0115
	SIII 7_22	25.07.14 11:40	28.9	0.0097
	SIII 7_23	28.07.14 13:20	32.0	0.0113

Annex 1 Table 2. Continuation.

		date/time	elapsed time [days]	biomass [g(dry)/kg]			date/time	elapsed time [days]	biomass [g(dry)/kg]
	SIII 3_24	29.07.14 13:45	33.0	0.1467		*SIII* 7_24	29.07.14 13:45	33.0	0.0099
	SIII 3_25	30.07.14 12:30	33.9	0.1471		*SIII* 7_25	30.07.14 12:30	33.9	0.0094
	SIII 3_26	01.08.14 11:30	35.9	0.1543		*SIII* 7_26	01.08.14 11:30	35.9	0.0115
***SIII* 4 500MS**						***SIII* 8 500MS, abiot. Ctrl.**			
	SIII 4_1	26.06.14 14:30	0.0	0.0329		*SIII* 8_1	26.06.14 14:30	0.0	0.0001
	SIII 4_2	27.06.14 12:15	0.9	0.0324		*SIII* 8_2	27.06.14 12:15	0.9	0.0001
	SIII 4_3	29.06.14 17:30	3.1	0.0498		*SIII* 8_3	29.06.14 17:30	3.1	0.0003
	SIII 4_4	30.06.14 16:25	4.1	0.0812		*SIII* 8_4	30.06.14 16:25	4.1	0.0005
	SIII 4_5	01.07.14 13:00	4.9	0.1002		*SIII* 8_5	01.07.14 13:00	4.9	0.0003
	SIII 4_6	02.07.14 13:25	6.0	0.1278		*SIII* 8_6	02.07.14 13:25	6.0	0.0003
	SIII 4_7	03.07.14 13:00	6.9	0.1312		*SIII* 8_7	03.07.14 13:00	6.9	0.0004
	SIII 4_8	04.07.14 12:50	7.9	0.1303		*SIII* 8_8	04.07.14 12:50	7.9	0.0006
	SIII 4_9	05.07.14 14:30	9.0	0.1342		*SIII* 8_9	05.07.14 14:30	9.0	0.0004
	SIII 4_10	07.07.14 13:10	10.9	0.1324		*SIII* 8_10	07.07.14 13:10	10.9	0.0004
	SIII 4_11	08.07.14 12:20	11.9	0.1338		*SIII* 8_11	08.07.14 12:20	11.9	0.0005
	SIII 4_12	09.07.14 12:45	12.9	0.1341		*SIII* 8_12	09.07.14 12:45	12.9	0.0004
	SIII 4_13	10.07.14 12:00	13.9	0.1354		*SIII* 8_13	10.07.14 12:00	13.9	0.0004
	SIII 4_14	11.07.14 12:30	14.9	0.1366		*SIII* 8_14	11.07.14 12:30	14.9	0.0004
	SIII 4_15	14.07.14 12:20	17.9	0.1348		*SIII* 8_15	14.07.14 12:20	17.9	0.0005
	SIII 4_16	16.07.14 12:00	19.9	0.1354		*SIII* 8_16	16.07.14 12:00	19.9	0.0005
	SIII 4_17	17.07.14 12:00	20.9	0.1381		*SIII* 8_17	17.07.14 12:00	20.9	0.0004
	SIII 4_18	21.07.14 13:45	25.0	0.1421		*SIII* 8_18	21.07.14 13:45	25.0	0.0006
	SIII 4_19	22.07.14 13:45	26.0	0.1439		*SIII* 8_19	22.07.14 13:45	26.0	0.0006
	SIII 4_20	23.07.14 13:45	27.0	0.1503		*SIII* 8_20	23.07.14 13:45	27.0	0.0006
	SIII 4_21	24.07.14 11:30	27.9	0.1478		*SIII* 8_21	24.07.14 11:30	27.9	0.0006
	SIII 4_22	25.07.14 11:40	28.9	0.1485		*SIII* 8_22	25.07.14 11:40	28.9	0.0006
	SIII 4_23	28.07.14 13:20	32.0	0.1500		*SIII* 8_23	28.07.14 13:20	32.0	0.0006
	SIII 4_24	29.07.14 13:45	33.0	0.1510		*SIII* 8_24	29.07.14 13:45	33.0	0.0008
	SIII 4_25	30.07.14 12:30	33.9	0.1506		*SIII* 8_25	30.07.14 12:30	33.9	0.0007
	SIII 4_26	01.08.14 11:30	35.9	0.1529		*SIII* 8_26	01.08.14 11:30	35.9	0.0008
***SIII* 5 1500MS**						***SIII* 9 1500MS, abiot. Ctrl.**			
	SIII 1_1	26.06.14 14:30	0.0	0.0336		*SIII* 9_1	26.06.14 14:30	0.0	0.0002
	SIII 1_2	27.06.14 12:15	0.9	0.0333		*SIII* 9_2	27.06.14 12:15	0.9	0.0005
	SIII 1_3	29.06.14 17:30	3.1	0.0640		*SIII* 9_3	29.06.14 17:30	3.1	0.0008
	SIII 1_4	30.06.14 16:25	4.1	0.0913		*SIII* 9_4	30.06.14 16:25	4.1	0.0008
	SIII 1_5	01.07.14 13:00	4.9	0.1279		*SIII* 9_5	01.07.14 13:00	4.9	0.0008
	SIII 1_6	02.07.14 13:25	6.0	0.1404		*SIII* 9_6	02.07.14 13:25	6.0	0.0010
	SIII 1_7	03.07.14 13:00	6.9	0.1437		*SIII* 9_7	03.07.14 13:00	6.9	0.0010
	SIII 1_8	04.07.14 12:50	7.9	0.1473		*SIII* 9_8	04.07.14 12:50	7.9	0.0009
	SIII 1_9	05.07.14 14:30	9.0	0.1502		*SIII* 9_9	05.07.14 14:30	9.0	0.0009
	SIII 1_10	07.07.14 13:10	10.9	0.1528		*SIII* 9_10	07.07.14 13:10	10.9	0.0010
	SIII 1_11	08.07.14 12:20	11.9	0.1594		*SIII* 9_11	08.07.14 12:20	11.9	0.0013
	SIII 1_12	09.07.14 12:45	12.9	0.1579		*SIII* 9_12	09.07.14 12:45	12.9	0.0010
	SIII 1_13	10.07.14 12:00	13.9	0.1681		*SIII* 9_13	10.07.14 12:00	13.9	0.0012
	SIII 1_14	11.07.14 12:30	14.9	0.1726		*SIII* 9_14	11.07.14 12:30	14.9	0.0012
	SIII 1_15	14.07.14 12:20	17.9	0.1777		*SIII* 9_15	14.07.14 12:20	17.9	0.0012
	SIII 1_16	16.07.14 12:00	19.9	0.1839		*SIII* 9_16	16.07.14 12:00	19.9	0.0013
	SIII 1_17	17.07.14 12:00	20.9	0.1908		*SIII* 9_17	17.07.14 12:00	20.9	0.0012
	SIII 1_18	21.07.14 13:45	25.0	0.1986		*SIII* 9_18	21.07.14 13:45	25.0	0.0015
	SIII 1_19	22.07.14 13:45	26.0	0.2016		*SIII* 9_19	22.07.14 13:45	26.0	0.0014
	SIII 1_20	23.07.14 13:45	27.0	0.2083		*SIII* 9_20	23.07.14 13:45	27.0	0.0014
	SIII 1_21	24.07.14 11:30	27.9	0.2037		*SIII* 9_21	24.07.14 11:30	27.9	0.0013
	SIII 1_22	25.07.14 11:40	28.9	0.2049		*SIII* 9_22	25.07.14 11:40	28.9	0.0016
	SIII 1_23	28.07.14 13:20	32.0	0.2076		*SIII* 9_23	28.07.14 13:20	32.0	0.0015
	SIII 1_24	29.07.14 13:45	33.0	0.2141		*SIII* 9_24	29.07.14 13:45	33.0	0.0016
	SIII 1_25	30.07.14 12:30	33.9	0.2157		*SIII* 9_25	30.07.14 12:30	33.9	0.0015
	SIII 1_26	01.08.14 11:30	35.9	0.2192		*SIII* 9_26	01.08.14 11:30	35.9	0.0016

Annex 1 Table 3. Table 3 of the Electronic supplement of Chapter 3 – Results of Experimental series S*IV*.

		date/time	elapsed time [days]	biomass [g(dry)/kg]	pH		date/time	elapsed time [days]	biomass [g(dry)/kg]	pH
***SIV* 1 biot. Ctrl**										
	SIV 1_1	08.10.14 16:00	0.0	0.0064	6.08					
	SIV 1_2	09.10.14 16:00	0.8	0.0063						
	SIV 1_3	10.10.14 16:00	1.8	0.0063	6.06					
	SIV 1_4	11.10.14 16:00	2.8	0.0058						
	SIV 1_5	12.10.14 16:00	4.8	0.0054	6.07					
	SIV 1_6	13.10.14 16:00	6.8	0.0046	6.26					
	SIV 1_7	14.10.14 16:00	8.8	0.0039	6.10					
	SIV 1_8	15.10.14 16:00	11.8	0.0029	6.10					
	SIV 1_9	16.10.14 16:00	12.8	0.0029	6.15					
	SIV 1_10	17.10.14 16:00	13.8							
	SIV 1_11	18.10.14 16:00	14.8							
	SIV 1_12	19.10.14 16:00	15.8	0.0026	6.14					

Annex 1 Table 3. Continuation.

		date/time	elapsed time [days]	biomass [g(dry)/kg]	pH
	SIV 1_13	20.10.14 16:00	18.8		
	SIV 1_14	21.10.14 16:00	19.8		
	SIV 1_15	22.10.14 16:00	20.8		
	SIV 1_16	23.10.14 16:00	21.8	0.0022	6.16
***SIV* 2 1500ICE**					
***SIV* 2, 1500 mg/l ICE, BG11 1:1000**	*SIV* 2_1	08.10.14 16:00	0.0	0.0064	7.02
	SIV 2_2	09.10.14 10:30	0.8	0.0067	
	SIV 2_3	10.10.14 10:30	1.8	0.0061	6.99
	SIV 2_4	11.10.14 10:45	2.8	0.0067	
	SIV 2_5	13.10.14 10:30	4.8	0.0061	7.04
	SIV 2_6	15.10.14 10:30	6.8	0.0064	7.01
	SIV 2_7	17.10.14 10:45	8.8	0.0074	7.11
	SIV 2_8	20.10.14 10:30	11.8	0.0180	7.73
	SIV 2_9	21.10.14 10:30	12.8	0.0265	8.12
	SIV 2_10	22.10.14 10:30	13.8	0.0402	
	SIV 2_11	23.10.14 10:30	14.8	0.0597	9.54
	SIV 2_12	24.10.14 10:30	15.8	0.0842	9.79
	SIV 2_13	27.10.14 10:30	18.8	0.1308	8.76
	SIV 2_14	28.10.14 10:30	19.8	0.1314	8.37
	SIV 2_15	29.10.14 10:30	20.8	0.1320	8.27
	SIV 2_16	30.10.14 10:30	21.8	0.1329	8.23
***SIV* 3 75ICE**					
***SIV* 3, 75 mg/l ICE, BG11 1:1000**	*SIV* 3_1	08.10.14 16:00	0.00	0.0065	6.20
	SIV 3_2	09.10.14 10:30	0.8	0.0063	
	SIV 3_3	10.10.14 10:30	1.8	0.0062	6.19
	SIV 3_4	11.10.14 10:45	2.8	0.0061	
	SIV 3_5	13.10.14 10:30	4.8	0.0051	6.09
	SIV 3_6	15.10.14 10:30	6.8	0.0052	6.12
	SIV 3_7	17.10.14 10:45	8.8	0.0042	6.18
	SIV 3_8	20.10.14 10:30	11.8	0.0033	6.17
	SIV 3_9	21.10.14 10:30	12.8	0.0032	6.27
	SIV 3_10	22.10.14 10:30	13.8		
	SIV 3_11	23.10.14 10:30	14.8		7.07
	SIV 3_12	24.10.14 10:30	15.8	0.0029	6.28
	SIV 3_13	27.10.14 10:30	18.8		
	SIV 3_14	28.10.14 10:30	19.8		
	SIV 3_15	29.10.14 10:30	20.8		
	SIV 3_16	30.10.14 10:30	21.8	0.0023	6.30
***SIV* 4 1500MS**					
***SIV* 4, 1500 mg/l MS, BG11 1:1000**	*SIV* 4_1	08.10.14 16:00	0.00	0.0072	7.31
	SIV 4_2	09.10.14 10:30	0.8	0.0071	
	SIV 4_3	10.10.14 10:30	1.8	0.0079	7.40
	SIV 4_4	11.10.14 10:45	2.8	0.0079	
	SIV 4_5	13.10.14 10:30	4.8	0.0085	7.42
	SIV 4_6	15.10.14 10:30	6.8	0.0093	7.52
	SIV 4_7	17.10.14 10:45	8.8	0.0133	7.76
	SIV 4_8	20.10.14 10:30	11.8	0.0572	10.20
	SIV 4_9	21.10.14 10:30	12.8	0.0830	10.46
	SIV 4_10	22.10.14 10:30	13.8	0.1113	
	SIV 4_11	23.10.14 10:30	14.8	0.1245	10.65
	SIV 4_12	24.10.14 10:30	15.8	0.1297	9.03
	SIV 4_13	27.10.14 10:30	18.8	0.1328	8.23
	SIV 4_14	28.10.14 10:30	19.8	0.1360	8.46
	SIV 4_15	29.10.14 10:30	20.8	0.1357	8.48
	SIV 4_16	30.10.14 10:30	21.8	0.1400	8.45
***SIV* 5 75MS**					
***SIV* 5, 75 mg/l MS, BG11 1:1000**	*SIV* 5_1	08.10.14 16:00	0.00	0.0065	6.29
	SIV 5_2	09.10.14 10:30	0.8	0.0067	
	SIV 5_3	10.10.14 10:30	1.8	0.0063	6.33
	SIV 5_4	11.10.14 10:45	2.8	0.0063	
	SIV 5_5	13.10.14 10:30	4.8	0.0057	6.32
	SIV 5_6	15.10.14 10:30	6.8	0.0054	6.35
	SIV 5_7	17.10.14 10:45	8.8	0.0049	6.41
	SIV 5_8	20.10.14 10:30	11.8	0.0037	6.45
	SIV 5_9	21.10.14 10:30	12.8	0.0036	6.53
	SIV 5_10	22.10.14 10:30	13.8		
	SIV 5_11	23.10.14 10:30	14.8		
	SIV 5_12	24.10.14 10:30	15.8	0.0033	6.51
	SIV 5_13	27.10.14 10:30	18.8		
	SIV 5_14	28.10.14 10:30	19.8		
	SIV 5_15	29.10.14 10:30	20.8		
	SIV 5_16	30.10.14 10:30	21.8	0.0031	6.68
***SIV* 6 1500ICE, abiot. Ctrl.**					
***SIV* 6, abiotic control, 1500 mg/l ICE, BG11 1:1000**	*SIV* 6_1	08.10.14 16:00	0.00	0.0031	6.89
	SIV 6_2	09.10.14 10:30	0.77	0.0031	
	SIV 6_3	10.10.14 10:30	1.77	0.0043	7.02
	SIV 6_4	11.10.14 10:45	2.78	0.0033	
	SIV 6_5	13.10.14 10:30	4.77	0.0048	7.03
	SIV 6_6	15.10.14 10:30	6.77	0.0043	6.98
	SIV 6_7	17.10.14 10:45	8.78	0.0052	6.99
	SIV 6_8	20.10.14 10:30	11.77	0.0055	7.09
	SIV 6_9	21.10.14 10:30	12.77	0.0062	7.13
	SIV 6_10	22.10.14 10:30	13.77	0.0069	
	SIV 6_11	23.10.14 10:30	14.77	0.0070	7.05
	SIV 6_12	24.10.14 10:30	15.77	0.0065	7.08
	SIV 6_13	27.10.14 10:30	18.77	0.0074	7.14
	SIV 6_14	28.10.14 10:30	19.77	0.0085	
	SIV 6_15	29.10.14 10:30	20.77	0.0086	
	SIV 6_16	30.10.14 10:30	21.77	0.0088	7.12
***SIV* 7 75ICE, abiot. Ctrl.**					
***SIV* 7, abiotic control, 75 mg/l ICE, BG11 1:1000**	*SIV* 7_1	08.10.14 16:00	0.00	0.0002	6.11
	SIV 7_2	09.10.14 10:30	0.77	0.0001	
	SIV 7_3	10.10.14 10:30	1.77	0.0003	6.25
	SIV 7_4	11.10.14 10:45	2.78	-0.0001	
	SIV 7_5	13.10.14 10:30	4.77	0.0003	6.18
	SIV 7_6	15.10.14 10:30	6.77	-0.0001	6.12
	SIV 7_7	17.10.14 10:45	8.78	0.0001	6.15
	SIV 7_8	20.10.14 10:30	11.77	0.0000	6.16
	SIV 7_9	21.10.14 10:30	12.77	-0.0002	6.19
	SIV 7_10	22.10.14 10:30	13.77	0.0000	
	SIV 7_11	23.10.14 10:30	14.77	0.0000	
	SIV 7_12	24.10.14 10:30	15.77	0.0001	6.17
	SIV 7_13	27.10.14 10:30	18.77	0.0000	
	SIV 7_14	28.10.14 10:30	19.77	0.0000	
	SIV 7_15	29.10.14 10:30	20.77	0.0000	
	SIV 7_16	30.10.14 10:30	21.77	0.0001	6.18
***SIV* 8 1500MS, abiot. Ctrl.**					
***SIV* 8, abiotic control, 1500 mg/l MS, BG11 1:1000**	*SIV* 8_1	08.10.14 16:00	0.00	0.0013	7.25
	SIV 8_2	09.10.14 10:30	0.77	0.0014	
	SIV 8_3	10.10.14 10:30	1.77	0.0014	7.45
	SIV 8_4	11.10.14 10:45	2.78	0.0012	
	SIV 8_5	13.10.14 10:30	4.77	0.0014	7.48
	SIV 8_6	15.10.14 10:30	6.77	0.0012	7.50
	SIV 8_7	17.10.14 10:45	8.78	0.0017	7.50
	SIV 8_8	20.10.14 10:30	11.77	0.0019	7.62
	SIV 8_9	21.10.14 10:30	12.77	0.0017	7.67
	SIV 8_10	22.10.14 10:30	13.77	0.0019	
	SIV 8_11	23.10.14 10:30	14.77	0.0022	7.66
	SIV 8_12	24.10.14 10:30	15.77	0.0019	7.66
	SIV 8_13	27.10.14 10:30	18.77	0.0025	7.73
	SIV 8_14	28.10.14 10:30	19.77	0.0027	
	SIV 8_15	29.10.14 10:30	20.77	0.0029	
	SIV 8_16	30.10.14 10:30	21.77	0.0028	7.76
***SIV* 9 75MS, abiot. Ctrl.**					
***SIV* 9, abiotic control, 75 mg/l MS, BG11 1:1000**	*SIV* 9_1	08.10.14 16:00	0.00	0.0002	6.28
	SIV 9_2	09.10.14 10:30	0.77	0.0000	
	SIV 9_3	10.10.14 10:30	1.77	0.0001	6.46
	SIV 9_4	11.10.14 10:45	2.78	-0.0001	
	SIV 9_5	13.10.14 10:30	4.77	0.0000	6.49
	SIV 9_6	15.10.14 10:30	6.77	-0.0002	6.41
	SIV 9_7	17.10.14 10:45	8.78	0.0002	6.43
	SIV 9_8	20.10.14 10:30	11.77	0.0001	6.49
	SIV 9_9	21.10.14 10:30	12.77	0.0001	6.55
	SIV 9_10	22.10.14 10:30	13.77	0.0000	
	SIV 9_11	23.10.14 10:30	14.77	0.0000	
	SIV 9_12	24.10.14 10:30	15.77	0.0001	6.51
	SIV 9_13	27.10.14 10:30	18.77	0.0000	
	SIV 9_14	28.10.14 10:30	19.77	0.0000	
	SIV 9_15	29.10.14 10:30	20.77	0.0000	
	SIV 9_16	30.10.14 10:30	21.77	0.0000	6.56

Annex 1 Table 4. Table 4 of the Electronic supplement of Chapter 3 – Results of Experimental series S*V*.

											Aqueous fluid composition - HR ICP-MS											
	date/ time	time [days]	biomass [g_{dry}/kg]	pH	DIC [ppm]	NPOC [ppm]	Si [ppb]	SD Si [ppb]	Al [ppb]	SD Al [ppb]	Ca [ppb]	SD Ca [ppb]	Mg [ppb]	SD Mg [ppb]	Mn [ppb]	SD Mn [ppb]	Fe [ppb]	SD Fe [ppb]	P [ppb]	SD P [ppb]
SV 1	**biot. ctrl.**																					
*SV*1_1	14.01.15 10:30	0		5.89	0.80	3.30																
*SV*1_2	14.01.15 16:30	0	0.0183	5.78	0.81	2.71	229.74	4.92	b.d.l.	0.11	294.39	2.37	371.01	1.63	26.33	0.12	38.91	0.06	185.23	1.81		
*SV*1_3	15.01.15 09:30	0.7	0.0179	5.86																		
*SV*1_4	16.01.15 09:15	1.7	0.0177	6.10	0.86	2.09																
*SV*1_5	18.01.15 09:30	3.7	0.0171	6.16			216.64	4.04	2.10	0.08	336.31	0.42	317.73	1.87	22.76	0.06	9.65	0.05	b.d.l.	0.20		
*SV*1_6	19.01.15 09:30	4.7	0.0169	6.19																		
*SV*1_7	20.01.15 09:40	5.7	0.0166	6.21																		
*SV*1_8	21.01.15 09:30	6.7	0.0163																			
*SV*1_9	22.01.15 09:35	7.7	0.0161																			
*SV*1_10	23.01.15 09:45	8.7	0.0157	6.30	0.79	3.13	202.49	4.38	1.34	0.03	363.53	1.40	335.88	0.50	24.09	0.09	6.44	0.05	7.90	0.10		
*SV*1_11	26.01.15 09:50	11.7	0.0139	6.37																		
*SV*1_12	27.01.15 09:40	12.7																				
*SV*1_13	29.01.15 09:30	14.7																				
*SV*1_14	30.01.15 09:30	15.7	0.0106	6.42	0.83	1.48	269.76	3.31	0.71	0.01	405.51	4.01	369.59	1.54	22.95	0.10	7.96	0.03	63.73	0.23		
*SV*1_15	02.02.15 09:30	18.7																				
*SV*1_16	04.02.15 09:30	20.7	0.0078	6.38																		
*SV*1_17	06.02.15 10:40	22.8																				
*SV*1_18	09.02.15 09:40	25.7																				
*SV*1_19	11.02.15 09:30	27.7	0.0053	6.57	0.69	1.45	173.53	2.14	0.52	0.02	432.10	3.26	411.85	3.69	24.83	0.07	16.24	0.10	166.16	2.86		
SV 2 **1500ICE**																						
*SV*2_1	14.01.15 10:30	0		5.81	0.87	2.86																
*SV*2_2	14.01.15 16:30	0	0.0167	6.35	0.97	2.89	143.78	1.14	15.31	0.02	956.19	5.26	378.07	3.79	17.12	0.13	34.82	0.44	144.40	0.81		
*SV*2_3	15.01.15 09:30	0.7	0.0167	6.74	1.23	3.25																
*SV*2_4	16.01.15 09:15	1.7	0.0170	6.75	1.63	3.21																
*SV*2_5	18.01.15 09:30	3.7	0.0210	7.62			804.46	5.43	45.96	0.11	1220.94	1.39	399.04	1.02	11.89	0.08	41.50	0.35	5.35	0.04		
*SV*2_6	19.01.15 09:30	4.7	0.0259	7.72																		
*SV*2_7	20.01.15 09:40	5.7	0.0344	8.83	2.41	2.57	1064.65	17.52	120.39	0.84	967.27	4.07	332.57	2.30	5.78	0.04	80.10	0.37	5.82	0.18		
*SV*2_8	21.01.15 09:30	6.7	0.0449	9.30																		
*SV*2_9	22.01.15 09:35	7.7	0.0552	9.51																		
*SV*2_10	23.01.15 09:45	8.7	0.0695	9.64	4.31	2.73	1938.90	2.94	388.31	0.52	510.45	1.84	157.31	0.95	2.32	0.02	87.49	0.62	6.66	0.25		
*SV*2_11	26.01.15 09:50	11.7	0.1148	9.98	6.36	5.24	3091.37	22.81	735.37	5.60	259.20	0.87	57.86	0.23	2.99	0.02	114.41	1.77	7.25	0.18		
*SV*2_12	27.01.15 09:40	12.7	0.1254	10.07																		
*SV*2_13	29.01.15 09:30	14.7	0.1299	8.73																		
*SV*2_14	30.01.15 09:30	15.7	0.1310	8.59	6.69	13.26	3549.18	10.92	463.59	1.22	234.27	0.66	67.36	0.13	3.08	0.01	116.16	0.30	10.75	0.29		
*SV*2_15	02.02.15 09:30	18.7	0.1338	8.21																		
*SV*2_16	04.02.15 09:30	20.7	0.1328	7.90	5.86	19.86																
*SV*2_17	06.02.15 10:40	22.8	0.1307	7.69			4011.90	97.44	345.83	0.98	250.89	0.92	138.58	0.76	7.17	0.06	251.09	5.32	18.78	0.27		
*SV*2_18	09.02.15 09:40	25.7	0.1306	7.75																		
*SV*2_19	11.02.15 09:30	27.7	0.1278	7.62	5.28	29.30	4360.15	7.47	287.43	1.39	339.29	1.63	171.95	0.55	8.88	0.05	265.80	3.71	24.01	0.18		
SV 3 **75ICE**																						
*SV*3_1	14.01.15 10:30	0		5.74																		
*SV*3_2	14.01.15 16:30	0	0.0180	5.78																		
*SV*3_3	15.01.15 09:30	0.7	0.0180	5.80																		
*SV*3_4	16.01.15 09:15	1.7	0.0174	5.89																		
*SV*3_5	18.01.15 09:30	3.7	0.0165	6.21																		
*SV*3_6	19.01.15 09:30	4.7	0.0156	6.29																		
*SV*3_7	20.01.15 09:40	5.7	0.0127	6.34																		
*SV*3_8	21.01.15 09:30	6.7	0.0099																			
*SV*3_9	22.01.15 09:35	7.7	0.0076																			
*SV*3_10	23.01.15 09:45	8.7	0.0058	6.44																		
*SV*3_11	26.01.15 09:50	11.7	0.0044	6.44																		
*SV*3_12	27.01.15 09:40	12.7																				
*SV*3_13	29.01.15 09:30	14.7																				

*SV*1, biotic control, BG11 1:1000

*SV*2, 1500 $mg_{/l}$ ICE, BG11 1:1000

*SV*3, 75 $mg_{/l}$ ICE, BG11 1:1000

Annex 1 Table 4. Continuation.

							Aqueous fluid composition - HR ICP-MS															
	date/ time	time [days]	biomass [g_{dw}/ kg]	pH	DIC [ppm]	NPOC [ppm]	Si [ppb]	SD Si [ppb]	Al [ppb]	SD Al [ppb]	Ca [ppb]	SD Ca [ppb]	Mg [ppb]	SD Mg [ppb]	Mn [ppb]	SD Mn [ppb]	Fe [ppb]	SD Fe [ppb]	P [ppb]	SD P [ppb]
	SV3_14	30.01.15 09:30	15.7	0.0040	6.50															
	SV3_15	02.02.15 09:30	18.7																	
	SV3_16	04.02.15 09:30	20.7	0.0040	6.50															
	SV3_17	06.02.15 10:40	22.8																	
	SV3_18	09.02.15 09:40	25.7																	
	SV3_19	11.02.15 09:30	27.7	0.0035	6.54															
SV 4 1500MS																				
SV 4, 1500 mg_{dw}/l MS, BG11 1:1000	*SV4_1*	14.01.15 10:30	0		5.88	0.99	2.59													
	SV4_2	14.01.15 16:30	0	0.0184	6.02	1.04	2.82	116.14	1.03	4.56	0.14	693.76	8.59	365.21	1.21	36.74	0.13	31.72	0.08	163.17	3.09
	SV4_3	15.01.15 09:30	0.7	0.0181	6.70	1.43	2.96														
	SV4_4	16.01.15 09:15	1.7	0.0187	7.20	2.61	2.52														
	SV4_5	18.01.15 09:30	3.7	0.0344	9.86			256.19	0.93	26.80	0.13	1220.75	2.01	516.21	1.74	3.42	0.04	15.02	0.08	2.09	0.06
	SV4_6	19.01.15 09:30	4.7	0.0466	10.17																
	SV4_7	20.01.15 09:40	5.7	0.0628	10.25	4.15	3.81	297.48	2.08	32.27	0.11	1019.11	8.62	432.29	1.19	2.19	0.01	16.37	0.19	b.d.l	0.12
	SV4_8	21.01.15 09:30	6.7	0.0795	10.47																
	SV4_9	22.01.15 09:35	7.7	0.0961	10.61																
	SV4_10	23.01.15 09:45	8.7	0.1124	10.58	7.09	2.47	376.11	0.82	28.65	0.61	344.13	2.24	96.28	0.16	1.40	0.02	11.48	0.12	b.d.l	0.09
	SV4_11	26.01.15 09:50	11.7	0.1277	8.34	8.50	2.96	352.77	0.86	10.61	0.08	320.58	1.11	421.92	0.10	2.89	0.02	4.48	0.03	1.67	0.04
	SV4_12	27.01.15 09:40	12.7	0.1293	8.46																
	SV4_13	29.01.15 09:30	14.7	0.1305	8.58																
	SV4_14	30.01.15 09:30	15.7	0.1305	8.70	8.81	2.91	374.60	2.26	12.53	0.19	355.59	2.47	673.77	3.73	3.74	0.03	2.48	0.08	b.d.l	0.19
	SV4_15	02.02.15 09:30	18.7	0.1347	8.58																
	SV4_16	04.02.15 09:30	20.7	0.1367	8.39	9.03	3.58														
	SV4_17	06.02.15 10:40	22.8	0.1369	8.12			386.07	3.55	10.09	0.13	217.63	1.17	843.54	2.54	6.67	0.08	4.20	0.07	1.61	0.04
	SV4_18	09.02.15 09:40	25.7	0.1396	8.01																
	SV4_19	11.02.15 09:30	27.7	0.1416	8.21	9.64	5.14	421.57	2.05	10.41	0.23	112.79	1.16	1025.4	3.59	9.95	0.10	4.53	0.19	b.d.l	0.19
SV 5 75MS																					
SV 5, 75 mg_{dw}/l MS, BG11 1:1000	*SV5_1*	14.01.15 10:30	0		5.78																
	SV5_2	14.01.15 16:30	0	0.0182	5.77																
	SV5_3	15.01.15 09:30	0.7	0.0179	5.95																
	SV5_4	16.01.15 09:15	1.7	0.0176	6.25																
	SV5_5	18.01.15 09:30	3.7	0.0170	6.35																
	SV5_6	19.01.15 09:30	4.7	0.0166	6.39																
	SV5_7	20.01.15 09:40	5.7	0.0162	6.38																
	SV5_8	21.01.15 09:30	6.7	0.0160																	
	SV5_9	22.01.15 09:35	7.7	0.0155																	
	SV5_10	23.01.15 09:45	8.7	0.0142	6.55																
	SV5_11	26.01.15 09:50	11.7	0.0130	6.58																
	SV5_12	27.01.15 09:40	12.7																		
	SV5_13	29.01.15 09:30	14.7																		
	SV5_14	30.01.15 09:30	15.7	0.0107	6.68																
	SV5_15	02.02.15 09:30	18.7																		
	SV5_16	04.02.15 09:30	20.7	0.0081	6.70																
	SV5_17	06.02.15 10:40	22.8																		
	SV5_18	09.02.15 09:40	25.7																		
	SV5_19	11.02.15 09:30	27.7	0.0073	6.86																
SV 6 1500ICE, abiot. Ctrl.																					
SV 6, abiotic control, 1500 mg_{dw}/l ICE, BG11 1:1000	*SV6_1*	14.01.15 10:30	0		5.89	0.84	2.87														
	SV6_2	14.01.15 16:30	0	0.0006	6.36	0.92	3.12	205.86	1.25	15.88	0.26	969.57	3.19	419.30	0.90	16.59	0.09	42.16	1.08	261.86	1.57
	SV6_3	15.01.15 09:30	0.7	0.0035	6.67																
	SV6_4	16.01.15 09:15	1.7	0.0058	6.64	1.20	3.97														
	SV6_5	18.01.15 09:30	3.7	0.0073	6.68			775.30	6.05	26.80	0.02	1342.48	12.83	502.95	3.00	16.64	0.06	33.67	0.19	183.99	0.61
	SV6_6	19.01.15 09:30	4.7	0.0063	6.84																
	SV6_7	20.01.15 09:40	5.7	0.0076	6.76			994.41	12.18	35.60	0.19	1435.41	6.42	527.37	2.67	17.31	0.04	42.15	0.57	175.58	1.58
	SV6_8	21.01.15 09:30	6.7	0.0070																	
	SV6_9	22.01.15 09:35	7.7	0.0095																	
	SV6_10	23.01.15 09:45	8.7	0.0089	6.89	1.28	3.77	1189.33	15.12	26.15	0.23	1478.34	4.93	542.11	3.31	17.75	0.04	30.43	1.34	157.08	2.29

Annex 1 Table 4. Continuation.

											Aqueous fluid composition - HR ICP-MS											
	date/ time	time [days]	biomass [g$_{dry}$/ kg]	pH	DIC [ppm]	NPOC [ppm]	Si [ppb]	SD Si [ppb]	Al [ppb]	SD Al [ppb]	Ca [ppb]	SD Ca [ppb]	Mg [ppb]	SD Mg [ppb]	Mn [ppb]	SD Mn [ppb]	Fe [ppb]	SD Fe [ppb]	P [ppb]	SD P [ppb]
	SY6_11	26.01.15 09:50	11.7	0.0085	6.87		1393.68	3.26	41.59	0.05	1533.71	5.12	558.81	4.53	18.74	0.05	43.88	0.31	144.31	0.94
	SY6_12	27.01.15 09:40	12.7	0.0089																
	SY6_13	29.01.15 09:30	14.7	0.0078																
	SY6_14	30.01.15 09:30	15.7	0.0095	6.95	1.44	2.10	1665.06	10.17	27.20	0.05	1575.07	16.56	567.20	2.29	17.89	0.09	28.12	0.40	132.35	0.31
	SY6_15	02.02.15 09:30	18.7	0.0087	6.91															
	SY6_16	04.02.15 09:30	20.7	0.0079	6.92															
	SY6_17	06.02.15 10:40	22.8	0.0081	6.91			1888.51	22.89	28.73	0.27	1652.41	9.87	588.80	3.81	18.80	0.10	29.22	0.35	114.78	0.59
	SY6_18	09.02.15 09:40	25.7	0.0084	6.97															
	SY6_19	11.02.15 09:30	27.7	0.0084	6.98	1.41	1.87	2221.04	7.61	52.85	0.23	1776.03	8.31	632.11	0.78	21.03	0.08	48.09	0.49	104.52	0.02
SY7 75ICE,	**abiot. Ctrl.**																				
	SY7_1	14.01.15 10:30	0		5.89																
	SY7_2	14.01.15 16:30	0	0.0000	5.89																
	SY7_3	15.01.15 09:30	0.7	0.0001	6.06																
	SY7_4	16.01.15 09:15	1.7	0.0001	6.13																
	SY7_5	18.01.15 09:30	3.7	0.0001	6.11																
	SY7_6	19.01.15 09:30	4.7	0.0001	6.17																
	SY7_7	20.01.15 09:40	5.7	0.0002	6.11																
	SY7_8	21.01.15 09:30	6.7	0.0001																	
	SY7_9	22.01.15 09:35	7.7	0.0003																	
	SY7_10	23.01.15 09:45	8.7	0.0003	6.18																
	SY7_11	26.01.15 09:50	11.7	0.0002	6.15																
	SY7_12	27.01.15 09:40	12.7	0.0000																	
	SY7_13	29.01.15 09:30	14.7	0.0000																	
	SY7_14	30.01.15 09:30	15.7	0.0001	6.21																
	SY7_15	02.02.15 09:30	18.7	0.0000																	
	SY7_16	04.02.15 09:30	20.7	0.0001	6.32																
	SY7_17	06.02.15 10:40	22.8	0.0000																	
	SY7_18	09.02.15 09:40	25.7	0.0000																	
	SY7_19	11.02.15 09:30	27.7	0.0001	6.42																
SY7, abiotic control, 75 mg/l ICE, BG11 1:1000																					
SY8 1500MS,	**abiot. Ctrl.**																				
	SY8_1	14.01.15 10:30	0		5.75	0.90	2.68														
	SY8_2	14.01.15 16:30	0	0.0003	5.96	0.80	3.05	225.05	0.34	3.93	0.13	802.73	4.96	360.72	2.83	35.03	0.08	26.46	0.01	264.84	2.53
	SY8_3	15.01.15 09:30	0.7	0.0010	6.68																
	SY8_4	16.01.15 09:15	1.7	0.0012	6.88	2.04	3.35														
	SY8_5	18.01.15 09:30	3.7	0.0014	7.09			322.54	0.92	20.41	0.20	1880.87	2.07	779.27	5.47	60.25	0.29	33.43	0.23	252.34	0.75
	SY8_6	19.01.15 09:30	4.7	0.0015	7.17																
	SY8_7	20.01.15 09:40	5.7	0.0015	7.20			356.44	1.94	36.07	0.44	2267.16	4.59	986.33	4.70	65.51	0.43	50.58	0.63	247.80	2.94
	SY8_8	21.01.15 09:30	6.7	0.0017																	
	SY8_9	22.01.15 09:35	7.7	0.0018																	
	SY8_10	23.01.15 09:45	8.7	0.0018	7.42	2.95	2.78	387.16	1.46	16.53	0.14	2845.49	10.80	1308.4	4.08	68.83	0.21	35.93	0.12	246.24	1.13
	SY8_11	26.01.15 09:50	11.7	0.0019	7.47			341.24	1.59	12.95	0.12	3259.45	7.55	1557.5	14.31	72.69	0.16	29.38	0.10	243.05	0.40
	SY8_12	27.01.15 09:40	12.7	0.0020	7.50																
	SY8_13	29.01.15 09:30	14.7	0.0021																	
	SY8_14	30.01.15 09:30	15.7	0.0022	7.61	3.81	2.20	368.36	2.83	17.08	0.12	3674.70	12.59	1809.3	15.33	71.71	0.22	21.63	0.23	236.20	1.06
	SY8_15	02.02.15 09:30	18.7	0.0022	7.59																
	SY8_16	04.02.15 09:30	20.7	0.0024	7.57																
	SY8_17	06.02.15 10:40	22.8	0.0023	7.57			325.34	5.14	7.23	0.04	4118.22	17.19	2088.7	9.61	73.14	0.17	14.60	0.12	275.51	0.44
	SY8_18	09.02.15 09:40	25.7	0.0026	7.56																
	SY8_19	11.02.15 09:30	27.7	0.0024	7.63	4.94	0.91	420.25	0.95	7.26	0.08	4566.51	15.83	2329.6	5.90	74.04	0.24	8.87	0.08	230.77	0.62
SY8, abiotic control, 1500 mg/l MS, BG11 1:1000																					
SY9 75MS,	**abiot. Ctrl.**																				
	SY9_1	14.01.15 10:30	0		5.72																
	SY9_2	14.01.15 16:30	0	0.0001	5.71																
	SY9_3	15.01.15 09:30	0.7	0.0000	5.94																
	SY9_4	16.01.15 09:15	1.7	0.0000	5.94																
	SY9_5	18.01.15 09:30	3.7	0.0000	6.25																
	SY9_6	19.01.15 09:30	4.7	0.0001	6.34																
	SY9_7	20.01.15 09:40	5.7	0.0001	6.35																
	SY9_8	21.01.15 09:30	6.7	0.0000																	
SY9, abiotic control, 75 mg/l MS, BG11																					

Annex 1 Table 4. Continuation.

	date/ time	time [days]	biomass [g$_{dw}$/kg]	pH	DIC [ppm]	NPOC [ppm]	Si [ppb]	SD Si [ppb]	Al [ppb]	SD Al [ppb]	Ca [ppb]	SD Ca [ppb]	Mg [ppb]	SD Mg [ppb]	Mn [ppb]	SD Mn [ppb]	Fe [ppb]	SD Fe [ppb]	P [ppb]	SD P [ppb]
								Aqueous fluid composition - HR ICP-MS												
*SV*9_9	22.01.15 09:35	7.7	0.0001																	
*SV*9_10	23.01.15 09:45	8.7	0.0001	6.47																
*SV*9_11	26.01.15 09:50	11.7	0.0001	6.48																
*SV*9_12	27.01.15 09:40	12.7																		
*SV*9_13	29.01.15 09:30	14.7																		
*SV*9_14	30.01.15 09:30	15.7	0.0000	6.56																
*SV*9_15	02.02.15 09:30	18.7																		
*SV*9_16	04.02.15 09:30	20.7	0.0001	6.53																
*SV*9_17	06.02.15 10:40	22.8																		
*SV*9_18	09.02.15 09:40	25.7																		
*SV*9_19	11.02.15 09:30	27.7	0.0000	6.69																
***SV*10 blank**																				
*SV*10_1	14.01.15 10:30	0		5.74																
*SV*10_2	14.01.15 16:30	0	0.0000	5.72			61.41	3.39	6.59	0.21	312.28	3.76	381.20	1.94	25.44	0.13	40.27	0.08	275.83	1.67
*SV*10_3	15.01.15 09:30	0.7	0.0001	5.79																
*SV*10_4	16.01.15 09:15	1.7	0.0000	5.79																
*SV*10_5	18.01.15 09:30	3.7	0.0001	5.78			67.50	0.49	1.64	0.15	297.51	2.56	382.65	0.80	23.90	0.08	6.93	0.43	263.70	1.87
*SV*10_6	19.01.15 09:30	4.7	0.0000	5.81																
*SV*10_7	20.01.15 09:40	5.7	0.0000	5.85																
*SV*10_8	21.01.15 09:30	6.7	0.0000																	
*SV*10_9	22.01.15 09:35	7.7	0.0001																	
*SV*10_10	23.01.15 09:45	8.7	0.0000	5.96			74.79	1.84	0.34	0.05	336.88	3.78	387.23	0.18	25.12	0.08	1.74	0.01	257.48	2.97
*SV*10_11	26.01.15 09:50	11.7	0.0001	6.01																
*SV*10_12	27.01.15 09:40	12.7	0.0000																	
*SV*10_13	29.01.15 09:30	14.7	0.0000																	
*SV*10_14	30.01.15 09:30	15.7	0.0001	6.09			91.43	1.46	0.53	0.10	297.03	0.70	387.44	2.65	25.26	0.16	1.24	0.02	251.51	2.08
*SV*10_15	02.02.15 09:30	18.7																		
*SV*10_16	04.02.15 09:30	20.7	0.0000	5.99																
*SV*10_17	06.02.15 10:40	22.8																		
*SV*10_18	09.02.15 09:40	25.7		6.08																
*SV*10_19	11.02.15 09:30	27.7	0.0000	6.17			101.07	2.07	0.52	0.02	352.80	3.48	395.54	0.86	25.79	0.34	0.76	0.03	250.32	1.12
***SV*10, blank, abiotic/no particulates, BG11 1:1000**																				

Annex 1 Table 5. Table 5 of the Electronic supplement of Chapter 3 – Results of Experimental series S*VI.*

		date/time	elapsed time [days]	biomass [g(dry)/kg]			date/time	elapsed time [days]	biomass [g(dry)/kg]
***SVb* 1 biot. Ctrl**									
***SVb* 1, biotic control, BG11 1:1000**	*SVb* 1_1	19.02.15 13:40	0.0	0.0189					
	SVb 1_2	20.02.15 09:35	0.8	0.0183					
	SVb 1_3	21.02.15 09:30	1.8	0.0172					
	SVb 1_4	23.02.15 09:35	3.8	0.0154					
	SVb 1_5	24.02.15 09:45	4.8	0.0147					
	SVb 1_6	25.02.15 09:45	5.8	0.0141					
	SVb 1_7	27.02.15 09:15	7.8	0.0131					
	SVb 1_8	02.03.15 09:30	10.8	0.0110					
	SVb 1_9	03.03.15 09:30	11.8	0.0103					
	SVb 1_10	04.03.15 09:40	12.8	0.0096					
	SVb 1_11	05.03.15 10:15	13.9	0.0089					
	SVb 1_12	06.03.15 09:20	14.8	0.0083					
	SVb 1_13	16.03.15 09:15	24.8	0.0042					
	SVb 1_14	17.03.15 09:40	25.8	0.0039					
	SVb 1_15	19.03.15 09:40	27.8	0.0035					
***SVb* 2 1500ICE**					***SVb* 4 1500MS**				
SVb 2, 1500 mg/l ICE, BG11 1:1000	*SVb* 2_1	19.02.15 13:40	0.0	0.0194	**SVb 4, 1500 mg/l MS, BG11 1:1000**	*SVb* 4_1	19.02.15 13:40	0.00	0.0190
	SVb 2_2	20.02.15 09:35	0.8	0.0214		*SVb* 4_2	20.02.15 09:35	0.83	0.0191
	SVb 2_3	21.02.15 09:30	1.8	0.0207		*SVb* 4_3	21.02.15 09:30	1.83	0.0191
	SVb 2_4	23.02.15 09:35	3.8	0.0225		*SVb* 4_4	23.02.15 09:35	3.83	0.0304
	SVb 2_5	24.02.15 09:45	4.8	0.0272		*SVb* 4_5	24.02.15 09:45	4.84	0.0504
	SVb 2_6	25.02.15 09:45	5.8	0.0393		*SVb* 4_6	25.02.15 09:45	5.84	0.0801
	SVb 2_7	27.02.15 09:15	7.8	0.0772		*SVb* 4_7	27.02.15 09:15	7.82	0.1319
	SVb 2_8	02.03.15 09:30	10.8	0.1396		*SVb* 4_8	02.03.15 09:30	10.83	0.1418
	SVb 2_9	03.03.15 09:30	11.8	0.1510		*SVb* 4_9	03.03.15 09:30	11.83	0.1429
	SVb 2_10	04.03.15 09:40	12.8	0.1569		*SVb* 4_10	04.03.15 09:40	12.83	0.1424
	SVb 2_11	05.03.15 10:15	13.9	0.1551		*SVb* 4_11	05.03.15 10:15	13.86	0.1461
	SVb 2_12	06.03.15 09:20	14.8	0.1561		*SVb* 4_12	06.03.15 09:20	14.82	0.1471
	SVb 2_13	16.03.15 09:15	24.8	0.1558		*SVb* 4_13	16.03.15 09:15	24.82	0.1574
	SVb 2_14	17.03.15 09:40	25.8	0.1559		*SVb* 4_14	17.03.15 09:40	25.83	0.1575
	SVb 2_15	19.03.15 09:40	27.8	0.1553		*SVb* 4_15	19.03.15 09:40	27.83	0.1594
***SVb* 3 1500ICE residual**					***SVb* 5 1500MS residual**				
***SVb* 3, residual FWSYN5 6, filtered, BG11 1:1000**	*SVb* 3_1	19.02.15 13:40	0.0	0.0185	***SVb* 5, residual FWSYN5 8, filtered, BG11 1:1000**	*SVb* 5_1	19.02.15 13:40	0.00	0.0188
	SVb 3_2	20.02.15 09:35	0.8	0.0181		*SVb* 5_2	20.02.15 09:35	0.83	0.0185
	SVb 3_3	21.02.15 09:30	1.8	0.0176		*SVb* 5_3	21.02.15 09:30	1.83	0.0184
	SVb 3_4	23.02.15 09:35	3.8	0.0182		*SVb* 5_4	23.02.15 09:35	3.83	0.0263
	SVb 3_5	24.02.15 09:45	4.8	0.0199		*SVb* 5_5	24.02.15 09:45	4.84	0.0342
	SVb 3_6	25.02.15 09:45	5.8	0.0247		*SVb* 5_6	25.02.15 09:45	5.84	0.0438
	SVb 3_7	27.02.15 09:15	7.8	0.0399		*SVb* 5_7	27.02.15 09:15	7.82	0.0630
	SVb 3_8	02.03.15 09:30	10.8	0.0603		*SVb* 5_8	02.03.15 09:30	10.83	0.0768
	SVb 3_9	03.03.15 09:30	11.8	0.0649		*SVb* 5_9	03.03.15 09:30	11.83	0.0774
	SVb 3_10	04.03.15 09:40	12.8	0.0657		*SVb* 5_10	04.03.15 09:40	12.83	0.0784
	SVb 3_11	05.03.15 10:15	13.9	0.0661		*SVb* 5_11	05.03.15 10:15	13.86	0.0787
	SVb 3_12	06.03.15 09:20	14.8	0.0669		*SVb* 5_12	06.03.15 09:20	14.82	0.0795
	SVb 3_13	16.03.15 09:15	24.8	0.0646		*SVb* 5_13	16.03.15 09:15	24.82	0.0783
	SVb 3_14	17.03.15 09:40	25.8	0.0643		*SVb* 5_14	17.03.15 09:40	25.83	0.0777
	SVb 3_15	19.03.15 09:40	27.8	0.0648		*SVb* 5_15	19.03.15 09:40	27.83	0.0771
***SVb* 6 1500ICE, abiot. Ctrl.**					***SVb* 7 1500MS, abiot. Ctrl.**				
***SVb* 6, abiotic control, 1500 mg/l ICE, BG11 1:1000**	*SVb* 6_1	19.02.15 13:40	0.0	0.0008	***SVb* 7, abiotic control, 1500 mg/l MS, BG11 1:1000**	*SVb* 7_1	19.02.15 13:40	0.00	0.0003
	SVb 6_2	20.02.15 09:35	0.8	0.0028		*SVb* 7_2	20.02.15 09:35	0.83	0.0005
	SVb 6_3	21.02.15 09:30	1.8	0.0033		*SVb* 7_3	21.02.15 09:30	1.83	0.0003
	SVb 6_4	23.02.15 09:35	3.8	0.0033		*SVb* 7_4	23.02.15 09:35	3.83	0.0005
	SVb 6_5	24.02.15 09:45	4.8	0.0029		*SVb* 7_5	24.02.15 09:45	4.84	0.0007
	SVb 6_6	25.02.15 09:45	5.8	0.0031		*SVb* 7_6	25.02.15 09:45	5.84	0.0005
	SVb 6_7	27.02.15 09:15	7.8	0.0023		*SVb* 7_7	27.02.15 09:15	7.82	0.0007
	SVb 6_8	02.03.15 09:30	10.8	0.0037		*SVb* 7_8	02.03.15 09:30	10.83	0.0007
	SVb 6_9	03.03.15 09:30	11.8	0.0033		*SVb* 7_9	03.03.15 09:30	11.83	0.0007
	SVb 6_10	04.03.15 09:40	12.8	0.0053		*SVb* 7_10	04.03.15 09:40	12.83	0.0008
	SVb 6_11	05.03.15 10:15	13.9	0.0034		*SVb* 7_11	05.03.15 10:15	13.86	0.0009
	SVb 6_12	06.03.15 09:20	14.8	0.0048		*SVb* 7_12	06.03.15 09:20	14.82	0.0009
	SVb 6_13	16.03.15 09:15	24.8	0.0064		*SVb* 7_13	16.03.15 09:15	24.82	0.0018
	SVb 6_14	17.03.15 09:40	25.8	0.0063		*SVb* 7_14	17.03.15 09:40	25.83	0.0017
	SVb 6_15	19.03.15 09:40	27.8	0.0069		*SVb* 7_15	19.03.15 09:40	27.83	0.0018

Annex 1 Table 6. Table 6 of the Electronic supplement of Chapter 3 – Results of Experimental series S*VII.*

		date/time	time [days]	biomass [$g_{(dry)}$/kg]	pH	Chl a [mg/l]			date/time	time [days]	biomass [$g_{(dry)}$/kg]	pH
***SVI* 1 biot. Ctrl., hpH, hOD**							***SVI* 4 blank, hpH**					
***SVI* 1, biotic control, BG11 1:1000 higher initial pH, hOD**	*SVI* 1_1	20.03.15 12:30	0.0		6.86		***SVI* 6, blank, abiotic/no particulates, BG11 1:1000 higher initial pH**	*SVI* 6_1	20.03.15 12:30	0.0		6.81
	SVI 1_2	20.03.15 12:30	0.0	0.0431	6.92			*SVI* 6_2	20.03.15 12:30	0.0		0.00
	SVI 1_3	23.03.15 09:45	2.9	0.0426	7.64	2.38		*SVI* 6_3	23.03.15 09:45	2.9		6.90
	SVI 1_4	24.03.15 09:40	3.9	0.0475	9.12			*SVI* 6_4	24.03.15 09:40	3.9		6.86
	SVI 1_5	25.03.15 09:30	4.9	0.0576	10.00	3.74		*SVI* 6_5	25.03.15 09:30	4.9		6.94
	SVI 1_6	26.03.15 09:45	5.9	0.0714	10.44			*SVI* 6_6	26.03.15 09:45	5.9		6.83
	SVI 1_7	27.03.15 09:45	6.9	0.0889	10.49	5.08		*SVI* 6_7	27.03.15 09:45	6.9		6.88
	SVI 1_8	30.03.15 09:50	9.9	0.1289	10.58			*SVI* 6_8	30.03.15 09:50	9.9		6.88
	SVI 1_9	31.03.15 09:35	10.9	0.1332	9.76	7.44		*SVI* 6_9	31.03.15 09:35	10.9		6.77
	SVI 1_10	02.04.15 09:35	12.9	0.1335	8.19	7.68		*SVI* 6_10	02.04.15 09:35	12.9		6.82
	SVI 1_11	03.04.15 09:20	13.9	0.1328	8.38			*SVI* 6_11	03.04.15 09:20	13.9		6.81
	SVI 1_12	06.04.15 09:55	16.9	0.1347	8.31	7.43		*SVI* 6_12	06.04.15 09:55	16.9		6.86
	SVI 1_13	07.04.15 09:30	17.9	0.1346	8.18			*SVI* 6_13	07.04.15 09:30	17.9		6.78
	SVI 1_14	09.04.15 09:30	19.9	0.1314	8.03	7.10		*SVI* 6_14	09.04.15 09:30	19.9		6.86
	SVI 1_15	10.04.15 09:35	20.9	0.1316	8.00	6.72		*SVI* 6_15	10.04.15 09:35	20.9		6.90
	SVI 1_16	13.04.15 09:35	23.9	0.1259	7.83	6.20		*SVI* 6_16	13.04.15 09:35	23.9		6.84
	SVI 1_17	15.04.15 09:30	25.9	0.1225	7.96	5.81		*SVI* 6_17	15.04.15 09:30	25.9		6.87
	SVI 1_18	17.04.15 09:40	27.9	0.1202	7.99			*SVI* 6_18	17.04.15 09:40	27.9		6.88
***SVI* 2 1500MS, hpH, hOD**							***SVI* 4 1500MS, abiot. Ctrl., hpH**					
***SVI* 2, 1500 mg/l MS, BG11 1:1000 higher initial pH, hOD**	*SVI* 2_1	20.03.15 12:30	0.0		6.82		***SVI* 4, abiotic control, 1500 mg/l MS, BG11 1:1000 higher initial pH**	*SVI* 4_1	20.03.15 12:30	0.0		6.80
	SVI 2_2	20.03.15 12:30	0.0	0.0429	7.06			*SVI* 4_2	20.03.15 12:30	0.0	0.0001	6.90
	SVI 2_3	23.03.15 09:45	2.9	0.0473	9.25	2.74		*SVI* 4_3	23.03.15 09:45	2.9	0.0002	7.21
	SVI 2_4	24.03.15 09:40	3.9	0.0582	9.91			*SVI* 4_4	24.03.15 09:40	3.9	0.0003	7.23
	SVI 2_5	25.03.15 09:30	4.9	0.0743	10.47	4.46		*SVI* 4_5	25.03.15 09:30	4.9	0.0005	7.37
	SVI 2_6	26.03.15 09:45	5.9	0.0868	10.64			*SVI* 4_6	26.03.15 09:45	5.9	0.0008	7.35
	SVI 2_7	27.03.15 09:45	6.9	0.1030	10.75	6.00		*SVI* 4_7	27.03.15 09:45	6.9	0.0009	7.44
	SVI 2_8	30.03.15 09:50	9.9	0.1530	10.77			*SVI* 4_8	30.03.15 09:50	9.9	0.0010	7.52
	SVI 2_9	31.03.15 09:35	10.9	0.1591	10.70	8.98		*SVI* 4_9	31.03.15 09:35	10.9	0.0010	7.49
	SVI 2_10	02.04.15 09:35	12.9	0.1621	9.05	8.49		*SVI* 4_10	02.04.15 09:35	12.9	0.0012	7.59
	SVI 2_11	03.04.15 09:20	13.9	0.1628	8.91			*SVI* 4_11	03.04.15 09:20	13.9	0.0013	7.56
	SVI 2_12	06.04.15 09:55	16.9	0.1671	8.73	8.98		*SVI* 4_12	06.04.15 09:55	16.9	0.0015	7.61
	SVI 2_13	07.04.15 09:30	17.9	0.1718	8.69			*SVI* 4_13	07.04.15 09:30	17.9	0.0015	7.56
	SVI 2_14	09.04.15 09:30	19.9	0.1727	8.57	8.69		*SVI* 4_14	09.04.15 09:30	19.9	0.0016	7.65
	SVI 2_15	10.04.15 09:35	20.9	0.1733	8.45	8.83		*SVI* 4_15	10.04.15 09:35	20.9	0.0018	7.66
	SVI 2_16	13.04.15 09:35	23.9	0.1749	8.28	8.66		*SVI* 4_16	13.04.15 09:35	23.9	0.0021	7.69
	SVI 2_17	15.04.15 09:30	25.9	0.1759	8.42	8.80		*SVI* 4_17	15.04.15 09:30	25.9	0.0023	7.74
	SVI 2_18	17.04.15 09:40	27.9	0.1783	8.41			*SVI* 4_18	17.04.15 09:40	27.9	0.0024	7.75
***SVI* 3 75MS, hpH, hOD**							***SVI* 5 75MS, abiot. Ctrl., hpH**					
***SVI* 3, 75 mg/l MS, BG11 1:1000 higher initial pH, hOD**	*SVI* 3_1	20.03.15 12:30	0.0		6.78		***SVI* 5, abiotic control, 75 mg/l MS, BG11 1:1000 higher initial pH**	*SVI* 5_1	20.03.15 12:30	0.0		6.82
	SVI 3_2	20.03.15 12:30	0.0	0.0429	6.86			*SVI* 5_2	20.03.15 12:30	0.0	0.0000	6.87
	SVI 3_3	23.03.15 09:45	2.9	0.0420	8.53	2.25		*SVI* 5_3	23.03.15 09:45	2.9	0.0000	6.92
	SVI 3_4	24.03.15 09:40	3.9	0.0489	9.91			*SVI* 5_4	24.03.15 09:40	3.9	0.0000	6.90
	SVI 3_5	25.03.15 09:30	4.9	0.0582	10.30	3.44		*SVI* 5_5	25.03.15 09:30	4.9	0.0000	6.98
	SVI 3_6	26.03.15 09:45	5.9	0.0731	10.46			*SVI* 5_6	26.03.15 09:45	5.9	0.0000	6.91
	SVI 3_7	27.03.15 09:45	6.9	0.0928	10.64	5.35		*SVI* 5_7	27.03.15 09:45	6.9	0.0000	6.96
	SVI 3_8	30.03.15 09:50	9.9	0.1342	9.88			*SVI* 5_8	30.03.15 09:50	9.9	0.0011	6.89
	SVI 3_9	31.03.15 09:35	10.9	0.1400	10.12	8.18		*SVI* 5_9	31.03.15 09:35	10.9	0.0006	6.81
	SVI 3_10	02.04.15 09:35	12.9	0.1405	8.58	8.12		*SVI* 5_10	02.04.15 09:35	12.9	0.0003	6.83
	SVI 3_11	03.04.15 09:20	13.9	0.1405	8.48			*SVI* 5_11	03.04.15 09:20	13.9	0.0003	6.81
	SVI 3_12	06.04.15 09:55	16.9	0.1418	8.18	7.87		*SVI* 5_12	06.04.15 09:55	16.9	0.0002	6.85
	SVI 3_13	07.04.15 09:30	17.9	0.1419	8.14			*SVI* 5_13	07.04.15 09:30	17.9	0.0003	6.75
	SVI 3_14	09.04.15 09:30	19.9	0.1399	8.11	7.64		*SVI* 5_14	09.04.15 09:30	19.9	0.0003	6.85
	SVI 3_15	10.04.15 09:35	20.9	0.1394	8.09	7.50		*SVI* 5_15	10.04.15 09:35	20.9	0.0002	6.90
	SVI 3_16	13.04.15 09:35	23.9	0.1365	7.94	7.46		*SVI* 5_16	13.04.15 09:35	23.9	0.0002	6.88
	SVI 3_17	15.04.15 09:30	25.9	0.1356	8.06	7.21		*SVI* 5_17	15.04.15 09:30	25.9	0.0002	6.94
	SVI 3_18	17.04.15 09:40	27.9	0.1332	8.10			*SVI* 5_18	17.04.15 09:40	27.9	0.0002	7.11
***SVI* 7 1000MS, hpH, hOD**							***SVI* 14 1000, abiot. Ctrl., hpH**					
***SVI* 7, 1000 mg/l MS, BG11 1:1000 higher initial pH, hOD**	*SVI* 7_1	20.03.15 12:30	0.0				***SVI* 14, 1000 mg/l MS, abiotic control, BG11 1:1000 higher initial pH**	*SVI* 14_1	20.03.15 12:30	0.0		
	SVI 7_2	20.03.15 12:30	0.0	0.0424				*SVI* 14_2	20.03.15 12:30	0.0	0.0001	
	SVI 7_3	23.03.15 09:45	2.9	0.0452				*SVI* 14_3	23.03.15 09:45	2.9	0.0004	
	SVI 7_4	24.03.15 09:40	3.9	0.0568				*SVI* 14_4	24.03.15 09:40	3.9	0.0004	
	SVI 7_5	25.03.15 09:30	4.9	0.0743				*SVI* 14_5	25.03.15 09:30	4.9	0.0004	
	SVI 7_6	26.03.15 09:45	5.9	0.0976				*SVI* 14_6	26.03.15 09:45	5.9	0.0005	
	SVI 7_7	27.03.15 09:45	6.9	0.1220				*SVI* 14_7	27.03.15 09:45	6.9	0.0005	
	SVI 7_8	30.03.15 09:50	9.9	0.1572				*SVI* 14_8	30.03.15 09:50	9.9	0.0006	
	SVI 7_9	31.03.15 09:35	10.9	0.1591				*SVI* 14_9	31.03.15 09:35	10.9	0.0006	
	SVI 7_10	02.04.15 09:35	12.9	0.1588				*SVI* 14_10	02.04.15 09:35	12.9	0.0007	
	SVI 7_11	03.04.15 09:20	13.9	0.1588				*SVI* 14_11	03.04.15 09:20	13.9	0.0007	
	SVI 7_12	06.04.15 09:55	16.9	0.1599				*SVI* 14_12	06.04.15 09:55	16.9	0.0007	
	SVI 7_13	07.04.15 09:30	17.9	0.1613				*SVI* 14_13	07.04.15 09:30	17.9	0.0008	
	SVI 7_14	09.04.15 09:30	19.9	0.1611				*SVI* 14_14	09.04.15 09:30	19.9	0.0009	
	SVI 7_15	10.04.15 09:35	20.9	0.1613				*SVI* 14_15	10.04.15 09:35	20.9	0.0009	
	SVI 7_16	13.04.15 09:35	23.9	0.1605				*SVI* 14_16	13.04.15 09:35	23.9	0.0011	
	SVI 7_17	15.04.15 09:30	25.9	0.1595				*SVI* 14_17	15.04.15 09:30	25.9	0.0013	

Annex 1 Table 6. Continuation.

		date/time	time [days]	biomass [$g_{(dry)}$/kg]	pH	Chl a [mg/l]
	SVI 7_18	17.04.15 09:40	27.9	0.1589		
***SVI* 8 500MS, hpH, hOD**						
***SVI* 8, 500 mg/l MS, BG11 1:1000 higher initial pH, hOD**	*SVI* 8_1	20.03.15 12:30	0.0			
	SVI 8_2	20.03.15 12:30	0.0	0.0426		
	SVI 8_3	23.03.15 09:45	2.9	0.0419		
	SVI 8_4	24.03.15 09:40	3.9	0.0498		
	SVI 8_5	25.03.15 09:30	4.9	0.0637		
	SVI 8_6	26.03.15 09:45	5.9	0.0840		
	SVI 8_7	27.03.15 09:45	6.9	0.1073		
	SVI 8_8	30.03.15 09:50	9.9	0.1534		
	SVI 8_9	31.03.15 09:35	10.9	0.1545		
	SVI 8_10	02.04.15 09:35	12.9	0.1551		
	SVI 8_11	03.04.15 09:20	13.9	0.1553		
	SVI 8_12	06.04.15 09:55	16.9	0.1555		
	SVI 8_13	07.04.15 09:30	17.9	0.1573		
	SVI 8_14	09.04.15 09:30	19.9	0.1555		
	SVI 8_15	10.04.15 09:35	20.9	0.1554		
	SVI 8_16	13.04.15 09:35	23.9	0.1538		
	SVI 8_17	15.04.15 09:30	25.9	0.1546		
	SVI 8_18	17.04.15 09:40	27.9	0.1538		
***SVI* 9 1000MS, hpH, mOD**						
***SVI* 9, 1000 mg/l MS, BG11 1:1000 higher initial pH, mOD**	*SVI* 9_1	20.03.15 12:30	0.0			
	SVI 9_2	20.03.15 12:30	0.0	0.0183		
	SVI 9_3	23.03.15 09:45	2.9	0.0190		
	SVI 9_4	24.03.15 09:40	3.9	0.0230		
	SVI 9_5	25.03.15 09:30	4.9	0.0315		
	SVI 9_6	26.03.15 09:45	5.9	0.0460		
	SVI 9_7	27.03.15 09:45	6.9	0.0644		
	SVI 9_8	30.03.15 09:50	9.9	0.1233		
	SVI 9_9	31.03.15 09:35	10.9	0.1354		
	SVI 9_10	02.04.15 09:35	12.9	0.1401		
	SVI 9_11	03.04.15 09:20	13.9	0.1400		
	SVI 9_12	06.04.15 09:55	16.9	0.1421		
	SVI 9_13	07.04.15 09:30	17.9	0.1413		
	SVI 9_14	09.04.15 09:30	19.9	0.1405		
	SVI 9_15	10.04.15 09:35	20.9	0.1415		
	SVI 9_16	13.04.15 09:35	23.9	0.1444		
	SVI 9_17	15.04.15 09:30	25.9	0.1445		
	SVI 9_18	17.04.15 09:40	27.9	0.1471		
***SVI* 11 1500MS, hpH, lOD**						
***SVI* 11, 1500 mg/l MS, BG11 1:1000 higher initial pH, lOD**	*SVI* 11_1	20.03.15 12:30	0.0			
	SVI 11_2	20.03.15 12:30	0.0	0.0069		
	SVI 11_3	23.03.15 09:45	2.9	0.0079		
	SVI 11_4	24.03.15 09:40	3.9	0.0104		
	SVI 11_5	25.03.15 09:30	4.9	0.0162		
	SVI 11_6	26.03.15 09:45	5.9	0.0263		
	SVI 11_7	27.03.15 09:45	6.9	0.0421		
	SVI 11_8	30.03.15 09:50	9.9	0.1040		
	SVI 11_9	31.03.15 09:35	10.9	0.1224		
	SVI 11_10	02.04.15 09:35	12.9	0.1299		
	SVI 11_11	03.04.15 09:20	13.9	0.1301		
	SVI 11_12	06.04.15 09:55	16.9	0.1321		
	SVI 11_13	07.04.15 09:30	17.9	0.1322		
	SVI 11_14	09.04.15 09:30	19.9	0.1329		
	SVI 11_15	10.04.15 09:35	20.9	0.1346		
	SVI 11_16	13.04.15 09:35	23.9	0.1386		
	SVI 11_17	15.04.15 09:30	25.9	0.1399		
	SVI 11_18	17.04.15 09:40	27.9	0.1424		
***SVI* 13 500MS, hpH, lOD**						
***SVI* 13, 500 mg/l MS, BG11 1:1000 higher initial pH, lOD**	*SVI* 13_1	20.03.15 12:30	0.0			
	SVI 13_2	20.03.15 12:30	0.0	0.0068		
	SVI 13_3	23.03.15 09:45	2.9	0.0064		
	SVI 13_4	24.03.15 09:40	3.9	0.0066		
	SVI 13_5	25.03.15 09:30	4.9	0.0080		
	SVI 13_6	26.03.15 09:45	5.9	0.0112		
	SVI 13_7	27.03.15 09:45	6.9	0.0172		
	SVI 13_8	30.03.15 09:50	9.9	0.0589		
	SVI 13_9	31.03.15 09:35	10.9	0.0788		
	SVI 13_10	02.04.15 09:35	12.9	0.1133		
	SVI 13_11	03.04.15 09:20	13.9	0.1174		
	SVI 13_12	06.04.15 09:55	16.9	0.1186		
	SVI 13_13	07.04.15 09:30	17.9	0.1196		
	SVI 13_14	09.04.15 09:30	19.9	0.1189		
	SVI 13_15	10.04.15 09:35	20.9	0.1182		
	SVI 13_16	13.04.15 09:35	23.9	0.1185		
***SVI* 15 500, abiot. Ctrl., hpH**						
***SVI* 15, 500 mg/l MS, abiotic control, BG11 1:1000 higher initial pH**	*SVI* 15_1	20.03.15 12:30	0.0			
	SVI 15_2	20.03.15 12:30	0.0	0.0001		
	SVI 15_3	23.03.15 09:45	2.9	0.0002		
	SVI 15_4	24.03.15 09:40	3.9	0.0002		
	SVI 15_5	25.03.15 09:30	4.9	0.0002		
	SVI 15_6	26.03.15 09:45	5.9	0.0003		
	SVI 15_7	27.03.15 09:45	6.9	0.0003		
	SVI 15_8	30.03.15 09:50	9.9	0.0004		
	SVI 15_9	31.03.15 09:35	10.9	0.0003		
	SVI 15_10	02.04.15 09:35	12.9	0.0004		
	SVI 15_11	03.04.15 09:20	13.9	0.0005		
	SVI 15_12	06.04.15 09:55	16.9	0.0005		
	SVI 15_13	07.04.15 09:30	17.9	0.0006		
	SVI 15_14	09.04.15 09:30	19.9	0.0006		
	SVI 15_15	10.04.15 09:35	20.9	0.0006		
	SVI 15_16	13.04.15 09:35	23.9	0.0008		
	SVI 15_17	15.04.15 09:30	25.9	0.0009		
	SVI 15_18	17.04.15 09:40	27.9	0.0008		
SVI 10 500MS, hpH, mOD						
***SVI* 10, 500 mg/l MS, BG11 1:1000 higher initial pH, mOD**	*SVI* 10_1	20.03.15 12:30	0.0			
	SVI 10_2	20.03.15 12:30	0.0	0.0184		
	SVI 10_3	23.03.15 09:45	2.9	0.0180		
	SVI 10_4	24.03.15 09:40	3.9	0.0198		
	SVI 10_5	25.03.15 09:30	4.9	0.0251		
	SVI 10_6	26.03.15 09:45	5.9	0.0352		
	SVI 10_7	27.03.15 09:45	6.9	0.0513		
	SVI 10_8	30.03.15 09:50	9.9	0.1067		
	SVI 10_9	31.03.15 09:35	10.9	0.1265		
	SVI 10_10	02.04.15 09:35	12.9	0.1323		
	SVI 10_11	03.04.15 09:20	13.9	0.1322		
	SVI 10_12	06.04.15 09:55	16.9	0.1332		
	SVI 10_13	07.04.15 09:30	17.9	0.1342		
	SVI 10_14	09.04.15 09:30	19.9	0.1334		
	SVI 10_15	10.04.15 09:35	20.9	0.1330		
	SVI 10_16	13.04.15 09:35	23.9	0.1318		
	SVI 10_17	15.04.15 09:30	25.9	0.1324		
	SVI 10_18	17.04.15 09:40	27.9	0.1325		
***SVI 12* 1000MS, hpH, lOD**						
***SVI* 12, 1000 mg/l MS, BG11 1:1000 higher initial pH, lOD**	*SVI* 12_1	20.03.15 12:30	0.0			
	SVI 12_2	20.03.15 12:30	0.0	0.0068		
	SVI 12_3	23.03.15 09:45	2.9	0.0068		
	SVI 12_4	24.03.15 09:40	3.9	0.0074		
	SVI 12_5	25.03.15 09:30	4.9	0.0092		
	SVI 12_6	26.03.15 09:45	5.9	0.0138		
	SVI 12_7	27.03.15 09:45	6.9	0.0216		
	SVI 12_8	30.03.15 09:50	9.9	0.0679		
	SVI 12_9	31.03.15 09:35	10.9	0.0889		
	SVI 12_10	02.04.15 09:35	12.9	0.1368		
	SVI 12_11	03.04.15 09:20	13.9	0.1516		
	SVI 12_12	06.04.15 09:55	16.9	0.1668		
	SVI 12_13	07.04.15 09:30	17.9	0.1661		
	SVI 12_14	09.04.15 09:30	19.9	0.1658		
	SVI 12_15	10.04.15 09:35	20.9	0.1663		
	SVI 12_16	13.04.15 09:35	23.9	0.1639		
	SVI 12_17	15.04.15 09:30	25.9	0.1634		
	SVI 12_18	17.04.15 09:40	27.9	0.1649		
***SVI* 16 biot. Ctrl., hN**						
***SVI* 16, biotic control, BG11 1:375**	*SVI* 16_1	20.03.15 12:30	0.0			
	SVI 16_2	20.03.15 12:30	0.0	0.0296		
	SVI 16_3	23.03.15 09:45	2.9	0.0265		
	SVI 16_4	24.03.15 09:40	3.9	0.0253		
	SVI 16_5	25.03.15 09:30	4.9	0.0250		
	SVI 16_6	26.03.15 09:45	5.9	0.0239		
	SVI 16_7	27.03.15 09:45	6.9	0.0233		
	SVI 16_8	30.03.15 09:50	9.9	0.0227		
	SVI 16_9	31.03.15 09:35	10.9	0.0233		
	SVI 16_10	02.04.15 09:35	12.9	0.0304		
	SVI 16_11	03.04.15 09:20	13.9	0.0392		
	SVI 16_12	06.04.15 09:55	16.9	0.1070		
	SVI 16_13	07.04.15 09:30	17.9	0.1374		
	SVI 16_14	09.04.15 09:30	19.9	0.1919		
	SVI 16_15	10.04.15 09:35	20.9	0.2164		
	SVI 16_16	13.04.15 09:35	23.9	0.2818		

Annex 1 Table 6. Continuation.

		date/time	time [days]	biomass [$g_{(dry)}$/kg]	pH	Chl a [mg/l]			date/time	time [days]	biomass [$g_{(dry)}$/kg]	pH
	SVI 13_17	15.04.15 09:30	25.9	0.1169				*SVI* 16_17	15.04.15 09:30	25.9	0.2865	
	SVI 13_18	17.04.15 09:40	27.9	0.1187				*SVI* 16_18	17.04.15 09:40	27.9	0.2852	
***SVI* 17 1500MS, hN**							***SVI* 17 1000MS, hN**					
	SVI 17_1	20.03.15 12:30	0.0					*SVI* 18_1	20.03.15 12:30	0.0		
	SVI 17_2	20.03.15 12:30	0.0	0.0311				*SVI* 18_2	20.03.15 12:30	0.0	0.0306	
	SVI 17_3	23.03.15 09:45	2.9	0.0350				*SVI* 18_3	23.03.15 09:45	2.9	0.0308	
	SVI 17_4	24.03.15 09:40	3.9	0.0461				*SVI* 18_4	24.03.15 09:40	3.9	0.0371	
	SVI 17_5	25.03.15 09:30	4.9	0.0644				*SVI* 18_5	25.03.15 09:30	4.9	0.0508	
	SVI 17_6	26.03.15 09:45	5.9	0.0884				*SVI* 18_6	26.03.15 09:45	5.9	0.0720	
	SVI 17_7	27.03.15 09:45	6.9	0.1185				*SVI* 18_7	27.03.15 09:45	6.9	0.0996	
	SVI 17_8	30.03.15 09:50	9.9	0.2266				*SVI* 18_8	30.03.15 09:50	9.9	0.2006	
	SVI 17_9	31.03.15 09:35	10.9	0.2675				*SVI* 18_9	31.03.15 09:35	10.9	0.2443	
	SVI 17_10	02.04.15 09:35	12.9	0.3261				*SVI* 18_10	02.04.15 09:35	12.9	0.3055	
	SVI 17_11	03.04.15 09:20	13.9	0.3235				*SVI* 18_11	03.04.15 09:20	13.9	0.3082	
	SVI 17_12	06.04.15 09:55	16.9	0.3430				*SVI* 18_12	06.04.15 09:55	16.9	0.3272	
	SVI 17_13	07.04.15 09:30	17.9	0.3462				*SVI* 18_13	07.04.15 09:30	17.9	0.3295	
	SVI 17_14	09.04.15 09:30	19.9	0.3460				*SVI* 18_14	09.04.15 09:30	19.9	0.3302	
	SVI 17_15	10.04.15 09:35	20.9	0.3443				*SVI* 18_15	10.04.15 09:35	20.9	0.3302	
	SVI 17_16	13.04.15 09:35	23.9	0.3439				*SVI* 18_16	13.04.15 09:35	23.9	0.3270	
	SVI 17_17	15.04.15 09:30	25.9	0.3435				*SVI* 18_17	15.04.15 09:30	25.9	0.3229	
	SVI 17_18	17.04.15 09:40	27.9	0.3441				*SVI* 18_18	17.04.15 09:40	27.9	0.3200	
***SVI* 19 500MS, hN**							***SVI* 20 75MS, hN**					
	SVI 19_1	20.03.15 12:30	0.0					*SVI* 20_1	20.03.15 12:30	0.0		
	SVI 19_2	20.03.15 12:30	0.0	0.0304				*SVI* 20_2	20.03.15 12:30	0.0	0.0301	
	SVI 19_3	23.03.15 09:45	2.9	0.0284				*SVI* 20_3	23.03.15 09:45	2.9	0.0278	
	SVI 19_4	24.03.15 09:40	3.9	0.0302				*SVI* 20_4	24.03.15 09:40	3.9	0.0268	
	SVI 19_5	25.03.15 09:30	4.9	0.0377				*SVI* 20_5	25.03.15 09:30	4.9	0.0262	
	SVI 19_6	26.03.15 09:45	5.9	0.0529				*SVI* 20_6	26.03.15 09:45	5.9	0.0266	
	SVI 19_7	27.03.15 09:45	6.9	0.0759				*SVI* 20_7	27.03.15 09:45	6.9	0.0282	
	SVI 19_8	30.03.15 09:50	9.9	0.1683				*SVI* 20_8	30.03.15 09:50	9.9	0.0531	
	SVI 19_9	31.03.15 09:35	10.9	0.2083				*SVI* 20_9	31.03.15 09:35	10.9	0.0721	
	SVI 19_10	02.04.15 09:35	12.9	0.2749				*SVI* 20_10	02.04.15 09:35	12.9	0.1311	
	SVI 19_11	03.04.15 09:20	13.9	0.2989				*SVI* 20_11	03.04.15 09:20	13.9	0.1679	
	SVI 19_12	06.04.15 09:55	16.9	0.3226				*SVI* 20_12	06.04.15 09:55	16.9	0.2553	
	SVI 19_13	07.04.15 09:30	17.9	0.3243				*SVI* 20_13	07.04.15 09:30	17.9	0.2767	
	SVI 19_14	09.04.15 09:30	19.9	0.3274				*SVI* 20_14	09.04.15 09:30	19.9	0.2963	
	SVI 19_15	10.04.15 09:35	20.9	0.3274				*SVI* 20_15	10.04.15 09:35	20.9	0.3017	
	SVI 19_16	13.04.15 09:35	23.9	0.3258				*SVI* 20_16	13.04.15 09:35	23.9	0.3027	
	SVI 19_17	15.04.15 09:30	25.9	0.3226				*SVI* 20_17	15.04.15 09:30	25.9	0.3003	
	SVI 19_18	17.04.15 09:40	27.9	0.3196				*SVI* 20_18	17.04.15 09:40	27.9	0.2996	

Annex 1 Table 7. Table 7 of the Electronic supplement of Chapter 3 – Results of Experimental series S*VII*.

SVII 1 biot. Ctrl., hpH, lOD						*SVII* 2 biot. Ctrl., hpH, mOD						*SVII* 3 biot. Ctrl., hpH, hOD					
SVII 1, biotic control, BG11 1:1000, high initial pH, lOD	date/time	time [days]	biomass [g_{dry}/kg]	pH	IS [µS/cm]	*SVII* 2, biotic control, BG11 1:1000, high initial pH, mOD	date/time	time [days]	biomass [g_{dry}/kg]	pH	IS [µS/cm]	*SVII* 3, biotic control, BG11 1:1000, high initial pH, hOD	date/time	time [days]	biomass [g_{dry}/kg]	pH	IS [µS/cm]
SVII 1_0	12.05.15 16:30	-0.8		7.43	133	*SVII* 2_0	12.05.15 16:30	-0.8		7.60	129	*SVII* 3_0	12.05.15 16:30	-0.8		7.64	130
SVII 1_1	13.05.15 10:30	0.0	0.0067	7.69	134	*SVII* 2_1	13.05.15 10:30	0.0	0.0183	7.96	135	*SVII* 3_1	13.05.15 10:30	0.0	0.0420	8.38	133
SVII 1_2	15.05.15 09:35	2.0	0.0137	8.36	126	*SVII* 2_2	15.05.15 09:35	2.0	0.0377	9.63	131	*SVII* 3_2	15.05.15 09:35	2.0	0.0696	10.08	140
SVII 1_3	17.05.15 09:30	4.0	0.0340	9.32	133	*SVII* 2_3	17.05.15 09:30	4.0	0.0722	9.67	134	*SVII* 3_3	17.05.15 09:30	4.0	0.1046	9.68	126
SVII 1_4	18.05.15 09:20	5.0	0.0460			*SVII* 2_4	18.05.15 09:20	5.0	0.0815			*SVII* 3_4	18.05.15 09:20	5.0	0.1137		
SVII 1_5	19.05.15 09:45	6.0	0.0595	9.44	133	*SVII* 2_5	19.05.15 09:45	6.0	0.0897	9.41	126	*SVII* 3_5	19.05.15 09:45	6.0	0.1210	9.21	119
SVII 1_6	20.05.15 09:30	7.0	0.0675			*SVII* 2_6	20.05.15 09:30	7.0	0.0948			*SVII* 3_6	20.05.15 09:30	7.0	0.1256		
SVII 1_7	21.05.15 09:40	8.0	0.0752	9.28	124	*SVII* 2_7	21.05.15 09:40	8.0	0.0976	8.76	112	*SVII* 3_7	21.05.15 09:40	8.0	0.1277	8.71	112
SVII 1_8	22.05.15 09:35	9.0	0.0787	8.50	112	*SVII* 2_8	22.05.15 09:35	9.0	0.0994	8.48	112	*SVII* 3_8	22.05.15 09:35	9.0	0.1266	8.46	112
SVII 1_9	26.05.15 09:40	13.0	0.0815	7.95	113	*SVII* 2_9	26.05.15 09:40	13.0	0.0971	8.13	112	*SVII* 3_9	26.05.15 09:40	13.0	0.1254	8.17	110
SVII 1_10	27.05.15 09:45	14.0	0.0810	8.25		*SVII* 2_10	27.05.15 09:45	14.0	0.0963	8.21		*SVII* 3_10	27.05.15 09:45	14.0	0.1235	8.23	
SVII 1_11	29.05.15 09:25	16.0	0.0790	7.90	116	*SVII* 2_11	29.05.15 09:25	16.0	0.0945	7.96	113.5	*SVII* 3_11	29.05.15 09:25	16.0	0.1207	8.03	110
SVII 1_12	01.06.15 09:25	19.0	0.0750	7.85	120	*SVII* 2_12	01.06.15 09:25	19.0	0.0899	7.95	117	*SVII* 3_12	01.06.15 09:25	19.0	0.1162	8.03	117
SVII 1_13	03.06.15 09:45	21.0	0.0715	8.27		*SVII* 2_13	03.06.15 09:45	21.0	0.0869	8.27		*SVII* 3_13	03.06.15 09:45	21.0	0.1150	8.27	
SVII 1_14	05.06.15 09:40	23.0	0.0688	7.94	119	*SVII* 2_14	05.06.15 09:40	23.0	0.0848	8.14	119	*SVII* 3_14	05.06.15 09:40	23.0	0.1104	8.08	116
SVII 1_15	09.06.15 09:35	27.0	0.0646	7.95	123	*SVII* 2_15	09.06.15 09:35	27.0	0.0822	8.05	122	*SVII* 3_15	09.06.15 09:35	27.0	0.1058	8.09	119
SVII 4 biot. Ctrl., hIS, lOD						*SVII* 5 biot. Ctrl., hIS, mOD						*SVII* 6 biot. Ctrl., hIS, hOD					
SVII 4, biotic control, BG11 1:1000, high initial IS, lOD	date/time	time [days]	biomass [g_{dry}/kg]	pH	IS [µS/cm]	*SVII* 5, biotic control, BG11 1:1000, high initial IS, mOD	date/time	time [days]	biomass [g_{dry}/kg]	pH	IS [µS/cm]	*SVII* 6, biotic control, BG11 1:1000, high initial IS, hOD	date/time	time [days]	biomass [g_{dry}/kg]	pH	IS [µS/cm]
SVII 4_0	12.05.15 16:30	-0.8		6.01	649	*SVII* 5_0	12.05.15 16:30	-0.8		6.03	649	*SVII* 6_0	12.05.15 16:30	-0.8		6.02	651
SVII 4_1	13.05.15 10:30	0.0	0.0068	6.05	659	*SVII* 5_1	13.05.15 10:30	0.0	0.0185	6.04	644	*SVII* 6_1	13.05.15 10:30	0.0	0.0422	5.85	650
SVII 4_2	15.05.15 09:35	2.0	0.0067	6.01	589	*SVII* 5_2	15.05.15 09:35	2.0	0.0182	5.96	590	*SVII* 6_2	15.05.15 09:35	2.0	0.0404		575
SVII 4_3	17.05.15 09:30	4.0	0.0059	6.26	655	*SVII* 5_3	17.05.15 09:30	4.0	0.0169	6.24	641	*SVII* 6_3	17.05.15 09:30	4.0	0.0379	6.17	651
SVII 4_4	18.05.15 09:20	5.0				*SVII* 5_4	18.05.15 09:20	5.0				*SVII* 6_4	18.05.15 09:20	5.0	0.0373		
SVII 4_5	19.05.15 09:45	6.0	0.0046	6.14	639	*SVII* 5_5	19.05.15 09:45	6.0	0.0147	6.13	629	*SVII* 6_5	19.05.15 09:45	6.0	0.0350	6.17	630
SVII 4_6	20.05.15 09:30	7.0				*SVII* 5_6	20.05.15 09:30	7.0				*SVII* 6_6	20.05.15 09:30	7.0			
SVII 4_7	21.05.15 09:40	8.0	0.0038	6.05	642	*SVII* 5_7	21.05.15 09:40	8.0	0.0113	6.11	635	*SVII* 6_7	21.05.15 09:40	8.0	0.0309	6.27	636
SVII 4_8	22.05.15 09:35	9.0				*SVII* 5_8	22.05.15 09:35	9.0				*SVII* 6_8	22.05.15 09:35	9.0			
SVII 4_9	26.05.15 09:40	13.0	0.0022	6.06	644	*SVII* 5_9	26.05.15 09:40	13.0	0.0066	6.18	636	*SVII* 6_9	26.05.15 09:40	13.0	0.0231	6.29	634
SVII 4_10	27.05.15 09:45	14.0				*SVII* 5_10	27.05.15 09:45	14.0				*SVII* 6_10	27.05.15 09:45	14.0			
SVII 4_11	29.05.15 09:25	16.0				*SVII* 5_11	29.05.15 09:25	16.0				*SVII* 6_11	29.05.15 09:25	16.0	0.0194	6.36	641
SVII 4_12	01.06.15 09:25	19.0				*SVII* 5_12	01.06.15 09:25	19.0				*SVII* 6_12	01.06.15 09:25	19.0	0.0163	6.40	
SVII 4_13	03.06.15 09:45	21.0				*SVII* 5_13	03.06.15 09:45	21.0				*SVII* 6_13	03.06.15 09:45	21.0			
SVII 4_14	05.06.15 09:40	23.0	0.0017	6.11	681	*SVII* 5_14	05.06.15 09:40	23.0	0.0043	6.27	680	*SVII* 6_14	05.06.15 09:40	23.0	0.0133	6.44	674
SVII 4_15	09.06.15 09:35	27.0	0.0017	6.11	695	*SVII* 5_15	09.06.15 09:35	27.0	0.0041	6.23	685	*SVII* 6_15	09.06.15 09:35	27.0	0.0118	6.46	676
SVII 7 biot. Ctrl., hpH&hIS, lOD						*SVII* 8 biot. Ctrl., hpH&hIS, mOD						*SVII* 9 biot. Ctrl., hpH&hIS, hOD					
SVII 7, biotic control, BG11 1:1000, high initial pHxIS, lOD	date/time	time [days]	biomass [g_{dry}/kg]	pH	IS [µS/cm]	*SVII* 8, biotic control, BG11 1:1000, high initial pHxIS, mOD	date/time	time [days]	biomass [g_{dry}/kg]	pH	IS [µS/cm]	*SVII* 9, biotic control, BG11 1:1000, high initial pHxIS, hOD	date/time	time [days]	biomass [g_{dry}/kg]	pH	IS [µS/cm]
SVII 7_0	12.05.15 16:30	-0.8		7.55	534	*SVII* 8_0	12.05.15 16:30	-0.8		7.58	538	*SVII* 9_0	12.05.15 16:30	-0.8		7.75	537
SVII 7_1	13.05.15 10:30	0.0	0.0071			*SVII* 8_1	13.05.15 10:30	0.0	0.0181	8.05	536	*SVII* 9_1	13.05.15 10:30	0.0	0.0420	8.34	535
SVII 7_2	15.05.15 09:35	2.0	0.0133	7.87	543	*SVII* 8_2	15.05.15 09:35	2.0	0.0388	9.46	502	*SVII* 9_2	15.05.15 09:35	2.0	0.0724	9.90	477
SVII 7_3	17.05.15 09:30	4.0	0.0500	8.25	508	*SVII* 8_3	17.05.15 09:30	4.0	0.0919	10.39	501	*SVII* 9_3	17.05.15 09:30	4.0	0.1375	10.57	496
SVII 7_4	18.05.15 09:20	5.0	0.0747	9.50	494	*SVII* 8_4	18.05.15 09:20	5.0	0.1137			*SVII* 9_4	18.05.15 09:20	5.0	0.1508		
SVII 7_5	19.05.15 09:45	6.0	0.0978			*SVII* 8_5	19.05.15 09:45	6.0	0.1210	9.62	465	*SVII* 9_5	19.05.15 09:45	6.0	0.1570	9.90	450
SVII 7_6	20.05.15 09:30	7.0	0.1061	9.90	485	*SVII* 8_6	20.05.15 09:30	7.0	0.1248			*SVII* 9_6	20.05.15 09:30	7.0	0.1599		
SVII 7_7	21.05.15 09:40	8.0	0.1067			*SVII* 8_7	21.05.15 09:40	8.0	0.1242	8.24	461	*SVII* 9_7	21.05.15 09:40	8.0	0.1590	8.61	450
SVII 7_8	22.05.15 09:35	9.0	0.1064	7.96	465	*SVII* 8_8	22.05.15 09:35	9.0	0.1242	8.01	468	*SVII* 9_8	22.05.15 09:35	9.0	0.1601	8.42	454
SVII 7_9	26.05.15 09:40	13.0	0.1074	8.21	468	*SVII* 8_9	26.05.15 09:40	13.0	0.1205	8.12	472	*SVII* 9_9	26.05.15 09:40	13.0	0.1576	8.37	464
SVII 7_10	27.05.15 09:45	14.0	0.1072	7.97	476	*SVII* 8_10	27.05.15 09:45	14.0	0.1199	8.28		*SVII* 9_10	27.05.15 09:45	14.0	0.1527	8.27	
SVII 7_11	29.05.15 09:25	16.0	0.1070			*SVII* 8_11	29.05.15 09:25	16.0	0.1176	7.80	465	*SVII* 9_11	29.05.15 09:25	16.0	0.1529	7.85	468
SVII 7_12	01.06.15 09:25	19.0	0.1020	8.30	480	*SVII* 8_12	01.06.15 09:25	19.0	0.1148	7.86	496	*SVII* 9_12	01.06.15 09:25	19.0	0.1455	7.86	481
SVII 7_13	03.06.15 09:45	21.0	0.1007	7.81	505	*SVII* 8_13	03.06.15 09:45	21.0	0.1124	8.14		*SVII* 9_13	03.06.15 09:45	21.0	0.1406	8.08	
SVII 7_14	05.06.15 09:40	23.0	0.0986	8.15		*SVII* 8_14	05.06.15 09:40	23.0	0.1106	7.88	507	*SVII* 9_14	05.06.15 09:40	23.0	0.1384	7.90	490
SVII 7_15	09.06.15 09:35	27.0	0.0944	7.81	513	*SVII* 8_15	09.06.15 09:35	27.0	0.1067	8.04	512	*SVII* 9_15	09.06.15 09:35	27.0	0.1318	8.00	498

Annex 1 Table 7. Continuation.

		date/time	time [days]	biomass [g(dry)/kg]	pH	IS [µS/cm]
SVII 10 biot. Ctrl., lOD						
SVII 10, biotic control, BG11 1:1000, lOD	*SVII* 10_0	12.05.15 16:30	-0.8		6.08	97.8
	SVII 10_1	13.05.15 10:30	0.0	0.0068	6.12	102
	SVII 10_2	15.05.15 09:35	2.0	0.0065	6.34	97.2
	SVII 10_3	17.05.15 09:30	4.0	0.0059	6.59	94.5
	SVII 10_4	18.05.15 09:20	5.0			
	SVII 10_5	19.05.15 09:45	6.0	0.0050	6.33	96.2
	SVII 10_6	20.05.15 09:30	7.0			
	SVII 10_7	21.05.15 09:40	8.0	0.0041	6.23	98.2
	SVII 10_8	22.05.15 09:35	9.0			
	SVII 10_9	26.05.15 09:40	13.0	0.0026	6.25	100
	SVII 10_10	27.05.15 09:45	14.0			
	SVII 10_11	29.05.15 09:25	16.0			
	SVII 10_12	01.06.15 09:25	19.0			
	SVII 10_13	03.06.15 09:45	21.0			
	SVII 10_14	05.06.15 09:40	23.0	0.0019	6.25	105
	SVII 10_15	09.06.15 09:35	27.0	0.0018	6.21	107
SVII 13 1500MS, lOD						
SVII 13, BG11 1:1000, 1500 mg/l MS, lOD	*SVII* 13_0	12.05.15 16:30	-0.8		5.95	98
	SVII 13_1	13.05.15 10:30	0.0	0.0061	6.21	104
	SVII 13_2	15.05.15 09:35	2.0	0.0073	7.51	102
	SVII 13_3	17.05.15 09:30	4.0	0.0221	8.67	104
	SVII 13_4	18.05.15 09:20	5.0	0.0378		
	SVII 13_5	19.05.15 09:45	6.0	0.0616	9.48	105
	SVII 13_6	20.05.15 09:30	7.0	0.0884		
	SVII 13_7	21.05.15 09:40	8.0	0.1141	10.25	105
	SVII 13_8	22.05.15 09:35	9.0	0.1250	10.12	97.4
	SVII 13_9	26.05.15 09:40	13.0	0.1301	8.48	81.9
	SVII 13_10	27.05.15 09:45	14.0	0.1306	8.52	
	SVII 13_11	29.05.15 09:25	16.0	0.1351	8.35	80.8
	SVII 13_12	01.06.15 09:25	19.0	0.1378	8.24	86.8
	SVII 13_13	03.06.15 09:45	21.0	0.1421	8.26	
	SVII 13_14	05.06.15 09:40	23.0	0.1425	8.12	88.1
	SVII 13_15	09.06.15 09:35	27.0	0.1416	8.26	91.7
SVII 17 1500MS - burned, lOD						
SVII 17, BG11 1:1000, 1500 mg/l MS - burned, lOD	*SVII* 17_1	13.05.15 10:30	0.0	0.0057		
	SVII 17_2	15.05.15 09:35	2.0	0.0060		
	SVII 17_3	17.05.15 09:30	4.0	0.0105		
	SVII 17_4	18.05.15 09:20	5.0	0.0183		
	SVII 17_5	19.05.15 09:45	6.0	0.0350		
	SVII 17_6	20.05.15 09:30	7.0	0.0564		
	SVII 17_7	21.05.15 09:40	8.0	0.0835		
	SVII 17_8	22.05.15 09:35	9.0	0.1099		
	SVII 17_9	26.05.15 09:40	13.0	0.1263		
	SVII 17_10	27.05.15 09:45	14.0	0.1270		
	SVII 17_11	29.05.15 09:25	16.0	0.1284		
	SVII 17_12	01.06.15 09:25	19.0	0.1340		
	SVII 17_13	03.06.15 09:45	21.0	0.1346		
	SVII 17_14	05.06.15 09:40	23.0	0.1370		
	SVII 17_15	09.06.15 09:35	27.0	0.1371		

		date/time	time [days]	biomass [g(dry)/kg]	pH	IS [µS/cm]
SVII 11 biot. Ctrl., mOD						
SVII 11, biotic control, BG11 1:1000, mOD	*SVII* 11_0	12.05.15 16:30	-0.8		6.05	97.8
	SVII 11_1	13.05.15 10:30	0.0	0.0181	6.10	102
	SVII 11_2	15.05.15 09:35	2.0	0.0176	6.21	95.4
	SVII 11_3	17.05.15 09:30	4.0	0.0164	6.54	96
	SVII 11_4	18.05.15 09:20	5.0			
	SVII 11_5	19.05.15 09:45	6.0	0.0141	6.41	95.6
	SVII 11_6	20.05.15 09:30	7.0			
	SVII 11_7	21.05.15 09:40	8.0	0.0110	6.35	97.8
	SVII 11_8	22.05.15 09:35	9.0			
	SVII 11_9	26.05.15 09:40	13.0	0.0064	6.36	102
	SVII 11_10	27.05.15 09:45	14.0			
	SVII 11_11	29.05.15 09:25	16.0			
	SVII 11_12	01.06.15 09:25	19.0			
	SVII 11_13	03.06.15 09:45	21.0			
	SVII 11_14	05.06.15 09:40	23.0	0.0044	6.35	105
	SVII 11_15	09.06.15 09:35	27.0	0.0041	6.34	107
SVII 14 1500MS, mOD						
SVII 14, BG11 1:1000, 1500 mg/l MS, mOD	*SVII* 14_0	12.05.15 16:30	-0.8		5.93	98.4
	SVII 14_1	13.05.15 10:30	0.0	0.0171	6.28	103
	SVII 14_2	15.05.15 09:35	2.0	0.0201	7.82	104
	SVII 14_3	17.05.15 09:30	4.0	0.0477	9.30	104
	SVII 14_4	18.05.15 09:20	5.0	0.0724		
	SVII 14_5	19.05.15 09:45	6.0	0.1014	9.98	110
	SVII 14_6	20.05.15 09:30	7.0	0.1273		
	SVII 14_7	21.05.15 09:40	8.0	0.1351	10.29	104
	SVII 14_8	22.05.15 09:35	9.0	0.1411	9.48	80.6
	SVII 14_9	26.05.15 09:40	13.0	0.1456	8.55	79.7
	SVII 14_10	27.05.15 09:45	14.0	0.1456	8.51	
	SVII 14_11	29.05.15 09:25	16.0	0.1506	8.39	79.6
	SVII 14_12	01.06.15 09:25	19.0	0.1531	8.23	84.5
	SVII 14_13	03.06.15 09:45	21.0	0.1553	8.24	
	SVII 14_14	05.06.15 09:40	23.0	0.1556	8.14	85.1
	SVII 14_15	09.06.15 09:35	27.0	0.1561	8.22	90.1
SVII 18 1500MS - burned, mOD						
SVII 18, BG11 1:1000, 1500 mg/l MS - burned, mOD	*SVII* 18_1	13.05.15 10:30	0.0	0.0166		
	SVII 18_2	15.05.15 09:35	2.0	0.0188		
	SVII 18_3	17.05.15 09:30	4.0	0.0487		
	SVII 18_4	18.05.15 09:20	5.0	0.0747		
	SVII 18_5	19.05.15 09:45	6.0	0.1106		
	SVII 18_6	20.05.15 09:30	7.0	0.1294		
	SVII 18_7	21.05.15 09:40	8.0	0.1352		
	SVII 18_8	22.05.15 09:35	9.0	0.1393		
	SVII 18_9	26.05.15 09:40	13.0	0.1399		
	SVII 18_10	27.05.15 09:45	14.0	0.1395		
	SVII 18_11	29.05.15 09:25	16.0	0.1430		
	SVII 18_12	01.06.15 09:25	19.0	0.1440		
	SVII 18_13	03.06.15 09:45	21.0	0.1458		
	SVII 18_14	05.06.15 09:40	23.0	0.1456		
	SVII 18_15	09.06.15 09:35	27.0	0.1481		

		date/time	time [days]	biomass [g(dry)/kg]	pH	IS [µS/cm]	Chl a [mg/kg]
SVII 12 biot. Ctrl., hOD							
SVII 12, biotic control, BG11 1:1000, hOD	*SVII* 12_0	12.05.15 16:30	-0.8		5.96	97.7	
	SVII 12_1	13.05.15 10:30	0.0	0.0420	5.88	104	2.95
	SVII 12_2	15.05.15 09:35	2.0	0.0409		96.2	2.58
	SVII 12_3	17.05.15 09:30	4.0	0.0384	6.43	97.9	2.37
	SVII 12_4	18.05.15 09:20	5.0	0.0374			
	SVII 12_5	19.05.15 09:45	6.0	0.0363	6.35	96.8	2.31
	SVII 12_6	20.05.15 09:30	7.0	0.0343			2.13
	SVII 12_7	21.05.15 09:40	8.0	0.0325	6.49	98.9	
	SVII 12_8	22.05.15 09:35	9.0	0.0301		99.9	1.54
	SVII 12_9	26.05.15 09:40	13.0	0.0218	6.47	102	0.92
	SVII 12_10	27.05.15 09:45	14.0				0.83
	SVII 12_11	29.05.15 09:25	16.0	0.0170	6.52	105	0.64
	SVII 12_12	01.06.15 09:25	19.0	0.0140	6.55	112	0.42
	SVII 12_13	03.06.15 09:45	21.0				
	SVII 12_14	05.06.15 09:40	23.0	0.0122	6.53	110	
	SVII 12_15	09.06.15 09:35	27.0	0.0107	6.53	113	0.26
SVII 15 1500MS, hOD							
SVII 15, BG11 1:1000, 1500 mg/l MS, hOD	*SVII* 15_0	12.05.15 16:30	-0.8		5.93	97.6	
	SVII 15_1	13.05.15 10:30	0.0	0.0411	6.24	104	2.90
	SVII 15_2	15.05.15 09:35	2.0	0.0580	9.61	104	3.59
	SVII 15_3	17.05.15 09:30	4.0	0.1174	10.35	115	7.66
	SVII 15_4	18.05.15 09:20	5.0	0.1496			
	SVII 15_5	19.05.15 09:45	6.0	0.1630	10.46	123	10.04
	SVII 15_6	20.05.15 09:30	7.0	0.1699			10.37
	SVII 15_7	21.05.15 09:40	8.0	0.1720	8.97	76.1	
	SVII 15_8	22.05.15 09:35	9.0	0.1711	9.04	77.7	10.20
	SVII 15_9	26.05.15 09:40	13.0	0.1806	8.87	79.5	10.29
	SVII 15_10	27.05.15 09:45	14.0	0.1819	8.78		10.07
	SVII 15_11	29.05.15 09:25	16.0	0.1859	8.50	79.6	10.11
	SVII 15_12	01.06.15 09:25	19.0	0.1892	8.37	84.1	10.12
	SVII 15_13	03.06.15 09:45	21.0	0.1940	8.39		
	SVII 15_14	05.06.15 09:40	23.0	0.1940	8.30	87.1	10.67
	SVII 15_15	09.06.15 09:35	27.0	0.1967	8.30	93.6	10.23
SVII 19 1500MS - burned, hOD							
SVII 19, BG11 1:1000, 1500 mg/l MS - burned, hOD	*SVII* 19_1	13.05.15 10:30	0.0	0.0410			
	SVII 19_2	15.05.15 09:35	2.0	0.0497			
	SVII 19_3	17.05.15 09:30	4.0	0.1082			
	SVII 19_4	18.05.15 09:20	5.0	0.1406			
	SVII 19_5	19.05.15 09:45	6.0	0.1576			
	SVII 19_6	20.05.15 09:30	7.0	0.1628			
	SVII 19_7	21.05.15 09:40	8.0	0.1645			
	SVII 19_8	22.05.15 09:35	9.0	0.1658			
	SVII 19_9	26.05.15 09:40	13.0	0.1690			
	SVII 19_10	27.05.15 09:45	14.0	0.1681			
	SVII 19_11	29.05.15 09:25	16.0	0.1690			
	SVII 19_12	01.06.15 09:25	19.0	0.1708			
	SVII 19_13	03.06.15 09:45	21.0	0.1710			
	SVII 19_14	05.06.15 09:40	23.0	0.1711			
	SVII 19_15	09.06.15 09:35	27.0	0.1690			

Annex 1 Table 7. Continuation.

	date/time	time [days]	biomass [g_{dry}/kg]	pH	IS [µS/cm]
***SVII* 20 1500Zrc, lOD**					
***SVII* 20, BG11 1:1000, 1500 mg/l Zircone, lOD**	*SVII* 20_1	13.05.15 10:30	0.0	0.0055	
	SVII 20_2	15.05.15 09:35	2.0	0.0050	
	SVII 20_3	17.05.15 09:30	4.0	0.0040	
	SVII 20_4	18.05.15 09:20	5.0		
	SVII 20_5	19.05.15 09:45	6.0	0.0026	
	SVII 20_6	20.05.15 09:30	7.0		
	SVII 20_7	21.05.15 09:40	8.0	0.0017	
	SVII 20_8	22.05.15 09:35	9.0		
	SVII 20_9	26.05.15 09:40	13.0	0.0010	
***SVII* 16 1000MS, lOD**					
***SVII* 16, BG11 1:1000, 1000 mg/l MS, lOD**	*SVII* 16_0	12.05.15 16:30	-0.8		
	SVII 16_1	13.05.15 10:30	0.0	0.0060	
	SVII 16_2	15.05.15 09:35	2.0	0.0074	
	SVII 16_3	17.05.15 09:30	4.0	0.0219	
	SVII 16_4	18.05.15 09:20	5.0	0.0377	
	SVII 16_5	19.05.15 09:45	6.0	0.0615	
	SVII 16_6	20.05.15 09:30	7.0	0.0888	
	SVII 16_7	21.05.15 09:40	8.0	0.1142	
	SVII 16_8	22.05.15 09:35	9.0	0.1228	
	SVII 16_9	26.05.15 09:40	13.0	0.1283	
	SVII 16_10	27.05.15 09:45	14.0	0.1294	
	SVII 16_11	29.05.15 09:25	16.0	0.1320	
	SVII 16_12	01.06.15 09:25	19.0	0.1340	
	SVII 16_13	03.06.15 09:45	21.0	0.1358	
	SVII 16_14	05.06.15 09:40	23.0	0.1359	
	SVII 16_15	09.06.15 09:35	27.0	0.1347	
***SVII* 22 1000MS, abiot. Ctrl**					
***SVII* 22, abiotic control, BG11 1:1000, 1000 mg/l MS**	*SVII* 22_0	12.05.15 16:30	-0.8		
	SVII 22_1	13.05.15 10:30	0.0		
	SVII 22_2	15.05.15 09:35	2.0	0.0016	
	SVII 22_3	17.05.15 09:30	4.0	0.0020	
	SVII 22_4	18.05.15 09:20	5.0		
	SVII 22_5	19.05.15 09:45	6.0	0.0023	
	SVII 22_6	20.05.15 09:30	7.0		
	SVII 22_7	21.05.15 09:40	8.0	0.0026	
	SVII 22_8	22.05.15 09:35	9.0		
	SVII 22_9	26.05.15 09:40	13.0	0.0030	
	SVII 22_10	27.05.15 09:45	14.0		
	SVII 22_11	29.05.15 09:25	16.0		
	SVII 22_12	01.06.15 09:25	19.0	0.0089	
	SVII 22_13	03.06.15 09:45	21.0		
	SVII 22_14	05.06.15 09:40	23.0		
	SVII 22_15	09.06.15 09:35	27.0	0.0050	
***SVII* 25 75MS, hOD**					
***SVII* 25, BG11 1:1000, 75 mg/l MS, hOD**	*SVII* 25_1	13.05.15 10:30	0.0	0.0421	
	SVII 25_2	15.05.15 09:35	2.0	0.0409	
	SVII 25_3	17.05.15 09:30	4.0	0.0385	
	SVII 25_4	18.05.15 09:20	5.0	0.0368	
	SVII 25_5	19.05.15 09:45	6.0	0.0344	
	SVII 25_6	20.05.15 09:30	7.0	0.0316	
	SVII 25_7	21.05.15 09:40	8.0	0.0289	
	SVII 25_8	22.05.15 09:35	9.0	0.0260	
	SVII 25_9	26.05.15 09:40	13.0	0.0182	
	SVII 25_10	27.05.15 09:45	14.0	0.0170	
	SVII 25_11	29.05.15 09:25	16.0	0.0161	
	SVII 25_12	01.06.15 09:25	19.0	0.0168	
	SVII 25_13	03.06.15 09:45	21.0	0.0243	
	SVII 25_14	05.06.15 09:40	23.0	0.0499	
	SVII 25_15	09.06.15 09:35	27.0	0.1390	
	SVII 25_16	10.06.15 09:40	28.0	0.1405	

	date/time	time [days]	biomass [g_{dry}/kg]	pH	IS [µS/cm]	Chl a [mg/kg]
***SVII* 21 1500Zrc, hOD**						
***SVII* 21, BG11 1:1000, 1500 mg/l Zircone, hOD**	*SVII* 21_1	13.05.15 10:30	0.0	0.0401		
	SVII 21_2	15.05.15 09:35	2.0	0.0380		
	SVII 21_3	17.05.15 09:30	4.0	0.0325		
	SVII 21_4	18.05.15 09:20	5.0			
	SVII 21_5	19.05.15 09:45	6.0	0.0219		
	SVII 21_6	20.05.15 09:30	7.0			
	SVII 21_7	21.05.15 09:40	8.0	0.0154		
	SVII 21_8	22.05.15 09:35	9.0			
	SVII 21_9	26.05.15 09:40	13.0	0.0102		
***SVII* 24 500MS, hOD**						
***SVII* 24, BG11 1:1000, 500 mg/l MS, hOD**	*SVII* 24_1	13.05.15 10:30	0.0	0.0417		2.85
	SVII 24_2	15.05.15 09:35	2.0	0.0464		2.79
	SVII 24_3	17.05.15 09:30	4.0	0.0880		5.63
	SVII 24_4	18.05.15 09:20	5.0	0.1170		
	SVII 24_5	19.05.15 09:45	6.0	0.1470		9.56
	SVII 24_6	20.05.15 09:30	7.0	0.1558		9.55
	SVII 24_7	21.05.15 09:40	8.0	0.1585		
	SVII 24_8	22.05.15 09:35	9.0	0.1608		9.46
	SVII 24_9	26.05.15 09:40	13.0	0.1635		9.75
	SVII 24_10	27.05.15 09:45	14.0	0.1626		9.07
	SVII 24_11	29.05.15 09:25	16.0	0.1626		9.38
	SVII 24_12	01.06.15 09:25	19.0	0.1603		9.14
	SVII 24_13	03.06.15 09:45	21.0	0.1594		
	SVII 24_14	05.06.15 09:40	23.0	0.1541		8.63
	SVII 24_15	09.06.15 09:35	27.0	0.1477		7.79
***SVII* 23 1000MS, hOD**						
***SVII* 23, BG11 1:1000, 1000 mg/l MS, hOD**	*SVII* 23_1	13.05.15 10:30	0.0	0.0412		
	SVII 23_2	15.05.15 09:35	2.0	0.0555		
	SVII 23_3	17.05.15 09:30	4.0	0.1163		
	SVII 23_4	18.05.15 09:20	5.0	0.1500		
	SVII 23_5	19.05.15 09:45	6.0	0.1606		
	SVII 23_6	20.05.15 09:30	7.0	0.1655		
	SVII 23_7	21.05.15 09:40	8.0	0.1661		
	SVII 23_8	22.05.15 09:35	9.0	0.1670		
	SVII 23_9	26.05.15 09:40	13.0	0.1702		
	SVII 23_10	27.05.15 09:45	14.0	0.1693		
	SVII 23_11	29.05.15 09:25	16.0	0.1720		
	SVII 23_12	01.06.15 09:25	19.0	0.1751		
	SVII 23_13	03.06.15 09:45	21.0	0.1750		
	SVII 23_14	05.06.15 09:40	23.0	0.1762		
	SVII 23_15	09.06.15 09:35	27.0	0.1757		

Annex 1 Table 8. Table 8 of the Electronic supplement of Chapter 3 – Results of Experimental series S*VIII*.

SVIII 1, biotic control, BGII 1:1000, higher initial pH, lOD					*SVIII* 2, biotic control, BGII 1:1000, higher initial pH, mOD				*SVIII* 3, biotic control, BGII 1:1000, higher initial pH, hOD				*SVIII* 4, 1000 mg/l MS, BGII 1:1000, hOD				*SVIII* 5, biotic control, BGII 1:1000, hOD				*SVIII* 6, biotic control, BGII 1:1000, hOD			
	date/time	elapsed time [days]	biomass [g(dry)/kg]	pH		date/time	elapsed time [days]	biomass [g(dry)/kg]	pH		date/time	elapsed time [days]	biomass [g(dry)/kg]	pH		date/time	elapsed time [days]	biomass [g(dry)/kg]	pH		date/time	elapsed time [days]	biomass [g(dry)/kg]	pH
***SVIII* 1 biot. Ctrl., hpH, lOD**					***SVIII* 2 biot. Ctrl., hpH, mOD**				***SVIII* 3 biot. Ctrl., hpH, hOD**								***SVIII* 5 biot. Ctrl., hOD**				***SVIII* 6 biot. Ctrl., hOD**			
*SVIII*1_0	03.06.15 11:20	0.0		7.09	*SVIII*2_0	03.06.15 11:20	0.0		7.09	*SVIII*3_0	03.06.15 11:20	0.0		7.09	*SVIII*4_0	03.06.15 11:20	0.0		6.14	*SVIII*5_0	03.06.15 11:20	0.0		6.09	*SVIII*6_0	03.06.15 11:20	0.0		6.11
*SVIII*1_1	03.06.15 11:30	0.0	0.0067	7.10	*SVIII*2_1	03.06.15 11:30	0.0	0.0189	7.01	*SVIII*3_1	03.06.15 11:30	0.0			*SVIII*4_1	03.06.15 11:30	0.0	0.0186	6.20	*SVIII*5_1	03.06.15 11:30	0.0	0.0419	6.02	*SVIII*6_1	03.06.15 11:30	0.0	0.0437	6.03
*SVIII*1_2	04.06.15 09:45	0.9	0.0070	7.06	*SVIII*2_2	04.06.15 09:45	0.9	0.0196	7.03	*SVIII*3_2	04.06.15 09:45	0.9			*SVIII*4_2	04.06.15 09:45	0.9	0.0200	7.06	*SVIII*5_2	04.06.15 09:45	0.9	0.0414	5.78	*SVIII*6_2	04.06.15 09:45	0.9	0.0428	5.79
*SVIII*1_3	05.06.15 09:50	1.9	0.0071	6.96	*SVIII*2_3	05.06.15 09:50	1.9	0.0194	7.07	*SVIII*3_3	05.06.15 09:50	1.9			*SVIII*4_3	05.06.15 09:50	1.9	0.0254	7.74	*SVIII*5_3	05.06.15 09:50	1.9	0.0404	6.01	*SVIII*6_3	05.06.15 09:50	1.9	0.0415	6.00
*SVIII*1_4	09.06.15 09:35	5.9	0.0273	7.58	*SVIII*2_4	09.06.15 09:35	5.9	0.0713	9.45	*SVIII*3_4	09.06.15 09:35	5.9			*SVIII*4_4	09.06.15 09:35	5.9	0.1307	10.14	*SVIII*5_4	09.06.15 09:35	5.9	0.0353	6.16	*SVIII*6_4	09.06.15 09:35	5.9	0.0367	6.23
*SVIII*1_5	10.06.15 09:40	6.9	0.0456	9.53	*SVIII*2_5	10.06.15 09:40	6.9	0.0777	5.77	*SVIII*3_5	10.06.15 09:40	6.9			*SVIII*4_5	10.06.15 09:40	6.9	0.1409		*SVIII*5_5	10.06.15 09:40	6.9	0.0339		*SVIII*6_5	10.06.15 09:40	6.9	0.0344	
*SVIII*1_6	12.06.15 09:35	8.9	0.0718	8.80	*SVIII*2_6	12.06.15 09:35	8.9	0.0832	8.23	*SVIII*3_6	12.06.15 09:35	8.9			*SVIII*4_6	12.06.15 09:35	8.9	0.1459		*SVIII*5_6	12.06.15 09:35	8.9	0.0307		*SVIII*6_6	12.06.15 09:35	8.9	0.0297	
*SVIII*1_7	15.06.15 09:35	11.9	0.0773	7.93	*SVIII*2_7	15.06.15 09:35	11.9	0.0922	8.21	*SVIII*3_7	15.06.15 09:35	11.9			*SVIII*4_7	15.06.15 09:35	11.9	0.1510		*SVIII*5_7	15.06.15 09:35	11.9	0.0262		*SVIII*6_7	15.06.15 09:35	11.9	0.0253	
*SVIII*1_8	17.06.15 09:30	13.9	0.0799	8.05	*SVIII*2_8	17.06.15 09:30	13.9	0.0931	7.81	*SVIII*3_8	17.06.15 09:30	13.9			*SVIII*4_8	17.06.15 09:30	13.9	0.1539	8.15										
*SVIII*1_9	19.06.15 09:20	15.9	0.0831		*SVIII*2_9	19.06.15 09:20	15.9	0.0926		*SVIII*3_9	19.06.15 09:20	15.9			*SVIII*4_9	19.06.15 09:20	15.9	0.1565											
*SVIII*1_10	22.06.15 09:40	18.9	0.0833	7.67	*SVIII*2_10	22.06.15 09:40	18.9	0.0913	7.59	*SVIII*3_10	22.06.15 09:40	18.9			*SVIII*4_10	22.06.15 09:40	18.9	0.1555	7.98										
*SVIII*1_11	24.06.15 09:45	20.9	0.0835	7.69	*SVIII*2_11	24.06.15 09:45	20.9	0.0898	7.63	*SVIII*3_11	24.06.15 09:45	20.9			*SVIII*4_11	24.06.15 09:45	20.9	0.1567											
*SVIII*1_12	26.06.15 09:35	22.9	0.0819	7.54	*SVIII*2_12	26.06.15 09:35	22.9	0.0885	7.54	*SVIII*3_12	26.06.15 09:35	22.9			*SVIII*4_12	26.06.15 09:35	22.9	0.1574											
*SVIII*1_13	29.06.15 09:45	25.9	0.0803	7.88	*SVIII*2_13	29.06.15 09:45	25.9	0.0875	7.82	*SVIII*3_13	29.06.15 09:45	25.9			*SVIII*4_13	29.06.15 09:45	25.9	0.1553											
*SVIII*1_14	30.06.15 09:15	26.9	0.0798	7.93	*SVIII*2_14	30.06.15 09:15	26.9	0.0867	7.86	*SVIII*3_14	30.06.15 09:15	26.9			*SVIII*4_14	30.06.15 09:15	26.9	0.1530											

Annex 1 Table 9. Table 9 of the Electronic supplement of Chapter 3 – Results of Experimental series S*IX*.

		date/time	elapsed time [days]	biomass [g(dry)/kg]	pH			date/time	elapsed time [days]	biomass [g(dry)/kg]	pH
***SIX* 1 biot. Ctrl., buff., lOD**						***SIX* 2 biot. Ctrl., buff., mOD**					
***SIX* 1, biotic control, BG11 1:1000, Carbonate buffer, lOD**	*SIX* 1_0	12.06.15 17:00	0.0		9.40	***SIX* 2, biotic control, BG11 1:1000, Carbonate buffer, mOD**	*SIX* 2_0	12.06.15 17:00	0.0		9.40
	SIX 1_1	12.06.15 17:10	0.0	0.0068	9.39		*SIX* 2_1	12.06.15 17:10	0.0	0.0181	9.39
	SIX 1_2	15.06.15 09:35	2.7	0.0293	9.42		*SIX* 2_2	15.06.15 09:35	2.7	0.0614	9.54
	SIX 1_3	16.06.15 09:40	3.7	0.0475	9.48		*SIX* 2_3	16.06.15 09:40	3.7	0.0876	9.70
	SIX 1_4	18.06.15 09:40	5.7	0.0874	9.62		*SIX* 2_4	18.06.15 09:40	5.7	0.1057	9.69
	SIX 1_5	19.06.15 09:20	6.7	0.0969			*SIX* 2_5	19.06.15 09:20	6.7	0.1081	
	SIX 1_6	22.06.15 09:40	9.7	0.1038	9.26		*SIX* 2_6	22.06.15 09:40	9.7	0.1119	9.31
	SIX 1_7	24.06.15 09:45	11.7	0.1026	9.28		*SIX* 2_7	24.06.15 09:45	11.7	0.1125	9.29
	SIX 1_8	26.06.15 09:35	13.7	0.1000	9.09		*SIX* 2_8	26.06.15 09:35	13.7	0.1107	9.12
	SIX 1_9	29.06.15 09:45	16.7	0.0915	9.27		*SIX* 2_9	29.06.15 09:45	16.7	0.1011	9.28
	SIX 1_10	01.07.15 09:29	18.7	0.0863			*SIX* 2_10	01.07.15 09:29	18.7	0.0967	
	SIX 1_11	03.07.15 09:30	20.7	0.0809	9.35		*SIX* 2_11	03.07.15 09:30	20.7	0.0904	9.33
	SIX 1_12	06.07.15 09:40	23.7	0.0763			*SIX* 2_12	06.07.15 09:40	23.7	0.0851	
***SIX* 3 500MS, buff., lOD**						***SIX* 4 500MS, buff., mOD**					
***SIX* 3, 500 mg/l MS, BG11 1:1000, Carbonate buffer, lOD**	*SIX* 3_0	12.06.15 17:00	0.0		9.39	***SIX* 4, 500 mg/l MS, BG11 1:1000, Carbonate buffer, mOD**	*SIX* 4_0	12.06.15 17:00	0.0		9.39
	SIX 3_1	12.06.15 17:10	0.0	0.0068	9.38		*SIX* 4_1	12.06.15 17:10	0.0	0.0180	9.37
	SIX 3_2	15.06.15 09:35	2.7	0.0258	9.33		*SIX* 4_2	15.06.15 09:35	2.7	0.0646	9.51
	SIX 3_3	16.06.15 09:40	3.7	0.0488	9.53		*SIX* 4_3	16.06.15 09:40	3.7	0.0999	9.64
	SIX 3_4	18.06.15 09:40	5.7	0.1054	9.83		*SIX* 4_4	18.06.15 09:40	5.7	0.1235	9.63
	SIX 3_5	19.06.15 09:20	6.7	0.1110			*SIX* 4_5	19.06.15 09:20	6.7	0.1271	
	SIX 3_6	22.06.15 09:40	9.7	0.1163	9.39		*SIX* 4_6	22.06.15 09:40	9.7	0.1341	9.28
	SIX 3_7	24.06.15 09:45	11.7	0.1164	9.31		*SIX* 4_7	24.06.15 09:45	11.7	0.1336	9.28
	SIX 3_8	26.06.15 09:35	13.7	0.1116	9.15		*SIX* 4_8	26.06.15 09:35	13.7	0.1291	9.15
	SIX 3_9	29.06.15 09:45	16.7	0.1053	9.30		*SIX* 4_9	29.06.15 09:45	16.7	0.1218	9.35
	SIX 3_10	01.07.15 09:29	18.7	0.1047			*SIX* 4_10	01.07.15 09:29	18.7	0.1177	
	SIX 3_11	03.07.15 09:30	20.7	0.0974	9.34		*SIX* 4_11	03.07.15 09:30	20.7	0.1115	9.34
	SIX 3_12	06.07.15 09:40	23.7	0.0911			*SIX* 4_12	06.07.15 09:40	23.7	0.1056	

Annex 1 Table 10. Table 10 of the Electronic supplement of Chapter 3 – Results of Experimental series S*X*

		date/time	time [days]	biomass [$g_{(dry)}$/kg]	pH	IS [µS/cm]	Chl a [mg/kg]		date/time	time [days]	biomass [$g_{(dry)}$/kg]	pH	IS [µS/cm]
***SX* 1 biot. Ctrl., lOD**								***SX* 2 1500ICE, lOD**					
***SX* 1, biotic control, BG11 1:1000, lOD**	*SX* 1_1	11.06.15 11:00	0.0	0.0069	5.81	107		***SX* 2, 1500 mg/l ICE, BG11 1:1000, lOD**	*SX* 2_1	11.06.15 11:00	0.0	0.0047	6.58	112
	SX 1_2	12.06.15 09:35	0.9	0.0068	5.71	94.7			*SX* 2_2	12.06.15 09:35	0.9	0.0081	6.83	100
	SX 1_3	15.06.15 09:35	3.9	0.0064	5.84	100			*SX* 2_3	15.06.15 09:35	3.9	0.0316	8.23	95.2
	SX 1_4	16.06.15 09:40	4.9						*SX* 2_4	16.06.15 09:40	4.9	0.0490	8.87	91.2
	SX 1_5	18.06.15 09:40	6.9	0.0060	5.96	104			*SX* 2_5	18.06.15 09:40	6.9	0.0980	9.97	108
	SX 1_6	19.06.15 09:20	7.9						*SX* 2_6	19.06.15 09:20	7.9	0.1182		
	SX 1_7	22.06.15 09:40	10.9	0.0046	5.99	102			*SX* 2_7	22.06.15 09:40	10.9	0.1337	7.94	75.2
	SX 1_8	24.06.15 09:45	12.9						*SX* 2_8	24.06.15 09:45	12.9	0.1363	8.08	73.1
	SX 1_9	26.06.15 09:35	14.9	0.0029	5.92	96.8			*SX* 2_9	26.06.15 09:35	14.9	0.1429	7.51	73.5
***SX 3* biot. Ctrl., mOD**								***SX 4* 1500ICE, mOD**					
***SX* 3, biotic control, BG11 1:1000, mOD**	*SX* 3_1	11.06.15 11:00	0.0	0.0193	5.83	107		***SX* 4, 1500 mg/l ICE, BG11 1:1000, mOD**	*SX* 4_1	11.06.15 11:00	0.0	0.0171	6.43	113
	SX 3_2	12.06.15 09:35	0.9	0.0194	5.83	94.6			*SX* 4_2	12.06.15 09:35	0.9	0.0214	7.13	98
	SX 3_3	15.06.15 09:35	3.9	0.0182	5.84	98.1			*SX* 4_3	15.06.15 09:35	3.9	0.0722	9.03	94.1
	SX 3_4	16.06.15 09:40	4.9						*SX* 4_4	16.06.15 09:40	4.9	0.0984	9.89	103
	SX 3_5	18.06.15 09:40	6.9	0.0169	6.08	102			*SX* 4_5	18.06.15 09:40	6.9	0.1339	9.96	100
	SX 3_6	19.06.15 09:20	7.9						*SX* 4_6	19.06.15 09:20	7.9	0.1405		
	SX 3_7	22.06.15 09:40	10.9	0.0141	6.14	101			*SX* 4_7	22.06.15 09:40	10.9	0.1478	8.12	72.8
	SX 3_8	24.06.15 09:45	12.9						*SX* 4_8	24.06.15 09:45	12.9	0.1543	8.09	71.5
	SX 3_9	26.06.15 09:35	14.9	0.0095	6.02	104			*SX* 4_9	26.06.15 09:35	14.9	0.1423	7.54	71.2
***SX* 5 biot. Ctrl., hOD**								***SX* 6 75ICE, hOD**					
***SX* 5, biotic control, BG11 1:1000, hOD**	*SX* 5_1	11.06.15 11:00	0.0	0.0426	5.78	104	2.21	***SX* 6, 75 mg/l ICE, BG11 1:1000, hOD**	*SX* 6_1	11.06.15 11:00	0.0	0.0424		
	SX 5_2	12.06.15 09:35	0.9	0.0416	5.61	94.9	1.98		*SX* 6_2	12.06.15 09:35	0.9	0.0413		
	SX 5_3	15.06.15 09:35	3.9	0.0380	5.88	98.8	1.85		*SX* 6_3	15.06.15 09:35	3.9	0.0320		
	SX 5_4	16.06.15 09:40	4.9						*SX* 6_4	16.06.15 09:40	4.9	0.0269		
	SX 5_5	18.06.15 09:40	6.9	0.0309	6.23	104			*SX* 6_5	18.06.15 09:40	6.9	0.0194		
	SX 5_6	19.06.15 09:20	7.9				1.19		*SX* 6_6	19.06.15 09:20	7.9			
	SX 5_7	22.06.15 09:40	10.9	0.0212	6.21	104			*SX* 6_7	22.06.15 09:40	10.9	0.0120		
	SX 5_8	24.06.15 09:45	12.9				0.13		*SX* 6_8	24.06.15 09:45	12.9			
	SX 5_9	26.06.15 09:35	14.9	0.0149	6.07	105			*SX* 6_9	26.06.15 09:35	14.9	0.0109		
***SX* 7 1500ICE, hOD**								***SX* 9 1500ICE - burned, mOD**					
***SX* 7, 1500 mg/l ICE, BG11 1:1000, hOD**	*SX* 7_1	11.06.15 11:00	0.0	0.0416	6.92	113	2.24	***SX* 9, 1500 mg/l ICE - burned, BG11 1:1000, mOD**	*SX* 9_0	11.06.15 10:30	0.0			
	SX 7_2	12.06.15 09:35	0.9	0.0465	8.09	104	2.36		*SX* 9_1	11.06.15 11:00	0.0	0.0167		
	SX 7_3	15.06.15 09:35	3.9	0.1372	10.15	110	9.16		*SX* 9_2	12.06.15 09:35	0.9	0.0188		
	SX 7_4	16.06.15 09:40	4.9	0.1608	10.39	117			*SX* 9_3	15.06.15 09:35	3.9	0.0758		
	SX 7_5	18.06.15 09:40	6.9	0.1738	8.87	76.6	10.70		*SX* 9_4	16.06.15 09:40	4.9	0.1061		
	SX 7_6	19.06.15 09:20	7.9	0.1859			10.87		*SX* 9_5	18.06.15 09:40	6.9	0.1459		
	SX 7_7	22.06.15 09:40	10.9	0.1853	8.25	76.2	10.34		*SX* 9_6	19.06.15 09:20	7.9	0.1491		
	SX 7_8	24.06.15 09:45	12.9	0.1863	8.01	74.9	10.66		*SX* 9_7	22.06.15 09:40	10.9	0.1585		
	SX 7_9	26.06.15 09:35	14.9	0.1777	7.56	74.4	11.11		*SX* 9_8	24.06.15 09:45	12.9	0.1590		
									SX 9_9	26.06.15 09:35	14.9	0.1489		

Annex 1 Table 10. Continuation.

		date/time	time [days]	biomass [$g_{(dry)}$/kg]	pH	IS [µS/cm]	Chl a [mg/kg]
***SX* 8 1500ICE abiot. Ctrl.**							
***SX* 8, abiotic control, 1500 mg/l ICE. BG11**	*SX* 8_1	11.06.15 11:00	0.0	0.0006	6.60	112	
	SX 8_2	12.06.15 09:35	0.9	0.0014	6.74	105	
	SX 8_3	15.06.15 09:35	3.9	0.0022	6.59	107	
	SX 8_4	16.06.15 09:40	4.9	0.0018	6.71	108	
	SX 8_5	18.06.15 09:40	6.9	0.0025	6.85	112	
	SX 8_6	19.06.15 09:20	7.9				
	SX 8_7	22.06.15 09:40	10.9	0.0023	6.78	113	
	SX 8_8	24.06.15 09:45	12.9	0.0026	6.82	110	
	SX 8_9	26.06.15 09:35	14.9	0.0023	6.65	112	
***SX* 11 biot. Ctrl., hpH, mOD**							
***SX* 11, biotic control, higher initial pH, BG11 1:1000, mOD**	*SX* 11_0	11.06.15 10:40	0.0		7.1		
	SX 11_1	11.06.15 11:00	0.0	0.0180	8.0		
	SX 11_2	12.06.15 09:35	0.9	0.0211	8.2		
	SX 11_3	15.06.15 09:35	3.9	0.0870	9.7		
	SX 11_4	16.06.15 09:40	4.9	0.1003	9.4		
	SX 11_5	18.06.15 09:40	6.9	0.1119	8.3		
	SX 11_6	19.06.15 09:20	7.9	0.1105			
	SX 11_7	22.06.15 09:40	10.9	0.1127	7.8		
	SX 11_8	24.06.15 09:45	12.9	0.1107	7.9		
	SX 11_9	26.06.15 09:35	14.9	0.1060	7.6		
	SX 11_10	29.06.15 09:45	17.9	0.1034	7.8		
	SX 11_11	01.07.15 09:20	19.9	0.1010			
	SX 11_12	03.07.15 09:30	21.9	0.1004	8.0		
	SX 11_13	06.07.15 09:40	24.9	0.0959			
***SX* 13 1500MS, lOD**							
***SX* 13, 1500 mg/l MS, BG11 1:1000, lOD**	SX 13_1	11.06.15 11:00	0.0	0.0070			
	SX 13_2	12.06.15 09:35	0.9	0.0083			
	SX 13_3	15.06.15 09:35	3.9	0.0487			
	SX 13_4	16.06.15 09:40	4.9	0.0778			
	SX 13_5	18.06.15 09:40	6.9	0.1194			
	SX 13_6	19.06.15 09:20	7.9	0.1240			
	SX 13_7	22.06.15 09:40	10.9	0.1268			
	SX 13_8	24.06.15 09:45	12.9	0.1292			
	SX 13_9	26.06.15 09:35	14.9	0.1301			
	SX 13_10	29.06.15 09:45	17.9	0.1339			
	SX 13_11	01.07.15 09:20	19.9	0.1344			
	SX 13_12	03.07.15 09:30	21.9	0.1344			
	SX 13_13	06.07.15 09:40	24.9	0.1347			
***SX* 12 1500MS abiot. Ctrl.**							
***SX* 12, abiotic control, 1500 mg/l MS, BG11 1:1000**	*SX* 12_1	11.06.15 11:00	0.0	0.0000	6.23	112	
	SX 12_2	12.06.15 09:35	0.9	0.0005	6.92	110	
	SX 12_3	15.06.15 09:35	3.9	0.0008	7.05	123	
	SX 12_4	16.06.15 09:40	4.9	0.0008	7.16	124	
	SX 12_5	18.06.15 09:40	6.9	0.0009	7.33	123	
	SX 12_6	19.06.15 09:20	7.9	0.0009			
	SX 12_7	22.06.15 09:40	10.9	0.0012	7.34	131	
	SX 12_8	24.06.15 09:45	12.9	0.0009	7.42	129	
	SX 12_9	26.06.15 09:35	14.9	0.0009	7.29	134	
	SX 12_10	29.06.15 09:45	17.9	0.0009	7.47	136	
	SX 12_11	01.07.15 09:20	19.9	0.0009			
	SX 12_12	03.07.15 09:30	21.9	0.0012	7.61	140	
	SX 12_13	06.07.15 09:40	24.9	0.0012			

		date/time	time [days]	biomass [$g_{(dry)}$/kg]	pH
***SX* 10 biot. Ctrl., hpH, hOD**					
***SX* 10, biotic control, higher initial pH, BG11 1:1000, mOD**	*SX* 10_0	11.06.15 10:40	0.0		7.1
	SX 10_1	11.06.15 11:00	0.0	0.0416	8.8
	SX 10_2	12.06.15 09:35	0.9	0.0489	9.3
	SX 10_3	15.06.15 09:35	3.9	0.1217	9.5
	SX 10_4	16.06.15 09:40	4.9	0.1332	9.7
	SX 10_5	18.06.15 09:40	6.9	0.1390	8.4
	SX 10_6	19.06.15 09:20	7.9	0.1373	
	SX 10_7	22.06.15 09:40	10.9	0.1392	7.9
	SX 10_8	24.06.15 09:45	12.9	0.1362	7.8
	SX 10_9	26.06.15 09:35	14.9	0.1326	7.6
	SX 10_10	29.06.15 09:45	17.9	0.1266	7.8
	SX 10_11	01.07.15 09:20	19.9	0.1256	
	SX 10_12	03.07.15 09:30	21.9	0.1233	8.0
	SX 10_13	06.07.15 09:40	24.9	0.1191	
***SX* 14 500MS, lOD**					
***SX* 14, 500 mg/l MS, BG11 1:1000,**	*SX* 14_1	11.06.15 11:00	0.0	0.0068	
	SX 14_2	12.06.15 09:35	0.9	0.0074	
	SX 14_3	15.06.15 09:35	3.9	0.0168	
	SX 14_4	16.06.15 09:40	4.9	0.0316	
	SX 14_5	18.06.15 09:40	6.9	0.0784	
	SX 14_6	19.06.15 09:20	7.9	0.1067	
	SX 14_7	22.06.15 09:40	10.9	0.1142	
	SX 14_8	24.06.15 09:45	12.9	0.1146	
	SX 14_9	26.06.15 09:35	14.9	0.1150	
	SX 14_10	29.06.15 09:45	17.9	0.1161	
	SX 14_11	01.07.15 09:20	19.9	0.1165	
	SX 14_12	03.07.15 09:30	21.9	0.1182	
	SX 14_13	06.07.15 09:40	24.9	0.1156	

Annex 2: Electronic supplement of Chapter 4

Annex 2 Table 1. Table 1 of the Electronic supplement of Chapter 4 – Results of Experimental series TW1.

ID	electrolyte	RPM [mg/kg]	date/time	duration [days]	Reactor ID	pH	TW x10^4 [cells/kg]	Reactor ID	pH	TW x10^4 [cells/kg]	Reactor ID	pH	TW x10^4 [cells/kg]
TW1 1	IO + 100 % f/2	biotic ctrl	02.03.16 18:00	0.0	TW1 1 R1-1	8.15	1.87	TW1 1 R2-1	8.21	1.91	TW1 1 R3-1	8.23	1.84
			03.03.16 16:30	0.9	TW1 1 R1-2	8.33	2.86	TW1 1 R2-2	8.38	2.45	TW1 1 R3-2	8.39	2.62
			04.03.16 10:20	1.7	TW1 1 R1-3	8.42	3.52	TW1 1 R2-3	8.44	3.80	TW1 1 R3-3	8.45	3.62
			07.03.16 15:10	4.9	TW1 1 R1-4	8.66	23.52	TW1 1 R2-4	8.78	24.30	TW1 1 R3-4	8.72	15.73
			08.03.16 16:15	5.9	TW1 1 R1-5		32.74	TW1 1 R2-5		41.33	TW1 1 R3-5		36.77
			09.03.16 07:25	6.6	TW1 1 R1-6	9.44	46.72	TW1 1 R2-6	9.48	43.90	TW1 1 R3-6	9.35	46.53
TW1 2	IO + 100 % f/2	500 MS	02.03.16 18:00	0.0	TW1 2 R1-1	8.21	1.80	TW1 2 R2-1	8.23	1.67	TW1 2 R3-1	8.23	1.82
			03.03.16 16:30	0.9	TW1 2 R1-2	8.42	2.69	TW1 2 R2-2	8.42	2.38	TW1 2 R3-2	8.42	2.95
			04.03.16 10:20	1.7	TW1 2 R1-3	8.45	4.33	TW1 2 R2-3	8.46	4.13	TW1 2 R3-3	8.47	4.46
			07.03.16 15:10	4.9	TW1 2 R1-4	8.66	19.02	TW1 2 R2-4	8.94	24.46	TW1 2 R3-4	9.41	36.93
			08.03.16 16:15	5.9	TW1 2 R1-5		34.80	TW1 2 R2-5		39.31	TW1 2 R3-5		39.74
			09.03.16 07:25	6.6	TW1 2 R1-6	9.33	43.90	TW1 2 R2-6	9.29	47.42	TW1 2 R3-6	9.32	46.98
TW1 3	IO + 100 % f/2	500 ICE	02.03.16 18:00	0.0	TW1 3 R1-1	8.22	1.82	TW1 3 R2-1	8.24	1.54	TW1 3 R3-1	8.24	1.64
			03.03.16 16:30	0.9	TW1 3 R1-2	8.40	2.53	TW1 3 R2-2	8.41	2.23	TW1 3 R3-2	8.42	2.75
			04.03.16 10:20	1.7	TW1 3 R1-3	8.46	4.19	TW1 3 R2-3	8.46	3.64	TW1 3 R3-3	8.48	4.08
			07.03.16 15:10	4.9	TW1 3 R1-4	8.80	21.58	TW1 3 R2-4	9.29	35.86	TW1 3 R3-4	9.26	39.49
			08.03.16 16:15	5.9	TW1 3 R1-5		39.65	TW1 3 R2-5		44.88	TW1 3 R3-5		47.33
			09.03.16 07:25	6.6	TW1 3 R1-6	9.18	44.42	TW1 3 R2-6	9.21	56.38	TW1 3 R3-6	9.22	54.02
TW1 4	IO + 100 % f/2	500 MS abiotic	02.03.16 18:00	0.0	TW1 4-1	8.2							
			03.03.16 16:30	0.9	TW1 4-2	8.37							
			04.03.16 10:20	1.7	TW1 4-3	8.42							
			07.03.16 15:10	4.9	TW1 4-4	8.36							
			08.03.16 16:15	5.9	TW1 4-5								
			09.03.16 07:25	6.6	TW1 4-6	8.41							
TW15	IO + 100 % f/2	500 ICE abiotic	02.03.16 18:00	0.0	TW1 5-1	8.18							
			03.03.16 16:30	0.9	TW1 5-2	8.3							
			04.03.16 10:20	1.7	TW1 5-3	8.4							
			07.03.16 15:10	4.9	TW1 5-4	8.34							
			08.03.16 16:15	5.9	TW1 5-5								
			09.03.16 07:25	6.6	TW1 5-6	8.39							

Annex 2 Table 2. Table 2 of the Electronic supplement of Chapter 4 – Results of Experimental series TW2.

ID	electrolyte	RPM [mg/kg]	date/time	Time [days]	Reactor ID	pH	TW x10^4 [cells/kg]	Reactor ID	pH	TW x10^4 [cells/kg]	Reactor ID	pH	TW x10^4 [cells/kg]
TW2 1	IO + 5 % f/2	biotic control	15.03.16 15:00	0.0	TW2 1 R1-1 B	8.34	0.96	TW2 1 R2-1	8.35	1.05	TW2 1 R3-1	8.35	0.92
			18.03.16 09:10	2.8	TW2 1 R1-2 B	8.44	2.14	TW2 1 R2-2	8.50	1.88	TW2 1 R3-2	8.51	1.98
			21.03.16 09:15	5.8	TW2 1 R1-3 B	8.57	6.83	TW2 1 R2-3	8.52	4.66	TW2 1 R3-3	8.53	4.83
			23.03.16 09:30	7.8	TW2 1 R1-4 B	8.53	11.01	TW2 1 R2-4	8.53	7.90	TW2 1 R3-4	8.54	7.10
			25.03.16 08:45	9.7	TW2 1 R1-5 B	8.39	10.50	TW2 1 R2-5	8.48	7.55	TW2 1 R3-5	8.51	8.26
			29.03.16 09:35	13.8	TW2 1 R1-6 B	8.19	12.62	TW2 1 R2-6	8.46	6.14	TW2 1 R3-6	8.47	8.02
			01.04.16 09:10	16.8	TW2 1 R1-7 B	8.16	10.68	TW2 1 R2-7	8.47	5.88	TW2 1 R3-7	8.44	5.96
			04.04.16 11:15	19.8	TW2 1 R1-8 B	8.16	11.38	TW2 1 R2-8	8.44	4.68	TW2 1 R3-8	8.29	5.40
			06.04.16 10:00	21.8	TW2 1 R1-9 B	8.14	10.51	TW2 1 R2-9	8.25	4.18	TW2 1 R3-9	8.25	5.36
TW2 2	IO + 5 % f/2	500 MS	15.03.16 15:00	0.0	TW2 2 R1-1 B	8.35	0.92	TW2 2 R2-1	8.35	1.06	TW2 2 R3-1	8.35	0.92
			18.03.16 09:10	2.8	TW2 2 R1-2 B	8.48	2.51	TW2 2 R2-2	8.50	2.35	TW2 2 R3-2	8.50	1.93
			21.03.16 09:15	5.8	TW2 2 R1-3 B	8.60	7.92	TW2 2 R2-3	8.56	7.34	TW2 2 R3-3	8.53	5.82
			23.03.16 09:30	7.8	TW2 2 R1-4 B	8.47	11.17	TW2 2 R2-4	8.48	12.90	TW2 2 R3-4	8.55	11.65
			25.03.16 08:45	9.7	TW2 2 R1-5 B	8.34	14.66	TW2 2 R2-5	8.35	14.27	TW2 2 R3-5	8.38	14.59
			29.03.16 09:35	13.8	TW2 2 R1-6 B	8.28	14.83	TW2 2 R2-6	8.28	12.48	TW2 2 R3-6	8.25	15.70
			01.04.16 09:10	16.8	TW2 2 R1-7 B	8.28	17.40	TW2 2 R2-7	8.27	14.56	TW2 2 R3-7	8.24	14.92
			04.04.16 11:15	19.8	TW2 2 R1-8 B	8.21	17.96	TW2 2 R2-8	8.24	14.64	TW2 2 R3-8	8.22	15.68
			06.04.16 10:00	21.8	TW2 2 R1-9 B	8.24	16.60	TW2 2 R2-9	8.27	13.28	TW2 2 R3-9	8.23	14.76
TW2 3	IO + 5 % f/2	500 ICE	15.03.16 15:00	0.0	TW2 3 R1-1 B	8.35	1.05	TW2 3 R2-1	8.35	0.88	TW2 3 R3-1	8.35	1.00
			18.03.16 09:10	2.8	TW2 3 R1-2 B	8.48	1.90	TW2 3 R2-2	8.49	2.01	TW2 3 R3-2	8.48	2.25
			21.03.16 09:15	5.8	TW2 3 R1-3 B	8.29	5.02	TW2 3 R2-3	8.21	4.46	TW2 3 R3-3	8.19	4.88
			23.03.16 09:30	7.8	TW2 3 R1-4 B	8.35	9.47	TW2 3 R2-4	8.26	7.49	TW2 3 R3-4	8.25	8.29
			25.03.16 08:45	9.7	TW2 3 R1-5 B	8.39	13.06	TW2 3 R2-5	8.28	9.66	TW2 3 R3-5	8.24	9.92
			29.03.16 09:35	13.8	TW2 3 R1-6 B	8.24	14.93	TW2 3 R2-6	8.20	12.05	TW2 3 R3-6	8.17	8.88
			01.04.16 09:10	16.8	TW2 3 R1-7 B	8.22	14.88	TW2 3 R2-7	8.19	9.72	TW2 3 R3-7	8.18	8.40
			04.04.16 11:15	19.8	TW2 3 R1-8 B	8.19	14.88	TW2 3 R2-8	8.15	9.08	TW2 3 R3-8	8.14	8.08
			06.04.16 10:00	21.8	TW2 3 R1-9 B	8.21	14.04	TW2 3 R2-9	8.19	8.31	TW2 3 R3-9	8.19	8.47
TW2 4	IO + 5 % f/2	75 MS	15.03.16 15:00	0.0	TW2 4 R1-1	8.35	0.88	TW2 4 R2-1	8.37	1.00	TW2 4 R3-1	8.37	0.94
			18.03.16 09:10	2.8	TW2 4 R1-2	8.50	2.14	TW2 4 R2-2	8.38	2.16	TW2 4 R3-2	8.51	2.34
			21.03.16 09:15	5.8	TW2 4 R1-3	8.49	4.29	TW2 4 R2-3	8.32	5.18	TW2 4 R3-3	8.51	5.70
			23.03.16 09:30	7.8	TW2 4 R1-4	8.51	7.07	TW2 4 R2-4	8.34	7.39	TW2 4 R3-4	8.52	6.69
			25.03.16 08:45	9.7	TW2 4 R1-5	8.47	6.85	TW2 4 R2-5	8.29	9.60	TW2 4 R3-5	8.48	8.83
			29.03.16 09:35	13.8	TW2 4 R1-6	8.47	7.15	TW2 4 R2-6	8.27	7.15	TW2 4 R3-6	8.47	7.10
			01.04.16 09:10	16.8	TW2 4 R1-7	8.47	6.72	TW2 4 R2-7	8.30	6.20	TW2 4 R3-7	8.46	7.84
			04.04.16 11:15	19.8	TW2 4 R1-8	8.40	5.09	TW2 4 R2-8	8.26	5.93	TW2 4 R3-8	8.26	4.90
			06.04.16 10:00	21.8	TW2 4 R1-9	8.40	4.82	TW2 4 R2-9	8.28	5.27	TW2 4 R3-9	8.23	6.72
TW2 5	IO + 5 % f/2	75 ICE	15.03.16 15:00	0.0	TW2 5 R1-1	8.36	1.03	TW2 5 R2-1	8.37	0.79	TW2 5 R3-1	8.37	0.99
			18.03.16 09:10	2.8	TW2 5 R1-2	8.52	1.82	TW2 5 R2-2	8.52	2.20	TW2 5 R3-2	8.52	1.85
			21.03.16 09:15	5.8	TW2 5 R1-3	8.47	5.90	TW2 5 R2-3	8.48	4.93	TW2 5 R3-3	8.45	4.69
			23.03.16 09:30	7.8	TW2 5 R1-4	8.43	8.96	TW2 5 R2-4	8.44	6.85	TW2 5 R3-4	8.39	6.27
			25.03.16 08:45	9.7	TW2 5 R1-5	8.37	9.34	TW2 5 R2-5	8.39	9.28	TW2 5 R3-5	8.32	6.08
			29.03.16 09:35	13.8	TW2 5 R1-6	8.35	8.98	TW2 5 R2-6	8.36	8.06	TW2 5 R3-6	8.32	8.06
			01.04.16 09:10	16.8	TW2 5 R1-7	8.36	8.64	TW2 5 R2-7	8.37	8.40	TW2 5 R3-7	8.34	6.68

Annex 2 Table 2. Continuation.

ID	electrolyte	RPM [mg/kg]	date/time	Time [days]	Reactor ID	pH	TW x10^4 [cells/kg]	Reactor ID	pH	TW x10^4 [cells/kg]	Reactor ID	pH	TW x10^4 [cells/kg]
			04.04.16 11:15	19.8	TW2 5 R1-8	8.31	7.92	TW2 5 R2-8	8.32	7.73	TW2 5 R3-8	8.30	5.16
			06.04.16 10:00	21.8	TW2 5 R1-9	8.31	7.14	TW2 5 R2-9	8.32	8.33	TW2 5 R3-9	8.31	5.93
TW2 6	IO + 5 % f/2	**500 MS abiotic**	15.03.16 15:00	0.0	TW2 6-1	8.35							
			18.03.16 09:10	2.8	TW2 6-2	8.47							
			21.03.16 09:15	5.8	TW2 6-3	8.48							
			23.03.16 09:30	7.8	TW2 6-4	8.46							
			25.03.16 08:45	9.7	TW2 6-5	8.43							
			29.03.16 09:35	13.8	TW2 6-6	8.48							
			01.04.16 09:10	16.8	TW2 6-7	8.50							
			04.04.16 11:15	19.8	TW2 6-8	8.49							
			06.04.16 10:00	21.8	TW2 6-9	8.51							
TW2 7	IO + 5 % f/2	**500 ICE abiotic**	15.03.16 15:00	0.0	TW2 7-1	8.35							
			18.03.16 09:10	2.8	TW2 7-2	8.46							
			21.03.16 09:15	5.8	TW2 7-3	8.46							
			23.03.16 09:30	7.8	TW2 7-4	8.46							
			25.03.16 08:45	9.7	TW2 7-5	8.40							
			29.03.16 09:35	13.8	TW2 7-6	8.46							
			01.04.16 09:10	16.8	TW2 7-7	8.48							
			04.04.16 11:15	19.8	TW2 7-8	8.46							
			06.04.16 10:00	21.8	TW2 7-9	8.27							
TW2 8	IO + 5 % f/2	**75 MS abiotic**	15.03.16 15:00	0.0	TW2 8-1	8.34							
			18.03.16 09:10	2.8	TW2 8-2	8.48							
			21.03.16 09:15	5.8	TW2 8-3	8.48							
			23.03.16 09:30	7.8	TW2 8-4	8.51							
			25.03.16 08:45	9.7	TW2 8-5	8.47							
			29.03.16 09:35	13.8	TW2 8-6	8.51							
			01.04.16 09:10	16.8	TW2 8-7	8.50							
			04.04.16 11:15	19.8	TW2 8-8	8.48							
			06.04.16 10:00	21.8	TW2 8-9	8.50							
TW2 9	IO + 5 % f/2	**75 ICE abiotic**	15.03.16 15:00	0.0	TW2 9-1	8.35							
			18.03.16 09:10	2.8	TW2 9-2	8.49							
			21.03.16 09:15	5.8	TW2 9-3	8.50							
			23.03.16 09:30	7.8	TW2 9-4	8.49							
			25.03.16 08:45	9.7	TW2 9-5	8.45							
			29.03.16 09:35	13.8	TW2 9-6	8.51							
			01.04.16 09:10	16.8	TW2 9-7	8.51							
			04.04.16 11:15	19.8	TW2 9-8	8.24							
			06.04.16 10:00	21.8	TW2 9-9	8.22							

Annex 2 Table 3. Table 3 of the Electronic supplement of Chapter 4 – Results of Experimental series TW3.

ID	electro lyte	RPM [mg/kg]	date/time	time [days]	Reactor ID	pH	TW x10^4 [cells/kg]	Reactor ID	pH	TW x10^4 [cells/kg]	Reactor ID	pH	TW x10^4 [cells/kg]
TW3 1	IO no f/2	biotic control	10.05.16 17:30	0.0	TW3 1 R1-1	8.32	1.10	TW3 1 R2-1	8.32	1.07	TW3 1 R3-1	8.33	1.08
			13.05.16 10.00	2.7	TW3 1 R1-2	8.36	1.00	TW3 1 R2-2	8.36	0.76	TW3 1 R3-2	8.37	0.98
			17.05.16 09:15	6.7	TW3 1 R1-3	8.34	0.86	TW3 1 R2-3	8.36	0.87	TW3 1 R3-3	8.37	0.90
			20.05.16 15:40	9.9	TW3 1 R1-4	8.37	0.76	TW3 1 R2-4	8.35	0.64	TW3 1 R3-4	8.35	0.83
			23.05.16 10:50	12.7	TW3 1 R1-5	8.34	0.61	TW3 1 R2-5	8.37	0.50	TW3 1 R3-5	8.35	0.62
			27.05.16 09:45	16.7	TW3 1 R1-6	8.32	0.54	TW3 1 R2-6	8.35	0.34	TW3 1 R3-6	8.33	0.54
			31.05.16 08:00	20.6	TW3 1 R1-7	8.41	0.18	TW3 1 R2-7	8.42	0.16	TW3 1 R3-7	8.38	0.37
			07.06.16 10:30	27.7	TW3 1 R1-8	8.30	0.13	TW3 1 R2-8	8.38	0.08	TW3 1 R3-8	8.32	0.14
TW3 2	IO no f/2	500 MS	10.05.16 17:30	0.0	TW3 2 R1-1	8.31	0.96	TW3 2 R2-1	8.31	0.91	TW3 2 R3-1	8.31	0.97
			13.05.16 10.00	2.7	TW3 2 R1-2	8.37	0.92	TW3 2 R2-2	8.36	0.75	TW3 2 R3-2	8.37	0.62
			17.05.16 09:15	6.7	TW3 2 R1-3	8.36	1.09	TW3 2 R2-3	8.37	0.96	TW3 2 R3-3	8.37	0.96
			20.05.16 15:40	9.9	TW3 2 R1-4	8.38	1.17	TW3 2 R2-4	8.36	1.06	TW3 2 R3-4	8.37	1.13
			23.05.16 10:50	12.7	TW3 2 R1-5	8.37	1.32	TW3 2 R2-5	8.37	1.17	TW3 2 R3-5	8.39	1.18
			27.05.16 09:45	16.7	TW3 2 R1-6	8.38	1.59	TW3 2 R2-6	8.37	1.44	TW3 2 R3-6	8.38	1.62
			31.05.16 08:00	20.6	TW3 2 R1-7	8.43	1.76	TW3 2 R2-7	8.42	1.66	TW3 2 R3-7	8.43	1.56
			07.06.16 10:30	27.7	TW3 2 R1-8	8.40	1.34	TW3 2 R2-8	8.38	1.54	TW3 2 R3-8	8.37	1.89
TW3 3	IO no f/2	500 ICE	10.05.16 17:30	0.0	TW3 3 R1-1	8.31	0.80	TW3 3 R2-1	8.31	0.78	TW3 3 R3-1	8.31	0.87
			13.05.16 10.00	2.7	TW3 3 R1-2	8.37	0.52	TW3 3 R2-2	8.37	0.55	TW3 3 R3-2	8.34	0.46
			17.05.16 09:15	6.7	TW3 3 R1-3	8.36	0.82	TW3 3 R2-3	8.34	0.79	TW3 3 R3-3	8.35	0.79
			20.05.16 15:40	9.9	TW3 3 R1-4	8.35	0.95	TW3 3 R2-4	8.33	0.83	TW3 3 R3-4	8.33	0.91
			23.05.16 10:50	12.7	TW3 3 R1-5	8.34	0.90	TW3 3 R2-5	8.32	0.87	TW3 3 R3-5	8.33	0.79
			27.05.16 09:45	16.7	TW3 3 R1-6	8.28	0.90	TW3 3 R2-6	8.25	0.97	TW3 3 R3-6	8.27	0.90
			31.05.16 08:00	20.6	TW3 3 R1-7	8.29	1.04	TW3 3 R2-7	8.28	0.91	TW3 3 R3-7	8.28	0.79
			07.06.16 10:30	27.7	TW3 3 R1-8	8.25	0.75	TW3 3 R2-8	8.24	0.68	TW3 3 R3-8	8.24	0.78
TW3 4	IO no f/2	100 MS	10.05.16 17:30	0.0	TW3 4 R1-1	8.32	0.98	TW3 4 R2-1	8.32	0.87	TW3 4 R3-1	8.32	0.99
			13.05.16 10.00	2.7	TW3 4 R1-2	8.36	0.71	TW3 4 R2-2	8.38	0.82	TW3 4 R3-2	8.37	0.90
			17.05.16 09:15	6.7	TW3 4 R1-3	8.34	0.97	TW3 4 R2-3	8.35	1.03	TW3 4 R3-3	8.33	0.96
			20.05.16 15:40	9.9	TW3 4 R1-4	8.38	0.90	TW3 4 R2-4	8.38	1.02	TW3 4 R3-4	8.38	0.94
			23.05.16 10:50	12.7	TW3 4 R1-5	8.39	1.01	TW3 4 R2-5	8.40	0.86	TW3 4 R3-5	8.40	0.77
			27.05.16 09:45	16.7	TW3 4 R1-6	8.38	0.74	TW3 4 R2-6	8.38	0.71	TW3 4 R3-6	8.37	0.75
			31.05.16 08:00	20.6	TW3 4 R1-7	8.41	0.63	TW3 4 R2-7	8.41	0.52	TW3 4 R3-7	8.40	0.52
			07.06.16 10:30	27.7	TW3 4 R1-8	8.38	0.54	TW3 4 R2-8	8.39	0.45	TW3 4 R3-8	8.39	0.38
TW3 5	IO no f/2	100 ICE	10.05.16 17:30	0.0	TW3 5 R1-1	8.33	0.94	TW3 5 R2-1	8.32	0.90	TW3 5 R3-1	8.32	0.82
			13.05.16 10.00	2.7	TW3 5 R1-2	8.36	0.70	TW3 5 R2-2	8.38	0.82	TW3 5 R3-2	8.36	0.62
			17.05.16 09:15	6.7	TW3 5 R1-3	8.29	0.69	TW3 5 R2-3	8.29	0.98	TW3 5 R3-3	8.31	0.87
			20.05.16 15:40	9.9	TW3 5 R1-4	8.29	0.69	TW3 5 R2-4	8.29	0.83	TW3 5 R3-4	8.30	0.73
			23.05.16 10:50	12.7	TW3 5 R1-5	8.29	0.66	TW3 5 R2-5	8.30	0.54	TW3 5 R3-5	8.30	0.78
			27.05.16 09:45	16.7	TW3 5 R1-6	8.24	0.53	TW3 5 R2-6	8.24	0.54	TW3 5 R3-6	8.24	0.51
			31.05.16 08:00	20.6	TW3 5 R1-7	8.25	0.44	TW3 5 R2-7	8.24	0.41	TW3 5 R3-7	8.25	0.37
			07.06.16 10:30	27.7	TW3 5 R1-8	8.21	0.24	TW3 5 R2-8	8.20	0.21	TW3 5 R3-8	8.20	0.31
TW3 6	IO no f/2	500 MS abiotic	10.05.16 17:30	0.0	TW3 6-1	8.30							
			13.05.16 10.00	2.7	TW3 6-2	8.36							
			17.05.16 09:15	6.7	TW3 6-3	8.34							
			20.05.16 15:40	9.9	TW3 6-4	8.35							
			23.05.16 10:50	12.7	TW3 6-5	8.40							
			27.05.16 09:45	16.7	TW3 6-6	8.36							
			31.05.16 08:00	20.6	TW3 6-7	8.40							
			07.06.16 10:30	27.7	TW3 6-8	8.38							
TW3 7	IO no f/2	500 ICE abiotic	10.05.16 17:30	0.0	TW3 7-1	8.32							
			13.05.16 10.00	2.7	TW3 7-2	8.37							
			17.05.16 09:15	6.7	TW3 7-3	8.36							
			20.05.16 15:40	9.9	TW3 7-4	8.34							
			23.05.16 10:50	12.7	TW3 7-5	8.39							
			27.05.16 09:45	16.7	TW3 7-6	8.36							
			31.05.16 08:00	20.6	TW3 7-7	8.40							
			07.06.16 10:30	27.7	TW3 7-8	8.37							
TW3 8	IO no f/2	100 MS abiotic	10.05.16 17:30	0.0	TW3 8-1	8.31							
			13.05.16 10.00	2.7	TW3 8-2	8.36							
			17.05.16 09:15	6.7	TW3 8-3	8.34							
			20.05.16 15:40	9.9	TW3 8-4	8.28							
			23.05.16 10:50	12.7	TW3 8-5	8.31							
			27.05.16 09:45	16.7	TW3 8-6	8.26							
			31.05.16 08:00	20.6	TW3 8-7	8.27							
			07.06.16 10:30	27.7	TW3 8-8	8.20							
TW3 9	IO no f/2	100 ICE abiotic	10.05.16 17:30	0.0	TW3 9-1	8.32							
			13.05.16 10.00	2.7	TW3 9-2	8.33							
			17.05.16 09:15	6.7	TW3 9-3	8.28							
			20.05.16 15:40	9.9	TW3 9-4	8.21							
			23.05.16 10:50	12.7	TW3 9-5	8.28							
			27.05.16 09:45	16.7	TW3 9-6	8.23							
			31.05.16 08:00	20.6	TW3 9-7	8.24							
			07.06.16 10:30	27.7	TW3 9-8	8.19							

Annex 2 Table 4. Table 4 of the Electronic supplement of Chapter 4 – Results of Experimental series TW4.

ID	electrolyte	RPM [mg/kg]	date/time	time [days]	Reactor ID	pH	TW x10^4 [cells/kg]	Reactor ID	pH	TW x10^4 [cells/kg]	Reactor ID	pH	TW x10^4 [cells/kg]
TW4 1	IO + 5 % f/2	biotic control	09.06.16 16:00	0.0	TW4 1 R1-1	8.44	0.90	TW4 1 R2-1	8.44	0.90	TW4 1 R3-1	8.44	0.80
			12.06.16 12:30	2.9	TW4 1 R1-2	8.34	1.31	TW4 1 R2-2	8.35	1.26	TW4 1 R3-2	8.32	1.08
			14.06.16 08:35	4.7	TW4 1 R1-3	8.33	1.86	TW4 1 R2-3	8.36	2.33	TW4 1 R3-3	8.32	1.96
			16.06.16 08:35	6.7	TW4 1 R1-4	8.35	3.06	TW4 1 R2-4	8.40	3.54	TW4 1 R3-4	8.34	3.58
			19.06.16 13:00	9.9	TW4 1 R1-5	8.39	5.93	TW4 1 R2-5	8.41	6.53	TW4 1 R3-5	8.37	6.38
			21.06.16 09:00	11.7	TW4 1 R1-6	8.29	6.14	TW4 1 R2-6	8.32	6.88	TW4 1 R3-6	8.28	6.24
			23.06.16 09:30	13.7	TW4 1 R1-7	8.32	6.34	TW4 1 R2-7	8.34	6.91	TW4 1 R3-7	8.29	7.23
			25.06.16 12:20	15.8	TW4 1 R1-8	8.34	5.82	TW4 1 R2-8	8.37	5.44	TW4 1 R3-8	8.33	6.40
			28.06.16 10:00	18.8	TW4 1 R1-9	8.33	4.16	TW4 1 R2-9	8.35	3.42	TW4 1 R3-9	8.32	4.67
			01.07.16 11:10	21.8	TW4 1 R1-10	8.35	3.42	TW4 1 R2-10	8.37	2.75	TW4 1 R3-10	8.34	3.33
TW4 2	IO + 5 % f/2	750 MS	09.06.16 16:00	0.0	TW4 2 R1-1	8.44	0.70	TW4 2 R2-1	8.43	0.86	TW4 2 R3-1	8.43	0.85
			12.06.16 12:30	2.9	TW4 2 R1-2	8.50	1.17	TW4 2 R2-2	8.51	1.20	TW4 2 R3-2	8.50	1.10
			14.06.16 08:35	4.7	TW4 2 R1-3	8.51	1.90	TW4 2 R2-3	8.52	2.06	TW4 2 R3-3	8.51	1.72
			16.06.16 08:35	6.7	TW4 2 R1-4	8.53	3.47	TW4 2 R2-4	8.54	3.33	TW4 2 R3-4	8.53	3.04
			19.06.16 13:00	9.9	TW4 2 R1-5	8.60	7.18	TW4 2 R2-5	8.62	7.87	TW4 2 R3-5	8.62	7.87
			21.06.16 09:00	11.7	TW4 2 R1-6	8.51	8.48	TW4 2 R2-6	8.51	8.12	TW4 2 R3-6	8.51	8.16
			23.06.16 09:30	13.7	TW4 2 R1-7	8.31	8.32	TW4 2 R2-7	8.32	8.99	TW4 2 R3-7	8.31	8.70
			25.06.16 12:20	15.8	TW4 2 R1-8	8.33	7.58	TW4 2 R2-8	8.34	7.68	TW4 2 R3-8	8.33	8.13
			28.06.16 10:00	18.8	TW4 2 R1-9	8.29	8.77	TW4 2 R2-9	8.29	8.51	TW4 2 R3-9	8.29	7.74
			01.07.16 11:10	21.8	TW4 2 R-.10	8.29	6.78	TW4 2 R2-10	8.30	7.78	TW4 2 R3-10	8.28	6.46
TW4 3	IO + 5 % f/2	750 ICE	09.06.16 16:00	0.0	TW4 3 R1-1	8.44	0.61	TW4 3 R2-1	8.44	0.72	TW4 3 R3-1	8.44	0.63
			12.06.16 12:30	2.9	TW4 3 R1-2	8.26	0.67	TW4 3 R2-2	8.24	0.93	TW4 3 R3-2	8.24	1.01
			14.06.16 08:35	4.7	TW4 3 R1-3	8.21	1.18	TW4 3 R2-3	8.21	1.20	TW4 3 R3-3	8.21	1.14
			16.06.16 08:35	6.7	TW4 3 R1-4	8.20	1.45	TW4 3 R2-4	8.21	1.86	TW4 3 R3-4	8.22	1.64
			19.06.16 13:00	9.9	TW4 3 R1-5	8.24	2.78	TW4 3 R2-5	8.24	3.46	TW4 3 R3-5	8.27	3.70
			21.06.16 09:00	11.7	TW4 3 R1-6	8.20	4.90	TW4 3 R2-6	8.19	5.18	TW4 3 R3-6	8.21	5.57
			23.06.16 09:30	13.7	TW4 3 R1-7	8.26	7.10	TW4 3 R2-7	8.20	7.07	TW4 3 R3-7	8.25	6.91
			25.06.16 12:20	15.8	TW4 3 R1-8	8.25	7.84	TW4 3 R2-8	8.25	6.27	TW4 3 R3-8	8.25	7.14
			28.06.16 10:00	18.8	TW4 3 R1-9	8.19	6.66	TW4 3 R2-9	8.19	6.24	TW4 3 R3-9	8.21	6.82
			01.07.16 11:10	21.8	TW4 3 R1-10	8.23	5.60	TW4 3 R2-10	8.21	4.80	TW4 3 R3-10	8.23	5.79
TW4 4	IO + 5 % f/2	250 MS	09.06.16 16:00	0.0	TW4 4 R1-1	8.44	0.89	TW4 4 R2-1	8.44	0.94	TW4 4 R3-1	8.44	0.90
			12.06.16 12:30	2.9	TW4 4 R1-2	8.50	1.34	TW4 4 R2-2	8.51	1.14	TW4 4 R3-2	8.52	1.10
			14.06.16 08:35	4.7	TW4 4 R1-3	8.52	1.91	TW4 4 R2-3	8.51	2.00	TW4 4 R3-3	8.51	1.81
			16.06.16 08:35	6.7	TW4 4 R1-4	8.51	2.98	TW4 4 R2-4	8.51	3.80	TW4 4 R3-4	8.51	2.99
			19.06.16 13:00	9.9	TW4 4 R1-5	8.54	5.21	TW4 4 R2-5	8.46	7.03	TW4 4 R3-5	8.39	6.74
			21.06.16 09:00	11.7	TW4 4 R1-6	8.42	6.88	TW4 4 R2-6	8.36	7.04	TW4 4 R3-6	8.32	6.66
			23.06.16 09:30	13.7	TW4 4 R1-7	8.28	7.36	TW4 4 R2-7	8.35	7.65	TW4 4 R3-7	8.32	7.62
			25.06.16 12:20	15.8	TW4 4 R1-8	8.30	6.78	TW4 4 R2-8	8.35	6.82	TW4 4 R3-8	8.33	6.43
			28.06.16 10:00	18.8	TW4 4 R1-9	8.23	5.79	TW4 4 R2-9	8.28	6.40	TW4 4 R3-9	8.27	4.29
			01.07.16 11:10	21.8	TW4 4 R1-10	8.27	5.70	TW4 4 R2-10	8.26	4.13	TW4 4 R3-10	8.27	3.65
TW4 5	IO + 5 % f/2	250 ICE	09.06.16 16:00	0.0	TW4 5 R1-1	8.44	0.64	TW4 5 R2-1	8.44	0.74	TW4 5 R3-1	8.44	0.71
			12.06.16 12:30	2.9	TW4 5 R1-2	8.26	1.07	TW4 5 R2-2	8.26	1.29	TW4 5 R3-2	8.25	1.32
			14.06.16 08:35	4.7	TW4 5 R1-3	8.24	1.90	TW4 5 R2-3	8.25	1.73	TW4 5 R3-3	8.25	1.79
			16.06.16 08:35	6.7	TW4 5 R1-4	8.26	3.18	TW4 5 R2-4	8.25	2.78	TW4 5 R3-4	8.25	3.22
			19.06.16 13:00	9.9	TW4 5 R1-5	8.32	5.83	TW4 5 R2-5	8.30	5.74	TW4 5 R3-5	8.30	5.16
			21.06.16 09:00	11.7	TW4 5 R1-6	8.22	6.53	TW4 5 R2-6	8.22	6.34	TW4 5 R3-6	8.21	6.50
			23.06.16 09:30	13.7	TW4 5 R1-7	8.24	7.87	TW4 5 R2-7	8.23	7.14	TW4 5 R3-7	8.23	7.17
			25.06.16 12:20	15.8	TW4 5 R1-8	8.24	6.40	TW4 5 R2-8	8.26	5.79	TW4 5 R3-8	8.24	6.30
			28.06.16 10:00	18.8	TW4 5 R1-9	8.22	4.96	TW4 5 R2-9	8.22	4.74	TW4 5 R3-9	8.22	4.29
			01.07.16 11:10	21.8	TW4 5 R1-10	8.26	3.55	TW4 5 R2-10	8.24	4.83	TW4 5 R3-10	8.25	3.65
TW4 6	IO + 5 % f/2	750 MS abiotic	09.06.16 16:00	0.0	TW4 6-1	8.43							
			12.06.16 12:30	2.9	TW4 6-2	8.48							
			14.06.16 08:35	4.7	TW4 6-3	8.48							
			16.06.16 08:35	6.7	TW4 6-4	8.48							
			19.06.16 13:00	9.9	TW4 6-5	8.49							
			21.06.16 09:00	11.7	TW4 6-6	8.46							
			23.06.16 09:30	13.7	TW4 6-7	8.48							
			25.06.16 12:20	15.8	TW4 6-8	8.50							
			28.06.16 10:00	18.8	TW4 6-9	8.53							
			01.07.16 11:10	21.8	TW4 6-10	8.55							
TW4 7	IO + 5 % f/2	750 ICE abiotic	09.06.16 16:00	0.0	TW4 7-1	8.43							
			12.06.16 12:30	2.9	TW4 7-2	8.47							
			14.06.16 08:35	4.7	TW4 7-3	8.49							
			16.06.16 08:35	6.7	TW4 7-4	8.47							
			19.06.16 13:00	9.9	TW4 7-5	8.50							
			21.06.16 09:00	11.7	TW4 7-6	8.44							
			23.06.16 09:30	13.7	TW4 7-7	8.39							
			25.06.16 12:20	15.8	TW4 7-8	8.29							
			28.06.16 10:00	18.8	TW4 7-9	8.21							
			01.07.16 11:10	21.8	TW4 7-10	8.19							
TW4 8	IO + 5 % f/2	250 MS abiotic	09.06.16 16:00	0.0	TW4 8-1	8.44							
			12.06.16 12:30	2.9	TW4 8-2	8.50							
			14.06.16 08:35	4.7	TW4 8-3	8.49							
			16.06.16 08:35	6.7	TW4 8-4	8.50							
			19.06.16 13:00	9.9	TW4 8-5	8.51							
			21.06.16 09:00	11.7	TW4 8-6	8.48							
			23.06.16 09:30	13.7	TW4 8-7	8.52							
			25.06.16 12:20	15.8	TW4 8-8	8.53							
			28.06.16 10:00	18.8	TW4 8-9	8.52							
			01.07.16 11:10	21.8	TW4 8-10	8.55							
TW4 9	IO + 5 % f/2	250 ICE abiotic	09.06.16 16:00	0.0	TW4 9-1	8.44							
			12.06.16 12:30	2.9	TW4 9-2	8.49							
			14.06.16 08:35	4.7	TW4 9-3	8.51							
			16.06.16 08:35	6.7	TW4 9-4	8.47							
			19.06.16 13:00	9.9	TW4 9-5	8.52							
			21.06.16 09:00	11.7	TW4 9-6	8.47							
			23.06.16 09:30	13.7	TW4 9-7	8.50							
			25.06.16 12:20	15.8	TW4 9-8	8.53							
			28.06.16 10:00	18.8	TW4 9-9	8.23							
			01.07.16 11:10	21.8	TW4 9-10	8.19							

Annex 2 Table 5. Table 5 of the Electronic supplement of Chapter 4 – Results of Experimental series TW5.

ID	electrolyte	RPM [mg/kg]	date/time	duration [days]	Reactor ID	pH	TW x10^4 [cells/kg]	Reactor ID	pH	TW x10^4 [cells/kg]	Reactor ID	pH	TW x10^4 [cells/kg]
TW5 1	IO no f/2	biotic control	07.07.16 10:45	0.0	TW5 1 R1-1	8.08	0.89	TW5 1 R2-1	8.11	0.94	TW5 1 R3-1	8.12	0.82
			08.07.16 14:30	1.2	TW5 1 R1-2	8.32	0.86	TW5 1 R2-2	8.32	0.90	TW5 1 R3-2	8.33	0.71
			11.07.16 09:20	3.9	TW5 1 R1-3	8.34	0.86	TW5 1 R2-3	8.34	0.82	TW5 1 R3-3	8.35	0.87
			13.07.16 08:30	5.9	TW5 1 R1-4	8.31	0.80	TW5 1 R2-4	8.30	0.89	TW5 1 R3-4	8.30	0.84
			16.07.16 09:30	8.9	TW5 1 R1-5	8.27	0.74	TW5 1 R2-5	8.29	0.86	TW5 1 R3-5	8.27	0.93
			19.07.16 13:30	12.1	TW5 1 R1-6	8.32	0.69	TW5 1 R2-6	8.34	0.58	TW5 1 R3-6	8.33	0.74
			22.07.16 08:30	14.9	TW5 1 R1-7	8.35	0.50	TW5 1 R2-7	8.35	0.54	TW5 1 R3-7	8.33	0.70
			25.07.16 08:40	17.9	TW5 1 R1-8	8.58	0.38	TW5 1 R2-8	8.58	0.32	TW5 1 R3-8	8.56	0.43
			28.07.16 11:00	21.0	TW5 1 R1-9	8.40	0.22	TW5 1 R2-9	8.41	0.29	TW5 1 R3-9	8.41	0.30
TW5 2	IO no f/2	750 MS	07.07.16 10:45	0.0	TW5 2 R1-1	8.09	0.73	TW5 2 R2-1	8.10	0.74	TW5 2 R3-1	8.08	0.74
			08.07.16 14:30	1.2	TW5 2 R1-2	8.30	0.59	TW5 2 R2-2	8.30	0.58	TW5 2 R3-2	8.30	0.65
			11.07.16 09:20	3.9	TW5 2 R1-3	8.33	0.66	TW5 2 R2-3	8.33	1.06	TW5 2 R3-3	8.31	0.96
			13.07.16 08:30	5.9	TW5 2 R1-4	8.32	1.06	TW5 2 R2-4	8.32	1.05	TW5 2 R3-4	8.32	1.32
			16.07.16 09:30	8.9	TW5 2 R1-5	8.28	1.33	TW5 2 R2-5	8.28	1.81	TW5 2 R3-5	8.27	1.26
			19.07.16 13:30	12.1	TW5 2 R1-6	8.33	1.32	TW5 2 R2-6	8.34	1.98	TW5 2 R3-6	8.34	1.68
			22.07.16 08:30	14.9	TW5 2 R1-7	8.35	1.81	TW5 2 R2-7	8.35	1.98	TW5 2 R3-7	8.35	1.97
			25.07.16 08:40	17.9	TW5 2 R1-8	8.56	1.95	TW5 2 R2-8	8.60	2.18	TW5 2 R3-8	8.58	2.01
			28.07.16 11:00	21.0	TW5 2 R1-9	8.42	2.24	TW5 2 R2-9	8.44	2.23	TW5 2 R3-9	8.44	1.95
TW5 3	IO no f/2	750 ICE	07.07.16 10:45	0.0	TW5 3 R1-1	8.09	0.68	TW5 3 R2-1	8.09	0.62	TW5 3 R3-1	8.08	0.71
			08.07.16 14:30	1.2	TW5 3 R1-2	8.29	0.55	TW5 3 R2-2	8.28	0.54	TW5 3 R3-2	8.29	0.46
			11.07.16 09:20	3.9	TW5 3 R1-3	8.31	0.64	TW5 3 R2-3	8.30	0.75	TW5 3 R3-3	8.31	0.78
			13.07.16 08:30	5.9	TW5 3 R1-4	8.30	0.79	TW5 3 R2-4	8.30	0.92	TW5 3 R3-4	8.30	0.88
			16.07.16 09:30	8.9	TW5 3 R1-5	8.27	1.05	TW5 3 R2-5	8.26	1.30	TW5 3 R3-5	8.27	1.01
			19.07.16 13:30	12.1	TW5 3 R1-6	8.30	1.22	TW5 3 R2-6	8.28	1.33	TW5 3 R3-6	8.29	1.14
			22.07.16 08:30	14.9	TW5 3 R1-7	8.45	1.44	TW5 3 R2-7	8.47	1.78	TW5 3 R3-7	8.47	1.26
			25.07.16 08:40	17.9	TW5 3 R1-8	8.58	1.52	TW5 3 R2-8	8.59	1.48	TW5 3 R3-8	8.58	1.38
			28.07.16 11:00	21.0	TW5 3 R1-9	8.40	1.04	TW5 3 R2-9	8.40	1.20	TW5 3 R3-9	8.41	1.23
TW5 4	IO no f/2	250 MS	07.07.16 10:45	0.0	TW5 4 R1-1	8.09	0.77	TW5 4 R2-1	8.10	0.75	TW5 4 R3-1	8.10	0.76
			08.07.16 14:30	1.2	TW5 4 R1-2	8.30	0.80	TW5 4 R2-2	8.32	0.60	TW5 4 R3-2	8.31	0.74
			11.07.16 09:20	3.9	TW5 4 R1-3	8.34	1.07	TW5 4 R2-3	8.33	0.97	TW5 4 R3-3	8.34	1.01
			13.07.16 08:30	5.9	TW5 4 R1-4	8.32	1.38	TW5 4 R2-4	8.31	1.24	TW5 4 R3-4	8.31	1.06
			16.07.16 09:30	8.9	TW5 4 R1-5	8.27	1.42	TW5 4 R2-5	8.28	1.34	TW5 4 R3-5	8.28	1.26
			19.07.16 13:30	12.1	TW5 4 R1-6	8.33	1.50	TW5 4 R2-6	8.31	1.12	TW5 4 R3-6	8.33	1.18
			22.07.16 08:30	14.9	TW5 4 R1-7	8.34	1.24	TW5 4 R2-7	8.34	1.21	TW5 4 R3-7	8.33	1.17
			25.07.16 08:40	17.9	TW5 4 R1-8	8.58	0.98	TW5 4 R2-8	8.58	0.89	TW5 4 R3-8	8.60	1.06
			28.07.16 11:00	21.0	TW5 4 R1-9	8.42	0.74	TW5 4 R2-9	8.42	0.86	TW5 4 R3-9	8.41	0.74
TW5 5	IO no f/2	250 ICE	07.07.16 10:45	0.0	TW5 5 R1-1	8.10	0.75	TW5 5 R2-1	8.10	0.58	TW5 5 R3-1	8.10	0.77
			08.07.16 14:30	1.2	TW5 5 R1-2	8.31	0.50	TW5 5 R2-2	8.31	0.55	TW5 5 R3-2	8.29	0.58
			11.07.16 09:20	3.9	TW5 5 R1-3	8.30	0.58	TW5 5 R2-3	8.32	0.78	TW5 5 R3-3	8.32	0.93
			13.07.16 08:30	5.9	TW5 5 R1-4	8.30	0.92	TW5 5 R2-4	8.30	0.90	TW5 5 R3-4	8.30	1.03
			16.07.16 09:30	8.9	TW5 5 R1-5	8.26	0.93	TW5 5 R2-5	8.27	0.94	TW5 5 R3-5	8.25	1.22
			19.07.16 13:30	12.1	TW5 5 R1-6	8.30	0.80	TW5 5 R2-6	8.30	0.78	TW5 5 R3-6	8.30	0.93
			22.07.16 08:30	14.9	TW5 5 R1-7	8.31	0.63	TW5 5 R2-7	8.32	0.67	TW5 5 R3-7	8.45	0.62
			25.07.16 08:40	17.9	TW5 5 R1-8	8.58	0.56	TW5 5 R2-8	8.58	0.46	TW5 5 R3-8	8.57	0.50
			28.07.16 11:00	21.0	TW5 5 R1-9	8.41	0.26	TW5 5 R2-9	8.39	0.36	TW5 5 R3-9	8.41	0.35
TW5 6	IO no f/2	750 MS abiotic	07.07.16 10:45	0.0	TW5 6-1	8.18							
			08.07.16 14:30	1.2	TW5 6-2	8.32							
			11.07.16 09:20	3.9	TW5 6-3	8.31							
			13.07.16 08:30	5.9	TW5 6-4	8.31							
			16.07.16 09:30	8.9	TW5 6-5	8.27							
			19.07.16 13:30	12.1	TW5 6-6	8.31							
			22.07.16 08:30	14.9	TW5 6-7	8.33							
			25.07.16 08:40	17.9	TW5 6-8	8.57							
			28.07.16 11:00	21.0	TW5 6-9	8.38							
TW5 7	IO no f/2	750 ICE abiotic	07.07.16 10:45	0.0	TW5 7-1	8.14							
			08.07.16 14:30	1.2	TW5 7-2	8.29							
			11.07.16 09:20	3.9	TW5 7-3	8.33							
			13.07.16 08:30	5.9	TW5 7-4	8.30							
			16.07.16 09:30	8.9	TW5 7-5	8.28							
			19.07.16 13:30	12.1	TW5 7-6	8.33							
			22.07.16 08:30	14.9	TW5 7-7	8.34							
			25.07.16 08:40	17.9	TW5 7-8	8.54							
			28.07.16 11:00	21.0	TW5 7-9	8.37							
TW5 8	IO no f/2	250 MS abiotic	07.07.16 10:45	0.0	TW5 8-1	8.14							
			08.07.16 14:30	1.2	TW5 8-2	8.30							
			11.07.16 09:20	3.9	TW5 8-3	8.34							
			13.07.16 08:30	5.9	TW5 8-4	8.31							
			16.07.16 09:30	8.9	TW5 8-5	8.29							
			19.07.16 13:30	12.1	TW5 8-6	8.34							
			22.07.16 08:30	14.9	TW5 8-7	8.35							
			25.07.16 08:40	17.9	TW5 8-8	8.59							
			28.07.16 11:00	21.0	TW5 8-9	8.40							
TW5 9	IO no f/2	250 ICE abiotic	07.07.16 10:45	0.0	TW5 9-1	8.14							
			08.07.16 14:30	1.2	TW5 9-2	8.32							
			11.07.16 09:20	3.9	TW5 9-3	8.34							
			13.07.16 08:30	5.9	TW5 9-4	8.31							
			16.07.16 09:30	8.9	TW5 9-5	8.29							
			19.07.16 13:30	12.1	TW5 9-6	8.31							
			22.07.16 08:30	14.9	TW5 9-7	8.36							
			25.07.16 08:40	17.9	TW5 9-8	8.58							
			28.07.16 11:00	21.0	TW5 9-9	8.38							

Annex 3: Co-author Publication in Applied Geochemistry

Effect of active freshwater *Synechococcus sp.* cyanobacteria on the precipitation kinetics of $CaCO_3$: implications for CO_2 sequestration

Raul E. Martinez[1*], Sebastian Weber[1], Christian Grimm[2]

[1] Geo- und Umweltnaturwissenschaften, Albert-Ludwigs Universität, 79104 Freiburg, Germany
[2] GET, CNRS/URM 5563, Université Paul-Sabatier, 14 avenue Edouard-Belin, 31400 Toulouse, France

* Corresponding author e-mail: raul.martinez@minpet.uni-freiburg.de

Keywords: CO_2 sequestration, flow-through bio-reactor, steady state, cyanobacteria, *Synechococcus sp*., calcite, air bubbling

Applied Geochemistry 75 (2016) 76–89

Contents lists available at ScienceDirect

Applied Geochemistry

journal homepage: www.elsevier.com/locate/apgeochem

Effects of freshwater *Synechococcus* sp. cyanobacteria pH buffering on $CaCO_3$ precipitation: Implications for CO_2 sequestration☆

Raul E. Martinez [a, *], Sebastian Weber [a], Christian Grimm [b]

[a] Institut für Geo- und Umweltnaturwissenschaften, Mineralogie-Petrologie, Albert-Ludwigs-Universität Freiburg, D-79104 Freiburg, Germany
[b] Laboratoire Géosciences Environnement Toulouse (GET), Université de Toulouse, CNRS-IRD-OMP, 14 Avenue Edouard Belin, 31400 Toulouse, France

ARTICLE INFO

Article history:
Received 23 June 2016
Received in revised form
23 September 2016
Accepted 24 October 2016
Available online 25 October 2016

Keywords:
CO_2 sequestration
Mixed-flow bio-reactor
Steady state
Freshwater cyanobacteria
Synechococcus sp.
Calcite
Air bubbling

ABSTRACT

In the present study, a mixed-flow steady-state bio-reactor was designed to biomineralize CO_2 as a consequence of photosynthesis from active *Synechococcus* sp. Dissolved CO_2, generated by constant air bubbling of inorganic and cyanobacteria stock solutions, was the only source of inorganic carbon. The release of hydroxide ion by cyanobacteria from photosynthesis maintained highly alkaline pH conditions. In the presence of Ca^{2+} and carbonate species, this led to calcite supersaturation under steady state conditions. Ca^{2+} remained constant throughout the experiments showing the presence of steady state conditions. Similarly, the *Synechococcus* sp. biomass concentration remained stable within uncertainty. A gradual pH decrease was observed for the highest Ca^{2+} condition coinciding with the formation of $CaCO_3$. The high degree of supersaturation, under steady-state conditions, contributed to the stabilization of calcite and maintained a constant driving force for the mineral nucleation and growth. For the highest Ca^{2+} condition a fast crystal growth rate was consistent with rapid calcite precipitation as suggested further by affinity calculations. Although saturation state based kinetic precipitation models cannot accurately reflect the controls on crystal growth kinetics or reliably predict growth mechanisms, the relatively reaction orders obtained from modeling of calcite precipitation rates as function of decreasing carbonate concentration suggest that the precipitation occurred via surface-controlled rate determining reactions. These high reaction orders support in addition the hypothesis that crystal growth proceeded through complex surface controlled mechanisms. In conclusion, the steady state supersaturated conditions generated by a constant cyanobacteria biomass and metabolic activity strongly suggest that these microorganisms could be used for the development of efficient CO_2 sequestration methods in a controlled large-scale environment.

1. Introduction

Today, the Earth's atmosphere records a CO_2 concentration of 403 ppm and 1100 ppm have been estimated by the year 2100 with detrimental and irreversible long-term effects on the quality of life of generations to come (Kharaka and Cole, 2011). As a consequence, carbon capture and storage (CCS) techniques need to be developed and quickly implemented in order to mitigate raising atmospheric CO_2 levels (Herzog, 2011). Among CCS methods, biological carbon sequestration by enhanced biomineralization has been investigated (Lee et al., 2004, 2006; Papazi et al., 2008; Dupraz et al., 2009; Obst et al., 2009; Dittrich and Sibler, 2010; Jansson and Northen, 2010; Martinez et al., 2010; Bundeleva et al., 2011, 2012, 2014; Zhu et al., 2015). However, further studies are needed to quantify the rates of biomediated carbonate precipitation under steady-state conditions.

CO_2 biomineralization in the form of calcium carbonate ($CaCO_3$) is ubiquitous in nature (Ferris et al., 1994; Millero, 2007; Cusack and Freer, 2008; Zhu et al., 2015). It is present in fresh- and seawater, and terrestrial ecosystems and is a key process of the global cycling of carbon (Ferris et al., 1994; Pokrovskiy and Savenko, 1995; Millero, 2007; Cusack and Freer, 2008; Jansson and Northen, 2010; Zhu et al., 2015). Particularly, cyanobacteria have played a major role in $CaCO_3$ precipitation since the Archean Eon (Thompson et al., 1997; Altermann et al., 2006; Power et al., 2007). These Gram negative microorganisms rely on oxygenic photosynthesis to metabolize CO_2 and produce organic macromolecules (Badger and Price, 2003; Price et al., 2002, 2008; Jansson and Northen, 2010).

☆ The paper has been recommended for acceptance by Dr. B. Ngwenya.

* Corresponding author.
E-mail address: raul.martinez@minpet.uni-freiburg.de (R.E. Martinez).

http://dx.doi.org/10.1016/j.apgeochem.2016.10.017
0883-2927/

Two cyanobacteria, namely *Synechococcus* sp. and *Prochlorococcus* sp., are responsible for more than 25% of the global photosynthesis (Dittrich and Obst, 2004; Rohwer and Thurber, 2009). Cyanobacteria, proposed to be responsible for whiting events, depend on a carbon concentrating mechanism (CCM), which allows them to enhance the amount of CO_2 at the site of their Rubisco enzyme in the Calvin cycle. This is the first step in the assimilation of CO_2 into organic biomolecules (Lee et al., 2004; Jansson and Northen, 2010).

CO_2 biomineralization to $CaCO_3$ at the alkaline pH conditions generated by active cyanobacteria is an important consequence of the CCM (Obst et al., 2009; Jansson and Northen, 2010). The CCM transports HCO_3^- across the cyanobacteria outer and plasma membranes. Once inside the cell, HCO_3^- enters the carboxysome. Within this protein-enclosed compartment, HCO_3^- is converted to CO_2 by carbonic anhydrase (Dupraz et al., 2009; Jansson and Northen, 2010). The activity of this enzyme generates an alkaline pH in the micro-environment of the cyanobacteria cell surface due to the production of OH^- ions (McConnaughey and Whelan, 1997; Martinez et al., 2008; Dupraz et al., 2009; Jansson and Northen, 2010). Under controlled conditions, a constant active cyanobacteria biomass concentration could sustain an alkaline bulk solution pH and supersaturated conditions for the nucleation and precipitation of calcium carbonate (Dupraz et al., 2009; Martinez et al., 2010; Bundeleva et al., 2012).

The nucleation, precipitation and crystal growth of biogenic $CaCO_3$ have been investigated with state-of-the art microscopic and spectroscopic methods (Teng et al., 2000; Benzerara et al., 2006; Aloisi et al., 2006; Kosamu and Obst, 2009; Obst et al., 2009; Rodríguez-Blanco et al., 2011; Bots et al., 2012; Ruiz-Agudo and Putnis, 2012; Urosevic et al., 2012; Bénézeth et al., 2013; Couradeau et al., 2013), however, although of utmost significance, these studies can be complemented by kinetic modeling of carbonate mineral formation derived from the monitoring of aqueous solution composition. So far, bulk kinetic measurements have not been able to accurately relate solution chemistry to the microscopic growth processes occurring at mineral surfaces, and batch reactors have been used extensively to quantify carbonate biomineral precipitation rates (Dittrich et al., 2003; Mitchell and Ferris, 2006; Obst et al., 2009; Martinez et al., 2010; Bundeleva et al., 2011, 2012, 2014). However, they are limited in their ability to control aqueous solution composition, including pH, pCO_2, saturation state, and biomass concentration (Martinez et al., 2010; Bundeleva et al., 2012). As such, it is impossible to develop robust rate equations describing CO_2 biomineralization. These limitations have been overcome by the development of mixed-flow reactors (Zhong and Mucci, 1993; Schott et al., 2009). They represent the first step in the development of CO_2 biomineralization methods because they allow rate quantification under controlled conditions. Mixed-flow reactors permit to study factors that influence mineralization reactions while varying a particular parameter and maintaining others constant. These constant addition systems maintain steady state conditions for CO_2 biomineralization, from which a kinetic description of the reaction mechanism can be derived (Zhong and Mucci, 1993; Schott et al., 2009).

In this study, a mixed-flow steady-state bio-reactor was designed to biomineralize CO_2 as calcium carbonate as a result of active *Synechococcus* sp. photosynthesis. Dissolved CO_2, generated by constant air bubbling of inorganic and cyanobacteria stock solutions, was the only source of inorganic carbon, as no bicarbonate or carbonate salts, or calcium carbonate seeds were added to experimental solutions. The release of hydroxide ion (OH^-) by cyanobacteria, as a waste product from photosynthesis, maintained highly alkaline pH conditions. In the presence of Ca^{2+} and the quasi-instantaneous carbonic acid dissociation reactions (Lasaga, 1981), this led to calcite supersaturation. Calcite precipitation rates were modeled as a function of decreasing carbonate activity as explained in Zhong and Mucci (1993), while other parameters remained constant. The calcite crystals generated were characterized with ESEM, EDS, XRD and Raman spectroscopy.

2. Materials and methods

2.1. Growth of Synechococcus sp. cyanobacteria culture stock

Synechococcus sp. cyanobacteria (PCC 7942) cultures were grown in sterile cyanobacteria BG-11 freshwater solution medium (Sigma-Aldrich C3061) for three weeks to the stationary growth phase, as described in Martinez et al., 2008, 2010. Stock cultures were kept at room temperature of (22 ± 1 °C), under a constant cool white fluorescent light illumination (5000 lux) on a rotatory shaker at 200 rpm. Aliquots were taken from the cyanobacteria stock culture for further preparation of the bacteria stock (BS) solution in Fig. 1.

2.2. Preparation of bacteria and inorganic stock solutions

In order to preserve freshwater electrolyte conditions, the inorganic stock (IS) solution in Fig. 1 was prepared by dissolving 3.25 g $NaNO_3$ and 0.375 g $MgSO_4 \cdot 7H_2O$ in 5 L of sterile double distilled water (0.055 μS/cm). To this 5 L background electrolyte solution, $CaCl_2$ was added to generate final nominal Ca^{2+} concentrations of 15, 150 or 300 ppm. A maximum value of 300 ppm Ca^{2+} was chosen to prevent detrimental ionic strength effects on cyanobacteria growth. These Ca^{2+} concentrations were chosen within the range for natural waters (e.g. $Ca^{2+}_{\text{river-water}} = 15$ ppm, $Ca^{2+}_{\text{sea-water}} = 400$ ppm). The cyanobacteria stock solution for kinetic experiments, BS in Fig. 1, was prepared by adding 10 mL of 50x cyanobacteria BG-11 freshwater medium solution (1/500 dilution), along with a 25 mL aliquot of cyanobacteria stock culture to 5 L of sterile double distilled water with 3.25 g $NaNO_3$ and 0.375 g $MgSO_4 \cdot 7H_2O$. For addition to the BS reactor, the 25 mL of cyanobacteria stock culture were washed by centrifuging at 10,000 × g for 10 min, to a final resuspension of the cells in 25 mL of the background electrolyte solution (i.e. 0.65 g/L $NaNO_3$ and 0.075 g/L $MgSO_4 \cdot 7H_2O$). Air, filtered through a 0.22 μm filter, and humidified within a gas wash bottle (Fig. 1), was bubbled constantly in the IS and BS solution for the duration of experiments with Optima aquarium pumps (Hagen Deutschland GmbH & Co., D-25488, Holm) exerting an excess pressure of approximately 8 psi, in an addition to an air pressure of 14.7 psi. The BS solution was constantly illuminated with cool white fluorescent light illumination (5000 lux).

2.3. Mixed-flow bio-reactor set up

The mixed flow bio-reactor set-up consisted of 2 stock solutions pumped through a sealed reactor vessel to maintain steady state conditions (Fig. 1). Custom made lids for the 5 L Schott® bottles containing inorganic and bacteria stock (IS and BS) solutions were fitted with flexible plastic tubing (Tygon® Formulation E-3603) for air bubbling and connection to the mixed-flow bio-reactor. IS and BS were input into the mixed-flow steady state bio-reactor by a high precision multi-channel peristaltic pump (Ismatec® Model ISM948C). IS and BS solutions were transferred simultaneously by this pump through two independent channels, at a rate of 200 μL/min, through stopper flexible plastic tubing (Tygon® Formulation LMT-55 Color code: purple). At the start of experiments (i.e. time zero), the mixed flow reactor was filled, to a final volume of 325 mL using the maximum speed of the peristaltic pump. Samples for solution monitoring were collected, at time zero and once every

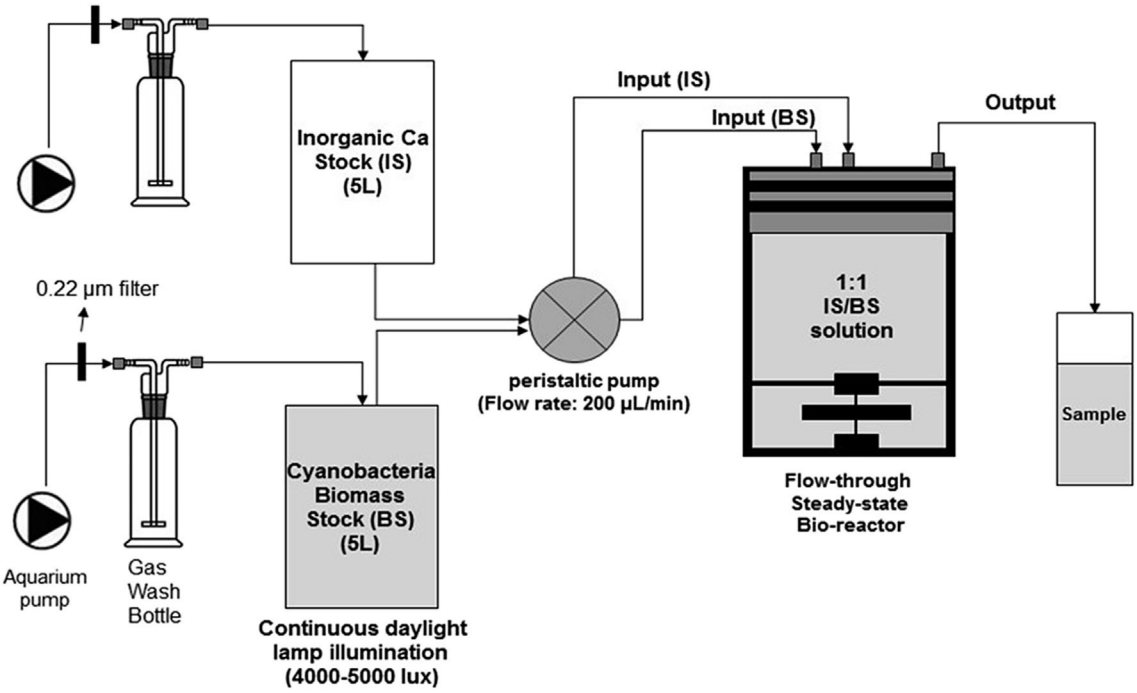

Fig. 1. Design of mixed-flow steady-state bio-reactor for quantification of calcite precipitation in the presence of active *Synechococcus* sp. cyanobacteria. "IS" and "BS" refer to the inorganic and bacteria stocks respectively prepared as explained in text. The solution inside the mixed-flow reactor was stirred by suspended stirring bar at 150 rpm.

24 h for period of 13 days, at the output of the bio-reactor in Fig. 1. The mixed-flow reactor consisted of a 400 mL borosilicate glass beaker, which was made air tight and closed from the atmosphere with an O-ring fitted custom made plastic lid (Fig. 1).

2.4. Monitoring of mixed-flow bio-reactor solution

Ca^{2+} concentration in the IS and its evolution inside the mixed-flow bio-reactor was monitored with a flame atomic absorption spectrometer (F-AAS vario 6 analytik Jena®) with a detection limit of >0.01 ppm. Monitoring of Synechococcus sp. cyanobacteria biomass in stock cultures and in the BS solution in Fig. 1 was achieved though spectrophotometric methods by measuring the solution absorbance at 750 nm using a Lambda 40 UV/Vis spectrophotometer (Perkin Elmer Instruments®) controlled by UV WinLab® software. A standard curve was constructed to correlate absorbance measurements to dry weight of cyanobacteria in mg and further estimate the biomass concentration in mg/L, for samples from the mixed-flow reactor. The pH, conductivity and total and carbonate alkalinities of each sampled aliquot were determined in the presence of cyanobacteria. The pH was measured using a pH electrode (Metrohm® 6.0257.000), four point calibrated with NIST standard buffers of pH 4.01 ± 0.01, 6.86 ± 0.01, 9.01 ± 0.01 and 11.01 ± 0.01 (CertiPUR® Buffer solutions – Merck KGaA, Darmstadt, Germany). The total and carbonate alkalinities were determined by titration with a 0.1 M HCl solution using an automated titrator system (Metrohm® 719S Titrino). To derive the solution ionic strength, the conductivity of each sample was measured, with a conductivity probe (Metrohm® 6.2324.010) previously calibrated with a 100 µS/cm standard solution (Metrohm® 6.2324.010) attached to a Metrohm 712 Conductometer.

2.5. Mineralogical characterization of precipitates in the mixed-flow bio-reactor

A qualitative mineralogical analysis of the crystals precipitated in the mixed-flow bio reactor was carried out with X-ray diffraction (XRD) using a Bruker AXS D8 Advance X-ray powder diffractometer, equipped with a Cu-Kα radiation source, a diffracted beam graphite monochromator, and a scintillation detector. The XRD patterns were collected from 2.0 to 60.0° 2θ, with a step size of 0.02 2θ, and a dwell time of 5 s at each step. The XRD patterns were evaluated with the DIFFRACplus 5.0 software.

Micro-Raman spectroscopy analyses of the same precipitates were performed to confirm the presence of calcite using a Renishaw inVia Raman spectrometer combined Leica DM 2500M Raman microscope with a 200× magnification and coupled to WiRE software (SSEF, Basel, Switzerland). The excitation source was an argon (Ar^{+}) laser at a wavelength of 514.5 nm.

Scanning electron microscopy/EDS analyses were performed at the Crystallography Department at the University of Freiburg, using a LEO 1525 field emission scanning electron microscope with an Oxford/Link electron backscattering detector (EBSD). High resolution electron microscopy images of the calcite crystals in the mixed-flow bio-reactor were obtained at the University of Leeds, U.K. with a Scanning Electron Microscope – FEI Quanta 650 FEG-ESEM with SE, BSE and full environmental (ESEM) capabilities. The ESEM was also fitted with a KE Centaurus panchromatic CL detector, an Oxford X-max 80 SDD EDS with AZtec software and an Oxford/HKL Nordlys S EBSD system.

Crystals precipitated from the mixed-flow bio-reactor solution at the highest Ca^{2+} activity were prepared for ESEM imaging by an ethanol exchange procedure. Samples containing calcite crystals were fixed by Glutaraldehyde treatment as follows: the sampled calcite was placed overnight in sterile 2.5% Glutaraldehyde (25% stock solution diluted in 50 mM Na_3PO_4) and subsequently ethanol exchanged by suspending them in continuously increasing ethanol concentrations through to pure ethanol. Finally samples were critical point dried, mounted on SEM sample stubs and gold coated.

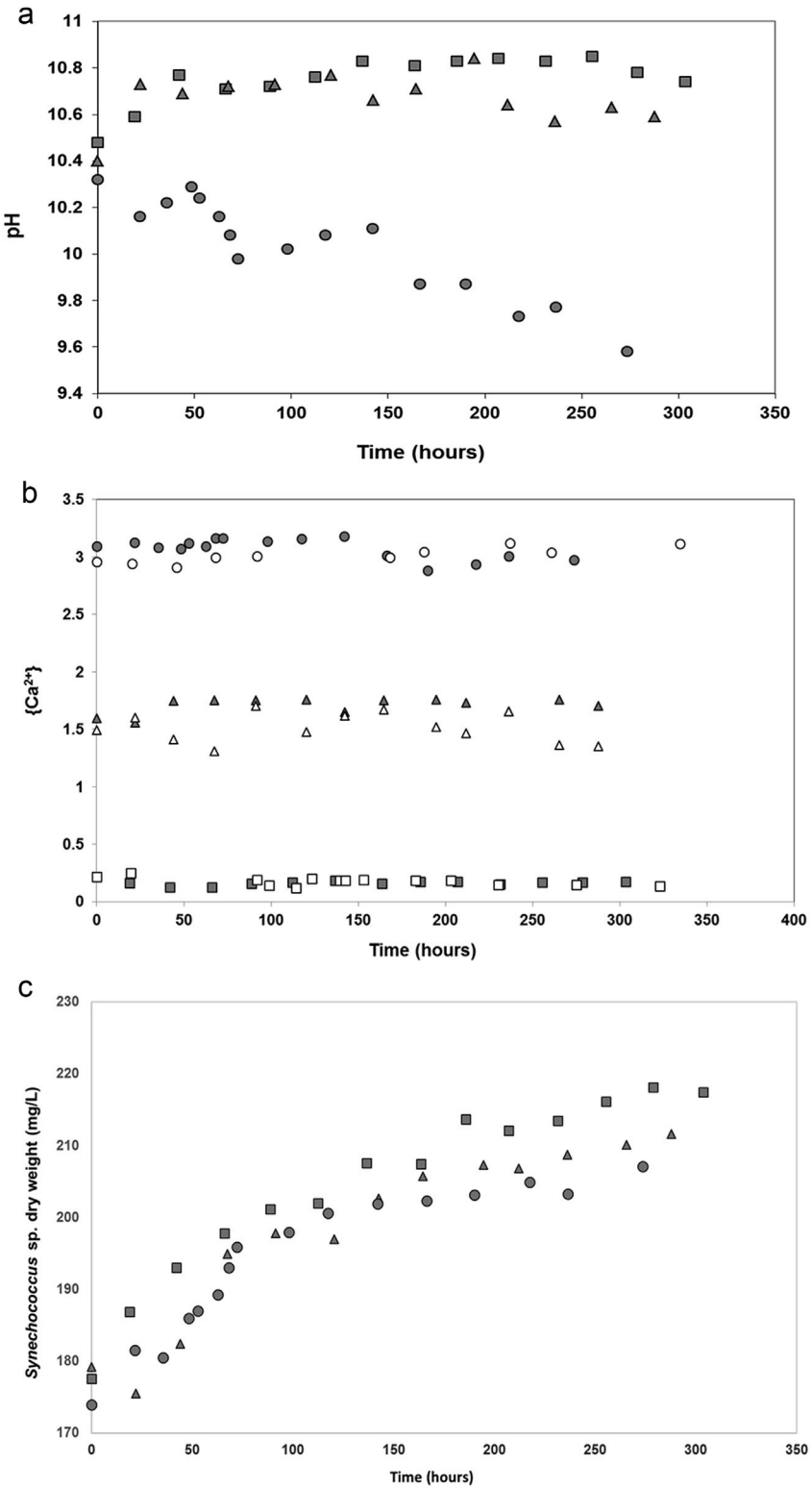

Fig. 2. a. This plot shows the evolution of pH for the duration of experiments in the presence of active cyanobacteria. Grey filled squares, triangles and circles correspond to calcium activities, $\{Ca^{2+}\}$, of 0.16 ± 0.02, 1.71 ± 0.07 and 3.07 ± 0.09. The gradual decrease in pH for the highest $\{Ca^{2+}\}$ suggests precipitation of calcium carbonate as per Eq. (1) in text. b. This figure shows the evolution of calcium activity for the duration of experimental runs in the presence of biomass (grey filled markers) and control inorganic conditions (open markers) for $\{Ca^{2+}\}$ of 0.16 ± 0.02, 1.71 ± 0.07 and 3.07 ± 0.09 as denoted by squares, triangles and circles respectively. The values shown correspond to the average in calcium activity from replicate experiments and the error in $\{Ca^{2+}\}$ measurements between replicate experiments ranged between 2 and 4%. c. Evolution of the *Synechococcus* sp. cyanobacteria biomass concentration as a function of time. For the first 48 h there is a slight increase in biomass from a lowest value of 180 mg/L to 200 mg/L, however, from 48 h to the end of experiments, the biomass remains stable within 200 and 220 mg/L. Square, triangle and circle markers correspond to Ca^{2+} activities of 0.16 ± 0.02, 1.71 ± 0.07 and 3.07 ± 0.09.

2.6. Modeling of calcite precipitation rates

The rate of calcite precipitation was modeled as: $R_1 = K_f^* [CO_3^{2-}]^{n1}$, or its logarithmic expression: $\log_{10}(R_1) = n_1^* \log_{10} [CO_3^{2-}] + \log_{10}(K_f)$, where K_f is the forward kinetic constant, and n_1 is the order of the reaction according to Zhong and Mucci, 1993. The results from these calculations were compared to those obtained from the empirical rate law: $R_2 = k_+^* (\Omega - 1)^{n2}$ or its logarithmic expression: $\log_{10} R_2 = n_2^* \log_{10}(\Omega - 1) + \log_{10}(k_+)$, where n_2 is the reaction order and k_+ is the forward rate constant (Lasaga, 1981; Morse, 1983). To calculate the experimental rate, $R_{exp} = d[CO_3^{2-}]/dt$, a polynomial fit of $[CO_3^{2-}]$ vs time data was generated. The first derivative of this polynomial fit was calculated from an observed calcite precipitation induction time of 48 h and used to calculate the rate of calcite precipitation, from the evolution of $[CO_3^{2-}]$, in moles/cm^3/s. R_{exp} was plotted as a function of both $\log_{10}[CO_3^{2-}]$ or $\log_{10}(\Omega - 1)$. Best fit values for the forward kinetic constants K_f and k_+, and the orders of reaction, n_1 and n_2 were obtained from linear regression of the resulting data.

3. Results and discussion

Fig. 2a, b and 2c show the evolution of the pH, Ca^{2+} activity and biomass concentration respectively, over a period of 13 days. The Ca^{2+} activities of 0.16 ± 0.02, 1.71 ± 0.07 and 3.07 ± 0.09, corresponding to ionic strengths (IS) of 0.08 ± 0.02, 0.09 ± 0.01 and 0.11 ± 0.01 M, remained constant within the stated uncertainty and were used to determine Ca^{2+} and carbonate activities and activity

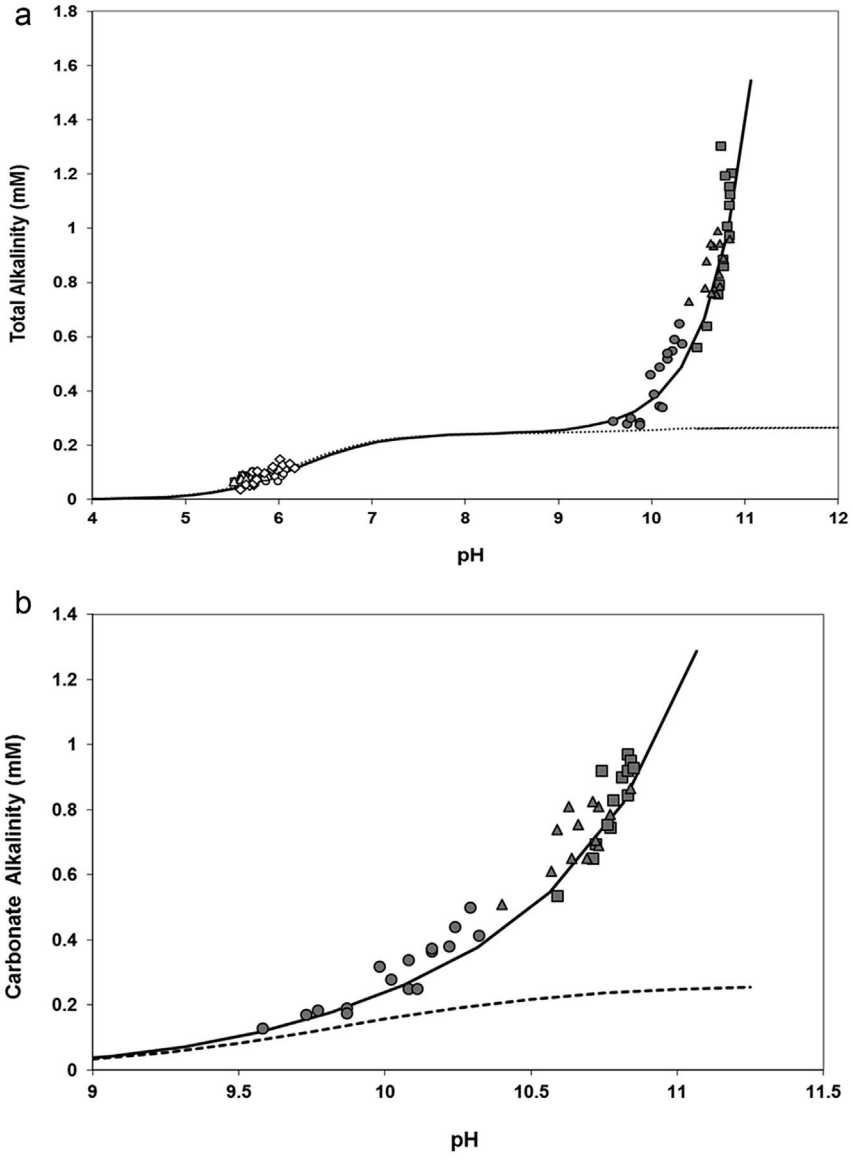

Fig. 3. a. Shows the evolution of modeled and experimental total alkalinity as a function of pH. The solid line represents the total alkalinity modeled from first principles for a total inorganic carbon concentration in the mixed-flow reactor of 0.29 ± 0.04 mM, as explained in text. The dotted line is the total alkalinity calculated only as a function of bicarbonate and carbonate species. Open markers at low pH, depict total alkalinities from replicate inorganic control experiments, and the grey squares, triangles and circles represent the measured total alkalinities corresponding to experiments with Ca^{2+} activities of 0.16 ± 0.02, 1.71 ± 0.07 and 3.07 ± 0.09 in the presence of active *Synechococcus* sp. The lowest values for the cyanobacteria data sets are those measured at the end of experimental runs. b. Shows the evolution of modeled and experimental carbonate alkalinity as a function of pH. The solid line represents the carbonate alkalinity modeled from first principles for a total inorganic carbon concentration in the mixed-flow reactor of 0.29 ± 0.04 mM, as explained in text. The dotted line is the carbonate alkalinity calculated only as a function of carbonate species. The grey squares, triangles and circles represent the carbonate alkalinities derived from measured total alkalinities corresponding to experiments with Ca^{2+} activities of 0.16 ± 0.02, 1.71 ± 0.07 and 3.07 ± 0.09 in the presence of active *Synechococcus* sp. The lowest values for the cyanobacteria data sets are those measured at the end of experimental runs.

coefficients when needed. Similarly, the *Synechococcus* sp. biomass concentrations did not change significantly, averaging 204 ± 12, 198 ± 13 and 197 ± 8 mg/L (Fig. 2b). These values were consistent with that of 202 ± 18 mg/L from control absorbance measurements in the absence of Ca^{2+}, suggesting no interferences from the precipitating calcium carbonate phase at 750 nm. For Ca^{2+} activities of 0.16 ± 0.02 and 1.71 ± 0.07 constant pH values of 10.75 ± 0.10 and 10.66 ± 0.11 were observed. For the highest Ca^{2+}, however, the pH dropped from 10.32 ± 0.17 to a final value of 9.54 ± 0.14 (Fig. 2a). This gradual pH decrease can be explained by the formation of $CaCO_3$ or $CaHCO_3^+$ complexes in alkaline solution with the rapid deprotonation of dissolved CO_2 (H_2CO_3) to CO_3^{2-} and HCO_3^- and the slow exchange of H_2CO_3 with the atmosphere (Plummer et al., 1978; Lasaga, 1981; Gómez-Morales et al., 1996). This supports the mechanism in Eqs. (1)–(4) where:

$$HCO_3^- + H_2O = CH_2O + O_2 + OH^- \quad (1)$$

$$HCO_3^- + OH^- = CO_3^{2-} + H_2O \quad (2)$$

$$Ca^{2+} + CO_3^{2-} = CaCO_3(s) \quad (3)$$

$$\text{Overall reaction}: \quad Ca^{2+} + 2HCO_3^- = CH_2O + O_2 + CaCO_3(s) \quad (4)$$

The overall reaction in Eq. (4) is consistent with the decrease in carbonate alkalinity in Fig. 3b and the consequent pH decrease for the highest Ca^{2+} condition (Fig. 2a). This scheme explains the chemical reactions leading to pH decrease: (1) HCO_3^- buffering by hydroxide ion produced by photosynthesis (Ferris et al., 1994; Pokrovskiy and Savenko, 1995; Morse et al., 2007; Dupraz et al., 2009), and (2) the consumption of carbonate ions by calcium carbonate precipitation, leading to a lower buffering capacity (Eq. (3)). The mechanism in Eq. (3) is confirmed by the results in Fig. 4 and Fig. 9, where a marked decrease in saturation index and $[CO_3^{2-}]$ are observed from maxima attained at 48 h from start of experiments. From this time on a continuous pH decrease is also observed in Fig. 2a suggesting an induction time of 48 h for calcium carbonate nucleation and precipitation in experiments with the highest Ca^{2+} activity. This is consistent with the results of He and Morse (1993) which showed that a supersaturation of at least 20 to 30 times with respect to calcite was necessary for nucleation of calcium carbonate within a few hours to a day. This value is also in good agreement with the study of Obst et al. (2009) where induction times of 25–50 h were observed as a function of supersaturation.

In the absence of added carbonate or bicarbonate salts, or calcium carbonate seeds, the mixed-flow bio-reactor (Fig. 1) relied exclusively on the constant air bubbling in the stock solutions (IS and BS) to generate calcium carbonate supersaturated conditions in the presence of active cyanobacteria. In the IS and BS, the total inorganic carbon, Ct, was determined from the excess pressure of approximately 8 psi exerted by the aquarium pump and the standard atmospheric air pressure of 14.7 psi. A total air pressure of 1.24 atm was then determined in equilibrium with the IS and BS solutions. As both stocks were open with respect to CO_2 exchange, the pCO_2 was calculated for a current atmospheric CO_2 concentration of 403 ppm, where the $\log_{10} pCO_2 = -2.20 \pm 0.09$. From these parameters and a Henry's law constant of 3.39×10^{-2} for 22 °C (Almeida et al., 2001), a Ct of 0.30 ± 0.05 mM was obtained for the IS solution with an equilibrium pH of 5.56 ± 0.22. For the bacteria stock (BS) however, Ct was calculated from the total alkalinity (TA) and the pCO_2. In the BS, two processes gave rise to alkalinity: (1) the constant dissolution and rapid ionization of dissolved CO_2 (i.e. H_2CO_3) to generate HCO_3^- and CO_3^{2-} and, (2) the OH^- ion released from cyanobacteria cells by photosynthesis. During the *Synechococcus* sp. stationary growth phase, the BS pH was stable at 10.65 ± 0.11 for 5 days prior to the start of experiments. This stock had a constant TA of 1.09 ± 0.19 mM and a $[OH^-]$ of 0.45 ± 0.13 mM. For the highly alkaline pH in the BS, carbonate ion was the dominant inorganic carbon species, and HCO_3^- was neglected. Ct was assumed to be equal to a $[CO_3^{2-}]$ of 0.32 ± 0.07 mM, as calculated from the carbonate alkalinity. No loss of Ct was expected upon transfer of IS and BS solutions to the mixed-flow bio-reactor by the peristaltic pump (Fig. 1).

Prior to the main experimental runs in presence of cyanobacteria, replicate controls were performed using the setup in Fig. 1, but with two inorganic stock (IS) solutions, to confirm the complete transfer of Ct to the mixed-flow reactor. A Ct value of 0.29 ± 0.04 mM was determined from these experiments. This

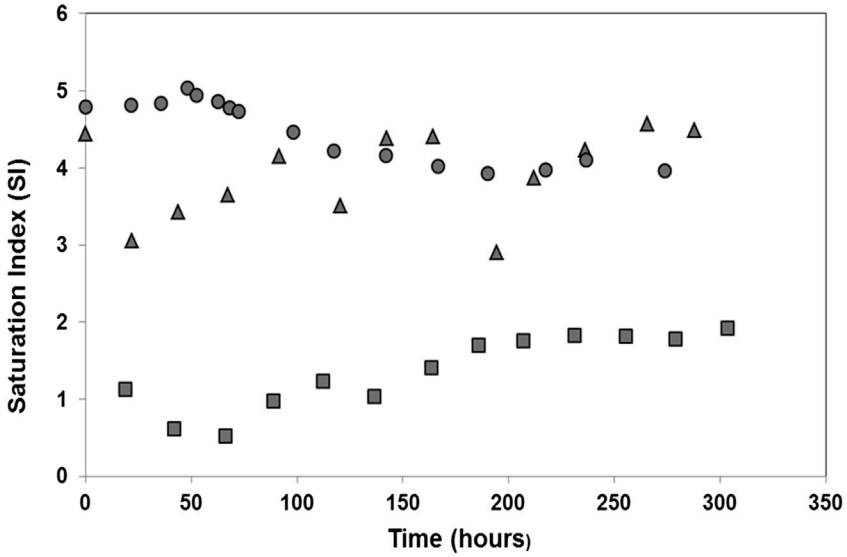

Fig. 4. Evolution of the saturation indeces (SI) for mixed-flow bio-reactor solutions. The grey squares, triangles and circles represent saturation indices calculated for experiments with Ca^{2+} activities of 0.16 ± 0.02, 1.71 ± 0.07 and 3.07 ± 0.09 in the presence of active *Synechococcus* sp. For the highest Ca^{2+} activity (grey circles) a maximum value of SI is observed at 48 h from the start of experiments. This time was regarded as the induction time for calcite precipitation in this system.

Table 1
Evolution of mixed-flow bio-reactor solution parameters over the course of control and biomass containing experimental runs.

Time (hours)	pH	$\{Ca^{2+}\}$[a]	Biomass[b] (mg/L)	Total Alk. (mM)	Carbonate Alk. (mM)	Ω[d]	$[CO_3^{2-}]$[c] (mM)
0	**5.64**	**0.16 ± 0.02**	**0**	**0.075**	**0**	**0.004**	**4.03×10^{-6}**
23	5.74			0.080	0	0.005	5.41×10^{-6}
95	5.71			0.080	0	0.005	5.05×10^{-6}
119	5.88			0.090	0	0.008	8.40×10^{-6}
153	5.66			0.085	0	0.004	4.78×10^{-6}
171	5.52			0.065	0	0.002	2.65×10^{-6}
183	5.88			0.090	0	0.008	8.40×10^{-6}
197	5.61			0.090	0	0.004	4.51×10^{-6}
203	5.7			0.080	0	0.005	4.93×10^{-6}
221	5.6			0.075	0	0.003	3.67×10^{-6}
231	5.65			0.075	0	0.004	4.12×10^{-6}
275	5.85			0.085	0	0.007	7.40×10^{-6}
323	5.74			0.080	0	0.005	5.41×10^{-6}
0	**5.77**	**1.71 ± 0.07**	**0**	**0.080**	**0**	**0.005**	**5.79×10^{-6}**
23	5.7			0.065	0	0.004	4.01×10^{-6}
45	6.07			0.110	0	0.015	1.59×10^{-6}
119	5.94			0.090	0	0.009	9.64×10^{-6}
143	6.03			0.085	0	0.010	1.12×10^{-5}
167	6.05			0.095	0	0.012	1.31×10^{-5}
192	5.96			0.085	0	0.009	9.53×10^{-6}
221	5.72			0.105	0	0.006	6.78×10^{-6}
263	5.86			0.065	0	0.005	5.79×10^{-6}
311	5.99			0.065	0	0.007	7.81×10^{-6}
0	**5.59**	**3.07 ± 0.09**	**0**	**0.037**	**0**	**0.002**	**1.77×10^{-6}**
20	5.69			0.049	0	0.003	2.95×10^{-6}
46	5.65			0.054	0	0.003	2.97×10^{-6}
68	5.73			0.053	0	0.003	3.50×10^{-6}
92	5.73			0.060	0	0.004	3.96×10^{-6}
168	5.76			0.072	0	0.005	5.10×10^{-6}
188	5.72			0.100	0	0.006	6.46×10^{-6}
237	5.85			0.097	0	0.008	8.45×10^{-6}
261	5.77			0.103	0	0.007	7.46×10^{-6}
335	5.93			0.111	0	0.011	1.16×10^{-5}
359	5.94			0.119	0	0.012	1.27×10^{-5}
379	6.01			0.148	0	0.017	1.86×10^{-5}
404	6.04			0.127	0	0.016	1.71×10^{-5}
428	6.04			0.126	0	0.016	1.70×10^{-5}
478	6.17			0.114	0	0.019	2.07×10^{-5}
502	6.12			0.131	0	0.020	2.12×10^{-5}
0	**10.48**	**0.16 ± 0.02**	**204 ± 12**	**0.560**	**nd**	**nd**	**nd**
19	10.59			0.640	0.535	3.096	6.39×10^{-2}
42	10.77			0.860	0.745	1.844	4.91×10^{-2}
66	10.71			0.755	0.650	1.676	4.51×10^{-2}
89	10.72			0.795	0.695	2.667	5.66×10^{-2}
112	10.76			0.885	0.755	3.443	6.87×10^{-2}
137	10.83			0.975	0.845	2.817	5.09×10^{-2}
164	10.81			1.010	0.900	4.067	8.56×10^{-2}
186	10.83			1.085	0.970	5.454	1.03×10^{-1}
207	10.84			1.125	0.950	5.817	1.12×10^{-1}
231	10.83			1.155	0.920	6.250	1.36×10^{-1}
255	10.85			1.165	0.930	6.146	1.22×10^{-1}
279	10.78			1.023	0.830	5.901	1.17×10^{-1}
304	10.74			0.984	0.920	6.838	1.30×10^{-1}
0	**10.40**	**1.71 ± 0.07**	**198 ± 13**	**0.730**	**0.510**	**84.57**	**1.76×10^{-1}**
22	10.73			0.785	0.690	21.05	4.48×10^{-2}
44	10.69			0.755	0.650	30.91	5.86×10^{-2}
67	10.72			0.830	0.705	38.51	7.29×10^{-2}
91	10.73			0.945	0.810	63.15	1.19×10^{-1}
120	10.77			0.890	0.785	33.53	6.31×10^{-2}
142	10.66			0.935	0.755	79.80	1.60×10^{-1}
165	10.71			0.990	0.825	81.55	1.54×10^{-1}
195	10.84			0.960	0.865	18.291	3.44×10^{-2}
212	10.64			0.760	0.650	47.901	9.16×10^{-2}
236	10.57			0.780	0.610	68.487	1.37×10^{-1}
266	10.63			0.945	0.810	96.501	1.82×10^{-1}
288	10.59			0.880	0.740	88.867	1.73×10^{-1}
0	**10.32**	**3.07 ± 0.09**	**197 ± 8**	**0.575**	**0.415**	**120.15**	**1.29×10^{-1}**
22	10.16			0.520	0.365	123.26	1.31×10^{-1}
35	10.22			0.550	0.380	126.04	1.35×10^{-1}
48	10.29			0.650	0.500	153.51	1.65×10^{-1}
53	10.24			0.590	0.440	140.32	1.49×10^{-1}
63	10.16			0.540	0.375	129.30	1.38×10^{-1}
68	10.08			0.490	0.340	119.82	1.25×10^{-1}

Table 1 (*continued*)

Time (hours)	pH	$\{Ca^{2+}\}$[a]	Biomass[b] (mg/L)	Total Alk. (mM)	Carbonate Alk. (mM)	Ω[d]	$[CO_3^{2-}]$[c] (mM)
72	9.98			0.460	0.320	113.20	1.18×10^{-1}
98	10.02			0.390	0.280	87.258	9.21×10^{-2}
117	10.08			0.345	0.250	68.038	7.13×10^{-2}
142	10.11			0.340	0.250	63.828	6.64×10^{-2}
166	9.87			0.285	0.190	55.795	6.13×10^{-2}
190	9.87			0.275	0.175	50.584	5.81×10^{-2}
217	9.73			0.280	0.170	53.295	6.01×10^{-2}
236	9.77			0.300	0.185	60.328	6.64×10^{-2}
274	9.58			0.290	0.130	52.346	5.83×10^{-2}

[a] Mean activity of calcium calculated using activity coefficients and ionic strength values over the course of experimental runs (Fig. 2b).
[b] A zero value of biomass corresponds to inorganic control experiments only in the presence of Ca^{2+}.
[c] Carbonate concentrations calculated from first principles with carbonate system acidity constants corrected for ionic strength.
[d] Ω refers to saturation state of solution with respect to calcite. Error from replicate experiments for alkalinity measurements was in the order of 0.5–1%, whereas the saturation state had an error of 1–2%. Alk refers to alkalinity. "nd" means that the parameter was not determined.

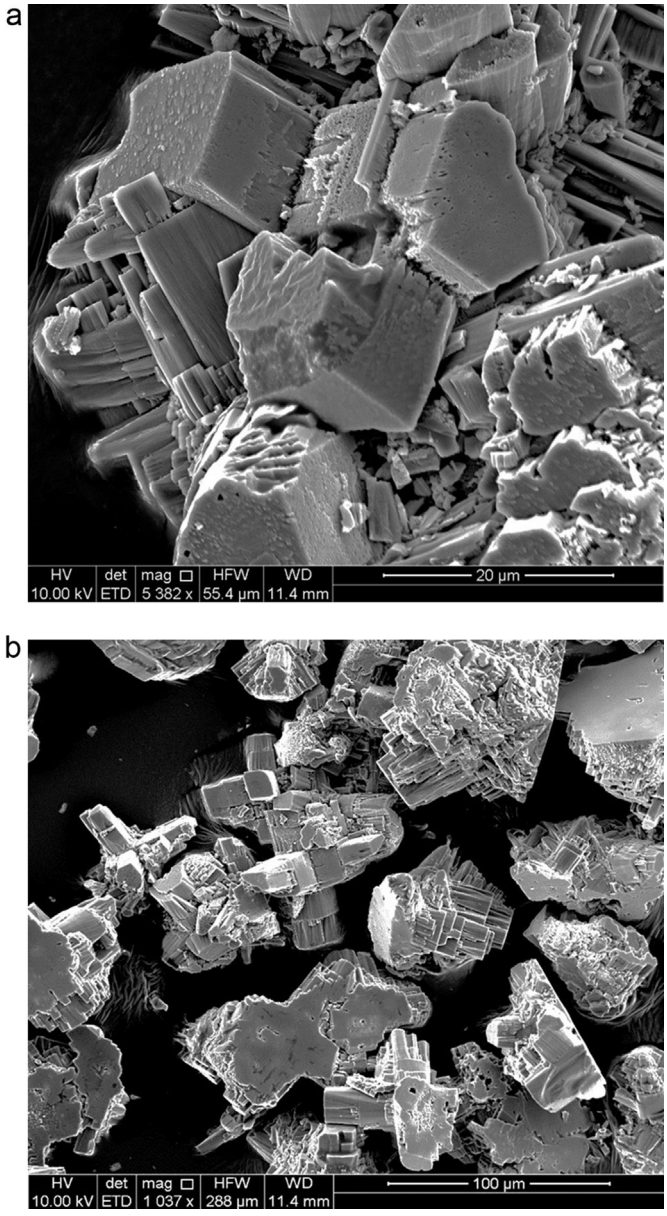

Fig. 5. ESEM Images (a) and (b) show calcite crystals generated in the mixed-flow steady state bio-reactor at the end of the experimental run at the highest Ca^{2+} activity (3.07 ± 0.09) and the presence of active *Synechococcus* sp. cyanobacteria. Both images show crystal features consistent with the inorganic formation of calcite, unaffected by the presence of organic matter as explained in text. In (b) flat crystal "sides" are observed, evidencing calcite nucleation and growth on the reactor glass walls.

value confirmed a complete transfer of Ct from stock solutions via the peristaltic pump (Fig. 1). Total and carbonate alkalinities were calculated from this value of Ct from the first principles of aquatic chemistry, and represented as solid lines in Fig. 3a and b. To emphasize the dominance of hydroxide ion activity on measured experimental alkalinities, dotted lines were plotted in these figures representing total and carbonate alkalinities computed in the absence of $[OH^-]$. Fig. 3a and b, and Table 1, show, in addition, the evolution of experimental total and carbonate alkalinities in the mixed-flow bio-reactor. In Fig. 3a, two data sets were plotted. The first, at the pH range of 5.52–6.17 and a total alkalinity of 0.04–0.14 mM, are the results of replicate inorganic control experiments (open markers). The second data group, at the pH interval of 9.54–10.85 and total alkalinities ranging from 0.29 to 1.31 mM, was recorded in the presence of active *Synechococcus* sp. cyanobacteria (grey filled markers). The higher total alkalinities measured were dominated by the $[OH^-]$ resulting from photosynthetic activity. Fig. 3b depicts experimental carbonate alkalinities for the same conditions, further emphasizing a strong influence of cyanobacteria metabolic activity (i.e. OH^- release) on the total and carbonate mixed-flow bio-reactor solution alkalinity.

Fig. 4 shows the evolution of saturation indeces (SI) in the presence of active cyanobacteria and Ca^{2+} at a temperature of 22 ± 1 °C. The SI was defined as the $\log_{10}(\Omega)$, where Ω is the saturation state with respect to calcite (Table 1). A temperature corrected solubility product ($K_{sp} = 10^{-8.46}$) was used to calculate the SI. The resulting values indicated supersaturated conditions for all experimental conditions (Fig. 4). The SI for the lowest Ca^{2+} activity ranged from 1.13 to 1.92 ($3.09 < \Omega < 6.84$) where no calcite crystal formation was observed after 13 days. This result is consistent with that of Zhong and Mucci, 1993 where no spontaneous nucleation of calcite took place in supersaturated solutions ($1 < \Omega < 15$) unless calcium carbonate seeds were introduced. This result further supports the idea that active cyanobacteria do not act as nucleation sites for calcite precipitation due to the development of a net positive surface charge at alkaline pH (Martinez et al., 2008, 2010). The SI oscillated between 3 and 4.6 for experiments with a Ca^{2+} activity of 1.71 ± 0.07. At the highest amount of Ca^{2+}, the SI reached a maximum value of 5.03 at 48 h from the start of experiments, decreasing gradually with time to a final value of 3.92. The high degree of supersaturation, under steady-state conditions, contributed to the stabilization of calcite and maintained a constant driving force for the mineral nucleation and growth. Under these highly supersaturated conditions the solution is expected to eventually crystallize, regardless of the critical size of nuclei or the presence of a foreign surface (DeYoreo and Vekilov, 2003).

ESEM imaging and EDS analyses confirmed the precipitation of calcite, in the presence of active cyanobacteria and the highest

Ca^{2+}, with a grain size ranging from 50 to 200 μm (Fig. 5a and b). Crystals showed a rhombohedral shape indicative of inorganic abiogenic precipitation (Gómez-Morales et al., 1996; Bundeleva et al., 2014). ESEM imaging revealed a surface roughness characteristic of crystals grown under significant supersaturation levels (Prieto et al., 1981; Astilleros et al., 2002; Teng et al., 2000). Another important morphological feature is the build-up of calcite crystals as elongated aggregates of echelon stacked flattened rhombs (Fig. 5a). Elongated calcite crystals have been suggested to occur from highly supersaturated solutions during rapid precipitation (James, 1972; Wright, 1984). These features can be indicative of homogeneous spontaneous nucleation, involving the formation of a precursor phase whose assembly and growth will evolve towards the properties of the bulk crystal (Mucci, 1986; Morse et al., 2007). The calcite crystals in Fig. 5a show cleavage and angular faces suggesting the absence of organic matter effects on crystal nucleation and morphology (Braissant et al., 2003; Bontognali et al., 2008; Bundeleva et al., 2012). The lack of round crystal edges or globular structures further supports the non-biogenic origin of these precipitates. The crystals in Fig. 5b, however, show distinct flat "sides" and suggest heterogeneous nucleation and growth of calcite on the reactor glass wall. As suggested by Brečević and Nielsen (1989) amorphous calcium carbonate (ACC) particles, in the order of 50–400 nm, may have been present at the start of experiments with the highest saturation state values and contributed to calcite nucleation and subsequent precipitation. EDS analysis of the precipitated mineral phase revealed C, O and Ca peaks, corresponding to those of a calcite standard (Fig. 6a).

Further characterization of the calcite crystals was accomplished by Raman spectroscopy. Two spectra are shown in Fig. 6b, the first corresponds to a Raman spectrum for synthetic calcite from the Laboratoire de Sciences de la Terre ENS-Lyon database and the second was obtained from crystals isolated from the mixed-flow bio-reactor at the highest Ca^{2+} activity. The latter showed four % transmission peaks at Raman shifts of 159, 285, 715 and 1086 cm^{-1} corresponding to those reported previously for calcite

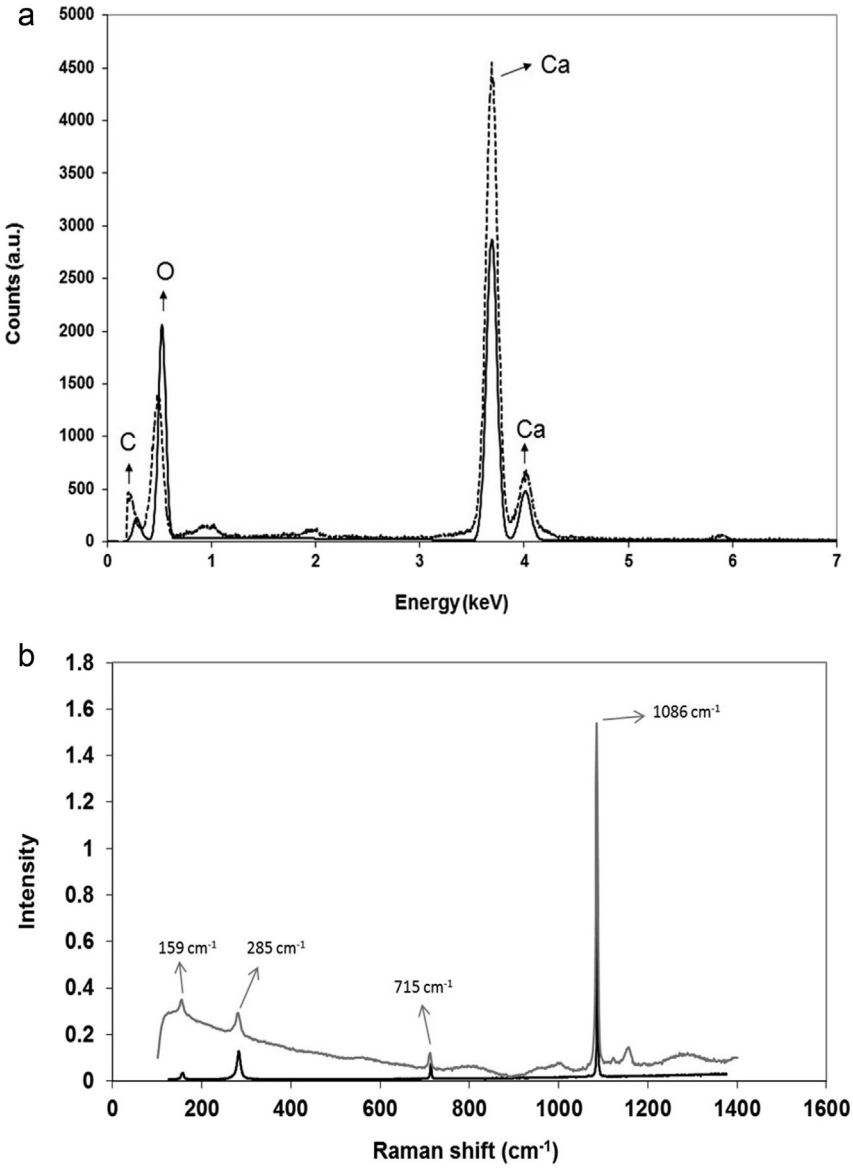

Fig. 6. (a) and (b) show EDS and Raman spectra respectively. Both spectra confirm the presence of calcite at the highest Ca^{2+} activity and active *Synechococcus* sp. cyanobacteria. In both (a) and (b) solid black line spectra correspond to standard pure calcite EDS and Raman spectra obtained from published databases (ENS-Lyon Raman Spectra Database).

Table 2
Affinity of mixed-flow reactor solution to form calcite and crystal growth rate of calcite crystals calculated from the evolution of solution parameters.

Ca2+	Biomass (mg/L)	Ω	Affinity, φ[a] (KJ/mol)	Crystal growth rate, G[b] (nm/s)
0.16 ± 0.02	**0**	**0.004**	**−13.72**	**nd**
		0.005	−13.00	nd
		0.005	−13.17	nd
		0.008	−11.92	nd
		0.004	−13.30	nd
		0.002	−14.75	nd
		0.008	−11.92	nd
		0.004	−13.44	nd
		0.005	−13.22	nd
		0.003	−13.94	nd
		0.004	−13.66	nd
		0.007	−12.23	nd
		0.005	−13.00	nd
1.71 ± 0.07	**0**	**0.005**	**−12.83**	**nd**
		0.004	−13.73	nd
		0.015	−10.35	nd
		0.009	−11.58	nd
		0.010	−11.21	nd
		0.012	−10.82	nd
		0.009	−11.60	nd
		0.006	−12.44	nd
		0.005	−12.83	nd
		0.007	−12.09	nd
3.07 ± 0.09	**0**	**0.002**	**−15.74**	**nd**
		0.003	−14.48	nd
		0.003	−14.47	nd
		0.003	−14.06	nd
		0.004	−13.76	nd
		0.005	−13.14	nd
		0.006	−12.56	nd
		0.008	−11.90	nd
		0.007	−12.21	nd
		0.011	−11.12	nd
		0.012	−10.89	nd
		0.017	−9.96	nd
		0.016	−10.17	nd
		0.016	−10.19	nd
		0.019	−9.70	nd
		0.020	−9.64	nd
0.16 ± 0.02	**204 ± 12**	**nd**	**nd**	**nd**
		3.096	2.77	0.002
		1.844	1.50	0.000
		1.676	1.27	0.000
		2.667	2.41	0.001
		3.443	3.03	0.002
		2.817	2.54	0.001
		4.067	3.44	0.003
		5.454	4.16	0.005
		5.817	4.32	0.005
		6.250	4.50	0.006
		6.146	4.46	0.006
		5.901	4.36	0.006
		6.838	4.72	0.008
1.71 ± 0.07	**198 ± 13**	**84.575**	**10.89**	**0.319**
		21.059	7.48	0.027
		30.914	8.42	0.050
		38.518	8.96	0.068
		63.153	10.17	0.143
		33.530	8.62	0.052
		79.800	10.75	0.222
		81.552	10.80	0.214
		18.291	7.13	0.019
		47.901	9.49	0.104
		68.487	10.37	0.194
		96.501	11.21	0.296
		88.867	11.01	0.276
3.07 ± 0.09	**197 ± 8**	**120.157**	**11.75**	**0.459**
		123.266	11.81	0.561
		126.043	11.87	0.547
		153.515	12.35	0.676
		140.324	12.13	0.622
		129.301	11.93	0.603
		119.825	11.74	0.584
		113.202	11.61	0.598
		87.258	10.97	0.393
		68.038	10.36	0.254
		63.828	10.20	0.223
		55.795	9.87	0.241
		50.584	9.63	0.211
		53.295	9.76	0.264
		60.328	10.06	0.302
		52.346	9.71	0.302

"nd" means indicates that the parameter was not determined.
[a] Affinity.
[b] Crystal growth rate were calculated as indicated in the text.

(Edwards et al., 2005; Bundeleva et al., 2014). In addition, these Raman shifts were in good agreement with those of the ENS-Lyon database spectrum for pure calcite at 156, 282, 713 and 1087 cm^{-1} (Fig. 6b). These results along with ESEM, EDS and XRD measurements (data not shown) confirmed the presence of calcite in supersaturated solutions generated by cyanobacteria metabolism.

To provide a measure of the ability of flow-through bio-reactor solutions to precipitate calcite, the affinity (Φ) was calculated (Table 2, Fig. 7). This is an intensive quantity measuring the driving force of a phase change and it represents the free energy difference between reactants and products (i.e. ΔG), such that $\Phi = -\Delta G$ (Nielsen, 1964; Pokrovsky and Schott, 2004; Benning and Waychunas, 2008; Schott et al., 2009). In this study, Φ, was calculated for each of the experiments as: $\Phi = kT^{*}\ln(\Omega)$, where T is the temperature in K, k is the Boltzmann constant in $KJ^{*}mol^{-1}{}^{*}K^{-1}$, and Ω refers to the saturation state. The larger Φ becomes, the greater the driving force for crystallization (Mullin, 1992; DeYoreo and Vekilov, 2003). When $\Phi > 0$ ($\Delta G < 0$), the transition from one phase to the other is considered a natural spontaneous process. If $\Phi < 0$, however, a phase transition is thermodynamically impossible. At $\Phi = 0$, there exists a condition for equilibrium with respect to the phase transition (Nielsen, 1964; Pokrovsky and Schott, 2004; Morse et al., 2007; Benning and Waychunas, 2008; Schott et al., 2009).

Fig. 7 shows a plot of affinity vs Ω. For inorganic control experiments, negative affinities ($\Phi < 0$) in the range of −15.7 to −10.3 $KJ^{*}mol^{-1}$, confirm the impossibility of a phase transition to form calcite under low alkalinity and pH conditions. Experiments in the presence of active *Synechococcus* sp., showed positive affinities ($\Phi > 0$). For the lowest Ca^{2+} activity however, affinities evolved from 0 to 4.7 kJ/mol. This result implies an equilibrium condition with a low driving force for calcite crystallization after 13 days of experiment. Higher affinities ranging from 7.48 to 11.2 and 9.6 to 12.4 kJ/mol were obtained for Ca^{2+} activities of 1.71 ± 0.07 and 3.07 ± 0.09 respectively. The larger values of Φ in the presence of high Ca^{2+} and the alkaline pH conditions generated by cyanobacteria metabolism, indicate a far from equilibrium condition showing a greatest driving force for phase transition (Table 2). For the highest Ca^{2+} activity data set in Fig. 7, the decrease in Φ as a function of time, along with the gradual pH and total alkalinity decrease in Figs. 2a and 3a, indicate a phase transition from a state of high free energy (solvated state) to one of low free energy state favoring calcite crystal nucleation and precipitation from the mixed-flow bio-reactor supersaturated solution generated as a result of continuous photosynthetic activity.

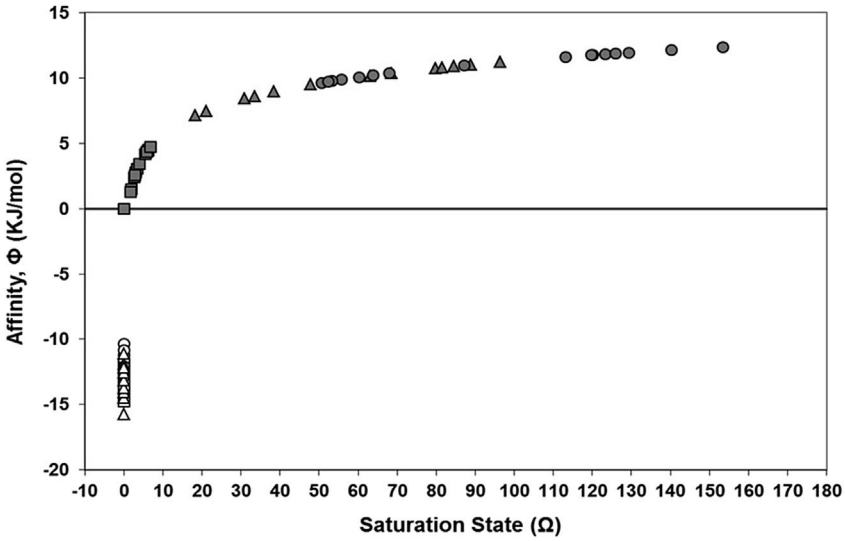

Fig. 7. Evolution of the affinity for mixed-flow bio-reactor solutions. The grey squares, triangles and circles represent affinities calculated for experiments with Ca^{2+} activities of 0.16 ± 0.02, 1.71 ± 0.07 and 3.07 ± 0.09 in the presence of active *Synechococcus* sp. Open markers represent affinity values calculated for control experiments in the absence of cyanobacteria biomass.

The chemical evolution of mixed-flow bio-reactor solutions in the presence of active cyanobacteria was used to determine calcite crystal growth rate, G. It was empirically defined as in Wolthers et al., 2012 such that, $G = IS^{-0.004} * pH^{-10.71} * r_{aq}^{-0.35} * (\Omega^{1/2} - 1)$, where IS is the ionic strength and r_{aq} is the ratio of carbonate and calcium activities. As shown in Fig. 8 and Table 2, for the lowest Ca^{2+} activity, G ranged from 0.00027 to 0.0079 nm/s, whereas for a Ca^{2+} activity of 1.71 ± 0.07, these values extended from 0.019 to 0.32 nm/s. For the highest Ca^{2+} activity of 3.07 ± 0.09, G varied from 0.21 to 0.67 nm/s. For similar solution ionic strengths and in the absence of significant concentrations of calcite inhibitors (e.g. PO_4^{3-}), G, would be mainly dependent on solution supersaturation. For the highest Ca^{2+} activity the fast crystal growth rate is consistent with a rapid calcite precipitation as suggested by affinity calculations (Fig. 7) and crystal morphologies (Fig. 5a and b). Under these conditions, the maximum value of G would correlate with highest supersaturation (Fig. 4) and affinity values (Fig. 7). These three parameters are controlled by the alkaline pH generated by the photosynthetic activity of *Synechococcus* sp. cyanobacteria. This further shows the feasibility of using active cyanobacteria to maintain highly supersaturated conditions and steady state conditions, for spontaneous nucleation and precipitation of calcite, leading to the biomineralization of excess atmospheric CO_2.

Fig. 9 and Table 1 show the evolution of $[CO_3^{2-}]$ for the duration of experiments. As explained earlier, a maximum $[CO_3^{2-}]$ is observed at 48 h followed by a gradual decrease. The time corresponding to the highest $[CO_3^{2-}]$ was taken as the induction time for calcite nucleation and precipitation as explained earlier. Fig. 10a and b shows plots of $\log_{10}R_{exp}$ vs $\log_{10}[CO_3^{2-}]$ and $\log_{10}R_{exp}$ vs $\log_{10}(\Omega\text{-}1)$ respectively, where R_{exp} refers to the calcite precipitation rate

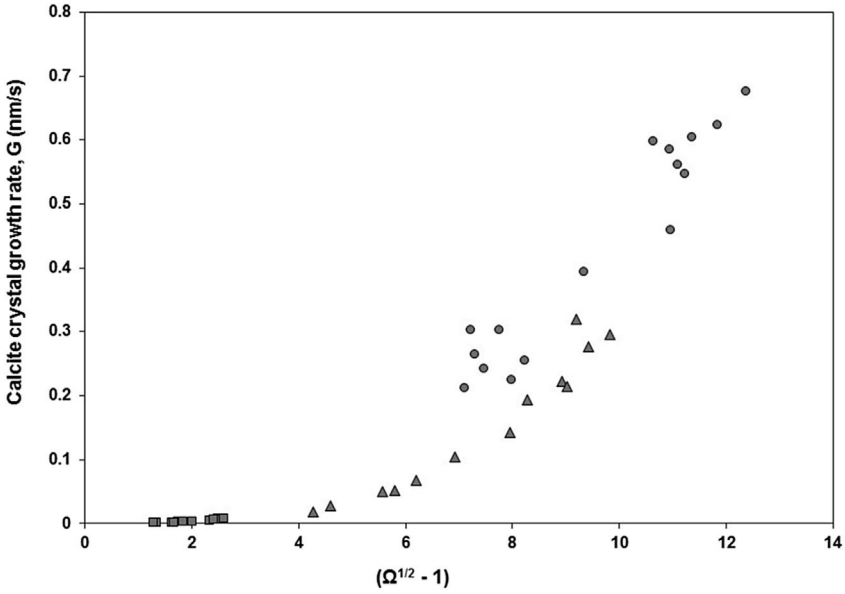

Fig. 8. The grey squares, triangles and circles represent the calcite crystal growth rates calculated from solution parameters as indicated in text for experiments with Ca^{2+} activities of 0.16 ± 0.02, 1.71 ± 0.07 and 3.07 ± 0.09 respectively, in the presence of active *Synechococcus* sp. cyanobacteria.

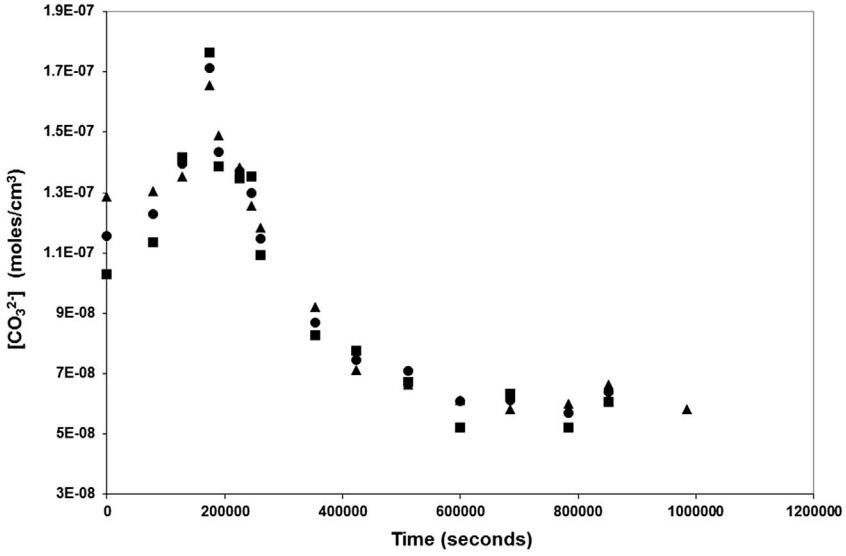

Fig. 9. Evolution of carbonate concentration as a function of time from three replicate experiments corresponding to the highest Ca^{2+} activity of 3.07 ± 0.09. The maximum carbonate concentration indicates an induction time of 48 h as explained in text.

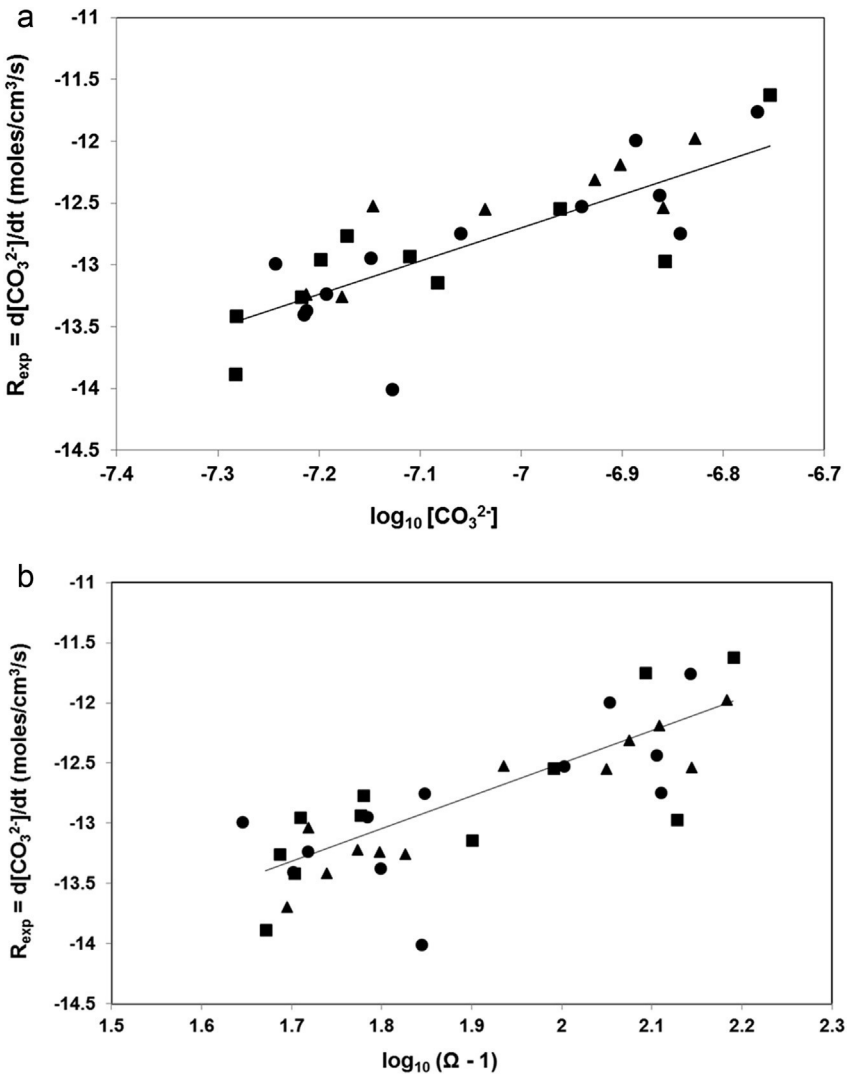

Fig. 10. (a) and (b) show log R_{exp} vs $\log_{10}[CO_3^{2-}]$ and $\log_{10}(\Omega\text{-}1)$ respectively, where R_{exp} was calculated as the first derivative of the data in Fig. 9. The solid lines in Figs. 10a and b represent the fit of the experimental rate data (R_{exp}) whose slope and intercept were used to obtain optimal kinetic parameters: n_1, n_2 and $\log_{10}K_f$ and $\log_{10}k_+$, as defined in text.

calculated as the first derivate of the data in Fig. 9. The solid lines in Figs. 10a and b are the regression lines of experimental calcite precipitation rates (R_{exp}). From these fits, n_1 and n_2 values of 2.71 ± 0.17 and 2.69 ± 0.11 were obtained, along with $\log_{10}K_f$ and $\log_{10}k_+$ of 6.37 ± 1.12 and −17.92 ± 0.28 respectively, when applying precipitation rate calculation methods from Zhong and Mucci (1993) and Morse (1983). The orders of reaction in this study are in good agreement with the n value of 2.83 ± 0.04 found by Zhong and Mucci (1993). As stated previously, saturation sate (Ω) or $[CO_3^{2-}]$ based rate laws, cannot reflect the controls on crystal growth kinetics or reliably predict growth mechanism (Teng et al., 2000). However the relatively high n_1 and n_2 values suggest that the precipitation of calcite, observed herein, occurred via surface-controlled rate determining reactions. These high reaction orders further support the hypothesis that calcite crystal growth proceeded through complex surface controlled mechanisms, as explained by Mucci and Morse, 1983.

4. Conclusion

This study quantified the kinetics of calcite precipitation using a novel steady state bio-reactor set up. Achievement of steady state conditions with respect to chemical parameters (e.g. Ca^{2+}), and most importantly biomass allowed quantification of the kinetics of calcite precipitation. Reaction orders and kinetic constant values obtained herein are consistent with those of previous studies. The results of this study propose that the photosynthetic activity of the planktonic cyanobacteria species *Synechococcus* sp. could aid in carbonate biomineralization at the large scale. This study showed the generation of a supersaturated solution with respect to calcite with dissolving CO_2 as the only source of inorganic carbon where active cyanobacteria maintained highly alkaline pH conditions. Although, in principle, this system has the potential to continuously biomineralize CO_2 as calcite, further studies would be needed before a large-scale application of this system can be implemented.

Acknowledgements

Funding for this project was obtained from a research grant provided to REM by the Science Support Center (SSC) at the University of Freiburg (Innovationsfonds Forschungs Kapitel: 1410, TG 99, BA 600197). The authors would like to thank Ms. Sigrid-Hirth Walther of the Institut für Geo-und Umweltwissenschaften at the University of Freiburg for F-AAS measurements. The authors are also grateful to Dr. Michael S. Krzemnicki of the Schweizerisches Gemmologisches Institut (SSEF) for providing access to their Raman Spectrometer. In addition, the authors would like to thank Prof. Dr. Liane G. Benning of the University of Leeds and for providing access to ESEM facilities.

References

Almeida, F.V., Guimarães, J.R., Jardim, W.F., 2001. Measuring the CO_2 flux at the air/water interface in lakes using flow injection analysis. J. Environ. Monit. 3, 317–321.
Aloisi, G., Gloter, A., Kruger, M., Wallman, K., Guyot, F., Zuddas, P., 2006. Nucleation of calcium carbonate on bacterial nanoglobules. Geology 34, 1017–1020.
Altermann, W., Kazmierczak, J., Oren, A., Wright, T., 2006. Cyanobacterial calcification and its rock-building potential during 3.5 billion years of Earth history. Geobiology 4, 147–166.
Astilleros, J.M., Pina, C.M., Fernández-Díaz, L., Putnis, A., 2002. Molecular-scale surface processes during the growth of calcite in the presence of manganese. Geochim. Cosmochim. Acta 66, 3177–3189.
Badger, M.R., Price, G.D., 2003. CO_2 concentrating mechanisms in cyanobacteria: molecular components, their diversity and evolution. J. Exp. Bot. 54, 609–622.
Bénézeth, P., Stefánsson, A., Gautier, Q., Schott, J., 2013. Mineral solubility and aqueous speciation under hydrothermal conditions to 300 °C – the carbonate system as an example. In: Stefánsson, A., Driesner, T., Bénézeth, P. (Eds.), Thermodynamics of Geothermal Fluids. Rev. Mineral. Geochem, vol. 76, pp. 81–133.
Benning, L.G., Waychunas, G.A., 2008. Nucleation, growth and aggregation of mineral phases: mechanisms and kinetic controls. In: Brantley, S.L., Kubicki, J.D., White, A.F. (Eds.), Kinetics of Water-rock Interaction. Springer Science+Business Media, LLC, New York, pp. 259–323.
Benzerara, K., Menguy, N., López-García, P., Yoon, T.-H., Kazmierczak, J., Tyliszczak, T., Guyot, F., Brown Jr., G.E., 2006. Nanoscale detection of organic signatures in carbonate microbialites. PNAS 103, 9440–9445.
Bontognali, T.R.R., Vasconcelos, C., Warthmann, R.J., Dupraz, C., Bernasconi, S.M., McKenzie, J.T., 2008. Microbes produce nanobacteria-like structures, avoiding cell entombment. Geology 36, 663–666.
Bots, P., Benning, L.G., Rodriguez-Blanco, J.-D., Roncal-Herrero, T., Shaw, S., 2012. Mechanistic insights into the crystallization of amorphous calcium carbonate (ACC). Cryst. Growth Des. 12, 3806–3814.
Braissant, O., Cailleau, G., Dupraz, C., Verrecchia, A.P., 2003. Bacterially induced mineralization of calcium carbonate in terrestrial environments: the role of exopolysaccharides and amino acids. J. Sediment. Res. 73, 485–490.
Brečević, L., Nielsen, A.E., 1989. Solubility of amorphous calcium carbonate. J. Cryst. Growth 1989 (98), 504–510.
Bundeleva, I.A., Shirokova, L.S., Bénézeth, P., Pokrovsky, O.S., Kompantseva, E.I., Balor, S., 2011. Zeta potential of anoxygenic phototrophic bacteria and Ca adsorption at the cell surface: possible implications for cell protection from $CaCO_3$ precipitation in alkaline solutions. J. Coll. Interf. Sci. 360, 100–109.
Bundeleva, I.A., Shirokova, L.S., Bénézeth, P., Pokrovsky, O.S., Kompantseva, E.I., Balor, S., 2012. Calcium carbonate precipitation by anoxygenic phototrophic bacteria. Chem. Geol. 291, 116–131.
Bundeleva, I.A., Shirokova, L.S., Pokrovsky, O.S., Bénézeth, P., Ménez, B., Gérard, E., Balor, S., 2014. Experimental modeling of calcium carbonate precipitation by cyanobacterium *Gloeocapsa* sp. Chem. Geol. 374–375, 44–60.
Couradeau, E., Benzerara, K., Gérard, E., Estève, I., Moreira, D., Tavera, R., López-García, P., 2013. Cyanobacterial calcification in modern microbialites at the submicrometer scale. Biogeosciences 10, 5255–5266.
Cusack, M., Freer, A., 2008. Biomineralization: elemental and organic influence in carbonate systems. Chem. Rev. 108, 4433–4454.
DeYoreo, J.J., Vekilov, P.G., 2003. Principles of crystal nucleation and growth. In: Dove, P.M., DeYoreo, J.J., Weiner, S. (Eds.), Biomineralization. Rev. Mineral Geochem, vol. 54, pp. 57–93.
Dittrich, M., Obst, M., 2004. Are picoplankton responsible for calcite precipitation in lakes? Ambio 33, 559–564.
Dittrich, M., Sibler, S., 2010. Calcium carbonate precipitation by cyanobacterial polysaccharides. Geol. Soc. Lond., Spec. Publ. 336, 51–63.
Dittrich, M., Müller, B., Mavrocordatos, D., Wehrli, B., 2003. Induced calcite precipitation by cyanobacterium *Synechococcus*. Acta Hydrochim. Hydrobiol. 31, 162–169.
Dupraz, C., Reid, R.P., Braissant, O., Decho, A.W., Norman, R.S., Visscher, P.T., 2009. Processes of carbonate precipitation in modern microbial mats. Earth-Sci. Rev. 96, 141–162.
Edwards, H.G.M., Jorge Villar, S.E., Jehlicka, J., Munshi, T., 2005. FT-Raman spectroscopic study of calcium-rich and magnesium-rich carbonate minerals. Spectrochim. Acta A 61, 2273–2280.
Ferris, F.G., Wiese, R.G., Fyfe, W.S., 1994. Precipitation of carbonate minerals by microorganisms: implications for silicate weathering and the global carbon dioxide budget. Geomicrobiol. J. 12, 1–13.
Gómez-Morales, J., Torrent-Burgués, J., Rodríguez-Clemente, R., 1996. Nucleation of calcium carbonate at different initial pH conditions. J. Cryst. Growth 169, 331–338.
He, S.L., Morse, J.W., 1993. The carbonic-acid system and calcite solubility in aqueous Na-K-Ca-Mg-Cl-SO_4 solutions from 0 to 90 °C. Geochim. Cosmochim. Acta 57, 3533–3554.
Herzog, H.J., 2011. Scaling up carbon dioxide capture and storage: from megatons to gigatons. Energ. Econ. 33, 597–604.
James, N.P., 1972. Holocene and Pleistocene calcareous crust (caliche) profiles: criteria for subaerial exposure. J. Sediment. Petrol 42, 817–836.
Jansson, C., Northen, T., 2010. Calcifying cyanobacteria – the potential of biomineralization for carbon capture and storage. Curr. Opin. Biotech. 21, 365–371.
Kharaka, Y.K., Cole, D.R., 2011. Geochemistry of geologic sequestration of carbon dioxide. In: Harmon, R.S., Parker, A. (Eds.), Frontiers in Geochemistry: Contribution of Geochemistry to the Study of the Earth. John Wiley & Sons Ltd., Chichester, West Sussex, UK.
Kosamu, I.B., Obst, M., 2009. The influence of picocyanobacterial photosynthesis on calcite precipitation. Int. J. Environ. Sci. Technol. 6, 557–562.
Lasaga, A.C., 1981. Rate laws of chemical reactions. In: Lasaga, A.C., Kirkpatrick, R.J. (Eds.), Kinetics of Geochemical Processes. Rev. Mineral. Geochem, vol. 8, pp. 1–68.
Lee, B.D., Apel, W.A., Walton, M.R., 2004. Screening of cyanobacterial species for calcification. Biotechnol. Prog. 20, 1345–1351. http://dx.doi.org/10.1021/bp0343561.
Lee, B.D., Apel, W.A., Walton, M.R., 2006. Calcium carbonate formation by Synechococcus sp. strain PCC 8806 and Synechococcus sp. strain PCC 8807. Bioresour. Technol. 97, 2427–2434.
Martinez, R.E., Pokrovsky, O.S., Schott, J., Oelkers, E.H., 2008. Surface charge and zeta potential of metabolically active and dead cyanobacteria. J. Coll. Interf. Sci. 323, 317–325.
Martinez, R.E., Gardés, E., Pokrovsky, O.S., Schott, J., Oelkers, E.H., 2010. Do photosynthetic bacteria have a protective mechanism against carbonate precipitation

at their surfaces? Geochim. Cosmochim. Acta 74, 1329–1337.
McConnaughey, T., Whelan, J.F., 1997. Calcification generates protons for nutrient and bicarbonate uptake. Earth Sci. Rev. 42, 95–117.
Millero, F.J., 2007. The marine inorganic carbon cycle. Chem. Rev. 107, 308–341.
Mitchell, A.C., Ferris, F.G., 2006. The Influence of Bacillus pasteurii on the nucleation and growth of calcium carbonate. Geomicrobiol. J. 23, 213–226.
Morse, J.W., 1983. The kinetics of calcium carbonate dissolution and precipitation. In: Reeder, R.J. (Ed.), Carbonates: Mineralogy and Chemistry. Rev. Mineral. Geochem, vol. 11, pp. 227–264.
Morse, J.W., Arvidson, R.S., Lüttge, A., 2007. Calcium carbonate formation and dissolution. Chem. Rev. 107, 342–381. http://dx.doi.org/10.1021/cr050358j.
Mucci, A., 1986. Growth kinetics and composition of magnesian calcite overgrowths precipitated form seawater: quantitative influence of orthophosphate ions. Geochim. Cosmochim. Acta 50, 2225–2265.
Mucci, A., Morse, J.W., 1983. The incorporation of $Mg^{2+}$and Sr^{2+} into calcite overgrowths: influences of growth rate and solution composition. Geochim. Cosmochim. Acta 47, 217–233.
Mullin, J.W., 1992. Crystallization, third ed. Butterworths, Oxford.
Nielsen, A.E., 1964. Kinetics of Precipitation. Pergamon Press, New York.
Obst, M., Dynes, J.J., Lawrence, J.R., Swerhone, G.D.W., Benzerara, K., Karunakaran, C., Kaznatcheev, K., Tyliszczak, T., Hitchcock, A.P., 2009. Precipitation of amorphous $CaCO_3$ (aragonite-like) by cyanobacteria: a STXM study of the influence of EPS on the nucleation process. Geochim. Cosmochim. Acta 73, 4180–4198.
Papazi, A., Makridis, P., Divanach, P., Kotzabasis, K., 2008. Bioenergetic changes in the microalgal photosynthetic apparatus by extremely high CO_2 concentrations induce an intense biomass production. Physiol. Plant. 132, 338–349.
Plummer, N.L., Wigley, T.M.L., Parkhurst, D.L., 1978. The kinetics of calcite dissolution in CO_2-water systems at 5° to 60°C and 0.0 to 1.0 atm CO_2. Am. J. Sci. 278, 179–216.
Pokrovskiy, O.S., Savenko, V.S., 1995. The role of magnesium at homogeneous precipitation of carbonate from seawater. Oceanology 34, 493–497.
Pokrovsky, O.S., Schott, J., 2004. Experimental study of brucite dissolution in aqueous solutions: surface speciation and chemical affinity control. Geochim. Cosmochim. Acta 68, 31–45.
Power, I.M., Wilson, S.A., Thom, J.M., Dipple, G.M., Southam, G., 2007. Biologically induced mineralization of dypingite by cyanobacteria from an alkaline wetland near Atlin, British Columbia, Canada. Geochem. Trans. 8, 1–16.
Price, G.D., Maeda, S., Omata, T., Badger, M.R., 2002. Modes of active inorganic carbon uptake in the cyanobacterium, *Synechococcus* sp. PCC7942. Funct. Plant Biol. 29, 131–149.
Price, G.D., Badger, M.R., Woodger, F.J., Long, B.M., 2008. Advances in understanding the cyanobacterial CO_2-concentratingmechanism (CCM): functional components, Ci transporters, diversity, genetic regulation and prospects for engineering into plants. J. Exp. Bot. 59, 1441–1461.
Prieto, M., García-Ruiz, J.M., Amorós, J.L., 1981. Growth of calcite crystals with nonsingluar phases. J. Cryst. Growth 52, 864–867.
Rodríguez-Blanco, J.D., Shaw, S., Benning, L.G., 2011. The kinetics and mechanisms of amorphous calcium carbonate (ACC) crystallization to calcite via vaterite. Nanoscale 3, 265–271.
Rohwer, F., Thurber, R.V., 2009. Viruses manipulate the marine environment. Nature 459, 207–212.
Ruiz-Agudo, E., Putnis, C.V., 2012. Direct observations of mineral-fluid reactions using atomic force microscopy: the specific example of calcite. Mineral. Mag. 76, 227–253.
Schott, J., Pokrovsky, O.S., Oelkers, E.H., 2009. The link between mineral dissolution/precipitation kinetics and solution chemistry. In: Oelkers, E.H., Schott, J. (Eds.), Thermodynamics and Kinetics of Water-rock Interaction. Rev. Mineral. Geochem, vol. 70, pp. 207–258.
Teng, H.H., Dove, P.M., DeYoreo, J.J., 2000. Kinetics of calcite growth: surface processes and relationships to macroscopic rate laws. Geochim. Cosmochim. Acta 64, 2255–2266.
Thompson, J.B., Shultze-Lam, S., Beveridge, T.J., Des Marais, D.J., 1997. Whiting events:biogenic origin due to the photosynthetic activity of cyanobacterial picoplankton. Limnol. Oceanogr. 42, 133–141.
Urosevic, M., Rodriguez-Navarro, C., Putnis, C.V., Cardell, C., Putnis, A., Ruiz-Agudo, E., 2012. In situ nanoscale observations of the dissolution of {10$\bar{1}$ 4} dolomite cleavage surfaces. Geochim. Cosmochim. Acta 80, 1–13.
Wolthers, M., Nehrke, G., Gustafsson, J.P., Van Cappellen, P., 2012. Calcite growth kinetics: modeling the effect of solution stoichiometry. Geochim. Cosmochim. Acta 77, 121–134. http://dx.doi.org/10.1016/j.gca2011.11003.
Wright, V.P., 1984. The significance of needle-fibre calcite in a lower carboniferous paleosol. Geol. J. 19, 23–32.
Zhong, S., Mucci, A., 1993. Calcite precipitation in seawater using a constant addition technique: a new overall reaction kinetic expression. Geochim. Cosmochim. Acta 57, 1409–1417.
Zhu, T., Paulo, C., Merroun, M.L., Dittrich, M., 2015. Potential application of biomineralization by *Synechococcus* PCC8806 for concrete restoration. Ecol. Eng. 82, 459–468. http://dx.doi.org/10.1016/j.ecoleng.2015.07.017.